Universidad de Huelva

Departamento de Ingeniería Electrónica, de Sistemas Informáticos y Automática

Contributions to smart grids based on renewable energy sources with hydrogen as backup system. Energy management system: design, modeling and physical implementation based on model predictive control theory

Memoria para optar al grado de doctor
presentada por:

Francisco José Vivas Fernández

Fecha de lectura: 5 de febrero de 2020

Bajo la dirección de los doctores:

José Manuel Andújar Márquez

Francisca Segura Manzano

Huelva, 2020

Universidad De Huelva

Programa de Doctorado de Ciencia y Tecnología Industrial y Ambiental
Línea de investigación
Ingeniería eléctrica, electrónica, de control y robótica

Contributions to smart grids based on renewable energy sources with hydrogen as backup system. Energy management system: design, modeling and physical implementation based on Model Predictive Control theory

Memoria para optar al grado de doctor presentada por:

Francisco José Vivas Fernández

Fecha de lectura:

Bajo la dirección de los doctores:

José Manuel Andújar Márquez

Francisca Segura Manzano

Huelva, 2019

UNIVERSITY OF HUELVA

Doctoral Program in Industrial and Environmental Science and Technology
Research line
Electrical, electronic, control and robotics engineering

CONTRIBUTIONS TO SMART GRIDS BASED ON RENEWABLE ENERGY SOURCES WITH HYDROGEN AS BACKUP SYSTEM. ENERGY MANAGEMENT SYSTEM: DESIGN, MODELING AND PHYSICAL IMPLEMENTATION BASED ON MODEL PREDICTIVE CONTROL THEORY

Ph. D. Thesis

FRANCISCO JOSÉ VIVAS FERNÁNDEZ

2019

Supervisors:

Dr. José Manuel Andújar Márquez

Dra. Francisca Segura Manzano

UNIVERSIDAD DE HUELVA

Programa de Doctorado de Ciencia y Tecnología Industrial y Ambiental
Línea de investigación
Ingeniería eléctrica, electrónica, de control y robótica

CONTRIBUCIONES A LAS MICRO REDES BASADAS EN FUENTES DE ENERGÍA RENOVABLE CON HIDRÓGENO COMO SISTEMA DE RESPALDO. SISTEMA DE GESTIÓN DE ENERGÍA: DISEÑO, MODELADO E IMPLEMENTACIÓN FÍSICA A PARTIR DE LA TEORÍA DE MODELO DE CONTROL PREDICTIVO

Tesis Doctoral

FRANCISCO JOSÉ VIVAS FERNÁNDEZ

2019

Directores:

Dr. José Manuel Andújar Márquez

Dra. Francisca Segura Manzano

D. José Manuel Andújar Márquez, Catedrático de Universidad de la Escuela Técnica Superior de Ingeniería de la Universidad de Huelva,

Dña. Francisca Segura Manzano, Profesora Titular de Universidad de la Escuela Técnica Superior de Ingeniería de la Universidad de Huelva,

CERTIFICAN:

Que D. Francisco José Vivas Fernández, Ingeniero Industrial por la Universidad de Huelva, ha realizado bajo nuestra dirección y dentro del programa de doctorado de Ciencia y Tecnología Industrial y ambiental (CyTIA) y en la línea de investigación de Ingeniería eléctrica, Electrónica, de Control y Robótica el trabajo correspondiente a su Tesis Doctoral titulada:

Contribuciones a las micro redes basadas en fuentes de energía renovable con hidrógeno como sistema de respaldo. Sistema de gestión de energía: diseño, modelado e implementación física a partir de la teoría de Modelo de Control Predictivo

Revisado el presente trabajo, estimamos que puede ser presentado al Tribunal que ha de juzgarlo.

Y para que así conste a efectos de lo establecido Real Decreto 99/2011 y por la normativa Reguladora del título de Doctor de la Universidad de Huelva, autorizamos la presentación de este trabajo en la Universidad de Huelva.

Huelva, a 22 de Noviembre de 2019

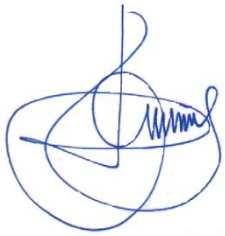

Director: Dr. José Manuel Andújar Márquez

Directora: Dra. Francisca Segura Manzano

Doctorando: D. Francisco José Vivas Fernández

CONTRIBUTIONS TO SMART GRIDS BASED ON RENEWABLE ENERGY SOURCES WITH HYDROGEN AS BACKUP SYSTEM. ENERGY MANAGEMENT SYSTEM: DESIGN, MODELING AND PHYSICAL IMPLEMENTATION BASED ON MODEL PREDICTIVE CONTROL THEORY

Research memory presented by Francisco José Vivas Fernández to apply for a PhD. Doctoral degree with International Mention at the University of Huelva.

Francisco José Vivas Fernández

The present Dissertation has been performed at the Control and Robotics Research Group, Ref. TEP192, from the University of Huelva, under the auspices of Dr. José Manuel Andújar Márquez and Dra. Francisca Segura Manzano, which approve its defence:

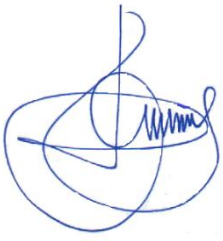

Dr. José Manuel Andújar Márquez

Dra. Francisca Segura Manzano

Huelva, November 22th, 2019

Acknowledgements

First of all I would like to thank my thesis directors, Dr. José Manuel Andújar and Dr. Paqui Segura, because their search for new projects makes it possible to maintain experimental works like this one, for teaching me to value the world of research from another point of view, for their infinite passion, confidence, dedication and patience during the development of this thesis.

To all my former INTA colleagues at the Energy Systems Laboratory (LSE-CEDEA) and the Astrobiology Center (CAB), whom I remember with great affection, thank you for making me a person who is curious for knowledge, and for making my stay there like being at home.

To all the members of the Control and Robotics Research Group TEP-192 of the University of Huelva, colleagues and friends, for sharing the days, hours, minutes, and for helping me in everything I needed, among them: Joaquín, Moisés, Julio, Daniel ...

To all the people who, to a greater or lesser extent, have shared during these years the hard but exciting stage of personal and professional growth that this thesis entails, especially Ainhoa.

And, finally, I want to thank my family, specifically my parents Francisco J. and Rocío. For their great personal sacrifice, for their affection, support and advice to make me a better person.

Thank you very much for your support and trust.

Agradecimientos

En primer lugar quiero dar las gracias a mis directores de Tesis, Dr. José Manuel Andújar y Dra. Paqui Segura, por su búsqueda de nuevos proyectos capaces de mantener trabajos experimentales como éste, por enseñarme a valorar el mundo de la investigación desde otro punto de vista, por su infinita pasión, confianza, entrega y paciencia durante al desarrollo de esta tesis.

A todos mis antiguos compañeros/as del INTA del Laboratorio de Sistemas de Energía (LSE-CEDEA) y del Centro de Astrobiología (CAB), a quienes les recuerdo con un gran cariño, gracias por haberme hecho una persona curiosa en el saber, y hacer que mi estancia allí fuera como estar en casa.

A todos los miembros del Grupo de Investigación de Control y Robótica TEP-192 de la Universidad de Huelva, compañeros y amigos, por compartir los días, horas, minutos, y haberme ayudado en todo lo que he necesitado, entre ellos: Joaquín, Moisés, Julio, Daniel…

A todas las personas que en mayor o menor medida han compartido durante estos años la dura pero apasionante etapa de crecimiento personal y profesional que conlleva la presente tesis, en especial a Ainhoa.

Y, finalmente quiero dar las gracias a mi familia, concretamente a mis padres Francisco J. y Rocío. Por su gran sacrificio personal, por su cariño, apoyo y sus consejos para hacer de mí una mejor persona.

Muchas gracias por vuestro apoyo y confianza.

Content

Chapter 1

General Approach of the Thesis

Chapter 1. General Approach of the Thesis

This Thesis is not conceived as an isolated work, but within the scientific production and the training capability that the Research Group TEP-192 from the University of Huelva has. This Thesis is part of the set of Theses that are being carried out simultaneously and that seek to solve the problem of *Configuration and management of a smart renewable micro-grid hybridized with hydrogen technology*; name and objective of the R&D project DPI2017-85540-R[1] that partially finances this Thesis.

Within the tasks of the research project mentioned above, this thesis aims to implement an energy management strategy based on the use of predictive control techniques, which optimizes the short- and long-term response of a renewable sources-based smart grid with hydrogen as backup. Hybridization for this case consists of the use of several renewable energy sources, solar and wind, connected to a common bus supported by a battery bank. Considering the use of hydrogen as an energy vector, it makes use of systems for the production and storage of hydrogen, and its subsequent conversion to electrical energy using electrolyzer, hydrogen storage tanks and fuel cell respectively.

In Article 1, there are studied all the topologies and typical configurations of this type of smart grids, the main problems associated with the use of renewable generation sources, as well as the use of storage technologies based on batteries and hydrogen as an energy vector. To solve the different problems in the management of the different devices, different technical and economic proposals are analysed, which largely determine the optimization of the system management. Based on the previous study, the Article 1 presents a detailed review and a critical analysis of the different management strategies proposed in the scientific literature, for smart grids with similar topology to the one studied in this thesis. In this sense, it is hard to find solutions that allow the technical and economic optimization of the system both in the short and in the long term. Therefore, it involve that there is a niche of improvements and new proposal in terms of system optimization.

Based on the main problems and technical and economic solutions studied in Article 1, it is necessary to test the system in order to solve the main deficiencies and needs found in the proposals analyzed in the scientific literature.

Due to the high economic and temporal cost required to test the behavior of these type of system, it is necessary to have a software tool that simulates its behavior in the short and long term, so that the results can be analyzed and allow to determine the relationships between operation criteria and equipment management and the response of the entire system in terms of

[1] R&D Project founded by the Spanish Government, RETOS programme.

performance, degradation, economical cost and quality of the electrical power supply.

To this end, and in the absence of flexible software solutions in the scientific literature, in Article 2 a powerful software tool developed in the Matlab Simulink® environment is presented, from which any system topology to be evaluated can be modelled, and in which different design criteria can be defined in the operation of the system, such as priorities in the performance of the equipment, grid connection, power constraints of the equipment, etc. Similarly, associated with each element of the system, different technical and economic parameters related to its operation are defined, such as cycles and operating times, accumulated degradation, operation and maintenance costs, hydrogen produced and/or consumed system performance, etc.

The analysis of the simulation results obtained will allow defining certain actions on the system, in such a way as to increase the performance of the system from a technical and economic point of view. These lines of action will allow defining the design criteria of the energy management strategy of the system, being therefore key for the definition of the predictive controller proposed in Article 5.

In response to the need to optimize the response of the management system, equipment degradation is a fundamental parameter in the of long-term technical and economic criteria optimization. To that end, Article 3 presents a novel system for individual cell detection for open-air-cooled cathode fuel cell stacks. This patented design allows to quantify the voltage degradation for each cell, as well as to identify the degradation ratios linked to the conditions of use, quantifying the individual degradation of the cell with respect to the current and operating temperature.

The use of the proposed system allows to know the degradation of the fuel cell stack with respect to the initial state, providing relevant information on the real state of the system in order to the controller acts accordingly.

To face the task of design and subsequent experimental implementation of the management strategy, it is necessary to have a model of the smart grid that serves as a background for the subsequent development of the predictive controller. In this sense, in Article 4 it is developed the non-linear state-space model of the smart grid consisting of renewable generation sources, energy storage systems, electrical grid input and load profile. To do it, a series of tests is carried out to characterize the dynamic behaviour of each device, as well as to obtain those mathematical expressions that allow, through an experimental identification process, to model the non-linearities of each equipment. Finally, the generalist model of the smart grid is linearized around different working points, in such a way that it is possible to obtain a Lineal Time Variant (LTV) model that allows considering the behaviour of the system throughout all its operating range.

Next, based on the proposed system state-space model, in Article 5 the theoretical study and

design of the proposed predictive controller for the implementation of the proposed energy management strategy is carried out. In this sense, the proposed management strategy determines the priority in the use of the equipment, the energy distribution between the different energy storage systems, the role of the electrical grid, as well as considerations in the operation of the different equipment that make up the smart grid system. In such a way that a safe and efficient operation of each of device is guaranteed. In order to guarantee the generality of the proposed controller, a methodology for calculating the main parameters of the predictive controller, prediction and control horizon, system references and weighting factors for the tracking problem and control variation defined by the cost function of the system, is presented.

Finally, it is proceeded to the physical implementation of the energy management strategy on the real smart grid. For this purpose, the design and development of the control, monitoring, visualization and power electronics, necessary for the correct management and interconnection of all the equipment to the smart grid is presented.

The experimental tests carried out on the real smart grid have allowed validating the design of the predictive controller and the proposed energy management strategy, on real renewable sources-based smart grid with the use of hydrogen as an energy carrier.

1.1. Summary of the Thesis

This Thesis is organized in seven Chapters according to the following order:

Chapter 1 deals with the *General Approach of the Thesis*, in which there is a description of the structure of the Thesis and a brief summary of each of the Chapters that integrate it, focusing on the main contributions. In addition, an analysis of the scientific contribution that has been produced by the completion of this Thesis is carried out.

Chapter 2, *Objectives and Methodology*, the individual objectives necessary to achieve the main objective of the thesis are presented, the design and implementation of a control system capable of managing energy based on technical and economic optimization criteria, both in the short and long term. According to the structure of the thesis, each of the scientific contributions included in Chapter 4, has the purpose of responding to each of the objectives set.

Finally, the working methodology used to achieve each and every one of the proposed objectives is presented.

In Chapter 3, *Materials*, the proposed micro grid architecture and the control, monitoring and power electronics developed for the correct integration of the equipment into the smart grid according to the selected topology are detailed.

Considering the power electronics developed, this section details the design of the power

converters and control algorithm used for the integration of renewable generation based on solar and hydrogen resources. It should be noted that boost converters have been developed with an MPPT algorithm to maximise the solar resource; as well as an isolated push-pull topology converter with power control based on discrete PID, with the aim of integrating the fuel cell subsystem into the smart grid.

In response to the monitoring and control electronics, all the electronics have been specifically designed to measure the main electrical parameters of each device.

In this sense, it has been designed and developed an electronic hardware to control and manage the balance of plant (BoP) of the fuel cell in order to guarantee the hydrogen supply, the hydrogen purges, the fuel cell thermal control and electrical insulation.

In the same way, it has been developed an electronic specially designed for individual cells voltage monitoring in the case of the fuel cell. This electronics allows to evaluate, detect and quantify the degradation associated to each of the cells depending on the polarization point, allowing having real data to update the different degradation parameters used in the model of the plant, as well as to detect any malfunction in any cell, which may negatively affect the operation of the entire stack.

Attending to the visualization and control solutions, a control and monitoring software (SCADA) has been developed, from which the individual control of each subsystem is allowed, as well as the detection of any problem associated with the operation of the smart grid.

In Chapter 4, *Results & Methods*, the set of scientific contributions that support this thesis is presented. In this sense, five scientific articles published in journals of high impact index are presented, as well as different contributions to international congress, referents of the renewable energy and hydrogen sector.

In the Chapter 5, *General Conclusions*, the most relevant conclusions obtained from this Thesis are discussed, and the research lines that have been opened by the developed work are framed, in addition to proposing strategies and actions in this sense.

Finally, Chapter 6, *Other scientific contributions*, a set of scientific contributions are presented in which the doctoral student has actively participated as co-author during the completion of the doctoral thesis. This compendium of works includes a series of research articles published in high impact index journals, as well as contributions to the main international congress of the renewable energies and hydrogen sector. These contributions complement the research activity of the doctoral student, and therefore are included in the set of contributions that support this thesis.

1.2. Innovations Provided by the Thesis

In this section, each of the Chapters that make up this Thesis are covered, highlighting the novel contributions that each Chapter adds with respect to the state of the art reviewed before, addressing the different tasks that make up each Article.

In the first instance, Article 1 presents an extensive scientific review that allows any technologist or researcher to identify the main characteristics of this type of smart grid and the different solutions in the field of energy management. For this, Article 1 analyses the main technical and economic problems associated with the operation of this type of systems, as well as the most widespread solutions in terms of optimization. An extensive review and critical analysis of the main works in the field of energy management in this type of systems allows contextualizing the reader in the state of technique and management algorithms used, allowing to identify niches of improvement.

In order to respond to the deficiencies found in the scientific literature, and identify the cause-effect relationships that the operation of a particular type of equipment may cause on the main technical and economic parameters of the system, in Article 2 a simulator has been developed. The use of this software solution allows to know the general functioning of the smart grid, taking into account all the restrictions imposed by the particularities in the use of each device related to the energy storage system, hydrogen and battery based systems, and the energy interactions between the hybrid system and the main grid. In this regard, it is worth mentioning: 1) the definition of a charging protocol to ensure a safe and efficient charging protocol of the batteries, 2) to establish minimum working power and restrictions in the variation of the working point for the hydrogen-based energy storage system, and 3) the definition of priorities about what subsystem must to act firstly in case of energy deficit and energy excess situation.

The definition of the present criteria will mark the design guidelines of the energy management strategy and therefore the predictive controller proposed in Article 5.

Attending to the optimization of the hydrogen-based storage system, and particularly the use of fuel cells, the detection, correction and mitigation of the occurrence of degradation associated with the start and stop cycles, as well as operating time, is crucial. The degradation parameter must be a fundamental point in the technical and economic criteria optimization of this type of equipment, known its reduced useful lifetime and high cost. For the detection of voltage and power degradation of the fuel cell, a patented electronic device specially designed for the application is presented in Article 3.

The use of this system allows to know in real time the voltage degradation of each of the cells that make up the fuel cell stack, and to identify if any of them suffer a high deterioration,

which can undermine the performance of the whole system. Based on this information, the control system that implements the energy management strategy will allow for a more conservative use of the fuel cell if necessary, increasing the lifetime of the hydrogen-based system, while reducing the costs associated with equipment maintenance and renovation.

In order to be able to study the system and define the proposed energy management strategy, in Article 4 a generalist mathematical model of the smart grid is presented, based on the use of recursive linearization. This allows us to model the behaviour of the system throughout all its operating range, thus increasing the quality of the prediction of the trajectory of the system in the operation of the predictive controller, unlike most solutions based on a linear model around a single operating point.

The proposed model includes all the technical and economic parameters to define the multi-objective function that will determine the cost function of the optimization problem of the proposed predictive controller. Thanks to the inclusion of these parameters, the evaluation of the temporary response of the system is allowed, so that the accumulated degradation of the system can be quantified, and therefore, corrective actions for the optimization can be established throughout the useful life of the system.

Based on the control proposed in Article 5, the novelty lies in the design of a tuning methodology for the controller parameters, based on the generalist model proposed in Article 4 and the design criteria defined in Article 2.

Unlike most of the scientific works reviewed, based on particular solutions depending on the topology and application of the system, to guarantee the generality of the controller, rules are defined for the tuning process. In such a way, it is allowed in the first instance to guarantee the closed loop stability of the system, as well how to correctly implement the energy management strategy based on the technical and economic optimization of the system both in the short and long term for any type of system.

For this, a careful study has been carried out with the aim to discern the relationships between the variations of the different parameters that define the controller, and the closed loop response of the plant-controller system in the short and long term. In this sense, a series of mathematical proposals based on fuzzy control and potential expressions obtained from the previous study are presented, which allow defining an adaptive controller whose function is to adapt the value of the weighting factor of the system based on the current situation and the past history of the system.

Finally, Article 5 presents the experimental implementation of the predictive control algorithm and therefore of the energy management strategy proposed on the real smart grid; as well as all the development of control, monitoring, visualization and power electronic required for the correct integration of all equipment in a topology based on a DC bus with direct battery

connection.

In this sense, unlike most works found in the scientific literature based mainly on simulation or small pilot plants, this Thesis validates the use of the proposed controller on a medium size smart grid, with a the power range of domestic consumption and small businesses.

In view of the above, the technical feasibility of using predictive control techniques in complex applications, such as the control of renewable generation systems with hydrogen as an energy vector is demonstrated.

1.3. Scientific Contribution of the Thesis

This section is dedicated to highlighting the scientific environment in which the Thesis has been developed and the results of each experiment carried out. For this purpose, relevant publications in indexed international journals will be detailed, as well as the national and international congresses in which the developed works have been disseminated. Moreover, within the scientific environment of the Thesis, the Research Projects, which have made possible the Thesis, will be emphasized. In short, the main objective of this section is to show that the memory, which is presented, constitutes the ordered and stitched the summary of a scientific production carried out during 4 years.

1.3.1. Scientific Projects that Fund the Thesis

1. Title: Configuration and management of an smart renewable hybridized micro-grid hybridized with hydrogen technology (DPI2017-85540-R)
   Type of Project: Spanish R&D&i Plan, Ministry of Economy and Competitiveness
   Cost total of the Project/contract: 196.000 €
   Main researcher: J. M. Andújar
   Period: 01/01/2018-31/12/2020
2. Title: Extension of the Laboratory of Autonomous Hybrid Systems of Renewable Energy (UNHU15-CE-3264)
   Type of Project: Call for European scientific infrastructure, Ministry of Economy and Competitiveness
   Cost total of the Project/contract: 442.318 €
   Main researcher: J. M. Andújar
   Period: 01/01/2016-31/12/2017
3. Title: Design, development and manufacturing of a modular polymer electrolyte fuel cell: instrumentation and control, online monitoring, study of deterioration effects (DPI2013-43870-R)

Type of Project: Spanish R&D&i Plan, Ministry of Economy and Competitiveness
Cost total of the Project/contract: 163.350 €
Main researcher: J. M. Andújar
Period: 01/01/2014-31/12/2016

1.3.2. Scientific Production (Publications in Journals and Congresses)

Article 1. *A review of Energy Management Strategies for Renewable Hybrid Energy Systems with Hydrogen Backup*

Title: A review of Energy Management Strategies for Renewable Hybrid Energy Systems with Hydrogen Backup

Authors: F.J. Vivas, A. De las Heras, F. Segura, J.M. Andújar
Journal: Renewable and Sustainable Energy Reviews
Reference: Vol. 81, pp. 126-155
Year: 2018
Quality index: Journal included in JCR, position 7/97 in the category of "Energy & Fuels, IF (2017): 9.184
Number of citations: 55

In this Article, a detailed study is made of the main problems and technical and economic solutions associated with the use of renewable generation systems with hydrogen as an energy vector; as well as a comparative study between the different solutions and algorithms proposed that are currently used in the scientific literature.

The present analytical and review study allows any technician or researcher to know the current state of the technique, as well as to know the operation and the main parameters to take into account in the design and management of renewable generation systems based on hydrogen as an energy vector.

Given the aforementioned situation, the Chapter has been written based on an exhaustive bibliographic research, since more than 250 references have been consulted, of which 138 have been included as bibliography.

Article 2. *H2RES2 simulator. A new solution for hydrogen hybridization with renewable energy sources-based systems*

Title: H2RES2 simulator. A new solution for hydrogen hybridization with renewable energy sources-based system

Authors: F.J. Vivas, A. De las Heras, F. Segura, J.M. Andújar
Journal: International Journal of Hydrogen Energy

Reference: Vol. 42, pp. 13510-13531

Year: 2017

Quality index: Journal included in JCR, position 24/97 in the category of "Energy & Fuels, IF (2017): 4.229

Number of citations: 8

This article presents a software tool for the simulation of renewable energy systems with hydrogen as an energy vector.

The flexibility in the selection of the operating conditions of each equipment, as well as the definition of the proposed energy management strategy, differ from the rest of the solutions studied in the scientific literature.

The simulator considers all the technical parameters necessary for the optimization of this type of systems. Among them, cycles and time of use of equipment, associated degradation, production and consumption of hydrogen, quality of electricity supply, operation and maintenance costs, as well as the cost associated with the purchase/sale of grid energy.

Based on the foregoing, the proposed software tool allows the evaluation of the main technical and economic parameters resulting from the operating conditions and the proposed energy management strategy, both in the short and long term.

The use of this powerful tool will allow, based on the micro grid topology under study, as well as the minute, hourly, daily and annual renewable generation and consumption profiles, to analyze and determine those design criteria, see operating margins, power constraints and priority in the use of systems, in the operation of each of the equipment that make up the energy storage system, as well as the role of the grid within the system.

Related with Article 2, the following contributions are presented:

Title: Configuration of a Fuel Cell system. Clues to choose between a modular or single stack-based design

Authors: F.J. Vivas, A. De las Heras, F. Segura, J.M. Andújar

Event: 42nd Annual Conference of IEEE Industrial Electronics Society (IECON2016)

Publication: Proceedings book. Vol. 1, pp. 5466-5472.

ISBN: 978-1-5090-3474-1

Date: The 24th-27th of October of 2016. Florence (Italy).

Title: A new simulator for hybrid renewable generation systems. A new solution for technological and economic analysis and energy/hydrogen management strategies

Authors: F.J. Vivas, A. De las Heras, F. Segura, J.M. Andújar

Event: 21st World Hydrogen Energy Conference (WHEC 2016)

Publication: Proceedings book. Vol. 1, pp. 114-115.

ISSN: 9781510838352

Date: The 13th-16th of June of 2016. Zaragoza (Spain).

Title: Optimal energy management strategy of a hybrid renewable energy system with hydrogen generation and storage

Authors: F.J. Vivas, A. De las Heras, F. Segura, J.M. Andújar

Event: 21st World Hydrogen Energy Conference (WHEC 2016)

Publication: Proceedings book. Vol. 1, pp. 796-797.

ISSN: 9781510838352

Date: The 13th-16th of June of 2016. Zaragoza (Spain).

Title: A proposal of energy management strategy on hybrid renewable system with hydrogen backup

Authors: F.J. Vivas, A. De las Heras, F. Segura, J.M. Andújar

Event: 7th International Renewable Energy Congress (IREC 2016)

Publication: Proceedings book. ID 16

Date: The 22th-24th of March of 2016. Hammamet (Tunisia).

Article 3. *Cell voltage monitoring All-in-One. A new low cost solution to perform degradation analysis on air cooled polymer electrolyte fuel cells*

This article presents a novel solution for degradation studies in air-cooled open cathode PEM type fuel cells.

The proposed system implements a low cost technical solution that allows individual cell monitoring of a fuel cell stack up to 100 cells, meeting all the precision and bandwidth requirements recommended for this type of application.

The use of this new system will allow real-time monitoring of the degradation of the stack according to its operating conditions, voltage, current and working temperature, so that the current state of the equipment is available in terms of degradation, performance and associated power loss.

These system parameters will be included in the system model, presented in Article 4, and therefore represent inputs of the main controller, keys for the definition of those decisions that determine the long-term optimization of the system, according to the tuning parameters of the model predictive controller, presented in Article 5.

Title: Cell Voltage Monitoring All-in-One. A new low cost solution to perform degradation analysis on Air-Cooled Polymer Electrolyte Fuel Cells

Authors: F.J. Vivas, J.J. Caparrós, F. Segura, J.M. Andújar

Journal: International Journal of Hydrogen Energy

Reference: Vol. 42, pp. 13510-13531

Year: 2018

Quality index: Journal included in JCR, position 24/97 in the category of "Energy & Fuels, IF (2017): 4.229

Associated with Article 3, the following contributions are presented:

Title: Cell voltage monitoring all in one. A new low cost solution for degradation analysis on polymer electrolyte fuel cells

Authors: F.J. Vivas, A. De las Heras, F. Segura, J.M. Andújar

Event: European Hydrogen Energy Conference 2018 (EHEC 2018)

Publication: Proceedings book. Vol. 1, pp. 33-34.

Date: The 14th -16th of March of 2018. Málaga (Spain).

Title: Fuel Cell Control and Supervisory System-F2C2S

Patent: Utility Model: 201731431

Ownership: University of Huelva

Date: 16/04/2018

Application number: U201731431

Publication number: ES1204161

Article 4. *A suitable space-state model for renewable sources-based microgrids with hydrogen as backup for the design of energy management systems*

Title: A suitable space-state model for renewable sources-based microgrids with hydrogen as backup for the design of energy management systems.

Authors: F.J. Vivas, J.J. Caparrós, F. Segura, J.M. Andújar

Journal: IEEE Access

Year: 2019

Quality index: Journal included in JCR, position 24/97 in the category of "Energy & Fuels, IF (2017): 4.229

The objective of this Article is to define a discrete general model in the state space form that can be used for any management system in any renewable micro-grid based on hydrogen as an energy carrier. In our case in particular, this model will be the key piece in the design of the predictive controller presented in Article 5.

The intrinsic novelty of this Article lies in the versatility and potential of the proposed model,

which allows the representation of all the technical and economic parameters necessary for the optimization of the renewable generation system both in the short and long term. For the definition of the model, a recursive linearization process was used, defining a Lineal Time Variant (LTV) model, which allows to increase the quality of the model with respect to the traditional linearization solutions around a single operating point, considering the behaviour of the smart grid in all its range of operation. The inclusion of all the parameters in the model allowed the possibility to define multi-objective optimization problems from the general formulation of the predictive control theory.

Article 5. *General MPC controller to develop energy management systems in renewable sources-based smart microgrids with hydrogen as backup. Theoretical foundation and case study*

Title: General MPC controller to develop energy management systems in renewable sources-based smart microgrids with hydrogen as backup. Theoretical foundation and case study

Authors: F.J. Vivas, J.J. Caparrós, F. Segura, J.M. Andújar

Journal: Applied Energy

Reference:

Year: 2019

Quality index: Journal included in JCR, position 24/97 in the category of "Energy & Fuels, IF (2017): 4.229

Article 5 presents the central core of the Thesis, and is dedicated to the design and validation of the MPC controller that performs the energy management strategy based on predictive control.

The novelty of this Article lies in the methodology used in the design of the controller, which is based on determining the optimal values of the main controller parameters, taking into account the closed loop stability of the system, the considerations imposed by the energy management strategy proposal and optimization of the system in the short and long term. Although the tuning process of the controller parameters depends largely on the plant, in this Article a general methodology is developed based on the model proposed in Article 4 and the design considerations obtained thanks to studies carried out using the software tool presented in Article 2. The implementation of this methodology will allow adapting the proposed controller to any smart grid topology simply by modifying the desired parameters of the plant model.

Finally, in this Article we analyse the behaviour of the proposed controller and energy management strategy on the real system, based on a series of previously designed empirical tests that allowed the validation of the control methodology established.

1.3.3. Others Scientific Contribution (Publications on Journals and Congresses)

In addition to above detailed scientific contributions, the doctoral student has been co-authors in the following contributions.

Publications in Scientific Journals

1. Title: Evaluation of fuel cell/battery passive hybrid power systems for unmanned vehicles
   Authors: Eduardo López González; Jaime Sáenz Cuesta; Francisco José Vivas Fernández; Fernando Isorna Llerena; Miguel A. Ridao Carlini; Carlos Bordons Alba; Emili Hernández; Alberto Efes
   Journal: International Journal of Hydrogen Energy
   Reference:
   Year: 2018
   Quality index: Journal included in JCR, position 5/90 in the category of "Energy & Fuels, IF (2017): 4,229

2. Title: From the cell to the stack. A chronological walk through the techniques to manufacture the PEFCs core
   Authors: A. De las Heras, F. J. Vivas, F. Segura, J. M. Andújar
   Journal: Renewable and Sustainable Energy Reviews
   Reference: Vol. 96, pp. 29-45.
   Year: 2018
   Quality index: Journal included in JCR, position 5/90 in the category of "Energy & Fuels, IF (2016): 8,050
   Number of citations: 1

3. Title: How the BoP configuration affects the performance in an Air-Cooled Polymer Electrolyte Fuel Cell. Keys to design the best configuration
   Authors: A. De las Heras, F. J. Vivas, F. Segura, J. M. Andújar
   Journal: International Journal of Hydrogen Energy
   Reference: Vol. 42(17) pp. 12841-12855
   Year: 2016
   Quality index: Journal included in JCR, position 28/90 in the category of "Energy & Fuels", IF (2016): 3,582

4. Title: Air-Cooled fuel cells: keys to design and build the oxidant/cooling system
   Authors: A. De las Heras, F. J. Vivas, F. Segura, J. M. Andújar
   Journal: Renewable Energy

Reference: Vol. 125 pp-1-20.
Year: 2018
Quality index: Journal included in JCR, position 18/90 in the category of "Energy & Fuels, IF (2016): 4,357
Number of citations: 3

Contributions to National and International Congress

5. Title: Comparative analysis of the efficiency of a classic MPPT system with location of sensors at the output of the converter, compared to the traditional approach of measurements at the output of the generator
   Authors: Juan Ríos Gutiérrez; Juan Manuel Enrique Gómez; Francisco José Vivas Fernández; José Manuel Andújar Márquez
   Event: International Congress on Engineering and Sustainability in the XXI Century (INCREASE 2019)
   Publication: Proceedings book. Vol. 1, pp. 377-384.
   Date: The 9th -11th of October of 2019. Faro (Portugal).

6. Title: Optimized Balance of Plant for a medium-size PEM electrolyzer. Design, Modelling and Control
   Authors: Julio Caparrós Mancera; Francisco José Vivas Fernández; Francisca Segura Manzano; José Manuel Andújar Márquez
   Event: 10th EUROSIM 2019
   Publication: Proceedings book. Vol. 1, pp. 24.
   Date: The 1st -5th of July of 2019. Logroño (Spain).

7. Title: Evaluation of fuel cell/battery passive hybrid power system for unmaned vehicles
   Authors: Alberto Efes; Eduardo López González; Jaime Sáenz Cuesta; Francisco José Vivas Fernández; Fernando Isorna Llerena; Miguel A. Ridao Carlini; Carlos Bordons Alba; Emili Hernández
   Event: European Hydrogen Energy Conference 2018 (EHEC 2018)
   Publication: Proceedings book. Vol. 1, pp. 176-177.
   Date: The 14th -16th of March of 2018. Málaga (Spain).

8. Title: In the path of H2020 targets. A new proposal and experimental case to reduce the cost of fuel cells
   Authors: A. De las Heras, F.J. Vivas, F. Segura, J.M. Andújar
   Event: European Hydrogen Energy Conference 2018 (EHEC 2018)
   Publication: Proceedings book. Vol. 1, pp. 101-102.
   Date: The 14th -16th of March of 2018. Málaga (Spain).

9. Title: Keys for the best selection of the Balance of Plant configuration in a fuel cell system based on a PE stack
   Authors: A. De las Heras, F.J. Vivas, F. Segura, J.M. Andújar
   Event: 21st World Hydrogen Energy Conference (WHEC 2016)
   Publication: Proceedings book. Vol. 1, pp. 312-313.
   ISSN: 9781510838352
   Date: The 13th -16th of June of 2016. Zaragoza (Spain).
10. Title: A review of BoP configurations for PEFCs. Experimental study of a suitable topology
    Authors: A. De las Heras, F.J. Vivas, F. Segura, J.M. Andújar
    Event: 7th International Renewable Energy Congress (IREC 2016)
    Publication: Minute book. Vol 1, pp. 231.
    Date: The 22 th -24th of March of 2016. Hammamet (Tunisia)

Chapter 2

Objectives and Methodology

Chapter 2. Objectives and Methodology

2.1 Objectives

The main objective of this thesis is the design and implementation of a distributed control system, which allows implementing an energy management strategy on an experimental renewable energy micro grid with the use of hydrogen as an energy vector. This management strategy must optimize the response of the system both in the short and long term, taking into account at all times the physical and operational restrictions necessary to operate the system safely and efficiently, while ensuring optimum operation of the system from the technical and economic point of view.

In order to reach the main goal of the Thesis, a series of specific objectives have been defined, which are described below:

- **Objective I: Identification of technical and economic considerations in the control and management of renewable energy system with hydrogen as energy vector**

Identification of technical and economic parameters in the operation of the equipment, operating criteria, safe operating margins, operation and maintenance costs, etc. Identification of niches for improvement regarding solutions proposed in the review of the state of the art.

- **Objective II: Design of the energy management strategy**

Definition of the energy management strategy according to the technical and economic criteria studied, depending on the topology and final application of the generation system.

Establishment of priorities for action against the energy situation of the system, criteria for energy distribution, definition of working powers for hydrogen equipment, criteria for charging and discharging of batteries, role of the main grid, etc.

- **Objective III: System modelling**

Obtaining the general system model in the state space representation.

This model provides the knowledge base necessary for the implementation of model-based control techniques (MPC). The objective model must provide all the necessary and sufficient information related to the behavior of the system, and therefore allow to define a multiobjective optimization problem to be raised, whose solution will optimize the response of the system according to the controller design criteria, both in the short and the long term.

- **Objective IV: Design, implementation and testing of the predictive controller**

Theoretical development of the MPC controller proposed in accordance with the model in the state space representation, presented in Article 4.

Implementation of the general cost function of the system, which will include all the technical and economic parameters, posing a multi-objective optimization problem according to the system's operating set-points. Generalist tuning proposal for predictive controller parameters.

Validation of controller behavior and proposed energy management strategy on simulation.

- **Objective V: Physical implementation of the micro grid**

Developed and validated on simulations the proposed controller and the energy management strategy, the next step is related to the experimental validation.

For the physical implementation of the micro grid, design and implementation tasks are required from the lowest level, that is, design and implementation of the electrical scheme, electrical protections, power electronics, acquisition systems, communication protocols, etc.

- **Objective VI: Experimental validation of the proposed management strategy and MPC controller**

Implementation, testing and validation of the MPC controller and the proposed energy management strategy in the experimental micro grid. The system will be validated in energy excess and deficit situations, based on certain system constraints and assuming different conditions of accumulated degradation of the system.

2.2 Methodology

In order to achieve the specific objectives defined in the previous section, a working methodology is defined, which is based, and will be implemented later in the different scientific contributions presented in Chapter 4.

The proposed methodology is established in accordance with the specific objectives of the Thesis defined in the previous section.

- **Objective I: Identification of technical and economic considerations in the control and management of renewable energy system with hydrogen as energy vector**

In the first instances, it was developed an extended review of the main topologies and configurations of hybrid renewable smart grids with the use of hydrogen as an energy carrier. From them, it was studied the main characteristics, advantages and disadvantages of the configurations according to the grid connection and the nature of the internal bus connection.

Next, all the technical and economic problems associated with the use of the renewable energy micro-grid, more specifically in the use of energy storage systems, were analysed in detail. Likewise, a review was made of the main technical solutions found in the scientific literature.

Finally, an exhaustive and critical study of the different energy management strategies solutions proposed in the scientific literature was presented, according to the topology, configuration, optimization and decision parameters, adopted solutions, purpose of the strategy, as well as control algorithms employees to implement the management strategy. From the previous study, it was determined that the multi-objective strategies present a small but growing number of solutions.

- **Objective II: Design of the energy management strategy**

System optimization begins with an exhaustive analysis of the main problems associated with the operation of each of the systems that make up the smart grid, emphasizing the operating conditions of the energy storage system based on batteries and hydrogen as an energy carrier.

From the previous analysis, a management solution was proposed with the aim of ensuring an efficient and responsible use of the system, in such a way that it is possible to guarantee the maximization of the useful lifetime, keeping commitments of cost, energy use and operation degradation. In this regard, it is worth mentioning the need to define a battery charging and discharging strategy, definition of the operation point and dynamics in the operation of the hydrogen-based energy storage system, as well as, criteria associated with the quality of the electricity supply, taking into account the energy dependence between the generation system and the electrical grid.

To do this, a study was made based on a proposed simulation tool, an expected load profile, and a historical of the renewable resources of the micro-grid location, evaluated during a year of operation. The results obtained allowed to define the operation points that optimize the long-term response of the system, which will be the references for the design of the predictive controller, responsible for implementing the energy management strategy.

The economic optimization of the system was evaluated based on the study of the cost problem proposed by the grid-connection topology, which determines an economic optimization problem based on the energy market price and the energy flows between systems.

Finally, the management strategy of the system was presented based on the situations of deficit and excess of energy, determining the criteria of priorities and energy distribution between the different elements that make up the energy storage system and the electrical grid, in accordance with the application in question.

- **Objective III: System modelling**

In this Objective all the modelling of the plant was done in the state space representation, based on the optimization parameters determined by the energy management strategy proposed

in Objective II, both in the short and long term. Among them, operating performance, operating cost, battery charging management, equipment degradation and power supply quality.

The definition of the proposed model was aimed at calculating the optimization parameters of the system based on the operating set-point of each equipment, so that the optimization of the system was determined at all times by the calculation of the optimal operating power.

The modelling of the smart grid was based on an identification process of the plant and a multivariable linearization process, which allows defining an LTV model that guarantees a linear relationship between the state variables and the input vector, throughout its operating range despite the nonlinearities present in the behaviour of the plant.

The proposed model allows generalization to any renewable generation system, regardless of the main generation system, battery technology or hydrogen generation and consumption system.

• Objective IV: Design, implementation and testing of the predictive controller

In the first instances, it was presented all the general mathematical foundation for the development of the constrained predictive control based on the state-space formulation, characterized in this case for the cost function and constraints that define the multi-objective optimization problem associated with the application in question.

In this particular case, the optimization problem is based on the minimization of a multi-objective function proposed by a tracking problem based on the achievement of a zero power balance, which defines a constrained quadratic programming problem.

In order to design a controller that includes all the energy management design criteria related to Objective II analysis, and taking into account the generalist model result of Objective III, a formal methodology for tuning the controller parameters was presented. It is based on the definition of the objectives of the smart grid; closed loop stability, operating prioritization, energy distribution of the energy storage system and minimum input from the electrical grid, as well as the desired dynamics of the plant. In particular, a practical case based on simulation demonstrate that both the tuning guidelines and the proposed controller are feasible for the real implementation if the smart grid.

Finally, from different simulations, the closed loop stability and the correct behaviour of the system for the proposed constrained optimization problem, both in the short and long term, were studied and validated.

- **Objective V: Physical implementation of the micro grid**

To reach this objective, it was necessary to develop all the necessary power, control and data acquisition electronics. In this regard, highlight the design of power converters for the

integration of solar panels and the modular fuel cell system. Similarly, it is important to highlight the design and implementation of a cell voltage detection system to determine the instantaneous degradation of the fuel cell stack with respect to the current operating point.

Finally, it was necessary to implement a user interface capable of developing the communication, control and management tasks of the micro grid. In this sense, different virtual instruments were developed in the LabVIEW® environment.

The different hardware and software developments designed specifically for this thesis are presented in more detail in section 3.

- **Objective VI: Experimental validation of the proposed management strategy and MPC controller**

Finally, the experimental results obtained from the implementation of the proposed energy management strategy were presented, through the use of predictive control over the real plant, determining a good behaviour in the closed loop response of the system, and therefore validating the design of the controller and the viability of the use of predictive control techniques in smart grids with renewable generation and the use of hydrogen as energy vector.

Chapter 3

Materials

Chapter 3. Materials

3.1. Description of the renewable sources-based smart grid with hydrogen as backup

The conception of the smart grid is based on the production of energy entirely obtained from renewable resources, which guarantees the production and storage of energy at zero cost in terms of CO_2 production.

Considering the topology of the smart grid under study, this allows bidirectional power flow between the electrical grid and the smart grid, so that it is possible to inject power towards and from the electrical grid. All this allows the economic factor to be a very important parameter in the energy management problem.

Considering the integration method, all the generation and consumption systems are connected to the internal DC bus, supported by the direct connection of the battery bank.

The main generation of the system is given at all times by renewable resources produced from the solar radiation, which allows the production of energy during the hours of greatest electrical demand.

To guarantee the power balance at all times, there are two energy storage systems available.

The first of these is a battery bank, which allows to act against fluctuations in the power balance, so it acts as a short/medium-term energy storage system. In addition to the above, the direct connection of the battery bank to the internal DC bus causes the voltage of DC bus to be stabilized within the operating range of the battery bank, without the need of using additional bidirectional converters that could complicate the control of the system.

As a long-term storage system, hydrogen-based subsystems are used, consisting of an electrolyzer as hydrogen production system, a fuel cell as an electrical production system, and storage tanks based on physical and chemical storage, with the aim of storing the hydrogen gas production.

The architecture of the renewable energy sources-based smart grid with hydrogen as backup installed at the University of Huelva is shown in Figure 3.1.

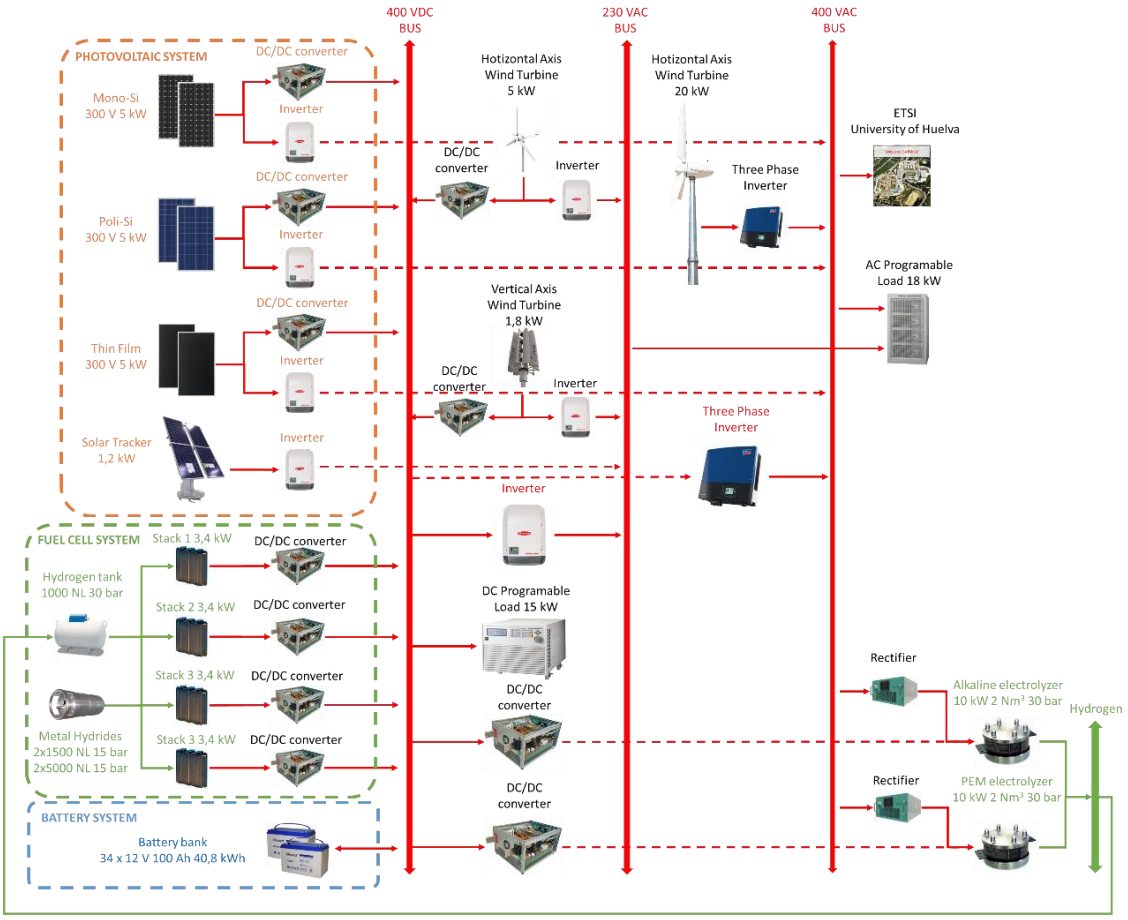

Figure 3.1. UHU Smart Grid architecture

In the following sections, each of the devices that compose the smart grid will be briefly described, as well as all the monitoring, power and control electronics for its management, developed specifically in the framework of the Thesis.

3.1.1. Renewable generation

The renewable generation is represented by photovoltaic generation, composed of three photovoltaic arrays of Monocrystalline, Polycrystalline and Thin film technology.

The power of the three photovoltaic fields is similar (5 kWp) and the assembly has been carried out under the same premises of tilt angle, with the aim of being able to evaluate the behaviour of the three technologies under the same conditions of solar radiation and ambient temperature.

In the case of the Monocrystalline technology photovoltaic field, 20 units, ISF-250 model panels from the ISOFOTON manufacturer are available, with a maximum power of 250 Wp, Figure 3.2.

The Polycrystalline technology photovoltaic field consists of a total of 50 panels model A-230P from the manufacturer ATERSA, with a maximum power of 230 Wp, Figure 3.2.

Finally, the Thin film technology photovoltaic field is composed of a total of 50 SCHOTT PROTECT ASI 100 panels from the manufacturer SCHOTT Solar AG, with a maximum power of 100 Wp, Figure 3.2.

a) b)

Figure 3.2. a) Monocrystaline and Polycrystaline solar panels. b) Thin film solar panels

With the objective of guaranteeing the maximum use of solar production, as well as the correct integration in the DC bus, a power converter has been developed that implements a Maximum Power Point Tracking algorithm (MPPT) for each of the technologies. The detailed description of the developed converter is studied in section 3.2.1.

In order to evaluate the behaviour of the controller on a first experimental phase, this Thesis will only use the photovoltaic field of Polycrystalline technology, due to its better performance in the field compared to Monocrystalline and Thin film technologies.

3.1.2. Battery Bank

As a short-term energy storage system, there is an AGM lead acid battery bank, consisting of 30 units connected in series. Each battery is model UP100-12 of 12 V and 100 Ah from the manufacturer U-POWER, Figure 3.3a. The battery bank has a rated voltage of 360 V and an energy storage capacity of 36 kWh, Figure 3.3b.

a) b)

Figure 3.3. Detail of the battery bank. a) UP100-12 single battery. b) Battery bank

As mentioned in previous sections, the battery bank is directly connected to the DC bus, which allows the stabilization of the bus voltage without the need of power converters or auxiliary control algorithms. On the other hand, the direct connection requires a more complex control system, in order to guarantee safe and efficient charging and discharging conditions.

3.1.3. Alkaline electrolyzer

As hydrogen production system, there is an alkaline technology electrolyzer with a production capacity of 2 Nm^3/ h, and a rated power of 10 kWp, manufactured by Nitidor, Figure 3.4.

a) b)

Figure 3.4. a) Electrolyzer control cabinet. b) Alkaline Electrolyzer

Although the electrolyzer has all the power and control electronics for its operation, it is necessary to include the connection between the power converter of the equipment with the DC

bus. For all these reasons, and in order to validate the behaviour of the controller in this first phase of development, in this Thesis, the alkaline electrolyser will be modelled by a load profile programmed into the system considering the minimum power and dynamics constraints.

3.1.4. Fuel cell

With the objective of producing electrical energy from hydrogen generated by electrolyzer, the smart grid includes a FC1020 fuel cell module composed of three stacks in parallel. Each stack is built from 80 PEM cells with a nominal power of 3.4 kWp from the manufacturer BALLARD, Figure 3.5. In this case, the rated power of the fuel cells, considering the converter, will be limited to 2 kW, in such a way that a safe operating range is allowed, considering the operating performance of the converter, as well as the degradation suffered by the use.

a) b)

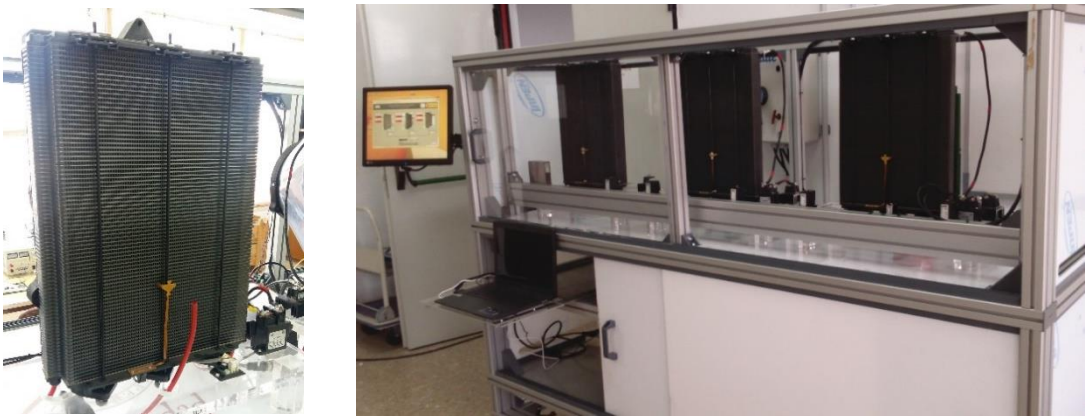

Figure 3.5. a) PEM fuel cell stack. b) PEM fuel cell module

Despite presenting a greater complexity in the control, the proposed parallel topology of the fuel cell module allows in the first instance adapting the generation and guaranteeing redundancy in the system in the event that some stack suffers a critical failure. In the same way, the possibility of selecting the stack to put in work allows distributing the operating time, and therefore guaranteeing a homogeneous degradation in the fuel cell module, that is, a modular structure help to prolong the useful lifetime.

Attending to the hydrogen management, the fuel cell module has all the necessary balance of plant (BoP) and associated control according to the manufacturer's specifications. The developed control electronics are studied more in detail in sections 3.2.3 and 3.2.4.

Similarly, for the correct connection of each fuel cell stack to the DC bus, a power DC/DC converter has been developed, see section 3.2.2.

In order to validate the behaviour of the energy management system, in the first phase studied in this Thesis, only one fuel cell stack will be used as an electric generation system.

3.1.5. Hydrogen storage system

Attending to the storage of the hydrogen generated by the electrolyzer, there are two types of storage, low-pressure tank and metal hydrides tank.

The low-pressure tank model LPS1000H from the manufacturer LAPESA has a nominal capacity of 1 Nm^3 and a design pressure of 30 bar, Figure 3.6a. The function of this tank is to serve as a hydrogen storage system in the first instance, as well as buffer between the electrolyzer and the metal hydride tanks.

a) b)

Figure 3.6. a) LPS1000H low-pressure tank. b) HB5000 & HB1500 metal hydrides tanks

In second instance, there is a hydrogen storage system based on metal hydrides tanks, being a chemical principle storage system. The metal hydride storage system consists of a total of four tanks, two tanks model HB5000 with nominal capacity of 5 Nm^3 and a maximum charge pressure of 15 bars, and two tanks model HB1500 with nominal capacity of 1.5 Nm^3 and a maximum charge pressure of 15 bars, both from the manufacturer LABTECH, Figure 3.6b.

To guarantee a charging and discharging process that maximizes the storage capacity of the metal hydride tank, it is necessary to manage the charging and discharging temperature in order to maximize the storage capacity.

In response to the management of the metal hydride system, the entire balance of plant is available, which guarantees a safe charging and discharging process. Analogously, taking into account the thermal constraints, a water-cooling circuit is available, Figure 3.7, which allows guaranteeing the optimum temperature conditions required for the charging and discharging processes.

Figure 3.7. Water cooling system

The consumption of the refrigeration system will not be considered as another load of the system. Likewise, it will not be considered a difference in the treatment of two hydrogen storage tanks, being modelled as a single deposit of nominal capacity calculated as the addition of the individual capacities.

3.1.6. Electrical grid

In the specific application, the use of the electrical grid is crucial to guarantee a technical and economic optimization of the complete system. In the current topology, there is a commercial three-phase solar inverter of 12 kWp model Sunny Tripower 12000TL-20 from the SMA manufacturer, Figure 3.8, adapted through a hardware and software reconfiguration to guarantee the extraction of energy directly from a bus supported by the battery bank. The adaptations are represented by the inclusion of a previous pre-charge stage and the implementation of an input voltage tracking algorithm as opposed to the MPPT algorithm used for the connection of solar panels.

To model the power input from the grid to the system, a programmable 15 kWp power supply model SGA 600/25 from the manufacturer AMETEK will be used, Figure 3.8. The source is directly connected by an anti-return diode.

a)

b)

Figure 3.8.SMA power inverter (left) and Programmable power supply (right)

The control of both systems is done remotely through the SCADA system, allowing to impose the desired power condition based on the current bus voltage and a working current set-point.

3.1.7. Load

The demand profile will be modelled at all times as a DC consumption, imposed at all times by a load demand whose profile is defined by means a programmable load of 10 kWp model 5VP10-32 of the manufacturer Adaptative Power Systems.

As previously mentioned in section 3.1.3, the electrolyzer consumption profile will be modelled by the programmable load according to its response dynamics and the constraints imposed by the control problem.

3.2. Power and control electronic

In order to integrate all the power sources, as well as carry out the necessary control actions to guarantee the operation point set by the response of the developed MPC controller, it is necessary to use power and control electronics specifically designed for the application.

Due to the chosen topology for the battery integration based on direct connection, together with the non-standard high DC bus voltage, as well as the particularity associated with the control and management of electrochemical systems, such as the fuel cell, it has not been possible to find commercial solutions that respond to the needs. For all these reasons, it was necessary to the design and development of all the power, control and monitoring electronics necessary to guarantee the operation of the Smart Grid.

3.2.1. Boost converter for solar panels integration

In order to guarantee the maximum power extraction, as well as the correct integration of renewable generation, a DC/DC power converter stage has been designed for each PV array. The developed DC/DC converter has a boost topology and implements a MPPT system based on the Perturbation and Observation (P&O) algorithm, Figure 3.9.

Figure 3.9.- Boost PV-converters prototype and final installation

Each power converters consists of two converters of 2.5 kWp in parallel in interleaved operating mode, with the aim of reducing current ripple at the input and the associated sizing, Figure 3.10.

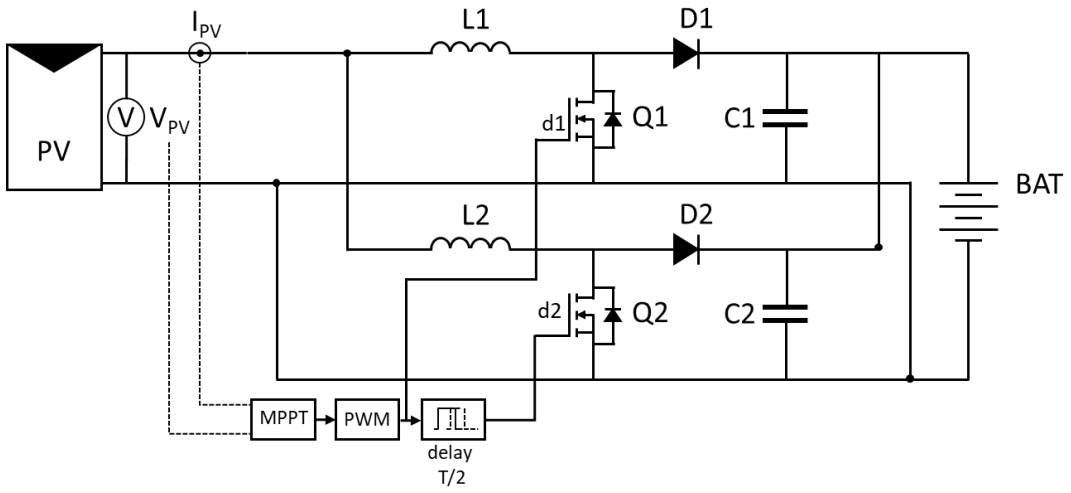

Figure 3.10.- Interleaved boost converter for PV array

In response to the management system, the power converter implements all the protections and pre-charge management in order to guarantee a safe operation within the operating range of the DC bus. To do this, the converter has the ability to detect system errors, and acts accordingly to prevent equipment malfunction. In this sense, the main errors are given by over voltage in the DC bus, as well as the operating temperature of the equipment. In case of low input voltage, the system allows the physical disconnection of the panels and its reconnection when a minimum open circuit voltage condition is reached again.

3.2.2. Push-pull converter for fuel cell system integration

For the correct integration of fuel cell system into the smart grid, it is necessary to use a DC/DC power converter, which guarantees on the one hand the high conversion ratio required for the application; and on the other hand, establish the power set-point calculated from the MPC controller.

Due to the high conversion ratio required (≈10), the use of non-isolated boost topologies are completely discarded, due to the real impossibility of reaching these elevation ratios with acceptable control capacity and operating performance. Within the isolated topologies, and due to the high working power, only the Push-Pull and Full-Bridge topologies guarantee a high operating efficiency.

For the specific application, a voltage feed Push-Pull isolated topology converter of 2.5 kWp has been developed, with an output power tracking performed through a PID controller, Figure 3.11 and Figure 3.12. The converter has the ability to detect system errors, and acts accordingly to prevent equipment malfunction. In this sense, the main errors are given by over voltage in the DC bus, low operating voltage of the fuel cell, as well as the operating temperature of the equipment itself.

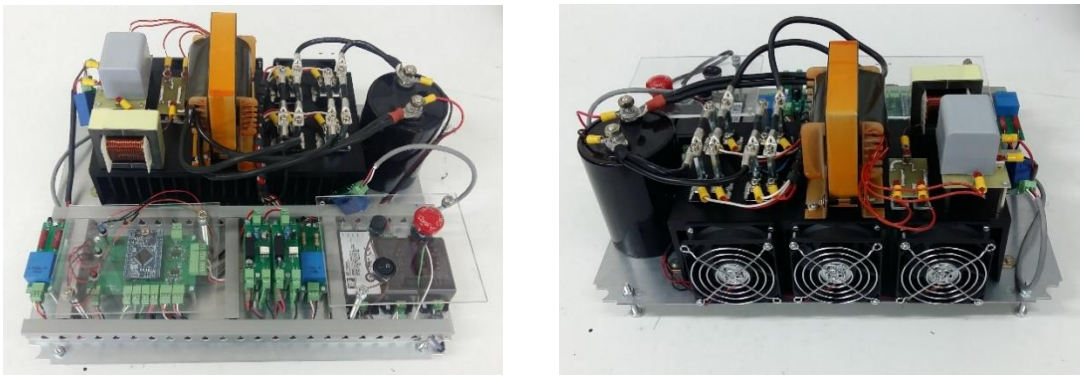

Figure 3.11. Push-Pull FC-converter prototype

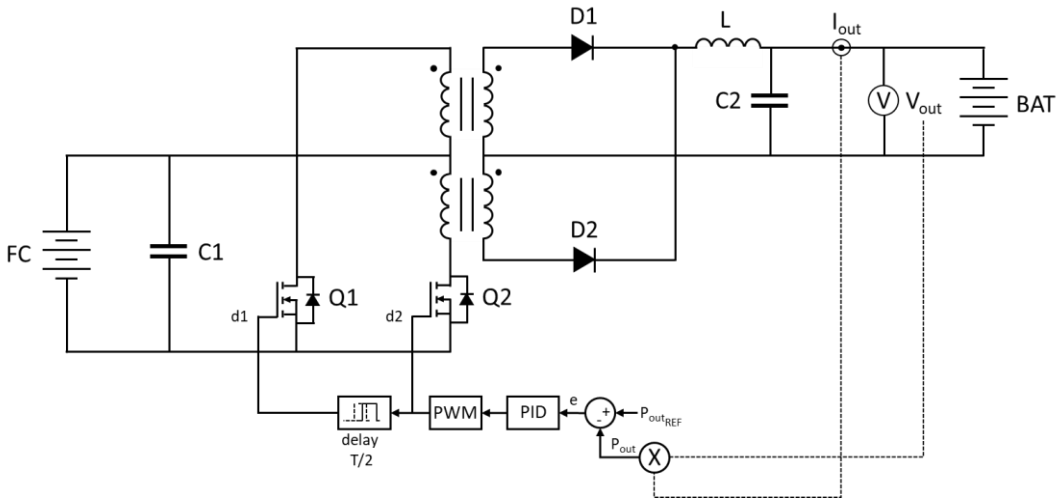

Figure 3.12. Push-Pull converter topology for Fuel Cell system

3.2.3. Fuel cell Balance of Plant

In order to guarantee the correct production of energy by means of fuel cell system, it is necessary to guarantee a correct hydrogen supply, a correct air flow for temperature control and the satisfaction of the stoichiometric coefficient, as well as a correct management of the purges in function from the current polarization point. In short, it is necessary to ensure the correct operation of the entire Balance of Plant (BoP) associated with the fuel cell system.

The proposed BoP is based on the manufacturer's recommendations, Figure 3.13. In the first instance, there is a hydrogen supply line, controlled and monitored from a supply valve and a pressure sensor respectively. To control the air flow, there is a fan with controlled speed which is set according to the optimal operating temperature provided by the manufacturer, based on a PID controller. Finally, a purge valve is available, which allows controlled purging in time depending on the operating power.

Regarding the electrical connection, the fuel cell is connected directly to the power converter through an anti-return diode and a cut-off relay, in order to isolate the fuel cell in case of malfunction.

Finally, taking into account the safety of the system, a hydrogen sensor is available, with the aim of detecting possible hydrogen leaks, allowing the quick stopping of the fuel cell.

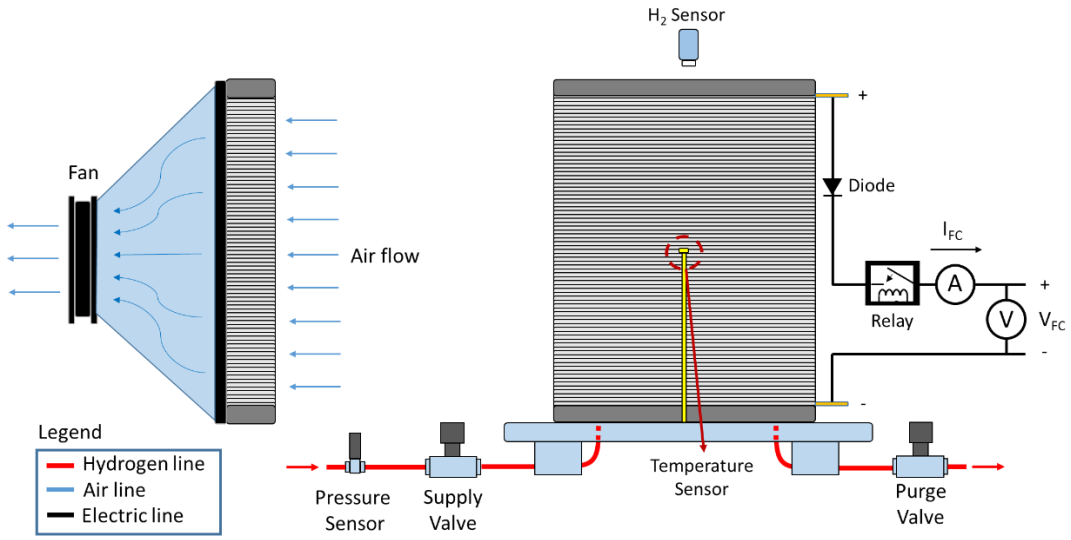

Figure 3.13. Balance of Plant

For the management of the fuel cell module (3 stacks), a control electronics has been developed, Figure 3.14, which allows managing their respective plant balances. The control electronics developed allows, in the first instance, managing the three stacks independently, operating the fuel cell system according to its working conditions. Likewise, it allows the early detection of any problem associated with the malfunction of the fuel cell system, due to the measurement of the chemical parameters (hydrogen leakage), physical (supply pressure and temperature), as well as electrical (voltage and operating current). In these cases, the controller acts to isolate electrically the fuel cell from the electrical load and the hydrogen supply in order to ensure safety in its operation.

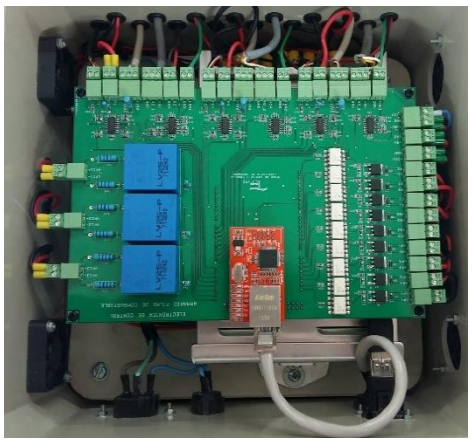

Figure 3.14. Fuel cell BoP control electronic

3.2.4. Cell Voltage Monitoring system

In order to detect and quantify the degradation associated with the operation of the fuel cell, an individual cell monitoring system (CVM All in One) has been developed. This monitoring electronics allows, on the one hand, the measurement of the individual cell voltage, as well as quantifying the degradation associated with each polarization point, thanks to the measurement of the current and working temperature, Figure 3.15.

The implementation of the CVM allows identifying the loss of performance of the fuel cell, due to the malfunction of any particular cell; and on the other hand, it allows quantifying the real degradation ratio of the fuel cell.

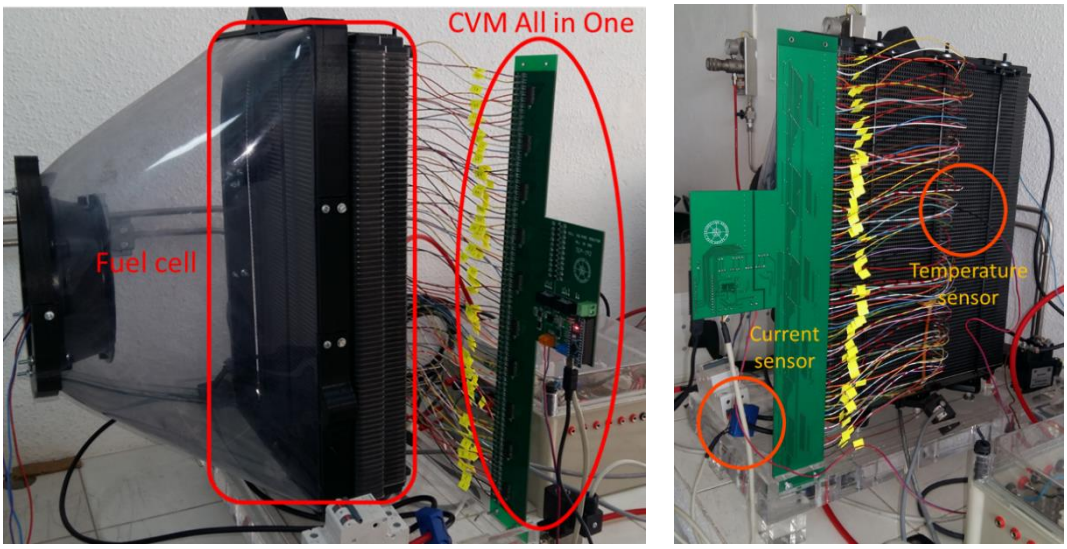

Figure 3.15. CVM All in One prototype

Associated to the developed hardware, a software tool is presented, which allows the use of the equipment based on the "plug and play" philosophy, Figure 3.16. This tool allows the real-

time representation of individual cell voltages, operating polarization point and working temperature.

a)

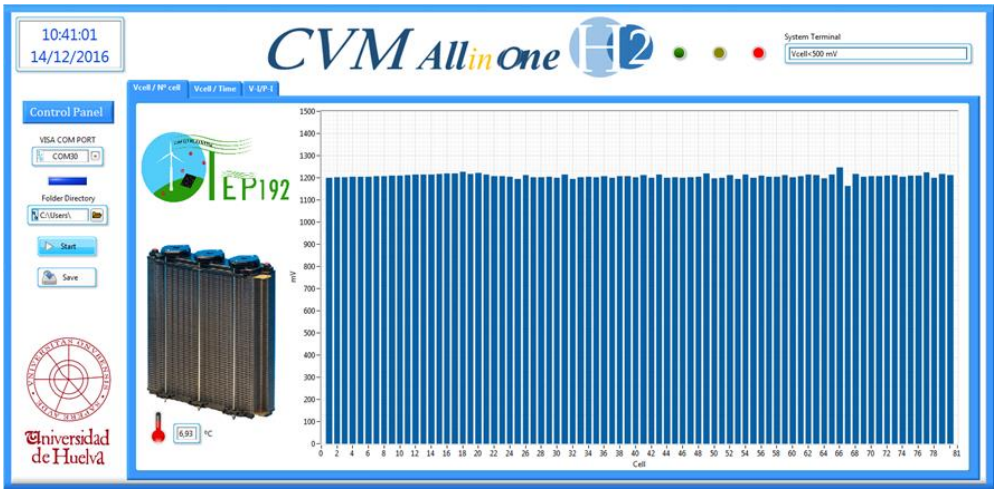

b)

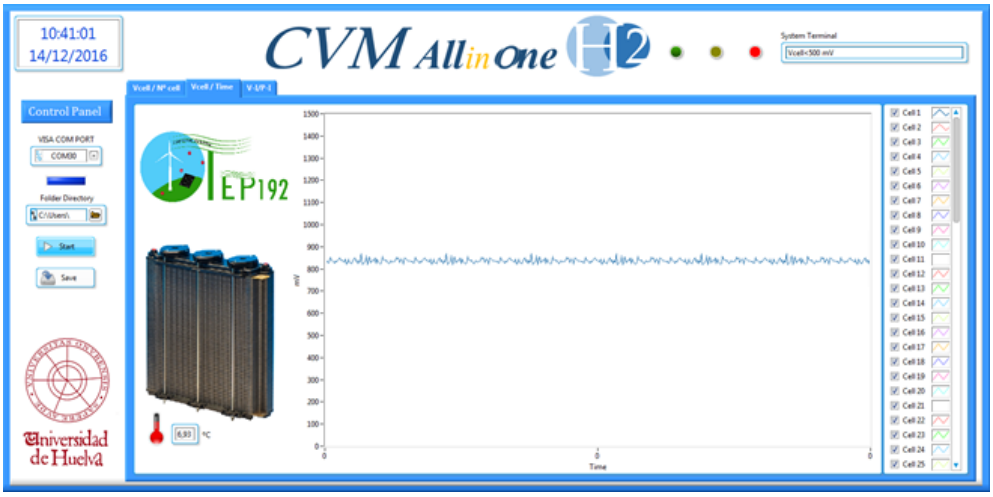

c)

Figure 3.16. CVM All in One Software tool. a) Example of bar graph interface. b) Example of real time plot interface. c) Example of polarization point representation

3.3. Monitoring and control software SCADA

In order to monitor, control and manage the complete smart grid, a SCADA system has been developed on the LabVIEW® platform, in which all the system parameters are centralized, and each device is individually controlled.

The developed SCADA system allows visualize quickly the operating status of the smart grid, as well as to identify any type of malfunction associated with any device.

From the main screen of the system, Figure 3.17, it is possible to control the start and stop of each device, as well as the navigation between the different windows related to the control and monitoring of the whole generation system.

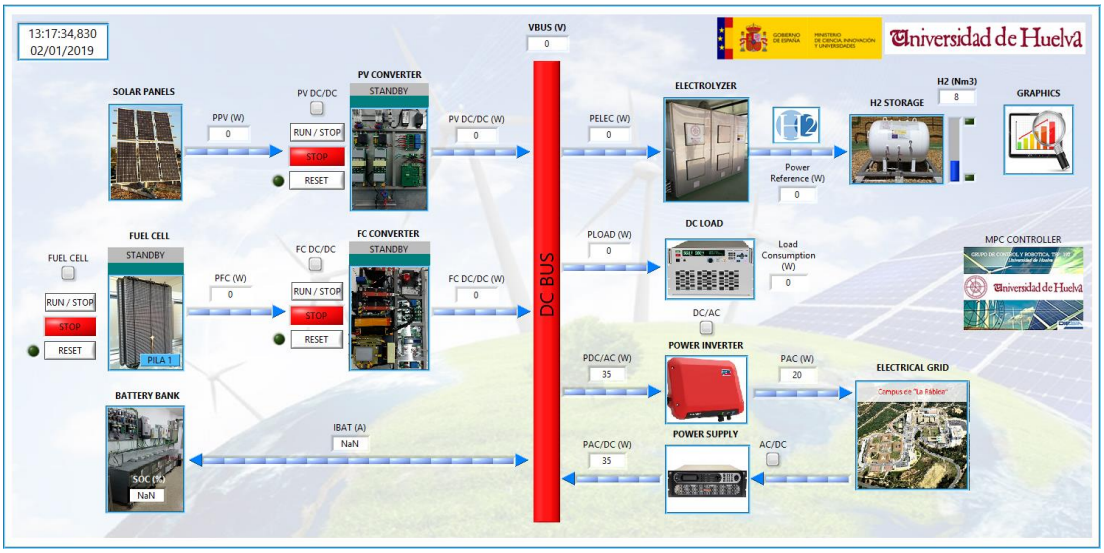

Figure 3.17. SCADA main window

Attending to the control of the developed power converters, the SCADA system allows controlling the start-up and stop actions, as well as the graphic representation of the electrical parameters, Figure 3.17 and Figure 3.18. In accordance with the security philosophy implemented in all the equipment, the SCADA system allows the user to show all the information based on the current status of each device, and in case of error, what anomaly causes it.

a)

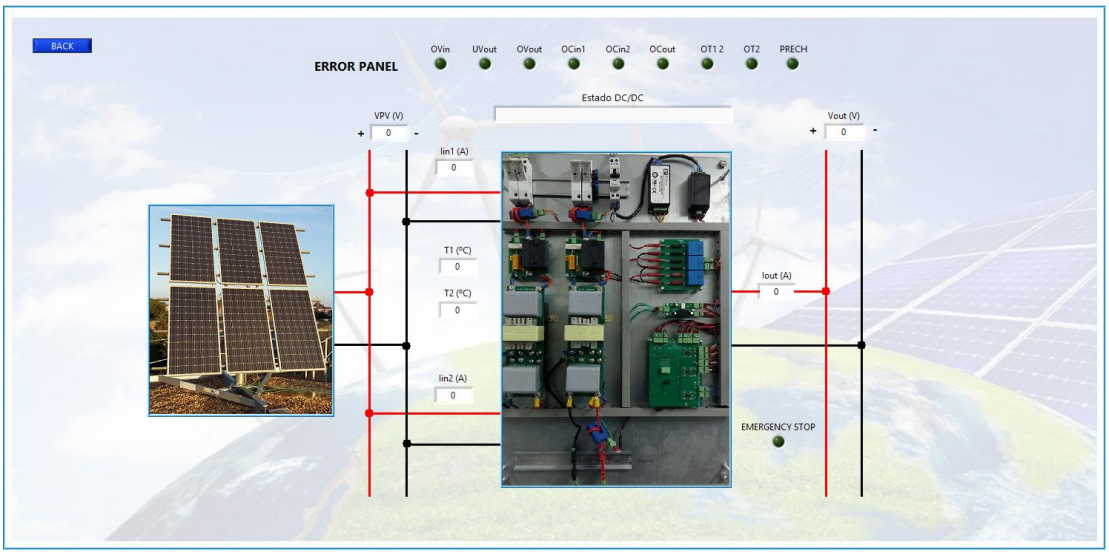

b)

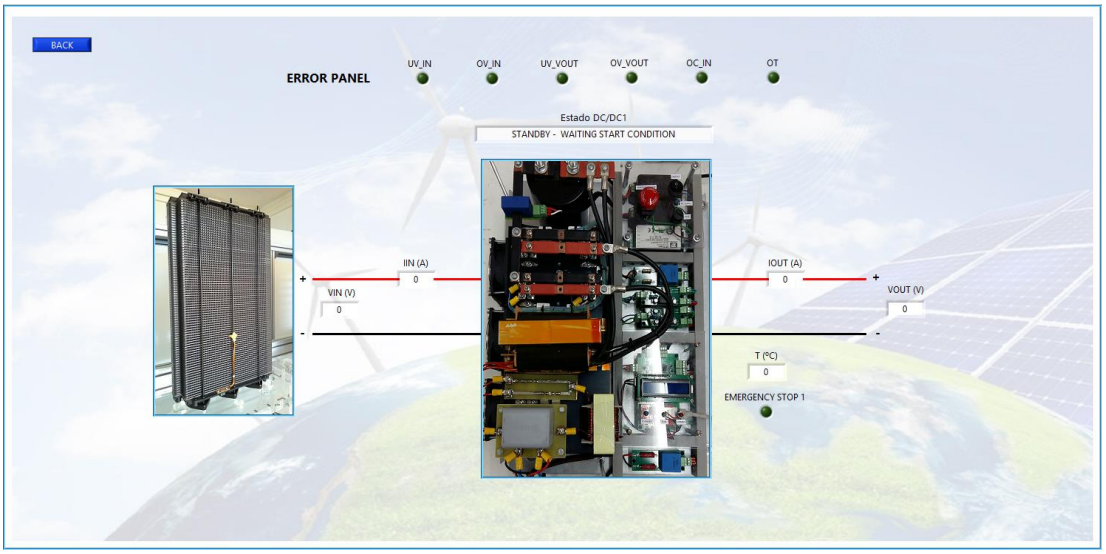

Figure 3.18. a) SCADA tab for PV-converter. b) SCADA tab for FC-converter

In case of management of the fuel cell BoP, the control electronics are monitored through the SCADA, which allows the visualization of the main operating parameters of the system, allowing visual identification of any malfunction in the system, Figure 3.19.

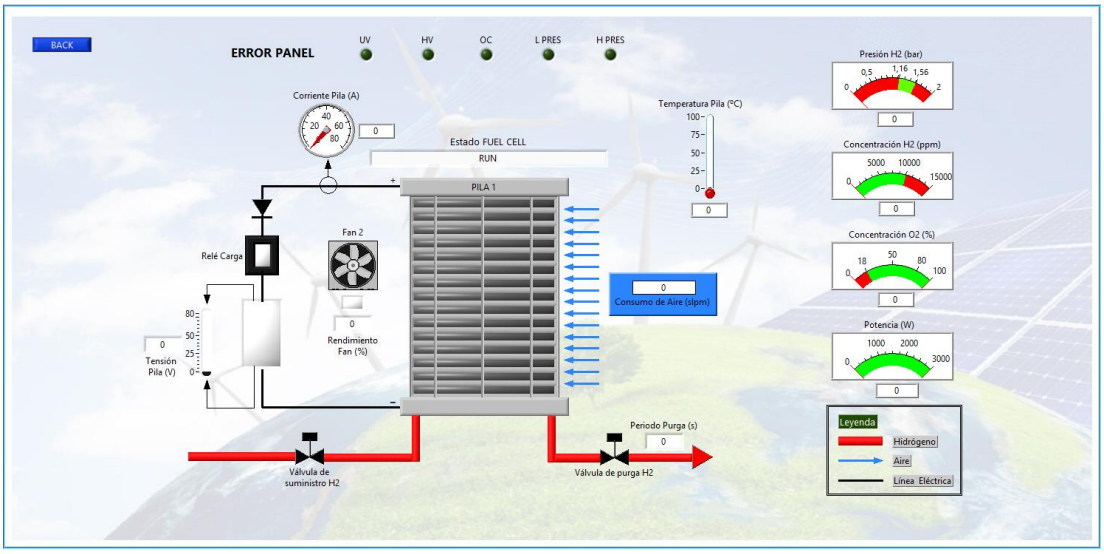

Figure 3.19. SCADA tab for Fuel cell BoP management

Finally, the SCADA system allows the real-time visualization of the control system. The proposed graphic representation allows identifying quickly the input and output parameters of the plant and the controller based on the typical representation of the control loop of an MPC controller, Figure 3.20.

Additionally, the most relevant information of the current state of the system is available based on the technical and economic parameters that define the multi-objective function of the optimization problem.

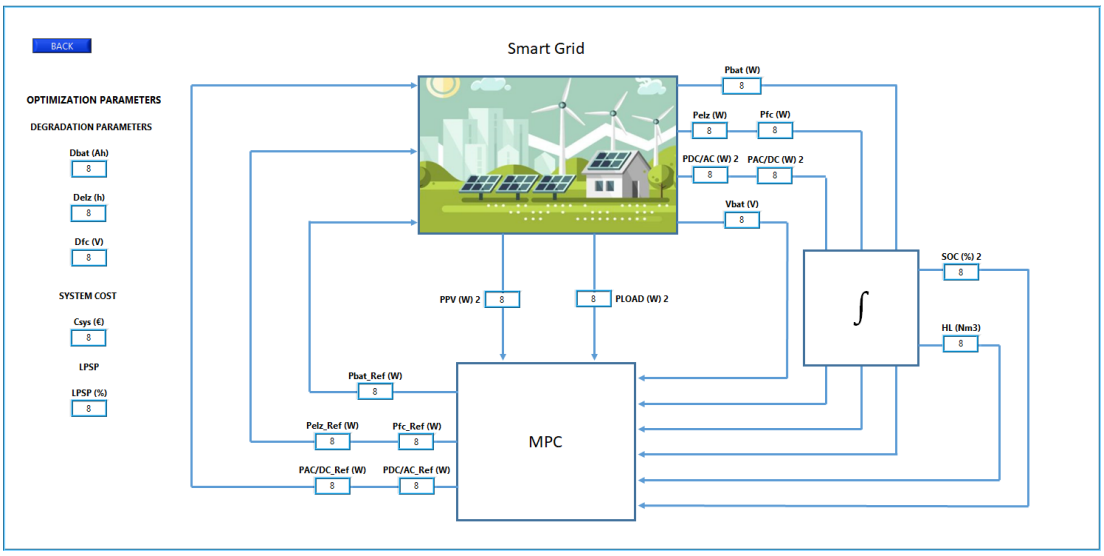

Figure 3.20. SCADA tab for MPC Control

Finally, there is a window in which the time evolution of all the electrical variables of the system is represented, Figure 3.21, in such a way that any anomaly can be identified, as well as it allows to test different energy management strategies into the smart grid.

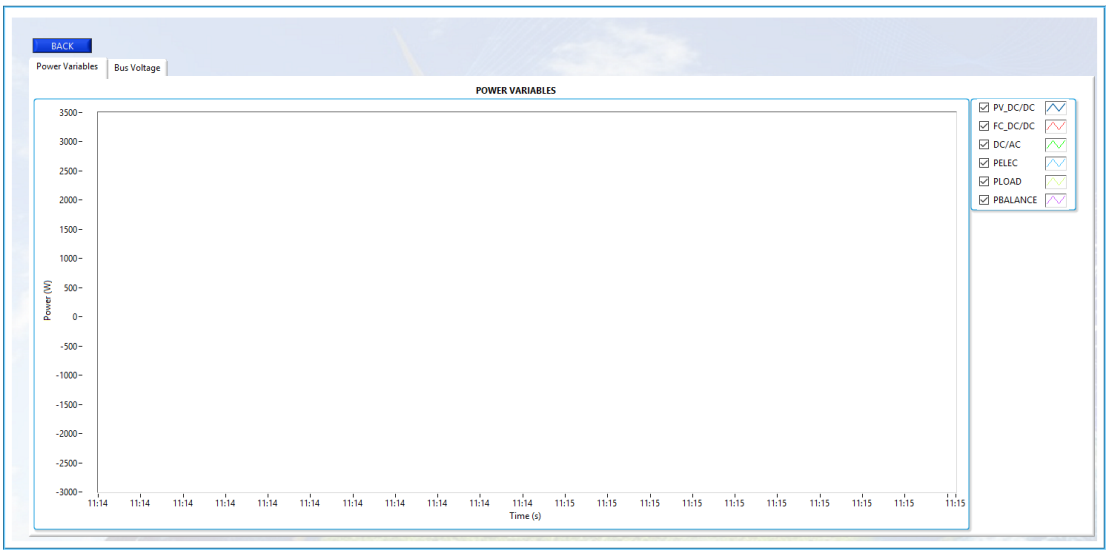

Figure 3.21. SCADA screen for Electrical variables representation

Chapter 4

Results & Methods

CHAPTER 4: RESULTS & METHODS

Las ponencias a Congresos, relacionadas más abajo, que forman parte del capítulo 4 “Results & Methods” han sido retiradas de la tesis debido a restricciones relativas a derechos de autor.

- Vivas, F.J, Heras, A. de las , Segura, F., Andújar, J.M.: “Cell Voltage Monitoring All in One. A new low cost solution for degradation analysis on Polymer Electrolyte Fuel Cells”. En: European Hydrogen Energy Conference (EHEC, Málaga, Spain. 2018).

- Vivas, F.J, Heras, A. de las , Segura, F., Andújar, J.M.: “Optimal energy management strategy of a hybrid renewable energy system with hydrogen generation and storage”. En: 21st World Hydrogen Energy Conference (WHEC. Zaragoza, Spain. 2016). ISBN 9781510838352.

- Vivas, F.J, Heras, A. de las , Segura, F., Andújar, J.M.: “A new simulator for hybrid renewable generation systems. A new solution for technological and economic analysis and energy/hydrogen management strategies”. En: 21st World Hydrogen Energy Conference (WHEC. Zaragoza, Spain. 2016). ISBN 9781510838352.

- Vivas, F.J, Heras, A. de las , Segura, F., Andújar, J.M.: “Configuration of a fuel cell system. Clues to choose between a modular or single stack-based design”. En: 42nd Annual Conference of IEEE Industrial Electronics Society (Florence, Italy. 2016). ISBN 9781509034741.

- Vivas, F.J, Heras, A. de las , Segura, F., Andújar, J.M.: “A proposal of energy management strategy on hybrid renewable system with hydrogen backup”. En: 7th International Renewable Energy Congress (Hammamet, Tunisia. 2016).

Chapter 4. Results & Methods

4.1. Article 1

A review of Energy Management Strategies for Renewable Hybrid Energy Systems with Hydrogen Backup

F.J. Vivas, A. De las Heras, F. Segura, J.M. Andújar

Published in:

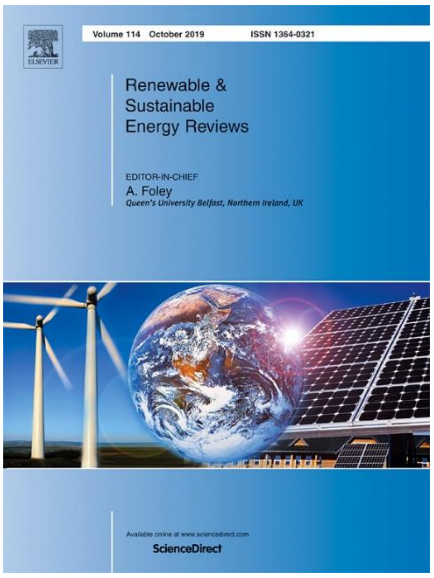

Journal: Renewable and Sustainable Energy Reviews
Editorial: ELSEVIER
Editor-in-Chief: Aoife M. Foley
Reference: Vol. 81, Part 1, pp. 126-155
Year: 2018
ISSN: 1364-0321
DOI 10.1016/j.rser.2017.09.014

Category	Journal Rank / Total journals	Quartile
Energy & Fuels	7 / 103	Q1
Green & sustainability science & technology	1 / 35	Q1
Impact Factor (2018)	10.556	
Citations	54	

Renewable and Sustainable Energy Reviews 82 (2018) 126–155

Contents lists available at ScienceDirect

Renewable and Sustainable Energy Reviews

journal homepage: www.elsevier.com/locate/rser

A review of energy management strategies for renewable hybrid energy systems with hydrogen backup

F.J. Vivas*, A. De las Heras, F. Segura, J.M. Andújar

Grupo de Investigación de Control y Robótica TEP-192, Departamento de Ingeniería Electrónica, de Sistemas Informáticos y Automática, Escuela Técnica Superior de Ingeniería, Universidad de Huelva, Spain

ARTICLE INFO

Keywords:
State of art revision
Energy management strategy
Hybrid renewable power systems
Hydrogen backup

ABSTRACT

Hybrid systems are presented as a viable, safe and effective solution to minimize the associated problems of the dependence on renewable energies with the environmental resources. In this way different renewable systems such as photovoltaic, wind, hydrogen and so on, can work together to configure hybrid renewable systems. However, to make them work properly in a holistic way by creating synergies among them is not an easy task. Recently hydrogen technology has appeared as a promising technology to hybridize renewable energy systems, since it allows the generation (by electrolyzers) and storage of hydrogen when there is a surplus of energy in the system, and at a later time (e.g. when there are insufficient renewable resources available) using the stored hydrogen to generate electrical energy by fuel cells. The choice of a correct energy management strategy should guarantee an optimum performance of the whole hybrid renewable system; therefore, it is necessary to know the most important criteria in order to define a management strategy that ensures the best solution from a technical and economic point of view. This paper presents a critical review and analysis of different energy management strategies for hybrid renewable systems based on hydrogen backup. In the same way, a review is also presented of the most important technical and economic optimization criteria, as well as problems and solutions studied in the scientific literature.

1. Introduction

With the advancement of civilization and evolution of technology, energy demand has become a basic issue for the development of a society today. The usual ways to address this demand today are based mostly on resources such as fossil or nuclear fuels [1–3], which have a negative impact on the environment, either contributing with greenhouse gases, or by production of radioactive or inert solid waste. For this reason, every day the need to migrate to more environmentally responsible energy production models becomes more evident.

Together with the above, due to the high-energy requirement, it is necessary to look for generation models to ensure maximum system performance, minimizing the use of resources, cost and thus the environmental impact. In recent decades, the use of distributed generation has emerged as a viable and safe solution to increase electrical system performance, reducing the distance between generation and demand [4,5].

The incorporation of renewable energies is a non-polluting solution for a distributed generation, allowing different generation points in the geography of a country, region or even district, as well as providing a viable alternative from a technical and economic point of view for isolated generation applications [6–9]. Among the main renewable energy sources for distributed generation, we can find photovoltaic panels, small and medium wind turbines, micro-hydro turbines, biomass and biogas [27]. The electricity production by hydropower, biomass and biogas need a constant supply of fuel and resources, which would imply a major economic commitment to such a sector and there are a lot of pollutant emissions in the case of the last two technologies; so they would not be suitable for small outlets in homes, small business systems etc. By contrast, wind and solar sources can be more suitable and they are nonpolluting [27]. This is why most applications choose these sources to implement hybrid systems based on renewable energies. The wind resource, despite being available throughout the day, has a high randomness and large variations in the short term, so it is not a reliable source for supplying a load [8]. On the other hand, although the solar resource is more predictable and suffers less pronounced variations, there can be no solar production during the night or at dawn or nightfall, so production is minimized due to the reduced amount of incident radiation, resulting in an energy deficit [28].

Despite the benefits of renewable energy, there are associated problems with each technology, such as dependence on environmental resources, high cost, etc. To minimize the negative impact of these

* Corresponding author.

http://dx.doi.org/10.1016/j.rser.2017.09.014
Received 26 April 2016; Received in revised form 20 August 2017; Accepted 2 September 2017

Nomenclature

BAT	Battery
CHP	Combined Heat and Power (cogeneration)
DOD	Depth Of Discharge
ELEC	Electrolyzer
FC	Fuel Cell
LPSP	Loss of Power Supply Probability
MH	Metal Hydride
MPPT	Maximum Power Point Tracker
MT	Micro Turbine
PV	Photovoltaic source
SC	Supercapacitor
SOC	State Of Charge
UC	Ultracapacitor
WT	Wind Turbine

disadvantages, hybrid systems are presented as a viable, safe and effective solution [10–16].

The use of hybrid systems with different generation sources is an acceptable solution to cover the deficiencies of the different elements, but a backup system is necessary for an optimal power supply [5,15]. Nowadays for small and medium scale, energy is stored mostly in batteries and, for specific applications, in supercapacitors. For larger scale storage, potential energy is used with hydro pumping in swamps. Because wind and solar resources have a stochastic behavior, and the supply of the load profile is the main objective of generation systems, the use of energy storage systems is necessary to ensure the demand is reached and the stability of the supply system [28]. In the short term, energy storage systems have the primary function of supporting excess/deficiency of energy, and guaranteeing system security and power supply when the load changes [1]. In contrast, in the long term, energy storage systems have the function of providing the demand for a long period when the generation is not sufficient to maintain the load [1].

Traditionally, batteries and more recently supercapacitors have been used as short-term energy storage systems. Supercapacitors have a better dynamic behavior than batteries, so they can respond to demand shocks and supply energy almost immediately [29]. Moreover, their lifetime is very high with a safe operation without emission of harmful gases [29]. Despite all these advantages, their low capacity restricts their use. In contrast, batteries are elements with worse dynamic response, and a limited lifetime based on the number of charge/discharge cycles. Additionally, batteries may suffer deterioration and during normal operation can produce harmful gases [30]. The fact that the batteries have gained greater prominence is mainly because of their high load capacity and the ability to support a higher density of discharge current in amplitude and time. These features ensure greater security in the system response, since batteries can withstand longer defects and deficiencies in generation and dynamic changes in demand.

The long-term energy storage systems have always been based on non-renewable energy sources, such as diesel generators. These generators require high maintenance cost and produce sound and environmental pollution.

Recently, the use of hydrogen technology is presented to have a future value [15,17]. The use of hydrogen as a fuel in fuel cells is showing its strengths compared to diesel systems. Fuel cells have higher performance, lower maintenance and no emissions. Because hydrogen is an energy vector and it can be produced renewably, it is ideal for use as renewable energy storage [18,19]. The use of hydrogen as an energy vector absorbs excess energy during generation and produce energy in stages of energy deficit [14]. This alternative decreases battery size and increases system performance by taking advantage of energy surplus. Despite the benefits of using hydrogen, it is true that greater control, security and associated equipment for proper operation is necessary [15].

The energy transformation based on electricity-hydrogen-electricity relation is a starting point for new models of energy storage for example: power to gas [20–27].

In order to ensure proper operation of hybrid systems based on renewable energy, guaranteeing the demand and increasing the system performance, it is necessary to use energy management strategies [6,28–30]. The goals of these strategies will determine the behavior of the system, so it is very important to define a proper management strategy. Therefore, this paper undertakes a review of different energy management systems on hybrid power systems based on renewable energies, with the use of hydrogen as an energy vector. Section 2 includes a review and a classification of the most common topologies studied in the scientific literature. In Section 3, a review of the main techno-economic criteria for designing energy management strategies is done. In Section 4 solutions adopted in the literature are presented. Section 5 reviews and analyses different strategies used in the scientific literature. Finally, Discussion and Conclusions are compiled in Sections 6 and 7 respectively.

2. Configuration of hybrid renewable systems

Hybrid systems can be classified in different ways; the most common are those which distinguish the different systems depending on their connection to the grid; as well as the method of integration of elements inside the system.

2.1. Classification according to grid connection

Hybrid generation equipment can be classified according to their stand-alone or grid connected operation. The use of one or another

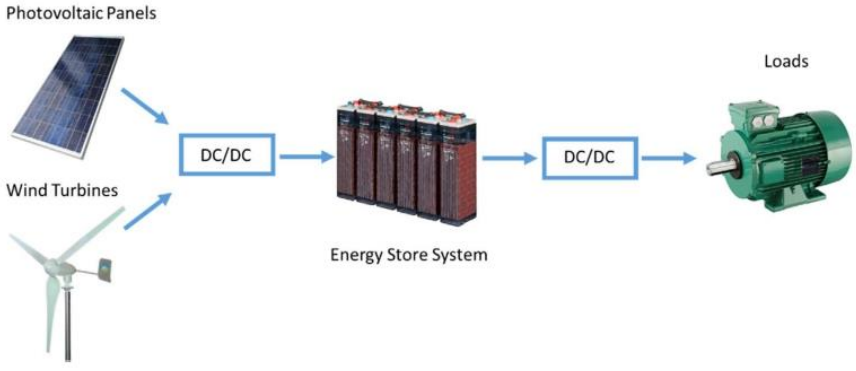

Fig. 1. Example of isolated topology.

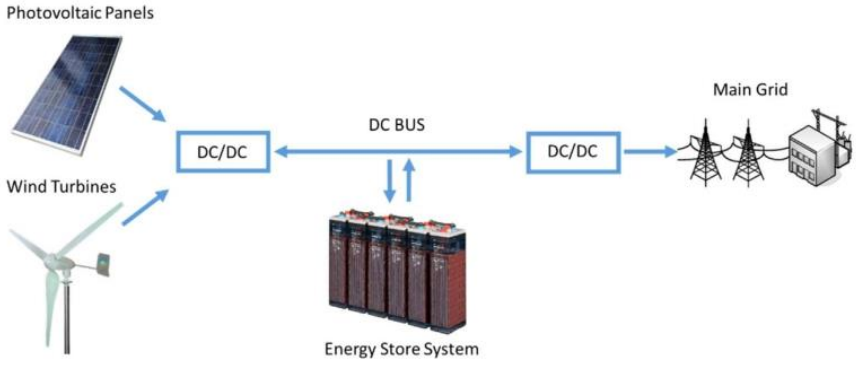

Fig. 2. Example of grid connected topology.

Table 1
Configuration and topology summary.

Ref.	Topology	Integration method
[2,3,19,30–45]	Grid connected	DC Bus
[5,8–12,28,29,46–93]	Isolated	DC Bus
[94–96]	Isolated	AC Bus
[97]	Isolated	Hybrid Bus

topology is mainly determined by the application and financial cost.

2.1.1. Isolated systems

In this topology, the system is isolated from the grid, so it is responsible for ensuring load demand at all times. The problems associated with this configuration are related to reliability and performance. Using a fully insulated system can endanger the security of the energy provided, due to the limited number of resources available. Similarly, the energy excess is a problem, and so it must be discarded, reducing system performance. For these reasons, this configuration has only technical and economic viability in applications where it is impossible or very expensive access to the grid connection. An example of isolated topology is presented in Fig. 1.

2.1.2. On-grid systems

In this configuration, the system is connected to the grid. This connection ensures demand is provided for in energy deficit situations, and increases system performance to take advantage of the energy excess for sale and distribution in the energy market. The use of this type of topology leads to new production models and energy management strategies based on consumption and distributed generation in small, medium or large scale. An example of a grid-connected configuration is presented in Fig. 2.

2.2. Classification by integration method

This type of classification distinguishes the system depending on the nature of the internal interconnection bus. The function of this bus is to create a physical link between all the elements, so generation and consumption is through the conditions imposed on the bus. Depending on the nature of the bus, we can distinguish between DC, AC or hybrid types. A summary table depending on grid connection and integration method is presented in Table 1.

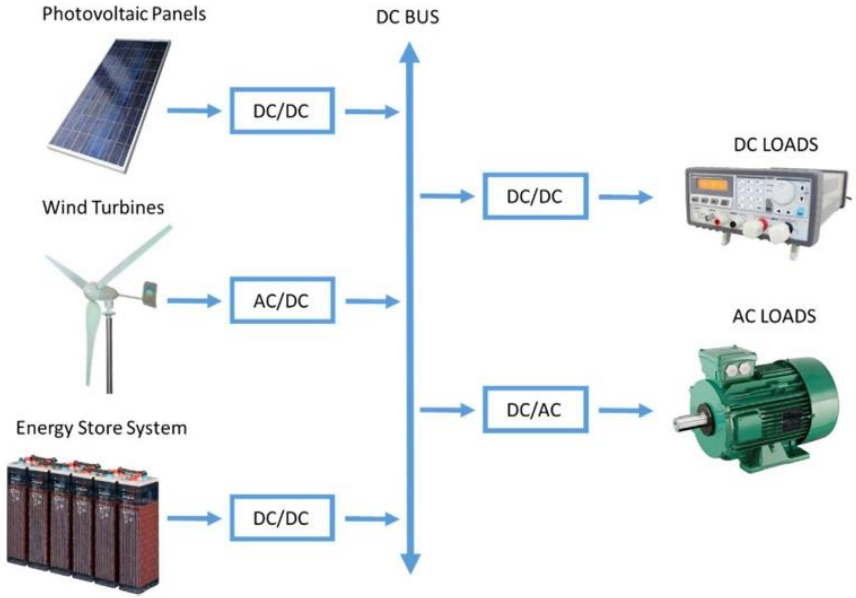

Fig. 3. Example of DC bus.

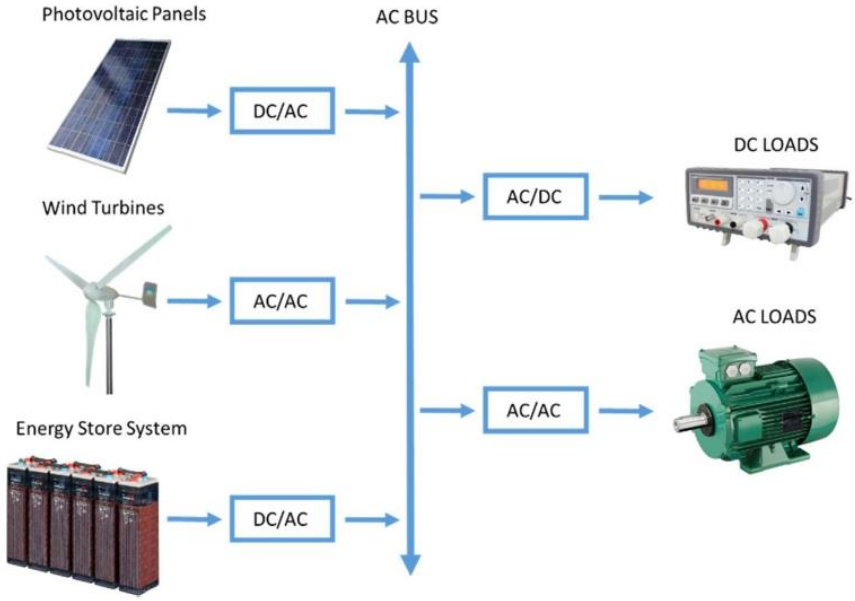

Fig. 4. Example of AC bus.

2.2.1. DC Bus

These buses are commonly used in low power applications because of a number of technical advantages that facilitate its use. Among these advantages, we can highlight their reduced losses and simplicity of use, avoiding technical problems related to power quality [1]. As a disadvantage, this configuration requires a larger number of conversion elements, because most of the loads must be supplied with AC. An example of topology based on a DC bus is presented in Fig. 3.

2.2.2. AC bus

AC buses are widely used in applications of medium and high production, due to the technical simplicity of operating at higher voltages than in DC, reducing internal losses of the system. The disadvantages of this configuration can often endanger the stability or integrity of the system. The main disadvantage is the need for elements for power quality correction [1]. It is increasingly common to find inductive and electronic loads that reduce the power factor and include harmonics respectively. A reduced power factor and high number of harmonics can damage the different generators, and requires the use of filtering and compensation elements, increasing the complexity and cost of the system. An example of AC bus-based configuration is presented in Fig. 4.

2.2.3. Hybrid bus

This configuration makes use of both buses (DC and AC) interconnecting generators and consumption which have the same nature. The principal advantage of this configuration is the reduction of power converters. As the main drawback of the system, it must be emphasized that the control is more complex, operating on two different networks, ensuring the balance of power at all times. An example of topology based on Hybrid bus is presented in Fig. 5.

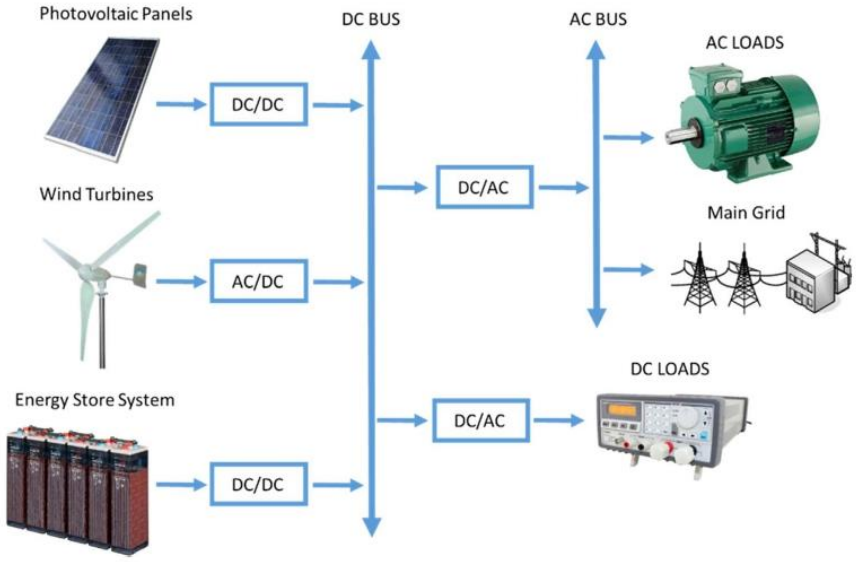

Fig. 5. Example of Hybrid bus.

2.3. Classification by integrated elements

The different integrated elements inside the hybrid system will define the generation, the energy storage system, or the demand. Next, the most common solutions adopted in the scientific literature are presented.

2.3.1. Generation

In case of generation, the most common solutions integrate renewable energy sources such as solar panels, wind turbines or hydro turbines. The use of solar panels guarantees generation during sun hours with an acceptable prediction margin. Wind turbines have a stochastic behavior so it provokes an unpredictable generation so the optimal use of the rest of the elements is necessary to guarantee the power balance. On the other hand, the wind generation is available during the entire day, intensified during the night. Wind turbines require special emplacement and environmental conditions, and therefore they are less used. According to the above, the hybridization of solar panel and wind turbines is considered an acceptable solution to generate energy from renewable sources.

In grid-connected topologies, the grid could be considered another generator if the renewable generation and energy storage system is not enough to guarantee the power balance.

2.3.2. Energy storage system

Batteries and/or supercapacitors seem to be the most important storage systems used in small applications. This solution permits the voltage stabilization of the internal DC bus, absorbing the transients during generation or load changes. Batteries and to a lesser extent supercapacitors represent the short-term storage system, and they are conceived as the main element of the system, whose parameters will define the operation of the other energy storage systems.

According to the goal of this paper, the hydrogen storage system is studied and evaluated in all the reviewed literature. This solution is a medium-long term storage system that is used to supply the demand when renewable generation and short-term storage systems are not enough. The main elements that compose the system are a fuel cell and hydrogen storage. The use of an electrolyzer or a reformer process (depending on application) is also extended and permits the utilization of excess energy to generate hydrogen and thus close the hydrogen energy cycle.

Other non-renewable storage systems are also used as the last resort to ensure demand. The most common solution is the use of diesel generators that are a synonym of pollution and fossil fuel consumption.

2.3.3. Demand

The demand will depend on the application in which the hybrid renewable system will be used. Desalinization processes, isolated telecommunication stations, distributed generation or residential uses are examples of different applications.

Finally, according to grid connection, the grid could be considered as another demand when it is necessary to guarantee the power balance during energy excess situations or when the purpose of the system is the energy injection to the national/regional/local energy system.

A summary based on all the previous classifications is shown in Table 1. Additionally, Appendix A includes an extended table where topology and integration methods, as well as constituent elements are also detailed for each reference.

2.4. Configurations review

Attending to the previous classifications and attending to different configurations and topologies, a brief analysis is performed bellow.

2.4.1. Single generation and single storage system

Configurations with DC bus and single generation which use only hydrogen storage systems are studied in these references: [10,38,39,63,67,73,85]. From the previous works in [10] and [38] an isolated and grid connected topology respectively use wind turbine as a renewable generator. Fuel cells represent the unique hydrogen backup system. Electrolyzers are included in isolated topologies in [63,67,73] and [39]. Solar panels are used as the main generator in [63] and [73], meanwhile in [67] and [39] the wind turbine replaces them.

2.4.2. Single generation and hybrid storage system

Configurations which include single generation, modeled by solar panels; and batteries and fuel cells/hydrogen as hybrid storage systems are presented in [5,31–33,48,49] and [40]. In [5,48,49] isolated applications are studied meanwhile grid connected topologies are studied in [31–33] and [40].

Electrolyzers are included in [9,41,50,64,65,71,77,80,83,91,92]. From previous configurations, only [9] and [41] present wind turbines as the only generator system. From the grid connection point of view, all the previous configurations except [41] present an isolated topology.

Finally, [83] presents an isolated application in which micro turbines are the main generator of the system, while batteries and fuel cells represent the hybrid storage system.

2.4.3. Hybrid generation and single storage system

In [2,34], and [36] a grid connected application based on DC bus integrates a hybrid generation composed of solar panels and wind turbines as main generators, and fuel cells/hydrogen as a unique storage system. On the other hand, [68] presents the same integrated elements in an isolated topology. Electrolyzers are included in the previous configurations in [8,19,29,37,43,60,66,69,70,84,88,94,95,97]; from which, [19,37,66,94] and [88] are developed in an isolated topology. A diesel generator is also included in an isolated application in [90].

Finally, from the integration method point of view, exceptions studied in [97] and [95] present a hybrid DC/AC and AC bus which are used respectively to integrate all the elements inside the hybrid system.

2.4.4. Hybrid generation and hybrid storage system

Isolated configurations which use solar panels and wind turbines as hybrid renewable generation, and batteries and fuel cells as hybrid storage systems are studied in [11,12,52,72] and [74]. In these configurations, hybrid generation and storage systems are used to solve the disadvantages of each technology taking advantage of the other ones. Hydrogen generation by electrolyzer is not considered in these applications.

The use of complete hybrid generation and hybrid storage systems under a DC bus in isolated application is presented in [28,30,32,46,51–59,61,62,75,76,78,79,81,82,86,87]. The use of hybrid generation is based on solar panels and wind turbines. On the other hand, the energy storage system is composed of batteries as a short-term storage solution, and fuel cells and electrolyzers as the hydrogen storage system. In these applications, electrolyzers take advantage of energy excess to produce hydrogen by electrolysis process. AC bus is used only in [96]. The same integrated elements are used on grid connected application in [3,30,35,42,44,45,93].

Finally, isolated configurations which also include diesel generators as long-term storage system are studied in [28,52,57,82,87,89,96].

3. Techno-economic criteria

To develop an energy management strategy in a hybrid renewable energy system it is necessary to take into account technical and economic criteria. These parameters will help to design a correct energy control, increasing the system performance. A description of the most important technical and economic criteria will be made below.

3.1. Technical criteria

Technical criteria are those that refer to the proper functioning of the equipment, in order to increase performance and reduce their degradation during normal system operation. A summary of technical considerations is presented in Table 2. The highlights to consider are presented below.

3.1.1. Solar & Wind sources

- MPPT techniques: The use of these techniques allow maximum performance and production for an environmental resource at a particular time [2,46].
- Wind turbine as main generator: Configurations that use wind turbines as the main generator can cause more changes in generation, so it will provoke an increased use of batteries and high number of start/stop cycles for electrolyzers and fuel cells. The use of solar panels and wind turbines enables a more consistent production during the day and takes advantage of the maximum wind resources overnight. With this topology, the use of energy storage equipment will be reduced and allows maximization of the environmental energy resources.

3.1.2. Battery

Short-medium term energy storage elements like batteries, can increase the system security under changes in consumption or production, and also during startups or shutdowns of the long-term storage equipment which has a slower dynamic [98–100]. In the same way, batteries will supply energy during energy deficit situations, allowing the reduction of hydrogen utilization, and therefore reduction in fuel cell and electrolyzer degradation by use.

- Battery discharge: The battery degradation is highly influenced by its own use. The use of high discharge depths may accelerate the battery deterioration, reducing its lifetime [101]. For lead acid batteries, a suitable sizing is one that estimates a running mode of operation around 20–30% of the DOD. Optimum replacement is determined when the maximum capacity of the battery has fallen to 80% of the initial nominal capacity [102].
- Battery charge: The charging process is crucial to operate the batteries safely and effectively [103–108]. There are different charging protocols depending on the battery technology and the desired charging rate. Despite this, a number of considerations need to be taken into account. The use of high charge currents can damage the cells and thus produce accelerated aging by corrosion [103–108]. Fast charging protocols require high voltages and high current, and therefore provoke an inefficient charge process, which can cause overcharge if it is not controlled. In spite of the above, the charge efficiency is very high even under fast charging processes.
  On the other hand, a slow charging process allows a safer and more efficient charge but it will cost some hours or even days [103–108]. Therefore, these charge processes would not be appropriate in hybrid systems whose generation is based on solar panels, because it will depend on weather conditions. In addition, a low voltage charge process can cause sulfation due to a low electrolyte renewal rate.
  Additionally, it is necessary to consider other factors such as the imbalance of charge between batteries, typical in series connection. In the long term, this problem can cause large voltage deviations between batteries causing non-homogeneous charging [107,108].
- Battery maintenance: The use of batteries requires basic maintenance principally to ensure correct operation and an increase in its lifetime. The main problem is related to self-discharge which causes capacity losses and even sulfation in case of long periods of inactivity [107,108].

3.1.3. Hydrogen resource

The proper use of hydrogen resources will increase the system performance in situations of excess or deficit of energy. In the case of using metal hydride tanks as storage technology, a proper management during the process of charge and discharge will be interesting to ensure a correct use.

- Hydrogen storage: Hydrogen storage systems are a safer solution which permits high energy density, high lifetime and a recharge time lower than that required by the batteries.
- Electrolyzer operation: Hydrogen based technology as electrolyzers and fuel cells has a proportional degradation with the number of start-stop cycles, as well as operating time [109,110]. An electrolyzer operating at low power can cause difference in pressures between the anode and cathode side, resulting in a flow of reagents from one electrode to another (crossover), obtaining products with low purity [111–113]. Similarly, operating at high powers causes a very high gas production, resulting in an accumulation of bubbles at the electrodes. This fact implies the reduction of the bonding surface between them and the electrolyte, increasing the electrical resistance and therefore reducing the performance [114–116]. Then the power operation will result from a combination between these previous processes.

Table 2
Summary of technical criteria.

				
Solar and wind based topology allow maximization of energy resources MPPT improve power generation Production depends on weather conditions		Batteries improve system security Reduce fuel cell and electrolyzer operation time, and therefore operation degradation Lifetime depends on DOD	Start-stop cycles in electrolyzers produce deterioration Low/High electrolysis power provokes low puricity and low efficiency respectively	Start-stop cycles and load changes in fuel cells produce deterioration Operation in ohmic region improves efficiency Power converter operation can cause deterioration

- Fuel cell operation: Fuel cells suffer deterioration in start-stop cycles and load changes [117]. During the processes of startup and shutdown, over voltages appear due to reverse current between cathode and anode in the presence of air in one of the electrodes. This problem causes the oxidation of carbon (CO_2) in the bipolar plates, decreasing catalyst surface due to platinum-CO_2 reactions, resulting in increasing of mass transport losses [118–126]. In case of load changes, a non-uniform temperature distribution can appear over the membrane and the catalyst surface, which may cause similar problems as start-stop cycles [17,118,121,123]. Finally, the use of fuel cells at very low and very high power causes a low performance operation. For this reason, the operation of fuel cells typically takes place in the ohmic operation zone [9].

Thus, the use of fuel cells as well as the operating point should be chosen taking into account the above restrictions.

- Effect of power converters over the fuel cell: The use of power converters can also have a negative influence on the degradation of fuel cells. The high operating frequencies can be filtered by the internal dynamics of the stack on the model of double capacitance [127]. Low frequencies, switching or harmonics between 0.1 and 100 Hz cannot be filtered, and so produce negative effects as discussed for load changes [126–130].

3.2. Economic criteria

The economic criteria are those that focus their efforts on economic decisions, trying to give a system response economically viable to compete with traditional systems. A summary of economic criteria is presented in Table 3. Main issues to consider when choosing generation and storage systems are presented below.

3.2.1. Solar & wind sources

The use of generators based on solar and wind energy, ensures long operating life and low operating and maintenance costs compared to other renewable technologies [1,131]. The use of renewable energy systems can impact discounts on energy invoices as well as facilitate the market entry of new methods of consumption, as a net balance system [132].

3.2.2. Energy management strategy

The use of a proper energy management strategy which takes into account the technical criteria presented in the previous section, will increase the lifetime of elements, and reduce replacement and operating and maintenance costs [133].

3.2.3. Battery

The use of short-term storage systems like batteries increases system security against the use of elements with slower dynamics such as fuel cells and electrolyzers [47–49]. A secure system is that which ensures critical loads at all times, minimizing damage and penalty cost by power failure situations.

In the same way, batteries present a more economical solution with respect to hydrogen storage systems.

3.2.4. Hydrogen resource

The use of hydrogen-based storage compared to fossil fuel based technologies such as diesel generators, allows the production of electricity with higher performance, low emission and reduced operating and maintenance costs [1,13,131].

– Electrolyzer:
PEM electrolyzers today constitute a promising technology but it is already under investigation. The reduced lifetime and the higher overall cost of this type of electrolyzer, are the main reason why alkaline electrolyzers are widely used, becoming a more competitive, safer and well known option for hydrogen production technologies [112,114,116].
The use of electrolyzers in isolated configurations increases system performance because they use energy excess to produce hydrogen.
– Fuel cell

The use of fuel cells will provide a faster response, working at lower temperatures than other technologies on the market [121,134,135]. This will enable a faster response under dynamic changes in demand or generation, reducing problems associated with the lack of power in heavy load situations.

4. Techno-economic solutions

In order to optimize the energy management strategy based on the criteria presented in the previous sections, the scientific literature includes different technical and economic solutions for the operation of the most vulnerable elements of the system, such as batteries and hydrogen-based elements for production and consumption as electrolyzers

Table 3
Summary of economic criteria.

					
Solar and wind syste s today have a good lifetime nd low maint nance and opera ion cost Help to introduce ne energy models	Bat eries help to ensure demand a all times, red cing penalty cost	Alkaline electrolyzer echnology is we l known Reduced initial ost with respect to o her technologi s Improve sys em erformance ab orbing energy exc ss	EM fuel cells rovide faster res onse to ensure demand Hi her efficiency t an traditional e ergy sources	Proper e ergy management strategy can reduce verall cost	

Table 4
Summary of techno-economic solutions.

			
The se of a DC Bus acilitates the system config ration	Direct con ection of batteries to DC Bus	Minimum ower electrolyzer o eration	U e of a modular uel cell system
Sup rcapacitors for ower factor correctio	Current/Volt ge charge modes	Variable power onditions	peration in Ohm c zone
Use f grid to ensure ower balance	Hysteresis operation mode		se of filters to r duce switching effects

and fuel cells respectively. A summary of techno-economic solutions is presented in Table 4. The main solutions proposed in the literature are described below.

4.1. System configuration

- The use of a DC bus provides a simple way to control the energy exchange between the elements, avoiding power quality problems and power factor correction. In the same way, it can reduce the number of devices needed to adapt the generation, because most generators produce in DC currents [1].
- In case of a grid-connected system, the use of supercapacitors allows the correction of the power factor by injecting reactive power into the internal bus [31].
- The use of the grid will help to ensure the power balance, and supply the demand or absorb energy in case of deficit/excess energy situations respectively.

4.2. Batteries

- Battery connection: Direct connection of batteries to the internal bus will save bidirectional converters. On the other hand, a more comprehensive power control is necessary in order to resolve the problem with DC bus voltage variation, and to protect batteries against excessive discharge or overcurrent situations [136]. The use of power converters will increase system cost but it allows different charge modes to protect batteries.
- Battery operation: In case of charging situations for batteries, the use of current mode will allow faster charges for low SOC. On the other hand, in case of high SOC, the voltage mode will protect the battery with a slower charge mode in which current will be imposed by battery voltage [50,137]. The use of a reduced depth of discharge will extend the lifetime of the battery [98,101,102,138].
- Hysteresis Band: The use of hysteresis based on the battery SOC will determine the start or stop conditions of fuel cell and electrolyzer. These strategies will reduce the number of operating cycles, and therefore increase the lifetime of the elements by minimizing their degradation [18,19,51–59,133]. Strategies with appropriate hysteresis bandwidths will increase the system performance, avoiding the overuse the batteries, and reducing start and stop cycles for electrolyzer and fuel cell [51,57].

4.3. Hydrogen resource

- Electrolyzer operation: Strategies which impose a minimum operating power for the electrolyzer, allow the operation in a high efficiency area, and high purity production [18,47,50,111–113]. The use of electrolyzers under variable power conditions can increase the hydrogen production [54,133].
- Fuel cell configuration: The use of a modular fuel cell system will help to increase the safety system response, just as it may be adapted to the demand in the proper way, regarding the use of a single fuel cell with high nominal power [29].
- Fuel cell operation: Fuel cells always operate in the ohmic zone, ensuring high performance and low degradation [9]. Similarly, the operation at constant power will reduce problems related to dynamic changes in the demand and damage associated [118,121,123].
- Power converter switching: The implementation of active or passive filters reduces the effect of switching of power converters for frequencies between 1 and 120 Hz [60,127,128].

5. Energy management strategies

To operate, integrate and interconnect several devices in a generation system, ensuring safe operating regime and fulfilling the goals, a control system to manage the energy is necessary. A proper energy management strategy enables the system to supply the demand, increase the lifetime of the elements, reduce operating costs and therefore maximize system performance, providing a technically and economically feasible option. The aims of the different management strategies influence the behavior of the system. Most of the works found in the scientific literature present simulated strategies for hybrid systems, in order to maintain the demand, obviating technical and economic optimization criteria and multiple problems associated with real systems, such as degradation of hydrogen equipment or a correct management energy vector. Next, a review of the different strategies used in the scientific literature can be found, analyzing the different objectives used in each one. A summary and description of all works studied in this section is presented in Appendix B-E according to the four strategies studied bellow.

5.1. Strategies in which the objective is to the ensure the demand

The main objective of this type of strategy is to satisfy the demand, and for that it bases its control algorithm mainly on three design criteria: power balance, state of charge of the batteries and hydrogen stock, depending on the elements which integrate the system (see Table 5). These design variables establish the operating limits of major energy storage systems, such as batteries to short-term storage, and fuel cells and electrolyzers to long-term storage.

The main advantage of this strategy is the simplicity in design and control, governed mainly by algorithms based on simple flow chart diagrams. In the same way, sizing applications that include this strategy

Table 5
Summary of strategies which objective is to ensure demand.

Ref.	Optimization objectives	Design constrains	Control Algorithm
[2,5,8–12,29,32–34,41,46,48,49,61–63,65–69,72,73,88–92,94,97]	Ensure Demand Sizing	Power balance SOC H_2 Stock	Flow Chart
[31]	Ensure Demand	Power balance Battery Voltage H_2 Stock	Linear Programming
[55]	Ensure Demand	Power balance SOC H_2 Stock	Model Predictive Control
[64]	Ensure Demand	Power balance SOC H_2 Stock	Fuzzy Logic
[70] [71]	Ensure Demand Sizing	Power balance SOC H_2 Stock	Pareto Optimal Solution
[35]	Ensure Demand	Power balance SOC H_2 Stock	Flow Chart & ANFIS

are also simplified. On the other hand, the non-use of optimization parameters based on equipment degradation, modes of operation or operating costs of the system, causes a non-optimal solution from a technical and economic point of view.

A summary scheme of the main characteristics of this strategy and a review of the optimization objectives, design constrains and control algorithm is presented in Fig. 6 and Table 5 respectively.

The operating priority is shared by almost all reviewed works, [9,11,12,32,33,35,41,46,48,49,55,61,62,65,71–73,88,90–92], and they give to the short-term storage system the responsibility for absorbing transients and stabilizing the power balance between a maximum and minimum state of charge. From these values, the fuel cell and electrolyzer will operate for the cases of excessive deficit or excess of energy respectively. The use of short-term storage systems implies having an element capable of dumping certain deviations in the power balance, and therefore limiting the use of the hydrogen storage system against situations of high excess or energy deficit. All this results in a lower degradation of these elements and therefore an increase in the useful lifetime of the system, to the detriment of the batteries.

There are other works whose strategies differ from the previous one. These other ones lack short-term storage elements, and therefore the SOC of the batteries/SC is not a design parameter. For example, in [2,8,29,34,63,66–70,89,90,94,97] the start/stop conditions of the hydrogen storage system will be determined by the value and sign of the power balance. This solution causes a high number of starts and stops of the fuel cell and electrolyzer, and consequently reduces the useful lifetime due to associated degradation.

With respect to the hydrogen-based energy storage system, the topologies studied in [8,9,29,35,41,46,55,65–67,69,72,73,88–92,94,97] have a hydrogen generating element, which allows the increase of the performance of the system by taking advantage of the excess energy and converting it into hydrogen. This hydrogen can be used by the fuel cell when it was necessary.

In the case of isolated topologies such as those presented in [5,8–12,29,35,46,48,49,55,61–63,65–68,73,88–92,94,97], the energy generation which cannot be stored by the energy storage systems is discarded through dumping loads. This fact implies a reduction in the operating performance of the system. Conversely, in case of excessive deficit, a prioritization of loads is necessary and in extreme cases, it is also necessary to disconnect the demand. This type of topology allows an operation strategy highly conditioned by the system sizing, and therefore the satisfaction of the demand can be put at risk.

On the other hand, in grid-connected topologies, the grid is an active element of the system and it allows maintaining the power balance

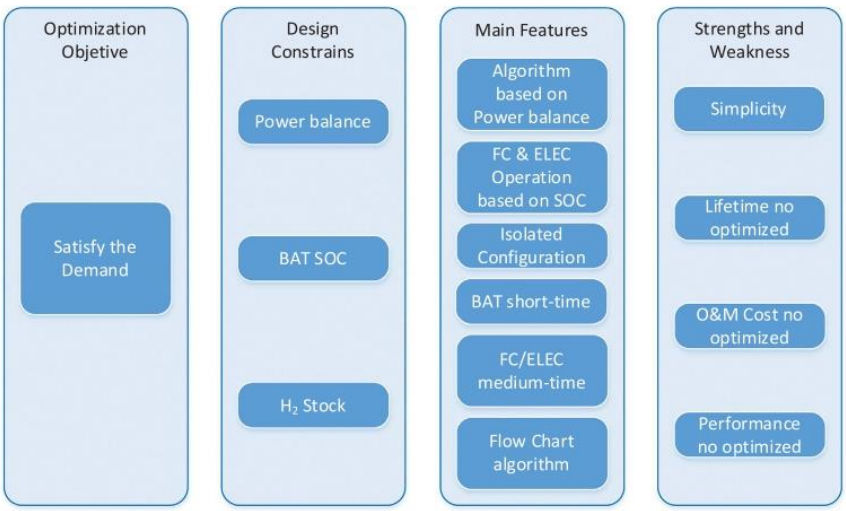

Fig. 6. Main characteristics of strategies for which objective is to ensure demand.

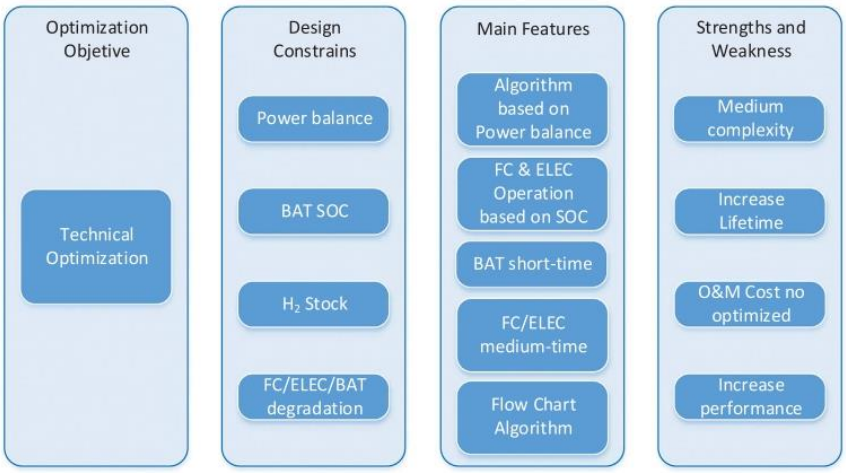

Fig. 7. Main characteristics of strategies whose objectives include technical decision factor.

by absorbing or supplying energy when the hydrogen stock is over its respective operating limits. In these topologies, such as those studied in [2,31–35,41], the excess or deficit of energy is corrected by the injection or purchase of energy from the grid. These topologies allow higher flexibility in the strategy and, also guarantee demand under any energetic situation.

Finally, based on the control algorithm, Flow Chart algorithm is the most extended solution, while other optimization algorithms are also used to calculate the reference power of the hydrogen energy system regarding the design constrains. As an example, Linear Programming in [31], Model Predictive Control in [55], Fuzzy Logic in [64], Pareto algorithm in [70] and [71] or Adaptative Neuro Fuzzy Inference System in [35]. The problem associated with these control algorithms is the need for accurate models of the overall system, demand and weather resources.

5.2. Strategies whose objectives include technical decision factor

These strategies, as well as ensuring demand at all times, take into account technical criteria in order to ensure the proper use of the equipment. The main target of these strategies is to reduce the degradation of the equipment more susceptible during operation of the system. These elements are battery, electrolyzer and fuel cell. The solutions adopted in the literature are diverse and depend on the main goal of the study. In order to perform the control algorithm, power balance, state of charge of the storage system and degradation parameters are defined as design constrains.

The main advantages of these strategies are their medium complexity design and control, and the good results in terms of system performance and/or lifetime, depending on the optimization objective. On the other hand, economic parameters are not taken into account, so the system response is not optimized.

A summary scheme of the main characteristics of this strategy and a review of the optimization objectives, design constrains and control algorithm is presented in Fig. 7 and Table 6 respectively.

As for the previous case, the most common solutions integrate short-term storage systems, and therefore, they will operate in first instance to absorb or supply energy when it is necessary. The use of long-term storage system based on hydrogen backup will operate when the maximum or minimum operating limits of batteries are reached. In the

Table 6
Summary of strategies whose objectives include technical decision factor.

Ref.	Optimization objectives	Design constrains	Control Algorithm
[19]	Ensure Demand Increase Lifetime	Power balance	Model Predictive Control
[30,47,50–,56–58,60,74,76,95]	Ensure Demand Increase Performance Increase Lifetime	Power balance SOC H_2 Stock	Flow Chart
[36]	Ensure Demand Stability	Power balance SC Energy function	Differential Flatness Based Control
[75]	Ensure Demand Maximize H_2 generation	Power balance SOC	Linear Programming
[77]	Ensure Demand Maximize H_2 generation Minimize Battery use	Power balance SOC	Fuzzy Logic
[78]	Ensure Demand Increase Lifetime	Power balance Load Forecast	Dynamic Real-Time Optimization
[79]	Ensure Demand Increase Lifetime	Power balance SOC	Fuzzy Logic
[80]	Ensure Demand Increase Lifetime	Power balance SOC H_2 Stock Weather Forecast	Flow Chart
[81]	Ensure Demand Increase Lifetime	Power balance SOC H_2 Stock	Artificial Neural Network Controller

case of isolated topology, the use of dumping loads and demand prioritizing are the most common solutions to solve the energy excess or high deficit of energy situations. On the other hand, in the case of grid connected topologies, the grid will absorb or supply energy when the energy storage system is over its operation limits. An example of application of these strategies are presented in [19,30,47,50–54,56–58,60,74,80,95].

Other works define the priority and the power reference of the elements based on the solution of different algorithms which have taken into account diverse parameters. Examples of that are studied in [36,75–79,81].

The main differences between these strategies and the ones studied in the previous section are based on the restrictions imposed to the operation points of the energy storage system to assure the different objectives, increase the system lifetime or increase the system performance.

In order to increase the system lifetime, different solutions are adopted to reduce the degradation caused by start/stop cycles of electrolyzers and fuel cells. [53][54][56][57][58] use a strategy based on hysteresis operation mode, which are defined by the predefined values of battery SOC. Despite being an important improvement from the point of view of degradation, the hysteresis bandwidth is fixed and modeled by a simple flow chart. For this reason, there is room for improvement in the storage system utilization.

In the same way, [19,52,79,80] use weather and demand prediction in order to determine if the use of hydrogen storage system in the next iteration step is necessary, reducing unnecessary start/stop cycles. To implement the control law, flow chart algorithm is used in [52] and [80], while [19] and [79] use Model Predictive Control and Fuzzy Logic respectively. According to above, the reliability of the strategy will depend on accurate forecast and reliable system models to perform a correct operation, and therefore the system performance will be conditioned by the accuracy of the models used.

Finally, [81] proposes a strategy in which Artificial Neural Network Controller is used to define the power reference of the hydrogen storage system in order to maintain the battery SOC in a fixed point. This strategy will increase the battery lifetime at expense of an intensive use of the fuel cell and electrolyzer. The system operating and maintenance cost in this strategy will be huge because of the higher degradation on the hydrogen storage system.

With the objective to increase the system performance, three solutions are adopted.

The first one tries to guarantee high purity products from electrolysis process. To get this target, in [30,47,51,95] a simple strategy based on flow chart and imposed minimum power to start up the electrolyzer is used. This constraint helps to solve degradation problems associated with the fuel contamination on fuel cells. On the other hand, higher utilization of batteries will be required to assure the minimum power of the electrolyzer in the case of a low power balance.

The second solution implemented in [74] modifies the fuel cell power in order to operate always in its maximum efficiency point. This strategy causes the fuel cell generation to not be synchronized with the energy requirements, and therefore implies a higher use of batteries and even start/stop cycles.

The last solution has the goal to maximize the hydrogen production. To get it, an optimization problem is defined in [75,77,78], and solved by different optimization algorithms: Linear Programming, Fuzzy Logic and Dynamic Real-Time Optimization Algorithm. The non-use of lifetime constraints could provoke high degradation of the energy storage system, so this strategy does not get an optimal solution.

5.3. Strategies whose objectives include economic decision factor

These strategies include an economic analysis in addition to a guarantee of the power balance. These economic parameters will help to determine an optimal solution from an economic point of view. In many cases, this optimal solution does not determine a favorable operation for equipment due to not having enough technical criteria to avoid problems associated with different operating regimes. These strategies have potential applications on sizing and long-term analysis.

The main advantage of these strategies is the optimal system response from an economic point of view. On the other hand, complex optimization algorithms are used, so it increases the complexity in real applications. In the same way, the reliability of the model to define the cost function is crucial to get the best performance. Finally, technical parameters are not taken into account, so the system lifetime might not be optimized.

A summary scheme of the main characteristics of this strategy and a review of the optimization objectives, design constrains and control algorithm is presented in the Fig. 8 and Table 7 respectively.

The solutions adopted in the literature are based on the use of different cost functions associated with the charge or discharge of the elements, which determine an optimization problem. Different algorithms are used to calculate the solution of the optimization problem. These determine the priority and the power reference of each element which guarantees the most economical utilization of the energy storage system during each integration period. As happened in previous cases, the solution implemented in extreme cases of high excess or energy deficit will depend on the topology.

The main difference between the consulted references is the optimization algorithm used to minimize the cost function (see Table 7). In the case of grid-connected applications, the interaction between grid and hybrid system is also taken into account. For this reason, the losses or benefits when buying or selling energy from the grid are taken into account as well.

5.4. Strategies whose objectives include technical and economic decision factors

Finally, this kind of strategy seeks to increase system performance,

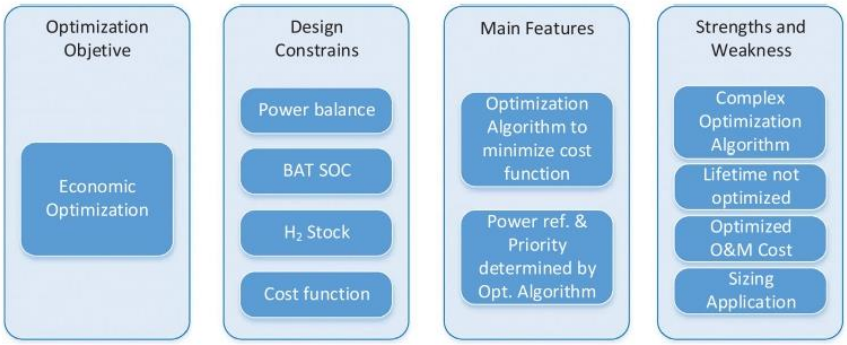

Fig. 8. Main characteristics of strategies whose objectives include economic decision factor.

Table 7
Summary of strategies whose objectives include economic decision factor.

Ref.	Optimization objectives	Design constrains	Control Algorithm
[3]	Ensure Demand Cost reduction	Power balance Cost function	Model Predictive Control
[28]	Ensure Demand Cost reduction	Power balance Cost function	Flow Chart & Genetic Algorithm
[82]	Ensure Demand Cost reduction	Power balance SOC Cost function LPSP CO_2 emissions	Fuzzy Logic & Differential Evolution Algorithm
[96]	Ensure Demand Cost reduction	Power balance SOC H_2 Stock Cost function Weather Forecast	Mixed-Integer Linear Programming
[83]	Ensure Demand Cost reduction	Power balance SOC H_2 Stock Cost function	Flow Chart
[37]	Ensure Demand Cost reduction	Power balance Cost function	Receding Horizon Optimization Algorithm
[38]	Ensure Demand Cost reduction	Power balance Cost function	Genetic Algorithm
[39]	Ensure Demand Cost reduction	Power balance Cost function	Receding Horizon Optimization Algorithm
[84]	Ensure Demand Cost reduction	Power balance Cost function	Gravitational Search Algorithm
[85]	Ensure Demand Cost reduction	Power balance Cost function Load Forecast	Particle Modified Swarm Optimization Algorithm
[40]	Ensure Demand Cost reduction	Power balance Cost function Load Forecast	Adaptive Model Predictive Control
[42]	Ensure Demand Cost reduction	Power balance SOC Cost function Weather Forecast	Fuzzy Logic
[43]	Ensure Demand Cost reduction	Power balance SOC H_2 Stock Cost function	Interior Search Algorithm

based on the proper supply to demand. Technical and economic criteria are taken into account to increase equipment life and reduce maintenance costs. This strategy has an optimal solution for a technical and economic point of view, compared to traditional generation alternative systems. The solutions adopted in the literature are based on nonlinear optimization problems, using cost and equipment depreciation integrated in a multi-objective function. The solution of this problem by various techniques, determines the reference power supplied by each element in each iteration, ensuring the power balance with optimal system performance. Finally, as the previous cases, the solution implemented in extreme cases of high excess or energy deficit will depend on the topology.

Table 8
Summary of strategies whose objectives include technical and economic decision factor.

Ref.	Optimization objectives	Design constrains	Control Algorithm
[59]	Ensure Demand Cost reduction Increase Lifetime	Power balance SOC H_2 Stock Cost function	Flow Chart
[86]	Ensure Demand Cost reduction Increase Lifetime	Power balance SOC H_2 Stock Cost function	Fuzzy Logic
[87]	Ensure Demand Cost reduction Increase Lifetime	Power balance SOC	Particle Swarm Optimization Algorithm
[44]	Ensure Demand Cost reduction Increase Lifetime Increase Performance	Power balance SOC H_2 Stock	Particle Swarm Optimization Algorithm
[93]	Ensure Demand Cost reduction Increase Lifetime	Power balance SOC H_2 Stock Cost function Degradation function	Flow Chart & Linear Programming
[45]	Ensure Demand Cost reduction Increase Lifetime Increase Performance	Power balance SOC H_2 Stock Cost function	Flow Chart

The main advantage of these strategies is the optimal system response from a technical and economic point of view. Lifetime and performance parameters are taken into account to define the cost function. On the other hand, complex optimization algorithms are used, so it increases the complexity to develop real applications.

A summary scheme of the main characteristics of this strategy and a review of the optimization objectives, design constrains and control algorithms is presented in the Fig. 9 and Table 8 respectively.

The main difference between the proposed strategies is based on the technical constraints, and also the optimization algorithm used to solve the nonlinear optimization problem.

In [44,86,93] Fuzzy Logic, Particle Swarm Optimization Algorithm and Linear Programming are used respectively to solve the multi-objective problem. The cost function includes lifetime parameters of each

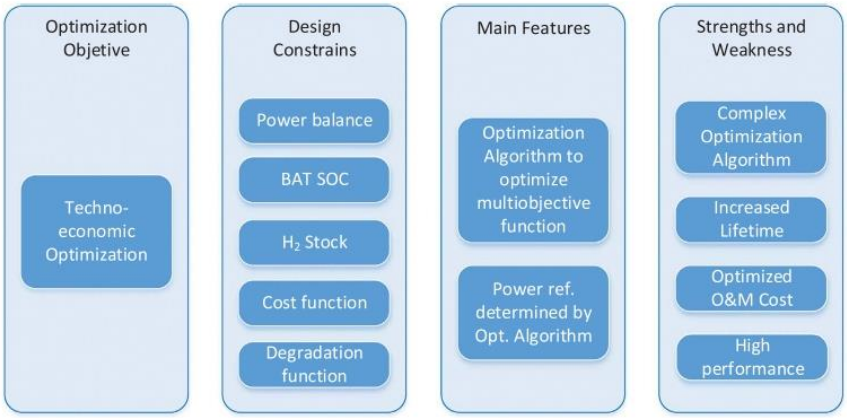

Fig. 9. Main characteristics of strategies whose objectives include technical and economic decision factor.

element and also the associated degradation cost. The priority and the power reference of each element are based on the response of the optimization problem.

In [87] a work is presented in which three different objectives are optimized with the use of Particle Swarm Optimization Algorithm. These objectives will define three different cost functions depending on the objective to minimize operation and maintenance cost, increase system efficiency or increase system lifetime.

In [59] the cost associated with the degradation process is included in the cost function. The priority of the energy storage system is based on the energy reserves of each storage system and the associated accumulated degradation cost.

Finally, [45] presents different cases and strategies based on a flow chart diagram in which different optimization objectives are studied. The short-term storage system is the core of the decision, and the start/stop conditions and power reference of the fuel cell and electrolyzer will depend on hysteresis operation mode and the optimization objective. Cost reduction, hydrogen maximization and system performance are the three main objectives studied in this work.

6. Discussion

Based on the structure of the paper and attending to all the issues developed in it, the Discussion Section will be classified in each of the topics analyzed along the manuscript.

6.1. Topologies and configurations

The chosen configuration, the topology and the elements which compose the system, will determine the operation and performance of it, (see Table 1 and Appendix A). The main problem to be solved in this area is the correct management of the energy in situations of excess and energy deficit, due to the stochastic production of the main sources of renewable generation.

Isolated topologies present problems related to low performance and low security to supply the demand. To solve the last problem it is common to oversize the storage equipment, increasing the investment cost. In the same way, in case of excess energy, the surplus energy must be discarded and therefore reduces the performance of the system.

Grid connected topologies allow the grid to be included as an active part of the system, and therefore optimize the system during excess or deficit of energy.

According to the energy storage system studied in Section 2.3, the use of batteries as a short-term storage element allows reduction of costs and the degradation related to the operation of the hydrogen storage systems. In addition to the above, simplicity, high efficiency and modularity help with the integration of these technologies. On the other hand, the charging process must be controlled and requires high charging time, caused mainly by the seasonality in photovoltaic or wind generation. All this has repercussions in a more complex system and the use of batteries with higher capacity.

Similarly, the use of hydrogen-based storage systems ensures a high energy density solution to guarantee a constant response against low state of charge of batteries, as well as a solution to evacuate the excess of energy in isolated systems. In addition to the above, it is presented as a clean and low maintenance system compared to traditional diesel systems. On the other hand, the complexity, the cost of these systems and their reduced useful lifetime, determine the need of a proper energy management strategy.

The use of hybrid storage systems will reduce the sizing of both technologies, as well as provide a more economical, simpler and more viable solution to the problem of energy storage.

The sizing criteria of these hybrid systems should respond to technical and economic criteria, as well as the topology used. Due to the above, grid-connected systems allow a cost reduction in batteries thanks to the reduction of its capacity. The stock of hydrogen can also be reduced because the grid can supply energy during low SOC situations. In the same way, during charging process, the grid can evacuate energy, so the hydrogen generator power could also be decreased.

In isolated applications, to guarantee the demand is the priority of the system, so a more comprehensive sizing process should be carried out in order to calculate the optimal storage capacity of the two storage systems. The maximum battery DOD, environmental conditions, demand profile as well as the cost of the different elements, will determine an optimization problem that requires a more exhaustive analysis.

6.2. Optimization objectives

The optimization objectives analyzed in Section 3, Tables 2, 3 will determine the performance and complexity of the system operation. Similarly, system configuration can limit the scope of these objectives.

The main objective of any generation system must be to satisfy the demand, so additional objectives will be determined by the possible options that the configuration and topology of the system allows. For example, isolated systems which only have a storage system based on batteries or hydrogen will not be able to implement other objectives than to guarantee the power balance at any moment.

The inclusion of new elements will allow including a degree of freedom on the decisions of the system against excess or deficit energy situations. The system response can be optimized according to technical and/or economic criteria, such as the operation of the system with a maximum performance or a minimum cost or a minimum degradation. Those works which integrate both criteria will allow an optimal performance of the system.

The study of new optimization objectives will allow renewable energy systems to be more competitive from a technical and economic point of view, thus encouraging the use of environmentally friendly technologies.

6.3. Techno-economic parameters

The technical and economic parameters are the baseline to define management strategies to fulfill different optimization objectives.

These parameters will largely depend on the topology and configuration used, as they will determine the advantages and disadvantages of the different technologies as well as the minimum criteria for a safe and efficient operation.

Taking into account the most used configurations, as has been studied in Section 4, Table 4 the most important parameters to guarantee the primary objective of satisfying the demand are the power balance, the batteries SOC and the available hydrogen stock. In the same way, in order to optimize system response, other criteria may be taken into account to meet secondary optimization objectives, such as equipment degradation, battery charging processes, the modularization of the fuel cell and the operation and maintenance cost.

The inclusion of new technical and economic parameters will allow a more secure and efficient management of the system, although more complex energy management strategies will be necessary.

6.4. Energy management strategies

The different energy management strategies are based on the achievement of different optimization objectives, based on different technical and economic criteria. These strategies are intended to define the energy flows during the normal operation of the system, and therefore to determine which equipment must operate and its power reference.

Depending on the optimization objectives and the topology and configuration of the system, the strategy can be more or less complex, requiring the use of more or less complex optimization algorithms.

In view of the classification of strategies according to their objectives, the simplest strategies are those in which the objective is to satisfy

the demand, (see Fig. 6, Table 5 and Appendix B). For that, it bases its control algorithm mainly on three design criteria: power balance, state of charge of the batteries and hydrogen stock, depending on the elements that integrate the system. These design variables establish the operating limits of major energy storage systems, such as batteries to short-term storage, and fuel cell and electrolyzer to long-term storage. From the point of view of system performance, these strategies do not optimize the use of equipment or operating costs, so they are recommended for systems with a very simple configuration such as isolated topology with a single energy storage system.

Strategies that take into account technical criteria, try to improve the system response with respect to the previous strategies, and a more complex configuration allows their implementation. The main target of these strategies is to reduce the degradation of the equipment more susceptible during operation of the system. These elements are battery, electrolyzer and fuel cell. The solutions adopted in the literature are diverse and depend on the main goal to study. In order to perform the control algorithm, power balance, state of charge of the storage system and degradation parameters are defined as design constrains. Other objectives that can integrate these strategies are increasing the useful lifetime, increasing the efficiency of a certain element, increasing the hydrogen production, etc. Depending on the previous objectives, the implemented solutions are different including hysteresis operation mode, minimum power condition for electrolyzer, or fixed operation power in the case of fuel cells, (see Fig. 7, Table 6 and Appendix C). These strategies are shown as an incomplete solution, due to the need for more competitive systems from an economic point of view.

On the other hand, strategies that only take into account economic criteria provide a solution that tries to minimize a cost function, and for this purpose, they use optimization algorithms which determine the priority and reference power of the elements, (see Fig. 8, Table 7 and Appendix D). This type of strategy increases complexity by introducing a more complex algorithm, so its implementation in real systems will require a large computational capacity of the control system. Although there is an apparent cost reduction with respect to the previous strategy, it is an incomplete analysis, since it does not take into account operation costs associated with certain operation modes, such as start and stop cycles of the fuel cell and electrolyzer.

Finally, we can find strategies which incorporate both criteria, technical and economic, in order to optimize the response of the system. These strategies are complex and consider a cost function that includes degradation parameters associated with each piece of equipment. Technical and economic criteria are examined to increase equipment life and reduce maintenance costs. This strategy has an optimal solution for a technical and economic point of view, compared to traditional generation alternative systems.

The solution of this problem by various techniques, determines the reference power supplied by each element in each iteration, ensuring the power balance with optimal system performance. This multi-objective problem requires a complex optimization algorithm, so it presents an added difficulty to be implemented in a real system, (see Fig. 9, Table 8 and Appendix E). Conversely, these types of strategies use the advantages of the elements to mitigate the effects of the main drawbacks. That is, despite the fact that complex optimization algorithms are required these strategies guarantee higher lifetime and better performance of the whole system at time that reduced cost.

7. Conclusions

In this paper, a thorough review of the energy management strategies for renewable hybrid energy systems with hydrogen backup has been carried out. It classifies and analyzes both the topologies of the systems as the criteria and techno-economic solutions until reaching the energy management strategies. In addition, the work is completed with an exhaustive discussion based on the obtained results.

Every day it becomes more evident that there is a need to migrate from a centralized electric model to a distributed model. Distribution systems based on fossil fuels require importing resources and producing pollution. Migration models based on renewable energies will allow generation of a low level of emissions and less dependence on oil.

Despite the benefits of renewable energy, there are problems related to each renewable source and associated technology, such as dependence on environmental resources, high cost, etc. To minimize the negative impact of these technologies, hybrid systems are presented as a viable, safe and effective solution. With them, the use of hydrogen technology is presented as a future value, mainly due to the high performance of the elements, and the possibility of energy storage in the form of hydrogen as an energy vector.

In order to ensure a proper operation mode of hybrid systems based on renewable energy, guaranteeing demand and increasing system performance, it is necessary to use energy management strategies. The objectives of these strategies will determine the behavior of the system, so it is very important to define a proper management strategy. The study of new technologies based on a technical-economic analysis is a key factor to make the hybrid system competitive.

For this reason, this paper has presented a comprehensive review and analysis of different energy management strategies for hybrid renewable systems based on hydrogen backup. For this purpose, the first step has been to classify hybrid systems in different ways. The most common are those which distinguish the different systems depending on their connection to the grid as well as the method of integration of elements inside the system.

Next, attending to the importance of developing an energy management strategy in a hybrid renewable energy system, technical and economic criteria have been described throughout. These parameters will help to design a correct energy control, increasing the system performance.

Once the technical and economic criteria have been studied, an analysis about the solutions found in the scientific literature is presented. In order to optimize the energy management strategy based on the chosen criteria, the literature includes different solutions for the operation of the most vulnerable elements of the system, such as batteries and hydrogen-based elements for production and consumption as electrolyzers and fuel cells respectively.

Finally, a review of the different strategies used in the scientific literature can be found, analyzing the different objectives used in each one. A summary and description of all works studied in this section has been presented in Appendix B–E according to the four strategies studied above. Moreover, benefits and problems associated with these systems are defined. The revision includes an analysis of the main characteristics, highlighting the strengths and weaknesses of each case. According to the latter, we can conclude that the most common strategies only try to satisfy demand, and in spite of their simplicity, show an inefficient behavior. Strategies that include technical and economic criteria are presented as the most efficient and secure, while they require more complex algorithms that are difficult to implement in a real control system.

Based on the study done and according to the results, it is necessary to continue advancing in the development of algorithms and multi-objective strategies that allow their application in real systems, permitting a more widespread use in distributed energy applications. Winning the bet on renewable hybrid energy systems with hydrogen backup depends fundamentally on this.

Appendix A

Ref.	Topology	Integration method	Integrated Elements
[2]	Grid connected	DC Bus	PV-WT-FC
[3]	Grid connected	DC Bus	PV-WT-BAT-FC-ELEC
[5]	Isolated	DC Bus	PV-FC-BAT
[8]	Isolated	DC Bus	PV-WT- FC-ELEC
[9]	Isolated	DC Bus	WT-BAT-FC-ELEC
[10]	Isolated	DC Bus	WT-FC-SC
[11]	Isolated	DC Bus	PV-WT-BAT-FC
[12]	Isolated	DC Bus	PV-WT-BAT-FC
[19]	Grid connected	DC Bus	PV-WT-FC-ELEC
[28]	Isolated	DC Bus	PV-WT-BAT-FC-ELEC-DIESEL
[29]	Isolated	DC Bus	PV-WT-FC-ELEC
[30]	Grid connected	DC Bus	PV-WT-BAT-FC-ELEC-CHP
[46]	Isolated	DC Bus	PV-WT-BAT-FC-ELEC-SC
[47]	Isolated	DC Bus	PV-WT-BAT-FC-ELEC
[48]	Isolated	DC Bus	PV-BAT-FC-SC
[49]	Isolated	DC Bus	PV-BAT-FC
[31]	Grid connected	DC Bus	PV-BAT-FC-SC
[50]	Isolated	DC Bus	PV-BAT-FC-ELEC
[51]	Isolated	DC Bus	PV-WT-BAT-FC-ELEC
[52]	Isolated	DC Bus	PV-WT-BAT-FC
[53]	Isolated	DC Bus	PV-WT-BAT-FC-ELEC-DIESEL
[54]	Isolated	DC Bus	PV-WT-BAT-FC-ELEC
[55]	Isolated	DC Bus	PV-WT-BAT-FC-ELEC
[56]	Isolated	DC Bus	PV-WT-BAT-FC-ELEC
[57]	Isolated	DC Bus	PV-WT-BAT-FC-ELEC-DIESEL
[58]	Isolated	DC Bus	PV-WT-BAT-FC-ELEC
[59]	Isolated	DC Bus	PV-WT-BAT-FC-ELEC
[60]	Isolated	DC Bus	PV-WT-FC-ELEC-SC
[32]	Grid connected	DC Bus	PV-BAT-FC
[33]	Grid connected	DC Bus	PV-BAT-FC
[61]	Isolated	DC Bus	PV-WT-BAT-FC-ELEC
[62]	Isolated	DC Bus	PV-WT-BAT-FC-ELEC
[63]	Isolated	DC Bus	PV-FC-ELEC
[64]	Isolated	DC Bus	PV-BAT-FC-ELEC
[65]	Isolated	DC Bus	PV-BAT-FC-ELEC
[66]	Isolated	DC Bus	PV-WT-FC-ELEC
[94]	Isolated	AC Bus	PV-WT-FC-ELEC
[67]	Isolated	DC Bus	WT-FC-ELEC
[97]	Isolated	Hybrid Bus	PV-WT-FC-ELEC
[68]	Isolated	DC Bus	PV-WT-FC
[69]	Isolated	DC Bus	PV-WT-FC-ELEC
[34]	Grid connected	DC Bus	PV-WT-FC
[70]	Isolated	DC Bus	PV-WT-FC-ELEC
[71]	Isolated	DC Bus	PV-BAT-FC-ELEC
[72]	Isolated	DC Bus	PV-WT-BAT-FC
[73]	Isolated	DC Bus	PV-FC-ELE C-SC
[35]	Grid connected	DC Bus	PV-WT-BAT-FC-ELEC
[74]	Isolated	DC Bus	PV-WT-BAT-FC
[36]	Grid connected	DC Bus	PV-WT-FC-SC
[75]	Isolated	DC Bus	PV-WT-BAT-FC-ELEC
[76]	Isolated	DC Bus	PV-WT-BAT-FC-ELEC
[77]	Isolated	DC Bus	PV-BAT-FC-ELEC
[95]	Isolated	AC Bus	PV-WT-FC-ELEC-SC
[78]	Isolated	DC Bus	PV-WT-BAT-FC-ELEC
[79]	Isolated	DC Bus	PV-WT-BAT-FC-ELEC
[80]	Isolated	DC Bus	PV-BAT-FC-ELEC
[81]	Isolated	DC Bus	PV-WT-BAT-FC-ELEC
[82]	Isolated	DC Bus	PV-WT-BAT-FC-ELEC-DIESEL
[96]	Isolated	AC Bus	PV-WT-BAT-FC-ELEC-DIESEL
[83]	Isolated	DC Bus	PV-BAT-FC-ELEC
[37]	Grid connected	DC Bus	PV-WT-FC-ELEC

[38]	Grid connected	DC Bus	WT-FC
[39]	Grid connected	DC Bus	WT-FC-ELEC-CHP
[84]	Isolated	DC Bus	PV-WT-FC-ELEC
[85]	Isolated	DC Bus	MT-BAT-FC
[40]	Grid connected	DC Bus	PV-BAT-FC
[86]	Isolated	DC Bus	PV-WT-BAT-FC-ELEC
[87]	Isolated	DC Bus	PV-WT-BAT-FC-ELEC-DIESEL
[88]	Isolated	DC Bus	PV,WT,FC,ELEC,BAT,DIESEL
[89]	Isolated	DC Bus	PV,WT,FC,ELEC
[41]	Grid connected	DC Bus	WT,BAT,FC,ELEC
[90]	Isolated	DC Bus	PV,WT,FC,ELEC,DIESEL
[91]	Isolated	DC Bus	PV, BAT,FC,ELEC
[92]	Isolated	DC Bus	PV,BAT,FC,ELEC
[42]	Grid connected	DC bus	PV,WT, BAT,FC,ELEC
[43]	Grid connected	DC bus	PV,WT,FC,ELEC
[44]	Grid connected	DC bus	PV,WT, BAT,FC,ELEC
[93]	Isolated	DC bus	PV,WT, BAT,FC,ELEC
[45]	Grid connected	DC bus	PV,WT, BAT,FC,ELEC

Appendix B

Ref	Elements of the hybrid system / Application	Optimization objectives	Design constraints	Outcome
Strategies which objective is to ensure the demand				
[2]	PV, WT, FC On-grid application DC bus Simulated	Ensure demand	Power balance	Strategy to ensure demand. Wind and solar generators are presented as the main sources of energy. In the case of excess energy, it is sold to the grid; the energy deficit is supplied by fuel cell or grid. It focuses mainly on the design of algorithms to control power converters, in order to interconnect the different elements and to establish the optimum operating point of each one.
[5]	PV, FC, BAT Isolated application DC bus Simulation results	Ensure demand	Power balance	A micro grid with solar source as the main generator. In the case of energy deficit, battery or fuel cell may supply demand. In the case of excess energy, batteries charge with constant current to a maximum value, after which the energy will be discarded by dumping load. The main objective is the study of different control algorithms for power converters, in order to ensure optimum operating point for generators.
[8]	PV, WT, FC, ELEC Isolated application DC bus Simulated	Ensure demand	Power balance	Strategy to ensure the power balance. The main generators are wind and solar sources. The excess energy is absorbed by the electrolyzer while energy deficit is supplied by the fuel cell. This work focuses on the design of control algorithms for power converters, which allow interconnection of generators and loads and operate all elements at optimum operating points.
[9]	WT, FC, ELEC, BAT Isolated application DC bus Simulated	Ensure demand	Power balance, SOC, FC power points, Wind forecast	The strategy presented is based on wind and demand forecast. For a known forecast, a study is performed based on the stock of energy stored in hydrogen tanks and batteries, determining the maximum acceptable load, including prioritizing if it is not possible to assure it. The operation of different elements is based on different operating points of the battery SOC. The optimal system response will depend on the accuracy of the forecast.
[10]	WT, FC, SC Isolated application DC bus Simulated	Ensure demand	Power balance, DC and SC energy	The strategy is based on keeping the DC bus energy, in order to ensure demand at all times. Wind generators and fuel cells are presented as the main generators of the system. In case of deficit/excess energy situations, the supercapacitor will supply or absorb energy to ensure energy stability in the bus. To calculate the reference power of the supercapacitor, the problem is based on state variables models, which are represented by the DC bus and supercapacitor energy. The resolution of the different trajectories of the state variables will be solved by a flatness based control.

[11]	PV, WT, FC, BAT, BIOETHANOL REFORMER Isolated application DC bus Simulated	Ensure demand	Power balance, SOC	The strategy presented tries to ensure the demand and to maximize the use of hydrogen obtained from a bioethanol reforming process. Wind and solar sources are the basic generators of the system. The battery is presented as the main backup element of the system, and hence the SOC is the most important decision parameter. In the case of excess energy, batteries assume the system load. In the opposite case, batteries and fuel cells with the bioethanol reformer will provide the necessary energy. This is an example of hydrogen resource use for chemical industry application.
[12]	PV, WT, FC, BAT Isolated application DC bus Simulation results	Ensure demand	Power balance	Simple strategy for an isolated application. The main generators are determined by wind and solar sources. In the case of excess energy, batteries will absorb it until their maximum capacity and then it will be discarded. In the case of energy deficit, batteries in the first instance and subsequently fuel cells will supply the needed energy to keep the power balance.
[29]	PV, WT, FC, ELEC Isolated application DC bus Simulated	Ensure demand	Power balance	The management strategy used is simple, wind and solar are presented as main generators of the system. In the case of excess energy, it will be converted into hydrogen by electrolysis. In the case of energy deficit, a fuel cell stack is used according to the rated power of each one. This system provides a security response to supply the load, ensuring demand in situations of excessive deterioration of any fuel cell, as well as a proportionate response to demand at all times.
[46]	PV, WT, FC, ELEC, BAT, UC Isolated application DC bus Simulated	Ensure demand	Power balance, SOC	In this application all the systems used in renewable energy generation are presented. Solar and wind are used as the main generators, while the other elements will be used to ensure the power balance. The use of batteries and supercapacitors is reduced to respond against transients, supporting the other elements with slower dynamics. In the case of excess energy, these fast response elements will absorb the energy until they reach their maximum SOC, and then the electrolyzer will absorb the excess energy. In the opposite situation, they are discharged to the minimum SOC, and then the fuel cell will supply the energy still necessary. The paper makes a study of different control algorithms for power converters in order to ensure optimum operating point for each element.
[48]	PV, FC, SC, BAT Isolated application DC bus Simulation results	Ensure demand	Power balance, DC bus voltage	The bus voltage is the main decision parameter for energy management. The batteries will determine bus voltage. The use of supercapacitors and fuel cells is limited to situations of temporary or peak demand and excessive energy deficits respectively.
[49]	PV, BAT, FC Isolated application DC bus Simulation results	Ensure demand	Power balance, DC bus voltage, Active and reactive power	Micro grid in which the main generator is the solar source, delegating fuel cells to supply energy in deficit situations and batteries to absorb energy and respond against transients. The main goal of this study is to control each element, so it focuses on PWM techniques using fuzzy logic to maintain stable bus voltage and supplying the active and reactive power demanded by the load.
[31]	PV, FC, SC, BAT On-grid application DC bus Empirical results	Ensure demand	Battery voltage	The strategy is based solely on observing the battery voltage and compares it with certain preset limits. The battery voltage will determine the energy situation, so this parameter is presented as the main decision variable of the system. The power balance is kept at all times with the main source (solar) and battery. If the battery level reaches its minimum reference voltage, the fuel cell is activated at its maximum operating point. In case the battery reaches its maximum value, supercapacitors and the grid will absorb the excess energy. The objective of using the battery voltage as an element of study, obviates SOC based methods, therefore current measurement which can produce medium and long-term integration errors.
[55]	PV, WT, FC, ELEC, BAT Isolated application DC bus Simulation results	Ensure demand	Power balance, SOC, stock H2	A strategy based on power balance, battery SOC and hydrogen stock is presented to compute the operating points of the different elements. The charge or discharge priority is given as result of calculating the remaining energy storage, prioritizing

				hydrogen stock. In the case of excess energy, the energy will be sent first to the electrolyzer, and then to battery. In the case of energy deficit, stored resources will be evaluated again, prioritizing hydrogen stock. In the case of equality of resources, a proportional charge/discharge operation will take place. The tool used in this case to determine the operating points of each element would be the Model Predictive Control, and it is based on a linear model of the system and hysteresis band for battery SOC and hydrogen stock. The solution of the algorithm will define the power reference of each element at all times.
[32]	PV, FC, BAT On-grid application DC bus Empirical results	Ensure demand	Power balance, SOC	This paper studies a power source application for a telecommunications antenna; therefore, the system's target is to supply the demand as long as possible. In this application, a solar source is the main generator of the system. Batteries respond in situations of excess or deficit of energy, in order to ensure the power balance at all times. Finally, in case of low battery SOC and energy deficit situations, fuel cells will supply the demand.
[33]	PV, FC, BAT On-grid application DC bus Simulated and empirical results	Ensure demand	Power balance, DC bus voltage, cost function	This work aims to increase economic and technical performance of the whole system. In this application, the solar source is the main generator, while the battery and the fuel cell are used as short and medium-long term storage elements respectively. The performance of the battery and the fuel cell depends on the SOC and hydrogen stock in the system. In this case, the battery SOC is related to the bus voltage, so the battery is the main element of the system. Finally, different simulations are presented for different allowed battery depths of discharge, and different fuel cell operating points. The results are intended to find an optimal sizing rather than to demonstrate the correct operation of the proposed strategy.
[61]	PV, WT, FC, ELEC, BAT Isolated application DC bus Simulated	Ensure demand	Power balance	The proposed strategy aims to ensure demand. The main energy sources will be represented by solar and wind generators, and the power balance will determine the power operation points of the other elements. Negative balances will cause the operation of fuel cell; positive balance operation will cause electrolyzer start condition. The battery function is limited to respond against transients during switching of the other components, so it does not require high capacity. In situations of overproduction, energy will be discarded by dumping load.
[62]	PV, WT, FC, ELEC, BAT Isolated application DC bus Empirical results	Ensure demand	Power balance, stock H_2	This paper presents a strategy that guarantees power balance with fuel cell and electrolyzer in case the hydrogen stock permits it. Solar and wind are the main generators of the system, while the use of electrolyzer and fuel cell are determined for excess and deficit energy situation respectively. The batteries will only be used to respond to transients while fuel cell or electrolyzer are under switching operation, ensuring system stability. This is an empirical application, so a detailed study of sensors and conditioning equipment is performed.
[63]	PV, FC, ELEC Isolated application DC bus Simulated	Ensure demand	Power balance, Weather & load forecast	The strategy target is to ensure the power balance. It uses predictive models for solar generation. The excess/deficit energy will be absorbed/supplied by electrolyzer and fuel cell respectively.
[64]	PV, FC, BAT, ELEC Isolated application DC bus Simulation results	Ensure demand	Power balance, SOC, stock H_2	Domestic application in which solar power is entirely used for the production of hydrogen by an electrolyzer. Batteries and fuel cells supply demand according to the SOC of the first and the level of hydrogen stored. Priority in discharge situation will be given for that element which has a greater amount of stored energy. The use of fuzzy logic will help the task of decision and determination of the optimum levels of charge or discharge of each element.
[65]	PV, FC, BAT, WASTEWATER Isolated application DC bus Simulation results	Ensure demand, Sizing, Cost	Power balance, SOC	Specific application of a hybrid renewable system and hydrogen recovery using wastewater plant. The management strategy is very simple and is based on batteries SOC. In the case of excess energy, batteries absorb the surplus energy. In case batteries reach the minimum SOC; the fuel cell with the

				hydrogen produced at the wastewater plant will maintain energy demand. Finally, an analysis is performed to verify the performance and safety of the system for the particular application.
[66]	PV, WT, FC, ELEC Isolated application DC bus Simulation results	Ensure demand, sizing	Power balance	Work oriented to optimal sizing strategy. In this case, wind and solar sources are main generators, while the fuel cell and electrolyzer should respond for deficit or excess energy respectively. To calculate the optimal sizing functions, equipment costs, performance features as LPSP and physical constraints associated with each element have been taken into account. An algorithm based on swarm intelligence determines the optimal configuration of each of the elements.
[94]	PV, WT, FC, ELEC Isolated application DC & AC bus Simulation results	Ensure demand, sizing	Power balance	The proposed strategy ignores short-term storage elements, so the management strategy is simpler. The main generators are wind and solar sources, while electrolyzers and fuel cells will absorb or supply energy depending on power balance. The aim of this work is to find an optimal sizing strategy.
[67]	WT, FC, ELEC, SYNC CAPACITOR Isolated application DC bus Simulation results	Ensure demand	Power balance	A very simple system in which wind turbines are the main generators. The electrolyzer and fuel cell will respond to energy excess/deficit respectively. In this application a synchronous condenser is reserved for the use of reactive compensation.
[97]	PV, WT, FC, ELEC,MHIDRO Isolated application AC bus Simulation results	Ensure demand, sizing	Power balance	The strategy used in this work is very simple and aims to ensure the power balance. A Particle Swarm Optimization algorithm is also presented for optimal sizing. The main sources of energy in this application are wind, solar and micro hydro. The hydrogen elements will ensure the power balance by consumption or energy production when necessary.
[68]	PV, WT, FC Isolated application DC bus Simulation results	Ensure demand	Power balance, DC bus voltage, Active and reactive power	In this application there is no short-term storage element, so the excess energy is discarded. Primary sources are solar and wind generators, delegating fuel cell response to energy deficit. The work focuses on the system control in order to ensure constant bus voltage, power factor correction and removal of any harmonics. Techniques for PWM control using fuzzy logic are studied.
[69]	PV, WT, FC, ELEC Isolated application DC bus Simulation results	Ensure demand, sizing	Power balance	An isolated application for a desalination plant is presented. The primary energy is obtained with solar and wind sources. In case of excess production, energy can be stored as hydrogen for later use in a fuel cell. The aim of this paper is the correct sizing of the system.
[34]	PV, WT, FC On-grid application DC bus Simulation results	Ensure demand	Power balance	This work is focused on the study of the control of power converters in the system. However, a management strategy is also presented. The primary generators are wind and solar sources, delegating the fuel cell the task of supplying energy in situations of energy deficit. In cases of excess energy or excessive deficit, the grid may act as a further element of the system, in order to ensure the power balance at all times.
[70]	PV, WT, FC, ELEC Isolated application DC bus Simulation results	Ensure demand, sizing	Power balance	This work is focused on a sizing algorithm using three-dimensional Pareto Optimal Solution, which will determine the optimum solution for a multi-objective problem. In this case, a management strategy for the system is also presented. In this application, wind and solar sources represent the main generators while the electrolyzer and fuel cells will absorb or supply energy respectively to ensure the power balance at every moment.
[71]	PV, FC, ELEC, BAT Isolated application DC bus Simulation results	Ensure demand	Power balance, SOC	Authors present three different strategies for energy management based on solar panels as the main generator in the system, and battery SOC as the most important decision parameter. The operations of the three strategies are very similar: the battery state of charge determines the start and stop conditions for the electrolyzer and the fuel cell. The differences between strategies reside in the power operation point of each element. In the first one, the power of each device will vary adapted at all times to the system demand. In the second strategy, the batteries will support fuel cells in case of low hydrogen stock. Finally, in the third strategy, all the equipment will operate at rated power; the battery will support the system:

				absorbing by fuel cell the excess produced energy or supplying the deficit energy for the rated operation of the electrolyzer. A comparison of the three strategies is not presented because the main goal of the system is the sizing and not the energy control.
[72]	PV, WT, FC, BAT Isolated application DC bus Experimental results	Ensure demand	Power balance, SOC	Strategy applied to a domestic application. The battery SOC will determine the start and stop conditions for the fuel cell. For other situations, the battery maintains the power balance. As a special feature, the use of a small starter battery in parallel with the fuel cell will absorb transients and avoid dynamic start/stop cycles.
[73]	PV, FC, ELEC, UC Isolated application DC bus Simulation results	Ensure demand	Power balance, SOC (UC,H2)	This paper proposes a simple strategy that uses short-term storage based on supercapacitors to solve problems of stability and transients. In the present application, a solar source is the main generator. The fuel cells are used as the main element to supply energy in case of deficit. In the case of excess energy, supercapacitors and then electrolyzers will absorb it. The remaining energy will be discarded through a dumping charge.
[35]	PV, WT, FC, ELEC, BAT On-grid application DC bus Simulation results	Ensure demand	Power balance, SOC, stock H2	The strategy is based on determining the amount of energy stored/generated by the energy storage equipment, in order to ensure the power balance among the main generators (wind and solar) and demand. To determine these variables, authors use a model based on adaptive neuro-fuzzy inference system (ANFIS) control, whose input variable values are the hydrogen stock, battery SOC and the net power at every moment. The result of the ANFIS method determines the optimum power reference for the battery. Depending on the sign of the power balance, the power reference of electrolyzer and fuel cell will be calculated according to the difference between net and battery power. A final study compares the results of the proposed strategy with another strategy based on state diagrams control, providing greater energy production and better efficiency.
[88]	PV,WT,FC,ELEC,BAT,DIESEL Isolated application DC bus	Ensure demand	Power balance, SOC, H_2 stock	Simple strategy. Solar Panels and Wind Turbines are the primary generators. The batteries will absorb or supply energy in short term. In the long term, fuel cell and electrolyzer will supply/absorb energy respectively. The use of Diesel generator is relegated to high deficit of energy.
[89]	WT,PV,FC,ELEC Isolated application DC bus	Ensure demand	Power balance, H2 stock, Water demand	This paper shows an application for water pumping. Solar panels and Wind Turbines will supply energy as much as possible, and the excess of energy will be used to produce Hydrogen or store water. In case of deficit of energy, the fuel cell will supply the demand. Finally, if necessary, the storage water can be used to supply the demand. A water limitation will occur when there is not enough energy to maintain the water flow rate.
[41]	WT,FC,BAT,ELEC On-grid application DC bus	Ensure demand, Voltage stability	Power balance, SOC, H_2 stock	In this paper, a simple on-grid application is presented. The battery is the main element of the system, absorbing or supplying energy during transients. Fuel cell and electrolyzer will operate to absorb or supply energy excess/deficit respectively. The use of grid is relegated to maintain the power balance when the hydrogen based system is not capable of it.
[90]	PV,WT,FC,ELEC,DIESEL, DUMPING LOAD Isolated application DC bus	Ensure demand	Power balance, H_2 stock	Solar panels and Wind turbines will supply energy depending on weather conditions. Fuel cell and electrolyzer will supply or absorb energy during deficit/excess situations respectively. In case of high hydrogen storage, the excess energy will be discarded by dumping load. In case of low hydrogen stock, a diesel generator will ensure power balance.
[91]	PV,ELEC,BAT,FC Isolated application DC bus	Ensure demand	Power balance, SOC, H_2 stock	Solar panel is the main generator of the system. Battery will absorb or supply energy in first instance, until it reaches its operation limits. Fuel cell will supply energy in case of energy deficit. On the other hand, electrolyzer will absorb the excess of energy. The authors use two battery banks which will alternate their operation in order to reduce cycled degradation.
[92]	PV,BAT,FC,ELEC Isolated application DC bus	Ensure demand	Power balance, SOC, H_2 stock	The paper presents a comparative between diesel and renewable solutions for a radio station application. The solar panels will supply energy as much as possible. The battery is

				the main element of the system, absorbing or supplying energy while it operates between predefined SOC limits. The use of fuel cell and electrolyzer is indicated when batteries are not capable of ensuring demand or power balance.

Appendix C

Ref.	Elements of the hybrid system / Application	Optimization objectives	Design constraints	Outcome
Strategies whose objectives include technical decision factor				
[19]	PV, WT, FC, ELEC On-grid application DC bus Simulated	Ensure demand, increase equipment lifetime	Power balance	The strategy uses a predictive control to minimize the degradation processes of the electrolyzer and fuel cell due to dynamic start/stop cycles. The main generators are wind and solar sources and the electrolyzer and fuel cell will ensure power balance in situations of excess/deficit energy respectively. In case of high or low production, the grid can act as a generator or load to support the system at all times assuring certain operating conditions such as minimum input power for the electrolyzer.
[30]	PV, WT, CHP, FC, ELEC, BAT On-grid application DC bus Simulated and empirical results	Ensure demand, improve performance	Power balance, SOC, SOC (H2)	Authors present a grid-connected system for a domestic application. The proposed strategy depends on the battery SOC and hydrogen stock available, therefore the use of each element will depend on them. The battery is presented as the most important element, supplying or absorbing energy under certain operating limits given for charge conditions. The maximum and minimum SOC will determine the start/stop conditions of the other components (electrolyzer and fuel cell). The use of minimum power conditions for the ignition of the electrolyzer and maximum depths of discharge for batteries are included in the energy management, in order to reduce degradation and increase the performance of elements. Finally, in case of high deficit/excess of energy, the grid can act as generator or load, increasing system security.
[74]	PV, WT, FC, BAT Isolated application DC bus Simulation results	Ensure demand, power quality, fuel cell efficiency	Power balance, Active and Reactive power	The goals of this work are to operate the fuel cell stack at its maximum efficiency operation point, while controlling the power factor. Although the work is mainly focused on control algorithms for power converters, an energy management strategy is proposed. This strategy is based on the use of solar and wind sources as main generators, while the fuel cell will operate against any energy deficit. The use of battery will be limited to absorb energy transients, excess energy and keep the fuel cell on its maximum efficiency power point, absorbing or giving power when necessary.
[36]	PV, WT, FC, SC On-grid application DC bus Experimental	Ensure demand, Stability	Power balance, SC energy function	Authors develop a control law and a nonlinear problem which aims to ensure the power balance. In this application, the wind and solar sources are the main generators of the system. To determine the contribution of the other elements, the power reference values depend on the sign of the power balance and the amount of available energy inside the storage systems. The response of the nonlinear optimization problem will be based on differential flatness-based control.
[47]	PV, WT, FC, ELEC, BAT Isolated application DC bus Simulation results	Ensure demand, increase performance	Power balance, SOC	In this paper, three strategies whose core decision is the batteries SOC are presented. The solar and wind sources are the main generators. The maximum and minimum values of the battery SOC will determine the start and stop conditions for the electrolyzer and fuel cell. The difference between the three strategies is given by the use of batteries for excess energy. In the first one, the electrolyzer will start if it reaches a minimum operating power, while batteries will assume the excess energy. In the second strategy, the batteries will

				support the electrolyzer to achieve a minimum power value. In the third and final strategy, the batteries will be disconnected to avoid overcharging them. Finally, authors present two sensitivity analyses based on the minimum battery SOC, and the use of a fixed and variable operating power for the fuel cell. Results determine that reducing the minimum SOC would increase the use of batteries and decrease the use of fuel cells. In case of a variable operating point of the fuel cell, the hydrogen consumption will be lower, adjusting it at all times to the required demand.
[50]	PV, FC, BAT, ELEC Isolated application DC bus Simulated	Ensure demand, improve performance, Battery management	Power balance, SOC, stock H_2	The target of the proposed management strategy is to keep power balance all times. The use of solar energy is considered to be the main generator of the system. Batteries assume the main role of the system, responding against situations of excess/deficit energy. Its SOC will determine the start/stop conditions for the electrolyzer and fuel cell. Two different controls for battery operation are studied depending on their SOC. First, the current control is used for fast charging in low SOC and the voltage control to protect the batteries at high charging conditions. When there is high excess energy, the solar generation will be limited and it will be used for hydrogen generation in order to absorb excess energy. The fuel cell will be used to supply demand and neutralize the power balance.
[51]	PV, WT, FC, ELEC, BAT Isolated application DC bus Simulation results	Ensure demand, increase equipment lifetime	Power balance, SOC	In this paper, the proposed strategy is based on hysteresis band operation determined for battery SOC. Hysteresis limits will determine the start/stop conditions for the electrolyzer and fuel cell. The aim of this work is to increase the useful lifetime of elements by reducing the degradation associated with dynamic operation. Additionally, the effect of using a minimum power for the electrolyzer to ensure optimum performance is studied. In order to reach the last target, two simulations of two different strategies are presented; the first one prevents electrolyzer operation while the excess energy is lower than the minimum power point, and the second one uses batteries to reach it. The result shows increased hydrogen production in the second strategy; increasing the overall system performance, with greater use of batteries. Finally, a parametric analysis based on the hysteresis bandwidth determines how it affects the battery lifetime as well as the use of other elements inside the system.
[52]	PV, WT, FC, BAT Isolated application DC bus Simulation results	Ensure demand, improve lifetime	Power balance, Weather forecast, SOC	Authors propose a strategy based on demand and production forecast in less than a two minute range. With the result of the forecast and the current state of the system, it will determine the actions required, allowing the charge/discharge of the batteries, or the start/stop conditions of the fuel cell and the reference power for each element. The use of this strategy will determine the efficiency of the fuel cell operation, and avoid unnecessary start/stop cycles thus reducing the degradation.
[53]	PV, WT, FC, ELEC, BAT, DIESEL Isolated application DC bus Simulation results	Ensure demand, improve lifetime	Power balance, SOC	In this paper the authors propose a study of a strategy based on hysteresis operation depending on maximum and minimum battery SOC. These levels determine the start and stop conditions of the fuel cell and electrolyzer. The use of hysteresis with minimum power conditions for the electrolyzer, tries to reduce degradation of the elements, and thus increases system lifetime. The use of diesel equipment will only operate in situations of high-energy deficit.
[54]	PV, FC, ELEC, BAT Isolated application DC bus Simulation results	Ensure demand, increase equipment lifetime	Power balance, SOC	The work presents a solution for degradation problems studied for fuel cells and electrolyzers. It implements a strategy based on hysteresis band operation for battery SOC. This strategy will determine the start/stop conditions of the electrolyzer and fuel cell. The strategy is based on the use of solar resources as the primary generator and a battery as a last resort. The excess/deficit energy is absorbed primarily by the battery if the SOC is within its operating limits, and

				then by the electrolyzer or fuel cell, depending on the energy situation. Besides the above, the fuel cell will operate in a fixed mode to avoid power transients operation and associated problems. Finally, the use of the electrolyzer in fixed or variable power mode is realized, determining that the variable operation mode is more efficient. This strategy shows many possible solutions to increase the lifetime of equipment, and thereby reduce costs and avoid malfunctions associated with incorrect operation of the system.
[56]	PV, FC, ELEC, BAT Isolated application DC bus Simulation results	Ensure demand, increase equipment lifetime	Power balance, SOC	In this paper, a proposed management strategy based on hysteresis operation depending on battery SOC is presented. This parameter will define the start/stop conditions of the electrolyzer and fuel cell. The target of the strategy is to reduce the size of the batteries and avoid extra degradation due to overuse. To achieve this, authors resolve to establish a battery range in which the system will operate in normal situations. In the case of high battery charge or discharge situations, the electrolyzer and fuel cell will be used at full power to bring the battery to the safe hysteresis band. In any situation, batteries will perform in the first instance to absorb or transfer the necessary energy to ensure the power balance. If that is not enough, the electrolyzer and fuel cell energy will support according to need.
[57]	PV, WT, FC, ELEC, BAT, DIESEL Isolated application DC bus Simulation results	Ensure demand, increase equipment lifetime, sizing	Power balance, SOC	In this paper, the strategy is based on the hysteresis band of battery SOC, which determines the start/stop conditions of the electrolyzer and fuel cell. The purpose of hysteresis is therefore to reduce the number of power cycles, avoiding the degradation associated with them. Besides operation with hysteresis, minimum power values for the electrolyzer and fuel cell are used in order to assure the optimal performance. If the minimum power of the electrolyzer is not reached, batteries will supply the remaining power. If the power operation of the fuel cells exceeds the energy deficit, batteries will absorb the excess energy. In extreme cases, the use of diesel equipment can supply the energy deficit necessary to ensure the power balance. Finally, a study of sizing based on a multi-objective problem is presented.
[58]	PV, WT, FC, ELEC, BAT Isolated application DC bus Simulation results	Ensure demand, increase equipment lifetime, sizing	Power balance, SOC	Authors present a simulation tool to study different scenarios in which solar and wind are the main generators. The simulator has a strategy based on the hysteresis band of the battery SOC. The maximum and minimum SOC will determine the start and stop conditions for the electrolyzer and fuel cell. There is no requirement to determine the operating point of the elements inside the system, so the energy excess or deficit will be absorbed or supplied by the battery, electrolyzer or fuel cell just based on power balance. Finally, a genetic algorithm is used to solve the multi-objective sizing problem which takes into account the costs and lifetime of each element.
[60]	WT, FC, ELEC, SC Isolated application DC bus Simulation results	Ensure demand, improve lifetime	Power balance	The work proposes a strategy that takes into account the deterioration of fuel cells due to the influence of high frequency switching. The proposed strategy is simple; wind is the main generator and uses supercapacitors to support the system during transients or load changes. The use of the electrolyzer and fuel cell are only justified to absorb or supply energy when supercapacitors are at their maximum or minimum charge respectively. The use of different low pass filters will help to reduce the problems associated with the switching of power converters over the fuel cell.
[75]	PV, WT, FC, ELEC, BAT Isolated application DC bus Simulated	Ensure demand, maximize Hydrogen production	Power balance, SOC	This study is based on three different strategies that differ in the method of using the excess energy. All the proposed strategies share the use of solar and wind sources as main generators and the rest of equipment as energy storage elements. The start/stop condition of the fuel cell and electrolyzer depends on the battery SOC. In the first strategy, the battery assists in the production of hydrogen with the

				main generators. The target of this strategy is to maximize the hydrogen production. In the second strategy, the electrolyzer will not be used, and therefore the battery will assume the full energy excess in order to increase the temporal response of the battery. Finally, the third strategy has a compromise between maximizing the production of hydrogen and maintaining an optimal battery SOC. The battery and electrolyzer will absorb the energy excess, while the deficit will be provided by battery and fuel cell, without specifying any priority.
[76]	PV, WT, FC, ELEC, BAT Isolated application DC bus Simulation results	Ensure demand, lifetime	Power balance, SOC, stock H2	This strategy aims to ensure the demand and increase the lifetime of the elements. In order to get it, authors present an analysis between two alternative strategies, depending on the priority of charge/discharge energy. In the present application, the main generators are wind and solar sources. The remaining elements form part of the energy storage system. The decision variables of the system will be the battery SOC and the hydrogen stock. The priority to charge or discharge energy is based on the stored energy inside the different elements. In case of equal resources, the element with the lowest deterioration accumulated by its operation will be responsible for guaranteeing the power balance.
[77]	PV, FC, ELEC, BAT Isolated application DC bus Simulation results	Ensure demand, maximize Hydrogen production, minimize battery usage	Power balance, SOC	The strategy has the target to ensure demand, increase hydrogen production, and minimize the use of batteries. To get it, batteries will operate in a narrow range of SOC, limiting their use to respond only against transients or short-term demands. In order to maximize the production of hydrogen, the electrolyzer will absorb the excess energy more often than batteries, while fuel cells will supply the energy deficit. Authors use a system based on fuzzy logic to decide which part of energy excess or deficit will be supplied/absorbed by the batteries, the electrolyzer or the fuel cell.
[95]	PV, WT, FC, ELEC, UC Isolated application AC bus Simulation results	Ensure demand, increase life time	Power balance, SOC (UC)	The implemented strategy has the target of guaranteeing the demand and increasing equipment lifetime, reducing transients and start/stop cycles for the electrolyzer and fuel cell. To solve the above problems, the electrolyzer will operate at different steps of continuous power, with a minimum starting power in order to avoid transients and associated deterioration. Fuel cells only come into operation when the supercapacitors SOC is lower than a defined set level. Finally, any short-term disruption will be absorbed by the supercapacitors, whose SOC should remain within safe operating ranges. The operation point of each device may be obtained at any time through the power balance equations.
[78]	PV, WT, FC, ELEC, BAT Isolated application DC bus Simulation results	Ensure demand, increase equipment lifetime	Power balance, Load and Resources estimation	An active strategy based on demand and production forecasts is presented. The use of forecast and the current battery SOC will determine a multi-objective function, designed to maximize hydrogen production and reduce start/stop cycles of the electrolyzer and fuel cell. The response to the algorithm will determine which element will absorb or supply energy at its rated power. Finally, to solve the nonlinear problem, the use of algorithms based on dynamic real-time optimization is performed.
[79]	PV, WT, FC, BAT, ELEC Isolated application DC bus Simulation results	Ensure demand, improve lifetime	Power balance, SOC	In this paper, fuzzy logic is used to implement a management strategy that will avoid unnecessary start/stop cycles, with the consequent degradation reduction. The decision parameters of this strategy will be the battery SOC and generation/demand forecast, which will determine the start or stop conditions of the electrolyzer and fuel cell. The use of fuzzy logic allows application of an algorithm which determines the operation point of the different elements, based on the previous parameters.
[80]	PV, FC, ELEC, BAT Isolated application DC bus	Ensure demand, improve lifetime	Power balance, SOC, stock H_2, Weather forecast	In this strategy, the solar source is the main generator of the system. The battery SOC and hydrogen stock represent the main decision parameters of the system, as well as the result

	Simulation and empirical results			of generation and demand forecasts. In the first instance, the battery will operate between preset maximum and minimum values, which determine the start and stop conditions of the electrolyzer and fuel cell. In order to increase the lifetime, reducing degradation of hydrogen elements, three different energy management strategies will be considered. The first one is based on ensuring minimum operating power to the electrolyzer with the discharge of battery if necessary. The second one refers to the operating point of the fuel cells. In order to operate the fuel cell in the maximum efficiency range, minimum and maximum power will be determined in order to get it. Finally, the third one is used to reduce the number of start/stop cycles of the elements and is based on the use of equipment in standby mode if the forecasting determines an imminent use of them.
[81]	PV, WT, FC, ELEC, BAT Isolated application DC bus Simulation results	Ensure demand, battery lifetime	Power balance, SOC, stock H_2	For this strategy, an artificial neural network controller is used in order to supply demand and preserve the battery SOC within preset limits. The main generators are represented by wind and solar sources, while the other elements are used for energy storage. In normal operation, the battery usages will respond against transient situations and start/stop cycles of the other elements. The strategy tries to maintain a battery SOC around 70%, so in the case of excess/deficit energy situations, the electrolyzer and fuel cell must respond to get it. Finally, the use of the algorithm is justified to determine the operating point of each element when excess/deficit energy situations occur while the battery is discharged or hydrogen stock is too low respectively.

Appendix D

Ref.	Elements of the hybrid system / Application	Optimization objectives	Design constraints	Outcome
Strategies whose objectives include economic decision factor				
[3]	PV, FC, BAT, ELEC On-grid application DC bus Experimental	Ensure demand, cost reduction	Power balance, cost function	The presented strategy attempts to ensure power balance at all times, by operating the system at the operation point that ensures the lowest value of the system-grid cost function. The technique uses an algorithm based on Model Predictive Control and a demand and generation forecast. This algorithm determines the operation points of the battery, fuel cell, and electrolyzer. During system operation, the purchase/sales price of grid energy is calculated at every moment, so the grid is an important element to consider for energy management.
[28]	PV, WT, MH, FC, ELEC, BAT, DIESEL Isolated application DC bus Simulated	Ensure demand, cost reduction	Power balance, cost function	This paper aims to ensure proper power supply to the load, optimizing operating costs. Authors present a cost function associated with the use of energy storage devices, such as batteries, electrolyzers, fuel cells or diesel generators. The use of physical constraints, current system status, and expected lifetime would determine a nonlinear optimization problem, which would be solved by genetic algorithms. The result determines at each time the cost of each element and the optimum operating point. The option to charge or discharge the system will be based on the element that keeps the lowest operation cost, within the range of optimal power for each one.
[82]	PV, WT, FC, ELEC, BAT, DIESEL Isolated application DC bus Simulation results	Ensure demand, cost reduction, sizing	Power balance, cost function, LPSP, CO_2 emissions, SOC	Authors present a strategy that aims to reduce costs, emissions, and ensure the power balance. The authors present some expressions which model each target depending on various parameters such as LPSP, CO_2 emissions, battery SOC, cost function... etc. Fuzzy logic and a differential evolution algorithm are used to solve the multi-objective problem. The result of this algorithm is the reference power for each of the elements in the

				different energy situations, giving priority to the use of batteries and renewable energy generators before diesel operation. In general, this is a sizing algorithm.
[96]	PV, WT, FC, ELEC, BAT, DIESEL Isolated application AC bus Simulation results	Ensure demand, cost reduction	Power balance, weather prediction, cost function, SOC, stock H_2	The aim of this study is to compare the proposed strategy regarding other strategies based on the battery SOC as the most important decision parameter. The presented strategy in the first instance is based on the generation and demand forecast, which is the input parameter to the decision algorithm. Considering the outcome of the previous forecast, the current state of the system (battery SOC and hydrogen stock) and the degradation, operation, maintenance and replacement costs, it will determine the reference power of each element. The operation will take place at each iteration by a linear simplified system model, in order to avoid heavy algorithms. The result of the comparison between strategies is the improvement in cost reduction, compared to traditional strategies, but the need for very accurate models and high processing capacity of the control system.
[83]	PV, FC, ELEC, BAT Isolated application DC bus Simulation results	Ensure demand, cost reduction	Power balance, SOC, stock hydrogen, cost function	The management strategy is based on hydrogen stock and batteries SOC. Depending on the previous decision parameters, it will determine the batteries charge/discharge and the start/stop conditions of the electrolyzer and fuel cell, prioritizing the element with higher energy stored. In case both parameters are equal, an economic decision factor represented by a cost function, determines the element with the lowest cost to charge or discharge inside the system.
[37]	PV, WT, FC, CHLOR-ALKALI PROCESS On-grid application DC bus Simulation results	Ensure demand, cost reduction	Power balance, cost function	This work is based on a particular application of the chemical production of chlorine. In the chemical process to obtain the product, hydrogen gas is generated, which can be stored for future use and conversion into electrical energy. The strategy is based on calculating the operation points of the fuel cell and the chlorine production system, with the target of minimizing operation costs, taking into account the benefits of injecting or buying power from the grid. A receding horizon optimization algorithm is used to solve the optimization problem.
[38]	WT, FC On-grid application DC bus Simulation results	Ensure demand, cost reduction	Power balance, cost function	The presented work studies the combination of wind power and a fuel cell to produce electricity and heat in a domestic application. Some expressions are presented to estimate the operation and maintenance costs of the use of the fuel cell or the grid. A genetic algorithm in any case allows calculating the cheaper option and determining the reference power of each element to support wind generation.
[39]	WT, FC, ELEC, HYDRAULIC GENERATOR, PUMP On-grid application DC bus Simulation results	Ensure demand, Cost reduction	Power balance, cost function	An application for a specific production model is presented. In this case, the main power generation is given by the wind source. In case of excess of energy, the system proposes two options. The first one proposes the conversion to hydrogen through electrolysis process; the second one uses a pumping station for water storage at high altitude. In the case of energy deficit situations, the required energy can be obtained through the production of electricity using fuel cells, or by generating electricity in a hydraulic plant. The most economically viable option will act at all times. The target strategy therefore is to maximize the wind resource, allowing the energy storage and subsequent use in the most economical way possible.
[84]	PV, WT, FC, ELEC Isolated application DC bus Simulation results	Ensure demand, cost reduction	Power balance, cost function	The target of this work is the optimal energy management from the economic point of view for a residential application. In order to get it, a cost function associated with energy production of each element is presented. The use of different physical constraints together with the previous cost functions will identify a nonlinear optimization problem. The problem will be solved with the use of gravitational search algorithms. The result is the reference power of each element, which assures the lowest production costs for system operation.
[85]	MT, FC, BAT Isolated application DC bus Simulation results	Ensure demand, cost reduction	Power balance, demand prediction, cost function	In this paper, a multi-objective function is presented to calculate the reference power of each element inside the system, knowing the costs associated with each item and demand forecasts for the next 24 h. The problem will be solved by an adaptive particle

				modified swarm optimization algorithm, which determines the energy delivered by each element according to the obtained estimator.
[40]	PV, FC, ELEC On-grid application DC bus Simulation results	Ensure demand, cost reduction	Power balance, weather prediction, cost function	In this paper a grid-connected system is studied in which solar energy is presented as the main generator. Authors present a function to model the operating costs of each element and power sale/purchase cost from the grid. The demand and solar generation forecast and the cost function, represent the input variables of an optimization algorithm, whose response will be calculated by adaptive model predictive control. The result of the optimization algorithm determines the elements' operating points for the most economical option, maintaining a minimum level of hydrogen in the energy storage system.
[42]	PV,WT,BAT,ELEC,FC On-grid application DC bus Simulation results	Ensure demand, cost reduction	Power balance, SOC, weather prediction, cost function	In this paper, a cost function is used to determine the power reference of grid, fuel cell and electrolyzer in order to minimize overall electricity cost. Battery SOC, power balance and a weather and demand forecast are used as input parameters of the optimization algorithm. The battery is used to absorb the transients during the generation and demand. The grid is another active element of the system.
[43]	WT,PV,FC,ELEC On-grid application DC bus	Ensure demand, cost reduction	Power balance, H_2 stock, cost function	A multi-objective function is developed to minimize the operation and maintenance cost of the system. The result of the optimization algorithm is the power reference of the grid, fuel cell and electrolyzer. The fuel cell will supply energy in case of energy deficit, while the electrolyzer will absorb energy during energy excess situations. The grid will operate as another active element inside the hybrid system.

Appendix E

Ref.	Elements of the hybrid system / Application	Optimization objectives	Design constraints	Outcome
Strategies whose objectives include technical and economic decision factor				
[59]	PV, WT, FC, ELEC, BAT Isolated application DC bus Simulation results	Ensure demand, cost reduction, Increase Lifetime	Power balance, SOC, stock H2, cost and life function	The presented strategy is based on hydrogen stock and battery SOC. The main generators of the system are wind and solar sources, while the other devices are part of the energy storage system. The charge or discharge of any element inside the system will depend on which element has the highest or lowest amount of energy stored respectively. In the case of equality of resources, a technical-economic factor will decide which element will supply or absorb the necessary energy to guarantee the power balance. This factor will be represented by a cost function, which integrates the cost associated with the degradation accumulated by the operating time.
[86]	PV, WT, FC, ELEC, BAT Isolated application DC bus Simulation results	Ensure demand, cost reduction, improve lifetime	Power balance, SOC, H_2 stock, cost function	In this paper, two targets are studied: reducing costs and increasing elements lifetimes at the same time. In the application, wind and solar sources are the main generators. To calculate the priority of each element, a multipurpose optimization problem is studied. Fuzzy logic will be used to calculate which element will be responsible for absorbing or supplying energy and its power reference. The inputs of the algorithm are represented by some cost expressions associated with each element, as well as estimation of the remaining lifetime and the current state of the energy of storage equipment.
[87]	PV, WT, FC, ELEC, BAT, DIESEL Isolated application DC bus	Ensure demand, improve lifetime, cost reduction	Power balance, SOC	Authors present three different strategies for different purposes in order to demonstrate the correct operation of the particle swarm optimization algorithm for solving nonlinear optimization problems. The response of the

	Simulation results			algorithm for different configurations is the reference power of the different elements, depending on the different targets: minimizing costs, increasing efficiency and equipment lifetime. Really, there is no priority in the use of the different elements, so this priority will be determined by the result of each algorithm calculation for each application.
[44]	PV,WT,FC,ELEC, BAT On-grid application DC bus Simulation results	Ensure demand, improve lifetime, cost reduction, improve performance	Power balance, SOC, H_2 stock	A multi-objective function based on degradation, performance and cost parameters is optimized in order to guarantee the optimal system response. The power reference of the fuel cell and electrolyzer will be defined by the optimization solution. Batteries are the core of the hybrid system and they will absorb or supply energy while they operate between prefixed states of charge limits. The fuel cell and electrolyzer will operate under high energy deficit or energy excess situations according to their optimal operation point. The grid will operate as a demand or generator depending on the sign of the power balance.
[93]	PV,WT,FC,ELEC,BAT Isolated application DC bus	Ensure demand, improve lifetime, cost reduction, improve performance	Power balance, SOC, H_2 stock, cost function, degradation function	This paper presents a multi-objective degradation-cost function which is minimized with an optimization algorithm. The result of the optimization is the power reference of the fuel cell, battery, and electrolyzer depending on state of charge of the battery and hydrogen stock. The hysteresis operation mode fixes the start/stop conditions of the electrolyzer and fuel cell.
[45]	PV,WT,FC,ELEC,BAT On-grid application DC bus Experimental	Ensure demand, improve lifetime, cost reduction, improve performance	Power balance, SOC, H_2 stock, cost function, performance function	In this work, authors studied the behavior of a hybrid system based on different strategies which integrate hysteresis operation mode. These strategies define different operation points for the fuel cell, electrolyzer, and battery, in order to show the response of the system under different goals, maximizing hydrogen production, increasing system performance, and the cases of rated operation mode for the three previous elements. The results of different strategies are compared based on technical and economic parameters to get the optimal solution. Advantages and disadvantages of the different configurations are also studied.

References

[1] Chauhan A, Saini RP. A review on Integrated Renewable Energy System based power generation for stand-alone applications: configurations, storage options, sizing methodologies and control. Renew Sustain Energy Rev 2014;38:99–120.

[2] Ahmed NA. On-grid hybrid wind/photovoltaic/fuel cell energy system. In: proceedings of the 10th international power & energy conference (IPEC), Ho Chi Minh City; 2012, p. 104–9. doi: http://dx.doi.org/10.1109/ASSCC.2012.6523247.

[3] Bordons C, García-Torres F, Valverde L. Gestión Óptima De La Energía En Microrredes Con Generación Renovable. Rev Iberoam Automática Inf Ind RIAI 2015;12(2):117–32.

[4] IEA (International Energy Agency. Renewable Energy Outlook, World Energy Outlook 2013; 2013, p. 197–232.

[5] Sun XSX, Lian ZLZ, Wang BWB, Li XLX. A Hybrid renewable DC microgrid voltage control, In: Proceedings of IEEE 6th international power electron. motion control conference, vol. 3; 2009. p. 725–9.

[6] Semaoui S, Hadj Arab a, Bacha S, Azoui B. The new strategy of energy management for a photovoltaic system without extra intended for remote-housing. Sol Energy 2013;94:71–85.

[7] Robitaille M, Agbossou K, and Doumbia ML. Modeling of an islanding protection method for a hybrid renewable distributed generator. In: Proceedings of IEEE Canadian conference on electrical and computer engineering, vol. 2005, no. May; 2005. p. 1485–9.

[8] Li X, Jiao X, and Wang L. Coordinated power control of wind-{PV}-fuel cell for hybrid distributed generation systems. In: SICE annual conference (SICE), 2013 Proceedings of ; 2013, p. 150–5.

[9] Osman Haruni a, Negnevitsky M, Haque ME, Gargoom A. A novel operation and control strategy for a standalone hybrid renewable power system. IEEE Trans Sustain Energy 2013;4(2):402–13.

[10] Tégani I, Aboubou A, Ayad MY, Becherif M, Bahri M. Power flow management in WT/FC/SC hybrid system using flatness based control. In: Proceedings of 3rd international symposium on environment-friendly energies and applications. EFEA; 2014.

[11] Feroldi D, Degliuomini LN, Basualdo M. Energy management of a hybrid system based on wind–solar power sources and bioethanol. Chem Eng Res Des 2013;91(8):1440–55.

[12] Mbarek E, Belhadj J, Le BP, Tunis B. Photovoltaic Wind hybrid system integrating a Permanent Exchange Membrane Fuel Cell (PEMFC). In: Proceedings of international multi-conference on systems, signals and devices; 2009, no. 1, 2009, p. 1–6.

[13] Fathima AH, Palanisamy K. Optimization in microgrids with hybrid energy systems – a review. Renew Sustain Energy Rev 2015;45:431–46.

[14] Vasallo MJ, Bravo JM, Andújar JM. Optimal sizing for UPS systems based on batteries and/or fuel cell. Appl Energy 2013;105:170–81.

[15] Segura F, Durán E, Andújar JM. Design, building and testing of a stand alone fuel cell hybrid system. J Power Sources 2009;193(1):276–84.

[16] Vasallo MJ, Andújar JM, García C, Brey JJ. A methodology for sizing backup fuel-cell/battery hybrid power systems. IEEE Trans Ind Electron 2010;57(6):1964–75.

[17] Segura F, Andújar JM. Step by step development of a real fuel cell system. Design, implementation, control and monitoring. Int J Hydrog Energy 2015;0:1–13.

[18] Valverde L, Ali D, and Gordo R. "A technical evaluation of Wind-Hydrogen (WH) demonstr ration projects in Eurrope. In: Proceedings of power engineering, energy and electrical drives (POWERENG), 2013 fourth international conference on, no. May; 2013. p. 13–7.

[19] Trifkovic M, Sheikhzadeh M, Nigim K, Daoutidis P. Modeling and control of a renewable hybrid energy system with hydrogen storage. IEEE Trans Control Syst Technol 2013;22(1). [1–1].

[20] Baumann C, Schuster R, Moser A. Economic potential of power-to-gas energy storages. In: Proceedings of international conference european energy market (EEM); 2013.

[21] Moskalenko N, Lombardi P, Komarnicki P. Multi-criteria optimization for determining installation locations for the power-to-gas technologies. In: IEEE PES General Meeting|Conference & Exposition, National Harbor, MD; 2014, p. 1–5. doi: http://dx.doi.org/10.1109/PESGM.2014.6939362.

[22] Clegg S, Mancarella P. Integrated modeling and assessment of the operational impact of power-to-gas (P2G) on electrical and gas transmission networks. IEEE Trans Sustain Energy 2015;6(4):1234–44.

[23] Belderbos A, Delarue E, D'haeseleer W. Possible role of power-to-gas in future energy systems. In: proceedings of the 12th International Conference on the European Energy Market (EEM), Lisbon; 2015, p. 1–5. doi: http://dx.doi.org/10.1109/EEM.2015.7216744.
[24] Heymann F, Bessa R. Power-to-gas potential assessment of Portugal under special consideration of LCOE. In: Proceedings of IEEE Eindh Power; 2015.
[25] Heinisch V. Effects of power-to-gas on power systems: a case study of Denmark. In: Proceedings of IEEE Eindh PowerTech; 2015, p.1–6.
[26] Alkano D, Kuiper I, Scherpen JMA. Distributed MPC for Power-to-Gas facilities embedded in the energy grids. In: European Control Conference (ECC), Linz; 2015, p. 1474–9. doi: http://dx.doi.org/10.1109/ECC.2015.7330747.
[27] Diaz I, Mendaza DC, Bhattarai BP, Optimal sizing and placement of power-to-gas systems in future active distribution networks. In: Proceedings of innovative smart grid technologies - Asia (ISGT ASIA); 2015 IEEE.
[28] Dufo-López R, Bernal-Agustín JL, Contreras J. Optimization of control strategies for stand-alone renewable energy systems with hydrogen storage. Renew Energy 2007;32(7):1102–26.
[29] El-Shatter TF, Eskander MN, El-Hagry MT. Energy flow and management of a hybrid wind/PV/fuel cell generation system. Energy Convers Manag 2006;47(9–10):1264–80.
[30] Baumann L, Boggasch E, Rylatt M, Wright A. Energy flow management of a hybrid renewable energy system with hydrogen, In: Proceedings of innovative technologies for an efficient and reliable electricity supply (CITRES), IEEE Conference on; 2010, p. 78–5.
[31] Karami N, Moubayed N, Outbib R. Energy management for a PEMFC-PV hybrid system. Energy Convers Manag 2014;82:154–68.
[32] Kato N, Kurozumi K, Susuld N, Muroyama S. Hybrid power-supply system composed of photovoltaic and fuel-cell systems. In: proceedings of the twenty-third International Telecommunications Energy Conference INTELEC 2001, Edinburgh, UK; 2001, p. 631–5. doi: http://dx.doi.org/10.1049/cp:20010663.
[33] Bruni G, Cordiner S, Galeotti M, Mulone V, Nobile M, Rocco V. Control strategy influence on the efficiency of a hybrid photovoltaic-battery-fuel cell system distributed generation system for domestic applications. Energy Procedia 2014;45:237–46.
[34] Das D, Esmaili R, Xu L, Nichols D. An optimal design of a grid connected hybrid wind/photovoltaic/fuel cell system for distributed energy production. In: Proceedings of IEEE industrial electronics society, IECON 2005. 31st annual conference; 2005. p. 2499–504.
[35] García P, García CA, Fernández LM, Llorens F, Jurado F. ANFIS-based control of a grid-connected hybrid system integrating renewable energies, hydrogen and batteries. IEEE Trans Ind Inform 2014;10(2):1107–17.
[36] Thounthong P, Sikkabut S, Mungporn P, Sethakul P, Pierfederici S, Davat B. Differential flatness based-control of fuel cell/photovoltaic/wind turbine/supercapacitor hybrid power plant, In: Proceedings of the 4th international conference clean electrical power, Renewable Energy Resources Impact, ICCE; 2013, p. 298–305.
[37] Wang X, Tong C, Palazoglu A, El-farra NH. Energy Management for the chlor-alkali process with hybrid renewable energy generation using receding horizon optimization. In: Proceedings of the 53rd IEEE conference on decision and control; 2014, p. 4838—43.
[38] Talebian ME, Sobhani S, Borzooi A. New hybrid system of fuel cell power plant and wind turbine for household consumption. In: proceedings of the 3rd International Conference on Electric Power and Energy Conversion Systems, Istanbul; 2013, p. 1–6. doi: http://dx.doi.org/10.1109/EPECS.2013.6713074.
[39] Dagdougui H, Minciardi R, Ouammi A, Robba M, Sacile R. A dynamic decision model for the real-time control of hybrid renewable energy production systems. IEEE Syst J 2010;4(3):323–33. http://dx.doi.org/10.1109/JSYST.2010.2059150. Sept.
[40] Zervas PL, Sarimveis H, Palyvos J a, Markatos NCG. "Model-based optimal control of a hybrid power generation system consisting of photovoltaic arrays and fuel cells. J Power Sources 2008;181(2):327–38.
[41] Kamal T, Hassan SZ, Li Hui, Mumtaz S, Khan L. Energy management and control of grid-connected wind/fuel cell/battery Hybrid Renewable Energy System. In: International Conference on Intelligent Systems Engineering (ICISE), Islamabad; 2016, p. 161–6. doi: http://dx.doi.org/10.1109/INTELSE.2016.7475114.
[42] Athari MH, Ardehali MM. Operational performance of energy storage as function of electricity prices for on-grid hybrid renewable energy system by optimized fuzzy logic controller. Renew Energy 2016;85:890–902.
[43] Rouholamini M, Mohammadian M. Heuristic-based power management of a grid-connected hybrid energy system combined with hydrogen storage. Renew Energy 2016;96:354–65.
[44] Fernandez-Ramírez LM, Garcıa-Tribiño P, Gil-mena AJ, Llorens-iborra F, Jurado F, García-V-azquez CA. Optimized operation combining costs, efficiency and lifetime of a hybrid renewable energy system with energy storage by battery and hydrogen in grid-connected applications. Int J Hydrog Energy 2016;41:23132–44.
[45] Valverde L, Pino F, Rosa F. Definition, analysis and experimental investigation of operaion modes in hydrogen-renewable-based power plants incorporating hybrid energy storage. Energy Convers Manag 2016;113:290–311.
[46] Bizon N, Oproescu M, Raceanu M. Efficient energy control strategies for a standalone renewable/fuel cell hybrid power source. Energy Convers Manag 2015;90:93–110.
[47] Ipsakis D, Voutetakis S, Seferlis P, Stergiopoulos F, Elmasides C. Power management strategies for a stand-alone power system using renewable energy sources and hydrogen storage. Int J Hydrog Energy 2009;34(16):7081–95.
[48] Samson GT, Undeland TM, Ulleberg O, Vie PJS. Optimal load sharing strategy in a hybrid power system based on PV/fuel cell/battery/supercapacitor, In: Proceedings of IEEE international conference on clean electrical power, no. 2027; 2009, p. 141–6.
[49] Mohammadi M, Nafar M. Fuzzy sliding-mode based control (FSMC) approach of hybrid micro-grid in power distribution systems. Int J Electr Power Energy Syst 2013;51:232–42.
[50] Dash V, Bajpai P. Power management control strategy for a stand-alone solar photovoltaic-fuel cell–battery hybrid system. Sustain Energy Technol Assess 2015;9:68–80.
[51] Ipsakis D, Voutetakis S, Seferlis P, Stergiopoulos F, Papadopoulou S, Elmasides C. The effect of the hysteresis band on power management strategies in a stand-alone power system. Energy 2008;33(10):1537–50.
[52] Brka A, Kothapalli G, Al-Abdeli YM. Predictive power management strategies for stand-alone hydrogen systems: lab-scale validation. Int J Hydrog Energy 2015;40(32):9907–16.
[53] Ziogou C, Ipsakis D, Elmasides C, Stergiopoulos F, Papadopoulou S, Seferlis P, Voutetakis S. Automation infrastructure and operation control strategy in a stand-alone power system based on renewable energy sources. J Power Sources 2011;196(22):9488–99.
[54] ZHOU K. Optimal energy management strategy and system sizing method for stand-alone photovoltaic-hydrogen systems. Int J Hydrog Energy 2008;33(2):477–89.
[55] Torreglosa JP, García P, Fernández LM, Jurado F. Energy dispatching based on predictive controller of an off-grid wind turbine/photovoltaic/hydrogen/battery hybrid system. Renew Energy 2015;74:326–36.
[56] Tesfahunegn SG, Ulleberg Ø, Vie PJS, Undeland TM. Optimal shifting of Photovoltaic and load fluctuations from fuel cell and electrolyzer to lead acid battery in a Photovoltaic/hydrogen standalone power system for improved performance and life time. J Power Sources 2011;196(23):10401–14.
[57] Giannakoudis G, Papadopoulos AI, Seferlis P, Voutetakis S. Optimum design and operation under uncertainty of power systems using renewable energy sources and hydrogen storage. Int J Hydrog Energy 2010;35(3):872–91.
[58] Carapellucci R, Giordano L. Modeling and optimization of an energy generation island based on renewable technologies and hydrogen storage systems. Int J Hydrog Energy 2012;37(3):2081–93.
[59] Torreglosa JP, García P, Fernández LM, Jurado F. Hierarchical energy management system for stand-alone hybrid system based on generation costs and cascade control. Energy Convers Manag 2014;77:514–26.
[60] More JJ, Puleston PF, Kunusch C, Fantova MA. Development and implementation of a supervisor strategy and sliding mode control setup for fuel-cell-based hybrid generation Systems. IEEE Trans Energy Convers 2015;30(1):218–25.
[61] Wang C, Nehrir MH. Power management of a stand-alone wind/photovoltaic/fuel cell energy system. IEEE Trans Energy Convers 2008;23(3):957–67.
[62] Calderón M, Calderón aJ, Ramiro a, González JF. Automatic management of energy flows of a stand-alone renewable energy supply with hydrogen support. Int J Hydrog Energy 2010;35(6):2226–35.
[63] Hatti M, Meharrar a, Tioursi M. Power management strategy in the alternative energy photovoltaic/PEM fuel cell hybrid system. Renew Sustain Energy Rev 2011;15(9):5104–10.
[64] Stewart EM, Lutz AE, Schoenung S, Chiesa M, Keller JO, Fletcher J, Ault G, McDonald J, Cruden A. Modeling, analysis and control system development for the Italian hydrogen house. Int J Hydrog Energy 2009;34(4):1638–46.
[65] Wu W, Christiana VI, Chen S-A, Hwang J-J. Design and techno-economic optimization of a stand-alone PV (photovoltaic)/FC (fuel cell)/battery hybrid power system connected to a wastewater-to-hydrogen processor. Energy 2015;84:462–72.
[66] Sanchez VM, Chavez-Ramirez AU, Duron-Torres SM, Hernandez J, Arriaga LG, Ramirez JM. Techno-economical optimization based on swarm intelligence algorithm for a stand-alone wind-photovoltaic-hydrogen power system at south-east region of Mexico. Int J Hydrog Energy 2014;39(29):16646–55.
[67] Mendis N, Sayeef S, Muttaqi KM, Perera S. Hydrogen energy storage for a permanent magnet wind turbine generator based autonomous hybrid power system. In: Proceedings of power and energy society general meeting, IEEE; 2011. p. 1–7.
[68] Eid A. Utility integration of PV-wind-fuel cell hybrid distributed generation systems under variable load demands. Int J Electr Power Energy Syst 2014;62:689–99.
[69] Chedid R, El Khoury H. Design of a hybrid wind-PV-fuel cell system for powering a desalination plant. In: Proceedings of power engineering society general meeting, IEEE PES; 2007. p. 1–6.
[70] Baghaee HR, Gharehpetian GB, Kaviani aK Three dimensional Pareto optimal solution to design a hybrid stand-alone Wind/PV generation system with hydrogen energy storage using multi-objective particle swarm optimization. In: Proceedings of second Iranian conference on renewable energy and distributed generation; 2012. p. 1–6.
[71] Behzadi MS, Niasati M. Comparative performance analysis of a hybrid PV/FC/battery stand-alone system using different power management strategies and sizing approaches. Int J Hydrog Energy 2015;40(1):538–48.
[72] Eroglu M, Dursun E, Sevencan S, Song J, Yazici S, Kilic O. A mobile renewable house using PV/wind/fuel cell hybrid power system. Int J Hydrog Energy 2011;36(13):7985–92.
[73] Uzunoglu M, Onar OC, Alam MS. Modeling, control and simulation of a PV/FC/UC based hybrid power generation system for stand-alone applications. Renew Energy 2009;34(3):509–20.
[74] Hussain EK, Member S, Bingham CM, Stone D, Hybrid stand-alone renewable energy system with high fuel-cell efficiency and unity power factor. In :Proceedings of IEEE PES conference on innovative smart grid technologies – Middle East (ISGT Middle East); 2011. p. 1–6.
[75] Dursun E, Kilic O. Comparative evaluation of different power management strategies of a stand-alone PV/Wind/PEMFC hybrid power system. Int J Electr Power Energy Syst 2012;34(1):81–9.
[76] García P, Torreglosa JP, Fernández LM, Jurado F. Improving long-term operation of power sources in off-grid hybrid systems based on renewable energy, hydrogen and battery. J Power Sources 2014;265:149–59.
[77] Zhang F, Thanapalan K, Procter A, Carr S, Maddy J, Premier G. Power management control for off-grid solar hydrogen production and utilisation system. Int J Hydrog Energy 2013;38(11):4334–41.
[78] Trifkovic M, Marvin WA, Sheikhzadehy M, Daoutidis P. Dynamic real-time

optimization and control of a hybrid energy system. In: European Control Conference (ECC), Zurich; 2013, p. 2669–74.
[79] Cano MH, Kelouwani S, Agbossou K, Dubé Y. Power management system for off-grid hydrogen production based on uncertainty. Int J Hydrog Energy 2015;40(23):7260–72.
[80] Miland H, Ulleberg Ø. Testing of a small-scale stand-alone power system based on solar energy and hydrogen. Sol Energy 2012;86(1):666–80.
[81] Yumurtaci R. Role of energy management in hybrid renewable energy systems: casecase study based analysis considering varying seasonal conditions. Turk J Electr Eng Comput Sci 2013;21(4):1077–91.
[82] Abedi S, Alimardani A, Gharehpetian GB, Riahy GH, Hosseinian SH. A comprehensive method for optimal power management and design of hybrid RES-based autonomous energy systems. Renew Sustain Energy Rev 2012;16(3):1577–87.
[83] Castañeda M, Cano A, Jurado F, Sánchez H, Fernández LM. Sizing optimization, dynamic modeling and energy management strategies of a stand-alone PV/hydrogen/battery-based hybrid system. Int J Hydrog Energy 2013;38(10):3830–45.
[84] Rouholamini M, Mohammadian M. Energy management of a grid-tied residential-scale hybrid renewable generation system incorporating fuel cell and electrolyzer. Energy Build 2015;102:406–16.
[85] Moghaddam AA, Seifi A, Niknam T, Alizadeh Pahlavani MR. "Multi-objective operation management of a renewable MG (micro-grid) with back-up micro-turbine/fuel cell/battery hybrid power source. Energy 2011;36(11):6490–507.
[86] García P, Torreglosa JP, Fernández LM, Jurado F. Optimal energy management system for stand-alone wind turbine/photovoltaic/hydrogen/battery hybrid system with supervisory control based on fuzzy logic. Int J Hydrog Energy 2013;38(33):14146–58.
[87] García-Triviño P, Llorens-Iborra F, García-Vázquez CA, Gil-Mena AJ, Fernández-Ramírez LM, Jurado F. Long-term optimization based on PSO of a grid-connected renewable energy/battery/hydrogen hybrid system. Int J Hydrog Energy 2014;39(21):10805–16.
[88] Cozzolino R, Tribioli L, Bella G. Power management of a hybrid renewable system for artificial islands: a case study. Energy 2016;106:774–89.
[89] Smaoui M, Krichen L. Control, energy management and performance evaluation of desalination unit based renewable energies using a graphical user interface. Energy 2016;114:1187–206. ISSN 0360-5442 http://dx.doi.org/10.1016/j.energy.2016.08.051.
[90] Achour D, Chaib A, Kesraoui M. Power control and load management of an isolated hybrid energy system, In: Proceedings of 7th international renewable energy congress (IREC); 2016.
[91] Miron C, Christov N. Energy management of photovoltaic systems using fuel cells. In: Proceedings of the 20th international conference on system theory, control and computing; 2016.
[92] Cordiner S, Mulone V, Giordani A, Savino M, Tomarchio G, Malkow T, Tsotridis G, Pilenga A, Karlsen ML, Jensen J. Fuel cell based hybrid renewable energy systems for off-grid telecom stations: data analysis from on field demonstration tests q. Appl Energy 2016.
[93] Torreglosa JP, García-triviño P, Fernández-ramirez LM, Jurado F. Control based on techno-economic optimization of renewable hybrid energy system for stand-alone applications. Exp Syst App 2016;51:59–75. ISSN 0957-4174 http://dx.doi.org/10.1016/j.eswa.2015.12.038.
[94] Zahedi A. Technical analysis of an electric power system consisting of solar PV energy, wind power, and hydrogen fuel cell. In: Proceedings of Australasian universities power engineering; 2007, p. 1–5.
[95] Patsios C, Antonakopoulos M, Chaniotis A, and Kladas A. Control and analysis of a hybrid renewable energy-based power system,. In: Proceedings of XIX international conference electrical machines, ICEM; 2010, p. 1–6.
[96] Cau G, Cocco D, Petrollese M, Knudsen Kær S, Milan C. Energy management strategy based on short-term generation scheduling for a renewable microgrid using a hydrogen storage system. Energy Convers Manag 2014;87:820–31.
[97] Ri YB, and Cell DMH. "Optimal design and performance evaluation of," no. Iconce; 2014. p. 89–93.
[98] Ng KS, Moo CS, Lin YC, Hsieh YC. Investigation on intermittent discharging for lead-acid batteries, In: Proceedings of IEEE power electronics, Special Conference; 2008, pp. 4683–8.
[99] Guinot B, Champel B, Montignac F, Lemaire E, Vannucci D, Sailler S, Bultel Y. Techno-economic study of a PV-hydrogen-battery hybrid system for off-grid power supply: impact of performances' ageing on optimal system sizing and competitiveness. Int J Hydrog Energy 2015;40(1):623–32.
[100] Segura F, Andújar JM, Tomé JM. "Solutions to power management based on voltage and current control methods applied to fuel cell hybrid systems. In: Proceedings of international conference on biosciences (BIOSCIENCESWORLD); 2010. p. 99–105.
[101] Dufo-López R, Lujano-Rojas JM, Bernal-Agustín JL. Comparison of different lead–acid battery lifetime prediction models for use in simulation of stand-alone photovoltaic systems. Appl Energy 2014;115:242–53.
[102] Crossland AF, Anuta OH, Wade NS. A socio-technical approach to increasing the battery lifetime of off-grid photovoltaic systems applied to a case study in Rwanda. Renew Energy 2015;83:30–40.
[103] Koutroulis E, Kalaitzakis K, Novel battery charging regulation system for photovoltaic applications, p. 191–7.
[104] Andrade AMSS, Mattos E, Gamba CO, Schuch L, Martins MLS. Design and implementation of PV power zeta converters for battery charger applications. In: Proceedings of energy conversion congress and exposition (ECCE), IEEE; 2015. p. 3135–42.
[105] Lee CS, Lin HC, and Lai S, "Development of fast large lead-acid battery charging system using multi-state strategy," vol. 2; 2013. no. 2, p. 56–65.
[106] Horkos PG, Yammine E, Karami N. "Review on different charging techniques of lead- acid batteries. In: Proceedings of technological advances in electrical, electronics and computer engineering (TAEECE), third international conference on; 2015. p. 27–32.
[107] Linden TB, David, Reddy. Handbook of batteries. McGraw-Hil; 2002.
[108] Linden D, Reddy TB, *HANDBOOK OF BATTERIES*.
[109] Chen H, Pei P, Song M. Lifetime prediction and the economic lifetime of proton exchange membrane fuel cells. Appl Energy 2015;142:154–63.
[110] Little M, Thomson M, Infield D. Electrical integration of renewable energy into stand-alone power supplies incorporating hydrogen storage. Int J Hydrog Energy 2007;32(10–11):1582–8.
[111] Leng Y, Chen G, Mendoza AJ, Tighe TB, Hickner M a, Wang CY. Solid-state water electrolysis with an alkaline membrane. J Am Chem Soc 2012;134(22):9054–7.
[112] Rashid MM, Al Mesfer MK, Naseem H, Danish M. Hydrogen production by water electrolysis: a review of alkaline water electrolysis, PEM water electrolysis and high temperature water electrolysis. Int J Eng Adv Technol 2015;4(3):80–93.
[113] Dutton aG, Bleijs J aM, Dienhart H, Falchetta M, Hug W, Prischich D, Ruddell aJ. Experience in the design, sizing, economics, and implementation of autonomous wind-powered hydrogen production systems. Int J Hydrog Energy 2000;25:705–22.
[114] Symes D, Al-Duri B, Bujalski W, Dhir a. Cost-effective design of the alkaline electrolyser for enhanced electrochemical performance and reduced electrode degradation. Int J Low-Carbon Technol 2013. [vol. -, no. -, p. -].
[115] Santos DMF, Sequeira CAC. Revisão. vol 36, no. 8; 2013. p. 1176–93.
[116] Zeng K, Zhang D. Recent progress in alkaline water electrolysis for hydrogen production and applications. Prog Energy Combust Sci 2010;36(3):307–26.
[117] Calderón A, González I, Calderón M, Segura F, Andújar J. A new, scalable and low cost multi-channel monitoring system for polymer electrolyte fuel cells. Sensors 2016;16(3):349.
[118] Jourdan Mohammed, Mounir H, Marjani AEl. Compilation of factors affecting durability of proton exchange membrane fuel cell (PEMFC), In: Proceedings of international renewable and sustainable energy conference; 2014. pp. 542–7.
[119] Janssen GJM, Sitters EF, Pfrang a. Proton-exchange-membrane fuel cells durability evaluated by load-on/off cycling. J Power Sources 2009;191:501–9.
[120] Kannan A, Kabza A, Scholta J. Long term testing of start–stop cycles on high temperature PEM fuel cell stack. J Power Sources 2015;277:312–6.
[121] Borup RL, Davey JR, Garzon FH, Wood DL, Inbody M a. PEM fuel cell electrocatalyst durability measurements. J Power Sources 2006;163(1):76–81.
[122] Bae SJ, Kim S-J, Park JI, Park CW, Lee J-H, Song I, Lee N, Kim K-B, Park J-Y. Lifetime prediction of a polymer electrolyte membrane fuel cell via an accelerated startup–shutdown cycle test. Int J Hydrog Energy 2012;37(12):9775–81.
[123] Yu Y, Li H, Wang H, Yuan X-Z, Wang G, Pan M. A review on performance degradation of proton exchange membrane fuel cells during startup and shutdown processes: causes, consequences, and mitigation strategies. J Power Sources 2012;205:10–23.
[124] Oyarce A, Zakrisson E, Ivity M, Lagergren C, Ofstad AB, Bodén A, Lindbergh G. Comparing shut-down strategies for proton exchange membrane fuel cells. J Power Sources 2014;254:232–40.
[125] Lin R, Cui X, Shan J, Técher L, Xiong F, Zhang Q. Investigating the effect of start-up and shut-down cycles on the performance of the proton exchange membrane fuel cell by segmented cell technology. Int J Hydrog Energy 2015;40(43):14952–62.
[126] Uno M, Tanaka K. Pt/C catalyst degradation in proton exchange membrane fuel cells due to high-frequency potential cycling induced by switching power converters. J Power Sources 2011;196(23):9884–9.
[127] Fontes G, Turpin C, Saisset R, Meynard T, Astier S. Interactions between fuel cells and power converters Influence of current harmonics on a fuel cell stack, In: Proceedings of IEEE transactions on power electronics, special conference., vol. 6, no. 2; 2004, p. 4729–35.
[128] Hoshi H, Aisaka Y, Control Method of Multiple Power Converter to Reduce Deterioration of Fuel Cells.
[129] Changrong L, Jih-Sheng L. Low frequency current ripple reduction technique with active control in a fuel cell power system with inverter load. Power Electron IEEE Trans 2007;22(4):1429–36.
[130] Choi W, Howze JW, Enjeti P. Development of an equivalent circuit model of a fuel cell to evaluate the effects of interter ripple current. J Power Sources 2006;158(C):1324–32.
[131] Upadhyay S, Sharma MP. A review on configurations, control and sizing methodologies of hybrid energy systems. Renew Sustain Energy Rev 2014;38:47–63.
[132] de E EyTG. Ministerio de Industrial, Plan Nacional De Acción De Eficiencia Energética 2014–2020; 2014 p. 1–156.
[133] Ulleberg Ø. The importance of control strategies in PV–hydrogen systems. Sol Energy 2004;76(1–3):323–9.
[134] Kim J, Kim M, Kang T, Sohn YJ, Song T, Choi KH. Degradation modeling and operational optimization for improving the lifetime of high-temperature PEM (proton exchange membrane) fuel cells. Energy 2014;66:41–9.
[135] Jouin M, Gouriveau R, Hissel D, Jouin M, Gouriveau R, Hissel D. Remaining useful life estimates of a PEM fuel cell stack by including characterization-induced disturbances in a particle filter model. Noureddine Zerhouni To cite this version; 2014.
[136] Segura F, Andújar JM. Power management based on sliding control applied to fuel cell systems: a further step towards the hybrid control concept. Appl Energy 2012;99:213–25.
[137] Sacarisen SP, Parvereshi JJP, Improveq Lead-Acid Battery Management Techniques.
[138] Duryea S, Islam S, Lawrance W. A battery management system for stand-alone photovoltaic energy systems. Ind Appl Mag IEEE 2001;7:67–72.

4.2. Article 2

H2RES2 simulator. A new solution for hydrogen hybridization with renewable energy sources-based system

F.J. Vivas, A. De las Heras, F. Segura, J.M. Andújar

Published in:

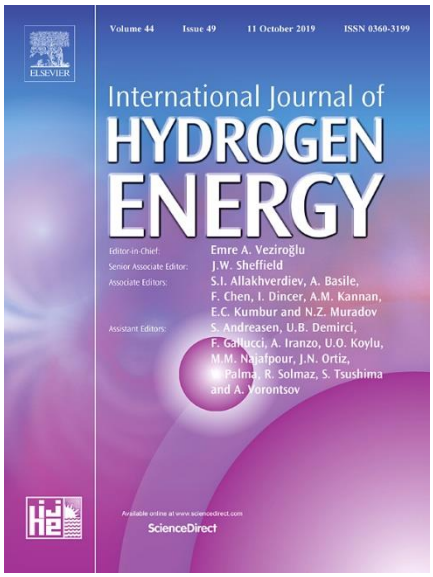

Journal: International Journal of Hydrogen Energy

Editorial: ELSEVIER

Editor-in-Chief: T. Nejat Veziroglu

Reference: Vol. 42, Issue 19, pp. 13510-13531

Year: 2017

ISSN: 0360-3199

DOI 10.1016/j.ijhydene.2017.02.139

Category	Journal Rank / Total journals	Quartile
Energy & Fuels	24 / 97	Q1
Electrochemistry	42 / 146	Q2
Chemistry	8 / 28	Q2
Impact Factor (2017)	3.581	
Citations	8	

INTERNATIONAL JOURNAL OF HYDROGEN ENERGY 42 (2017) 13510–13531

Available online at www.sciencedirect.com

ScienceDirect

journal homepage: www.elsevier.com/locate/he

H2RES2 simulator. A new solution for hydrogen hybridization with renewable energy sources-based systems

F.J. Vivas[*], *A. De las Heras*, *F. Segura*, *J.M. Andújar*

Grupo de Investigación de Control y Robótica TEP-192, Departamento de Ingeniería Electrónica, de Sistemas Informáticos y Automática, Escuela Técnica Superior de Ingeniería, Universidad de Huelva, Carretera Huelva - Palos de la Frontera, 21819, La Rábida - Palos de la Frontera, Huelva, Spain

ARTICLE INFO

Article history:
Received 7 October 2016
Received in revised form
14 February 2017
Accepted 17 February 2017
Available online 18 March 2017

Keywords:
Simulator
Energy management strategy
Hybrid renewable systems
Hydrogen hybridization
Technical and economic analysis

ABSTRACT

This paper presents a new simulator for Hydrogen hybridization with Renewable Energy based Systems. The aim of this simulator is to provide a new solution for testing different energy management strategies of hydrogen hybridization based on renewable systems, in order to optimize them for implementation. The simulator uses the open architecture philosophy and has been developed in MATLAB®-SIMULINK environment. Its main feature is calculating technical and economical parameters for a deepened analysis of influences on energy management strategies. It considers each element of the hybrid system and the whole system function. A simulation case shows the proper functioning of the simulator.

Introduction

More and more companies and governments are committed to a change in energy policies, always oriented towards more energy efficient actions and more renewable energy use. Currently, there are many research groups encouraging and working on a change in the recent energy model, trying to integrate the use of renewable energy sources in our lives.

Thus renewable energy technologies cause high costs and a high dependence on climatic factors [1–3], the use of hybrid power systems is presented as an ideal solution to fill the gaps in the energy supply that the different renewable energy sources may provoke. Due to the fact that some of renewable energy sources are still not entirely developed, the costs for their utilization and lifetime depend largely on the used technology and the operating system. As a result, performance improvements in terms of life and cost reduction of this new energy generation technology, will allow better integration and acceptance in future applications [4,5].

To operate and interconnect different elements of a hybrid generation system, ensuring safe operation and fulfilling the objectives, it is necessary to sufficiently control the system to manage the energy supply by each source. A proper energy management strategy guarantees the load supply, increases the lifetime of each system element, reduces operating costs, and therefore maximizes system performance, providing a technical and economical feasible solution [6–8]. There are

* *Corresponding author.*
http://dx.doi.org/10.1016/j.ijhydene.2017.02.139

Nomenclature

PV	Photovoltaic source
WT	Wind Turbine
ELEC	Electrolyzer
FC	Fuel Cell
MH	Metal Hydride tank
BAT	Battery
DOD	Depth Of Discharge
SOC	State Of Charge
E_{GRID_IN}	Input energy from grid
E_{GRID_OUT}	Output energy to grid
E_{BAT}	Battery energy supplied
E_{FC}	Fuel cell generation
E_{ELEC}	Electrolyzer consumption
E_{LOAD}	Load consumption
$Loss_{CHA}$	Battery charging losses
$Loss_{FC}$	Fuel cell average losses per cell
FC_{CYCLE}	Fuel cell start/stop cycles
FC_{TIME}	Fuel cell operation time
$ELEC_{CYCLE}$	Electrolyzer start/stop cycles
$ELEC_{TIME}$	Electrolyzer operation time
BAY_{CYCLE}	Battery operation cycles
$ELEC_{H2}$	Produced hydrogen
CO&M	Operation and maintenance cost

many research works which propose different configurations of hybrid power systems based on renewable energy sources. These configurations have different energy management strategies, most of them focused on guaranteeing the demand [1–3,9,56], and are regardless of technical and economic optimization criteria, or problems associated with real equipment such as transients, stability, security, equipment degradation, hydrogen management, etc.

For all these reasons, the use of software tools is necessary. These tools allow us to perform simulations and previous analysis to enable an implementation, taking into account different management strategies, including genuine parameters for sensitivity analysis.

Recently, there exist plenty of simulators on the market (AEOLIUS, BALOMOREL, COMPOSE, E4CAST, EMCAS, EMINENT, EMPS, ENERGYPLAN, ENERGY PRO, GTMAX, INFORSE, INVERT, LEAP, MESAP, NEMOS, ORCED, PERSEUS, PRIMES, PRODRISK, RAMSES, SIVAEL, STREAM, UNISYD3.0, WASP or WILMAR), which are used to model different power generation systems and loads.

Most of these simulators allow the modeling of power generation systems connected to a grid, or a system integrated into microgrids, giving an optimal solution for economic and power management in the middle and long-term [10–13]. A reduced number of simulators include the ability to combine renewable energy generation equipment and their auxiliary systems. Additionally they permit the use of hydrogen as energy vector in all its phases: hydrogen production, storage and consumption (HOMER, RETSCREEN, HYBRID DESIGNER, HYBRID2, iHOGA, MATLAB or TRNSYS16) [10–13,47].

The above list of recent software tools can be basically divided into four categories according to their purpose [14,47].

Tools of the first tool category can be called *pre-feasibility* tools, which are tools for preliminary estimation, in order to study the feasibility of a project [14]. To this category belong tools like RETSCREEN or EXCELL (Really: Excel is a specialized spreadsheet that can be used for almost any application).

The second tool category refers to *sizing*. These tools' purpose is to generate a technical and economic long term study in order to obtain an optimum sizing [10,11,14]. These tools are very useful for economic viability studies, but they lack the possibility of studies of different energy management strategies, due to their closed software with little or no flexibility, as well as their use of very high integration periods. The most common ones to distinguish are the tools HYBRID DESIGNER and HOMER.

The third tool category includes *simulation*, that is intended to reproduce the behavior of a system based on fixed sizing and fixed operation parameters [10,11,14]. The main problem with this type of software tools is the low flexibility to modify simulation parameters, in order to carry out a study of different management strategies. Prominent examples of this type of software are HYBRID2 and iHOGA.

The fourth and last tool category unites open architecture software which offers better flexibility and is more suitable for analytical studies varying in the energy management strategy [14]. The main problem of this type of software is the high need of programming environment knowledge. TRNSYS16 and MATLAB are the most known software tools for this kind of applications.

Table 1 shows the principal drawbacks associated with the most used software tools.

Following the analysis of Table 1, we can deduce that simulation software tools with open architecture software would be the most useful for the study of different energy management strategies. Additionally, the fourth category of tools compiles software tools that could provide a solution capable of combining all the possibilities of analysis. Therefore, the developed simulator presented in this paper has been designed, according to the common characteristics of this category.

Regarding the software tools included in the last category, the main advantages of MATLAB over TRNSYS16 are its greater computational power and widely establishment [14]. In addition, MATLAB has the ability to be integrated into acquisition systems. This way it is possible to implement all the previously developed control logic into genuine future systems. However, MATLAB requires higher processing times (about 4 times) compared to other software tools based on different programming languages such as C, Fortran, Java, Julia or Phyton [53]. For this reason, a proper programming is necessary, to simplify the simulation tool and perform tests, resulting in more reasonable processing times.

In basis on all exposed above, this paper presents a simulator based on MATLAB-Simulink environment. The simulator allows modeling isolated or grid connected hybrid power systems. These systems allow the integration of hydrogen technology and renewable energy sources from different nature and energy storage systems. Additionally, the presented simulator offers the possibility of testing different energy management strategies, running simulations in the short-term time scale and improving sensitivity analysis attending

Table 1 – Simulators classification.

Software category	Software tool	Drawback
Pre-feasibility	RETSCREEN	Only for basic feasibility studies
	EXCELL	
Sizing tool	HOMER	Doesn't consider variations in bus voltage
		DOD is not considered, only in sensitive analysis
		Low and closed energy dispatching options
		Only minimize net present cost
	HYBRID DESIGNED	Focused on isolated applications
		Doesn't consider technical optimization
Simulation tool	HYBRID2	High learning time requirements
		Low and closed energy dispatching options
	iHOGA	Fixed optimization algorithm (GA)
		Difficult to extrapolate optimization algorithm to real implementation
		Complex models for elements
Open architecture software	TRNSYS16	Fortran knowledge is required
		For H_2 storage analysis, it needs HYDROGEMS tool
	MATLAB	C programming skills are required
		Structure programming notions are required

to cost and lifetime of the devices which integrate the hybrid power system. These features give benefit to the developed simulator, overtaking the main shortcomings that the authors have found in other software tools available in the scientific literature or in the market. All the developed functions are accessible and therefore adapting to user requirements.

In the next section, a detailed description of the proposed simulator is done. Section "Energy management study" presents the developed energy management strategy by authors and used in the simulator. In Section "technical and economic parameters" the technical and economical parameters considered by the simulator and needed for sensitive analysis are presented. In order to show the proper functioning of the simulator as well as its particular features, a simulation case of a practical system is carried out in Section "Simulation case". Finally, Conclusions and future works close the paper.

Simulator: architecture and interface description

The simulator proposed in this work has been developed under MATLAB-Simulink environment. It is a powerful tool, user friendly and very intuitive. It can be used already with very little training.

Regarding the software implementation, the simulator has been developed maintaining a modular structure in order to guarantee the highest level of scalability and flexibility.

The simulator provides default configuration and can be adapted to the user needs, allowing to update input data related to weather, load profile, base time, model used for each element as well as its size. The guiding thread the authors have followed in their development has been the possibility to perform realistic energy simulations of **H**ydrogen **H**ybridization with **R**enewable **E**nergy **S**ources-based **S**ystems (H2RES2). A general view of the simulator is shown in Fig. 1.

H2RES2 simulator architecture

The default hybrid system architecture (see in Fig. 2a a schematic representation) consists of two different sources of renewable energy as the primary energy source: photovoltaic panels and wind turbines. It is assuming a common hybrid power system supply of electric power to an electrical network. In case of isolated applications, the grid energy will define the energy deficit of the proposed energy management strategy and system sizing. This parameter indicates the difference between the generated and the consumed energy, providing the user a way to test the viability of his configuration.

In the hybrid system has to include different energy backup elements to ensure the load demand and grid stability in situations of energy deficit. In this case, a battery bank is used as the primary short- and middle-term energy backup. A modular fuel cell should be used secondary for a long-time energy backup. The use of a modular fuel cell (built out of single stacks) improves the performance of the whole configuration and guarantees the energy supply even in cases of stack failure [48]. However, the fuel cell configuration can be chosen by the user. It is possible to define one or more fuel cells built from one single stack. To guarantee an accurate fuel cell operation the use of hydrogen storage technology is required. For this target, in this topology there are metal hydrides tanks and high pressure tanks used. Finally, an electrolyzer is included to ensure a precise energy balance in situations of electrical overproduction and convert the overproduced electrical energy into chemical energy while producing hydrogen. In order to generate any consumption profile, we consider that the network has programmable AC and DC loads.

The H2RES2 simulator includes the ability to define different energy management strategies, as well as it includes auxiliary functions, state diagrams and truth tables that are derived from the established strategy, Fig. 2b.

Although MATLAB-Simulink is a powerful tool, the use of this program requires high computing times [53]. In order to mitigate this problem, all functions have been programmed with the aim of reducing the computation time. In this manner, the one-year simulation is performed in less than one and a half minutes, with a time step of seconds.

Besides, the H2RES2 simulator includes mathematical expressions to model the effect of the battery bank voltage and

Fig. 1 – H2RES2: General view.

charge efficiency, in order to calculate the energy losses associated with this process.

Moreover, based on system parameters (like the battery State Of Charge, hydrogen tanks level, fuel cell and electrolyzer start–stop cycles, run times, SOC hysteresis-based operation mode, etc.), it is possible to perform a sensitivity analysis of the lifetime of the involved devices [15–18], comparing them after the implementation of different management strategies or configuration parameters.

Similarly, the H2RES2 simulator performs short-term time simulations, to tender the user detailed information of the system response with transients in a short time scale (seconds). Moreover it enables the user to study the system stability while accessing all electrical and physical parameters that are required for technical and economic analysis under different strategies and configurations. Additionally, this option allows the user to conclude causes of risks, damages or malfunction of all subsystems.

Results & graphical interface

Finally (see Fig. 2a), the simulator provides a graphical environment in which the user is able to choose any variable to be represented. This allows a fast location and simple definition of parameters or phenomena that may affect the proper functioning of the system as well as it compares the power generation of different sources and the amount of the produced, stored or consumed hydrogen.

In particular, the H2RES2 simulator has a graphical environment in which all system variables (physical, chemical and economical) can be represented (Fig. 3). Furthermore, it includes a summary window which shows global parameters (electrical and economic) obtained from the simulation (Fig. 4).

The results presented by the H2RES2 simulator include both, the power and energy associated with each element. They can be associated as well for electrolyzers, fuel cells, hydrogen storage tanks, the hydrogen production, the hydrogen consumption and hydrogen stocks. In case of fuel cells, battery banks and electrolyzers, the number of operation cycles can be displayed if necessary.

Particularly, the fuel cell deterioration, battery bank SOC, battery bank charge losses and real nominal capacity are represented in order to get enough information to develop various sensitivity analysis.

Finally, the overall operation and the maintenance costs are presented in the summary window.

Energy management study

The energy management strategy is responsible for solving the problem of the power balance as well as for the load demand at all time. Additionally, it must guarantee the hydrogen production, storage and consumption of each element; and all of this taking into account technical and economic optimization criteria with the aim of increasing the performance of the system.

Energy management criteria

Before a description of the different energy management strategies, we are going to define the parameters on which the proposed strategies are based. In case of the H2RES2 simulator, the control laws are established according to the priority of the elements, the power balance, the SOC hysteresis band-based operation mode and operation conditions.

Priority of the elements

Since the renewable energy hybrid system architecture of the H2RES2 simulator is composed of various generation and consumption subsystems, it is necessary to establish a hierarchical structure to determine the usage of them in different situations.

With this aim, the energy stored in the battery bank plays a special role [21]. In fact, it is the key given to define the energy management strategy. Remember this device should respond in situations of energy deficit and support with security and stability the transients both in the demand and the generation.

The use of primary generators of solar and wind energy is not causing any other certain requirements for the reason,

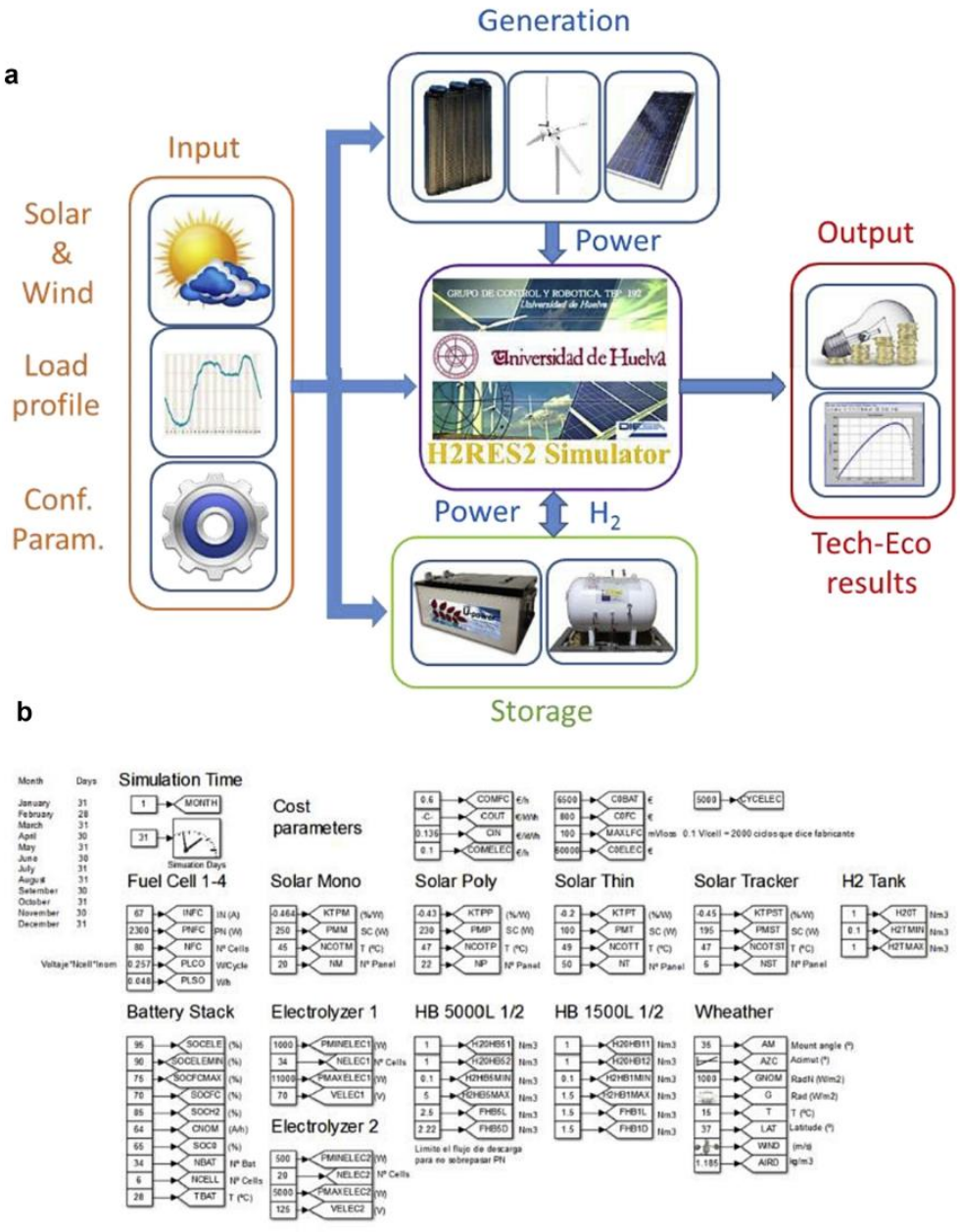

Fig. 2 – a. Default hybrid system schematic architecture, b. Simulator architecture implementation.

that these elements will supply energy whenever environmental resources are available.

The other elements of the hybrid system, like fuel cells and electrolyzers, have a secondary priority, due to their operation conditions that depend on the battery bank SOC level.

Power balance

The energy management strategy is based on the calculation of the power balance. The expression that models it is presented below Eq. (1):

$$P_{net} = P_{PV} + P_{WT} - P_{load} - P_{loss} \quad (1)$$

Where,

P_{net}: Hybrid system net power (W)
P_{PV}: Solar panels power (W)
P_{WT}: Wind turbine power (W)
P_{load}: Load power (W)
P_{loss}: Loss power (W)

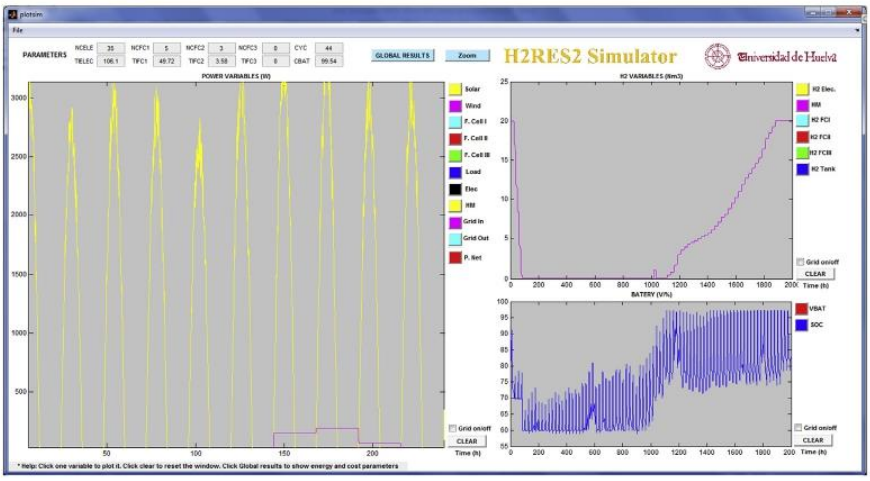

Fig. 3 – H2RES2 simulator: Simulation results window.

Fig. 4 – H2RES2 simulator: Summary window.

The sign and value of the power balance is determined system situations: deficit, balance or excess energy situation.

Hysteresis

In order to avoid a high degradation due to the number of operation cycles, the proposed strategy for electrolyzers and fuel cells is based on SOC hysteresis bandwidth.

This way the strategy consists on determining the start and stop conditions of fuel cells and electrolyzers in while using the battery bank SOC level [29–32].

The operation of the battery bank, the fuel cell and the electrolyzer inside the hysteresis band will be defined by the last element that was operating on the previous time step. The H2RES2 simulator facilitates the flexibility of modifying the hysteresis bandwidth values or even to removing them. In this last case, the user is given the chance to try other energy management strategy not based on the SOC hysteresis operation mode.

The values used in the definition of the hysteresis operation scheme are defined below (Fig. 5):

- **SOClow**: Allowed minimum SOC value. Below this level, the grid will supply demand and the fuel cell will be disconnected in order to save energy from the battery bank.
- **SOCmin**: Minimum SOC recommended to guarantee the lifetime of the battery bank. This value coincides with the start condition of the fuel cell.
- **SOCfcmax**: SOC value which indicates the stop condition of the fuel cell concerning the battery bank has enough stored energy to supply the load demand.
- **SOCH_2**: Minimum SOC value which indicates the stop condition for the hydrogen charging process from high pressure tanks towards the metal hydride tanks. This value is necessary for its absorption of energy in this charging process absorbs energy (please see Annex A, Section "Pressurized gas") It will affect the remaining energy in situations of low SOC value.
- **SOCelemin**: SOC value below which the electrolyzer must be stopped.
- **SOCmax:** Maximum SOC value required for a reliable. This value matches the SOC value at which the electrolyzer should start, since this SOC value is the maximum allowed.

Operation conditions

The last criteria around that defines the energy management strategy is related to operations conditions of the fuel cell and the electrolyzer. H2RES2 simulator has the possibility to choose between fixed or variable power conditions for the fuel cell and the electrolyzer. This gives the possibility to perform an analytical study of the effect on the operation of these devices under the demand (Fig. 6).

Additionally, in case of the electrolyzer, a minimum power point from which the electrolysis reaction is produced is necessary. This also guarantees the minimum crossover effect [24,33].

Energy management strategy definition

The energy management strategy can be differentiated in the charging process (energy excess), the discharging process (energy deficit) and additionally the hydrogen storage strategy.

Charging strategy

During energy excess situations, the power balance of the system will be positive and as discussed above, the SOC value will determine which element is to operate. As a conclusion, it

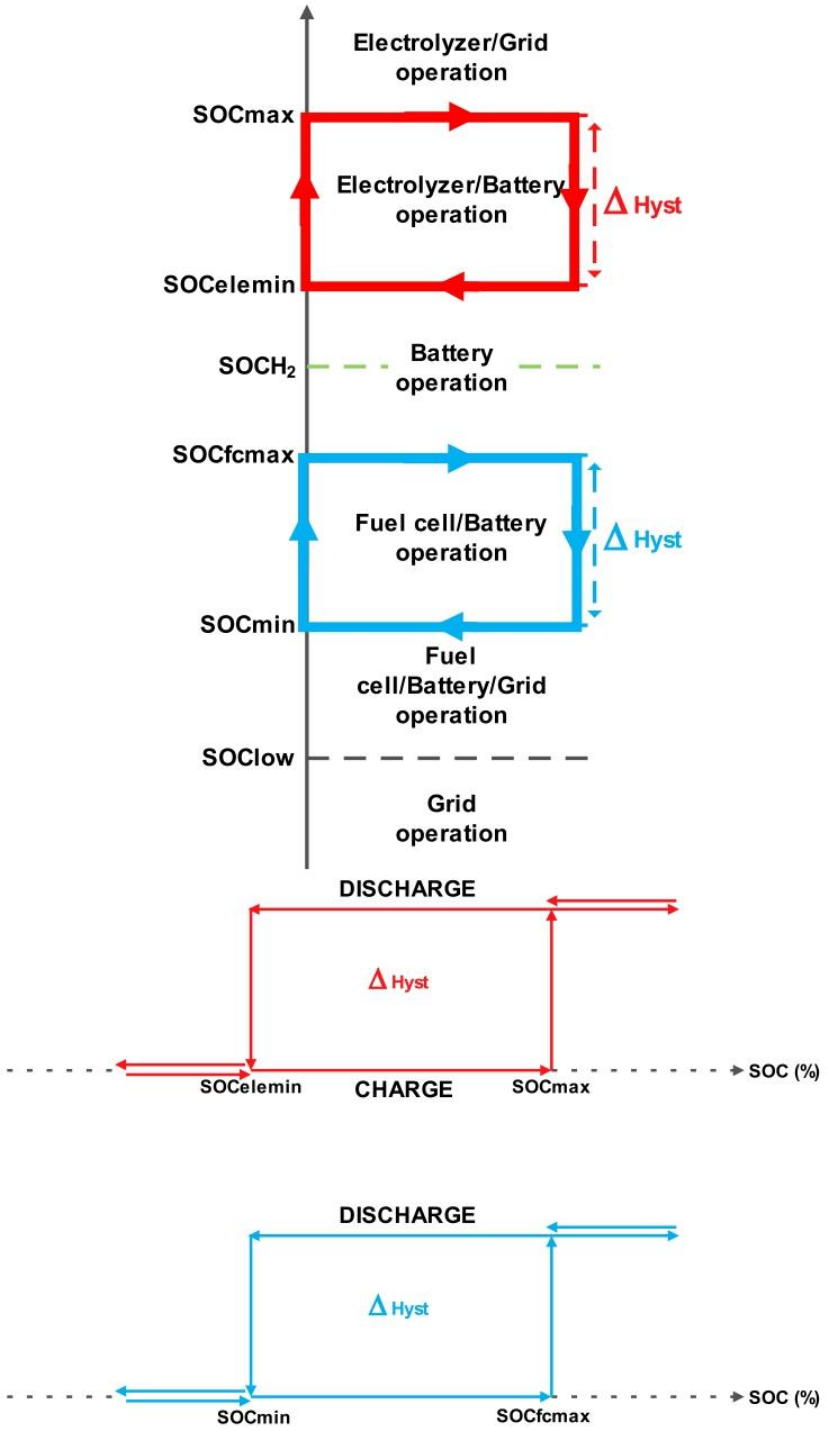

Fig. 5 – Hysteresis bandwidth-based operation diagram.

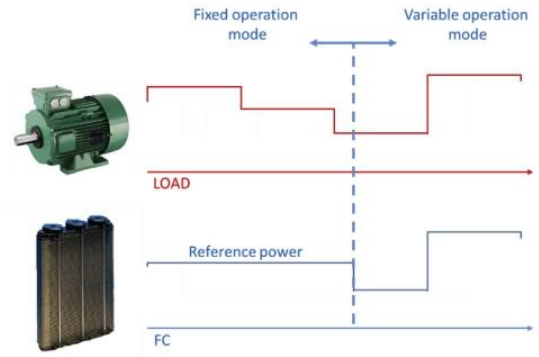

Fig. 6 – Fuel cell operation modes allowed by H2RES2 simulator.

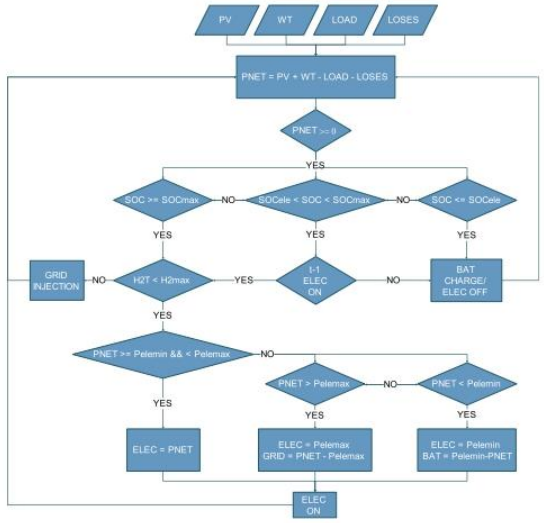

Fig. 7 – Energy management strategy: Charging process diagram.

is possible to distinguish between three possible situations (Fig. 7):

SOC ≤ SOCelemin

If the SOC is lower than for the electrolyzer start condition, all the excess of energy will be used to charge the battery bank, in order to have enough energy to provide energy in cases of an energy deficit.

SOC ≥ SOCmax

In this case, the battery bank is at its maximum charge capacity, so it should not admit more energy. The energy excess should be absorbed by other elements.

In the first instance, any energy excess is absorbed by the electrolyzer, taking advantage of it to produce hydrogen. If the energy excess is insufficient to guarantee the minimum power required by the electrolysis process, it is ensured at all times with the support of the battery bank.

In case the energy excess is higher than the electrolyzer rated power, or the hydrogen storage system is at its maximum capacity, the remaining energy is injected to the grid.

SOCelemin < SOC < SOCmax

During this situation the battery bank SOC is high enough and electrolyzer and battery bank will operate in basis on the hysteresis bandwidth strategy explained in Section "Hysteresis".

Discharging strategy

During an energy deficit situation, the SOC level will impose again the operation conditions of the rest of the elements of the system.

Since the battery bank is less expensive and more durable than the fuel cell, it reserves the use of the last one for cases in which the battery bank is not able to respond to the demand.

If the amount of hydrogen is enough negotiate the energy deficit, the fuel cell will supply the load demand until the SOC reaches the fuel cell's stop value. Conversely, if it is insufficient, the fuel cell will operate until the amount of hydrogen reaches its minimum value, then the battery bank or grid have to supply the demand. There are four operation zones distinguished, depending on the SOC value (Fig. 8):

SOC ≥ SOCfcmax

During this situation, the battery bank has enough charge capacity to keep the load demand under security conditions, therefore it is not necessary to use the fuel cell.

SOCmin < SOC < SOCfc

During this situation the SOC is low, the fuel cell and battery bank will operate based on the hysteresis strategy explained in Section "Hysteresis".

SOClow ≤ SOC ≤ SOCmin

This is case represents the limit situation of the system. On this occasion, the battery bank is at very low SOC. For this reason, all of the demand must be supplied by the fuel cell and/or an auxiliary grid (which can be, with the switching elements due, the same grid that is supplying the hybrid system; as long as it is not isolated).

SOC ≤ SOClow

This situation is given due to a lack of capacity of the fuel cell to supply the demand. All the demand is satisfied by the grid.

Hydrogen storage strategy

The hydrogen production will take place in situations of energy excess. The produced hydrogen must be stored in the

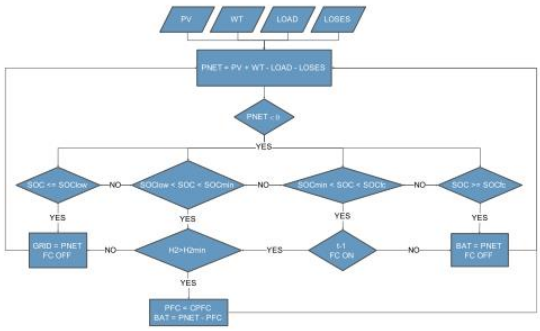

Fig. 8 – Energy management strategy: Discharging process diagram.

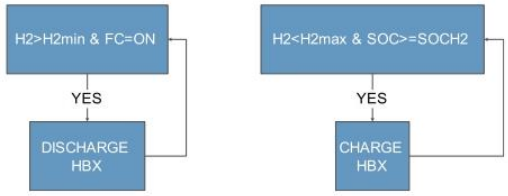

Fig. 9 – Hydrogen storage charging/discharging diagram.

hydrides metal tanks for its future use in situations of energy deficit.

The process of hydrogen storage only occurs in generation situations (energy excess) and for values of SOC > SOCH2, in order to guarantee the minimum charge level at all times. A States diagram that models the hydrogen storage strategy is presented in Fig. 9.

Technical and economic parameters

The H2RES2 simulator has been developed with the aim to test different energy management strategies, however, it also includes the possibility of a sensitivity analysis attending to lifetime and costs of the devices which are integrated in the hybrid power system. To conclude this section, technical and economic parameters calculated by H2RES2 are presented.

Technical parameters

As it happens to the entirely equipment, the useful lifetime of the elements that are integrated in the renewable energy hybrid system object of the H2RES2 simulator, depend on their use and work conditions [58].

Considering an expected lifetime by the whole hybrid system of typically 20–25 years, there are elements whose lifetime coincide with these values. In this case, for the cost analysis it is enough to assume the acquisition costs; this is the case in solar panels, wind turbines, and hydrogen storage equipment.

On the other hand, there are other elements whose useful lifetime depends on the number of working hours or operation cycles, for instance battery banks, fuel cells and electrolyzers. These elements' lifetime depends on the established management strategy.

Additionally, due to their extending acquisition costs, and to ensure the demanded supply as long as possible, a technical devise deterioration analysis is performed to increase the system performance.

Battery bank deterioration

According to scientific literature, operating temperature affects the battery lifetime [34–36]. High operating temperatures trigger a series of parasitic reactions which provoke the reduction of its nominal capacity (2):

$$Det_{BAT}(T) = Det_{BAT\_0}(T = 20^{\circ}C)*2^{\left(\frac{T-20}{10}\right)} \quad (2)$$

Where,

$Det_{BAT}(T)$: Battery deterioration associated with operation temperature (Ah)
$Det_{BAT\_0}(T = 20^{\circ}C)$: Battery deterioration at 20 °C operation temperature (Ah)
T: Battery operation temperature (°C)

From this expression, H2RES2 simulator estimates the nominal capacity degradation according to expressions (3) and (4):

$$Cnom(t) = Cnom(t-1),\ T \leq 20^{\circ}C \quad (3)$$

$$Cnom(t) = Cnom(t-1) - 0.2*Cnom(t-1)* *2^{\left(\frac{T-20}{10}\right)}*\Delta t,\ T > 20^{\circ}C \quad (4)$$

Lead-acid batteries degradation can be modeled with complex models that accurately estimate the battery lifetime. As an example [49], presents a degradation model based on operating conditions during a discharge process with the use of the weight factor. This parameter represents the loss of degradation due to current rate, depth of discharge, acid stratification, corrosion, etc. This model was validated in Ref. [50], and it is used in iHOGA software.

A linear aging coefficient function is presented in Refs. [51,52], and was validated in Ref. [52]. The battery deterioration can be reflected over the nominal capacity deterioration with the use of the linear aging coefficient according to Eqs. (5) and (6). For lead acid battery technology, an aging coefficient value of $3*10^{-4}$ can be considered as a good approximation [52].

$$Cnom(t) = Cnom(t-1) - Cnom(0)*\alpha* *(SOC(t-1) - SOC(t),\ T \leq 20^{\circ}C \quad (5)$$

$$Cnom(t) = Cnom(t-1) - Cnom(t=0)*\alpha* *2^{\left(\frac{T-20}{10}\right)}*(SOC(t-1) - SOC(t)),\ T > 20^{\circ}C \quad (6)$$

Where,

α: Estimated aging coefficient associated in the instantaneous discharging process.

Electrolyzer deterioration

The electrolyzer, mostly alkaline technology, is a high performance operation device which has an estimated lifetime of several years and even decades. The deterioration associated with the electrolysis process is minimal and therefore it can be considered negligible. At the end of the lifetime of an electrolyzer the deterioration is associated to the number of start–stop cycles [16,18].

To calculate the associated electrolyzer deterioration, the H2RES2 simulator uses the relationship between accumulated start.-stop cycles and the expected lifecycles (please see Section "Unitary cost function for each element"; expression (11)), given in typical electrolyzer technical handbooks/documents.

Fuel cell deterioration

Experimental studies on fuel cells agree that the most common processes, which have an influence on the fuel cell degradation, are related to start–stop cycles, the long operation time, and very fast demand variations [19,37,54]. The effect on the fuel cell is an increase of the kinetic losses due to the destruction of the catalytic layer and the reduction of the membrane thickness [38–40,54].

In practice, the deterioration results in a voltage drop which considered the effects commented above [41].

The assumptions used by the H2RES2 simulator to model the fuel cell voltage losses are presented in Eq. (7):

$$LOSS_{FC} = \Delta V_{CYCLE} * FC_{CYCLE} + \Delta V_{TIME} * FC_{TIME} \quad (7)$$

Where:

ΔV_{FC}: Overall fuel cell voltage losses (V/cell)
ΔV_{CYCLE}: Fuel cell voltage losses per operation cycle (V/operation cycle)
FC_{CYCLE}: Fuel cell operation cycles (operation cycles)
V_{TIME}: Fuel cell voltage losses per operation time (V/hr)
FC_{TIME}: Fuel cell operation time (hr)

The fuel cell net power results from the subtraction of the gross generated power minus and the power associated to the fuel cell (8):

$$P_{FC\_NET} = P_{FC\_GROSS} - LOSS_{FC} * I_{FC} \quad (8)$$

Where:

P_{FC_NET}: Fuel cell net power (W)
P_{FC_GROSS}: Gross power generated (W) by the fuel cell (please see Annex A)
I_{FC}: Fuel cell current (A)

Hybrid system reliability

Finally, the H2RES2 simulator offers the possibility to evaluate the system reliability. For this purpose the simulator includes the calculation of parameters called *Loss of Power Supply Probability* (LPSP).

The goal of any power generation system must be the demand satisfaction at all times. However, it is possible for autonomous systems or under operation failures, that the demand can not be guaranteed. Potentially, this results in non-continuous operations, that cause the destruction of elements and the economic detriment.

The simulator defines the LPSP index according to expression (9). This index allows it to compare the tested energy management strategies and decide over an optimal response. Furthermore, this index provides enough certainty to decide over the element sizing to form a proper hybrid system [42,43].

$$LPSP = \frac{\sum_{t=1}^{T} PDo}{\sum_{t=1}^{T} PD} * 100\ (\%) \quad (9)$$

Where:

PDo: Power demand no supplied by the system (W)
PD: Total power demand (W)
T: Period of time

Economical parameters

Up to now we have described the energy management strategies based on the H2RES2 simulator, allowing the analysis of the operational feasibility. Additionally the technical parameters have been observed, to understand how the H2RES2 simulator processes information for and evaluates the lifetime of the whole hybrid system, foreseeing a necessary displacement of devices.

To increase feature advantages of the H2RES2 simulator and complete it with respect to the simulators reviewed in Section "Introduction", a cost analysis is included. This allows the user to study the operational, technical and the economic viability of its project.

Nowadays, one of the drawbacks in renewable energy-based technologies is their high costs [1,2,9]. Nevertheless, possible changes in the legislation as well as new energy policies (in fact today all this is very different depending on the country concerned) increase the demand of auto consumption and distributed generation based on renewable energies presents to a remarkably boom in the upcoming decades. Moreover, in isolated applications, renewable energy sources-based hybrid systems are already economically justified.

To carry out an economic analysis of all the devices which integrate the hybrid system, the H2RES2 simulator involves the costs associated with each element as well as the lifetime of each, in order to compare the economic viability and the system behavior for different configurations.

Remembering the primary goal of the simulator, being a software tool to study different energy management strategies, the H2RES2 simulator takes those parameters into account, which vary during the operation and lifetime of the system. These parameters conclude the Operation & Maintenance and degradation costs.

Unitary cost function for each element

The H2RES2 simulator includes the expression that models the total costs of each element, according to Eq. (10). This unitary cost function, particularized by each element, reflects the contribution of the acquisition costs, its operation and maintenance costs, the expected lifetime and the expected lifetime of the whole hybrid system.

$$Cx(€) = Cox|_{L_x} + CO\&Mx * \left(\frac{i(1+i)^n}{(1+i)^n - 1}\right)$$

$$Cox|_{L_x} = \begin{cases} Cox, & if\ L_X \geq L_S \\ \sum_{1}^{r} Cox * \left(\frac{i(1+i)^{L_X * r}}{(1+i)^{L_X * r} - 1}\right), & if\ L_X < L_S \end{cases} \quad (10)$$

$$r = \frac{L_S}{L_X}$$

Where,

Cx: Unitary cost function for device x (€)
Cox: Acquisition cost of the device x (€)
$Cox|_{L_x}$: Actualized acquisition cost depending on lifetime (€)
L_{HS}: Lifetime of the hybrid system (years)

L_X: Lifetime of device x (years)
$CO\&Mx$: Operation & Maintenance costs of the device x (€)
i: Annual interest rate (%)
n: Years
r: Number of expected replacement of device x

As it can be observed in Eq. (10), the effect of interest rates or inflation is considers the costs for each element, including the annual interest rate, the number of years and its lifetime. In case the user needs to change this relation, he can modify the interest rate expression by its own auxiliary function. Nevertheless, as has been mentioned before, the H2RES2 is not meant to provide an economic analysis software tool but its goal is to test different energy management strategies, evolving simulations in a one-year period.

Distinguishing the elements, of solar panels and wind turbines, their useful lifetime coincides practically with the expected lifetime of the whole hybrid system (20–25 years), so we just have to compute the acquisition costs at the beginning of the project.

Additionally, for those elements whose expected lifetime depends on operating conditions, such as the battery bank, the electrolyzer and the fuel cell, it is necessary to integrate the degradation expressions (please see Section "Technical parameters") into the expected lifetime model.

The associated lifetime of the electrolyzer is depending on the number of operation cycles and the maximum expected operation cycles according to the following expression (11):

$$L_{ELEC} = \frac{ELEC_{CYCLE\_MAX}}{ELEC_{CYCLE}} * t\ (years) \tag{11}$$

Where,

L_{ELEC}: Electrolyzer expected lifetime (years)
$ELEC_{CYCLE\_MAX}$: Maximum expected start–stop cycles for the electrolyzer during its lifetime
$ELEC_{CYCLE}$: Accumulated start–stop cycles of the electrolyzer
t: Accumulated operating time (years)

On the other hand, in case of the fuel cell, the simulator includes the degradation costs depending on the maximum voltage losses of expression (12). The fuel cell degradation is determined by the operation cycles and operation time, as it was studied in Section "Fuel cell deterioration":

$$L_{FC} = \frac{LOSS_{FC\_MAX}}{LOSS_{FC}} * t\ (years) \tag{12}$$

Where,

L_{FC}: Fuel cell expected lifetime (years)
$LOSS_{FC\_MAX}$: Maximum voltage losses permitted for the fuel cell operation (V/cell)

And finally, in case of the battery bank, the H2RES2 simulator calculates two expressions for the lifetime parameter ((13) and (14)). The first one depends on the operation cycles, while the second one depends on the capacity losses respect to its initial value (please see Annex A. Lead-acid battery. State of charge estimation). Comparing results from both expressions, the one which provides the highest degradation value determines the lowest battery bank lifetime, and this one will be chosen by H2RES2 simulator for a conservative design.

$$L_{BAT} = \frac{BAT_{CYCLE\_MAX}}{BAT_{CYCLE}} * t \tag{13}$$

$$L_{BAT} = \frac{C_{NOM0} * 0.2}{\Delta C_{NOM}} * t \tag{14}$$

Where,

L_{BAT}: Battery expected lifetime (years)
BAT_{CYCLE_MAX}: Maximum expected battery operation cycles associated with DOD design
BAT_{CYCLE}: Accumulated battery operation cycles
C_{NOM0}: Initial nominal battery capacity
ΔC_{NOM}: Battery nominal capacity degradation
t: Accumulated operating time (years)

System cost function

The cost function of the whole system includes all the unitary cost functions calculated for each element. Additionally, in case of non-isolated systems, the H2RES2 simulator includes a term associated with the costs derived from the energy acquisition from the grid, or the benefits of energy injection in situations of energy excess. These factors can be decisive when choosing one or another energy management strategy. The cost function of the overall system is presented in Eq. (15).

$$C(€) = \sum Cx + C_{GRID} \tag{15}$$

Where,

C: Overall system cost (€)
C_{GRID}: Grid operation cost (€)

The grid operation cost is calculated as following:

$$C_{GRID} = E_{GRID\_IN} * C_{GRID\_IN} - E_{GRID\_OUT} * C_{GRID\_OUT} \tag{16}$$

Where,

E_{GRID_IN}: Input energy from the grid to the hybrid system (kWh)
C_{GRID_IN}: Cost to buy energy from grid (€/kWh)
E_{GRID_OUT}: Output energy from the hybrid system to the grid (kWh)
C_{GRID_OUT}: Cost to sell energy to grid (€/kWh)

Simulation case

Summarizing what has been presented up to now, a general description of the H2RES2 simulator has been done (description based on simulator structure, implementation and user interface) as well as a review of the energy management strategies that the H2RES2 simulator develops and the sensitivity analysis it offers according to studied technical and economic parameters.

Arriving at this point and in order to show the correct operation of the simulator as well as to know its genuine features, two simulation cases have been developed. For this purpose, authors have selected an energy management strategy based on hysteresis bandwidth, with a variable operating mode for the fuel cell and the electrolyzer. In the first simulation case, a detailed description of obtained results is presented attending to the power balance and technical and economic parameters. The second simulation case is proposed to show the sensitivity analysis allowed by the H2RES2 simulator.

Case I

For this case, the equipment characteristics like sizing, power rate, costs and degradation parameters of each element are shown in Table 2. There are 95% and 60% SOC values chosen for SOCmax and SOClow, in order to charge the batteries as much as possible and keep the maximum DOD under recommended values to keep a higher useful lifetime.

The system configuration, cost and degradation parameters as well as the weather and the load profile (Fig. 10), are based on a real prototype implementation developed by different authors [45,46].

In Fig. 11 the different results obtained for the simulation case are presented.

These results monitor the system behavior under energy excess and deficit situations, based on the hysteresis band strategy studied in Section "Hysteresis".

In Fig. 11 the battery bank SOC value is presented, which determines the charge state of the system. As it is presented, during the summer months the battery SOC is always remarkably high due to the high solar energy generation. During this period hydrogen is produced by electrolysis processes until the metal hydride tanks reach their maximum level (see Fig. 11, days 50–80) Then the energy excess is injected to the grid in order to keep the power balance at all time (Fig. 11, days 80–285).

Table 2 – Parameters selected for the simulation case I.

Sim. time: 1 year			
Element	**Resource**	**BAT SOC**	**%**
PV	7.5 kW	SOCmax	95
WT	2 kW	SOCelemin	90
MH	20 Nm^3	SOCH2	85
ELEC	5 kW, 1 Nm^3	SOCfcmax	75
FC	3.4 kW × 2	SOCmin	70
BAT	400 V, 100 Ah	SOClow	60
Equipment cost	**Units**		
CO&MFC	0.6 €/h		
CO&MELEC	0.1 €/h		
C_{GRID_IN}	0.136 €/kWh		
C_{GRID_OUT}	−0.03 €/kWh		
CoFC	8000 €		
CoELEC	75,000 €		
CoBAT	7650 €		
Degradation	**Units**		
V_{time}	9 μV/cell/h		
V_{cyc}	48 μV/cell/cyc		
ΔV_{FC_max}	150 mV/cell		
$N_{ELECcycmax}$	5000 cycles		

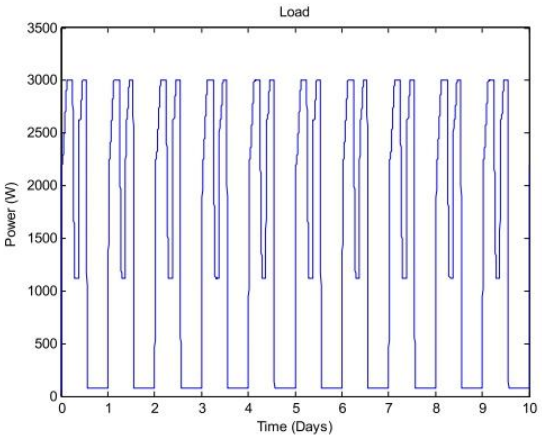

Fig. 10 – Load profile.

On the other hand, during winter months, the system experiences a constant energy deficit due to the low solar generation. During this period, the battery bank is more requested and therefore, the battery SOC is lower than the previous one.

In order to preserve the defined SOClow value, the fuel cell is used while the hydrogen resource is available. In the case that fuel cell generation is too low or zero, the grid (in an uninsulated configuration of course) will supply the necessary energy to guarantee the power balance and the minimum SOC value.

To detail the system behavior explained above, Figs. 12–17 show the SOC values, the hydrogen consumption and generation and the fuel cell, the electrolyzer and the grid power for different days and energy situations.

In the case of an energy deficit situation (days between 304 and 310), it is seen, how the battery reaches its minimum level, and the fuel cell operates in order to keep it. In this case, the fuel cell supplies the demand under variable operation mode. When there is enough energy to charge the battery, the fuel cell stops according to the hysteresis-band operation.

Finally, when the hydrogen stock is very low (from days 306–310), the fuel cell is not able to generate any energy, so it is the grid's responsibility to assure the demanded energy and keep the SOClow level balanced.

In the case of an energy excess situation (days 75–80), the battery SOC reaches its maximum value. The electrolyzer's start conditions are defined. The electrolyzer needs the extra energy of 1 kW of the minimum power operation condition (minimum power to start the electrolysis).

The overall simulation parameters are summarized in Table 3.

As we can extract from Table 3, the H2RES2 simulator provides all the electrical, technical and economic parameters necessary to perform a sensitivity analysis based on different energy management strategies.

Case II. Sensitivity analysis example

In order to show how to develop a sensitivity analysis with the H2RES2 simulator, a second case is simulated. In this case the

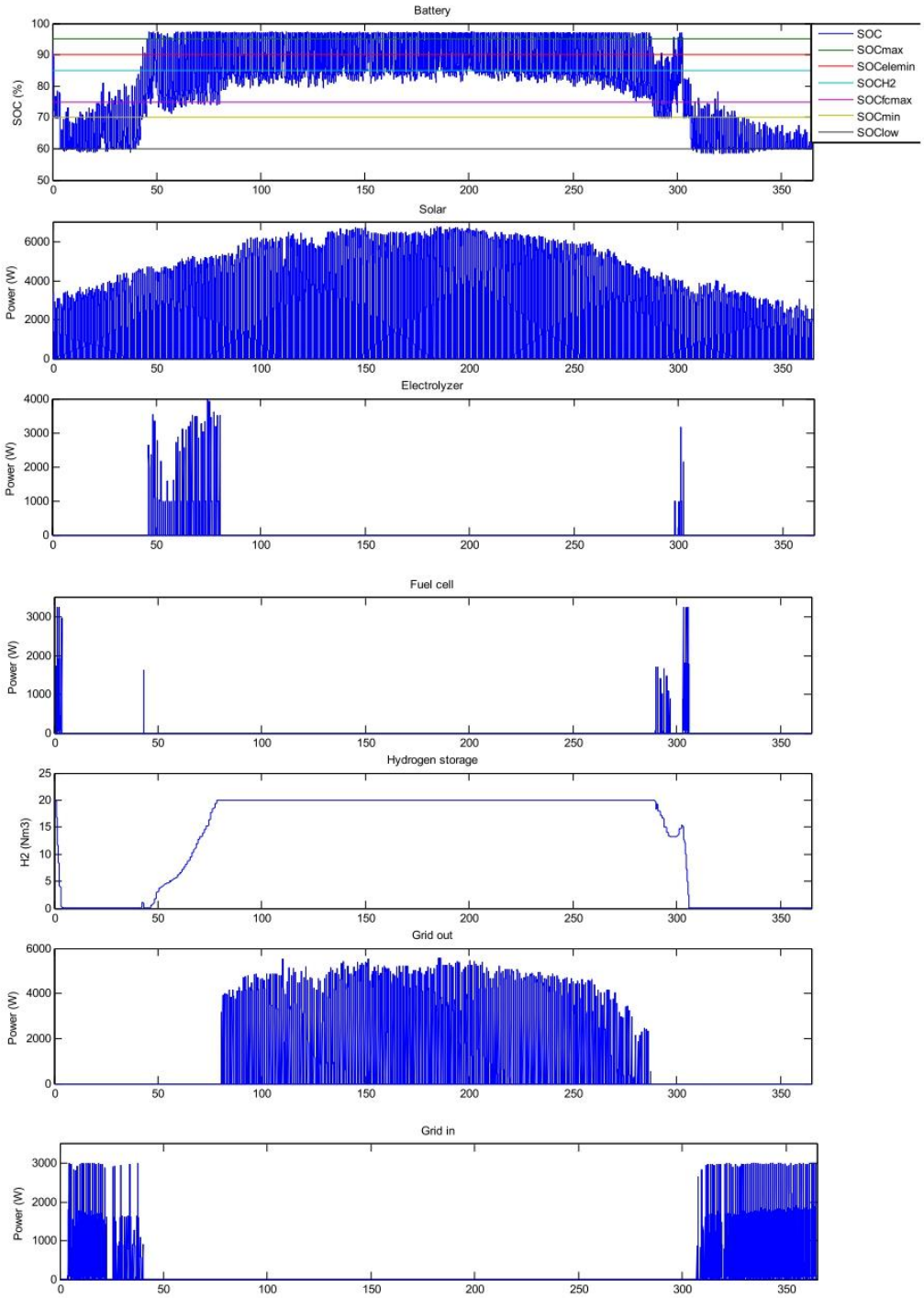

Fig. 11 – Overall system simulation results.

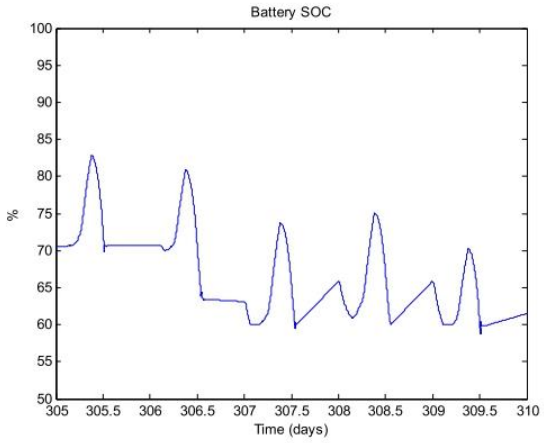

Fig. 12 – Battery SOC under energy deficit situation.

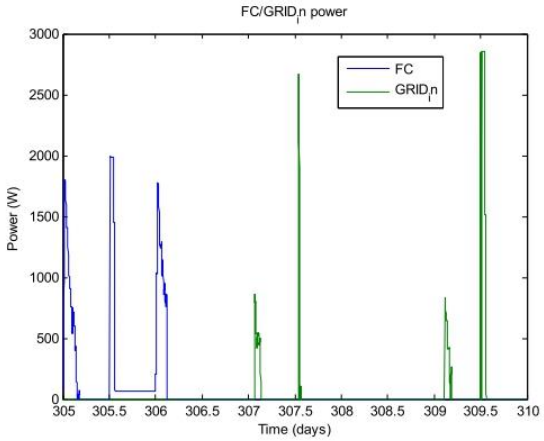

Fig. 13 – Fuel cell and grid power during energy deficit situation.

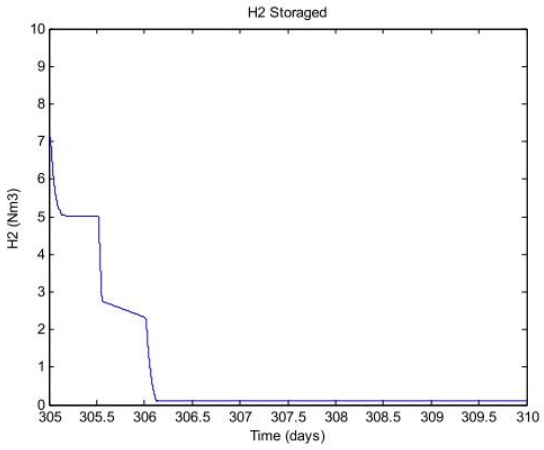

Fig. 14 – Hydrogen level in metal hydride tanks.

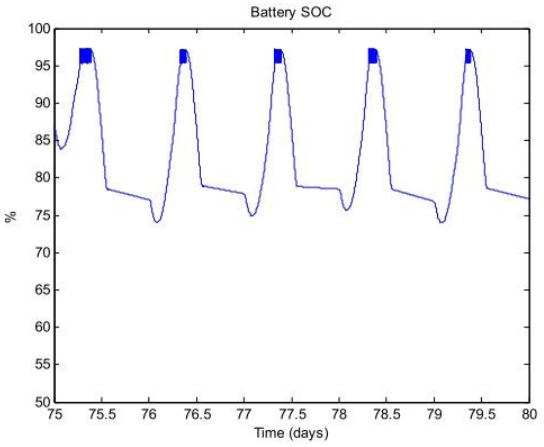

Fig. 15 – Battery bank SOC under energy excess situation.

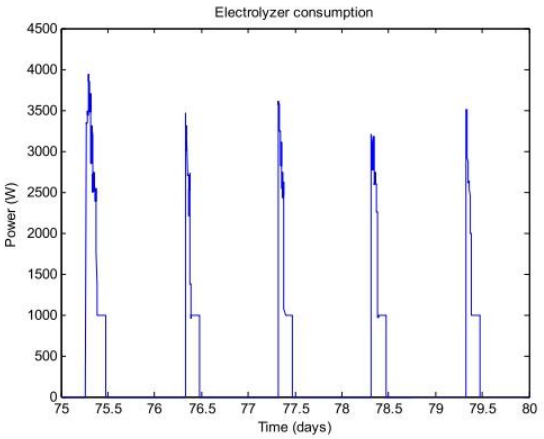

Fig. 16 – Electrolyzer power during energy excess situation.

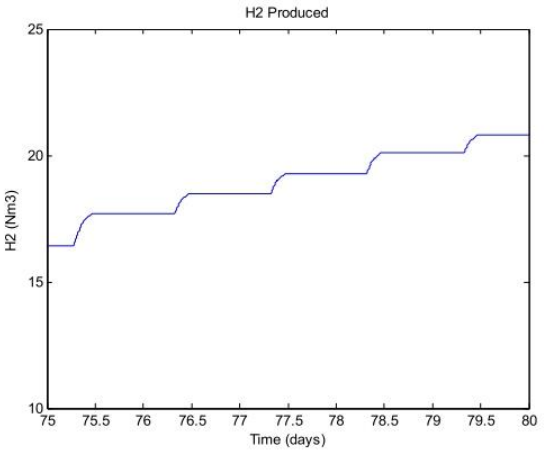

Fig. 17 – H_2 production during energy excess situation.

Table 3 – Summary of technical–economical parameters.

E_{GRID_IN} (kWh)	710.47
E_{GRID_OUT} (kWh)	2908.397
E_{ELEC} (kWh)	180.33
E_{FC} (kWh)	64.35
E_{BAT} (kWh)	2635.58
E_{LOAD} (kWh)	11,967.03
$LOSS_{CHA}$ (kWh)	209.54
$ELEC_{H_2}$ (Nm^3)	23.15
$ELEC_{CYCLE}$	39
$ELEC_{TIME}$ (h)	117.37
$FCI_{CYCLE}/FCII_{CYCLE}$	17/6
$FCI_{TIME}/FCII_{TIME}$ (h)	165.58/6.08
$\Delta V_{FCI}/\Delta V_{FCII}$ (mV/cell)	2.31/0.34
$N_{BATCcyc}$	68
ΔC_{NOM} (%)	2.12
LPSP (%)	5.94
CO&Mx (€)	1247.76

Table 5 – Summary of technical and economical parameters.

E_{GRID_IN} (kWh)	709.69
E_{GRID_OUT} (kWh)	2908.97
E_{ELEC} (kWh)	180.28
E_{FC} (kWh)	65.08
E_{BAT} (kWh)	2635.57
E_{LOAD} (kWh)	11,967.03
$LOSS_{CHA}$ (kWh)	209.54
$ELEC_{H2}$ (Nm^3)	23.14
$ELEC_{CYCLE}$	39
$ELEC_{TIME}$ (h)	117.32
$FCI_{CYCLE}/FCII_{CYCLE}$	31/15
$FCI_{TIME}/FCII_{TIME}$ (h)	128.97/6.3
$\Delta V_{FCI}/\Delta V_{FCII}$ (mV/cell)	2.65/0.78
$N_{BATCcyc}$	67
ΔC_{NOM} (%)	2.12
LPSP (%)	5.93
CO&Mx (€)	1263.81

different authors have eliminated the hysteresis bandwidth of the fuel cell operation (Table 4), maintaining the same SOCmin value and the rest of the simulation parameters similar to Case I.

According to the results obtained from Case I and Case II, Tables 3 and 5 respectively, we can state that the use of the hysteresis band mode can reduce the start–stop cycles of the fuel cell [45,46]. Besides, it requires higher operation time to reach the SOCfcmax value [45,46]. Depending on the hydrogen storage capacity, the difference between the fuel cell degradation of both strategies can be determined by one of the previous parameters.

In both cases, the hydrogen storage capacity is too low considering the demand. All the hydrogen resource is consumed and the fuel cell energy production is practically the same. However, the overall fuel cell degradation is higher in Case II due to the higher number of start–stop cycles. All of this causes a low increase in the fuel cell's costs (C_{FC}), and therefore an increase in the overall system costs.

Thanks to this sensitivity analysis, the user can propose different solutions for its simulation cases in order to minimize the equipment deterioration and the system costs. As an example, in the simulation case studied by various/the authors a possible solution increases the hydrogen storage capacity and allows a longer operating time of the fuel cell without start–stop cycles. This option reduces the degradation associated with operation time respect to the Case I.

Table 4 – Parameters defined for the simulation case II.

Sim. time: 1 year			
Element	**Resource**	**BAT SOC**	**%**
PV	7.5 kW	SOCmax	95
WT	2 kW	SOCelemin	90
MH	20 Nm^3	SOCH2	85
ELEC	5 kW, 1 Nm^3	SOCfcmax	70
FC	3.4 kW × 2	SOCmin	70
BAT	400 V, 100 Ah	SOClow	60
Equipment cost	**Units**		
CO&MFC	0.6 €/h		
CO&MELEC	0.1 €/h		
C_{GRID_IN}	0.136 €/kWh		
C_{GRID_OUT}	−0.03 €/kWh		
CoFC	8000 €		
CoELEC	75,000 €		
CoBAT	7650 €		
Degradation	**Units**		
V_{time}	9 μV/cell/h		
V_{cyc}	48 μV/cell/cyc		
ΔV_{FC_max}	150 mV/cell		
$N_{ELECcycmax}$	5000 cycles		

Conclusions

There is an increasing commitment of governments and companies to change their energy policies, orienting them towards higher energy efficiencies and renewable energy sources. This leads to the need of a control system required by hybrid renewable energy-based systems to manage the energy supplied by each source ensuring safe operation and fulfilling the objectives. This control system must be based on a proper energy management strategy which guarantees the load supply, increases the lifetime of the elements, reduces the operating costs, and therefore maximizes the system performance and providing a technical and economical feasible solution. For this purpose the use of software tools which allow us to perform simulations and previous analysis before the real implementation is necessary.

The software tools found in the scientific literature include some restrictions, so that the development of new simulators is necessary. The H2RES2 simulator presented in this paper overtakes these restrictions and it allows the testing of different energy management strategies, providing simulations in the short-term time scale. Additionally it offers a sensitivity analysis attending to costs and lifetimes of the devices which are integrated in the hybrid power system. The presented simulator allows the user to choose a configuration and management strategy using a user-friendly interface, providing a useful tool which offers detailed information for

technical and economic data analysis, that is needed before any genuine implementation is possible. Additionally, the H2RES2 simulator has been developed in MATLAB Simulink environment adding helpful computing power and security.

Simulation cases studied in the last section demonstrate a proper H2RES2 performance and show its features: energy management strategy selection as well as a technical and economic study.

Future work

The H2RES2 is in a constant evolution process in order to expand its architecture (generators, elements backups and kind of loads) and integrate new tools and functions to improve it.

New economic functions are developed in order to test the effect of interest rates of inflation over the economical results for long term simulations.

As a future task, H2RES2 simulator may also be used as a SCADA (Supervisory Control And Data Acquisition) system, taking advantage of all the previous studies performed under simulation conditions. This involves the integration of sensors replacing the previous simulation variables and communication protocols of electronics and the PC hosting the SCADA system. Finally, new kinds of elements and different nature elements are going to be added in order to increase the applications range of H2RES2.

Annex A. Simulator. Hybrid system models

Since the H2RES2 Simulator is intended to be a tool for testing different energy management strategies, it is not necessary to use excessively complex models that require a tedious programming. The models used for the generators and auxiliary elements have been widely studied; they are based on empirical curves and parameters obtained from technical documentation, so they represent faithfully the behavior of different elements of the real systems.

Renewable resources and demand

Renewable resources

Solar radiation will be an input parameter to H2RES2 simulator so it can be adapted to different weather resources of different locations. The radiation series is considered to be a file data with radiation data of every 10 min expressed in W/m^2.

Solar radiation and wind speed are other possible input parameters for the H2RES2 simulator, that are used to estimate the production of the wind turbine. Wind speed series is a file with speed data every 10 min expressed in m/s.

Demand

H2RES2 allows to define different load profiles. The goal is a simulator with the possibility to simulate both, typical demand profiles and extreme conditions, in order to analyze the system response. The demand load profile must have at least involved data of every 10 min expressed in watts.

Photovoltaic panels

Photovoltaic (PV) panels are arrays of serial and parallel connections. The model used to represent them is based on the empirical behavior of the panel current and voltage regarding the radiation and operating temperature. According to Figs. A1 and A2, in a PV panel the behavior of the short circuit current regarding the incident irradiance is almost linear. Conversely, the open circuit voltage hardly suffers variations with irradiance, so it can be assumed as practically independent of it [20].

In the same way, the short circuit current is maintained virtually invariant with respect to the cell temperature. The open circuit voltage behaves similar to a linear function with a negative slope [20].

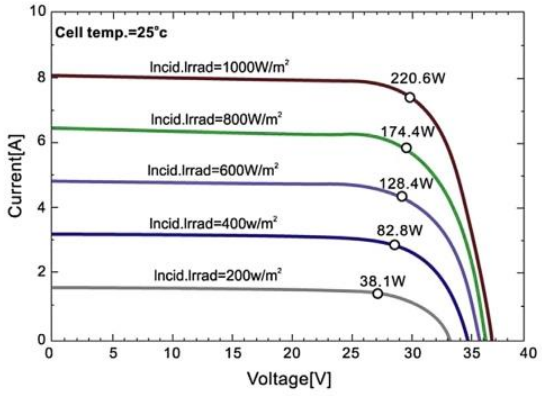

Fig. A1 – PV (60 cells) polarization curves dependency with irradiance.

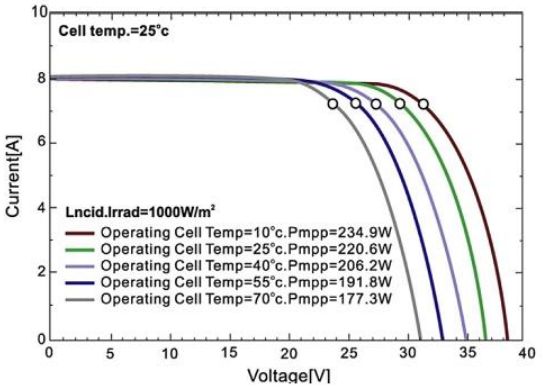

Fig. A2 – PV (60 cells) polarization curves dependency with cell temperature.

Based on the above, the equations that model the behavior of a PV panel regarding the irradiance (G) and temperature (T) can be written with a good approximation as:

$$Isc(G,T) = Isc_{ref} * G/G_{ref} \quad (1)$$

$$Voc(G,T) = V_{OCref} * (1 - kv * T_{cell}) \quad (2)$$

Where,

I_{SC} : PV panel short circuit current (A)
Isc_{ref}: PV panel short circuit current (A) at reference irradiance
V_{OC} : PV panel open circuit voltage (V)
V_{OCref} : PV panel open circuit voltage at reference temperature (V)
G_{ref} : Reference irradiance (W/m^2)
G : Incident Irradiance (W/m^2)
T_{cell}: Cell temperature (°C)
kv: Voltage temperature coefficient (V/°C)

To calculate the generated power at any irradiance, it is common to use the NOCT (Nominal operating cell temperature) conditions as reference, because it determines real power, voltage and current under nominal cell temperature operation. Then the generated power dependence with irradiance follows expression (3):

$$P(G) = P_{NOCT} * G/G_{NOCT} \quad (3)$$

Where,

P_{NOCT} : Generated power at NOCT condition (W)

After this, for given conditions of irradiance and cell temperature, the real generated power by the PV panel can be calculated from Eq. (4):

$$P(G,T) = P(G) * (1 - K_{PT} * T_{cell}) \quad (4)$$

Where,

K_{PT} : Thermal power variation coefficient (W/°C)

Finally, to calculate the cell temperature (°C) we can use Eq. (5) [20]:

$$T_{cell} = T_{amb} + \frac{T_{NOCT} - 20}{G_{NOCT}} * G \quad (5)$$

Wind turbines

The wind turbine model used in H2RES2 is based on the power curve relating the generated power with the wind speed and referring to electrical and mechanical losses.

According to Ref. [22], we can define the following areas in a wind turbine power curve (Fig. A3):

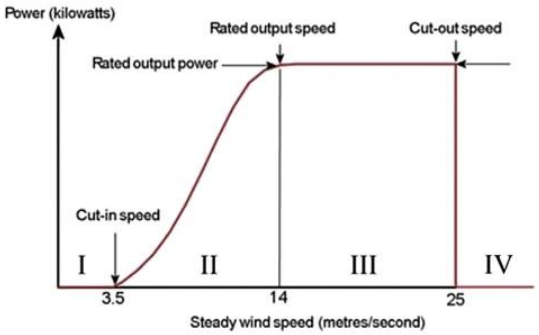

Fig. A3 – Wind turbine power curve.

Zone I: This zone corresponds to the area between a null and the cut-in wind speed.

Zone II or partial cargo area: This area is defined by the cut-in speed and the operation rated speed of the machine. In this area, the generated power is lower than the nominal power and it follows a cubic function with respect to the wind speed.

Zone III or full load area: In this area the wind speed is higher than the rated speed. To avoid any damage in the wind turbine, it is common to use a power control technique whose aim is to keep the machine running at rated power.

Zone IV: This area is defined by wind speeds higher than the cut-out speed. In order to protect the wind turbine, mechanical breaking techniques are used to cut down the generation.

Expression (6) shows the relation of generated power regarding wind speed, differencing each above described zones.

$$P_{WT} = \begin{cases} 0; \ v \le v_{cut-in} \\ \eta_m \eta_e Cp \frac{1}{2} \rho A v^3; \ v_{cut-in} < v < v_{rated} \\ \eta_m \eta_e P_N; \ v_{rated} \le v \le v_{cut-out} \\ 0; \ v_{cut-out} < v \end{cases} \quad (6)$$

Where,

η_m: Mechanical efficiency of the wind turbine
η_e: Electrical efficiency of the wind turbine
Cp: Power coefficient
ρ: Air density (kg/m^3)
A: Rotor area (m^2)
v: Wind speed (m/s)
P_N: Nominal power of the wind turbine

Lead-acid battery

For the needs of the H2RES2 simulator, the energy that the battery is able to absorb and the transfer during the charging/discharging cycles is modeled. It is necessary to model the

battery state of charge (SOC) as well, due to the fact, that it represents a fundamental decision parameter in every energy management strategy. It determines start–stop conditions of other elements of the system.

Battery electrical model

The battery electrical model is obtained from its Thevenin simplification (Fig. A4). From here we can propose the battery current dependence on the net power (Eq. (7)) and consequently the battery voltage, (Eqs. (8) and (9)) according to Ref. [23].

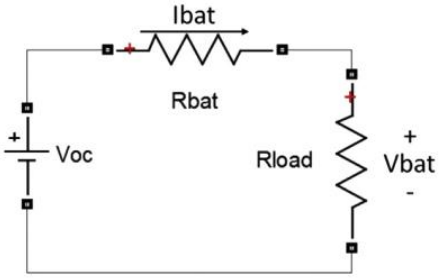

Fig. A4 – Battery simplified model.

$$I_{BAT} = \frac{P_{net}}{V_{BAT}} \quad (7)$$

$$V_{BAT} = V_{oc} - I_{BAT} * R_{BAT} \quad (8)$$

$$R_{BAT} \cong \left(\frac{1.89}{SOC} - 0.0150\right) \quad (9)$$

Where,

P_{net} : Net battery power (W)
I_{BAT}: Battery current (A)
V_{BAT}: Battery terminal voltage (V)
V_{oc}: Battery open circuit voltage (V)
R_{BAT}: Battery internal resistance (Ω)

State of charge estimation

In H2RES2 simulator *Coulomb counting method* has been used as SOC estimator.

SOC estimator algorithm. The Coulomb counting method calculates the capacity balance during charging and discharging processes. To improve the algorithm accuracy, it is necessary to use short time samples and high accuracy sensors. However, this method is an open loop estimator, so external correction after a certain period of time is required [23,55].

The equation that models the Coulomb algorithm is presented in Eq. (10):

$$SOC(t) = SOC(0) \pm \int_0^t \frac{I_{BAT}(t) * \eta_C\ (t)\ dt}{Cap(t)} \quad (10)$$

Where:

SOC(0): Initial battery SOC value (%)
$I_{BAT}(t)$: Battery current (A)
η_C (t): Coulomb efficiency (%)
Cap(t): Battery current capacity (Ah)

Equation (10) can be solved using numerical integration (11):

$$SOC\ (t) = SOC(t-1) \pm \frac{\eta_C\ (t) * I_{BAT}(t) * \Delta t}{Cap\ (t)} \quad (11)$$

These expressions can be separated for charging process:

$\eta_C < 100\ \%$

$$Cap(t) = Cnom(t)$$

Where Cnom is the nominal capacity of the battery.

And discharging process, according to Peuckert' law:

$\eta_C \cong 100\ \%$

$$Cap(t) = \frac{Cnom(t) * I^{1-n}}{Inom^{1-n}}$$

Where Cnom integrates the deterioration associated with the different charging/discharging processes.

Electrolyzer

There are several electrolyzer technologies in the market, while alkaline electrolysis is the most widely used, due to its price and demonstrated performance [24,25]. Reactions occurring within an electrolytic cell regardless of the technology are:

$$\text{Anode}: \ 2OH\ aq \rightarrow 1/O_2\ g + H_2O + 2e^- \quad (12)$$

$$\text{Cathode}: \ H_2O + 2e^- \rightarrow 1/2H_2 + 2\ OH\ aq \quad (13)$$

Hydrogen production

As opposed to what happens with photovoltaic panels and wind turbines as electrolyzers, it is not very common to find power-hydrogen generation curves in its technical characteristics. For this reason authors have opted for using a model based on Faraday's law, which relates the amount of input current regarding the produced hydrogen [26,57].

$$\text{mols } H_2 = \frac{\eta_F * I_{ELEC} * t}{F * z} \quad (14)$$

Where,

η_F: Faraday's efficiency
I_{ELEC}: Electrolysis current (A)
t: Time (s)
F: Faraday's constant (96,485 C/mol)
z: Number of electrons which play in the reaction (z = 2)

According to the electrical power definition and considering the nominal operation voltage, a relationship between input power and hydrogen production is easily found (15):

$$P_{ELEC} = V_{ELEC} * I_{ELEC} \Rightarrow \text{mols } H_2 = \frac{\eta_F * P_{ELEC} * t}{F * z * V_{ELEC}} \quad (15)$$

In a real system this expression needs to be corrected to take into account the auxiliary loads consumption (P_{aux}). Auxiliary loads usually represent 10–20% of the total consumed power, and mainly used to feed the refrigeration system, and the control and operation electronics. Finally, expression (16) allows the calculation of the hydrogen production based on the supplied power and the auxiliary loads consumption:

$$\text{mol } H_2 = \frac{\eta_F * (P_{ELEC} - P_{aux}) * t}{F * z * V_{ELEC}} \quad (16)$$

Fuel cell

In a fuel cell, the processes of oxidation and reduction of hydrogen and oxygen at the anode and cathode respectively follow the equations:

$$\text{Anode}: 2H_2 \rightarrow 4H^+ + 4e^- \quad (17)$$

$$\text{Cathode}: O_2 + 4e^- + 4H^+ \rightarrow 2H_2O \quad (18)$$

Fuel cell power curve model

In the case of fuel cells, polarization and power curves in technical documentation are commonly provided by manufacturers. Taking advantage of this, the model used by the H2RES2 simulator corresponds to the least squares method of the voltage versus current curve provided by the manufacturer (19). The greater number of points that are used is, the better the accuracy achieved. Fig. A5 shows the real performance of a fuel cell developed by authors and based on the stack FC1020 from Ballard® [44].

$$V_{FC} = a * I_{FC}^3 + b * I_{FC}^2 + c * I_{FC} + d \quad (19)$$

$$P_{FC\_gross} = V_{FC} * I_{FC} \quad (20)$$

Where,

V_{FC}: Fuel cell voltage (V)
I_{FC}: Fuel cell current (A)
P_{FC_gross}: Gross power generated (W) by the fuel cell

Fuel cell consumption model

Similar to what was done in electrolyzer modeling, the Faraday's law will be used again to calculate the hydrogen consumption based on the fuel cell operating point [27,28]. Knowing the operation point of the fuel cell, the hydrogen consumption can be determined.

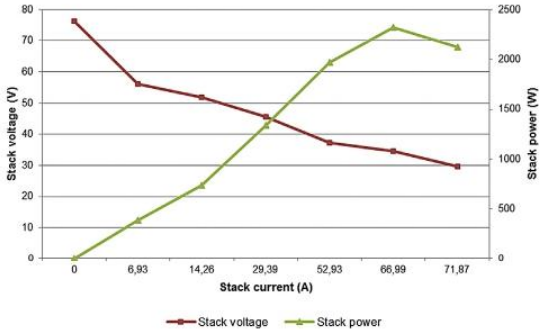

Fig. A5 – V–I, P–I curve for FC1020 from Ballard®.

$$\text{mol } H_2 = \frac{I_{FC} * t}{F * z * Eff} \quad (21)$$

Where,

mol H_2: Produced hydrogen (mol)
Eff: Fuel cell efficiency (%)

The efficiency is calculated from the quotient between the electrical power produced by the fuel cell and the hydrogen heat power, expression (22):

$$Eff = \left(\frac{P_{FC_{gross}}}{P_{H_2}}\right) = \frac{V_{FC} * I_{FC}}{\text{mol } H_2 * LHV * I_{FC}} \quad (22)$$

Where,

$P_{FC_{gross}}$: Fuel cell output power (W)
P_{H_2}: Chemical power associated to determined hydrogen consumption (W)
LHV: Hydrogen lower heating value

Hydrogen storage

Regarding hydrogen storage, H2RES2 simulator implements the two most widely used hydrogen storage technologies currently: pressurized gas and metal hydrides.

Pressurized gas

The considered parameters regarding pressurized hydrogen in a tank are the hydrogen input (Nm^3) (this hydrogen has been generated by the electrolyzer), consumed hydrogen by the fuel cell, initial level of the hydrogen tank (H_{2_0}), as well as the maximum and minimum levels which guarantee the proper tank operation. Since the input and output flow rate capacity is higher than metal hydrides tanks can support, it can be assumed, that the flow rate is imposed by the maximum capacity of hydrogen absorption of metal hydrides tanks.

The hydrogen balance inside the tank is given at every moment by the amount of hydrogen input and hydrogen output, adding the initial hydrogen stock.

$$H_2(Nm^3) = H_{2\_in} - H_{2\_out} + H_{2\_0} \quad (23)$$

Metal hydrides tank

Unlike high pressure tanks, metal hydrides tanks need a power supply to stabilize the temperature of the cooling water during the hydrogen charge and discharge processes. This means that the power consumption by hydride metals can be considered as another load with respect to the power balance. The metal hydrides model includes the hydrogen balance, similar to the one for high-pressure tanks, and a model that reflects the power consumption of the cooling system.

The power consumption of the cooling system can be obtained from the manufacturer's data, and in general it is given as a function of the input/output hydrogen flow rate. Given a particular operation flow rate, it is possible to calculate the metal hydride tanks power consumption according to expression (24):

$$P_{HM} = FR_{H_2} * P_{cool}\ (H_2) \quad (24)$$

Where,

P_{HM}: Metal hydride tank power consumption (W)
FR_{H_2}: Inlet/outlet hydrogen flow rate (Nm^3/h)
P_{cool} (H_2): Cooler/heater power consumption per Nm^3/h (W)

To distinguish the charging and discharging process of the metal hydride tanks, the model includes a way to check the derivative of the hydrogen balance. If the derivative is not zero, the metal hydride tank is charging or discharging and the derivative sign will define it.

The hydrogen balance model is similar to the high pressure tank model. The model takes considers the hydrogen input (from high pressure tank), the hydrogen output (towards the fuel cell), the initial hydrogen level and the maximum and minimum limits which ensure the safe operation of the system.

Grid

As it has been mentioned above, H2RES2 allows modeling isolated or grid connected hybrid power systems.

In case of grid connected systems, the grid is represented by a model that is recommended to solve two different situations (deficit and overproduction). In energy deficit situations, the grid behaves as an additional generator that injects the needed power to guarantee the power balance of the system.

On the other hand, when the system provide an over production, the grid is supposed to behave as a variable charge that consumes as much power as needed to achieve the power balance.

Finally, in case of isolated applications, the *grid* concept which appears in the simulator defines and allows quantifying the energy deficit or energy overproduction of the studied hybrid system. This parameter indicates the difference between the generated and the consumed energy, providing the user an opportunity to test the viability of his configurations. Based on the obtained results, the user is enabled to look over the proposed energy management strategy and the system sizing.

REFERENCES

[1] Tégani I, Aboubou A, Ayad MY, Becherif M, Bahri M. Power flow management in WT/FC/SC hybrid system using flatness based control. In: 3rd Int Symp Environ Friendly Energies Appl EFEA 2014; 2014. http://dx.doi.org/10.1109/EFEA.2014.7059962.

[2] Feroldi D, Degliuomini LN, Basualdo M. Energy management of a hybrid system based on wind–solar power sources and bioethanol. Chem Eng Res Des 2013;91:1440–55. http://dx.doi.org/10.1016/j.cherd.2013.03.007.

[3] Fathima AH, Palanisamy K. Optimization in microgrids with hybrid energy systems – a review. Renew Sustain Energy Rev 2015;45:431–46. http://dx.doi.org/10.1016/j.rser.2015.01.059.

[4] Dufo-López R, Bernal-Agustín JL, Contreras J. Optimization of control strategies for stand-alone renewable energy systems with hydrogen storage. Renew Energy 2007;32:1102–26. http://dx.doi.org/10.1016/j.renene.2006.04.013.

[5] El-Shatter TF, Eskander MN, El-Hagry MT. Energy flow and management of a hybrid wind/PV/fuel cell generation system. Energy Convers Manag 2006;47:1264–80. http://dx.doi.org/10.1016/j.enconman.2005.06.022.

[6] Baumann L, Boggasch E, Rylatt M, Wright A. Energy flow management of a hybrid renewable energy system with hydrogen. IEEE Conf Innov Technol Effic Reliab Electr Supply 2010:78–85.

[7] Wang C, Nehrir MH. Power management of a stand-alone wind/photovoltaic/fuel cell energy system. IEEE Trans Energy Convers 2008;23:957–67. http://dx.doi.org/10.1109/TEC.2007.914200.

[8] Cau G, Cocco D, Petrollese M, Knudsen Kær S, Milan C. Energy management strategy based on short-term generation scheduling for a renewable microgrid using a hydrogen storage system. Energy Convers Manag 2014;87:820–31. http://dx.doi.org/10.1016/j.enconman.2014.07.078.

[9] Mbarek E, Belhadj J, Le BP, Tunis B. Photovoltaic wind hybrid system integrating a Permanent Exchange Membrane Fuel Cell (PEMFC). Int Multi-Conference Syst Signals Devices 2009;2009:1–6. http://dx.doi.org/10.1109/SSD.2009.4956782.

[10] L. Arribas, G. Bopp, M. Vetter, A. Lippkau, K. Mauch, Worldwide overview of design and simulation tools for hybrid PV systems. International Energy Agency (IEA), Report IEA-PVPS T11-01:2011

[11] Sinha S, Chandel SS. Review of software tools for hybrid renewable energy systems. Renew Sustain Energy Rev 2014;32:192–205. http://dx.doi.org/10.1016/j.rser.2014.01.035.

[12] Lambert T, Gilman P, Lilienthal P. Micropower system modeling with Homer. Integr Altern Sources Energy 2006:379–418. http://dx.doi.org/10.1002/0471755621.ch15.

[13] Connolly D, Lund H, Mathiesen BV, Leahy M. A review of computer tools for analysing the integration of renewable energy into various energy systems. Appl Energy 2010;87:1059–82. http://dx.doi.org/10.1016/j.apenergy.2009.09.026.

[14] Turcotte D, Ross M, Sheriff F, Blvd L, Tel C. Photovoltaic hybrid system sizing and simulation tools. 2001. p. 1–10.

[15] Layadi TM, Champenois G, Mostefai M, Abbes D. Lifetime estimation tool of lead–acid batteries for hybrid power sources design. Simul Model Pract Theory 2015;54:36–48. http://dx.doi.org/10.1016/j.simpat.2015.03.001.

[16] Chen H, Pei P, Song M. Lifetime prediction and the economic lifetime of Proton Exchange Membrane fuel cells. Appl Energy 2015;142:154–63. http://dx.doi.org/10.1016/j.apenergy.2014.12.062.

[17] Bae SJ, Kim S-J, Park JI, Park CW, Lee J-H, Song I, et al. Lifetime prediction of a polymer electrolyte membrane fuel cell via an accelerated startup–shutdown cycle test. Int J Hydrogen Energy 2012;37:9775–81. http://dx.doi.org/10.1016/j.ijhydene.2012.03.104.

[18] Little M, Thomson M, Infield D. Electrical integration of renewable energy into stand-alone power supplies incorporating hydrogen storage. Int J Hydrogen Energy 2007;32:1582–8. http://dx.doi.org/10.1016/j.ijhydene.2006.10.035.

[19] Segura F, Durán E, Andújar JM. Design, building and testing of a stand alone fuel cell hybrid system. J Power Sources 2009;193(1):276–84. http://dx.doi.org/10.1016/j.jpowsour.2008.12.111.

[20] Siv Helene Nordahl. Norwegian University of Science and Technology. Design of roof PV in Oslo.

[21] Vasallo MJ, Bravo JM, Andújar JM. Optimal sizing for UPS systems based on batteries and/or fuel cell. Appl Energy 2013;10:170–81. http://dx.doi.org/10.1016/j.apenergy.2012.12.058.

[22] Edition E. Gary L. Johnson. Wind energy systems.
[23] Pang SPS, Farrell J, Du JDJ, Barth M. Battery state-of-charge estimation. In: Proc 2001 Am Control Conf (Cat No01CH37148)2; 2001. p. 1644–9. http://dx.doi.org/10.1109/ACC.2001.945964.
[24] Rashid MM, Al Mesfer MK, Naseem H, Danish M. Hydrogen production by water electrolysis : a review of alkaline water electrolysis, PEM water electrolysis and high temperature water electrolysis. Int J Eng Adv Technol 2015;4:80–93.
[25] Symes D, Al-Duri B, Bujalski W, Dhir A. Cost-effective design of the alkaline electrolyser for enhanced electrochemical performance and reduced electrode degradation. Int J Low-Carbon Technol 2014;10(4):452–9. http://dx.doi.org/10.1093/ijlct/ctt034.
[26] Ulleberg I. Modeling of advanced alkaline electrolyzers: a system simulation approach. Int J Hydrogen Energy 2003;28(1):21–33. http://dx.doi.org/10.1016/S0360-3199(02)00033-2.
[27] Edition S, Virginia W. Fuel cell handbook. 2004.
[28] Hydrogen fuel: production, transport, and storage. Edited by Ram B. Gupta, CRC Press, 2008, ISBN 9781420045758
[29] Ipsakis D, Voutetakis S, Seferlis P, Stergiopoulos F, Papadopoulou S, Elmasides C. The effect of the hysteresis band on power management strategies in a stand-alone power system. Energy 2008;33:1537–50. http://dx.doi.org/10.1016/j.energy.2008.07.012.
[30] Ziogou C, Ipsakis D, Seferlis P, Bezergianni S, Papadopoulou S, Voutetakis S. Optimal production of renewable hydrogen based on an efficient energy management strategy. Energy 2013;55:58–67. http://dx.doi.org/10.1016/j.energy.2013.03.017.
[31] Tesfahunegn SG, Ulleberg Ø, Vie PJS, Undeland TM. Optimal shifting of photovoltaic and load fluctuations from fuel cell and electrolyzer to lead acid battery in a photovoltaic/hydrogen standalone power system for improved performance and life time. J Power Sources 2011;196:10401–14. http://dx.doi.org/10.1016/j.jpowsour.2011.06.037.
[32] Carapellucci R, Giordano L. Modeling and optimization of an energy generation island based on renewable technologies and hydrogen storage systems. Int J Hydrogen Energy 2012;37:2081–93. http://dx.doi.org/10.1016/j.ijhydene.2011.10.073.
[33] Leng Y, Chen G, Mendoza AJ, Tighe TB, Hickner MA, Wang CY. Solid-state water electrolysis with an alkaline membrane. J Am Chem Soc 2012;134:9054–7. http://dx.doi.org/10.1021/ja302439z.
[34] Leng F, Tan CM, Pecht M. Effect of temperature on the aging rate of Li ion battery operating above room temperature. Nat Publ Gr 2015:1–12. http://dx.doi.org/10.1038/srep12967.
[35] PowerTHRU. Technical paper lead acid battery working – lifetime study Valve Regulated Lead Acid (VRLA) batteries factors affecting battery life ; n.d.:1–13.
[36] Linden David, Reddy TB. Handbook of batteries. McGraw-Hil 2002.
[37] Andújar JM, Segura F. PEFC simulator and real time monitoring system. Fuel Cells 2015;15:813–25. http://dx.doi.org/10.1002/fuce.201500128/epdf.
[38] Jourdan M, Mounir H, El Marjani A. Compilation of factors affecting durability of Proton Exchange Membrane Fuel Cell (PEMFC). Int Renew Sustain Energy Conf (IRESC) 2014:542–7. http://dx.doi.org/10.1109/IRSEC.2014.7059906.
[39] Janssen GJM, Sitters EF, Pfrang A. Proton-exchange-membrane fuel cells durability evaluated by load-on/off cycling. J Power Sources 2009;191:501–9. http://dx.doi.org/10.1016/j.jpowsour.2009.02.027.
[40] Yu Y, Li H, Wang H, Yuan X-Z, Wang G, Pan M. A review on performance degradation of proton exchange membrane fuel cells during startup and shutdown processes: causes, consequences, and mitigation strategies. J Power Sources 2012;205:10–23. http://dx.doi.org/10.1016/j.jpowsour.2012.01.059.
[41] Manual P, Guide I. Putting fuel cells to work FCgen ® -1020ACS fuel cell stack FCvelocity ® -1020ACS fuel cell stack product manual and integration guide. 2014.
[42] Semaoui S, Hadj Arab A, Bacha S, Azoui B. The new strategy of energy management for a photovoltaic system without extra intended for remote-housing. Sol Energy 2013;94:71–85. http://dx.doi.org/10.1016/j.solener.2013.04.029.
[43] Chauhan A, Saini RP. A review on Integrated Renewable Energy System based power generation for stand-alone applications: configurations, storage options, sizing methodologies and control. Renew Sustain Energy Rev 2014;38:99–120. http://dx.doi.org/10.1016/j.rser.2014.05.079.
[44] Segura F, Andújar JM. Step by step development of a real fuel cell system. Design, implementation, control and monitoring. Int J Hydrogen Energy 2015;40(15):5496–508.
[45] Vivas FJ, De las Heras A, Segura F, Andújar JM. A proposal of energy management strategy on hybrid renewable system with hydrogen backup. In: 7th International Renewable Energy Congress (IREC); 2016.
[46] Vivas FJ, De las Heras A, Segura F, Andújar JM. A new simulator for hybrid renewable generation systems. A new solution for technological and economic analysis and energy/hydrogen management strategies. 21 st World Hydrogen Energy Congress (WHEC). 2016.
[47] Phrakonkham S, Le Chenadec J, Diallo D, Ieee SM. Optimization software tool review and the need of alternative means for handling the problems of excess energy and mini-grid configuration : a case study from Laos n.d. Eng J 2010;14(3):15–34.
[48] Andújar JM, Segura F. Electric generating system power. WO 2015169979 A1. November 12, 2015.
[49] Schiffer J, Uwe D, Bindner H, Cronin T, Lundsager P, Kaiser R. Model prediction for ranking lead-acid batteries according to expected lifetime in renewable energy systems and autonomous power-supply systems. J Power Sources 2007;168(1):66–78. http://dx.doi.org/10.1016/j.jpowsour.2006.11.092.
[50] Dufo-López R, Lujano-Rojas JM, Bernal-Agustín JL. Comparison of different lead–acid battery lifetime prediction models for use in simulation of stand-alone photovoltaic systems. Appl Energy 2014;115:242–53. http://dx.doi.org/10.1016/j.apenergy.2013.11.021.
[51] Lemaire-Potteau E, Mattera F, Delaille A, Malbranche P. Assessment of storage ageing in different types of PV systems technical and economical aspects. In: Proc. 24th EU photovoltaic solar energy conf., Valencia, Spain; 2008.
[52] Delaille A. Development of new state-of-charge and state-of-health criteria for batteries used in photovoltaic systems. University Pierre et Marie Curie, [Ph.D Report (French)]. 2006.
[53] Bora S, Fernández-villaverde J. A comparison of programming languages in macroeconomics. J Econ Dyn Control 2015;58:265–73. http://dx.doi.org/10.1016/j.jedc.2015.05.009.
[54] Lin R, Cui X, Shan J, Técher L, Xiong F, Zhang Q. Investigating the effect of start-up and shut-down cycles on the performance of the proton exchange membrane fuel cell by segmented cell technology. Int J Hydrogen Energy 2015;40:14952–62. http://dx.doi.org/10.1016/j.ijhydene.2015.09.042.

[55] González I, Ramiro A, Calderón M, Calderón AJ, González JF. Estimation of the state-of-charge of gel lead-acid batteries and application to the control of a stand-alone wind-solar test-bed with hydrogen support. Int J Hydrogen Energy 2012;37:11090–103. http://dx.doi.org/10.1016/j.ijhydene.2012.05.001.

[56] Fernandez-Ramírez LM, Garcıa-Tribiño P, Gil-mena AJ, Llorens-iborra F, Jurado F, García-V-azquez CA. Optimized operation combining costs, efficiency and lifetime of a hybrid renewable energy system with energy storage by battery and hydrogen in grid-connected applications. Int J Hydrogen Energy 2016;41:23132–44. http://dx.doi.org/10.1016/j.ijhydene.2016.09.140.

[57] Ulleberg I. Modeling of advanced alkaline electrolyzers : a system simulation approach. Int J Hydrogen Energy 2003;28:21–33.

[58] Behzadi MS, Niasati M. Comparative performance analysis of a hybrid PV/FC/battery stand-alone system using different power management strategies and sizing approaches. Int J Hydrogen Energy 2015;40:538–48. http://dx.doi.org/10.1016/j.ijhydene.2014.10.097.

4.3. Article 3

Cell Voltage Monitoring All-in-One. A new low cost solution to perform degradation analysis on Air-Cooled Polymer Electrolyte Fuel Cells

F.J. Vivas, A. De las Heras, F. Segura, J.M. Andújar

Published in:

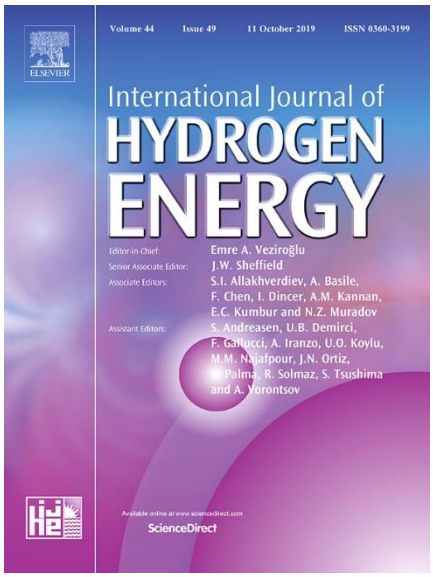

Journal: International Journal of Hydrogen Energy
Editorial: ELSEVIER
Editor-in-Chief: T. Nejat Veziroglu
Reference: Vol. 44, Issue 25, pp. 12842-12856
Year: 2018
ISSN: 0360-3199
DOI 10.1016/j.ijhydene.2018.12.172

Category	Journal Rank / Total journals	Quartile
Energy & Fuels	31 / 103	Q2
Electrochemistry	48 / 148	Q2
Chemistry	8 / 26	Q2
Impact Factor (2018)	4.084	
Citations	8	

INTERNATIONAL JOURNAL OF HYDROGEN ENERGY 44 (2019) 12842–12856

Available online at www.sciencedirect.com

ScienceDirect

journal homepage: www.elsevier.com/locate/he

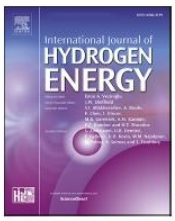

Cell voltage monitoring All-in-One. A new low cost solution to perform degradation analysis on air-cooled polymer electrolyte fuel cells

Francisco José Vivas[*], *Ainhoa de las Heras, Francisca Segura, José Manuel Andújar*

Grupo de Investigación TEP-192. Departamento de Ingeniería Electrónica, de Sistemas Informáticos y Automática, University of Huelva. Crta. Huelva-Palos de La Frontera, Palos de La Frontera, Huelva 21919, Spain

ARTICLE INFO

Article history:
Received 5 July 2018
Received in revised form
17 December 2018
Accepted 20 December 2018
Available online 24 January 2019

Keywords:
Cell voltage monitoring
Data acquisition
Air-cooled fuel cell
Cell faults detection
Degradation analysis

ABSTRACT

In this work, a new low-cost and high-performance system for cells voltage monitoring and degradation studies in air-cooled polymer electrolyte fuel cells has been designed, built and validated in the laboratory under experimental conditions.

This system allows monitoring in real time the cells' voltages, the stack current and temperature in fuel cells made of up to 100 cells. The developed system consists of an acquisition system, which complies with all the recommendations and features necessary to perform degradation tests. It is a scalable configuration with a low number of components and great simplicity. Additionally, the cell voltage monitoring (CVM) system offers high rate of accuracy and high reliability and low cost in comparison with other commercial systems.

In the same way, looking for an "All-in-One" solution, the acquisition hardware is accompanied by a software tool based on the "plug and play" philosophy. It allows in a simple way obtaining information from the cells and performing a degradation analysis based on the study of the polarisation curve. The different options and tools included in the CVM system permit, in a very intuitive and graphical way, detecting and quantifying the cell degradation without the need of isolating the stack from the system.

Experimental tests carried out on the system validate its performance and show the great applicability of the system in cases where cell faults detection and degradation analysis are required.

Introduction

Due to the imperative need to find new sustainable energy models from the economic and environmental point of view [1], the use of hydrogen, and associated with it, the use of fuel cells is presented as an impending solution [2,3].

Among the main benefits of the hydrogen technology compared to traditional battery-based systems is highlighted the higher energy density, short charge/discharge times, as well as large-scale storage and expansion capacity [2,4,5]. In contrast, fuel cells have a very important handicap in terms of cost and degradation ratios, which greatly damages the lifetime of this kind of systems [6–8].

* *Corresponding author.*
E-mail address: francisco.vivas@diesia.uhu.es (F.J. Vivas).
https://doi.org/10.1016/j.ijhydene.2018.12.172

The degradation processes associated with the reduction of performance affect all the constituent parts of the fuel cell [9]. These processes can have different origins, chemical, electrical, thermal, mechanical, and usually follow a specific pattern of action [10–12].

In this sense, demonstrations show that the operation of fuel cells under low and high current density conditions can increase the carbon corrosion process on bipolar plates, causing changes in the mechanical structure of the platinum support [11,13–15]; as well as the agglomeration of the platinum particles with the consequent active surface loss [8,13,16,17]. Alternatively, carbon corrosion will result in poor management of the flow of gases in the bipolar plates with the resultant lost due to mass transfer [16,18,19]. Similarly, the production of water is reduced and therefore tends to dry the membrane and reduce its proton activity [19–21].

Similarly, operation at high current densities tends to produce high amounts of water at the cathode, and this can cause flooding of the gas diffusion channels and consequently the gas starvation phenomenon [18,21,22].

Conversely, the operation under cyclical conditions will accentuate the previous problems, besides causing a mechanical stress to the membrane favouring the appearance of cracks, pinholes, crossover gas and ultimately a reduction of the active surface [10,23,24].

The increase of the gas crossover will cause the appearance of peroxide radicals that will favour the chemical attack of membrane and catalytic layer [25,26]. The reduction of these pollutants is produced by a strongly exothermic reaction, which will cause hot spots in the membrane, favouring the appearance of new cracks and therefore a greater gas crossover effect and a fatal chain reaction [18,20,27].

From the thermal point of view, the operation at a high temperature favours the catalytic effect on degradation reactions and the production of pollutants [20,28,29]. Then again, the operation at low temperatures tends to reduce the activity of the membrane, in addition to being able to even form ice inside the fuel cell provoking a collapse in the water management system [28–30].

Based on the foregoing, we can conclude that the operating conditions determine the degradation of the different parts of the fuel cell and, therefore, have influence on the performance and useful lifetime, Table 1, [31–33].

However, there is a lack of hardware-software tools focused on detecting the relation between the operating conditions and the associated degradation. These tools would allow carrying out degradation studies directly on the device during its operation in the final application [34,35], and they would favour the fuel cell technology penetration into the industry.

So far, there are three main methods to perform degradation diagnostics studies on fuel cells: the study of the polarisation curve, the study of impedance by electrochemical spectroscopy, and current interruption method [31,36].

The study of the polarisation curve is based on the comparison between the real polarisation curve of the fuel cell respect the original one. The overall degradation process can be modelled using different mathematical expressions as the Nerst's Law, the Taffel equation, etc [37–39]. Tey are observed as a voltage drop respect to the original polarisation curve and, therefore, the fuel cell is unable to supply the nominal current.

The study of impedance by electrochemical spectroscopy (IES) is based on the frequency response of the fuel cell under low amplitude sinusoidal signal with certain frequency values, depending on the different operation zones on the polarisation curve [12,40–42]. This method aims at identifying the electrical model based on the RC circuit that describes the double-layer effect on the fuel cell [42–44].

The last method, current interruption, has the same goal as the IES, but it is simpler. The fuel cell model parameters are obtained from the voltage transient response of the fuel cell during a step/impulse change in the current [45–47]. This method is restricted to the possibility of obtaining only certain values for ohmic and activation losses [48,49].

Then, based on the above, only the polarisation curve method could be used in the final application without the need to isolate the stack from the rest of the fuel cell system [36,37,41,50], simplifying its use. In the same way, the implementation based on individual cells voltage monitoring versus operating current allows detecting and quantifying at the same time the degradation accumulated by each cell in the different zones of the polarisation curve [16,51]. Therefore, the degradation study based on the polarisation curve is the most widespread solution [9,49,52], and the use of cell voltage monitoring (CVM) systems as the physical tool to carry it out.

Despite being a very important tool, CVM systems are usually very expensive (please see Table 2), mostly conceived for its use in laboratories and test benches, making difficult their use directly into the final application by either design

Table 1 – Summary of degradation processes that have effects on the fuel cell performance.

Process	Effect	
Electrical	**Low current density**	**High current density**
	Carbon corrosion on bipolar plates	Flooding of gas diffusion channels
	Changes in mechanical structure of the platinum	Fuel starvation
	Active surface losses	
Mechanical	**Cyclical operating conditions**	
	Cracks apparition	Pinholes on MEA
	Gas Crossover	Active surface reduction
Thermal	**Low temperature**	**High temperature**
	Membrane activity reduction	Catalytic effect on degradation reactions
	Ice formation	Production of pollutants
	Water management system collapsed	

Table 2 – Technical characteristics of CVM systems. Proposal by authors and commercial and patented solutions.

Device	Channels	Resol. (bits)	Accu. (mV)	Sampling frequency	CMRR	Elect. connection	Isolation Voltage	Power supply	Power consumption	Price (€)
CVM All-in-One	100	24	5	10 Hz	120 V	Probes/Cable	1 kV	USB/External	<1.5 W	120
[62]	144	–	10	7 Hz	300 V	Cable	3 kV	External	4.3 W	2880
[74]	10	16	6	100 Hz	–	Cable	1.4 kV	External	0.8 W	>2000
[75]	128	10	3	50 Hz	600 V	Cable	–	External	<5 W	1900
[59]	90	12	6	10 Hz	200 V	Cable	1 kV	External	4 W	5000
[60]	32	16	5	5 Hz	300 V	Cable	1 kV	External/Fuel cell	120 W	>2000
[61]	128	12	5	–	130 V	Cable	–	External/Fuel cell	3 W	>2000
[76]	32	16	4	30 Hz	85 V	Cable	1 kV	USB	<2.5 W	1875
[77]	90	12	3	12.5 Hz	85 V	Cable	1 kV	External	6 W	7706
[69]	70	12	1	10 Hz	80 V	Cable	1 kV	External	35 W	9655
[56]	80	12	5	0.75 Hz	200 V	Cable	–	External	<5 W	460

criteria, dimensions or overall project cost [53]. All these reasons lead ultimately to the no use of this type of systems directly into the final application. Therefore, this hinders the availability of an experimental base of knowledge to detect and quantify the degradation rate that the fuel cell suffers when it works at different operating conditions. Consequently, studies oriented to improve the useful lifetime of fuel cell are missing.

For all the above, the aim of this article is to present a new hardware-software solution that allows to perform degradation studies based on the analysis of the fuel cell polarisation curve. For this, a high-performance, safe, easy-to-design and low-cost CVM solution is presented. It can be adapted at any time to any type of application in terms of operating conditions and sizing, also reducing the economic impact on the overall system cost.

This article is organized as follows. A brief review of the different CVM requirements and solutions available in the scientific literature or in the market, is presented in Section Cell voltage monitoring systems. requirements and commercial solutions. The proposed hardware/software solution for CVM is described and analysed in detail in Section Cell voltage monitoring "All-in-One". prototype description. Experimental results obtained from tests applied over the developed CVM system are presented in Section Validation test. Experimental results and Discussion and, finally, conclusions and future works are outlined in Section Conclusions.

Cell voltage monitoring systems. Requirements and commercial solutions

For the correct implementation of degradation analysis tools based on the study of the polarisation curve, it is necessary to monitor the cells' voltages and their relationship with the working current in order to be able to define the current polarisation point of each cell [36]. Likewise, the monitoring of the stack operating temperature will also allow determining cause-effect relationships between the detected degradation and problems associated with different possible causes, such as high current densities, inverse polarisation currents, thermal management and humidification deficiencies, etc. [30,54,55].

For a proper implementation of an acquisition system associated with this type of applications, it is necessary previously to define some minimum requirements to be met, in order to guarantee an accurate and safe measurement. These requirements are summarised below.

Requirements

Depending on the study to be carried out, CVM systems must meet the minimum constraints to ensure accurate readings. As a general rule, it is estimated that these systems should measure at a minimum sampling frequency of 1–4 Hz, and they have an accuracy of ±100 mV to detect significant faults and ±10 mV to perform degradation analysis [36,56].

According to the above, it is necessary to design an equipment with a sampling rate according to the number of cells, or to develop an instrumentation channel per cell. Normally, the first option implies a decrease in the overall accuracy of the CVM system by increasing the sampling frequency (reduce free noise bits), while the second alternative increases the hardware cost and complexity exponentially.

Instead, from the security point of view, it is necessary the use of electrical insulation to prevent damages both in the electronics and cells [56]. In the same way, the system has to take into account different actions to avoid reverse current or short circuit situations between cells in a possible failure during the acquisition process. This requires a more comprehensive design and the use of components that make it rather expensive.

Taking into account the manoeuvrability of the system, it is necessary to develop a cell voltage acquisition system that facilitates the interface with the fuel cell. The current solutions require large quantity of crimped cables [53,56–70]. This means a greater complexity of assembly, and the possibility of bad connections putting at risk the integrity of the stack.

Finally, low-cost systems and a "plug and play" philosophy are needed in order to promote the use of CVM systems and to facilitate the design, study and operation of fuel cells in the industrial, research and university realm.

Overview of CVM commercial solutions

Currently, the most common CVM systems are high-cost systems that provide a hardware/software solution for the acquisition and monitoring of cells' voltage in the fuel cell. Nevertheless, these systems obviate other important

parameters such as the stack current and temperature, which are fundamental to analyse the polarisation curve of the fuel cell [38,39]. In some cases, these systems only act as an alarm generator when certain levels of minimum operating voltage are exceeded [58,64,65,68,71]; thus, they do not allow degradation studies.

From the hardware point of view, there are several solutions based on the non-multiplexed systems [58,60], or partially multiplexed [62,64,65,68], which cause an increase on the number of components and, thus, on the associated cost and complexity.

Other solutions opt for multiplexing after the conditioning stage using a single analog-to-digital converter (ADC) [72], which reduces the cost compared to previous solutions, but it requires a more complex sizing and error correction actions associated with tolerances of components. In any case, this is a high cost solution that does not include isolation between the power equipment and the control unit.

Conversely, there are solutions that use full multiplexing and a single front-end stage [53,56,63,67]. These solutions are usually low-accuracy, low-cost and non-isolated systems. In addition, the multiplexing leads to low sampling frequencies, not recommended for stacks with high number of cells (>50). As an exception, in Ref. [59] an isolated configuration that allows a higher sampling frequency is presented, but it is more expensive than the previous solutions.

According to the electrical coupling between acquisition hardware and fuel cell stack, the most common solution is the direct connection point to point through wiring [39–41,43–54], which leads to more vulnerable connection due to surrounding electromagnetic noise. This fact, together with the difficult task of ensuring a correct electrical coupling can lead to false contacts, which can cause short circuits, incorrect measurements, or simply no measurement, putting at risk the test and the veracity of the results.

In contrast, there are several solutions that propose only a coupling based on retractable probes that ensure a correct electrical contact even under irregular cell surface, but they avert the subsequent acquisition hardware [71,73].

Finally, the cost of commercial solutions makes these devices are almost prohibitive to the end user. This is why fuel cell degradation analysis are given up and, consequently, all the information they can supply is neglected.

Table 2 shows the main characteristics of the CVM system proposed in this paper, and it can be compared with commercial and patented systems found in the scientific literature.

Cell voltage monitoring "All-in-One". Prototype description

The developed prototype allows cell voltage monitoring, including current and temperature sensing for a fuel cell stack up to 100 cells and a maximum current of 100 A. The number of cells and the maximum current of the stack can be expanded according to user needs.

The system consists of a perfectly interconnected hardware and software component, which allows its use based on the "plug and play" philosophy through a USB connection to any PC. The hardware component has been designed with the aim of guaranteeing a low-cost solution with sufficient accuracy and safety features for the designed application. The proposed system reduces the necessary hardware, coupling directly on the fuel cell stack and powered mainly from a USB connection.

The monitoring software allows real time measurements of the cells' voltages, simultaneously with the stack current and temperature, allowing at any time to associate the degradation causes (observable mainly by the value of each cell voltage) and the operating point, according to the polarisation curve of the fuel cell to be tested.

The purpose of the developed CVM system is to provide a complete low-cost and easy-to-use solution that can be utilised in any sector involving the usage of fuel cells.

The elements that integrate the proposed system are described below.

Hardware implementation and assembly on the stack

Hardware implementation

The CVM acquisition hardware can be divided into four subsystems that have been designed taking into account safety, accuracy and economic principles.

The system has been implemented according to three electrically isolated zones: high voltage zone, acquisition zone and control zone. The complete system scheme is presented in Fig. 1.

Front-end subsystem. This subsystem includes all the necessary elements to define the first conditioning stage of the signals obtained from the sensors, or direct measurements from cells voltage.

Voltage divider. Firstly, a 1:8 gain stage has been implemented with the aim of reducing common mode voltages, which can reach as high as n volts, where n is the number of stack cells. This results in a practically unassuming voltage value by commercial analog multiplexers and amplifiers [56]. This first stage simplifies the design and reduces the cost of the following steps. Contrariwise, it is necessary to use more accurate and higher resolution acquisition systems, because the differential cells voltage is reduced up to eight units.

The use of this pre-multiplexing step also helps to reduce ohmic losses associated with the leakage current of various multiplexer's connections, because there is no voltage drop just before the instrumentation amplifier. In addition, it allows to increase the security of the system in case of a fault during multiplexing cycles, providing a high impedance between cells and avoiding the occurrence of short circuits.

Multiplexing. The multiplexing stage allows reducing the number of conditioning amplifiers and front-ends stages; therefore, it promotes a cost reduction and a simpler acquisition solution [78]. Oppositely, it increases the performance of the system as long as all the signals are conditioned and acquired by the same circuit; accordingly, it avoids problems associated with differences in circuits offset, linear response, bandwidth, thermal drift, filtering stages, tolerance of components, etc.

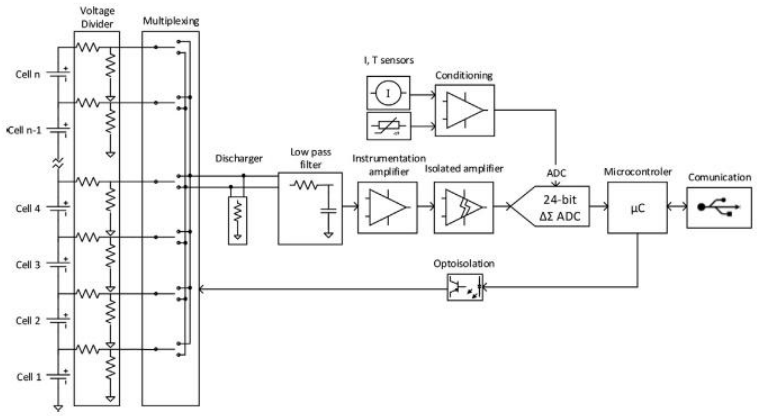

Fig. 1 – Electrical scheme of acquisition and control hardware.

Dischargie ng stage. Becausof the inclusion of multiplexing, the effect of the multiplexer parasitic capacitors, and the filter capacitance effect must be taken into account. These capacitances may cause the appearance of residual voltage during the multiplexer transitions and, therefore, the reverse current flow towards the cells. This occurrence can have irreversibly effects on the fuel cell, so it is important to prevent it [2,47]. The most common solutions are to use of discharging resistors at the output of the multiplexer, or to increase the death time during switching.

The first solution, discharging resistors, introduces a parasitic resistance that causes a resulting parallel resistance which modifies the gain of the resistive divider and, hence, the accuracy of the CVM system.

The second solution, to increase the death time, avoids the previous problem, but it requires longer multiplexing times and, therefore, reduces the sampling frequency, causing non-compliance of the minimal frequency requirements.

The solution adopted in the CVM system proposed in this paper is the use of a selective discharging resistor, controlled by microcontroller through an opto-coupler, which allows discharging the parasitic capacitance through the resistor only during a short death time between commutations. This solution combines the advantages of the both proposed alternatives and it allows obtaining an accurate measurement without barely reducing the sampling frequency of the system.

Filtering. In order to filter the effect of possible radiated or conducted noise, a first-order analogue low pass filter is used based on passive RC components. This stage will mitigate the noise effect over the signal before its conditioning, preventing the noise spreading to later stages.

Cell voltage signal conditioning. For the signal conditioning, a low-cost and high accuracy instrumentation amplifier model INA128 is used. It allows obtaining an output signal identical to the differential voltage between two electrical terminals (n-1 and n), associated with nth cell.

The use of a differential amplifier is essential to ensure the common mode voltage rejection and the cancellation of differential noise.

Insulation. In order to guarantee the safety of the subsequent stages, the use of a low-cost and high-performance isolation amplifier model ACPL-C78A has been chosen to apply an 8:1 gain to the input signal. This gain stage allows recovering the original voltage values and, therefore, increasing the accuracy of the system taking advantage of the overall analog-to-digital converter (ADC) operating range. Alternatively, the use of this isolated amplifier keeps an electrical insulation between the high voltage circuitry and the acquisition and control circuitry, avoiding the propagation of possible failures in the first stages.

Current and temperature conditioning. For current sensing a closed-loop Hall effect sensor is used, which guarantees a high linearity response over a wide range of currents and electrical insulation. In the case of temperature measurement, a NTC thermistor is used because their exponential response makes it capable to detect small changes in the stack temperature with high accuracy [39].

For this purpose, operational amplifiers model TL081 with a voltage follower (buffer) configuration have been used in order to increase the impedance of the output sensor line and, thus, reduce losses associated with current consumption during the acquisition stage. This solution will therefore increase the accuracy of the CVM system.

The current and temperature measurements and condition stages are carried out in the low voltage zone, because the nature of the sensors permits an isolated measure with respect to the high voltage zone and, therefore, no further actions are required.

Acquisition subsystem. The acquisition subsystem consists on a low-cost ΔΣ ADC model ADS1220 with 24-bits resolution and up to 2 kHz sample rate. The low noise, high linearity and low thermal drift of the ADC allows obtaining high precision measurements, necessary for this type of applications.

The noise of this ADC can be optimized reducing the output data rate; however, it is necessary to get a commitment between noise and the output data rate required for this application. In our case, it is enough 10 samples per second in order to capture the dynamic of each cell. So, 1000 Hz sampling

frequency has been chosen (10 samples per second for a 100 cells stack). At this frequency, the noise-free bits from peak-to-peak noise is 14.4.

The number of cells can be modified at any time, guaranteeing a number of samples per cell of 1000/N, in which N represents the number of cells and 1000 the frequency in Hz. In this way, in the case of, for example, a single cell stack, the number of samples per second can reach 1000, enough to perform very fast dynamic studies such as current interruption.

Control and communications subsystem. In order to keep the system robustness, easy-to-use and low-cost solution, an open hardware Arduino Nano board [79] is used (which can be replaced by another similar, according to needs of the final application) as microcontroller to manage communications and switching. The use of this type of open source platform allows the immediate replacement due to any failure, and even the reprogramming by the end-user in case of the need to modify the sampling rate, to develop digital filtering interface, or the need to modify the number of cells to be monitored.

In order to guarantee the safety of the control and acquisition subsystem, the control interface used to manage the multiplexing stage is performed through low-cost opto-couplers, which allows the isolation of the high voltage circuitry from the control zone.

Finally, the communications between the acquisition hardware and the monitoring software is performed through a USB port, allowing for the "plug and play" philosophy.

Power supply subsystem. The main power of the system is obtained from the USB connection, since a current consumption less than 300 mA is guaranteed and, therefore, the use of external electronics is not necessary. In any case, there is an extra input which permit an auxiliary source connection to guarantee the power supply in case of one of the sensors is replaced by other with higher consumption.

The acquisition and front-end subsystems are powered through two converters with galvanic isolation, allowing the electrical insulation previously guaranteed by opto-couplers and the isolation amplifier.

Assembly on the stack

The developed CVM acquisition hardware has been designed to guarantee an easy integration into commercial open-cathode PEM fuel cell systems (see Fig. 2). Owing to the holes in the cells' cathodes, the connection pins of the CVM system acquisition system can be inserted into them.

The coupling takes advantage of the physical geometry and the assembly parts of the fuel cell stack to have a firm and precise connection. For this purpose, a specially adapted PCB coupling has been designed for this application.

In the same way, in order to guarantee a secure electrical connection, special spring probes are used that ensure the contact even with irregular cell surfaces. The connection is made through an array of this type of probes as shown in Fig. 2. In any case, wiring connection is also available.

Software development of the monitoring tool

The software tool has been developed under graphic programming language through the LabVIEW software platform [80] in parallel to the acquisition hardware, which allows extracting its maximum performance.

The developed software is able to read immediately physical variables following the "plug and play" philosophy. No pre-configuration is required and the reading is very fast and intuitive.

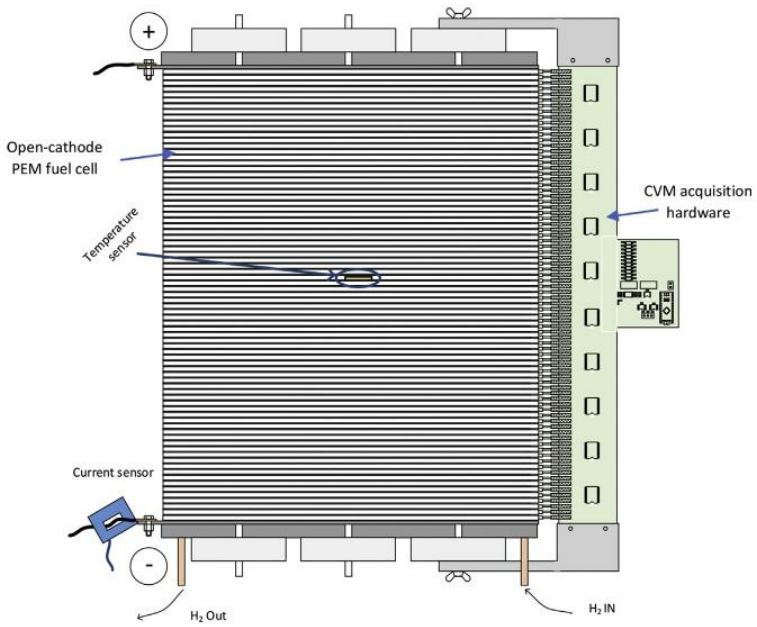

Fig. 2 – CVM acquisition hardware assembled on the fuel cell stack.

Fig. 3 – CVM "All-in-One". Software tool: example of bar graph interface.

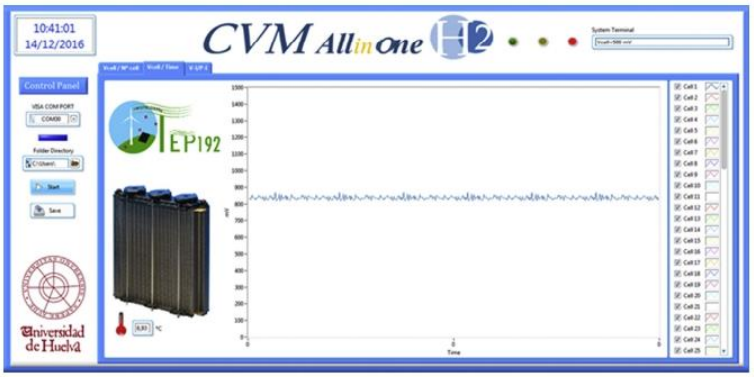

Fig. 4 – CVM "All-in-One". Software tool: example of real time plot interface.

The software tool developed allows for the cell voltage monitoring in two different formats: the first, in form of a bar graph (Fig. 3), allows the rapid verification of discrepancies between cells' voltages; and the second permits the visualisation of the temporal history of each cell as well as the current, power and temperature of the stack (Fig. 4).

Moreover, the software tool has additional auxiliary functions that help the user analyse the degradation and behaviour of the stack. These functions are listed below:

- Graphical information about the real operation point display with respect to the theoretical or original V-I, P-I curves. This information allows the user to detect the

Fig. 5 – CVM "All-in-One". Software tool: interface to compare real fuel cell operating point with respect to theoretical polarisation and power curves.

degradation of the fuel cell performance produced along the useful lifetime of the stack as well as to determine what kind of losses within the polarisation curve have been accentuated (Fig. 5).
- Programmed alarms. The software tool allows defining prefixed values of cell voltage, stack current and stack temperature from which a warning is activated in the front panel.

System operation

The sequence followed by the developed CVM system is presented in Fig. 6. Firstly, the system waits for a scan command from the monitoring software and then it begins the initialization process, where all the measurements are updated. Next, the scan process begins and creates an internal loop in order to measure all the cells' voltages and the temperature and current sensors. This internal loop will increase an auxiliary variable, x, which corresponds with the number of the cell to be measured.

This process will finish when the auxiliary variable, x, gets to N, i.e., the number of cells that makes up the stack.

Finally, the microprocessor sends the information to the monitoring software through the USB communication interface. The monitoring software will read, upload and plot the new measures and will save then in an.txt file. In the same way, the warnings subroutine will check all the cells' voltages and will generate the consequent message to the user according to predefined alarm limits. The monitoring software operation flowchart is shown in Fig. 7.

Empirical error calculation

To determine the overall empirical error, a test was performed with a high accuracy voltage reference circuit that generates a 1 V-reference signal. To ensure consistent results, 150 samples of each channel have been used and a statistical analysis was carried out.

The test consisted in comparing the measures obtained by each channel from the proposed acquisition hardware and the reference voltage generated by a 14 bits resolution-DAC integrated circuit to obtain the values of precision and accuracy of the proposed CVM system. The 1 V-reference signal was measured with a calibrated high accuracy acquisition hardware ARBIN LBT21084, guaranteeing 0.5 mV accuracy. Before carrying out the test, the entire system was calibrated.

As a measure of accuracy, the mean deviation between both signals has been used and is shown in Fig. 8. In this case, the measurement error of the reference is considered negligible. According to the statistical results, the mean deviation of all channels is always lower or equal to 1 mV; thus, we may conclude that the overall accuracy of the system is better than the maximum mean deviation of 1 mV.

To know the precision of the developed CVM system, the standard deviation of the measures has been used and it is shown in Fig. 9. To identify the differences, we assumed that the measurement error is distributed normally; hence, the maximum precision error (with 99.7% of certainty) will be included in the range of $[\mu-3\sigma, \mu+3\sigma]$, where μ represents the mean, and σ the standard deviation. Taking into account this statistical ground, the maximum error is defined by 3σ, being in this case lower than 4 mV.

According to the experimental results, the maximum error of the system can be assumed lower than 5 mV, equivalent to an error rate of 0.5% for 1 V-signal. This error rate is under the

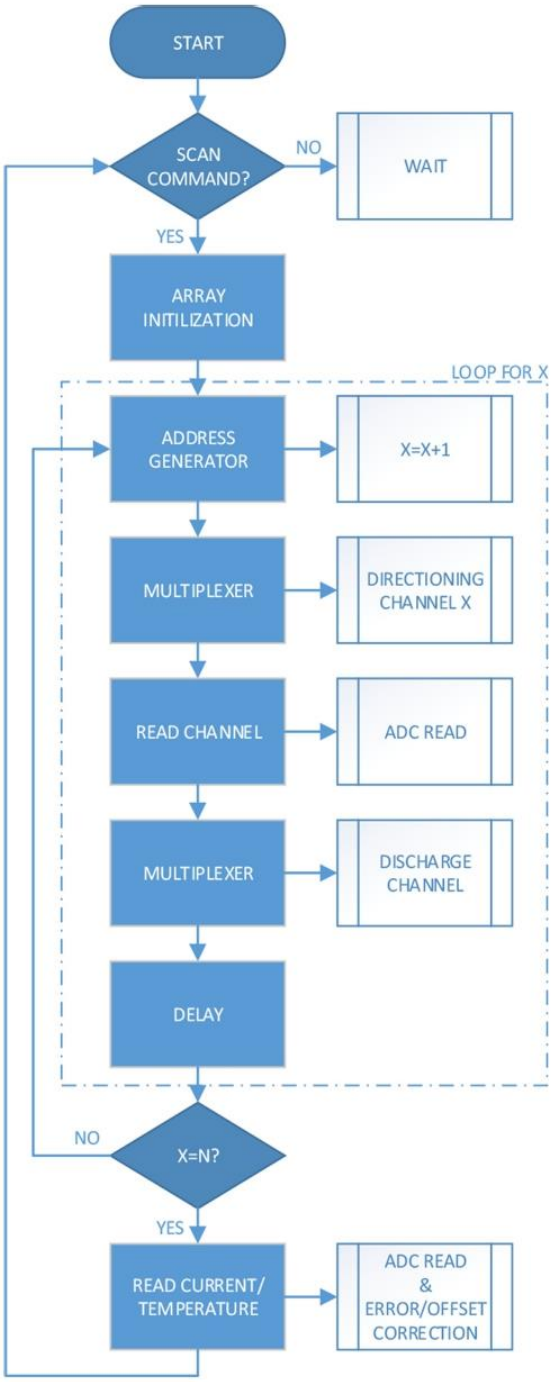

Fig. 6 – CVM acquisition hardware: operation flowchart.

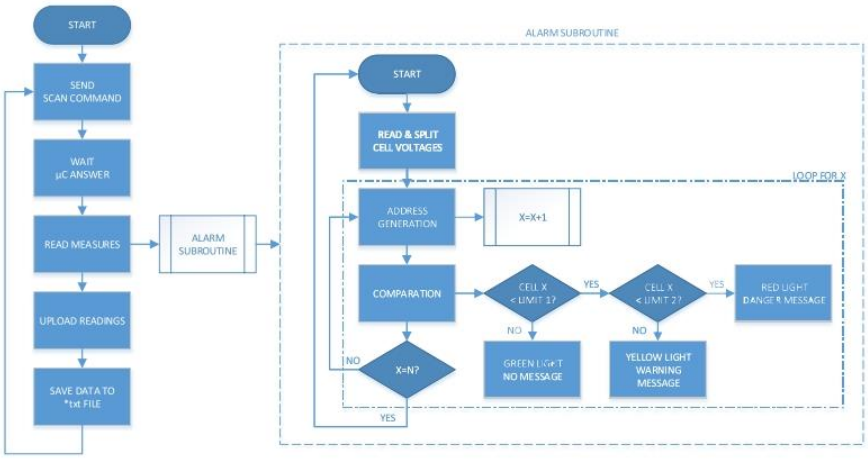

Fig. 7 – CVM monitoring software: operation flowchart.

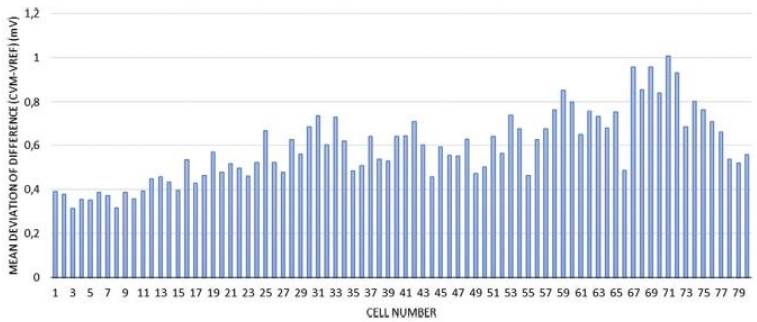

Fig. 8 – Accuracy of voltage of CVM.

recommended limits to perform degradation analysis and, therefore, the good accuracy of the proposed CVM system is demonstrated.

Validation test. Experimental results and discussion

With the aim of validating the developed data acquisition system and monitoring software, the CVM "All-in-One" has been subjected to different experimental tests. The experimentation has been carried out at the Hydrogen Research Laboratory of the University of Huelva (Spain).

The first test demonstrates the effectiveness of the acquisition hardware over short and long operation time and different load profiles.

Fig. 10 illustrates the laboratory setup. The monitored air-cooled PEFC is built with a 80-cells stack from Ballard [81], and it achieves up to 3 kW of nominal power. In order to validate the experimental trial, authors tested a damaged stack from which it is impossible to obtain a net power greater than 1.5 kW in the current state.

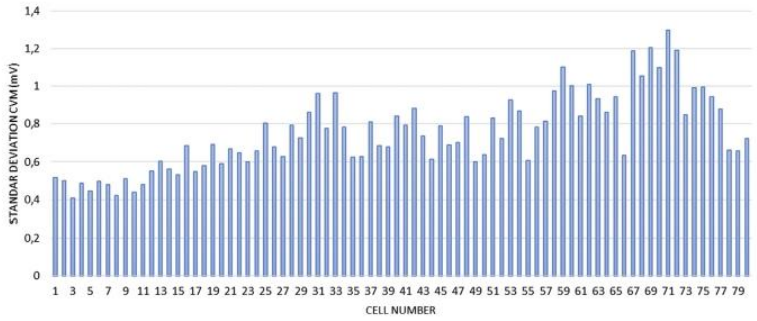

Fig. 9 – Precision measurement of the developed CVM.

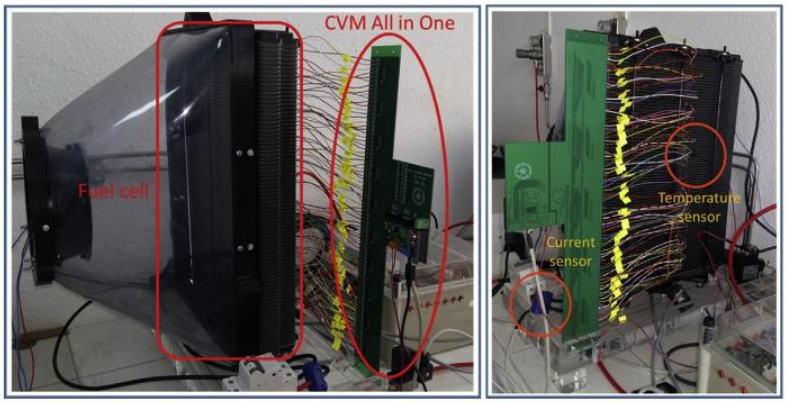

Fig. 10 – Laboratory setup for experimental tests.

Other auxiliary devices are used to carry out the experimental test. A Fluke 177 multimeter is used to validate the measurements as well as a programmable DC electronic load to configure the load profile to be applied to the fuel cell.

The test performed was reproduced for 17 min and consists of a progressive increase of the load profile in such a way that slight differences in temperature and cell operating voltages can be appreciated. For this, a conditioning stage was previously carried out on the fuel cell until it reached the nominal operating temperature conditions. The stop condition of the test was given in case the cell voltage was below 150 mV to avoid inverse polarisations and irreversible damage.

According to the experimental results, the stack voltage decreased while the load current demand was increasing (Fig. 11). This experimental response can be compared with theoretical V-I and P-I curves provided by fuel cell manufacturer (Fig. 12). In spite of being an expected response, it is appreciated that there is a variation with respect to the theoretical polarisation curve, which denotes an associated degradation. Due to the losses appear early, at low current values and they continue along the polarisation curve (the distance from the real polarisation curve to the theoretical curve is practically the same along all the operating range), the activation losses, those that mainly affect the stack degradation versus the ohmic or concentration losses, are deduced for this case. Nevertheless, a slight progressive increase in the losses is appreciated; the distance from the real to the theoretical curve somewhat rises while the load current is moving upwards. Let us observe the individual cell voltage to explain this issue.

Taking into account the individual cell voltages (Figs. 13 and 14), there is an excessive difference between cell voltage for cells from 6 to 24 and, particularly, cell 18 is deeply damaged when compared to the rest of the cells in the stack. This voltage drop increases exponentially while the load current rises, which indicates a high deterioration or malfunction reducing the performance of the whole stack, as it is shown in Fig. 12.

In view of the foregoing, it can be deduced that the degradation of the stack is not uniform, demonstrating that the cells of medium-high position (cells > cell #25) have a good behaviour along all the test, while those of lower position (cells < cell #25) have suffered a substantial voltage degradation. In principle the possible causes are unknown, although they can be attributed in a first instance to problems in the management of hydrogen (leaks caused by a bad seal), or a high deterioration of the electro-catalytic layer, which would denote the above-mentioned increase of activation losses.

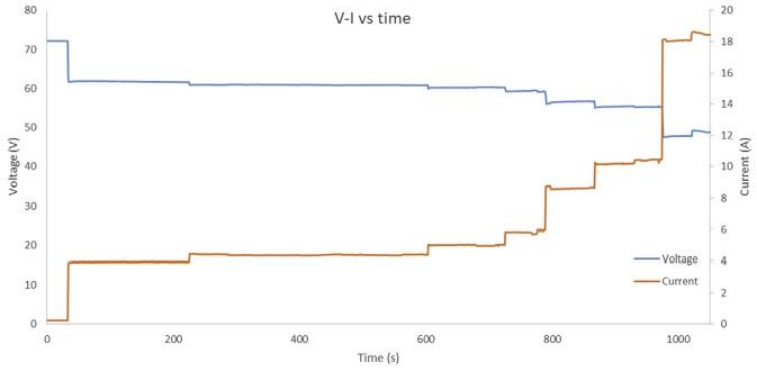

Fig. 11 – Stack voltage and current response during the experimental test.

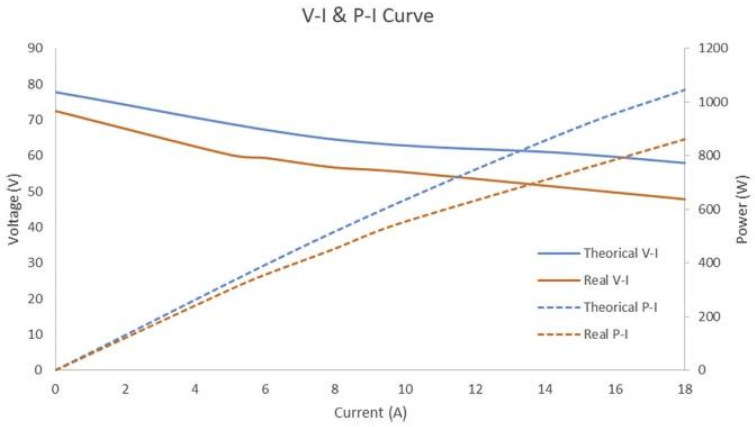

Fig. 12 – V-I (continuous line) and P-I (dotted line) curves for theoretical (blue) and real (orange) state of the fuel cell. (For interpretation of the references to color in this figure legend, the reader is referred to the Web version of this article.)

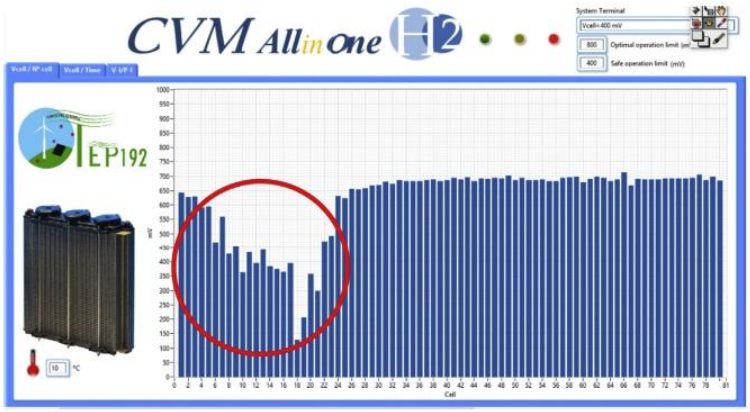

Fig. 13 – Individual cell voltage at high current (t = 1000 s).

From the thermal point of view (Fig. 15), no huge changes can be observed between the real stack operating temperature and the optimum operating temperature recommended by the manufacturer. Only at the beginning of the test, the difference between real and recommended operating temperature was recognised. This is due to the initial operating condition. In the case of the experimental test, the warmed environmental conditions justified the initial stack

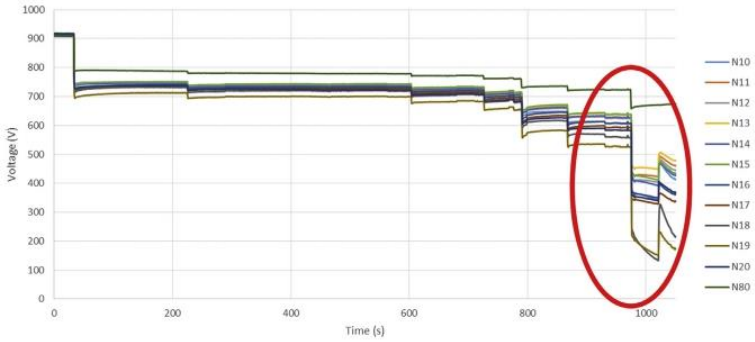

Fig. 14 – Cell voltageO time evolution during the performance test.

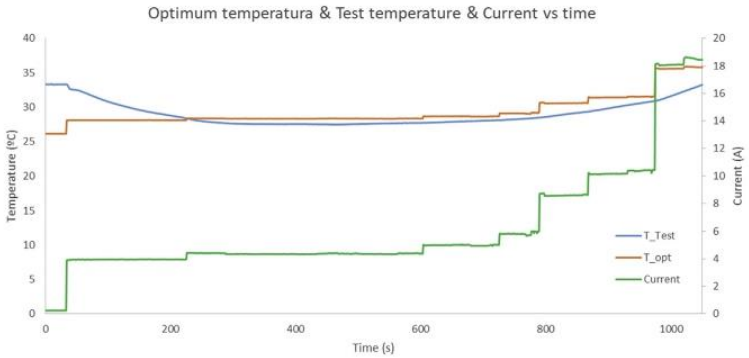

Fig. 15 – Temperature and current evolution during experimental test.

temperature. But, fortunately, owing to the proper thermal management of the cooling system, the real stack temperature was adjusted with the aim of following the optimum value. For this reason, deterioration problems due to thermal malfunction or excessive humidity can be discarded.

From the point of view of the acquisition system and control software, the accuracy of the developed CVM system can be affirmed, together with the ability to monitor current and operating temperature have enabled the evaluation of the fuel cell degradation in the first instance. Additionally, the CVM system favours the detection, visualisation and quantification of the losses associated at each cell and, consequently, of the whole stack.

Conclusions

One of the most important drawbacks of the fuel cells is their short lifetime due to their susceptibility to different electrochemical processes that lead to irreversible degradation. This problem provokes a reduced use of fuel cells outside the scope of research laboratories. In order to increase the competitiveness of the fuel cells, it is necessary to mitigate the degradation process that they can suffered. To this end, the use of degradation analysis is necessary to detect the relationship between degradation causes and the effect over the fuel cell. The most extended solution is the analysis of the polarisation curve, and it implies the monitoring of certain parameters during the normal operation, mainly voltage (on the entire stack and on each cell), and the stack current and temperature. Therefore, the use of a CVM system looks like as crucial support to improve the fuel cell lifetime.

In this sense, both commercial and patented CVM solutions available in the scientific literature or in the market are usually expensive and in some cases inaccurate to develop degradation tests. In addition, the majority of these solutions only are able to measure voltage values without including stack current and temperature information, and its coupling to the stack requires tedious connection procedures. For this reason, it is necessary to develop new CVM system that facilitates its use and the acquisition process.

In this work, the design, development and experimental testing of a new low-cost CVM system is expounded. This system, CVM "All-in-One" more than meets the recommended requirements to perform degradation analysis on the fuel cell. Additionally, it has proved an accurate and secure operation under laboratory conditions. In addition to above, the easy coupling to the stack, its low-cost, extended software functions and the "plug and play" philosophy, makes the proposed system a powerful and intuitive tool to help researchers and industry technicians to advance in new research lines, such as analysis and detection of new degradation causes, define accurate electrochemical models, etc.

As a forthcoming work, the integration of new parameters such as hydrogen pressure, fan speed, cell temperature, etc., will be carried out. In the same way, output channels will be included to act over common actuators such as fan or hydrogen valves. The software will also be updated to include control functions and, thus, to provide the system with all the degrees of freedom to perform any test for fuel cells.

Acknowledgements

This work is a contribution of the DPI2017-85540-R Project supported by the Spanish Ministry of Economy and Competitiveness and by the European Union Regional Development Fund.

REFERENCES

[1] García E, Correcher A, Quiles E. FM. Renewable energy resources of the marine environment and its control requirements. RIAI - Rev Iberoam Automática e Informática Ind 2016;13(2):141–61.
[2] Vivas FJ, De Las Heras A, Segura F, Andújar JM. A review of energy management strategies for renewable hybrid energy system with hydrogen backup. Renew Sustain Energy Rev 2018;82:126–55. https://doi.org/10.1109/IREC.2016.7478902.
[3] Vasallo MJ, Bravo JM, Andújar JM. Optimal sizing for UPS systems based on batteries and/or fuel cell. Appl Energy 2013;105:170–81. https://doi.org/10.1016/j.apenergy.2012.12.058.

[4] Vasallo MJ, Andújar JM, García C, Brey JJ. A methodology for sizing backup fuel-cell/battery hybrid power systems. IEEE Trans Ind Electron 2010;57:1964–75. https://doi.org/10.1109/TIE.2009.2021171.

[5] Fernández RÁ, Cilleruelo FB, Martínez IV. A new approach to battery powered electric vehicles: a hydrogen fuel-cell-based range extender system. Int J Hydrogen Energy 2016;41:4808–19. https://doi.org/10.1016/j.ijhydene.2016.01.035.

[6] Lin RH, Xi XN, Wang PN, Wu BD, Tian SM. Review on hydrogen fuel cell condition monitoring and prediction methods. Int J Hydrogen Energy 2018:1–11. https://doi.org/10.1016/j.ijhydene.2018.09.085.

[7] Ozden E, Tari I. PEM fuel cell degradation effects on the performance of a stand-alone solar energy system. Int J Hydrogen Energy 2017;42:13217–25. https://doi.org/10.1016/j.ijhydene.2017.04.017.

[8] Franck-Lacaze L, Bonnet C, Choi E, Moss J, Pontvianne S, Poirot H, et al. Ageing of PEMFC's due to operation at low current density: investigation of oxidative degradation. Int J Hydrogen Energy 2010;35:10472–81. https://doi.org/10.1016/j.ijhydene.2010.07.180.

[9] Hu Z, Xu L, Huang Y, Li J, Ouyang M, Du X. Comprehensive analysis of galvanostatic charge method for fuel cell degradation diagnosis 2018;212:1321–32.

[10] Zhang X, Yang D, Luo M, Dong Z. Load profile based empirical model for the lifetime prediction of an automotive PEM fuel cell. Int J Hydrogen Energy 2017;42:11868–78. https://doi.org/10.1016/j.ijhydene.2017.02.146.

[11] Xiao S, Zhang H, Bi C, Zhang Y, Zhang Y, Dai H, et al. Degradation location study of proton exchange membrane at open circuit operation. J Power Sources 2010;195:5305–11. https://doi.org/10.1016/j.jpowsour.2010.03.010.

[12] Pivac I, Bezmalinovi D. Catalyst degradation diagnostics of proton exchange membrane fuel cells using electrochemical impedance spectroscopy. Int J Hydrogen Energy 2018;3:0–8. https://doi.org/10.1016/j.ijhydene.2018.05.095.

[13] Shin H, Kwon O, Oh BS. Correlation between performance of polymer electrolyte membrane fuel cell and degradation of the carbon support in the membrane electrode assembly using image processing method. Int J Hydrogen Energy 2018:3.

[14] Erbach S, Pribyl B, Klages M, Spitthoff L, Borah K, Epple S, et al. Influence of operating conditions on permeation of CO2 through the membrane in an automotive PEMFC system. Int J Hydrogen Energy 2018:1–12. https://doi.org/10.1016/j.ijhydene.2018.10.033.

[15] Bae SJ, Kim SJ, Lee JH, Song I, Kim NI, Seo Y, et al. Degradation pattern prediction of a polymer electrolyte membrane fuel cell stack with series reliability structure via durability data of single cells. Appl Energy 2014;131:48–55. https://doi.org/10.1016/j.apenergy.2014.05.064.

[16] Baricci A, Bonanomi M, Yu H, Guetaz L, Maric R, Casalegno A. Modelling analysis of low platinum polymer fuel cell degradation under voltage cycling : gradient catalyst layers with improved durability. J Power Sources 2018;405:89–100. https://doi.org/10.1016/j.jpowsour.2018.09.092.

[17] Zhao M, Shi W, Wu B, Liu W, Liu J, Xing D, et al. Influence of membrane thickness on membrane degradation and platinum agglomeration under long-term open circuit voltage conditions. Electrochim Acta 2015;153:254–62. https://doi.org/10.1016/j.electacta.2014.12.024.

[18] Wu J, Yuan XZ, Martin JJ, Wang H, Zhang J, Shen J, et al. A review of PEM fuel cell durability: degradation mechanisms and mitigation strategies. J Power Sources 2008;184:104–19. https://doi.org/10.1016/j.jpowsour.2008.06.006.

[19] Yousfi-Steiner N, Moçotéguy P, Candusso D, Hissel D, Hernandez A, Aslanides A. A review on PEM voltage degradation associated with water management: impacts, influent factors and characterization. J Power Sources 2008;183:260–74. https://doi.org/10.1016/j.jpowsour.2008.04.037.

[20] Zhang S, Yuan X, Wang H, Mérida W, Zhu H, Shen J, et al. A review of accelerated stress tests of MEA durability in PEM fuel cells. Int J Hydrogen Energy 2009;34:388–404. https://doi.org/10.1016/j.ijhydene.2008.10.012.

[21] Hu Z, Xu L, Li J, Gan Q, Xu L, Ouyang M, et al. A multipoint voltage-monitoring method for fuel cell inconsistency analysis. Energy Convers Manag 2018;177:572–81. https://doi.org/10.1016/j.enconman.2018.09.077.

[22] Schmittinger W, Vahidi A. A review of the main parameters influencing long-term performance and durability of PEM fuel cells. J Power Sources 2008;180:1–14. https://doi.org/10.1016/j.jpowsour.2008.01.070.

[23] Büsselmann J, Rastedt M, Tullius V, Yezerska K, Dyck A, Wagner P. Evaluation of HT-PEM MEAs: load cycling versus start/stop cycling. Int J Hydrogen Energy 2018:1–11. https://doi.org/10.1016/j.ijhydene.2018.07.181.

[24] Moein-Jahromi M, Kermani MJ, Movahed S. Degradation forecast for PEMFC cathode-catalysts under cyclic loads. J Power Sources 2017;359:611–25. https://doi.org/10.1016/j.jpowsour.2017.05.102.

[25] Placca L, Kouta R. Fault tree analysis for PEM fuel cell degradation process modelling. Int J Hydrogen Energy 2011;36:12393–405. https://doi.org/10.1016/j.ijhydene.2011.06.093.

[26] Chung CG, Kim L, Sung YW, Lee J, Chung JS. Degradation mechanism of electrocatalyst during long-term operation of PEMFC. Int J Hydrogen Energy 2009;34:8974–81. https://doi.org/10.1016/j.ijhydene.2009.08.094.

[27] Chang Y, Zhao J, Shahgaldi S, Qin Y, Yin Y, Li X. Modelling of mechanical microstructure changes in the catalyst layer of a polymer electrolyte membrane fuel cell. Int J Hydrogen Energy 2018:1–13. https://doi.org/10.1016/j.ijhydene.2018.10.157.

[28] Ozden A, Shahgaldi S, Zhao J, Li X, Hamdullahpur F. Degradations in porous components of a proton exchange membrane fuel cell under freeze-thaw cycles : morphology and microstructure effects. Int J Hydrogen Energy 2018. https://doi.org/10.1016/j.ijhydene.2018.10.209.

[29] Yousfi-Steiner N, Moçotéguy P, Candusso D, Hissel D. A review on polymer electrolyte membrane fuel cell catalyst degradation and starvation issues: causes, consequences and diagnostic for mitigation. J Power Sources 2009;194:130–45. https://doi.org/10.1016/j.jpowsour.2009.03.060.

[30] Dafalla AM, Jiang F. Stresses and their impacts on proton exchange membrane fuel cells: a review. Int J Hydrogen Energy 2018;43:2327–48.

[31] Benouioua D, Candusso D, Harel F, Oukhellou L. The dynamic multifractality in PEMFC stack voltage signal as a tool for the aging monitoring. Int J Hydrogen Energy 2017;42:1466–71. https://doi.org/10.1016/j.ijhydene.2016.04.033.

[32] Benmouna A, Becherif M, Depernet D, Gustin F, Ramadan HS, Fukuhara S. Fault diagnosis methods for proton exchange membrane fuel cell system. Int J Hydrogen Energy 2017;42:1534–43. https://doi.org/10.1016/j.ijhydene.2016.07.181.

[33] Macauley N, Watson M, Lauritzen M, Knights S, Wang GG, Kjeang E. Empirical membrane lifetime model for heavy duty fuel cell systems. J Power Sources 2016;336:240–50. https://doi.org/10.1016/j.jpowsour.2016.10.068.

[34] Gazdzick P, Mitzel J, Garcia Sanchez D, Schulze M, Friedrich KA. Evaluation of reversible and irreversible degradation rates of polymer electrolyte membrane fuel cells tested in automotive conditions. J Power Sources

2016;327:86–95. https://doi.org/10.1016/j.jpowsour.2016.07.049.
[35] Li J, Hu Z, Xu L, Ouyang M, Fang C, Hu J, et al. Fuel cell system degradation analysis of a Chinese plug-in hybrid fuel cell city bus. Int J Hydrogen Energy 2016;41:15295–310. https://doi.org/10.1016/j.ijhydene.2016.06.136.
[36] Mulder G, De Ridder F, Coenen P, Weyen D, Martens A. Evaluation of an on-site cell voltage monitor for fuel cell systems. Int J Hydrogen Energy 2008;33:5728–37. https://doi.org/10.1016/j.ijhydene.2008.07.017.
[37] Wu J, Yuan XZ, Wang H, Blanco M, Martin JJ, Zhang J. Diagnostic tools in PEM fuel cell research: Part I Electrochemical techniques. Int J Hydrogen Energy 2008;33:1735–46. https://doi.org/10.1016/j.ijhydene.2008.01.013.
[38] Bezmalinovic D, Simic B, Barbir F. Characterization of PEM fuel cell degradation by polarization change curves. J Power Sources 2015;294:82–7. https://doi.org/10.1016/j.jpowsour.2015.06.047.
[39] Segura F, Andújar JM. Step by step development of a real fuel cell system. Design, implementation, control and monitoring. Int J Hydrogen Energy 2015;40:5496–508. https://doi.org/10.1016/j.ijhydene.2015.01.178.
[40] Ri R, Qhuj E, Ulg V, Lg K, Dkpdghlg P, Ruj L, et al. &rqwuro ri +\eulg (qhuj\ 6\vwhpv 0lfur *ulg [n.d].
[41] Darowicki K, Janicka E, Mielniczek M, Zielinski A, Gawel L, Mitzel J, et al. Implementation of DEIS for reliable fault monitoring and detection in PEMFC single cells and stacks. Electrochim Acta 2018;292:383–9. https://doi.org/10.1016/j.electacta.2018.09.105.
[42] Wang H, Gaillard A, Hissel D. Online electrochemical impedance spectroscopy detection integrated with step-up converter for fuel cell electric vehicle. Int J Hydrogen Energy 2019;44:1110–21.
[43] Brunetto C, Moschetto A, Tina G. PEM fuel cell testing by electrochemical impedance spectroscopy. Electr Power Syst Res 2009;79:17–26. https://doi.org/10.1016/j.epsr.2008.05.012.
[44] Tant S, Rosini S, Thivel P-X, Druart F, Rakotondrainibe A, Geneston T, et al. An algorithm for diagnosis of proton exchange membrane fuel cells by electrochemical impedance spectroscopy. Electrochim Acta 2014;135:368–79. https://doi.org/10.1016/j.electacta.2014.04.108.
[45] Rubio MA, Urquia A, Dormido S. Diagnosis of PEM fuel cells through current interruption. J Power Sources 2007;171:670–7. https://doi.org/10.1016/j.jpowsour.2007.06.072.
[46] LIU M, WANG J, WANG S, XIE X, ZHOU T, Mathur VK. On-line measurement for ohmic resistance in direct methanol fuel cell by current interruption method. Chin J Chem Eng 2010;18:843–7. https://doi.org/10.1016/S1004-9541(09)60137-3.
[47] Jo YY, Cho E, Kim JH, Lim T-H, Oh I-H, Kim S-K, et al. Degradation of polymer electrolyte membrane fuel cells repetitively exposed to reverse current condition under different temperature. J Power Sources 2011;196:9906–15. https://doi.org/10.1016/j.jpowsour.2011.08.035.
[48] Page SC, Anbuky a H, Krumdieck SP, Brouwer J. Test method and equivalent circuit modeling of a PEM fuel cell in a passive state. Energy conversion. IEEE Trans 2007;22:764–73. https://doi.org/10.1109/tec.2007.895857.
[49] Cooper KR, Smith M. Electrical test methods for on-line fuel cell ohmic resistance measurement. J Power Sources 2006;160:1088–95. https://doi.org/10.1016/j.jpowsour.2006.02.086.
[50] Cadet C. Jeme?? S, Druart F, Hissel D. Diagnostic tools for PEMFCs: from conception to implementation. Int J Hydrogen Energy 2014;39:10613–26. https://doi.org/10.1016/j.ijhydene.2014.04.163.
[51] Li Z, Outbib R, Giurgea S, Hissel D, Giraud A, Couderc P. Fault diagnosis for fuel cell systems : a data-driven approach using high-precise voltage sensors. Renew Energy 2018:1–10. https://doi.org/10.1016/j.renene.2018.09.077.
[52] Cole BA, Kepros MA, Schmitt RJ. A discussion about water loss, compression and the VRLA cell. In: Proceedings of power and energy systems in converging markets, Melbourne, Victoria, Australia; 1997. p. 221–9. https://doi.org/10.1109/INTLEC.1997.645892.
[53] Brunner D, Prasad AK, Advani SG, Peticolas BW. A robust cell voltage monitoring system for analysis and diagnosis of fuel cell or battery systems. J Power Sources 2010;195:8006–12. https://doi.org/10.1016/j.jpowsour.2010.06.054.
[54] De las Heras A, Vivas FJ, Segura F, Redondo MJ, Andújar JM. Air-Cooled fuel cells: keys to design and build the oxidant/cooling system. Renew Energy 2018;125:1–20. https://doi.org/10.1016/j.renene.2018.02.077.
[55] Whiteley M, Dunnett S, Jackson L. Failure mode and effect analysis, and fault tree analysis of polymer electrolyte membrane fuel cells. Int J Hydrogen Energy 2016;41:1187–202. https://doi.org/10.1016/j.ijhydene.2015.11.007.
[56] Webb D, Møller-Holst S. Measuring individual cell voltages in fuel cell stacks. J Power Sources 2001;103:54–60. https://doi.org/10.1016/S0378-7753(01)00831-X.
[57] Schuster M. Our flyer Your contact person MCM-IntelliProbe 10-Channel. 2016. p. 1–6.
[58] Summers WS, Charest FG. Intrinsically Powered Electronic Monitor for Fuel Cells. 1974. U.S. 3,808,534.
[59] http://www.quintech.de/englisch/products/research/uebersicht-cell-voltage-measurement.php [n.d].
[60] Http://www.greenlightinnovation.com/diagnostics/data-acquisition.php [n.d].
[61] http://www.scribner.com/products/896-stack-monitor-system/[n.d].
[62] https://www.cellsense.eu/[n.d].
[63] Becker-Irvin CH. Battery Cell Voltage Monitor and Method. U.S. Patent 1999;6. 406,806 B1.
[64] Blair JD, Dircks K. Method and Apparatus for Monitoring Fuel Cell Performance. 1997. https://doi.org/10.1145/634067.634234. U.S.005170124A.
[65] Heskula DH, Clingerman BJ, Chalfant RW. Fuel Cell Voltage Monitoring and System Control. U.S. 2002. 6,406,806 B1.
[66] Lacy RA. Measuring Cell Voltages of a Fuel Cell Stack. U.S. 2001. 6,313,750 B1.
[67] Masse; S, Gopal RB. Fuel Cell Voltage Monitoring and the method Thereof. U.S. 2002. 20020180447A1.
[68] Meltser MA, Grot SA. PEM Fuel Cell Monitoring System. 1998. https://doi.org/10.1145/634067.634234. U.S.005763113A.
[69] http://www.fuelcon.com/fileadmin/FuelCon/Dokumente/BZMs/BZM000/BZM087_01_15.pdf [n.d].
[70] http://fuelcellsetc.com/products-services/cell-voltage-monitor/[n.d].
[71] Barbetta Joseph P, Oradell N. Device and Method for Monitoring Fuel Cell Performance and Controlling A Fuel Cell System. 2004. https://doi.org/10.1016/j.(73). U.S. 6,762,587 B1.
[72] Calderón AJ, González I, Calderón M, Segura F, Andújar JM. A new, scalable and low cost multi-channel monitoring system for polymer electrolyte fuel cells. Sensors 2016;16:1–19. https://doi.org/10.3390/s16030349.
[73] Chang H-L, Huang J-L. Fuel Cell Voltage Measurement Device. 2009. U.S.007639023B2.
[74] https://www.smart-testsolutions.de/products-detailed-view/batterie-brennstoffzellenueberwachung-mcm-intelliprobe-linkmodul/subkategorie/mess-und-

simulationstechnik-batterie-brennstoffzellenueberwachung.html [n.d].
[75] http://www.quintech.de/englisch/products/research/lena-pro.php [n.d].
[76] http://fuelcellsetc.com/2012/06/fuel-cell-voltage-monitoring/ [n.d].
[77] https://www.smart-testsolutions.de/tl_files/smart_files/Produktblaetter/CVMprox0-R3_Datenblatt.pdf [n.d].
[78] Leal DL, Celi EÁ MR. Integral computer-aided system for control design and implementation. RIAI - Rev Iberoam Automática e Informática Ind 2016;13(2):228–37.
[79] https://www.arduino.cc/[n.d]. https://www.arduino.cc/.
[80] http://www.ni.com/es-es/shop/labview.html [n.d].
[81] BALLARD. FCgen ® -1020ACS Fuel cell Stack Product Manual and Integration Guide. 2011.

4.4. Article 4

A suitable space-state model for renewable sources-based microgrids with hydrogen as backup for the design of energy management systems

F.J. Vivas, J.J. Caparrós, F. Segura, J.M. Andújar

Submited in:

Journal: International Journal of Hydrogen Energy
Editorial: IEEE
Editor-in-Chief: T. Nejat Veziroglu
ISSN: 0360-3199
In review process

Category	Journal Rank / Total journals	Quartile
Computer Science, Information system	23 / 155	Q1
Engineering, electrical & electronic	52 / 265	Q1
Telecommunications	19 / 88	Q1
Impact Factor (2018)	4.098	

IEEE Access
Multidisciplinary | Rapid Review | Open Access Journal

Date of publication xxxx 00, 0000, date of current version xxxx 00, 0000.

Digital Object Identifier 10.1109/ACCESS.2017.Doi Number

A suitable space-state model for renewable sources-based microgrids with hydrogen as backup for the design of energy management systems

Vivas F.J.[1], Caparrós J.J.[1], Segura F.[1], Andújar J.M[1] (Senior Member, IEEE).

[1] Grupo de Investigación de Control y Robótica TEP-192, Departamento de Ingeniería Electrónica, de Sistemas Informáticos y Automática, Escuela Técnica Superior de Ingeniería. Universidad de Huelva, Spain

Corresponding author: Francisco José Vivas Fernández (e-mail: francisco.vivas@diesia.uhu.es).

ABSTRACT

When a microgrid includes control and management smart technology, it becomes a smart microgrid. The term smart means that the microgrid has a control system with its own energy management system (EMS) that is able to meet with the demand requirements, to increase the lifetime of the devices, to reduce operating costs and to maximize the microgrid efficiency. But, the increasing complexity of microgrids due to the many different renewable sources involved and the minimum quality and competitiveness restrictions, it requires to have accuracy and practical models (useful for both simulation and control) that reflects as well as possible the real performing of the microgrid. This paper develops a general space-state model that allows modelling the performance of a complete renewable sources-based microgrid with hydrogen as backup throughout all its operating range. This approach guarantees a better approximation with respect to those models mostly used in the scientific literature because those one are linearized systems around a single operating point. Additionally, apart from describing electrical performance for each device that makes up the microgrid, the proposed modelling formulation also includes technical and economical parameters as operating efficiency, degradation, losses and costs needed for the microgrid optimization. The paper includes experimental results that show the quality and excellent performance of the developed model. This can be an excellent starting point for develop accuracy simulation tools as well as energy management controllers to be used in renewable sources-based microgrids with hydrogen as backup.

INDEX TERMS Energy management system, State-space model, renewable sources-based smart microgrids, hydrogen backup systems.

LIST OF ACRONYMS

BoP: Balance of plant
EMS: Energy management system
HL: Hydrogen level
LTI: Linear time invariant
LTV: Linear time variant
MPPT: Maximum power point tracking
O&M: Operation and maintenance
PEM: Proton exchange membrane
SCADA: Supervisory control and data acquisition
SOC: State of charge

I. INTRODUCTION

Microgrid are closely linked to the use of renewable energy sources [1]. Despite the benefits of these systems, their dependence on environmental resources does not guarantee a zero net power balance at any time. To solve this problem, hybridization is presented as a viable technical and economic solution [2]. For this purpose, the use of energy storage systems, which allows absorbing the excess energy and supplies energy when the renewable resource is insufficient, is necessary. In this sense, the utilization of hydrogen as an energy vector is a promising solution [3][4].

Most renewable microgrids with hydrogen as backup have an underlying structure similar to that shown in Fig. 1. Renewable generation is usually represented by traditional sources based on solar panels or wind turbines [2][5][6]; although there are other applications based on biomass [7], tidal energy [8], etc. Considering the energy storage system, regardless of the use of power converters and the nature of the internal bus (DC or AC), a battery bank is normally designed to absorb the transients in the power balance and, therefore, represents the short-term storage system [2][5]. In contrast, the hydrogen-based storage system usually faces more stable power imbalances and, consequently, acts as a long-term storage system [2][9]. Depending on the application, the hydrogen generation system can be represented by the use of an electrolyser (usually alkaline or proton-exchange membrane (PEM) apropos the available technology) as the first option [2], or by replacing a reforming process [10], or by decomposing matter through bacteria [11], etc.

With the increasing complexity of microgrids due to the many different renewable sources involved and the required quality and competitiveness constraints, it is inevitable to incorporate a certain degree of intelligence in the micro network through an energy management system (EMS), Fig. 1, which must ensure that all critical parameters of the micro network (both from the user's point of view and from the elements of the microgrid) be satisfied at all time. This lead the microgrid to a smart microgrid.

FIGURE. 1. Typical architecture and power balance of a renewable sources-based microgrid with hydrogen as backup.

Regardless of the system sizing or technology used, the main target of a hybrid renewable energy microgrid must be meeting the load demand at all times; however, secondary objectives such as the technical and economic viability must be also taken into account to allow the hybrid renewable energy microgrid being really competitive with conventional sources-based grid [12]. These technical and economic objectives can be thus included in any of the following categories: minimization of the operation costs, maximization of useful lifetime of the equipment or minimization of operational losses. The optimization parameters related to above-cited objectives are identified by each application, optimization horizon (short- or long-term), system topology and nature of the devices.

Regarding the technical objectives, to guarantee an efficient and safe use of batteries, it is necessary to impose certain restrictions regarding the battery charging and discharging processes [3][13][14] by implementing a charging protocol based on voltage control to avoid excessive degradation, to guarantee maximum energy use in terms of efficiency [13][15][16], to limit the maximum depth of discharge, or increase the useful lifetime of the batteries [17][18].

In this sense, it is also necessary to analyse the use of the hydrogen-based energy systems. In the case of the electrolyser, the degradation is associated with its use, and it is directly related with the power and the operating time [19][20]. Considering the operating efficiency, its value will depend directly on the temperature conditions, and inversely with the operating voltage and power [21].

The operating conditions of the fuel cell determine its useful lifetime [22]–[24]. Thus, avoiding problems associated with thermal management or the balance of plant (BoP), the main causes of operational degradation are given by the cycling, operating time at high voltages-low currents, due to carbon corrosion process [25][26], and the lack of reactants caused by sudden changes in the load demand due to the fuel starvation phenomenon [27][28]. The value of the fuel cell efficiency directly depends on the operating voltage; the higher the operating voltages, the higher efficiency [29]. Coming to terms, there is a split-up between selecting an efficient operating point or considering a conservative use of the fuel cell [9].

Finally, taking into account the economic optimization of the microgrid, it is necessary to consider the depreciation, operation and maintenance (O&M) costs of each of its elements, as well as to regard the price of buy/sale energy from/to the external electrical grid (see Fig.s 1), with the objective of maximizing the economic benefit based on the integration of the microgrid into the intraday electricity market [30].

In view of the foregoing, there is a high quantity of parameters and factors that should be considered in the microgrid operation, which will largely determine its behaviour. In order to optimize the microgrid response, it is necessary to design and develop control algorithms that implement an EMS that permits, on the one hand, to guarantee the demand at all times and, on the other, to optimize the response of the microgrid according to the studied technical and economic parameters [3][31]–[33]. But as important as the above, is the fact that it would be very useful to carry out precise simulations to verify the operation of the microgrid under different conditions. When managing tens or hundreds of kilowatts, it is not advisable to make decisions or even perform operations without knowing the expected results. Therefore, for the best simulation of the microgrid and to help design of appropriate EMS, it is pivotal to have the best possible microgrid model. This explains the objective of this article: to develop a good microgrid model that, taking into account all the parameters

(technical and economic) explained above, allows precision simulations and the design of appropriate EMS systems.

Then, regarding microgrid modelling process, most of the solutions presented in the scientific literature, carry out an extensive and complex formulation, particularly for the technology and configuration of the devices that make up the microgrid, which greatly hinders its use, generalization and extrapolation to other cases [34][35]. Thus, the models used are oriented to the calculation of the main electrical and physical-chemical parameters of the device, typically oriented to the design of the local controllers instead of EMS. In many cases, the calculation of the main parameters of these models is not a trivial task, and therefore the use of simplifications or assumptions that may have impact on the quality of the model are applied [34][1]. Examples of these complex models are the model based on One/Two-diode for solar cells [34][36]–[39]; or the most extended electrolyser and fuel cell models, based on voltage losses due to physical-chemical parameters, defined by operating conditions such as partial reagent pressures, operating temperature, membrane electrical conductivity, stoichiometry, etc. [34][35][39]–[43].

Considering the inclusion in the model of technical and economic parameters of the microgrid, it is possible to find in the scientific literature different solutions, which are described below.

1. Based on the calculation of the devices depreciation and their associated cost, the widespread solution are based on expressions that are independent of the operating power, especially in the case of electrolyser and fuel cell, being a function only of the operating time of the device to be modelled [5][42], [44]–[46], or including certain operating conditions, such as number of start and stop cycles [30][47]. This leads to a simplification of the problem, because although fixed costs associated with the use of these systems can be determined, there are other variable costs depending on the operating regime, associated with depreciation, cooling needs, water consumption, etc.

2. Regarding the calculation of the operating efficiency of the devices, although in the case of electrolyser and fuel cell the formulation to calculate the operating efficiency is perfectly defined, there is no expressions that allow modelling the efficiency of battery operation, essential for the correct estimation of the battery state of charge depending on voltage, temperature, and charging current [34] [41][47]–[49].

Then, the modelling of the optimization parameters is based on multiple simplifications, particularized in each model and for each application, and therefore they move away from the real performance of the devices and they lack the required generality.

Finally, according to the type of model proposed, due to the complexity associated with the use of non-linear models, the widely adopted solution is the use of Linear Time Invariant (LTI) models calculated from the linearization around a single working point [30][50]–[54], which negatively affects the quality of the model and the results derived from its use [55][56], since in a real microgrid the operating range is very wide.

Therefore, attending to the previous considerations, the objective of this paper is to propose a generalized mathematical model of a renewable sources-based microgrid that allows, independently of the topology and equipment technology used, to determine the technical and economic parameters associated with its operation based on the operating point of each of its elements. The proposed formulation is based on an extended Linear Time Variant (LTV) model, calculated from a recursive linearization process, which allows to faithfully model the system behaviour throughout its entire operating range. The proposed model will allow, on the one hand, to quantify the performance of the system associated exclusively with the energy management strategy used, as well as serve as a knowledge base for the design and analysis of model-based controllers.

The paper organization is as follows: Section II presents the materials used in this research, which is essentially a real renewable sources-based microgrid with hydrogen as backup. Section III presents the developed methodology to obtain the general space-state model of the microgrid. Section IV deals with the real experimental tests carried out to validate the model accuracy and to demonstrate its application. The model performance discussion is contained in section IV and, finally, Section V presents the main conclusions obtained from the developed work.

II. MATERIALS

With the objective of being able to validate the proposed model, and without loss of any generality, all the experimental tests have been carried out on the resources available in the research laboratory, in accordance with the general scheme of the micro grid under study, proposed in Fig. 1.

In the following sections the equipment used for the identification process and experimental validation will be described in more detail.

2.1-BATTERY BANK

For the validation of the proposed model, an AGM lead-acid technology battery bank is available. The battery bank is made up of a total of 30 units of 12 VDC and 100 Ah batteries in a serial configuration (Fig. 2), providing a nominal voltage of 360 VDC and a storage capacity of 36 kWh.

With the objective of supervising the operation during the charging and discharging processes, a local acquisition system is available, which allows the monitoring of the main system variables (battery voltage, battery current and battery temperature), in such a way that it is allowed to ensure that the operating parameters are within the safety ranges established by the manufacturer.

Finally, the battery bank has all the necessary electrical protections to guarantee safety in its operation.

a)

b)

FIGURE. 2. Detail of the Lead-acid battery bank.

2.2- Hydrogen-based systems

According to the general model of the micro grid presented in Fig. 1, a hydrogen generation system is necessary, which allows the excess energy to be stored in the form of hydrogen for its subsequent conversion to electrical energy.

In this case, an alkaline technology electrolyzer of 2 Nm3/h is available (Fig. 3). The electrolyser has all the Balance of Plant (BoP), sensors, actuators and auxiliary equipment necessary for the correct management of the system, so that the operation of the electrolyser is carried out within the conditions defined by the manufacturer and based on the established power setpoint.

In response to the power stage for the electrolysis process, a rectifier stage is available in the first instance, which allows the stack to be fed from a three-phase AC outlet or from a regulated DC voltage. Subsequently, a DC/DC buck converter implements a control based on the current supplied to the stack, in such a way that it guarantees the working power of the electrolyser, while monitoring that the operating voltage is within the established limits by the manufacturer.

Finally, the electrolyser has a PLC from the manufacturer ABB® which acts as an acquisition and control system, allowing the reading and storage of the main operating parameters of the electrolyser, necessary for the validation of the proposed model.

a)

b)

c)

FIGURE. 3. Detail of the Alkaline electrolyser (a and b); Power electronics and control cabinet (c).

In accordance with the configuration presented in Fig. 1, and as a core of the hydrogen-based storage system, a 3.4 kW PEM technology fuel cell is available (Fig. 4a). In order to guarantee the operating conditions, in terms of supply pressure, operating temperature, cooling/oxidant flow rate, etc; as well as regulating the working point of the fuel cell, control electronics and power converters specially designed for the application are available, Fig. 4b and Fig. 4c respectively.

Attending to the operation variables of the fuel cell, the stack temperature monitoring is carried out through an NTC type surface temperature sensor integrated in the fuel cell itself. To guarantee the supply pressure and measure the supplied hydrogen flow rate, an inlet pressure sensor, as well as a mass flow meter is available respectively. The use of this sensor allows the calculation of the hydrogen consumption, and consequently the operating performance of the fuel cell.

In accordance with the thermal control of the system, a fan with speed control is available. The use of this fan allows the fuel cell to operate within the safe temperature operating range, depending on the operating point, through the use of a local controller. In the same way, the use of the fan guarantees the minimum stoichiometric coefficient to produce the main

reactions. Similarly, discrete control signals are available to act on the different supply and purge solenoid valves, as well as the electrical connection relay.

All the conditioning and signal processing electronics described have been specifically designed for the application, and are integrated into the control electronics presented in Fig. 4c.

Attending the conversion and power stage, in this particular case, the designed power converter is based on a 3.4 kW Push-Pull topology (Fig. 4b) and has all the necessary sensors to measure the main electrical parameters of the fuel cell. The internal control of the power converter allows to implement operating modes based on working power, voltage or current setpoints of the fuel cell, which allows in addition to its integration in any system, the testing of the potentiostatic and galvanostatic operating modes depending on the application.

a)

b)

c)

FIGURE. 4. a) PEM fuel cell; b) DC-DC Push-Pull converter; c) BoP controller.

In order to store the hydrogen produced by the electrolyser, and supply the fuel cell, it is available a 1 Nm3, 25 bar high pressure tank (Fig. 5). This tank has all the valves and sensors necessary for the monitoring of inlet pressure and hydrogen flowrate in order to ensure proper use within the physical limits determined by the manufacturer.

FIGURE. 5. Hydrogen high pressure tank.

2.3- Programmable power source and electronic load

With the objective to simulate any demand profile, and thus allow the characterization of the different equipment, batteries and fuel cell, a 10 kW programmable electronic DC load is available (Fig. 6a). The programmable electronic load incorporates its own data acquisition system and communications via Ethernet, and therefore the measurements of all the electrical parameters, voltage and current, necessary for the models validation are available.

Finally, in order to validate the proposed battery model, a 15 kW DC programmable power supply is used (Fig. 6b), which allows to implement any desired generation profile from an imposed power, current or voltage setpoint. Similarly to the programmable electronic load, the programmable power supply has its own data acquisition system and communications via Ethernet, and therefore current and voltage measurements necessary for the validation of the battery charging model are available.

a)

b)

FIGURE. 6. a) DC programmable electronic load; b) DC programmable power supply.

The system main parameters and system configuration are shown in Table 1.

TABLE I
SYSTEM PARAMETERS

Component	Parameter	Value	Manufacturer
Lead acid Battery bank	Rated capacity (C_{10})	100 Ah	U-Power®
	Battery voltage	12 V	
	Number of batteries (series configuration)	30	
High Pressure tank	Rated capacity	1 Nm^3, 25 bar	Lapesa®
Alkaline electrolyser	Rated power	10 kW	ARIEMA®
	Hydrogen production rate	2 Nm3/h	
	Number of cells	28	
PEM Fuel cell	Rated Power	3.4 kW	BALLLARD®
	Number of cells	80	
DC Programmable power supply	Rated Power	15 kW	SORENSEN®
DC Programmable load	Rated Power	10 kW	AMREL®

III. MICROGRID MODELLING. METHODOLOGICAL FOUNDATION PROPOSAL

With the objective to simulate any demand profile, and thus allow the characterization of the different equipment, batteries and fuel cell, a 10 kW programmable electronic DC load is available (Fig. 6a). The programmable electronic load incorporates The modelling process has the objective to obtain a mathematical model that represents the performance of a renewable sources-based microgrid with hydrogen as backup (similar to that of Figure 1) throughout its complete operating range and includes all the parameters necessary to perform an optimal energy management from a technical and economic point of view. As the objective is not only to be able to obtain an accurate model to simulate the network, but also to obtain a model suitable for control, the model to be developed will be a state-space model. That is, the usual model used in control for both linear and non-linear multivariable systems. In this case, to solve the problem associated with nonlinearities in the modelling, a recursive linearization process will be used in such a way that the non-linear terms will be calculated and linearized in each sampling period, defining a linear time variant (LTV) model.

In the following sections, the model of each device (battery and hydrogen-based equipment since, as stated before, regarding renewable generation devices, the only variable that the model must take into account is the available renewable power on the DC bus) that integrates the renewable sources-based microgrid with hydrogen as backup will be depicted (see Figure 1). Each model describes the electrical performance for each element and also includes the technical (operating efficiency, degradation, losses and useful lifetime) and economical (costs) parameters needed for system performance optimization. Additionally, due to the particular dynamics of the application (renewable sources with slow response), relatively large sample time is allowed, in terms of tens of seconds (even minutes), which facilitates the use of the modelling process from static models with a small margin of error.

Finally, without losing generality, the proposed model will be validated (Section IV) on the experimental microgrid of our University, described in Section II.

3.1- Equipment Modelling: Battery and hydrogen-based systems

3.1.1- Battery performance modelling

In cases where a microgrid is supported by a battery bank, Figure 1, it is necessary that the EMS integrates a battery charging protocol with the aim of prolonging the battery's useful lifetime. For this purpose, a model of the battery bank should be developed. The parameters to be into account for the battery modelling are: battery voltage, battery efficiency and battery state of charge.

3.1.1.1- Battery Voltage

There are different papers that present static models of battery voltage, both for the charging and discharging processes. These models are mainly based on resistive circuits in which the polarization resistances are obtained from the mass balance available in the electrodes, and they have different relationships with respect to the current and the battery state of charge [57], [58].

The best known and widely used models, due to their simplicity and good approximation, are those presented by Copetti [58] (specific for lead-acid batteries) and Tremblay [57] (general model).

Copetti's proposal is shown in equations (1) and (2):

$$V_{bat_{char}}(k) = \left(2 + a_c SOC(k)\right) - \\ -\frac{i_{bat}(k)}{C_N(k)}\left(\frac{b_c}{1+\left(i_{bat}(k)\right)^{c_c}} + \frac{d_c}{\left(1-SOC(k)\right)^{e_c}} + f_c\right) \quad (1)$$

$$V_{bat_{disch}}(k) = \left(2.085 - a_d\left(1-SOC(k)\right)\right) - \\ -\frac{i_{bat}(k)}{C_N(k)}\left(\frac{b_d}{1+\left(i_{bat}(k)\right)^{c_d}} + \frac{d_d}{SOC(k)^{e_d}} + f_d\right) \quad (2)$$

Where:

$V_{bat_{disch}}(k)$: Battery voltage during the discharge at sampling time k (V).

$V_{bat_{char}}(k)$: Battery voltage during the charge at sampling time k (V).

$a_c, a_d, \dots g_c, g_d$: Battery parameters for charging and discharging model respectively.

$SOC(k)$: Battery state of charge at sampling time k.

$i_{bat}(k)$: Battery current at sampling time k (A).

$C_N(k)$: Nominal battery capacity at sampling time k (Ah).

Tremblay's model is summarized in equations (3) and (4):

$$V_{bat_{disch}}(k) = E_0 - Ri_{bat}(k) - \\ -K\left(\frac{C_N(k)}{C_N(k) - C_N(k)\left(1 - SOC(k)\right)}\right) \\ \left(C_N(k)\left(1 - SOC(k)\right) + i_{bat}(k)\right) + Ae^{-Bi_{bat}(k)T_s} \quad (3)$$

$$V_{bat_{char}}(k) = E_0 + Ri_{bat}(k) - \\ -K\left(\frac{C_N(k)}{C_N(k) - C_N(k)\left(1 - SOC(k)\right)}\right) \\ \left(C_N(k)\left(1 - SOC(k)\right)\right) + \\ +K\left(\frac{C_N(k)}{C_N(k)\left(1 - SOC(k)\right) - 0.1C_N(k)}\right) i_{bat}(k) + \\ +Ae^{-Bi_{bat}(k)T_s} \quad (4)$$

Where:
E_0: Battery open circuit voltage (V).
R: Battery internal resistance (Ω).
$i_{bat}(k)$: Battery current at sampling time k (A).
K: Polarization constant (V/Ah).
$C_N(k)$: Nominal battery capacity at sampling time k (Ah).
$SOC(k)$: Battery state of charge at sampling time k.
A: Exponential zone amplitude (V).
B: Exponential zone time constant inverse (Ah^{-1}).
The different coefficients of the models can be obtained through an identification process from empirical tests for different charging and discharging currents throughout the operating range of the battery's state of charge (SOC).
Regardless of the voltage model used, and based on the model parameters obtained through the identification process, it can be obtained a linearized model of the battery voltage, which can be calculated by a recursive linearization process based on the Taylor approximation method for the current operating power. According to the dimensions of the model, the surfaces obtained based on the recursive linearization process will be defined by equation (5).

$$V_{bat}(k) \approx f\left(i_{bat_0}(k), SOC_0(k)\right) + \\ + \left.\frac{\partial f(i_{bat}, SOC)}{\partial i_{bat}}\right|_{i_{bat_0}(k), SOC_0(k)} \left(i_{bat}(k) - i_{bat_0}(k)\right) + \\ + \left.\frac{\partial f(i_{bat}, SOC)}{\partial SOC}\right|_{i_{bat_0}(k), SOC_0(k)} \left(SOC(k) - SOC_0(k)\right) \quad (5)$$

Where:
$V_{bat}(k)$: Battery voltage at sampling time k (V).
$f(i_{bat}, SOC)$: Non lineal battery model (Copetti or Tremblay)
$SOC(k)$: Battery state of charge at sampling time k.
$i_{bat}(k)$: Battery current at sampling time k (A).
$i_{bat_0}(k)$: Battery current at linearization point at sampling time k (A).
$SOC_0(k)$: Battery state of charge at linearization point at sampling time k.
Assuming a minimum variation of the battery voltage $V_{bat}(k)$with respect to the previous value at time $k-1$, the term of battery current can be replaced by a term dependent on battery power, incorporating the voltage term in the parameter associated with the battery current resulting from the linearization process, expressed in the general equation (6).

$$V_{bat}(k) = SV(k) \cdot SOC(k) + VP(k) \cdot P_{bat}(k) + C(k) \quad \textbf{(6)}$$

Where:
$V_{bat}(k)$: Battery voltage at sampling time k (V).
$SV(k)$: Coefficient associated to SOC term at sampling time k.
$VP(k)$: Coefficient associated to battery power term at sampling time k.
$SOC(k)$: Battery state of charge at sampling time k.
$P_{bat}(k)$: Battery power at sampling time k (W).
$C(k)$: Independent term result of the linearization process at sampling time k.
In accordance with the Taylor approach, the terms $SV(k)$, $VP(k)$ and $C(k)$ can be calculated according to the expressions (7), (8) and (10) respectively for each linearization point.

$$SV(k) = \left.\frac{\partial f(i_{bat}, SOC)}{\partial SOC}\right|_{i_{bat_0}(k), SOC_0(k)} \quad (7)$$

$$VP(k) = \frac{1}{V_{bat}(k-1)} \cdot \left.\frac{\partial f(i_{bat}, SOC)}{\partial i_{bat}}\right|_{i_{bat_0}(k), SOC_0(k)} \quad (8)$$

$$C(k) = f\left(i_{bat_0}(k), SOC_0(k)\right) - \\ - \frac{i_{bat_0}(k)}{V_{bat}(k-1)} \cdot \left.\frac{\partial f(i_{bat}, SOC)}{\partial i_{bat}}\right|_{i_{bat_0}(k), SOC_0(k)} - \\ - SOC_0(k) \cdot \left.\frac{\partial f(i_{bat}, SOC)}{\partial SOC}\right|_{i_{bat_0}(k), SOC_0(k)} \quad (9)$$

3.1.1.2.- Battery Efficiency

The battery efficiency is defined by the amount of energy actually used by the battery to produce the main reactions, which defines the chemistry of the charging and discharging processes [59][60].
Focusing the problem for lead-acid batteries, the main phenomena that affect the battery efficiency (η_{bat}) are given by the internal resistance due to the Joule Law as well as the effect of secondary reactions, such as corrosion and electrolysis of the electrolyte during the charging process [14][15][61]. Because Joule losses usually represents a very low percentage with respect to the operating power of the battery, the discharge efficiency is normally considered unitary, (10).

$$\eta_{bat_{disch}}(k) \approx 1 \quad (10)$$

Where k is the sampling time.
During the charging process, the amount of current that the battery is able to accept depends mainly on the number of reactants available to produce the main reaction. In case the battery SOC is low or medium, the battery has a large reserve of material to produce the main reaction and, therefore, can accept large amounts of charge. As the battery increases its SOC, the amount of available active material is reduced and, therefore, its ability to accept current decreases. If the battery is forced to be charged at a higher current than can be accepted, an accelerated increase in the battery voltage occurs, while causing the increase in secondary reactions (mainly electrolysis and corrosion) [15][60].
In view of the above, the charging current of the battery $\left(i_{bat_{char}}(k)\right)$ at sampling time k can be defined at all times by a usable component to contribute to the main reaction, $I_{MR}(k)$, and another component used in secondary or side reactions, $I_{SR}(k)$, (11):

$$i_{bat_{char}}(k) = I_{MR}(k) + I_{SR}(k) \tag{11}$$

The term related to side reactions can be approached to the current consumed during the electrolysis process, also known as gassing current, since the effect of the corrosion is negligible with respect to it [14][60][62]. The current generated during the electrolysis process has an exponential function with respect to the battery voltage and temperature according to the Butler-Volmer equation [15][60], (12).

$$I_{SR}(k) \approx I_G(k) = \\ = I_{G_o} e^{\left(K_V\left(V_{bat_{char}}(k) - V_{bat_o}\right) + K_T\left(T_{bat}(k) - T_{bat_o}\right)\right)} \tag{12}$$

Where:
$I_G(k)$: Current consumed during the electrolysis process (Gassing current) at sampling time k (A).
I_{G_o}: Exchange current (A).
K_V: Voltage coefficient (V-1).
K_T: Temperature coefficient (T-1).
$V_{bat_{char}}(k)$: Battery voltage at sampling time k (V).
V_{bat_o}: Reference battery voltage (V).
$T_{bat}(k)$: Battery temperature at sampling time k (K).
T_{bat_o}: Reference temperature (K).
The coefficients of the Butler-Volmer equation can be obtained through experimental identification tests under different charging voltage and temperature conditions.
From (12), a mathematical relationship of the battery efficiency during the charge can be obtained as a function of the charging current and, analogously, as a function of charging voltage and battery charging power, (13).

$$\eta_{bat_{char}}(k) = \frac{i_{bat_{char}}(k) - I_{SR}(k)}{i_{bat_{char}}(k)} = \\ 1 - \frac{V_{bat_{char}}(k) \cdot I_{G_o} \cdot e^{\left(K_V\left(V_{bat_{char}}(k) - V_{bat_o}\right) + K_T\left(T_{bat}(k) - T_{bat_o}\right)\right)}}{P_{bat_{char}}(k)} \tag{13}$$

According to equation (13), in order to estimate the charging efficiency, it is necessary to know the actual battery voltage and power values. If these parameters cannot be measured directly in the system, they can be approximated from the value obtained at the previous instance. The use of reduced sampling period and the slow dynamics of the system will allow a reduced error in the approach.

3.1.1.3.- Battery State of Charge Estimation

The battery's state of charge (SOC) is determined from the amount of charge available in the battery with respect to the maximum charge storage capacity, i.e., its nominal capacity [63][64], (14).

$$SOC(t) = SOC(t_0) + \frac{\eta_{bat}(t)}{C_N(t)} \int_{t_o}^{t_o+t} i_{bat}(t)\, dt \tag{14}$$

Where:
$SOC(t)$: Battery state of charge (%).
$\eta_{bat}(t)$: Overall battery efficiency (%).
$C_N(t)$: Battery nominal capacity (Ah).
$i_{bat}(t)$ Battery charging/discharging current (A); loss reactions included.
Equation (14) can be represented in terms of battery instantaneous power, P_{bat}.

$$SOC(t) = SOC(t_0) + \frac{\eta_{bat}(t)}{C_N(t)} \int_{t_o}^{t_o+t} \frac{P_{bat}(t)}{V_{bat}(t)} dt \tag{15}$$

With the discretizing equation (15) according to the backward-Euler method a linear model can be used to determine the instantaneous charging/discharging power, (16).

$$SOC(k+1) = SOC(k) + \\ + \frac{P_{bat}(k) \cdot \eta_{bat}(k) \cdot \frac{1\,h}{3600\,s} T_s}{C_N(k) \cdot V_{bat}(k)} \\ \rightarrow SOC(k+1) = SOC(k) + P_{bat}(k) \cdot S_1(k) \tag{16}$$

Where:
$SOC(k+1)$: Battery SOC at sampling time k +1 (%).
$SOC(k)$: Battery SOC at sampling time k (%).
$P_{bat}(k)$: Battery power at sampling time k (W).
$V_{bat}(k)$: Battery voltage at sampling time k (V).
$C_N(k)$: Nominal battery capacity at sampling time k (Ah).
T_s: Sampling period (s).
$S_1(k)$: All the terms that multiply $P_{bat}(k)$, (%/W).
In order to define the parameter $S_1(k)$, it is necessary to have the existing values of operating efficiency, nominal capacity and battery voltage. Due to the normally slow dynamics of the batteries SOC, these parameters can be approximated from the value calculated at the previous sampling. In any case, the

error of this approach can be minimized by reducing the sampling period.

3.1.2- Modelling of the Hydrogen-based Storage Systems

In cases where a microgrid integrates hydrogen-based storage systems, Figure 1, it is necessary that the EMS controls the hydrogen level, hydrogen generation/consumption ratio and operating efficiency. Only in this way hydrogen availability will be guaranteed at any time as well as better system efficiency.

3.1.2.1.- Estimation of the Hydrogen Level

The hydrogen level (HL) available will be given by the mass balance associated with the generation and consumption of hydrogen by the electrolyser and fuel cell respectively, (17).

$$HL(t) = HL(t_0) + \\ + \int_{t_0}^{t_0+t} \left(P_{els}(t) r_{els}(t) - P_{fc}(t) r_{fc}(t) \right) dt \quad (17)$$

Where:
$HL(t)$: Hydrogen storage level (Nm3).
$P_{els}(t)$: Electrolyser power (W).
$r_{els}(t)$: Hydrogen generation ratio associated to electrolyser production (Nm3/h).
$P_{fc}(t)$: Fuel cell power (W).
$r_{fc}(t)$: Hydrogen consumption ratio associated to fuel cell (Nm3/h).
Discretizing the equation according to the Backward-Euler method, a linear model with respect to the electrolyser and fuel cell power can be determined, equation (18).

$$HL(k+1) = HL(k) + \\ + \left(P_{els}(k).r_{els}(k) - P_{fc}(k).r_{fc}(k) \right) \frac{1\ h}{3600\ s} T_s \quad (18)$$

3.1.2.2.- Hydrogen generation/consumption ratio

To determine the value of the hydrogen generation/consumption ratio according to the electrolyser and fuel cell operation point, the Faraday Law is used [21][65], (19).

$$r_{els}(k), r_{fc}(k) = \frac{\dot{n_{H2}}(k) \cdot M_{H2}}{\rho_{H2}} = \\ = \frac{i_{els,fc}(k) \cdot N_{cell(els,fc)} \cdot M_{H2}}{z \cdot F \cdot \rho_{H2}} = \\ = 4.17 \times 10^{-4} i_{els,fc}(k) \cdot N_{cell(els,fc)} \quad (19)$$

Where:
$\dot{n_{H2}}(k)$: Hydrogen production/consumption ratio (Nm3/h).
M_{H2}: Molecular hydrogen molar mass (2.02 g/mol).
ρ_{H2}: Molecular hydrogen gas density (0.0899 Kg/Nm3).
$i_{els,fc}(k)$: Current consumed/provided by the electrolyser (els) /fuel cell (fc) at sampling time k (A).
$N_{cell(els,fc)}$: Number of cells of the electrolyser or fuel cell stack.
z: Number of electrons involved in the reduction-oxidation reaction ($z = 2$).
F: Faraday constant (26.81 Ah/eq).
From the previous expression, the parameter for hydrogen consumption/generation based on the operating current of each hydrogen device can be determined. Once the working voltage is known, this ratio can be easily related with the operating power, (20) and (21) respectively for electrolyser and fuel cell.

$$r_{els}(k) = 4.17 \times 10^{-4} \frac{P_{els}(k)}{V_{els}(k)} N_{cell(els)} \frac{1\ h}{3600\ s} T_s \\ \rightarrow r_{els}(k) = P_{els}(k) \cdot r_1(k) \quad (20)$$

Where:
$r_{els}(k)$: Hydrogen generation ratio associated to electrolyser at sampling time k (Nm3/h).
$r_{fc}(k)$: Hydrogen consumption ratio associated fuel cell at sampling time k (Nm3/h).
$V_{els}(k)$: Electrolyser operating voltage at sampling time k (V).
$P_{els}(k)$: Electrolyser operating power at sampling time k (W).
T_s: Sampling period (s).
$r_1(k)$: All the terms that multiply $P_{els}(k)$, (Nm3/Wh).

$$r_{fc}(k) = 4.17 \times 10^{-4} \frac{P_{fc}(k)}{V_{fc}(k)} N_{cell(fc)} \frac{1\ h}{3600\ s} T_s \\ \rightarrow r_{fc}(k) = P_{fc}(k) \cdot r_2(k) \quad (21)$$

Where:
$r_{fc}(k)$: Hydrogen consumption ratio associated to fuel cell at sampling time k.
$V_{fc}(k)$: Fuel cell voltage at sampling time k (V).
$P_{fc}(k)$: Fuel cell operating power at sampling time k (W).
T_s: Sampling period (s).
$r_2(k)$: All the terms that multiply $P_{fc}(k)$, (Nm3/Wh).
If the values of the electrolyser and fuel cell operating voltages cannot be obtained through direct measurement, each power value can be estimated from their polarization curve. This approach, despite being a static model, allows for an acceptable result because the normally slow dynamics of the hydrogen devices permits sampling period of tens of seconds (even more) without negatively affecting the performance of the system.

3.1.2.3.- Hydrogen-based systems: Operating Efficiency

In case of the electrolyser, the operating efficiency, η_{els}, is defined by the quotient between the chemical power associated with the produced hydrogen, P_{H_2}, and the electrical power consumed, P_{els}, [21][29]. Therefore, at sampling time k (22) is obtained.

$$\eta_{els}(k) = \frac{P_{H_2}(k)}{P_{els}(k)} = \frac{r_{els}(k)LHV}{P_{els}(k)} \quad (22)$$

Where LHV is the hydrogen lower heating value (2993 Wh/Nm3)
Equation (17) verifies that electrolyser efficiency, η_{els}, is inversely proportional to its operating voltage [21][65], which can be easily shown in (23).

$$\eta_{els}(k) = \frac{P_{H_2}(k)}{P_{els}(k)} = \\ = \frac{4.17 \times 10^{-4} \frac{P_{els}(k)}{V_{els}(k)} N_{cell(els)} LHV}{P_{els}(k)} \\ \rightarrow \eta_{els}(k) = \frac{K_{els}}{V_{els}(k)} \quad (23)$$

Where K_{els} (V) represents the result of operating with all terms that multiply $V_{els}(k)$.
In the case of the fuel cell, its efficiency, η_{fc}, is defined by the quotient between the generated electric power, P_{fc}, and the chemical power associated with the hydrogen consumed, P_{H_2}, [29]. Again, at sampling time k (24) is obtained.

$$\eta_{fc}(k) = \frac{P_{fc}(k)}{P_{H_2}(k)} = \frac{P_{fc}(k)}{r_{fc}(k)LHV} \quad (24)$$

Equation (24) verifies that, unlike the case of the electrolyser, the efficiency of the fuel cell is directly proportional to its operating voltage (25).

$$\eta_{fc}(k) = \frac{P_{fc}(k)}{P_{H_2}(k)} = \frac{P_{fc}(k)}{4.17 \times 10^{-4} \frac{P_{fc}(k)}{V_{fc}(k)} N_{cell(fc)} LVH} \\ \rightarrow \eta_{fc}(k) = \frac{V_{fc}(k)}{K_{fc}} \quad (25)$$

Where K_{fc} (V) represents the result of operating with all terms that multiply $V_{fc}(k)$.

3.2.- Technical and Economic Parameters Modelling: Life Time, Operating Costs and Losses

The lifetime, operating costs and losses included in the model will take into account the degradation of the smart grid elements, costs (differentiating operating and maintenance costs from depreciation costs) and losses; all this, obviously, under the consideration to meet with the power balance. Considering the huge difference between the lifetime of photovoltaic panels (25 years or more) and wind turbines (similar to photovoltaic panels) as well as their operating costs with respect to batteries and hydrogen system, the model only considers these last two. Regarding the losses, the referred to photovoltaic panels and wind turbines are well-known and they are ignored because there is no point to carry out any control over them, i.e., it is assumed the power available at the DC/AC bus after losses (P_{ren} in Figure 1). In fact, the modelling process considers that while there are renewable resources, photovoltaic panels and wind turbines are delivering all the available power to the renewable microgrid. The EMS controls the power balance in the microgrid and, in case batteries fully charged and hydrogen tanks at its maximum level,there is an energy surplus, and it is spilt to the grid.

3.2.1.- Life time and degradation

3.2.1.1- Battery Degradation

As a general rule, manufacturers provide experimental curves that relate the loss of nominal capacity to the number of operating cycles under certain conditions of maximum depth of discharge (DOD) [15][66][67]. This kind of approximations can differ quite a bit from the real value owing to the parameters associated with the use of the battery during charging and discharging processes such as partial charges, current and charge voltage, and operating temperature, which are not always similar to those used during the test conditions. Nevertheless, it can be a good starting point for an approximate model [15][66][67].
In this case, a linear model of capacity degradation is proposed, which is based on the curves for an expected average DOD. The equation is conceived from a relationship defined by the expected amount of energy cycled for the number of expected operating cycles and the maximum loss of capacity, $loss_{bat_{max}}$, (26), which determines the end of the useful lifespan.

$$\alpha = \frac{loss_{bat_{max}}}{\int SOC} \quad (26)$$

Where:
α: Battery degradation ratio (Ah).
$loss_{bat_{max}}$: Battery maximum loss of capacity (Ah).
From the battery degradation ratio, the nominal capacity losses, C_N, can be established from the cycled energy in terms of variations of the battery SOC (27).

$$C_N(k) = C_N(k-1) \cdot \alpha\big(SOC(k) - SOC(k-1)\big) \quad (27)$$

In general, the battery degradation can be calculated from the expected capacity losses and the cycled energy, obtaining the linear degradation model given in (28). A model similar to the one presented is used in [68].

$$D_{bat}(k+1) = P_{bat}(k) \cdot \alpha \cdot \frac{\frac{1\,h}{3600s}\eta_{bat}(k) \cdot T_s}{C_N(k) \cdot V_{bat}(k)} = \\ = P_{bat}(k) \cdot D_1(k) \quad (28)$$

Where:
$D_{bat}(k)$: Battery degradation at sampling time k + 1 (Ah).

$P_{bat}(k)$: Battery power at sampling time k (W).
$\eta_{bat}(k)$: Overall battery efficiency at sampling time k.
T_s: Sampling period (s).
$C_N(k)$: Nominal battery capacity at sampling time k (Ah).
$V_{bat}(k)$: Battery voltage at sampling time k (V).
$D_1(k)$: All the terms that multiply $P_{bat}(k)$, (V/h).

3.2.1.2.- Electrolyser Degradation

In case of the electrolyser, it is very common to associate the degradation with the number of working hours. For simplicity, it has been assumed that the electrolyser degradation, in terms of operating power (in number of operating hours), can follow a linear relationship with respect to the rated power [19][20], (29). This approximation considers that the degradation of the electrolyser, D_{els}, is proportional to the operating regime.

$$D_{els}(k+1) = P_{els}(k) \cdot \frac{1}{P_{els_N}} \cdot \frac{1\,h}{3600\,s} T_s = \\ = P_{els}(k) \cdot D_2(k) \quad (29)$$

Where:
$D_{els}(k+1)$: Electrolyser degradation at sampling time k + 1 (h).
$P_{els}(k)$: Electrolyser operating power at sampling time k (W).
P_{els_N}: Nominal electrolyser power (W).
T_s: Sampling period (s).
$D_2(k)$: All the terms that multiply $P_{els}(k)$, (h/W).

3.2.1.3.- Fuel Cell Degradation

In the case of the fuel cell, it is very common to relate the degradation with the number of operating cycles or working hours. This approach can be very far from reality because the operating conditions of the fuel cell strongly influence its lifetime [22]. For this reason, it has been decided to quantify the degradation as voltage drop of a fuel cell with respect to the nominal operating voltage. For this type of assumption, manufacturers provide experimentally calculated parameters, which quantify the voltage drop of one cell based on the number of hours and operation cycles under nominal operating conditions [69]. For simplicity, the two terms have been considered in a single parameter that relates the voltage drop with respect to the operating time, assuming linearity between this parameter regarding the fuel cell nominal power (30).

$$D_{fc}(k+1) = P_{fc}(k) \cdot \frac{\Delta V_{fc_{time}}}{P_{fc_N}} \cdot \frac{1\,h}{3600\,s} T_s = \\ = P_{fc}(k) \cdot D_3(k) \quad (30)$$

Where:

$D_{fc}(k+1)$: Fuel cell degradation at sampling time k + 1 (V).
$P_{fc}(k)$: Fuel cell operating power at sampling time k (W).
$\Delta V_{fc_{time}}$: Fuel cell voltage drop considering the operation hours and cycles (V/h).
P_{fc_N}: Nominal fuel cell power at sampling time k (W).
T_s: Sampling period (s).
$D_3(k)$: All the terms that multiply $P_{fc}(k)$, (h/A).

3.2.2- System Operating Costs

In a microgrid based on Figure 1, the system's operating costs will be given by the addition of the individual operating costs of the battery, the fuel cell and the electrolyser, while neglecting, for being comparatively much smaller and as already discussed, the operating costs related to photovoltaic panels and wind turbines. In the case of grid-connected topology, the costs associated with the exchange of energy between the electrical grid and the renewable generation must also be taken into account.
Considering battery and hydrogen-based elements, the operating cost of each will be defined by two power variable terms associated to firstly, the operation and maintenance costs and, secondly, the depreciation cost [46][70]. The latter will be defined according to the equipment acquisition cost, the degradation associated with the operating power and the useful lifetime determined by the maximum expected degradation, (31).

$$C_x(k+1) = P_x(k) \\ \left(C_{O\&M_x} + C_{x_o} \frac{loss_x(k)}{loss_{x_{max}}}\right) \cdot \frac{1\,h}{3600\,s} \cdot T_s \quad (31)$$

Where:
$C_x(k+1)$: Total operating cost of the element x (battery: bat; electrolyser: els, and fuel cell: fc) at sampling time k + 1 (€).
$P_x(k)$: Operating power of the element x at sampling time k (W).
$C_{O\&M_x}$: Operation and maintenance cost of the element x at sampling time k (€/Wh).
C_{x_o}: Depreciation cost of the element x at sampling time k (€).
$loss_x(k)$: Losses of the element x associated with its operating power (units according to element).
$loss_{x_{max}}$: Maximum expected losses of the element x (units according to element).
T_s: Sampling period (s).
Particularizing for each element, the linear models that relate the operating cost of the battery, electrolyser and fuel cell with its operation power are settled in the following subsections.

3.2.2.1- Battery Operating Cost

As for the battery operating cost, the degradation associated with the operating power is defined by the variation of the nominal capacity of the battery according to the proposed degradation model (32).

$$C_{bat}(k+1) = P_{bat}(k) \\ \left(C_{O\&M_{bat}}(k) + C_{bat_o}(k) \frac{\alpha \frac{\eta_{bat}(k)}{C_N(k) \cdot V_{bat}(k)}}{loss_{bat_{max}}}\right) \quad (32)$$

$$\cdot \frac{1\,h}{3600\,s} \cdot T_s \rightarrow C_{bat}(k+1) = P_{bat}(k) \cdot C_1(k)$$

Where:
$C_{bat}(k+1)$: Total operating cost of the battery at sampling time k + 1 (€).
$P_{bat}(k)$: Operating power of the battery at sampling time k (W).
$C_{O\&M_{bat}}(k)$: Operation and maintenance cost of the battery at sampling time k (€/Wh).
$C_{bat_o}(k)$: Depreciation cost of the battery at sampling time k (€).
α: Battery degradation ratio (Ah).
$\eta_{bat}(k)$: Overall battery efficiency at sampling time k.
$C_N(k)$: Nominal battery capacity at sampling time k (Ah).
$V_{bat}(k)$: Battery voltage at sampling time k (V).
$loss_{bat_{max}}$: Maximum expected losses of the battery (Ah).
$C_1(k)$: Groups all the terms that multiply $P_{bat}(k)$, (€/W).

3.2.2.2- Electrolyser Operating Cost

In case of electrolyser operating cost, the degradation term is calculated from the equivalent hours of operation at nominal power according to the proposed degradation model (33).

$$C_{els}(k+1) = P_{els}(k)$$
$$\left(C_{O\&M_{els}}(k) + C_{els_o}(k)\frac{1}{life_{els}P_{els_N}(k)}\right) \cdot \frac{1\,h}{3600\,s} \cdot T_s \qquad (33)$$
$$\rightarrow C_{els}(k+1) = P_{els}(k) \cdot C_2(k)$$

Where:
$C_{els}(k+1)$: Total operating cost of the electrolyser at sampling time k + 1 (€).
$P_{els}(k)$: Operating power of the electrolyser at sampling time k (W).
$C_{O\&M_{els}}(k)$: Operation and maintenance cost of the electrolyser at sampling time k (€/Wh).
$C_{els_o}(k)$: Depreciation cost of the electrolyser at sampling time k (€).
$life_{els}$: Useful lifetime of the electrolyser (hours).
$P_{els_N}(k)$: Nominal electrolyser power at sampling time k (W).
$C_2(k)$: All the terms that multiply $P_{els}(k)$, (€/W).

3.2.2.3- Fuel Cell Operating Cost

Fuel cell operating cost is determined by the voltage drop associated with the operation power according to the proposed degradation model (34).

$$C_{fc}(k+1) = P_{fc}(k)$$
$$\left(C_{O\&M_{fc}}(k) + C_{fc_o}(k)\frac{\Delta V_{fc_{time}}}{\Delta V_{fc_{Max}} \cdot P_{fc_N}(k)}\right) \cdot \frac{1\,h}{3600\,s} \cdot T_s \qquad (34)$$
$$\rightarrow C_{fc}(k+1) = P_{fc}(k) \cdot C_3(k)$$

Where:
$C_{fc}(k+1)$: Total operating cost of the fuel cell at sampling time k + 1 (€).
$P_{fc}(k)$: Operating power of the fuel cell at sampling time k (W).
$C_{O\&M_{fc}}(k)$: Operation and maintenance cost of the fuel cell at sampling time k (€/Wh).
$C_{fc_o}(k)$: Depreciation cost of the fuel cell at sampling time k (€).
$\Delta V_{fc_{time}}$: Fuel cell voltage drop considering the operating hours and cycles (V/h).
$\Delta V_{fc_{Max}}$: Maximum expected fuel cell voltage drop considering the operating hours and cycles (V/h).
$P_{fc_N}(k)$: Nominal fuel cell power at sampling time k (W).
$C_3(k)$: All the terms that multiply $P_{fc}(k)$.

3.2.2.4- Grid Operation Cost

In relation to grid costs, assuming a grid-connected topology (see Figure 1), a direct relationship of the grid cost (C_{grid}) associated with the incoming (bought, C_{in}) or outgoing (sold, C_{out}) power can be exemplified (35).

$$C_{grid}(k+1) =$$
$$= \begin{cases} P_{grid}(k)C_{in}(k); if\ P_{grid} = P_{grid_{in}}(k) \\ P_{grid}(k)C_{out}(k); if\ P_{grid} = P_{grid_{out}}(k) \end{cases} \qquad (35)$$
$$\rightarrow C_{grid}(k+1) = P_{grid}(k) \cdot C_4(k)$$

Where: $C_4(k)$ is $C_{in}(k)$ or $C_{out}(k)$. The sign is defined by $P_{grid}(k)$.
Then, the total operating costs of the whole microgrid (c_{sys}) can be defined by the addition of the previously calculated individual costs (36):

$$C_{sys}(k+1) = C_{bat}(k+1) + C_{els}(k+1) +$$
$$+ C_{fc}(k+1) + C_{grid}(k+1) \rightarrow$$
$$C_{sys}(k+1) = P_{bat}(k) \cdot C_1(k) + P_{els}(k) \cdot C_2(k) + \qquad \textbf{(36)}$$
$$+ P_{fc}(k) \cdot C_3(k) + P_{grid}(k) \cdot C_4(k)$$

3.2.3.- Operating Losses

The losses associated to the most sensitive part of the microgrid (the losses due to photovoltaic panels and wind turbines are intrinsic in the model; in the sense that they are considered in the total power that both systems deliver to the microgrid, i.e., their local controllers guarantee that the maximum power is transferred to the microgrid, so, this is not a EMS task) can be modelled based on the current working power each device (battery , electrolyser and fuel cell) and its operating efficiency. Despite the fact that the current efficiency value is unknown, an approximation can be estimated from the value of the previous instant with a reduced margin of error (37).

$$Loss_x(k+1) = P_x(k)\left(\frac{1-\eta_x(k)}{\eta_x(k)}\right) \quad (37)$$

Where:
$Loss_x(k+1)$: Operating losses of the element x at sampling time k +1 (W); x = bat, els or fc.
$P_x(k)$: Operating power of the element x at sampling time k (W).
$\eta_x(k)$: Operating efficiency of the element x at sampling time k.
Particularizing for each element, a linear model that relates the operation losses of the battery, electrolyser and fuel cell can be obtained according to their operating power and instantaneous performance, respectively (38), (39) and (40).

$$Loss_{bat}(k+1) = P_{bat}(k)\left(\frac{1-\eta_{bat}(k)}{\eta_{bat}(k)}\right) \rightarrow Loss_{bat_k} = P_{bat}(k)\cdot L_1(k) \quad (38)$$

$$Loss_{els}(k+1) = P_{els}(k)\left(\frac{1-\eta_{els}(k)}{\eta_{els}(k)}\right) \rightarrow Loss_{els}(k) = P_{els}(k)\cdot L_2(k) \quad (39)$$

$$Loss_{fc}(k+1) = P_{fc}(k)\left(\frac{1-\eta_{fc}(k)}{\eta_{fc}(k)}\right) \rightarrow Loss_{fc}(k) = P_{fc}(k)\cdot L_3(k) \quad (40)$$

Where: $L_1(k), L_2(k)$ and $L_3(k)$ are, respectively, all terms multiplying $P_{bat}(k), P_{els}(k)$ and $P_{fc}(k)$.
For grid-connected topologies, it is also necessary to consider the losses associated with the use of power electronic devices: DC/AC converters used during the injection to grid; and AC/DC converters utilised during the electrical consumption from the grid (41).

$$Loss_{grid}(k+1) = \begin{cases} P_{grid}(k)\left(\frac{1-\eta_{AC/DC}(k)}{\eta_{AC/DC}(k)}\right); if\ P_{grid}(k) = P_{grid_{in}}(k) \\ P_{grid}(k)\left(\frac{1-\eta_{DC/AC}(k)}{\eta_{DC/AC}(k)}\right); if\ P_{grid}(k) = P_{grid_{out}}(k) \end{cases} \rightarrow Loss_{grid_k} = P_{grid}(k)\cdot L_4(k) \quad (41)$$

Where:
$Loss_{grid}(k+1)$: Losses related to the grid connection at sampling time k + 1 (W).
$P_{grid}(k)$: $P_{grid_{in}}(k)$ or $P_{grid_{out}}(k)$ (W).
$\eta_{DC/AC}(k)$: Power electronics efficiency in case of injection to the grid.
$\eta_{AC/DC}(k)$: Power electronics efficiency in case of consumption from the grid.
$L_4(k)$: All the terms that multiply $P_{grid}(k)$.

The operating losses associated to the whole microgrid is resolved by the addition of the individual losses associated to each element (42):

$$\begin{aligned} &Loss(k+1) = Loss_{bat}(k+1) + Loss_{els}(k+1) + \\ &+ Loss_{fc}(k+1) + Loss_{grid} \rightarrow Loss(k+1) = \\ &= P_{bat}(k)\cdot L_1(k) + P_{els}(k)\cdot L_2(k) + \\ &+ P_{fc}(k)\cdot L_3(k) + P_{grid}(k)\cdot L_4(k) \end{aligned} \quad (42)$$

3.3.- Power Balance in the Microgrid

Real microgrids based on renewable generation should guarantee a minimum quality in the electricity supply [71][72]. The loss of power supply probability (LPSP) parameter is defined by the ratio between the total losses of power supply to total demand for a considered period of time. Regarding the model and indirect way, the closer LPSP to one is achieved guaranteeing the power balance in the microgrid. Following Figure 1, the power balance at sampling time k is determined by the addition of the input power, i.e., the only primary power available (renewable: solar and wind) and the output power at this time (43).

$$\begin{aligned} &P_{balance}(k) = -P_{ren}(k) + P_{load}(k) + P_{bat}(k) + \\ &+ P_{H2}(k) + P_{grid}(k) + Loss(k) \end{aligned} \quad (43)$$

Where, the used criterion has been that the delivered power to the DC/AC bus is negative and the consumed from it is positive. Regarding $P_{H2}(k)$ it means (see Figure 1) the power of the hydrogen-based systems, i.e., fuel cell or electrolyser (both are complementary: the fuel cell operates when there is energy deficit in the microgrid and the electrolyser enters into operation when there is energy excess, so, both do not work together). Then, depending on the state of the microgrid, $P_{H2}(k)$ can be $P_{els}(k)$ or $-P_{fc}(k)$, and following the same rule: $P_{grid}(k)$ can be $P_{grid_{out}}(k)$ or $-P_{grid_{in}}(k)$, and $P_{bat}(k)$ can be $-P_{bat_{disch}}(k)$ or $P_{bat_{char}}(k)$. In any case, if the microgrid operates properly, thank of the EMS, $P_{balance}$must be zero all the time.

3.4.- Discrete State-space Model

From the models developed for each device and for a given sampling period T_s, it is possible to put them together in an equation as (44), corresponding with a Linear Time Variant (LVT) discrete state-space model of the whole microgrid. A very important issue regarding the model (44) must be taken into account: in order to distinguish which element of the hydrogen-based system is working on k, the P_{H2} sign has been used, i.e., when it is positive the electrolyser is working and when is negative the fuel cell is who works.

$$
\begin{bmatrix} SOC(k+1) \\ HL(k+1) \\ V_{bat}(k+1) \\ C_{sys}(k+1) \\ D_{bat}(k+1) \\ D_{H2}(k+1) \\ Loss(k+1) \\ P_{H2}(k+1) \\ P_{grid}(k+1) \\ P_{net}(k+1) \end{bmatrix} =
$$

$$
= \begin{bmatrix} 1 & 0 & 0 & 0 & 0 & 0 & 0 & 0 & 0 & 0 \\ 0 & 1 & 0 & 0 & 0 & 0 & 0 & 0 & 0 & 0 \\ SV(k) & 0 & 0 & 0 & 0 & 0 & 0 & 0 & 0 & 0 \\ 0 & 0 & 0 & 0 & 0 & 0 & 0 & 0 & 0 & 0 \\ 0 & 0 & 0 & 0 & 0 & 0 & 0 & 0 & 0 & 0 \\ 0 & 0 & 0 & 0 & 0 & 0 & 0 & 0 & 0 & 0 \\ 0 & 0 & 0 & 0 & 0 & 0 & 0 & 0 & 0 & 0 \\ 0 & 0 & 0 & 0 & 0 & 0 & 0 & 0 & 0 & 0 \\ 0 & 0 & 0 & 0 & 0 & 0 & 0 & 0 & 0 & 0 \\ 0 & 0 & 0 & 0 & 0 & 0 & 0 & 0 & 0 & 0 \end{bmatrix} \begin{bmatrix} SOC(k) \\ HL(k) \\ V_{bat}(k) \\ C_{sys}(k) \\ D_{bat}(k) \\ D_{H2}(k) \\ Loss(k) \\ P_{H2}(k) \\ P_{grid}(k) \\ P_{net}(k) \end{bmatrix} +
$$

$$
+ \begin{bmatrix} S_1(k) & 0 & 0 \\ 0 & r_{els}(k) \text{ or } r_{fc}(k) & 0 \\ VP(k) & 0 & 0 \\ C_1(k) & C_2(k) \text{ or } -C_3(k) & C_4(k) \\ D_1(k) & 0 & 0 \\ 0 & D_2(k) \text{ or } -D_3(k) & 0 \\ L_1(k) & L_2(k) \text{ or } -L_3(k) & L_4(k) \\ 0 & 1 & 0 \\ 0 & 0 & 1 \\ 1 & 1 & 1 \end{bmatrix} \begin{bmatrix} P_{bat}(k) \\ P_{H2}(k) \\ P_{grid}(k) \end{bmatrix} + \tag{44}
$$

$$
+ \begin{bmatrix} 1 & 0 & 0 \\ 0 & 1 & 0 \\ 0 & 0 & 1 \\ 0 & 0 & 0 \\ 0 & 0 & 0 \\ 0 & 0 & 0 \\ 0 & 0 & 0 \\ 0 & 0 & 0 \\ 0 & 0 & 0 \\ 0 & 0 & 0 \end{bmatrix} \begin{bmatrix} v_1(k) \\ v_2(k) \\ v_3(k) \end{bmatrix}
$$

$$
\begin{bmatrix} SOC(k) \\ HL(k) \\ V_{bat}(k) \\ C_{sys}(k) \\ D_{bat}(k) \\ D_{H2}(k) \\ Loss(k) \\ P_{H2}(k) \\ P_{grid}(k) \\ P_{net}(k) \end{bmatrix} = \begin{bmatrix} 1 & 0 & 0 & 0 & 0 & 0 & 0 & 0 & 0 & 0 \\ 0 & 1 & 0 & 0 & 0 & 0 & 0 & 0 & 0 & 0 \\ 0 & 0 & 1 & 0 & 0 & 0 & 0 & 0 & 0 & 0 \\ 0 & 0 & 0 & 1 & 0 & 0 & 0 & 0 & 0 & 0 \\ 0 & 0 & 0 & 0 & 1 & 0 & 0 & 0 & 0 & 0 \\ 0 & 0 & 0 & 0 & 0 & 1 & 0 & 0 & 0 & 0 \\ 0 & 0 & 0 & 0 & 0 & 0 & 1 & 0 & 0 & 0 \\ 0 & 0 & 0 & 0 & 0 & 0 & 0 & 1 & 0 & 0 \\ 0 & 0 & 0 & 0 & 0 & 0 & 0 & 0 & 1 & 0 \\ 0 & 0 & 0 & 0 & 0 & 0 & 0 & 0 & 0 & 1 \end{bmatrix} \begin{bmatrix} SOC(k) \\ HL(k) \\ V_{bat}(k) \\ C_{sys}(k) \\ D_{bat}(k) \\ D_{H2}(k) \\ Loss(k) \\ P_{H2}(k) \\ P_{grid}(k) \\ P_{net}(k) \end{bmatrix}
$$

$$
+ \begin{bmatrix} 0 & 0 & 0 \\ 0 & 0 & 0 \\ 0 & 0 & 0 \\ 0 & 0 & 0 \\ 0 & 0 & 0 \\ 0 & 0 & 0 \\ 0 & 0 & 0 \\ 0 & 0 & 0 \\ 0 & 0 & 0 \\ 0 & 0 & 0 \end{bmatrix} \begin{bmatrix} P_{bat}(k) \\ P_{H2}(k) \\ P_{grid}(k) \end{bmatrix} + \begin{bmatrix} 1 & 0 & 0 \\ 0 & 1 & 0 \\ 0 & 0 & 1 \\ 0 & 0 & 0 \\ 0 & 0 & 0 \\ 0 & 0 & 0 \\ 0 & 0 & 0 \\ 0 & 0 & 0 \\ 0 & 0 & 0 \\ 0 & 0 & 0 \end{bmatrix} \begin{bmatrix} d_{SOC}(k) \\ d_{HL}(k) \\ d_{V_{bat}}(k) \end{bmatrix}
$$

Each one of the rows of the state equation given in (44) can be obtained in the following way: $SOC(k+1)$ from (16) and $HL(k+1)$ from (18); note that in order to distinguish who is working (electrolyser or fuel cell), r_{els} or r_{fc} need to be used. Regarding $v_1(k)$ and $v_2(k)$, both represent model disturbances. Of course, if at sampling time k neither the electrolyser nor the fuel cell is working, the second row in (44) is zero.

Now, focusing on $V_{bat}(k+1)$, its row represents the linearization result of (1) or (2) and (3) or (4); where, for both, $V_{bat}(k+1) = f_k(i_{bat}(k), SOC(k))$ i.e., considering that the nominal capacity of the battery is substantially constant. From here, writing the current in function of the power under the condition that from k to $k+1$ the V_{bat} remains constant, it is easy to show that $V_{bat}(k+1) = SV(k) \cdot SOC(k) + VP(k).P_{bat}(k) + v_3(k)$, where $SV(k)$ and $VP(k)$ are coefficients depending on the linearization plane of (1) or (2) and (3) or (4); obviously, the EMS will need to know the working region in order to apply in each one the suitable linearized model) and $v_3(k)$ represents the sum of the independent term (result of the linearization) and model disturbances.

Regarding forth row, $C_{sys}(k+1)$ comes from (36) and it groups all operating cost: (32), (33), (34) and (35). Of course, there is no point to have negative costs resulting of the assumed criterion for $P_{els}(k)$ and $P_{fc}(k)$, $P_{bat}(k)$ or $-P_{bat}$ (depending if the battery is powering from the bus or supplying to it) and P_{grid} or $-P_{grid}$(depending if the smart grid is powering from the electrical grid or supplying to it). This apparent incongruence is very easy to solve in the programming stage: only to change the sign is needed.

Equations (28), (30) or (31) build, respectively, rows fifth and sixth. Again, in order to avoid negative deterioration, the battery and hydrogen system power criterion need to be taken into account and resolving in the programming stage. Seventh row groups all the microgrid operating losses (42) and, one more time, in order to avoid negative losses, the power criterion for the hydrogen-based system, battery and grid needs to be taken into account in the programming stage.

Eighth and ninth rows are identical to the corresponding input vector coordinates. Their presence in the state vector is due to give uniformity to the model but, obviously, they might not be taken into account. Finally, tenth row represents the net power of the microgrid, which can be obtain from (43) taking into account that the only primary source is P_{ren}; so, the net power is the one that remains of the primary one, once extracted the consumed by the loads and the losses. This is, matching (40) to zero, $P_{net}(k) = P_{ren}(k) - P_{load}(k) - Loss(k) = P_{bat}(k) + P_{H2}(k) + P_{grid}(k)$.

Equation (44) can be expressed in the well-known control way (45):

$$
\begin{aligned} x(k+1) &= Ax(k) + Bu(k) + Gv(k) \\ y(k) &= Cx(k) + Du(k) + Ed(k) \end{aligned} \tag{45}
$$

Where, for a given sampling period T_s,

$x(k)$: Discretized state vector

$[SOC(k)HL(k)V_{bat}(k)\ C_{sys}(k)D_{bat}(k)D_{H2}(k)\ Loss(k)P_{H2}(k)$ ...

... $P_{grid}(k)\ P_{net}(k)]^T$.
$u(k)$: Discretized input vector $[P_{bat}(k) P_{H2}(k)\ P_{grid}(k)]^T$.
$v(k)$: Discretized model disturbances $[v_1(k)\ v_2(k) v_3(k)]^T$.
$y(k)$: Discretized output vector
$[SOC(k) HL(k) V_{bat}(k)\ C_{sys}(k) D_{bat}(k) D_{H2}(k)\ Loss(k) P_{H2}(k)$ ...
... $P_{grid}(k)\ P_{net}(k)]^T$.
$d(k)$: Discretized vector of measurable output disturbances $[d_{SOC}(k)\ d_{HL}(k)\ d_{V_{bat}}(k)]^T$.

So far, a general model has been developed that allows modelling the performance of a complete renewable sources-based microgrid with hydrogen as backup throughout all its operating range. This general model extended to all the operating range of the microgrid guarantees a better approximation with respect to those models mostly used in the scientific literature because those one are linearized systems around a single operating point. Additionally, apart from describing electrical performance for each device that makes up the microgrid, the proposed modelling formulation also includes technical and economical parameters as operating efficiency, degradation, losses and costs needed for the microgrid optimization. In case the microgrid under study would not include any of the generation elements shown in Figure 1, the equivalent discretized state-space model would be obtained from expression (44) simply removing the rows corresponding to the elements not included.

IV. EXPERIMENTAL RESULTS

In order to validate the proposed model, a series of experimental tests on the equipment defined in Section II have been developed, in accordance with the system configuration shown in Figure 1.

In the following sections, the different experimental tests developed will be detailed and the experimental results will be presented against those obtained by applying the proposed model.

In this particular case, the proposed battery voltage and charge efficiency models, as well as the efficiency, hydrogen generation and consumption models for the case of the electrolyser and fuel cell will be individually validated.

4.1- Battery voltage

4.1.1- Battery voltage model identification

To identify the coefficient of the static models of the battery voltage, a series of empirical charging and discharging tests have been carried out over the battery bank at a controlled and constant temperature of 20 °C. In order to guarantee repeatability in the tests, the results used for the identification process have been obtained from an average of three identical tests.

The battery voltage model must represent the battery voltage behaviour throughout its operating range for both charging and discharging process. Based on the above, a test with three clearly differentiated phases will be developed; a first initial phase of full battery charging based on a two stage-based charging protocol; a second resting phase; and a last phase in which a constant current discharge is made up to a minimum value of battery state of charge. The test procedures are described below.

Charge phase

The objective of this first phase is to achieve the full charge of the battery, allowing a known initial condition for the subsequent discharge procedure (SOC ≈ 100%), and obtaining an empirical relationship between the battery voltage, the battery state of charge and charge current for the charging process.

The charging phase is given by a two stage-based charging protocol, given by a first initial constant current charging stage until the desired charge voltage is reached (bulk stage), and a subsequent constant voltage charging stage until the full charge condition is reached (boost stage).

In this case, specifically, the bulk stage is determined in the first instance by a constant current charging protocol at different current values 3 A, 5 A, 7.5 A, 10 A, 15 A and 25 A, until the desired battery voltage has been reached (2.4 V/cell ≈ 400 VDC). The use of different charge currents will allow for a greater number of experimental data for the identification process.

During the boost stage, a constant voltage charging protocol is performed until the battery float current is reached (1 A), or the float current remains constant for at least one hour, determining the full charge.

In order to implement the described charging protocol, the programmable power supply described in section II is used according to the connection scheme described in Figure 7a. The mode of operation, constant current or constant voltage, will be given by the stage of the charging process to be developed. The measurements of the main electrical parameters, voltage and battery current, have been obtained from the programmable power supply acquisitions system

Rest phase

In order to guarantee the parasitic reactions cease in the battery, the battery is left open circuit for 5 hours.

Discharge phase

This phase implements the desired discharge test procedure, making use of a constant current discharging protocol, for different discharge current values 5 A, 10 A, 15 A, 20 A, 25 A and 30 A until reaching a SOC of 50% with respect to the initial nominal capacity, that is 50 Ah. The objective is to obtain an empirical relationship between the battery voltage and the battery state of charge and discharge current for the discharging process. The use of different discharge currents will allow for a greater number of experimental data for the identification process.

In order to implement the described discharging protocol, the programmable electronic load described in section II is used according to the connection scheme described in Figure 7b. In

this specific case, a constant current operation mode has been used. The measurements of the main electrical parameters, voltage and battery current, have been obtained from the programmable electronic load acquisitions system.

a)

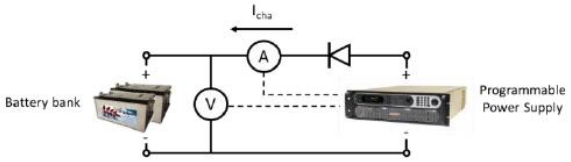

b)

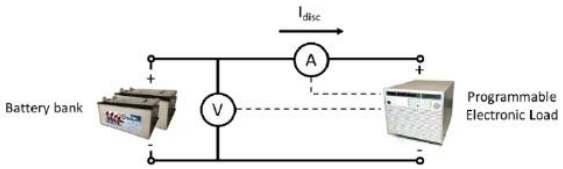

FIGURE. 7. a) Set-up for charging phase; b) Set-up for discharging phase.

Table 2 and Table 3 include the parameters values for the Copetti and Tremblay models respectively for the battery bank described in section II, obtained from identification process from the experimental test under charging and discharging profiles. For the identification process, the Matlab® curve fitting toolbox has been used.

TABLE II
COPETTI BATTERY MODEL PARAMETERS

Parameter	Value	Parameter	Value
a_d	0.2936	d_d	-10.09
a_c	-1.311	d_c	0.3656
b_d	-1.355	e_d	1.5
b_c	0.0743	e_c	1.5
c_d	0.054	f_d	10.15
c_c	-19.09	f_c	19.11

TABLE III
TREMBLAY BATTERY MODEL PARAMETERS

Parameter	Value
E_0	395 V
R	0.005 Ω
K	0.37 V/Ah
C_N	100 Ah
A	0.053 V
B	0.13 Ah^{-1}

For the battery bank described in section II, the model surfaces for charging and discharging process defined by the Copetti and Tremblay model obtained from identification process are presented in Figure 8. Table 4 contains the statistical parameters that define the behaviour of the studied models.

a)

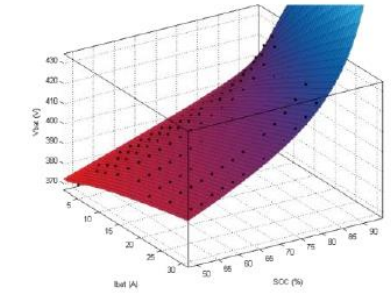

b)

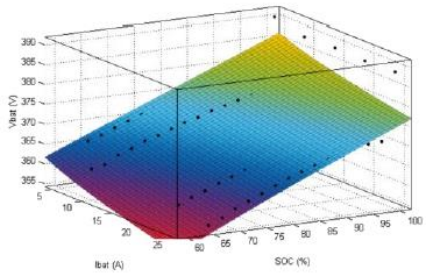

c)

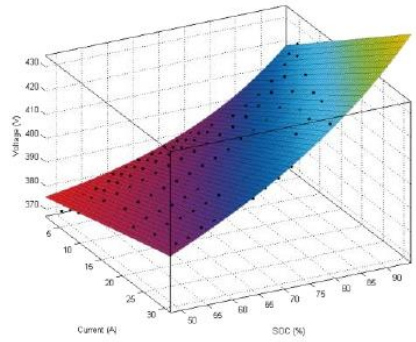

d)

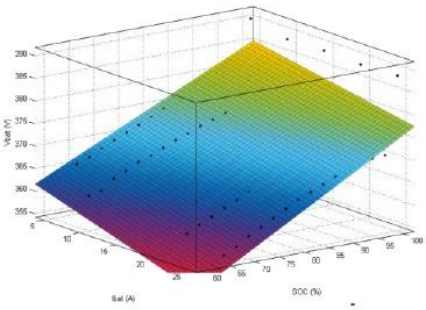

FIGURE. 8. a) Copetti surface model for battery charging; b) Copetti surface model for battery discharging; c) Tremblay surface model for battery charging; d) Tremblay surface model for battery discharging.

TABLE IV
COPETTI AND TREMBLAY MODEL STATISTICAL PARAMETERS

		(SSE)	(RMSE)	R^2	Adj R^2
Charging	Coppeti	167.4	1.162	0.993	0.9928
	Tremblay	473.6	1.954	0.9802	0.9795

Discharging	Copetti	690.1	3.054	0.8506	0.8524
	Tremblay	684.8	3.042	0.8517	0.8437

4.1.2- Battery voltage model validation

The behaviour of the proposed models has been validated on the lead-acid battery bank. Both models have been compared with the experimental results obtained under charging and discharging profiles for different operating currents. In order to ensure a correct reading of the battery voltage, taking into account the time scale of the model, the voltage measurements were made every minute, so that the voltage transients associated with changes in the charging/discharging current were completely filtered. The test results are shown in Figure 9.

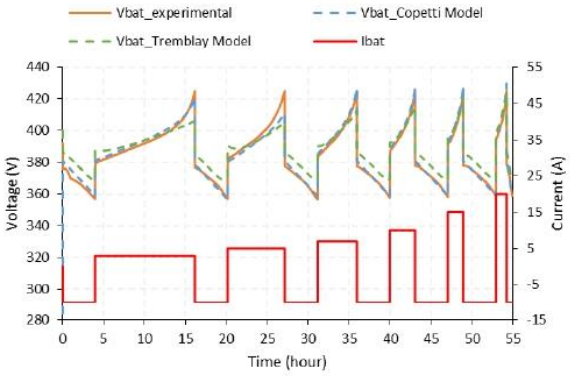

FIGURE. 9. Comparison between battery experimental voltage and Copetti and Tremblay linearized model for charging and discharging test.

4.2- Battery efficiency

4.2.1- Battery charge efficiency model identification

To determine the coefficients of the Butler-Volmer equation, an experimental tests have been carried out under the same initial conditions. The test procedure starts from a battery fully charge, proceeding with a constant voltage charging protocol at different charging voltages, 2.25 V/cell (405 VDC), 2.275 V/cell (410 VDC), 2.3 V/cell (414 VDC), 2.325 V/cell (419 VDC), 2.35 V/cell (423 VDC), 2.375 V/cell (427 VDC), and 2.4 V/cell (432 VDC), and operating temperatures, 15 °C, 20 °C, 25 °C and 30 °C. The charging current for each voltage and operating temperature will be determined by the float current, which will practically represent the current associated with the parasitic reactions in the battery (gassing current), and therefore will determine the efficiency in the charging process. The battery float current was determined as that current that remained constant after one hour of constant voltage charging. In order to guarantee a precise model, the values used for the experimental identification procedure were obtained from the average of three different tests.

In this particular test, the programmable power supply described in section II is used according to the connection scheme described in Figure 7a. According to the test performed, a constant voltage operation mode has been used. The measurements of the main electrical parameters, voltage and battery current, have been obtained from the programmable power supply acquisitions system. The temperature measurement has been carried out through the use of surface temperature sensors type Pt100 and conditioning electronics.

Table 5 include the parameters values for Butler-Volmer equation for the battery bank described in section II, obtained from identification process from the experimental test under charging profile. For the identification process, the Matlab® curve fitting toolbox has been used.

TABLE V
COPETTI AND TREMBLAY MODEL STATISTICAL PARAMETERS

Parameter	Value
I_{G_o}	0.22 A
K_V:	0.096 V^{-1}
K_T:	0.05 $ºC^{-1}$
V_{bat_o}	414 V
T_{bat_o}	25 ºC

For the battery bank described in section II, the model surface for gassing current defined by the Butler-Volmer equation obtained from identification process are presented in Figure 10. Table 6 contains the statistical parameters that define the behaviour of the identified model.

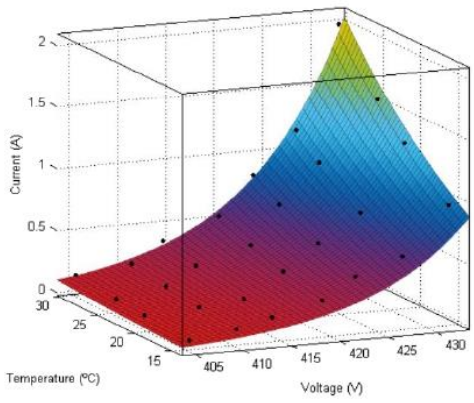

FIGURE. 10. Gassing current surface model for battery.

TABLE VI
BUTLET-VOLMER MODEL STATISTICAL PARAMETERS

Sum of squared error (SSE)	Root-mean-square deviation (RMSE)	R^2	Adjusted R^2
0.4535	0.1296	0.929	0.929

4.2.2- Battery charge efficiency model validation

The behaviour of the proposed models has been validated on the lead-acid battery bank. The Butler-Volmer equation have been compared with the experimental results obtained under charging profiles for different operating voltages and two different temperatures. With the aim of guaranteeing a correct

reading of the battery floating current, avoiding the effect of transients in the charging process, the current measurements were made one hour after the test voltage and temperature conditions were reached. The test results are shown in Figure 11.

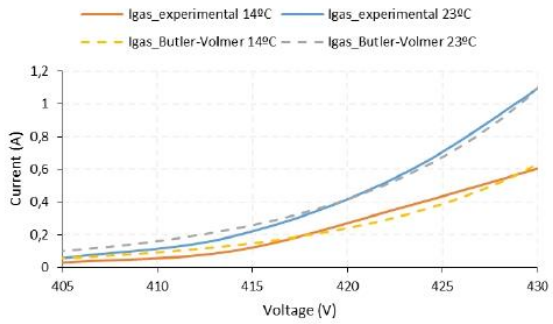

FIGURE. 11. Comparison between battery experimental gassing current and Butler-Volmer model for charging test.

4.3- Electrolyser generation ratio and efficiency model validation

The behaviour of the proposed hydrogen generation ratio and electrolyser efficiency model has been validated on the alkaline electrolyser explained in section II, whose main parameters were presented in Table 1.

In this particular test, the power stage of the electrolyser is supplied from a three-phase AC connection. The rectifier stage and subsequent DC/DC buck converter allows to supply DC current to the electrolyser stack based on a ramp-type programmed power profile (Figure 14a), which starts from a minimum power value of 5 kW, up to the nominal power value (10 kW). In order to neglect the thermal effect on the system response, the test was performed after operating the electrolyser for 2 hours at nominal power, in order to reach the nominal operating temperature, and it is kept established along the test duration thanks to the auxiliary cooling system.

Finally, the produced hydrogen is stored in the high pressure tank described in section II. The connection scheme is shown in Figure 12.

To validate the proposed hydrogen generation and efficiency model, all the sensors and acquisition and control electronics integrated in the same equipment are used. In this sense, the measurement of the produced hydrogen flow through the use of a mass flow meter will allow to determine the instantaneous generation ratio, as well as the electrolyzer performance from the relationship between the electric power consumed and the chemical power extracted, according to the equation (22).

The experimental test results for hydrogen generation ratio and electrolyser efficiency are shown in Figure 13 and Figure 14 respectively.

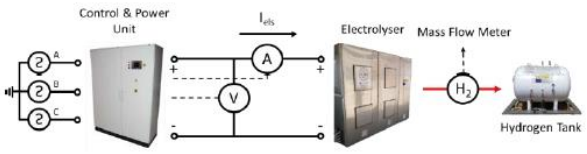

FIGURE. 12. Set-up for electrolyser test.

a)

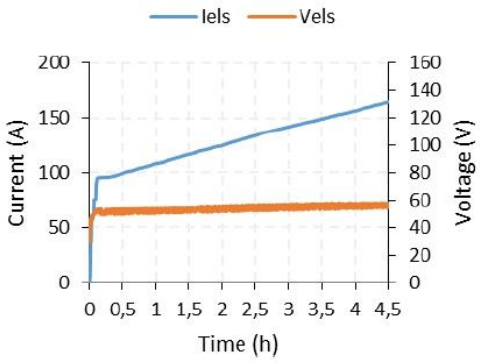

b)

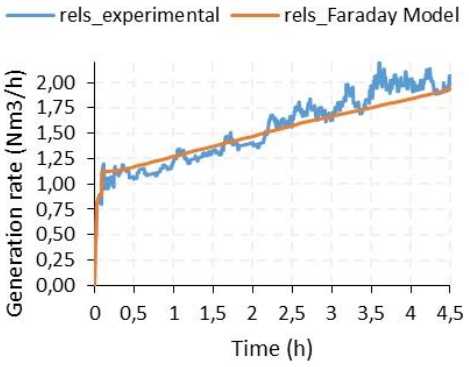

FIGURE. 13. a) Electrolyser voltage and current for experimental test; b) Comparison between experimental hydrogen generation ratio and Faraday model.

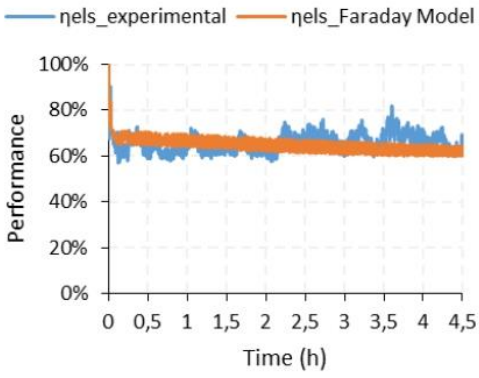

FIGURE. 14. Comparison between experimental electrolyser efficiency and Faraday-based model.

4.4- Fuel cell consumption ratio and efficiency model validation

The behaviour of the proposed hydrogen consumption ratio and fuel cell efficiency model has been validated on the PEM fuel cell explained in section II, whose main parameters were presented in Table 1.

In this particular test, the fuel cell has been subjected to a stair-type up-down load profile (Figure 16a), with the aim of validating the behaviour of the system during the increasing and decreasing of the current setpoint. In this case, in order to be able to regulate the working current of the fuel cell and take advantage of the energy produced for recharging the battery bank, a high-ratio lifting Push-Pull topology DC/DC converter has been used (Figure 4b). The design and application of this converter allows the power regulation, electrical interconnection and measurement of the main electrical parameters of the fuel cell. The measurement of the consumed hydrogen flow through the use of a mass flow meter will allow to determine the instantaneous consumption ratio, as well as the fuel cell performance from the relationship between the chemical energy stored in hydrogen and the extracted electric power, according to equation (25). The connection scheme is shown in Figure 15.

The experimental test results for hydrogen consumption ratio and fuel cell efficiency are shown in Figure 16 and Figure 17 respectively.

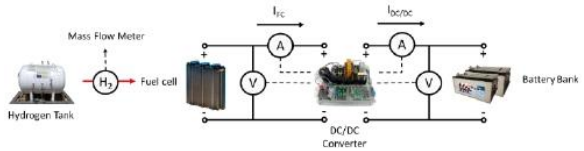

FIGURE. 15. Set-up for fuel cell test.

a)

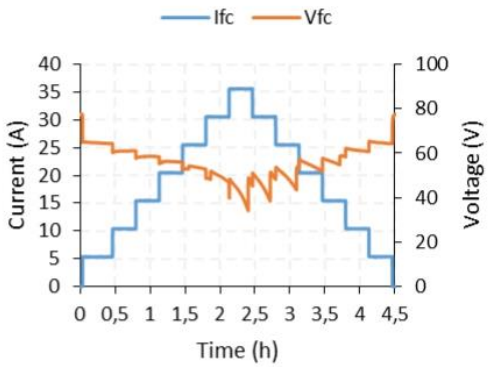

b)

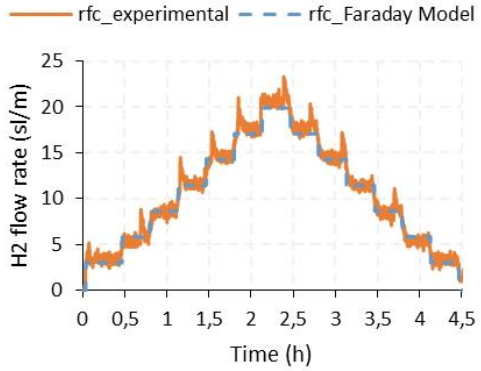

FIGURE. 16. a) Fuel cell voltage and current for experimental test; b) Comparison between experimental hydrogen consumption ratio and Faraday model.

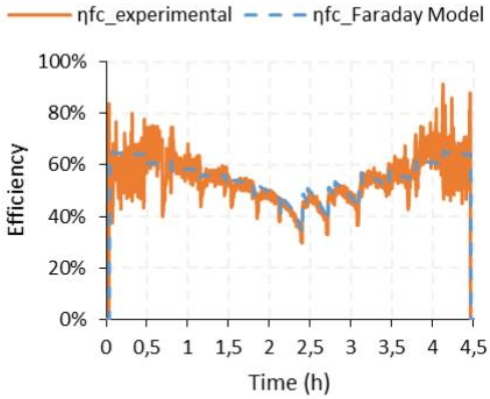

FIGURE. 17. Comparison between experimental fuel cell efficiency and Faraday-based model.

V. DISCUSSION

In this section, the results obtained from the validation tests of the proposed models will be analysed.

Attending to the battery voltage model, a series of experimental tests were carried out that allowed, through an identification process, to obtain the parameters of Coppeti and Tremblay models (Table 2 and Table 3), resulting in a state surfaces (Figure 8) which represents a mathematical model with a very high coefficient of determination, as well as a reduced average error (Table 4), which determines the correct adjustment with respect to the reference data matrix.

Considering the parameters obtained from the identification process, each of the previous models was validated on the same charging and discharging profile according to the experimental test presented in section 4.1.2 and collected in Figure 9.

From the previous results it follows that Coppeti model reflects faithful the real behaviour of battery thanks to it is a model designed specifically for lead-acid batteries. Attending to the representation of the experimental vs simulated curves (Figure 9), the good behaviour of the model is checked, which presents a very small percentage error in its entire operating

range characterized by an average percentage error less than 0.2% and a standard deviation of 0.62%, presenting a maximum percentage error (absolute value) less than 4.2% given for the load change transitions (Figure 18a).

In case of the Tremblay model, despite presenting good results, since it is a generalized model for any battery technology, it presents an average error significantly higher than the Coppeti model (Figure 18b). In this particular case, the error is present in practically the entire operating area, characterized by an average percentage error close to 1% and a standard deviation of 1.9%. The maximum percentage error, as in the previous case is given for load changes transitions, reaching in this case a maximum value (absolute value) of 5.2%.

Attending to the results, the Coppeti model presents a better performance for the modelling of lead acid batteries. In any case, both models presents a good approximation. In the case that control actions aimed at implementing charge management algorithms are considered, the Coppeti model presents better results with a reduced modelling error for both charge and discharge process.

Based on the above, the use of the static Coppeti model in micro grids with energy storage system based on lead acid technology batteries is recommended. For the rest of the technologies, the Tremblay model presents a mathematical solution that should be evaluated depending on the application.

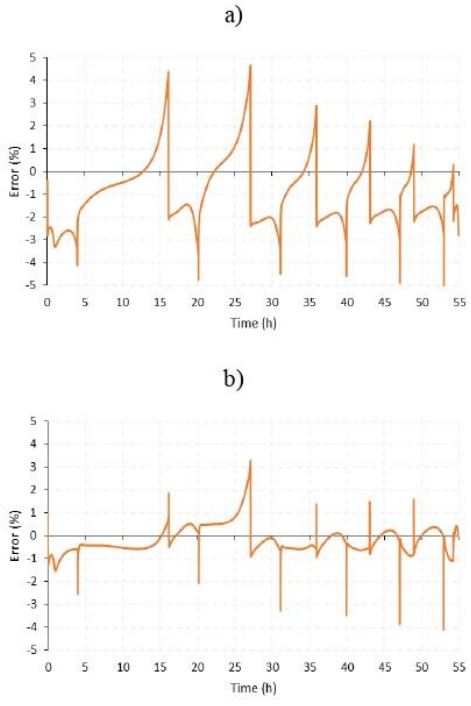

FIGURE. 18. a) Percentage error profile Coppeti model; b) Percentage error profile Tremblay model.

Attending to the battery efficiency, model based on Butler-Volmer equation, a series of experimental tests were carried out that allowed, through an identification process, to obtain the main model parameters and define the proposed charge efficiency model (Table 5). As a result from the identification process, a state surface was obtained (Figure 10), which represents a mathematical model with a very high coefficient of determination, as well as a reduced average error (Table 6), which determines the correct adjustment with respect to the reference data matrix.

The behaviour of the proposed model was validated by experimental tests for the voltages range defined by the floating voltage and the maximum charge voltage recommended by the manufacturer, as well as different operating temperatures (Figure 11).

Based on the gassing current error profile (Figure 19), it reaches its highest percentage value for the lowest current range, reaching peak values close to 70%, Figure 19a. This problem is mainly due to three factors:

The first one is due to the exponential relationship proposed by the Butler-Volmer model for the gassing current with respect to the battery operating voltage and temperature. Although for high values of voltage and/or charge temperature, the experimental relationship respond to an exponential function, for low values, the gassing current profile tends to resemble a linear type relationship (Figure 11, $V_{bat} \leq 415$ V).

The second one is due to the reduced magnitude of the operating current, which has a very low weight in the identification process in favour of a better parametric adjustment for more significant charging currents.

Finally, the reduced gassing current values determine the need for high accuracy in the current measurement, which will be determined in general by the performance of the sensor and acquisition system used.

On the contrary, for voltage values greater than 415 V, the gassing current follows a clearly exponential profile and that is why the percentage error decreases rapidly, limited to a maximum value of 20%, thanks to a considerable increase in the gassing current (Figure 11 and Figure 19a-19b). This current magnitude increase has a greater influence on the parameters identification process, which directly affects the quality of the model, while its high value allows it to be measured with greater accuracy.

Although the error in the calculation of the gassing current can be high in percentage terms (Figure 19a-19b), the error in terms of operating current is very small (Figure 19c-19d), and therefore, the error made in the calculation of the battery efficiency, according to the equation (13) can be considered negligible. Thus, for 2 A charge current (very low current C/50), the maximum error in the model would be associated with a maximum efficiency absolute error less than 5%.

In accordance to above, it is confirmed that the presented model to determine the battery charging efficiency has a good

performance, and therefore allows its application in systems based on lead acid technology batteries.

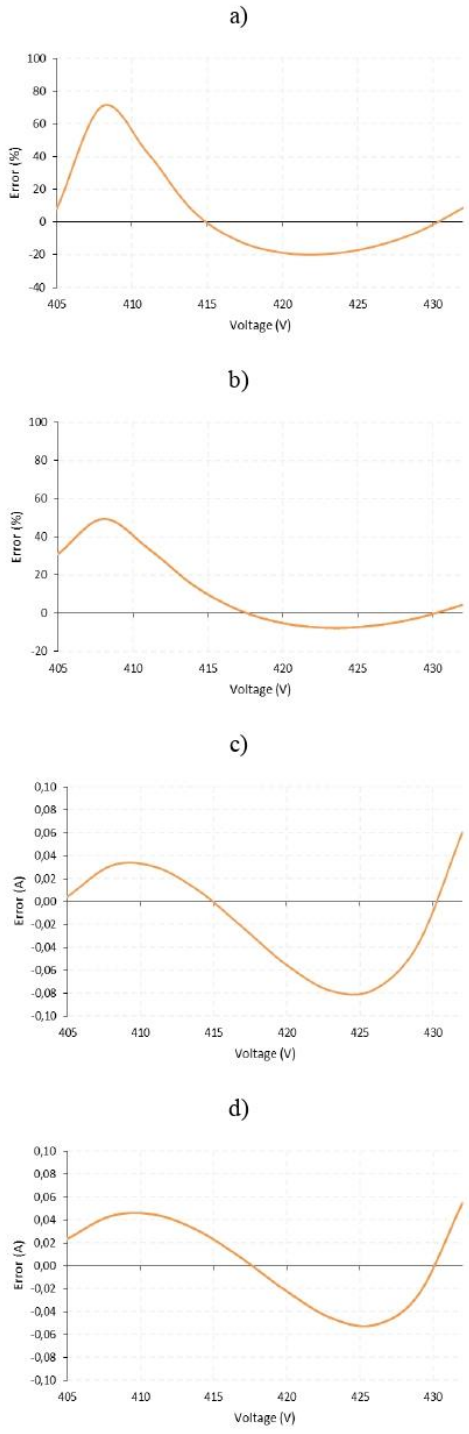

FIGURE. 19. a) Gassing current percentage error profile (14ºC); b) Gassing current percentage error profile (23ºC); c) Gassing current error profile (14ºC); d) Gassing current error profile (23ºC).

Unlike the case of the battery bank, the proposed model for the electrolyser and fuel cell hydrogen production/consumption ratio and operating efficiency is based on Faraday's Law, and therefore do not require the calculation of additional parameters that require a prior identification process.

The validation of the hydrogen generation profile model and consequently the electrolyser efficiency model was carried out in the experimental test presented in section 4.3 and collected in Figure 13 and Figure 14.

Attending to experimental results, it is easy to check how despite imposing a low dynamic ramp current profile, there are large fluctuations in the measured generated hydrogen flow rate profile (Figure 13b). These fluctuations are result from the operation mode of the DC/DC converter that supplies DC regulated power to the electrolysis stack. The converter selected for this application implements a power control stage, which regulates the working current based on the RMS value of a step type current profile (the current and voltage values obtained from the electrolyser data acquisition system have been subjected to a low-pass filter process). Continuous fluctuations in the current regulation stage cause variations in the instantaneous working power, and therefore in the production hydrogen flow rate.

According to the error profile resulting from the validation test (Figures 20a-20b), and despite the presence of fluctuations, the model error is reduced, presenting an average error close to 0.4%, with a maximum error (absolute value) less than 20%, and a standard deviation of 9.2%.

Based on validation test and error profile, it can easily verified that the hydrogen generation flow rate profile presents a direct and proportional relationship with the electrolysis current (Figure 13), in accordance with the proposed model based on the Faraday Law, equation (19). It follows that the proposed model present a reliable behaviour and permits to estimate the hydrogen generation profile during the electrolysis process.

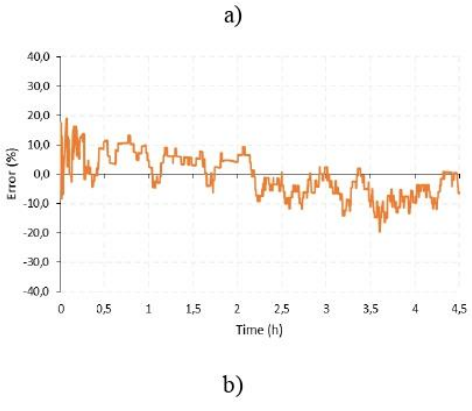

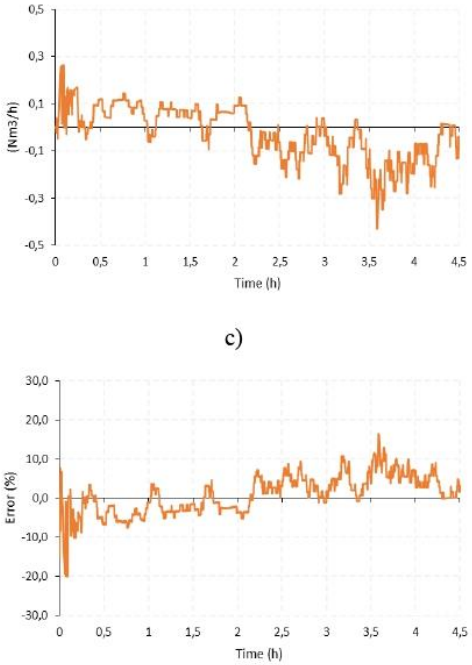

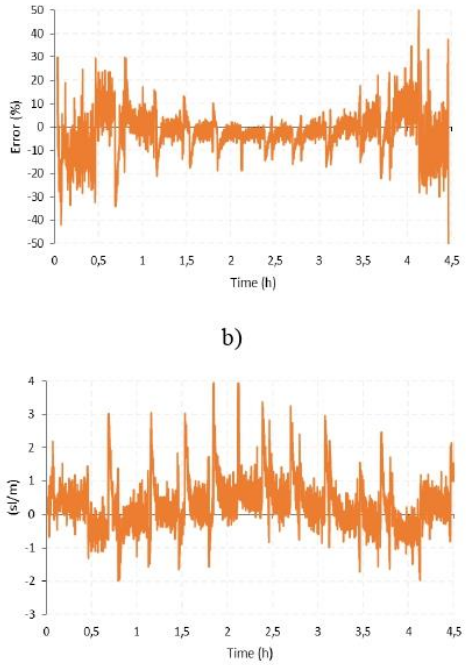

FIGURE. 20. a) Hydrogen generation percentage error profile; b) Hydrogen generation error profile; c) Electrolyser efficiency percentage error profile.

Based on the experimental and simulated hydrogen generation profile obtained for the described validation test, and based on the relationship between the electrical input energy and chemical output energy, equation (22), the operating electrolyzer efficiency profile is presented in Figure 14.

Similarly to the hydrogen generation profile, the presence of fluctuations in the current profile causes a greater error in the efficiency model (Figure 14). In spite of the above, it is verified that the electrolyser operating profile remains practically constant regardless of the working current, as derived from the proposed model, equation (23). The main reason is the direct dependence between electrolysis efficiency and operating voltage, which has remained practically constant for the entire test.

Following the error profile of the electrolyser efficiency model (Figure 20c), despite the fluctuations present in the hydrogen generation profile, good performance of the model is achieved, characterized by an average error is around 0.8%, with a maximum error (absolute value) always less than 20% and a standard deviation of 5.20%.

Based on the results obtained, and independently of the technology, the proposed model for the calculation of the electrolyser efficiency can be validated.

a)

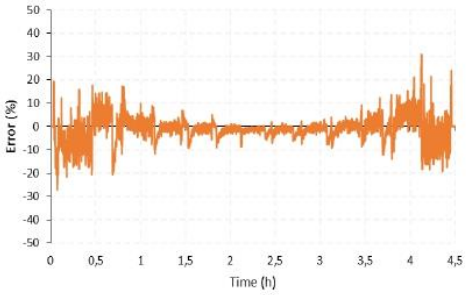

c)

FIGURE. 21. a) Hydrogen consumption percentage error profile; b) Hydrogen consumption error profile; c) Fuel cell efficiency percentage error profile.

Similar to the case of the electrolyser, the proposed model for the hydrogen consumption rate and efficiency of the fuel cell does not require a prior identification process as it is based on Faraday's Law, in accordance with equations (21) and (24).

According to the fuel cell hydrogen consumption model, these errors are determined by changes in the load, which cause an instantaneous peak consumption (Figure 16b and Figure 21a-21b). Similarly, the occurrence of periodic purges negatively affects the measure. Discarding the peaks derived from changes in the load, and the area of low operating power, it is verified that the maximum error in terms of absolute value is below 10%, with an average error close to 0.5% and a standard deviation less than 2.5% (Figure 21a).

In the case of low current operation the percentage consumption error is high, mainly because the hydrogen consumed value is very low and any small error in the

measurement has a great impact on the final value. In the low power area, the measurement range of the mass flow meter is far from the nominal design operating range, this fact, together with the output range of the flow meter sensor is 15-20 mA, causes that the resolution in the measure can be greatly affected in this working area.

In response to the errors previously analysed, the experimental results compared to the model based on Faraday's Law are compromised in the low current operation zone and during load changes. Although the average efficiency error is low, with an approximate value of 1,20%, the high percentage error in the measurement of hydrogen consumption for low operating power causes a high maximum error (in absolute value) close to 30%, and a standard deviation close to 5,52% (Figure 21c).

Considering that the low power region is a transit zone until reaching a minimum working point determined by 1 kW, equivalent to 30% of the nominal power ($1h \leq t \leq 3.5$ h), the error of this area can be considered negligible and therefore the benefits of the model increase in the nominal operating area, reaching maximum errors (absolute value) less than 10%, given for load change situations, with an average error of 0.73% and a standard deviation of 2.10% (Figure 21c). Based on the above, it is demonstrated that the proposed model is valid for determining the working efficiency of the fuel cell within the described operating range.

Finally, the proposed model for equipment degradation, and depending on it, the cost of the system, has not been possible for experimental validation.

The experimental validation of the equipment degradation model requires an exhaustive control and a history of use, due to its high dependence on the operating conditions of the systems; as well as the implementation of a long-term test, or accelerated life test (ALT) whose purpose is exclusively to determine the degradation rates according to the current regime, operating cycles, etc.

Due to the high cost of the equipment, the high availability required, the high temporal cost, as well as the lack of historical data, the experimental validation of these models has not been possible. For all the above, in this work the system degradation model is based on typical parameters provided by the manufacturer, which are a good starting point.

In the case that degradation parameters associated with the systems in use are available, the generality of the LTV model makes possible to easily modify the degradation rates according to the operation point at each sampling period.

VI. DISCUSSION

Despite the benefits of renewable sources-based microgrids, they need to be hybridized with the aim to mitigate their dependence on environmental resources and to guarantee a zero net power balance at any time. In the hybridization task, the use of different types of energy storage systems like battery and hydrogen-based system is promising solution. Hydrogen-based storage systems usually faces more stable power imbalances and, consequently, acts as a long-term storage system.

Regarding a renewable sources-based microgrid, it is not the load demand the only criteria to satisfy, but also there are technical and economic parameters to take into account by the EMS. Then, in order to optimize the microgrid response, it is necessary to design and develop control algorithms that implement an EMS that permits, on the one hand, to guarantee the demand at all times and, on the other, to optimize the response of the microgrid according to the studied technical and economic parameters. Therefore, it is crucial to have an accurate model of the microgrid that allows to have enough knowledge about it to design and analysis the controller.

But, the particularity and high complexity of the models widely used in the scientific literature, makes the process of designing controllers oriented to the implementation of management strategies a complicated task.

With the aim of simplifying the modelling task and centralizing design efforts exclusively at the level of supervision and management of the system, this paper presents a methodological foundation to obtain a generalized model of the whole system. The modelling methodology used is based on the operating philosophy of an EMS, developing a general formulation based on the operating powers of each device, based on the main parameters of the plant, which allows a sufficient level of abstraction for its generalization and use in any other microgrid with a similar configuration, regardless of technology, or working power range of the equipment used.

The general model has been developed and tested with experimental results. There has been proven that the proposed model describes the performance of a complete renewable sources-based microgrid with hydrogen as backup throughout all its operating range. This general model extended to all the operating range of the microgrid guarantees a better approximation with respect to those models mostly used in the scientific literature because those one are linearized systems around a single operating point. Additionally, apart from describing electrical performance for each device that makes up the microgrid, the proposed modelling formulation also includes technical and economical parameters as operating efficiency, degradation, losses and costs needed for the microgrid optimization.

To use the proposed methodology to other microgrid applications that do not include any of the studied devices, the equivalent discretized state-space model would be obtained by simply removing the rows corresponding to the devices not included.

The features of the generalized model obtained from the proposed methodology (model based on the entire operating point of each device and inclusion of the technical and economic parameters) help to define multi-objective optimization problems, as well as serving as a knowledge base in the design and implementation of model-based controllers.

The experimental results on each device and on the complete hydrogen-based microgrid allow validating the correct behaviour of the proposed model under long-term simulations.

REFERENCES

[1] J. M. Andújar, A. J. Barragán, J. M. Córdoba, and I. F. De Viana, "DISEÑO DE SISTEMAS DE CONTROL BORROSO: MODELADO DE LA PLANTA José M. Andújar, Antonio J. Barragán, Juan M. Córdoba, Iñaki Fernández de Viana," vol. 3, pp. 75–81, 2006.
[2] F. J. Vivas, A. De Las Heras, F. Segura, and J. M. Andújar, "A review of energy management strategies for renewable hybrid energy system with hydrogen backup," Renew. Sustain. Energy Rev., vol. 82, no. September 2018, pp. 126–155, 2018.
[3] F. J. Vivas, A. De las Heras, F. Segura, and J. M. Andújar, "A review of energy management strategies for renewable hybrid energy systems with hydrogen backup," Renew. Sustain. Energy Rev., vol. 82, 2018.
[4] A. De las Heras, F. J. Vivas, F. Segura, and J. M. Andújar, "From the cell to the stack. A chronological walk through the techniques to manufacture the PEFCs core," Renew. Sustain. Energy Rev., vol. 96, no. July, pp. 29–45, 2018.
[5] P. García, J. P. Torreglosa, L. M. Fernández, and F. Jurado, "Optimal energy management system for stand-alone wind turbine/photovoltaic/ hydrogen/battery hybrid system with supervisory control based on fuzzy logic," Int. J. Hydrogen Energy, vol. 38, no. 33, pp. 14146–14158, 2013.
[6] R. Dufo-López, "Dimensionado y Control Óptimos de Sistemas Híbridos Aplicando Algoritmos Evolutivos," p. 511, 2007.
[7] C. Y. Acevedo-Arenas et al., "MPC for optimal dispatch of an AC-linked hybrid PV/wind/biomass/H2 system incorporating demand response," Energy Convers. Manag., vol. 186, no. December 2018, pp. 241–257, 2019.
[8] A. Osman Haruni, M. Negnevitsky, M. E. Haque, and A. Gargoom, "A novel operation and control strategy for a standalone hybrid renewable power system," IEEE Trans. Sustain. Energy, vol. 4, no. 2, pp. 402–413, 2013.
[9] Ø. Ulleberg, "The importance of control strategies in PV – hydrogen systems," Sol. Energy, vol. 76, pp. 323–329, 2004.
[10] D. Feroldi, L. N. Degliuomini, and M. Basualdo, "Energy management of a hybrid system based on wind-solar power sources and bioethanol," Chem. Eng. Res. Des., vol. 91, no. 8, pp. 1440–1455, 2013.
[11] N. Moskalenko, P. Lombardi, and P. Komarnicki, "Multi-criteria optimization for determining installation locations for the power-to-gas technologies," IEEE Power Energy Soc. Gen. Meet., vol. 2014-Octob, no. October, pp. 1–5, 2014.
[12] M. J. G. R. Real-Calvo, A. Moreno-Munoz, V. Pallares-Lopez and E. J. P. I. M. Moreno-Garcia, "Intelligent Electronic System to Control the Interconnection Between Distributed Generation Resources and Power Grid," RIAI - Rev. Iberoam. Automática e Informática Ind., vol. 14(1), pp. 56–69, 2016.
[13] J. W. Stevens and G. P. Corey, "A Study of Lead-Acid Battery Efficiency Near Top-of-Charge and the Impact on PV System Design."
[14] K. Brik and F. Ben Ammar, "Causal tree analysis of depth degradation of the lead acid battery," J. Power Sources, vol. 228, pp. 39–46, 2013.
[15] J. Schiffer, D. U. Sauer, H. Bindner, T. Cronin, P. Lundsager, and R. Kaiser, "Model prediction for ranking lead-acid batteries according to expected lifetime in renewable energy systems and autonomous power-supply systems," J. Power Sources, vol. 168, no. 1 SPEC. ISS., pp. 66–78, 2007.
[16] C. Karnjanapiboon, K. Jirasereeamornkul, and V. Monyakul, "The high efficiency charge equalized system for serially connected VRLA battery string using synchronous flyback converter," 2010 Int. Power Electron. Conf. - ECCE Asia -, IPEC 2010, pp. 1185–1188, 2010.
[17] E. Potteau, D. Desmettre, F. Mattera, O. Bach, J. L. Martin, and P. Malbranche, "Results and comparison of seven accelerated cycling test procedures for the photovoltaic application," J. Power Sources, vol. 113, no. 2, pp. 408–413, 2003.
[18] P. Ruetschi, "Aging mechanisms and service life of lead-acid batteries," J. Power Sources, vol. 127, no. 1–2, pp. 33–44, 2004.
[19] M. Chandesris, V. Médeau, N. Guillet, S. Chelghoum, D. Thoby, and F. Fouda-Onana, "Membrane degradation in PEM water electrolyzer: Numerical modeling and experimental evidence of the influence of temperature and current density," Int. J. Hydrogen Energy, vol. 40, no. 3, pp. 1353–1366, Jan. 2015.
[20] P. Millet, A. Ranjbari, F. De Guglielmo, S. A. Grigoriev, and F. Auprêtre, "Cell failure mechanisms in PEM water electrolyzers," Int. J. Hydrogen Energy, vol. 37, no. 22, pp. 17478–17487, 2012.
[21] A. Kosonen, J. Ahola, M. Niemelä, J. Koponen, K. Huoman, and V. Ruuskanen, "Control and energy efficiency of PEM water electrolyzers in renewable energy systems," Int. J. Hydrogen Energy, vol. 42, no. 50, pp. 29648–29660, 2017.
[22] F. J. Vivas, A. de las Heras, F. Segura, and J. M. Andújar, "Cell voltage monitoring All-in-One. A new low cost solution to perform degradation analysis on air-cooled polymer electrolyte fuel cells," Int. J. Hydrogen Energy, no. xxxx, 2019.
[23] A. Benmouna, M. Becherif, D. Depernet, F. Gustin, H. S. Ramadan, and S. Fukuhara, "Fault diagnosis methods for Proton Exchange Membrane Fuel Cell system," Int. J. Hydrogen Energy, vol. 42, no. 2, pp. 1534–1543, 2017.
[24] N. Macauley, M. Watson, M. Lauritzen, S. Knights, G. G. Wang, and E. Kjeang, "Empirical membrane lifetime model for heavy duty fuel cell systems," J. Power Sources, vol. 336, pp. 240–250, 2016.
[25] H. Shin, O. Kwon, and B. S. Oh, "Correlation between performance of polymer electrolyte membrane fuel cell and degradation of the carbon support in the membrane electrode assembly using image processing method," vol. 3, 2018.
[26] S. Xiao et al., "Degradation location study of proton exchange membrane at open circuit operation," J. Power Sources, vol. 195, no. 16, pp. 5305–5311, 2010.
[27] J. Büsselmann, M. Rastedt, V. Tullius, K. Yezerska, A. Dyck, and P. Wagner, "Evaluation of HT-PEM MEAs: Load cycling versus start/stop cycling," Int. J. Hydrogen Energy, pp. 1–11, 2018.
[28] M. Moein-Jahromi, M. J. Kermani, and S. Movahed, "Degradation forecast for PEMFC cathode-catalysts under cyclic loads," J. Power Sources, vol. 359, pp. 611–625, 2017.
[29] F. J. Vivas, A. De las Heras, F. Segura, and J. M. Andújar, "H2RES2 simulator. A new solution for hydrogen hybridization with renewable energy sources-based systems," Int. J. Hydrogen Energy, vol. 42, no. 19, pp. 13510–13531, 2017.
[30] C. Bordons, F. García-Torres, and L. Valverde, "Gestión Óptima de la Energía en Microrredes con Generación Renovable," RIAI - Rev. Iberoam. Autom. e Inform. Ind., vol. 12, no. 2, pp. 117–132, 2015.
[31] I. Tégani, A. Aboubou, M. Y. Ayad, M. Becherif, and M. Bahri, "Power flow management in WT/FC/SC hybrid system using flatness based control," 3rd Int. Symp. Environ. Friendly Energies Appl. EFEA 2014, 2014.
[32] M. J. Vasallo, J. M. Bravo, and J. M. Andújar, "Optimal sizing for UPS systems based on batteries and/or fuel cell," Appl. Energy, vol. 105, pp. 170–181, 2013.
[33] D. Feroldi, L. N. Degliuomini, and M. Basualdo, "Energy management of a hybrid system based on wind–solar power sources and bioethanol," Chem. Eng. Res. Des., vol. 91, no. 8, pp. 1440–1455, 2013.
[34] L. Valverde, F. Rosa, A. J. Del Real, A. Arce, and C. Bordons, "Modeling, simulation and experimental set-up of a renewable hydrogen-based domestic microgrid," Int. J. Hydrogen Energy, vol. 38, no. 27, pp. 11672–11684, 2013.
[35] S. Sen and V. Kumar, "Microgrid modelling: A comprehensive survey," Annu. Rev. Control, vol. 46, pp. 216–250, 2018.
[36] D. Morin, Y. Stevenin, C. Grolleau, and P. Brault, "Evaluation of performance improvement by model predictive control in a renewable energy system with hydrogen storage," Int. J. Hydrogen Energy, vol. 43, no. 45, pp. 21017–21029, 2018.
[37] A. Alzahrani, M. Ferdowsi, P. Shamsi, and C. H. Dagli, "Modeling and Simulation of Microgrid," Procedia Comput. Sci., vol. 114, pp. 392–400, 2017.
[38] R. Darbali-Zamora, J. E. Quiroz, J. Hernández-Alvidrez, J. Johnson, and E. I. Ortiz-Rivera, "Implementation of a Dynamic Real Time Grid-Connected DC Microgrid Simulation Model for Power Management in Small Communities," 2018 IEEE 7th World Conf. Photovolt. Energy Conversion, WCPEC 2018 - A Jt. Conf. 45th IEEE PVSC, 28th PVSEC 34th EU PVSEC, pp. 1179–1184, 2018.

[39] Q. Niu, H. Zhang, and K. Li, "An improved TLBO with elite strategy for parameters identification of PEM fuel cell and solar cell models," Int. J. Hydrogen Energy, vol. 39, no. 8, pp. 3837–3854, 2014.
[40] S. S. Deshmukh and R. F. Boehm, "Review of modeling details related to renewably powered hydrogen systems," Renew. Sustain. Energy Rev., vol. 12, no. 9, pp. 2301–2330, 2008.
[41] S. A. Konstantinopoulos, A. G. Anastasiadis, G. A. Vokas, G. P. Kondylis, and A. Polyzakis, "Optimal management of hydrogen storage in stochastic smart microgrid operation," Int. J. Hydrogen Energy, vol. 43, no. 1, pp. 490–499, 2018.
[42] G. Cau, D. Cocco, M. Petrollese, S. Knudsen K??r, and C. Milan, "Energy management strategy based on short-term generation scheduling for a renewable microgrid using a hydrogen storage system," Energy Convers. Manag., vol. 87, pp. 820–831, 2014.
[43] T. Niknam, F. Golestaneh, and M. Shafiei, "Probabilistic energy management of a renewable microgrid with hydrogen storage using self-adaptive charge search algorithm," Energy, vol. 49, no. 1, pp. 252–267, 2013.
[44] R. Dufo-López, J. L. Bernal-Agustín, and J. Contreras, "Optimization of control strategies for stand-alone renewable energy systems with hydrogen storage," Renew. Energy, vol. 32, no. 7, pp. 1102–1126, 2007.
[45] J. P. Torreglosa, P. García-Triviño, L. M. Fernández-Ramirez, and F. Jurado, "Control based on techno-economic optimization of renewable hybrid energy system for stand-alone applications," Expert Syst. Appl., vol. 51, pp. 59–75, 2016.
[46] M. Castañeda, A. Cano, F. Jurado, H. Sánchez, and L. M. Fernández, "Sizing optimization, dynamic modeling and energy management strategies of a stand-alone PV/hydrogen/battery-based hybrid system," Int. J. Hydrogen Energy, vol. 38, no. 10, pp. 3830–3845, 2013.
[47] F. Garcia-torres and C. Bordons, "Optimal Economical Schedule of Hydrogen-Based Microgrids With Hybrid Storage Using Model Predictive Control," IEEE Trans. Ind. Electron., vol. 62, no. 8, pp. 5195–5207, 2015.
[48] G. Cau, D. Cocco, and M. Petrollese, "Modeling and simulation of an isolated hybrid micro-grid with hydrogen production and storage," Energy Procedia, vol. 45, pp. 12–21, 2014.
[49] M. Gulin, J. Matusko, and M. Vasak, "Stochastic model predictive control for optimal economic operation of a residential DC microgrid," Proc. IEEE Int. Conf. Ind. Technol., vol. 2015-June, no. June, pp. 505–510, 2015.
[50] L. Valverde, C. Bordons, and F. Rosa, "Power management using model predictive control in a hydrogen-based microgrid," IECON 2012 - 38th Annu. Conf. IEEE Ind. Electron. Soc., pp. 5669–5676, 2012.
[51] L. Valverde, F. Rosa, C. Bordons, and J. Guerra, "Energy Management Strategies in hydrogen Smart-Grids: A laboratory experience," Int. J. Hydrogen Energy, vol. 41, no. 31, pp. 13715–13725, 2016.
[52] A. Parisio, E. Rikos, and L. Glielmo, "Stochastic model predictive control for economic/environmental operation management of microgrids: An experimental case study," J. Process Control, vol. 43, pp. 24–37, 2016.
[53] M. Pereira, D. Limon, D. M. De La Peña, L. Valverde, and T. Alamo, "Periodic Economic Control of a Nonisolated Microgrid," IEEE Trans. Ind. Electron., vol. 62, no. 8, pp. 5247–5255, 2015.
[54] F. R. S. Sevilla, C. Park, V. Knazkins, and P. Korba, "Model predictive control of energy systems with hybrid storage," IEEE Power Energy Soc. Gen. Meet., vol. 2016-Novem, pp. 1–5, 2016.
[55] G. C. Goodwin, M. G. Cea, M. M. Seron, D. Ferris, R. H. Middleton, and B. Campos, Opportunities and challenges in the application of nonlinear MPC to industrial problems, vol. 4, no. PART 1. IFAC, 2012.
[56] N. Blet, D. Megías, J. Serrano, and C. de Prada, "Nonlinear Mpc Versus Mpc Using on-Line Linearisation — a Comparative Study," IFAC Proc. Vol., vol. 35, no. 1, pp. 147–152, 2002.
[57] O. Tremblay and L. A. Dessaint, "Experimental validation of a battery dynamic model for EV applications," World Electr. Veh. J., vol. 3, no. 1, pp. 289–298, 2009.
[58] J. B. Copetti, E. Lorenzo, and F. Chenlo, "A general battery model for PV system simulation," Prog. Photovoltaics Res. Appl., vol. 1, no. 4, pp. 283–292, 1993.
[59] N. Achaibou, M. Haddadi, and A. Malek, "Modeling of lead acid batteries in PV systems," Energy Procedia, vol. 18, pp. 538–544, 2012.
[60] H. Wenzl, "BATTERIES AND FUEL CELLS | Efficiency," Encycl. Electrochem. Power Sources, pp. 544–551, Jan. 2009.
[61] J. Xiang, P. Ding, H. Zhang, X. Wu, J. Chen, and Y. Yang, "Beneficial effects of activated carbon additives on the performance of negative lead-acid battery electrode for high-rate partial-state-of-charge operation," J. Power Sources, vol. 241, pp. 150–158, 2013.
[62] V. T. Arioli Maria F N C Rosolem Thais T de Sousa Thiago C do Nascimento CPqD CPqD CPqD CPqD Campinas, B. Campinas, and B. S. Cesar Vieira Dresser-Rand Guascor do Brasil São Paulo, "Ageing Evaluation of Lead-Acid Battery Used in Off-Grid Photovoltaic System," pp. 1–11.
[63] S. Piller, M. Perrin, and A. Jossen, "Methods for state-of-charge determination and their applications," J. Power Sources, vol. 96, no. 1, pp. 113–120, 2001.
[64] M. H. Chang, H. P. Huang, and S. W. Chang, "A new state of charge estimation method for LiFePO4 battery packs used in robots," Energies, vol. 6, no. 4, pp. 2007–2030, 2013.
[65] H. Görgün, "Dynamic modelling of a proton exchange membrane (PEM) electrolyzer," Int. J. Hydrogen Energy, vol. 31, no. 1, pp. 29–38, 2006.
[66] R. Dufo-López, J. M. Lujano-Rojas, and J. L. Bernal-Agustín, "Comparison of different lead-acid battery lifetime prediction models for use in simulation of stand-alone photovoltaic systems," Appl. Energy, vol. 115, pp. 242–253, 2014.
[67] T. M. Layadi, G. Champenois, M. Mostefai, and D. Abbes, "Lifetime estimation tool of lead-acid batteries for hybrid power sources design," Simul. Model. Pract. Theory, vol. 54, pp. 36–48, 2015.
[68] D. Ipsakis, S. Voutetakis, P. Seferlis, F. Stergiopoulos, and C. Elmasides, "Power management strategies for a stand-alone power system using renewable energy sources and hydrogen storage," Int. J. Hydrogen Energy, vol. 34, no. 16, pp. 7081–7095, 2009.
[69] BALLARD, "FCgen ® -1020ACS Fuel Cell Stack Product Manual and Integration Guide." 2011.
[70] M. Petrollese, L. Valverde, D. Cocco, G. Cau, and J. Guerra, "Real-time integration of optimal generation scheduling with MPC for the energy management of a renewable hydrogen-based microgrid," Appl. Energy, vol. 166, pp. 96–106, 2016.
[71] W. Wu, V. I. Christiana, S. A. Chen, and J. J. Hwang, "Design and techno-economic optimization of a stand-alone PV (photovoltaic)/FC (fuel cell)/battery hybrid power system connected toa wastewater-to-hydrogen processor," Energy, vol. 84, pp. 462–472, 2015.
[72] A. H. Fathima and K. Palanisamy, "Optimization in microgrids with hybrid energy systems - A review," Renew. Sustain. Energy Rev., vol. 45, pp. 431–446, 2015.

4.5. Article 5

General MPC controller to develop energy management systems in renewable sources-based smart micro grids with hydrogen as backup. Theoretical foundation and case study

F.J. Vivas, J.J. Caparrós, F. Segura, J.M. Andújar

Submited in:

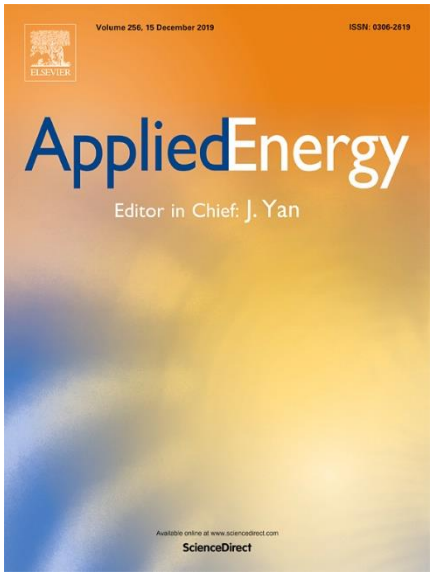

Journal: Applied Energy
Editorial: ELSEVIER
Editor-in-Chief: Jinyue Yan
ISSN: 0306-2619
In review process

Category	Journal Rank / Total journals	Quartile
Energy & Fuels	8 / 103	Q1
Engineering, chemical	5 / 138	Q1
Impact Factor (2018)	8.426	

General MPC controller to develop energy management systems in renewable sources-based smart microgrids with hydrogen as backup. Theoretical foundation and case study

Vivas F.J., Caparrós J.J., Segura F., Andújar J.M.

Grupo de Investigación de Control y Robótica TEP-192, Departamento de Ingeniería Electrónica, de Sistemas Informáticos y Automática, Escuela Técnica Superior de Ingeniería. Universidad de Huelva, Spain

Abstract

This article presents a methodological foundation to design and test experimentally a Model Predictive Control (MPC)-based controller to be applied in renewable sources-based microgrids with hydrogen as backup. The MPC controller has been developed with the aim to guarantee the best energy distribution at the same time that it is optimized the microgrid operation considering both technical and economic parameters. For this purpose, it has been defined an multiobjective function that takes into account the energy demand, operating cost, system performance and the suffered and accumulated degradation by the microgrid elements throughout their lifetime. That is, the proposed MPC controller solves the optimization of the microgrid operation both in the short and in the long-term basis. The MPC controller has been validated by simulation and experimental tests in a case study, where the performance of the microgrid under excess energy and deficit situations has been tested, acting as constrains the various degrees of degradation of the systems that make up the microgrid. The MPC controller results have been excellent both by simulation and by experimental tests.

Keywords: model predictive control, energy management system, renewable sources-based smart microgrid, hydrogen backup systems, technical and economic parameters, lifetime, power balance, energy balance.

LIST OF ACRONYMS

EMS: Energy Management System
HL: Hydrogen level
LTI: Linear Time Invariant
MILP: Mixed Integer Linear Programming
MIQP: Mixed Integer Quadratic Programming
MPC: Model Predictive Control
O&M: Operating maintenance
PV: Photovoltaic
SOC: State of Charge

I. INTRODUCTION

In general, a smart grid is a concept that comprises an efficient way to manage the electricity and that uses different technologies and tools (control, computers, communications, instrumentation, etc.) to optimize the production and distribution of the electricity, pursuing the balance between producers and consumers [1–3]. Therefore, a smart grid must secure a sustainable and resourceful energy system, with few losses and high-quality power as well as to guarantee the electrical supply [1,4,5].

Specifically, in the case of renewable sources-based microgrids with hydrogen as backup (Figure 1 shows the one used in the case study of this article), the intelligent management system must be responsible not only satisfying the load at all times, optimizing production and distribution but also accomplishing pivotal goals in case of hydrogen systems (electrolyser and fuel cell) as lifetime, degradation, costs, operating time and losses [3,6,7]. Only in that way, renewable sources-based microgrids with hydrogen as backup will be able to compete successfully with traditional electric power generation grids [1][2][8][9].

According to the control structure, for the implementation of the energy management strategy (EMS), the most used solution is based on a two-level structure (Figure 2 shows the designed control architecture in the case study of this article), in which there is a centralized controller that regarding the current energy situation of the system, it determines the optimal energy distribution based on the desired decision criteria

[1][10][11]. The power set points generated from the main controller are imposed on each system from the use of local controllers, which can implement different control algorithms depending on the topology and nature of the equipment.

The EMS provides a wide variety of control solutions from the simple heuristic strategies, based on the hysteresis operation mode [12–14]; methods focused on artificial intelligence by the use of fuzzy logic [15–17]; as well as complex control algorithms oriented at optimizing multi-objective functions [18–20]. In the latter cited category, the use of techniques based on MPC theory has been gaining relevance in recent years, due to its simplicity and good performance [21–23].

As it is well-known, MPC theory is a multivariable control method to predict future plant behaviour (in this case, the plant consists on a renewable sources-based microgrid with hydrogen as backup) that depends on future inputs and known measurable variables at a given sampling time. Additionally, the MPC is based on an optimization function [24–26], so if a suitable model plant is available, MPC theory drives the predicted plant output to the desired reference as close as possible, taking into account prediction and control horizons and constraints supported by the plant [27,28].

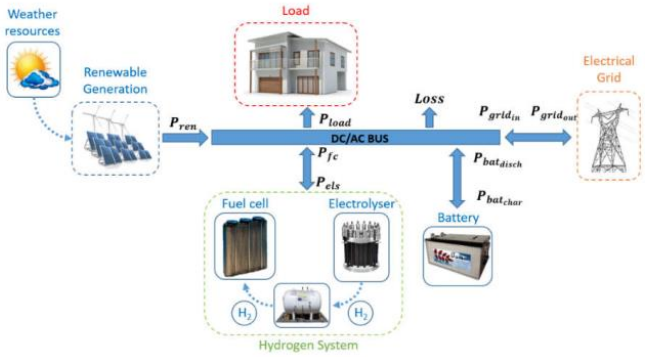

Figure 1. Architecture and power balance of the renewable sources-based microgrid with hydrogen as backup used as case study.

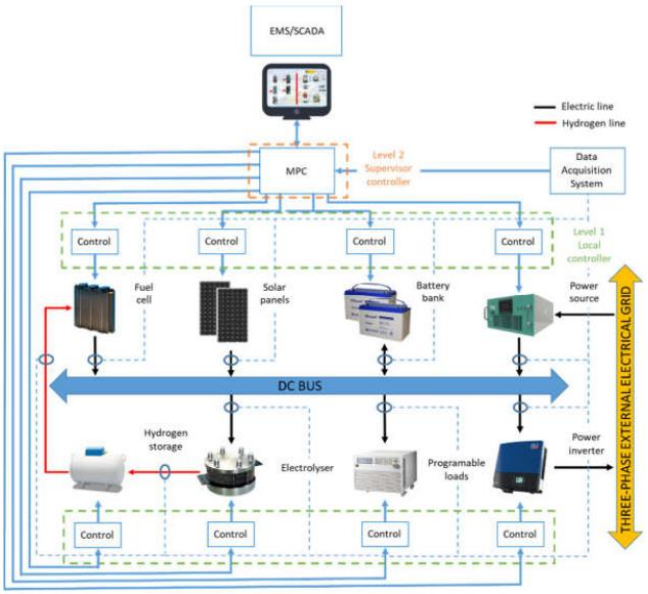

Figure 2. Designed control structure of the renewable sources-based microgrid with hydrogen as backup used as case study.

It is possible to find in the scientific literature configurations of microgrid with similar structure to that presented in Figure 1 and 2, where the MPC controller is based on a simplified LTI model of the plant. In these cases, the controller function is to determine the energy distribution of the microgrid, taking into

account exclusively the power balance and predefined set points for the energy storage system [12],[22,23],[29–33]. Then, these solutions present a very simple proposal because it obviates the influence of economic cost, operating efficiency, equipment degradation, as well as criteria associated with battery charge/discharge management.

By contrast, other works based on the economic optimization of the microgrid have been presented. For this purpose, it is proposed a cost function that includes economic terms associated with the operation and maintenance cost of the systems, as well as the cost related to the energy flow between the microgrid and the electrical grid. In spite of this, the systems operation is only linked to economic terms and therefore no actions are carried out with the objective of establishing technical optimization criteria.

Thus, in [25] and [34] an MPC controller is used based on simplified LTI models which seeks to maximize the economic performance of the microgrid. For this, the behaviour of the microgrid is validated through simulations in a residential application for different annual generation and consumption profiles.

Variants of the previous MPC controller are shown in [35]. This paper presents an MPC controller based on evolutionary algorithms, which starts from a complex nonlinear model of the microgrid and proposes an objective function that minimizes its operating costs in economic terms.

Unlike previous work, [36] presents an objective function which takes into account the microgrid operating costs based on equipment depreciation costs. The cost function includes terms associated with the amortization of the systems, without addressing specific solutions based on the technical criteria presented. This work was validated through experimentation in a residential application.

Finally, in [37–40], strategies based on MILP (Mixed Integer Linear Programming) and MIQP (Mixed Integer Quadratic Programming) theory are presented. These solutions are used to solve the optimization problem posed by the use of a hybrid model, which makes use of discrete variables to define operating cycles, as well as the charging and discharging cycles of batteries and hydrogen system. The use of discrete variables is used to quantify the cost associated with the cyclic use of the equipment, without considering technical optimization criteria. The results were validated through experimentation and simulation in residential applications.

Finally, there are different solutions in the scientific literature in which the objective function allows optimizing not only the operating cost, but also the equipment lifetime. These solutions present a more complex multi-objective optimization problem based on system cost functions and MIQP, dependent on the current operating parameters of the system.

In the papers presented in [18][41–45], the optimization problem is based on complex particular cost functions for all systems, defining a global cost function that integrates the economic cost associated with the purchase/sale of energy to the grid, as well as the equipment's amortization cost. The proposed energy management problem is based on the minimization of costs, as well as the maintenance of certain levels of energy stored in the energy storage systems, posing a tracking problem. These solutions are based on determining the degradation of the equipment in terms of operating cycles and changes in the power set point for each discretization period, without taking into account the historical state of the system.

Based on the literature review, most of the solutions reviewed are based on simple LTI models, linearized around a single working point, which only include the model of the energy state of the system in terms of battery SOC, as well as the level of hydrogen stored. The use of these types of solutions can have a negative impact on the prediction capability of the controller, and therefore on the system behaviour [24,28,46–48].

Based on the application of the different proposals, most of the works focus their studies and validations on simulations [25,33–35,38–41], presenting great difficulties in real applications under variations of generation, demand, equipment performance, safety criteria, etc. In this sense, attending to the safety and management of batteries, no scientific work proposes solutions in terms of battery charge management beyond the limitation of the battery SOC, which may be insufficient in terms of efficiency and safety in real battery operation.

Similarly, the solutions that include the degradation of the systems in the cost function, are based solely on the short term [36,41,43,49]. That is, the equipment degradation in each sample time is evaluated, without taking into account the system past history. Therefore, the controller bases its operation on the assumption that the performance of the devices remains constant throughout their lifetime. Notwithstanding the foregoing, in no case, the losses of efficiency or reduction in nominal power in accordance with the degradation accumulated by the systems are considered. Based on this assumption, the controller does not have accurate information of the current state of the microgrid, so the decision it takes will not be suitable in the long-term prediction horizon.

Finally, most of the reviewed works [25,33–36,38–41,43,49,50] present particular solutions according to the topology, application and objectives of the microgrid, starting from the modelling phase until the choice of the cost function and tuning the control parameters. This particularity makes difficult to extrapolate the methodology proposed in each paper to any other configuration that differ from the used model.

In order to respond to the shortages found in the literature review, this paper presents a generalized formulation for the design of MPC controllers applied to renewable energy microgrids with hydrogen as energy carrier. The solution is based on the proposal of generalized LTV (Linear Time Variant) model

presented in [X], which allows integrating in a state space model all the necessary parameters and considerations for the suitable operation of the microgrid throughout all its operating range. According to the MPC controller design, the generality of the proposed methodology allows to adapt the parameters of the controller according to the objectives, topology and application of the microgrid. In such a way, it is possible to enhance the microgrid performance both in the short- and long-term, guaranteeing the optimization of the plant from technical and economic point of view all over its lifetime.

The paper is organized as follows: Section II presents the theoretical foundation for the design of the generalized MPC controller, as well as the tuning methodology guidelines of the controller parameters. Section III shows a case study, developed and validated by simulation and experimental tests, which demonstrates the proper operation of the MPC controller. Finally, Section IV and Section V presents the discussions and the main conclusions, respectively, from the developed work.

II. MPC CONTROLLER

2.1.- General model for renewable sources-based microgrid with hydrogen as backup

In order to guarantee a correct behaviour of the microgrid controller, as well as providing the mathematical knowledge basis for the MPC-based controller design, it is necessary to have a suitable model of the renewable sources-based microgrid with hydrogen as backup shown in Figure 1. The model is fully developed in [X] and, in order to make this article self-contained, the linear time variant (LVT) discrete state-space model of the microgrid for a given sampling time T_s is again reproduced in (1). This can be expressed in the most compact way (2).

$$\begin{bmatrix} SOC(k+1) \\ HL(k+1) \\ V_{bat}(k+1) \\ C_{sys}(k+1) \\ D_{bat}(k+1) \\ D_{H2}(k+1) \\ Loss(k+1) \\ P_{H2}(k+1) \\ P_{grid}(k+1) \\ P_{net}(k+1) \end{bmatrix} = \begin{bmatrix} 1 & 0 & 0 & 0 & 0 & 0 & 0 & 0 & 0 & 0 \\ 0 & 1 & 0 & 0 & 0 & 0 & 0 & 0 & 0 & 0 \\ SV(k) & 0 & 0 & 0 & 0 & 0 & 0 & 0 & 0 & 0 \\ 0 & 0 & 0 & 0 & 0 & 0 & 0 & 0 & 0 & 0 \\ 0 & 0 & 0 & 0 & 0 & 0 & 0 & 0 & 0 & 0 \\ 0 & 0 & 0 & 0 & 0 & 0 & 0 & 0 & 0 & 0 \\ 0 & 0 & 0 & 0 & 0 & 0 & 0 & 0 & 0 & 0 \\ 0 & 0 & 0 & 0 & 0 & 0 & 0 & 0 & 0 & 0 \\ 0 & 0 & 0 & 0 & 0 & 0 & 0 & 0 & 0 & 0 \\ 0 & 0 & 0 & 0 & 0 & 0 & 0 & 0 & 0 & 0 \end{bmatrix} \begin{bmatrix} SOC(k) \\ HL(k) \\ V_{bat}(k) \\ C_{sys}(k) \\ D_{bat}(k) \\ D_{H2}(k) \\ Loss(k) \\ P_{H2}(k) \\ P_{grid}(k) \\ P_{net}(k) \end{bmatrix} +$$

$$+ \begin{bmatrix} S_1(k) & 0 & 0 \\ 0 & r_{els}(k) \text{ or } r_{fc}(k) & 0 \\ VP(k) & 0 & 0 \\ C_1(k) & C_2(k) \text{ or } -C_3(k) & C_4(k) \\ D_1(k) & 0 & 0 \\ 0 & D_2(k) \text{ or } -D_3(k) & 0 \\ L_1(k) & L_2(k) \text{ or } -L_3(k) & L_4(k) \\ 0 & 1 & 0 \\ 0 & 0 & 1 \\ 1 & 1 & 1 \end{bmatrix} \begin{bmatrix} P_{bat}(k) \\ P_{H2}(k) \\ P_{grid}(k) \end{bmatrix} + \begin{bmatrix} 1 & 0 & 0 \\ 0 & 1 & 0 \\ 0 & 0 & 1 \\ 0 & 0 & 0 \\ 0 & 0 & 0 \\ 0 & 0 & 0 \\ 0 & 0 & 0 \\ 0 & 0 & 0 \\ 0 & 0 & 0 \\ 0 & 0 & 0 \end{bmatrix} \begin{bmatrix} v_1(k) \\ v_2(k) \\ v_3(k) \end{bmatrix} \quad (1)$$

$$\begin{bmatrix} SOC(k) \\ HL(k) \\ V_{bat}(k) \\ C_{sys}(k) \\ D_{bat}(k) \\ D_{H2}(k) \\ Loss(k) \\ P_{H2}(k) \\ P_{grid}(k) \\ P_{net}(k) \end{bmatrix} = \begin{bmatrix} 1 & 0 & 0 & 0 & 0 & 0 & 0 & 0 & 0 & 0 \\ 0 & 1 & 0 & 0 & 0 & 0 & 0 & 0 & 0 & 0 \\ 0 & 0 & 1 & 0 & 0 & 0 & 0 & 0 & 0 & 0 \\ 0 & 0 & 0 & 1 & 0 & 0 & 0 & 0 & 0 & 0 \\ 0 & 0 & 0 & 0 & 1 & 0 & 0 & 0 & 0 & 0 \\ 0 & 0 & 0 & 0 & 0 & 1 & 0 & 0 & 0 & 0 \\ 0 & 0 & 0 & 0 & 0 & 0 & 1 & 0 & 0 & 0 \\ 0 & 0 & 0 & 0 & 0 & 0 & 0 & 1 & 0 & 0 \\ 0 & 0 & 0 & 0 & 0 & 0 & 0 & 0 & 1 & 0 \\ 0 & 0 & 0 & 0 & 0 & 0 & 0 & 0 & 0 & 1 \end{bmatrix} \begin{bmatrix} SOC(k) \\ HL(k) \\ V_{bat}(k) \\ C_{sys}(k) \\ D_{bat}(k) \\ D_{H2}(k) \\ Loss(k) \\ P_{H2}(k) \\ P_{grid}(k) \\ P_{net}(k) \end{bmatrix} + \begin{bmatrix} 0 & 0 & 0 \\ 0 & 0 & 0 \\ 0 & 0 & 0 \\ 0 & 0 & 0 \\ 0 & 0 & 0 \\ 0 & 0 & 0 \\ 0 & 0 & 0 \\ 0 & 0 & 0 \\ 0 & 0 & 0 \\ 0 & 0 & 0 \end{bmatrix} \begin{bmatrix} P_{bat}(k) \\ P_{H2}(k) \\ P_{grid}(k) \end{bmatrix} + \begin{bmatrix} 1 & 0 & 0 \\ 0 & 1 & 0 \\ 0 & 0 & 1 \\ 0 & 0 & 0 \\ 0 & 0 & 0 \\ 0 & 0 & 0 \\ 0 & 0 & 0 \\ 0 & 0 & 0 \\ 0 & 0 & 0 \\ 0 & 0 & 0 \end{bmatrix} \begin{bmatrix} d_{SOC}(k) \\ d_{HL}(k) \\ d_{V_{bat}}(k) \end{bmatrix}$$

Where:

SOC: Battery bank state of charge (%).
HL: Hydrogen level (Nm^3).
V_{bat}: Battery bank voltage (V).
C_{sys}: System operating cost ($€/T_s$).
D_{bat}: Battery bank degradation (Ah).
D_{H2}: H_2 system degradation; (h/T_s) for the electrolyser and (V/T_s) for the fuel cell.
$Loss$: System total losses (W).
P_{H2}: Following Figure 1, power consumed (if electrolyser in on, P_{els})/supplied (if fuel cell is on, P_{fc}) by the hydrogen system (W).
P_{grid}: Following Figure 1, power consumed ($P_{grid_{in}}$)/supplied ($P_{grid_{out}}$)/from/to the electrical grid (W).

P_{net}: Net power in the microgrid (W). Following Figure 1: $P_{net}(k) = P_{ren}(k) - P_{load}(k) - Loss(k) = \pm P_{bat}(k) \pm P_{H2}(k) \pm P_{grid}$. The used signs criterion is that the delivered power to the DC/AC bus is negative and the consumed is positive. So, P_{bat} is positive when is $P_{bat_{char}}$ and negative when is $P_{bat_{disch}}$.

$$\begin{aligned} x(k+1) &= Ax(k) + Bu(k) + Gv(k) \\ y(k) &= Cx(k) + Du(k) + Ed(k) \end{aligned} \tag{2}$$

Where,

$x(k)$: State vector $[SOC(k)\ HL(k)\ V_{bat}(k)\ C_{sys}(k)\ D_{bat}(k)\ D_{H2}(k)\ Loss(k)\ P_{H2}(k)\ P_{grid}(k)\ P_{net}(k)]^T$.
$u(k)$: Input vector $[P_{bat}(k) P_{H2}(k)\ P_{grid}(k)]^T$.
$v(k)$: Model disturbances vector $[v_1(k)\ v_2(k) v_3(k)]^T$.
$y(k)$: Output vector $[SOC(k)\ HL(k)\ V_{bat}(k)\ C_{sys}(k)\ D_{bat}(k)\ D_{H2}(k)\ Loss(k)\ P_{H2}(k)\ P_{grid}(k)\ P_{net}(k)]^T$.
$d(k)$: Measurable output disturbances vector $[d_{SOC}(k)\ d_{HL}(k)\ d_{V_{bat}}(k)]^T$.

The presented LTV model allows in a general way the calculation of the technical and economic microgrid parameters, guaranteeing a good performance all over its operating range.

Then, according to the model, the use of the variable P_{net} allows to establish the power balance. On the other hand, the term of amortization and operation and maintenance cost, allows taking into account the changes in the intraday electricity market without the need to act on the controller cost function.

2.2.- General Formulation of the Extended Model

In the first instance and from the control point of view, it is necessary to carry out some manipulation on the microgrid model (2). In general, and in this case in particular, the state control model produces a Type 0 system, that is, without integrators. Hence, as it is well known, such kind of control model cannot follow without error a step signal, i.e., a set point. This means that the stationary output vector will contain errors, which could be considerable. The solution is to insert an integrator in the direct path to the plant [51][52][53]. Then, considering $\Delta u(k)$ the input of the inserted integrator and $u(k)$ its output (plant input), the result is (3).

$$\Delta u(k) = u(k) - u(k-1) \tag{3}$$

Therefore, (2) can be expressed based on (3) as (4).

$$\begin{aligned} x(k+1) &= Ax(k) + B(\Delta u(k) + u(k-1)) + Gv(k) \\ y(k) &= Cx(k) + D(\Delta u(k) + u(k-1)) + Ed(k) \end{aligned} \tag{4}$$

As only future control actions can affect the system output, matrix D in (4) must be null. This allows defining the reduced discretized state-space model as (5).

$$\begin{aligned} x(k+1) &= Ax(k) + B(\Delta u(k) + u(k-1)) + Gv(k) \\ y(k) &= Cx(k) + Ed(k) \end{aligned} \tag{5}$$

In order to express the previous model according to the base form represented in (2), a new extended state vector, $\bar{x}(k)$, is defined including the control term, $u(k-1)$, (6).

$$\bar{x}(k) = \begin{bmatrix} x(k) \\ u(k-1) \end{bmatrix} \tag{6}$$

In response to the new state vector, (5) is redefined in the extended state space representation as (7):

$$\begin{aligned} \begin{bmatrix} x(k+1) \\ u(k) \end{bmatrix} &= \begin{bmatrix} A & B \\ 0 & I \end{bmatrix} \begin{bmatrix} x(k) \\ u(k-1) \end{bmatrix} + \begin{bmatrix} B \\ I \end{bmatrix} \Delta u(k) + \begin{bmatrix} G \\ 0 \end{bmatrix} v(k) \\ y(k) &= [C \quad 0] \begin{bmatrix} x(k) \\ u(k-1) \end{bmatrix} + Ed(k) \end{aligned} \tag{7}$$

In a simplified way, the extended state-space model can be written as (8):

$$\begin{aligned} \bar{x}(k+1) &= \bar{A}\bar{x}(k) + \bar{B}\Delta u(k) + \bar{G}v(k) \\ y(k) &= \bar{C}\bar{x}(k) + Ed(k) \end{aligned} \tag{8}$$

Where $\bar{A}, \bar{B}, \bar{C}$ and $\bar{G}$ are, following the same criterion as for $\bar{x}$, extended state matrices.

2.3.- Output Prediction

The MPC approach predicts future values of the controlled variables as a function of possible control action based on measurements known at a specific sampling time. Then, following this approach $\hat{y}(k+n|k)$ means the MPC output prediction in the sampling time $k+n$ based on measurements known at sampling time k. Then, output vector from (8) can be expressed as (9).

$$\hat{y}(k+1|k) = \bar{C}\bar{x}(k+1) + Ed(k+1) \tag{9}$$

For the output disturbance $d(k)$, a good approximation is to make it equal to the perturbation at the previous sampling $(k-1)$, i.e., $d(k) = d(k-1)$ [53][54]. Then, based on this approach and considering (8), it is possible to redefine the output prediction vector (9) as (10):

$$\hat{y}(k+1|k) = \bar{C}\bar{A}\bar{x}(k) + \bar{C}\bar{B}\Delta u(k) + \bar{C}\bar{G}v(k) + Ed(k) \tag{10}$$

By applying the procedure recursively, the prediction of the output vector can be obtain from (11).

$$\hat{y}(k+N_p|k) = \bar{C}\bar{A}^{N_p}\bar{x}(k) + \sum_{i=0}^{N_p-1}\left(\bar{C}\bar{A}^{N_p-i-1}\bar{B}\Delta u(k+i) + \bar{C}\bar{A}^{N_p-i-1}\bar{G}v(k+i)\right) + Ed(k+N_p-1) \tag{11}$$

Where N_p is an integer that represents the prediction horizon (output horizon). Developing (11) for each sampling, from 1 to N_p, the prediction of the output vector from measurements known at sampling time k, can be expressed in matrix form as (12):

$$\begin{bmatrix} \hat{y}(k+1|k) \\ \hat{y}(k+2|k) \\ \vdots \\ \hat{y}(k+N_p|k) \end{bmatrix} = \begin{bmatrix} \bar{C}\bar{A}\bar{x}(k) + \bar{C}\bar{B}\Delta u(k) + \bar{C}\bar{G}v(k) + Ed(k) \\ \bar{C}\bar{A}^2\bar{x}(k) + \sum_{i=0}^{1}\left(\bar{C}\bar{A}^{2-i-1}\bar{B}\Delta u(k+i) + \bar{C}\bar{A}^{2-i-1}\bar{G}v(k+i)\right) + Ed(k+1) \\ \vdots \\ \bar{C}\bar{A}^{N_p}\bar{x}(k) + \sum_{i=0}^{N_p-1}(\bar{C}\bar{A}^{N_p-i-1}\bar{B}\Delta u(k+i) + \bar{C}\bar{A}^{N_p-i-1}\bar{G}v(k+i)) + Ed(k+N_p-1) \end{bmatrix} \tag{12}$$

This general expression of the output prediction vector, $\hat{y}(k+j|k)$, can be expressed as a matrix equation in terms of the future control actions $\Delta u = [\Delta u(k)\ \Delta u(k+1) \ldots \Delta u(k+N_u-1)]^T$, being $N_u = i+1$ the control signal horizon; as well as terms based on the known extended state vector, $\bar{x}(k)$, at past sampling time k, $\bar{x}(k)$, and disturbances v and d, (13).

$$\hat{y} = \underbrace{F\bar{x}(k) + Kv + \tilde{E}d}_{yp} + \underbrace{H\Delta u}_{y_f} \tag{13}$$

Where y_p represents the free response of the system and y_f the response forced by action control. Regarding matrices $F, K, \tilde{E}$ and H are given, respectively, by (14):

$$F = \begin{bmatrix} \bar{C}\bar{A} \\ \bar{C}\bar{A}^2 \\ \vdots \\ \bar{C}\bar{A}^{N_p} \end{bmatrix};\ K = \begin{bmatrix} \bar{C}\bar{G} & \cdots & 0 \\ \bar{C}\bar{A}\bar{G} & & 0 \\ \vdots & \ddots & \vdots \\ \bar{C}\bar{A}^{N_p-1}\bar{G} & \cdots & \bar{C}\bar{G} \end{bmatrix};\ \tilde{E} = \begin{bmatrix} E & \cdots & 0 \\ 0 & & 0 \\ \vdots & \ddots & \vdots \\ 0 & \cdots & E \end{bmatrix} \text{ and } H = \begin{bmatrix} \bar{C}\bar{B} & \cdots & 0 \\ \bar{C}\bar{A}\bar{B} & & 0 \\ \vdots & \ddots & \vdots \\ \bar{C}\bar{A}^{N_p-1}\bar{B} & \cdots & \bar{C}\bar{B} \end{bmatrix} \tag{14}$$

2.4.- Objective Function

As discussed previously, the multivariable control method to predict future system output, $\hat{y}(k+j|k)$, which depends on future system inputs $\Delta u(k+N_u-1)$, based on measurements known at sampling time k, and that is based on an optimized criterion function of $\hat{y}$ and Δu, is called model predictive control (MPC). If a suitable model plant is available, this control method guarantees the best behaviour of the plant.

Given the model plant of the hydrogen-based microgrid, expression (8), and the output vector prediction, expression (13), the following step regarding microgrid is to choose the optimization criterion based on $\hat{y}$ and Δu. For that, the use of a well-known generalized cost function J, (15) is proposed: a quadratic function whose weights are related to the tracking error between the output and the reference, and

the effort of the control action to achieve them [52]. Thus, the control law would be the result of the minimization of (15).

$$J = \sum_{j=1}^{N_p} \alpha(j)[\hat{y}(k+j|k) - r(k+j)]^2 + \sum_{j=1}^{N_u} \lambda(j)[\Delta u(k+j-1)]^2 \quad (15)$$

Where:

$\alpha(j)$: Weighting factor of tracking error.
$\hat{y}(k+j|k)$: Output prediction at the sampling time $k+j$ based on measurements known at sampling time k.
$r(k+j)$: Output reference at the sampling time $k+j$.
$\lambda(j)$: Weighting factor that penalizes, from the sampling time k, large changes of the control action.
$\Delta u(k+j-1)$: control action at the sampling time $k+j-1$.

According to the prediction model of the output vector determined in (13), the cost function (15) can be transformed into an equivalent matrix as (16):

$$\begin{aligned} J &= \alpha[\hat{y} - r]^2 + \lambda[\Delta u]^2 \\ &= [F\bar{x}(k) + Kv + \bar{E}d + H\Delta u - r]^T \alpha[F\bar{x}(k) + Kv + \bar{E}d + H\Delta u - r] + \Delta u^T \lambda \Delta u \end{aligned} \quad (16)$$

Note that $[\hat{y} - r]^2$ implies to multiply two matrices $[\hat{y} - r]$ of dimension $N_y N_p \times 1$ (N_y is the number of outputs) which is not possible. So, defining α as a diagonal matrix whose dimension is $N_y N_p \times N_y N_p$, it is easy to show that $\alpha[\hat{y} - r]^2 = [\hat{y} - r]^T \alpha[\hat{y} - r]$, and the result is obviously a scalar. In the same way, $[\Delta u]^2$ needs to carry out the multiplication of two matrices $N_{\Delta u} N_u \times 1$ ($N_{\Delta u}$ is the number of inputs); a solution is again to define λ as a diagonal matrix of dimension $N_{\Delta u} N_u \times N_{\Delta u} N_u$ to get a scalar again. The minimization of (15), whose matrix development is (16), can be presented as the usual quadratic programming problem (QP) shown in (17).

$$J = \frac{1}{2} z^T Q z + c^T z \quad (17)$$

Where J is the function to minimize, and it is subjected to the constraints in the form: $Pz \leq \delta$, where z is the vector to find (in our case the control vector (Δu) that minimizes J). The given values are: Q (a symmetric matrix), the vector c and the constraints characterised for the matrix P and the restricted values δ.

The cost function (15) must be manipulate in order to obtain an expression comparable with (17) that allows identifying each of its terms. To this aim, from (15), taking the transpose of $H\Delta u$ in the first square bracket, operating and applying again the transpose to get $\alpha H \Delta u$ twice, results (18).

$$\begin{aligned} J &= [\Delta u^T H^T \alpha H \Delta u + [F\bar{x}(k) + Kv + \bar{E}d - r]^T \alpha H \Delta u + [F\bar{x}(k) + Kv + \bar{E}d - r]^T \alpha H \Delta u + \\ &+ [F\bar{x}(k) + Kv + \bar{E}d - r]^T \alpha [F\bar{x}(k) + Kv + \bar{E}d - r] + \Delta u^T \lambda \Delta u \end{aligned} \quad (18)$$

From this last equation, grouping terms and taking common factor Δu^T, (19) is obtained.

$$\begin{aligned} J &= [\Delta u^T (H^T \alpha H + \lambda) \Delta u + 2[F\bar{x}(k) + Kv + \bar{E}d - r]^T \alpha H \Delta u + \\ &+ [F\bar{x}(k) + Kv + \bar{E}d - r]^T \alpha [F\bar{x}(k) + Kv + \bar{E}d - r] \end{aligned} \quad (19)$$

Obviating the terms that do not depend on the control vector, because they will be eliminated in the derivation process to obtain the minimum (optimization), and multiplying the whole expression by $1/2$, (20) is obtained.

$$J = \frac{1}{2}[\Delta u^T (H^T \alpha H + \lambda) \Delta u] + [F\bar{x}(k) + Kv + \bar{E}d - r]^T \alpha H \Delta u] \quad (20)$$

Now, it is easy to compare (20) with (17), which is shown in (21).

$$\begin{aligned} z &= \Delta u \\ Q &= (H^T \alpha H + \lambda) \\ c^T &= [F\bar{x}(k) + Kv + \bar{E}d - r]^T \alpha H \end{aligned} \quad (21)$$

2.5.- Constraints

The great advantage of the MPC approach does not lie in the solution of the analytical minimization of a quadratic criterion such as (17), but in that it is easy to handle constraints (needed in a real plant), C, with the input and output of the plant ($|u| \leq C_u$ and $|y| \leq C_y$). Then, with the objective of establishing the operation limits of the microgrid, it is necessary to define the constraints that will delimit the space of possible solutions for the multi-objective problem, calculated from the quadratic optimization algorithm [52]. In general, the constraints must be defined considering the boundaries of the control action and the desired system response, (22):

$$\begin{aligned} &\Delta u_{min} \leq \Delta u \leq \Delta u_{max} \\ &u_{min} \leq u \leq u_{max} \\ &y_{min} \leq y \leq y_{max} \end{aligned} \tag{22}$$

Where Δu represents the input vector to the plant before the integrators, whose output vector is u. Obviously, in the microgrid presented in Figure 1 and expressions (1)-(2), the constraints are closely related to its physical limits as shown in (23):

$$\begin{aligned} &SOCmin \leq SOC \leq SOCmax \\ &HLmin \leq HL \leq HLmax \\ &V_{bat}min \leq V_{bat} \leq V_{bat}max \\ &C_{sys} \geq 0 \\ &D_{bat} \geq 0 \\ &D_{H2} \geq 0 \\ &Loss \geq 0 \\ &LPSP \geq 0 \\ &-Pmax_{bat_{disc}} \leq P_{bat} \leq Pmax_{bat_{char}} \\ &-Pmax_{fc} \leq P_{H2} \leq Pmax_{els} \\ &-Pmax_{grid_{in}} \leq P_{grid} \leq Pmax_{grid_{out}} \\ &P_{net}min \leq P_{net} \leq P_{net}max \\ &-\Delta Pmax_{bat\_disc} \leq \Delta P_{bat} \leq \Delta Pmax_{bat_{char}} \\ &-\Delta Pmax_{fc} \leq \Delta P_{H2} \leq \Delta Pmax_{els} \\ &-\Delta Pmax_{grid_{in}} \leq \Delta P_{grid} \leq \Delta Pmax_{grid_{out}} \end{aligned} \tag{23}$$

Where the criterion taken regarding Figure 1, following the state-space discrete model (2) has been that the delivered power is negative and the consumed is positive. This is the sense of signs in term that involves P and ΔP constraints. Then, for example, $-Pmax_{bat_{disc}}$ represents the highest battery bank power value (negative because it is supplied to the bus) allowed during the battery bank discharge. However, the case of P_{net}, as assessed in [X], represents the net power of the micro grid; thus, taking into account that the only primary source is renewable, the net power is the one that remains from the primary source once extracted that consumed by the loads and the losses. Then, from Figure 1, considering that the microgrid must be balanced all the time $P_{net} = P_{ren} - P_{load} - Loss = P_{bat} + P_{H2} + P_{grid}$. The maximum and minimum values will be given for situations of maximum renewable production and zero demand (positive); and maximum demand with zero production (negative) respectively.

In order to make the correspondence between the constraints shown in (23) with those of the standard form $Pz \leq \delta$, the problem is reduced to three inequalities: future control actions constraints; plant input constraints; and plant output constraints.

2.5.1.- Constraints of the Future Control Actions

Future control actions can be positive or negative, and following the optimization procedure ($Pz \leq \delta$), the constraints can be defined, taking into account (22), from the two following inequalities: $\Delta u \leq \Delta u_{max}$ and $-\Delta u \leq -\Delta u_{min}$, i.e., as (24).

$$\overbrace{\begin{bmatrix} 1 & \cdots & 0 \\ \vdots & \ddots & \vdots \\ 0 & \cdots & 1 \end{bmatrix}}^{P} \overbrace{\begin{bmatrix} \Delta u(k) \\ \Delta u(k+1) \\ \vdots \\ \Delta u(k+N_u-1) \end{bmatrix}}^{z} \leq \overbrace{\begin{bmatrix} \Delta u_{max} \\ \Delta u_{max} \\ \vdots \\ \Delta u_{max} \end{bmatrix}}^{\delta}$$
$$\begin{bmatrix} -1 & \cdots & 0 \\ \vdots & \ddots & \vdots \\ 0 & \cdots & -1 \end{bmatrix} \begin{bmatrix} \Delta u(k) \\ \Delta u(k+1) \\ \vdots \\ \Delta u(k+N_u-1) \end{bmatrix} \begin{bmatrix} -\Delta u_{min} \\ -\Delta u_{min} \\ \vdots \\ -\Delta u_{min} \end{bmatrix} \quad (24)$$

2.5.2.- Constraints of the Plant Inputs

Following expression (22), the constraints of the plant inputs (after integrators) can be defined from the two following inequalities: $u \leq u_{max}$ and $-u \leq -u_{min}$. Hence, taking into account (3) and operating as in (24), the result is (25).

$$\overbrace{\begin{bmatrix} 1 & \cdots & 0 \\ \vdots & \ddots & \vdots \\ 1 & \cdots & 1 \end{bmatrix}}^{P} \overbrace{\begin{bmatrix} \Delta u(k) \\ \Delta u(k+1) \\ \vdots \\ \Delta u(k+N_u-1) \end{bmatrix}}^{z} \leq \overbrace{\begin{bmatrix} u_{max} - u(k-1) \\ u_{max} - u(k-1) \\ \vdots \\ u_{max} - u(k-1) \end{bmatrix}}^{\delta}$$
$$\begin{bmatrix} -1 & \cdots & 0 \\ \vdots & \ddots & \vdots \\ -1 & \cdots & -1 \end{bmatrix} \begin{bmatrix} \Delta u(k) \\ \Delta u(k+1) \\ \vdots \\ \Delta u(k+N_u-1) \end{bmatrix} \begin{bmatrix} -u_{min} + u(k-1) \\ -u_{min} + u(k-1) \\ \vdots \\ -u_{min} + u(k-1) \end{bmatrix} \quad (25)$$

2.5.3.- Constraints of the Plant Output

From (22) and the model of the plant output prediction (13), the constraints can be defined from two inequalities: $F\bar{x}(k) + Kv + \bar{E}d + H\Delta u \leq y_{max}$ and $-(F\bar{x}(k) + Kv + \bar{E}d + H\Delta u) \leq -y_{min}$. Accordingly, the equivalent matrix inequations are (26).

$$\overbrace{\begin{bmatrix} H \\ -H \end{bmatrix}}^{P} \overbrace{\begin{bmatrix} \Delta u(k) \\ \Delta u(k+1) \\ \vdots \\ \Delta u(k+N_u-1) \end{bmatrix}}^{z} \leq \overbrace{\begin{bmatrix} y_{max} - \left(F\bar{x}(k) + Kv + \bar{E}d\right) \\ -y_{min} + \left(F\bar{x}(k) + Kv + \bar{E}d\right) \end{bmatrix}}^{\delta} \quad (26)$$

2.6.- MPC Cost function. Guidelines for Parameters Tuning

To define the cost function of the MPC controller proposed for the general microgrid presented in Figure 1, the variables included into the microgrid model, expression (1), will be included into the general expression of the cost function (15). Then the cost function of the microgrid will be (27).

$$\begin{aligned} J_k = {} & \alpha_1(k)\left(SOC(k) - SOC_r(k)\right)^2 + \alpha_2(k)\left(HL(k) - HL_r(k)\right)^2 + \alpha_3(k)\left(V_{bat}(k) - V_{bat_r}(k)\right)^2 + \\ & + \alpha_4(k)C_{sys}^2(k) + \alpha_5(k)D_{bat}^2(k) + \alpha_6(k)D_{H2}^2(k) + \alpha_7(k)Loss^2(k) + \alpha_8(k)P_{H2}^2(k) + \alpha_9(k)P_{grid}^2 + \\ & + \alpha_{10}(k)\left(P_{net}(k) - P_{net_r}(k)\right)^2 + \lambda_1(k)\Delta P_{bat}^2(k) + \lambda_2(k)\Delta P_{H2}^2(k) + \lambda_3(k)\Delta P_{grid}^2(k) \end{aligned} \quad (27)$$

Where at sampling time k, α_i are weighting factors corresponding to the first addend of (15), i.e., outputs deviations; and λ_i to the second addend of (15), i.e., control efforts. Figure 3 shows the general scheme of the system: renewable sources-based smart microgrid with hydrogen as backup + MPC controller + Cost Function. The meaning of each parameter is:
SOC: Measured battery bank state of charge (%).
SOC_r: Reference of the battery bank state of charge (%).
HL: Measured hydrogen level (Nm^3).
HL_r: Reference of the hydrogen level (Nm^3).
V_{bat}: Measured battery bank voltage (V).
V_{bat_r}: Reference battery bank voltage (V).

C_{sys}: System cost (€/T_s).
D_{bat}: Battery bank degradation (Ah/T_s).
D_{H2}: H_2 system degradation; (h/T_s) for the electrolyser and (V/T_s) for the fuel cell.
$Loss$: System total losses (W).
P_{H2}: Power consumed/supplied by H_2 system (W).
P_{grid}: Power consumed/supplied from/to the electrical grid (W).
P_{net}: Net power in the microgrid (W).
P_{net_r}: Reference net power in the microgrid (W).
P_{bat}: Battery bank power (W).

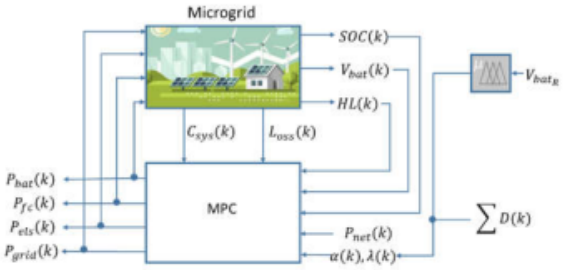

Figure 3. MPC controller architecture over the proposed hydrogen-based microgrid.

Once the objective function to be minimized has been defined in (27), as well as the constraints to take into account from (23) to (26), it is necessary to calculate the values for the weighting factors α_i and λ_i, as well as the control and the prediction horizons N_u and N_p, respectively (15), to obtain a desired system response [55][48] on the short- and long-term basis.

For this purpose, taking into account there is available a great amount of measured data and the "intelligence" that it has over its operation, the tuning process can be faced in a heuristic way. There is a set of cause-effect relationships that can help the tuning process.

2.6.1.- Short-term Optimization

In the microgrid short-term operation, the aim is to guarantee the power balance with the most renewable generation input as possible, while the battery bank charging process follows a controlled voltage protocol. Then, the parameters to take into account in the short-term are control and prediction horizons N_u and N_p, and from the cost function (27) are: the weighting factors related to the battery bank (α_1, α_3); stored hydrogen level (α_2) and power balance (α_{10}); also the weighting factors related with general losses (α_7) and H_2 system operation (α_8). Additionally, the weighting factor α_9 related to P_{grid} should be included in the short-term because in case of excess energy or deficit the microgrid must be connected to the external grid selling or buying energy to/from it.

2.6.1.1.- Control and Prediction Horizon

The selection of the control and prediction horizons N_u and N_p, respectively, are intimately linked with the system dynamics and the close loop stability. In the case of a fast dynamic system, it is unnecessary to use high control and prediction horizons because it must reach shortly its permanent regime. From this moment on, the output signal remains constant and, therefore, the subsequent temporal evaluation is needless. In contrast, for a slow dynamic system, the use of a relatively high control and prediction horizons is necessary in order to evaluate the performance of the system throughout its transient response.

In this case, where the plant is the hydrogen-based microgrid shown in Figure 1, the choice of the control and prediction horizons will depend on the desired behaviour as well as the dynamics of electrical generation and demand. It is advisable to use medium control and prediction horizons, due to the need of implementing constraints in the variation of the control signal, which will impose a slower system dynamic. If the constraint of the control variation is very strict, it can cause the multi-objective problem to be unfeasible. In order to find a reasonable solution, it is recommended to increase the control and prediction horizons so that the controller can evaluate the transient response impose by the constraints.

2.6.1.2.- Weighting Factors of the Reference Tracking Error

The weighting factors of the reference tracking error ($\alpha_1, \alpha_2, \alpha_3, \alpha_{10}$) provide the controller to impose the priority of the objectives according to the current state of the microgrid.

The main objective of short-term optimization is to safeguard the power balance at any time. For this reason, the weighting factor associated with the net power tracking error (α_{10}) must have a high value (it is a strong constraint), in such a way that a high difference between P_{net} and P_{net_r} should be punished.

Weighting factors α_1 and α_2 are related to energy storage systems (battery bank and hydrogen respectively), so they must guarantee the following: α_1 is responsible for maintaining of optimum battery bank SOC; and α_2 preservers the optimum stored hydrogen level. Therefore, both weighing factor need to have high values because the MPC controller must respond quickly if there is an increasing error in the tracking reference. However, the key is the ratio between both weighting factors, which will permit to define the optimal energy distribution between batteries and hydrogen storage system.

In special applications, where it is required from the microgrid to maintain a certain level of hydrogen, α_2 must be considered a high value, and therefore, the use of electrolyser and fuel cell will be made solely based on the hydrogen stock. In this sense, electrolyser and fuel cell will be putted into operation when the current hydrogen level is lower or higher than the reference level respectively, independently of the power balance and energy requirements.

On the other hand, in cases where the objective of the system does not require maximizing hydrogen production, but maintaining a desired reference hydrogen level, α_2 will have a low value, and the use of electrolyser and fuel cell will depend mainly on the battery bank SOC and the current energy situation. In this way, the use of electrolyser and fuel cell will be given for excess energy and energy deficit situations, respectively.

Finally, the weighting factor α_3 regulates the battery bank charge voltage control necessary to warrant a safe and efficient charging process. The importance of this parameter will only make sense when the battery bank voltage reaches a high level and there is an excess energy. For all other situations, this parameter must have a low value to avoid indiscriminate use of the rest of the elements in order to guarantee the reference voltage. Hence, α_3 must not have a fixed value but an adaptive value according to the energy situation at each time. A way to solve α_3 tuning can be by using a fuzzy controller as can be seen in Section 3.2.

2.6.1.3.- Weighting Factors of H2 system operation and total Losses

As in the short-term optimization the main objective is to safeguard the power balance at any time, the term in (27) related to operating power of H_2 system, α_8, must be low, even more taking into account that the term P_{H2} is squared. In this sense, a reduced value of the parameter α_8, will favour the use of the H_2 storage system as another key element in the problem of energy distribution, making use of the system's own resources when the battery-based storage system cannot cope with the energy imbalance. On the other hand, the weighting factor α_7, linked to total $Loss$ (losses in battery bank, fuel cell, electrolyser and losses associated with power electronic systems), must be small. In order to safeguard the power balance at any time, the losses in the microgrid must not determine its operation.

2.6.1.4.- Grid exchange energy flow

The use of the grid will be determined by the definition of dependence and interaction between the microgrid and the general electrical grid. Then, it is possible to define as many cases as possibilities, depending on the energetic situation, regulatory framework, etc.

Thus, isolated topologies or configurations whose objectives are to maximize the production/consumption of hydrogen, the weighting factor of the use of the general grid (α_9) must be represented by a high value. The purchase/sale of energy is penalized to the detriment of a more intensive use of the battery bank and H_2 system.

By contrast, in the case where it is desired that the microgrid acts as an active generation/storage system within the local electrical system, constantly allowing bidirectional energy exchange according to the intraday electricity market, the weighting factor α_9 should be reduced.

Finally, it can be found hybrid solutions, in which the energy flow between the microgrid and the electrical grid is only penalized in one way, that is, in the purchase or sale of energy. In this type of applications, the solution is a hybrid of the previous cases, in which a high value of the weighting factor will be used for the vetoed action, while for the favourable case, reduced values will be used. An example of this type of applications can be found in microgrids based on recent regulations of the Spanish electricity system. Here the objective is to guarantee maximum dependence on the grid, and at the same time the sale of energy can be considered as a positive contribution representing an economic benefit, or a reduction in the annual amount of the electric bill.

2.6.1.5.- Weighting factors of the Control Vector

The weighting factor of the control vector, λ_1, λ_2 and λ_3, allows the MPC controller to define the desired dynamics of the microgrid punishing strong variations of the operating point of those systems that better work under low dynamic operation, i.e. electrolyser and fuel cell. In this case, the weighting factors allow defining which subsystem will supply or absorb energy based on power balance dynamics.

Then, a reduced value of the weighting factor related to the battery bank power, λ_1, is recommended, but always above zero to guarantee the convexity of the objective function. Battery bank must present fast response dynamics versus transients. In contrast, the H_2 systems require more conservative operation, so, λ_2, will have a medium-high value.

The weighting factor associated with the use of the external electrical grid, λ_3, will depend on its role and the priority of the economic term in the cost function. In this sense, if it is necessary to maximize the economic performance of the microgrid based on the electricity market, it is important to reduce this weighting factor (always greater than the battery bank factor) with the aim of being considered an alternative in the energy distribution thanks to a reduced punishment.

Nonetheless, if it is necessary to prioritize the use of the renewable resources instead of the external electrical grid, it is advisable to increase the weighting factor λ_3 to punish the exchange of energy between the micro grid and the external grid.

2.6.2.- Long-term Optimization

The weighting factors of the long-term optimization ($\alpha_4, \alpha_5, \alpha_6$) seeks the most out of the performance of the microgrid while prolonging its useful lifetime. The optimization should respond to the objective of costs minimization ($\alpha_4 C_{sys}^2$) and the minimization of the battery bank and H_2 systems degradation ($\alpha_5 D_{bat}^2$ and $\alpha_6 D_{H2}^2$), while they guarantee a minimum electrical importation from the external grid.

2.6.2.1.- Operation Costs

The weighting factor α_4 determines the weight of the economic objective in the energy management strategy. Therefore, this parameter should have a high value when the microgrid is designed to provide maximum economic benefits.

2.6.2.2.- Lifetime

The weighting factors that represent the battery bank and H_2 system degradation (α_5, α_6), should not have fixed values but adaptive according to the cumulative degradation of the systems in such a way as to avoid the use of the most degraded ones.

For this purpose, a linear function is proposed (28), which allows calculating the updated weighting factor based on the accumulated degradation.

$$\alpha_x(k+1) = a\frac{\sum_{i=0}^{i=k} D_x(i)}{D_{x_{max}}} + b \tag{28}$$

Where:

$\alpha_x(k+1)$: Degradation weighting factor of the element x at sampling time $k+1$, with $x = 5$ (battery bank) or 6 (H_2 system).
$D_x(i)$: Current degradation of the element x at sampling time i, with $x = 5$ (battery bank) or 6 (H_2 system).
$D_{x_{max}}$: Maximum expected degradation of the element x, with $x = 5$ (battery bank), 6 (H_2 system).

Expression (28) can be tailored to the case of the battery bank (29), electrolyser (30) and fuel cell (31), respectively.

$$\alpha_5(k+1) = a_1\frac{\sum_{i=0}^{i=k} D_{bat}(i)}{D_{bat_{max}}} + b_1 \tag{29}$$

$$\alpha_{6\_els}(k+1) = a_2\frac{\sum_{i=0}^{i=k} D_{els}(i)}{D_{els_{max}}} + b_2 \tag{30}$$

$$\alpha_{6\_fc}(k+1) = a_3\frac{\sum_{i=0}^{i=k} D_{fc}(i)}{D_{fc_{max}}} + b_3 \tag{31}$$

Scalar coefficients, from a_1 to b_3, can be estimated from the manufactures' datasheets and/or by a trial and error procedure based on experimental tests. If a data historical series of the different elements is available, a precise assessment can be carry out.

Finally, based on the proposed tuning methodology, Table 1 summarizes the cause-effect relationships of each weighting factor on the performance of the microgrid MPC controller.

Table 1 – Cause-effects relationship between control parameters and microgrid response.

Parameter	Means	↑increase ↓decrease	Effect

Nu, Np	Determine the prediction and control horizons of the plant response based on the plant model	↑	• Facilitates solubility of the optimization problem in presence of slow dynamics and constrains. • Increase computational cost.
		↓	• Difficulties solubility of the optimization problem, especially in operating conditions close to design constraints. • Reduce computational cost.
α_1	Weighting of the tracking error of SOC setpoint	↑	• H_2 system and grid operation is defined based on SOC. • Very high values forces H_2 system and grid operate exclusively based on SOC setpoint and not on the energy situation. • Reduces battery bank degradation and increases lifetime.
		↓	• Indiscriminate battery bank use. • H_2 system and grid operation is defined exclusively by SOC limits. • Increases battery bank degradation and reduces its lifetime.
α_2	Weighting of the tracking error of HL setpoint	↑	• The operation of the H_2 system conditions the microgrid. • H_2 system operates based on HL set point. It is prioritized to keep the level of hydrogen stored independent on the energy situation.
		↓	• The operation of the H_2 system does not condition the microgrid. • The use of H_2 system is determined by other objectives.
α_3	Weighting of the tracking error of V_{bat} setpoint	↑	• Maximum battery bank voltage assured. • H_2 system and grid will be forced to guarantee the voltage set point (desirable in excess energy situations, undesirable in energy deficit situations). In case of energy deficit situation, the microgrid + MPC controller is reduced to a simple battery bank charge controller. • Controlled battery bank voltage assures low battery bank degradation, high charge performance and secure operation.
		↓	• Maximum battery voltage not assured. • High voltage cause excessive battery bank degradation, low charge performance and risk situation.
α_4	Weighting of system operating costs (C_{sys}). Influence of the economic objective.	↑	• The energy distribution in the use of battery bank, H_2 system and grid meets economic criteria. • The operating cost of the system decreases.
		↓	• The selection of the equipment and its operating power barely meets economic criteria. • The operating cost of the system increases.
α_5	Weighting of battery degradation (D_{bat}). Technical objective, increases lifetime.	↑	• The use of batteries is strongly penalized. • H_2 system and/or grid as a short-term storage system is required. • Increased H_2 system degradation and reduced lifetime.
		↓	• The use of batteries is indiscriminate, reduced use of H_2 system. • Increased batteries degradation and reduced lifetime.
α_6	Weighting of H_2 system degradation (D_{H2}). Technical objective: increases lifetime.	↑	• Reduced H_2 system degradation and increased lifetime. • The use of H_2 system is strongly penalized.
		↓	• Increased H_2 system degradation and reduced lifetime. • The use of H_2 system is indiscriminate, reduced use of batteries.
α_7	Weighting of operating losses. Technical objective: increases operating efficiency.	↑	• High penalty on equipment with low efficiency (H_2 system). • The grid acts as the main long-term energy storage system. • Higher efficiency operation.
		↓	• Reduced penalty on equipment with low efficiency (H_2 system). • The H_2 system acts as the main long-term energy storage system. • Lower efficiency operation.
α_8	Weighting factor of operation set point of H_2 system, P_{H2} (control signal)	↑	• Reduced use of H_2 system. • The grid acts as the main long-term energy storage system. • High grid dependence.
		↓	• Prioritization of H_2 system. • H2 system acts as the main long-term energy storage system. • Low grid dependence.
α_9	Weighting of the control signal P_{grid}	↑	• Prioritization of H_2 system and, to a lesser extent batteries. • The H_2 system acts as the main long-term energy storage system. • Low grid dependence.
		↓	• Reduced use of H_2 system and batteries as well. • The grid acts as the main long-term energy storage system. • High grid dependence.
α_{10}	Weighting of the tracking error of P_{net} set point P_{net_r}	↑	• Reduced (null) P_{net} tracking error. • The power balance is guaranteed from controller response.
		↓	• High P_{net} tracking error. • The power balance is not guaranteed based on the established criteria.

λ_1	Defines battery bank dynamics. Penalises ΔP_{bat}	↑	• High limitation of ΔP_{bat}. Slow dynamic response versus transients. • H_2 system or grid must deal with transients in the power balance. • Degradation increase and lower efficiency operation of H_2 system.
		↓	• Reduced limitation of ΔP_{bat}. Fast dynamic response versus transients. • H_2 system or grid operates in conditions of slow dynamics. • More efficient and conservative operation of H_2 system.
λ_2	Defines H_2 system dynamics. Penalises ΔP_{H2}	↑	• High limitation of ΔP_{H2}. Slow dynamic response versus transients. • Battery bank or grid must deal with transients in the power balance. • More efficient and conservative operation of H_2 system.
		↓	• Reduced limitation of ΔP_{H2}. Fast dynamic response versus transients. • Battery bank or external grid operates in conditions of slow dynamics. • Degradation increases and lower operation efficiency of H_2 system.
λ_3	Define grid dynamics. Penalises ΔP_{grid}	↑	• High limitation of ΔP_{grid}. Slow dynamic response versus transients. • H_2 system or battery bank must deal with transients in the power balance. • Degradation increases and lower operation efficiency of H_2 system.
		↓	• Reduced limitation of ΔP_{grid}. Fast dynamic response versus transients. • H_2 system operates in conditions of slow dynamics. • More efficient and conservative operation of H_2 system.

III. CASE STUDY

In order to validate the proposed MPC controller and tuning methodology, a case study is used that consists on the renewable sources-based microgrid with hydrogen as backup, made available for this research by our Research Group at the University of Huelva (UHU). In this section, the microgrid will be firstly described giving its technical characteristics. Next, the parameters tuning calculation used in the MPC controller as well as the constraints considered will be justified. Finally, simulations results corroborated with experimentation will show the performance of the microgrid both on the short- and long-term basis. The software tool used to implement the state-space model developed in [X] and the MPC controller designed in Section II is Matlab®.

3.1.- Description of the renewable sources-based microgrid with hydrogen as backup

In the renewable sources-based microgrid with hydrogen as backup available by the Research Group TEP192 at the (UHU), Figure 4, there are two main renewable generation sources: a photovoltaic (PV) array based on monocrystalline technology and a wind turbine with horizontal axis.

In the first instance, as energy storage systems there is a lead-acid battery bank with direct connection to a high voltage DC bus. Due to the direct connection of the battery bank to the DC bus, it is necessary to implement a charging control protocol for guaranteeing an optimum voltage operating range.

Additionally, the micro grid includes a H_2 backup system that is integrated by an alkaline electrolyser (for hydrogen generation), a PEM fuel cell (for electricity generation from hydrogen consumption), a medium pressure hydrogen gas tank and metal hydride tanks for the hydrogen storage.

To allow the energy exchange between the external electrical grid and the renewable sources-based microgrid, there is a commercial inverter (for injection to grid), and a programmable DC source (for consumption from grid). The programmable DC load can be used to simulate the load demand profile.

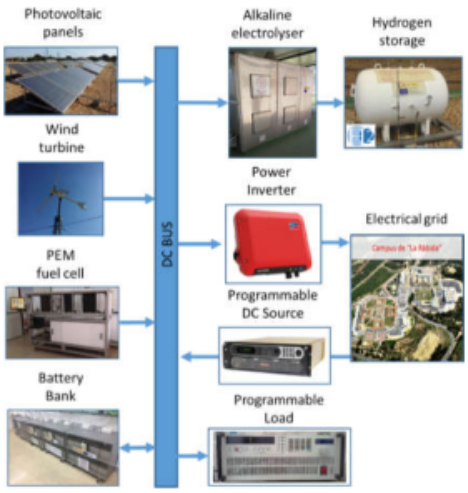

Figure 4. UHU renewable sources-based microgrid with hydrogen as backup.

The technical characteristics of the different systems s are summarized in Table 2.

Table 2 – Main parameters of the UHU renewable sources-based microgrid with hydrogen as backup

Equipment	Nominal capacity	Cost	Degradation
Photovoltaic panels	5 kW		
Wind turbine	2 kW		
Hydrogen storage	5 Nm^3		
Electrolyser	5 kW, 1N m^3	Electrolyser cost: 75000 € Electrolyser O&M cost: 0.1 €/h	$D_{els_{max}}$: 10000 h
Fuel cell	2 kW, 80 cells	Fuel cell cost: 8000 € Fuel cell O&M(1) cost: 0.1 €/h	$D_{fc_{max}}$: 100 mV/cell Fuel cell deg. Ratio: 10 µV/cell/h
Battery bank	400 V, 100Ah	Battery bank cost: 7650 € Battery bank O&M cost: 0.001 €/h	Bat deg. Ratio: 0.000676 $D_{bat_{max}}$: 40 Ah
Power inverter	2.5 kW	Grid selling cost: -0.03 €/kWh	
Programmable DC source	15 kW		
Programmable load	10 kW		

(1) Operation and maintenance

3.2.- MPC Controller and Tuning Parameters

The MPC controller is based on the developed state-space model (1) and the developed theoretical MPC foundation in Section II, considering the output prediction model (13) and the obtained cost function (27).

The weighting factors have been calculated following the design guidelines presented in Section 2.6. In order to implement the proposed tuning methodology, based on the comparison between the values of the weighting factors, all system outputs have been scaled at a rate of 0-1 based on the maximum and minimum limits established by the actual constraints of the microgrid (33). Then, applying a weighting factor of value 300 on an output variable and a value of 30 to another output variable indicates that the ratio of importance of the first with respect to the second is 10 directly.

In this particular case, the main objective of the microgrid is to guarantee at all times the power balance, from a safe, conservative and efficient use of the battery bank, electrolyser and fuel cell, giving priority to the use of the microgrid's resources, instead of the external grid utilization. For this, the battery bank operation is defined as a short-medium term energy storage system, while the electrolyser and fuel cell will act as a long-term energy storage system in such a way that they support the battery bank operation in extreme cases while the hydrogen level permits it.

Mentioning the foregoing, the use of the external grid will be limited to the objective of making a more conservative use of electrolyser and fuel cell, while at the same time it is possible to obtain an economic performance with the sale of the energy surplus.

Based on the above, a very high value of the net power weighting factor (α_{10}) has been defined, with the aim of guaranteeing at all times the power balance in each sampling period. Similarly, a controller based

on fuzzy logic has been proposed for the calculation of the weighting factor of the battery bank voltage (α_3), so that depending on the sign of the power balance, the working voltage and the energy surplus, it allows to control the battery bank charging voltage within established limits in accordance with the manufacturer's specifications.

Finally, in order to define the operation of the battery bank, electrolyser and fuel cell, a high value of the weighting factor of the battery bank SOC (α_1), and a reduced value of the weighting factor of the hydrogen level (α_2) have been used. With this, the use of electrolyser and fuel cell is determined exclusively by the energy situation of the system, and not by the hydrogen stock. Based on the above, the operation around the SOC reference defines the role of batteries as a short and medium term storage system, while the H_2 system acts as a long term storage system, acting in support of battery bank in situations of high and reduced SOC.

In order to define the priority in the use of the equipment, H_2 system vs. external grid, a very low value of the weighting factor of H_2 system (α_8) has been opted against a high value of the weighting factor of the grid (α_9), in such a way that the use of the external grid is strongly penalized against the H_2 system.

Because in this case the economic optimization is not the main objective of the microgrid operation, a low-medium value of the operation cost weighting factor (α_4) has been considered. So that the use of systems within the microgrid, as well as the energy flows between the microgrid and the general grid, are mainly defined by technical criteria, although cost minimization criteria are also contemplated in second instance.

The degradation parameters for battery bank (α_5), electrolyser (α_{6_els}) and fuel cell (α_{6_fc}) have been defined based on the linear function presented in (28). In this way, the degradation weighting factor will increase with the use of the systems. The slope of the linear function gives the maximum value of the weighting factor. In this case, taking into account the high cost associated with electrolyser and fuel cell, the slopes of their associated degradation functions (a_2 and a_3) are considerably higher than that of the battery bank degradation (a_1). Then, H_2 system degradation is more penalized and allows a longer lifetime. In this case, a similar function for electrolyser and fuel cell has been chosen because they have very similar established operating characteristics.

Finally, according to the objective of taking advantage of the internal resources of the microgrid, the weighting factor associated with the operating losses (α_7) has been kept very low, so that it does not influence the energy distribution between systems, penalizing the use of H_2 system.

Based on the weighting factors of the control signal variation (λ_1, λ_2 and λ_3), very small values have been chosen, because the terms of the control signal have not been scaled, and therefore the square of the values of any power increase causes a very high value with respect to the parameters associated with the output tracking errors.

In this case, the use of the battery bank as a short-term storage system has been chosen, acting against any transient in the microgrid, and that is why the weighting factor λ_1, acquires the lowest value. In order to maintain a safe and efficient operation of the electrolyser and fuel cell, a relatively high weighting factor of λ_2, has been chosen, which ensures slow dynamic operation. Finally, to guarantee the use of battery bank in the first instance, as well as to preserve the slow dynamics of the H_2 system, the weighting factor of the grid power variation, λ_3, has a value ten times lower than the parameter λ_2. This allows absorbing slow dynamic changes in the power balance, in favour of electrolyser and fuel cell; as well as a value much higher than λ_1, guaranteeing the role of the battery bank in the energy storage system. The main parameters of the MPC controller (except α_3) are summarized in Table 3.

Table 3 – Controller parameters and weighting factors.

Parameter	Value	Parameter	Value
Nu, Np	10	α_{10}	5000
α_1	300	λ_1	10^{-8}
α_2	0.01	λ_2	5×10^{-4}
α_4	2	λ_3	5×10^{-5}
α_5	$4\frac{\sum_{i=0}^{i=k} Dbat_i}{Dbat_{max}} + 0.1$	T_s	30 s
α_6	$20\frac{\sum_{i=0}^{i=k} Dels_i}{Dels_{max}} + 0.1;\ if\ P_{els} > 0$ $20\frac{\sum_{i=0}^{i=k} Dfc_i}{Dfc_{max}} + 0.1;\ if\ P_{fc} > 0$	SOC_{ref}	85%
α_7	0.01	HL_{ref}	4 Nm^3
α_8	0.01	$V_{bat_{ref}}$	400 V
α_9	20	P_{net}	$P_{ren} - P_{load}{}^{(1)}$

Finally, in order to fit the weighting factor of the battery bank voltage α_3, a Mandani fuzzy controller has been implemented that allows for calculating the optimal weighting factor regarding the power balance

and the current battery bank voltage. Table 4 and Figure 5 show, respectively, the inference matrix as well as the membership functions and the output surface of the proposed fuzzy controller.

Table 4 – Inference matrix of the fuzzy controller.

	Vbat				
Pnet	VL	L	M	H	VH
VL	VL	VL	L	M	H
L	VL	L	L	M	H
M	L	L	M	H	VH
H	L	H	H	VH	VH
VH	M	H	H	VH	VH

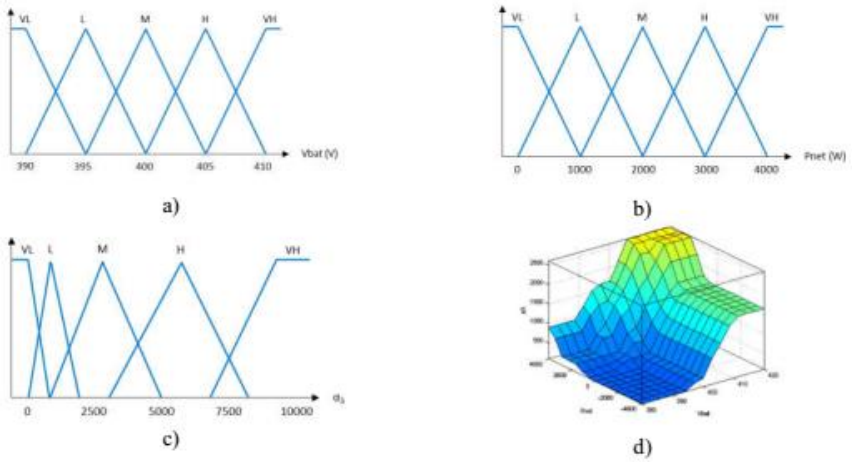

Figure 5. (a) Battery bank voltage membership functions. (b) Microgrid net power membership functions. (c) Weighting factor α_3 membership functions. (d) Fuzzy controller output surface.

3.2.2.- MPC Constraints

Considering the size of the actual microgrid, its maximum power capability and the manufacturer's recommendations for each connected system, the multi-objective function is subjected to the following constraints, (33):

$$
\begin{aligned}
&55\% \leq SOC \leq 90\% \\
&2\ \mathrm{Nm^3} \leq HL \leq 5\ \mathrm{Nm^3} \\
&330\ \mathrm{V} \leq V_{bat} \leq 430\ \mathrm{V} \\
&C_{sys} \geq 0 \\
&D_{bat} \geq 0 \\
&D_{H2} \geq 0 \\
&Loss \geq 0 \\
&LPSP \geq 0 \\
&-5000\ \mathrm{W} \leq P_{bat} \leq 5000\ \mathrm{W} \\
&-2000\ \mathrm{W} \leq P_{H2} \leq 5000\ \mathrm{W} \\
&-5000\ \mathrm{W} \leq P_{grid} \leq 5000\ \mathrm{W} \\
&-5000\ \mathrm{W} \leq P_{net} \leq 5000\ \mathrm{W} \\
&-5000\ \mathrm{W} \leq \Delta P_{bat} \leq 5000\ \mathrm{W} \\
&-500\ \mathrm{W} \leq \Delta P_{H2} \leq 500\ \mathrm{W} \\
&-1000\ \mathrm{W} \leq \Delta P_{grid} \leq 1000\ \mathrm{W}
\end{aligned}
\tag{33}
$$

3.3.- Simulation & Experimental Tests

In order to validate the design methodology of the MPC controller and tuning guidelines, the proposed algorithm has been evaluated both on the short- and long-term basis. In each case, the plant response (hydrogen-based microgrid + controller) is tested under these two situations. On the short-term basis, the plant is checked for excess energy and deficit situations (case I). In contrast, in the long-term case, it is analysed the response of the plant when battery bank and H_2 system suffer high degradation (case II and case III respectively). In order to subject the microgrid to greater stress, it is considered the most unfavourable situation in the microgrid area, i. e., there is no wind (at the microgrid site, the average sunshine hours per year is 3.120, the highest in Spain; however, there are often days with virtually no wind, at least the minimum necessary to start the wind turbine).

3.3.1.- Case I. Short-term Optimization. Simulation test

In this case, the aim is validating the performance of the microgrid under conditions of high excess energy and high deficit. This case represents the most unfavourable situation for the controller. The initial conditions of the plant are defined by a battery bank SOC of 65% and a hydrogen level of 4.5 Nm^3. An equivalent degradation (0%) is considered in all systems. The renewable generation and load profile is shown in Figure 6a.

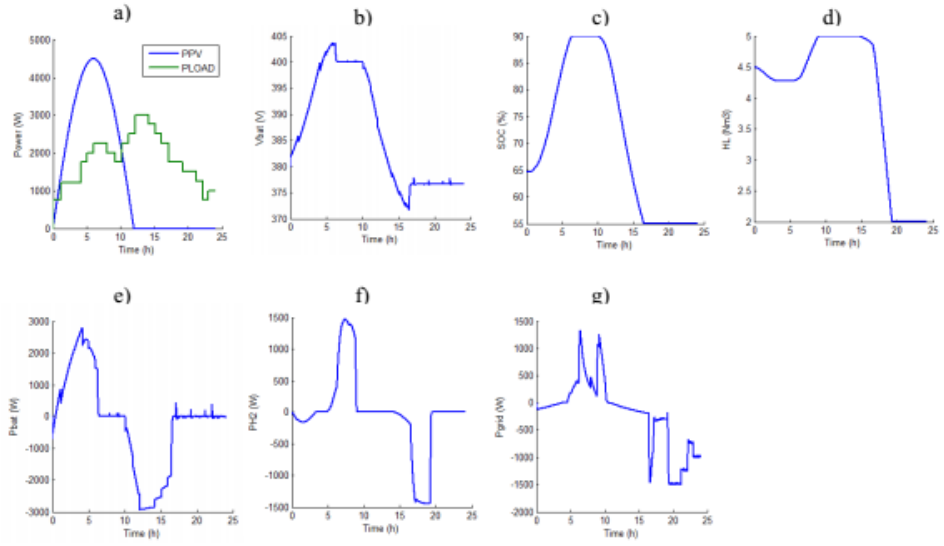

Figure 6. Performance of the plant + MPC controller in case I: high excess energy and high deficit. a) Renewable power (there is no wind, only PV) and load power; b) battery bank voltage; c) battery bank SOC; d) stored hydrogen level; e) battery bank power; f) H_2 system power; g) external grid power.

3.3.2.- Case II and III. Long-term optimization. Simulation test

The objective of the simulations presented in case II and case III is to validate the tuning methodology of the MPC controller parameters in the long-term optimization. For this purpose, the controller and the microgrid are subjected to situations of high battery bank degradation (case II) and high fuel cell and electrolyser degradation (case III).

a) Case II. Long-term optimization. High battery bank degradation

In this particular case, a high degradation of the battery bank is considered (75% of maximum degradation), while the degradation associated to the H_2 system is relatively low (25% of maximum degradation). The initial conditions of the system are similar to those used in the Case I. The renewable generation and load profile is shown in Figure 7a.

a) b) c) d)

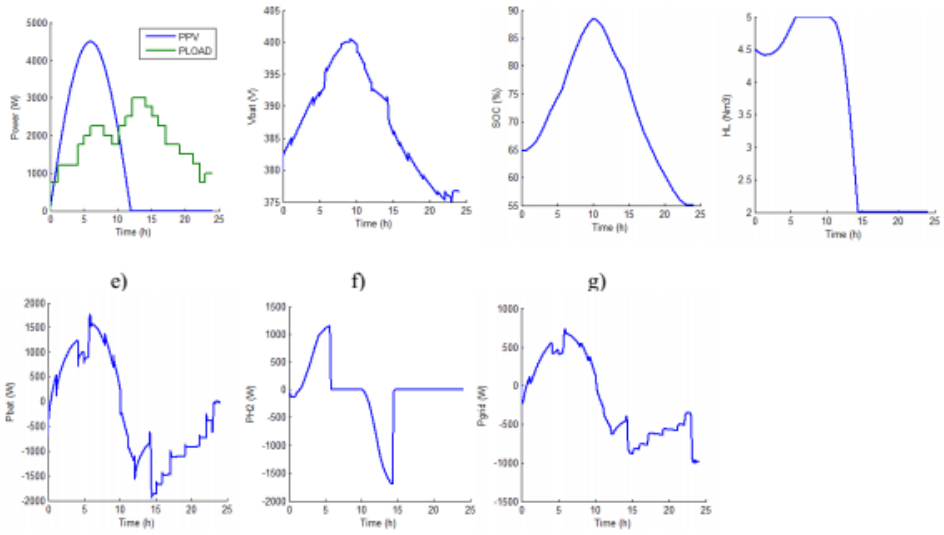

Figure 7. Performance of the microgrid + MPC controller in Case II: high battery bank degradation. a) Renewable power (there is no wind, only PV) and load power; b) battery bank voltage; c) battery bank SOC; d) stored hydrogen level; e) battery bank power; f) H_2 system power; g) external grid power.

b) Case III. Long-term optimization. High electrolyser and fuel cell degradation

In this particular case, a high degradation of electrolyser and fuel cell is considered (75% of maximum degradation), while the degradation associated to the battery bank is considered low (25% of maximum degradation). The initial conditions of the system are similar to those used in Case I. The renewable generation and load profile is shown in Figure 8a.

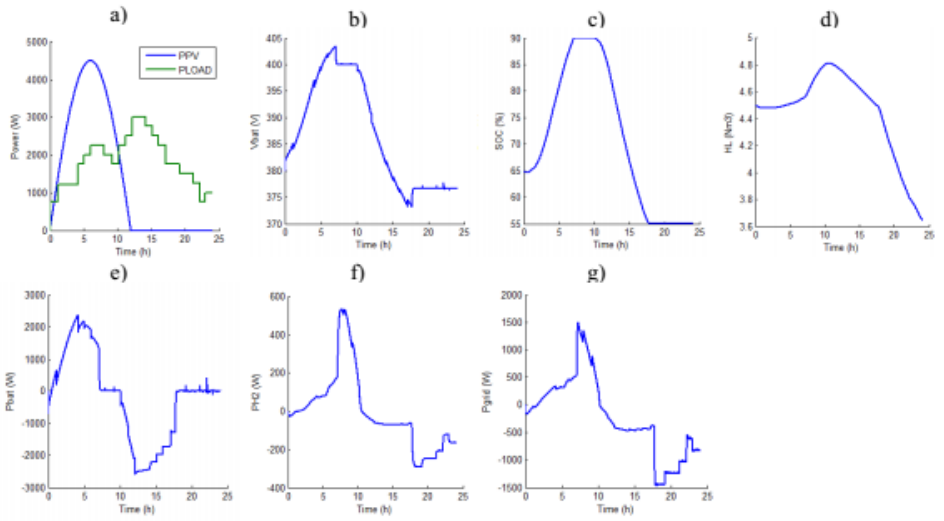

Figure 8. Performance of the microgrid + MPC controller in Case III: High degradation on H_2 system. a) Renewable power (there is no wind, only PV) and load power; b) battery bank voltage; c) battery bank SOC; d) stored hydrogen level; e) battery bank power; f) H_2 system power; g) external grid power.

3.3.3.- Case IV and V. Short-term optimization. Experimental test

Now, the results of several experimental tests on the microgrid of Figure 4 are presented. The actual control architecture of the microgrid is based on the two-level structure presented in Figure 2. The main objective of these tests is to validate the behaviour of the designed controller under real short-term operating

conditions. Due to the high cost of the equipment and the need for a large number of tests, long-term tests have been validated only by simulation.

In order to check the response of the microgrid-controller set against any possible energy situation, the system will be tested against cases of excess energy and deficit for operating limits situation, which define the most restrictive operating conditions of the system.

c) Case IV. Excess energy situation

In this case, the plant has been subjected to an excess energy condition under a stored energy level, given by the SOC and the HL close to their higher limit. For this, two different tests have been carried out in which the microgrid is studied against a situation of excess energy for a variable operation (1); and another low dynamic operation with saturation in hydrogen production (2). The objective is to validate the behaviour of the MPC controller in the face of a limit charge situation. The initial conditions of the microgrid are defined by a battery bank SOC of 70% and 80%, and a hydrogen level of 4.5 Nm^3 and 4.8 Nm^3. An equivalent degradation (10%) is considered in all systems. The renewable generation and load profiles are shown in Figure 9a and Figure 10a respectively for (1) and (2) situations.

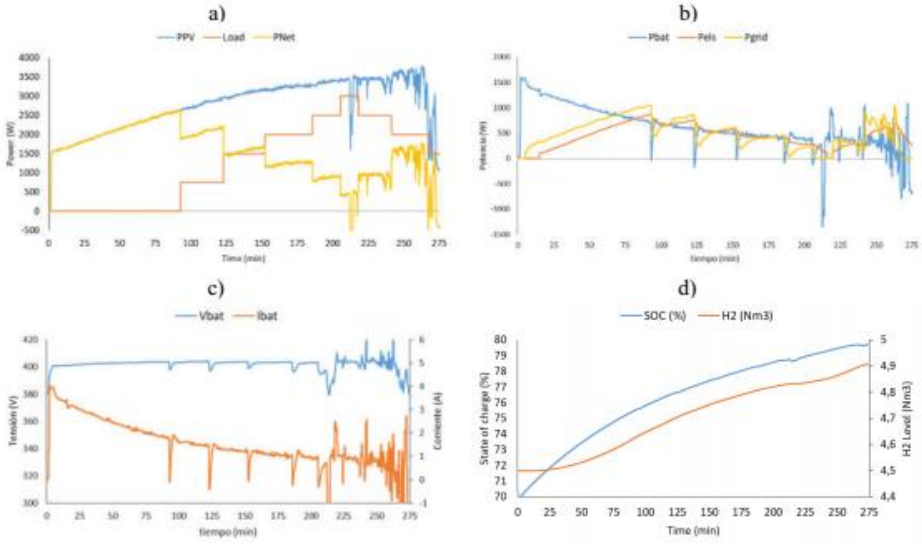

Figure 9. Actual microgrid performance + MPC controller in case IV: excess energy for a variable operation (1). a) Renewable power (there is no wind, only PV) and net power in the microgrid; b) battery bank power and H_2 system power; c) battery bank voltage and current; d) battery bank SOC and stored hydrogen level.

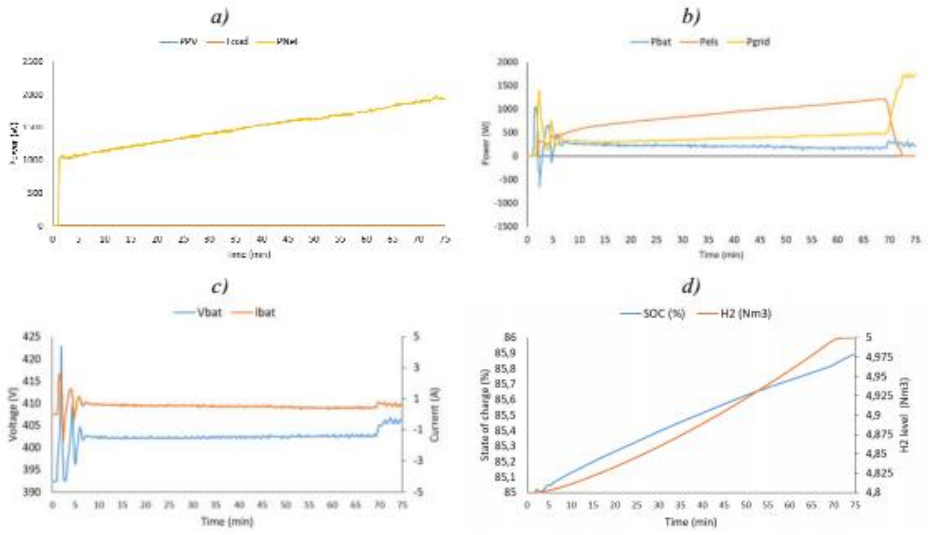

Figure 10.Actual microgrid performance + MPC controller in case IV: saturation in hydrogen production (2). a) Renewable power (there is no wind, only PV) and net power in the microgrid; b) battery bank power and H_2 system power; c) battery bank voltage and current; d) battery bank SOC and stored hydrogen level.

d) Case V. Energy deficit situation

Unlike the previous case, in this test the system has been subjected to an energy deficit condition under a stored energy level, given by SOC and HL, close to their lower limit. The objective of this case study is to validate the behaviour of the MPC controller in the face of a limit discharge situation. The initial conditions of the system are defined by a battery bank SOC of 57.5% and a hydrogen level of 3.6 Nm^3. An equivalent degradation (10%) is considered in all systems. The renewable generation and load profile is shown in Figure 11a.

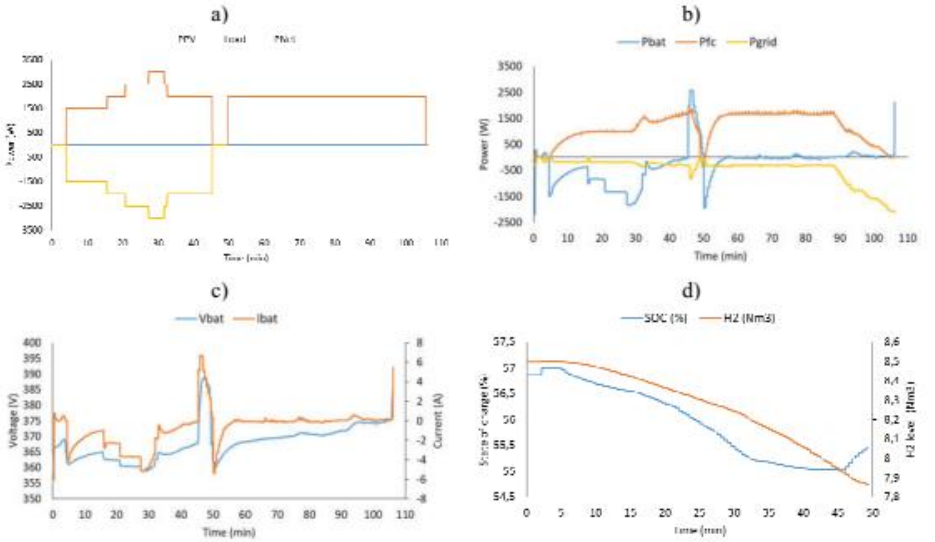

Figure 11. Actual microgrid performance + MPC controller in Case V: energy deficit situation. a) Renewable power (there is no wind, only PV) and net power in the microgrid; b) battery bank power and H_2 system power; c) battery bank voltage and current; d) battery bank SOC and stored hydrogen level.

IV. Discussions

Regardless of the case study, on excess energy situation, the battery bank deals firstly with excess energy, due to its priority of action defined by the reduced value of the weighting factor of the control signal variation (λ_1), until it reaches the desired charging voltage (400 VDC). Please see Figures 6e (t < 10 h), 7e (t < 10 h), 8e (t < 10 h) as well as even faster in 9b and 10b. Thereafter, the MPC controller regulates the charging power to keep the battery bank voltage around the reference with an error lower than 1%, regardless of the case under study (Case I-IV) and the system operating conditions: low dynamic (Case I, II, III) or variable operation (Case IV). Please see Figures 6b (4 h < t < 10 h), 8b (7.5 h < t < 10 h), 9c (t > 0 min) and 10c (t > 0 min). From this moment, the charging battery bank protocol based on fuzzy logic controller guarantees a safe and efficient charging process according to the battery bank charge acceptance curve, up to the maximum SOC defined by the system constraints (SOC = 90%). Please see Figures 6c and 8c (7.5 h < t < 10 h).

Based on the proposed tuning method, the MPC controller regulates the charging process making use of a perfect synchronism between battery bank, electrolyser and external grid, based on the battery bank charge acceptance curve and system dynamics; according to the weighting factors of control signal variation (λ_1, λ_2 and λ_3), battery bank and H_2 system accumulated degradation and performance priority of each system (determined by α_5 and α_6). In this sense, the excess energy is used in the safest and most efficient way following design considerations, i. e., prioritizing the hydrogen production instead of selling energy to the external grid. This can be clearly seen in the battery bank, electrolyser and external grid operating power profiles presented in Figures 6e-g (t < 10 h), 7e-g (t < 10 h), 8e-g (t < 10 h) as well as even faster in 9b and 10b.

Attending exclusively to the control signal variation, it is verified that under dynamic operating conditions (Case IV, excess energy situation (1)), the use of the electrolyser is heavily penalized due to the specified constrains in the operating power variation. In accordance with the above, the external grid acts virtually as a battery bank charge regulation system, Figure 9a-9b (t > 215 min).

In contrast, being an operation with a much lower dynamics (Case I and Case IV excess energy situation (2)), it is allowed to prevail the operation of the electrolyser against a small percentage of energy destined for sale to the external grid, Figures 6e-6g (5 h < t < 10 h) and 10a-10b (t > 5 min).

Similarly, based on the influence of systems degradation, the increase in the use of the electrolyser will be associated with an increase in its degradation and, therefore, a more conservative use will be required to make the system degradation more representative. The proposed adaptive tuning method for the weighting factor of the electrolyser degradation (α_6), will allow to increase the associated term on the cost function of the system (27), which will result in less use of the electrolyser to the detriment of greater use of batteries and external grid. Please see case III in Figures 8e-8g (10 h < t).

Finally, in case that the hydrogen level approaches the maximum capacity of the hydrogen tank (5 Nm^3), a controlled switch-off of the electrolyser is carried out. Then, the external grid is responsible for guaranteeing the power balance and the management of the battery bank charging protocol. Please see Figures 6d-6g (8 h < t < 16 h), 7d-7g (6 h < t < 12 h), 10b and 10d (t > 70 min).

Given the energy deficit situation (Case V), the reduced weighting factor of the battery bank power variation term (λ_1), makes the battery bank absorb instantaneously the transients in the net power set point in order to cover the demand. Please see Figures 6e (t > 10 h), 7e (t > 10 h), 8e (t > 10 h) and 11b (around 50 min). Once the battery bank SOC is lower than that designated as optimal by the reference (SOC = 85%), the fuel cell and, in less intensity, the external grid, go into operation to reduce the excessive use of batteries. Please, see Figures 6c, 6e and 6f (t > 15 h); Figures 7c and 7e-7f (t > 10 h); Figures 8c and 8e-8f (t > 12.5 h) and Figures 11b-c (t > 0 min). The energy distribution between battery bank and fuel cell is defined mainly from the term associated with the tracking error of the reference of the battery bank SOC, the dynamic impose by the weighting factors associated with the control signal variation (λ_1 and λ_2) and the current degradation, which directly influences the weighting factors of the degradation of batteries and the H_2 system (α_5 and α_6).

According to the proposed tuning method, the increase in the use of the battery bank will be associated with an increase in its degradation and, therefore, a more conservative use will be required to make the battery bank degradation more representative. The adaptive tuning method for the battery bank degradation weighting factor (α_5) will allow to increase the associated term on the cost function of the microgrid (27), which will result in a lower use of the battery bank to the detriment of greater use of fuel cell and external grid, Case II, Figures 7e-7g (t > 10 h).

Having reached the minimum battery bank SOC (55%), it is the fuel cell and the external grid which guarantees the power balance. Please see Figures 6c and 6e-6f (t > 17 h), 8c and 8e-8f (t > 18 h), and 11b-c (t > 47 min)). The energy distribution between battery bank and fuel cell is defined mainly from the weighting factors associated with the use of each system (α_8 and α_9), the dynamic impose by the weighting factors associated with the control signal variation (λ_2 and λ_3) and the current degradation which directly influences the weighting factor of the H_2 system (α_6).

Thus, in case of reduced degradation of the fuel cell, its operation prevails over the use of the external grid, thanks to the use of a lower weighting factor ($\alpha_8 < \alpha_9$) to maximize the use of the energy resource

available, Please, see Figures 6e-6g (t > 10 h) and 11 b (5 min < t < 90 min). Although the priority is established by the design considerations, the external grid will behave like a backup system to act against changes in the net power set point, thanks to the lower restriction in the variation of the working power ($\lambda_3 < \lambda_2$), in order to maintain a low dynamic and more conservative fuel cell operation.

According to the proposed tuning method, the increase in the use of the fuel cell will be associated with an increase in its degradation and, therefore, a more conservative use will be required to make the fuel cell degradation more representative. The adaptive tuning method for the weighting factor of the fuel cell degradation (α_6) will allow to increase the associated term on the cost function of the microgrid (27), which will result in a lower use of the fuel cell to the detriment of greater use of battery bank and external grid, Case III, Figures 8e-8g (t > 10 h).

Once the hydrogen level approaches the lower limit (Figures 6d (t > 20 h), 7d (t > 15 h) and 11d (t > 105 min)), the controlled shut down of the fuel cell proceeds and it is ultimately the external grid which meets the demand (Figures 6g (t > 20 h), 7g (t > 15 h) and 11b (t > 105 min)), in order to prioritize satisfying the demand through the microgrid resources. Unlike the previous case, due to energy deficit in the system, the implementation of battery bank charge voltage controller is not required.

V. Conclusions

In order to ensure a safe and efficient operation of renewable energy microgrids, it is necessary the implementation of energy management strategies, which take into account all the characteristics of the microgrid and allow the supply of demand to be guaranteed at all times, optimizing the response of the microgrid based on technical and economic criteria. This is especially important when the microgrid includes hydrogen systems (electrolysers and fuel cells), due to its high cost and rapid degradation due to misuse.

Based on the needs raised, MPC-based techniques place it as a powerful tool for the design of multivariable controllers that optimize the response of the closed-loop system (microgrid + controller), taking into account the restrictions associated with the physical or operating limits of the systems connected to the microgrid. All this, together with the ability to predict and precede any change in the entrance, makes the use of MPC controllers show great advantages over traditional control techniques.

Although previous works can be found in which the theory of predictive control is applied to hydrogen-based microgrids, most present particularized solutions for the topology and application in question, greatly hindering their dissemination and reproduction in other cases. These works present particular solutions, which focus on the short-term operation of the microgrid, ignoring pivotal technical-economic criteria for the optimization and operation of actual microgrids, both short and long term.

In order to respond to the lack of general solutions based on predictive control applied to renewable sources-based microgrid, this paper has presented a methodological foundation to design a MPC controller that can be applied to renewable sources-based microgrid with hydrogen as backup. The methodology is general enough that it can be used independently of the micro grid topology.

The resolution of the multi-objective optimization problem has been carried out using a generalized quadratic cost function. The weighting factors have been calculated taking into account the role of each system connected to the microgrid, as well as technical and economic parameters based on the performance of the actual systems, including considerations related to battery bank charging strategy, systems efficiency, operating degradation or systems cost in accordance with the selected topology and application both in the short and long-term.

The intrinsic difficulty in optimizing the multi-objective functions, as well as the large number of parameters to be optimized, make the tuning process a very complex task. Although a mathematical method to calculate the weighting factors is not presented, because they depends strongly on the microgrid topology and the final application, different cause-effect relationships have been explained and guidelines that facilitate the tuning process have been provided.

The MPC controller and the tuning methodology proposed have been checked in a case study, both by simulation and experimental tests.

Attending to the test results, thanks to the predictive action of the MPC controller, the goodness of the model used, as well as the proposed tuning method, it has been demonstrated the ability of the controller to establish the proposed energy management strategy based on the design criteria and the operating limits defined by the equipment restrictions.

Results obtained in the case study show the validity of the model and tuning methodology of the MPC controller, offering a powerful tool to other researchers in the tasks of designing, controlling and managing microgrids with renewable generation and the use of hydrogen as an energy carrier.

Acknowledgements

This work is a contribution of the DPI2017-85540-R Project supported by the Spanish Ministry of Economy and Competitiveness and by the European Union Regional Development Fund.

REFERENCES

[1] Vivas FJ, De Las Heras A, Segura F, Andújar JM. A review of energy management strategies for renewable hybrid energy system with hydrogen backup. Renew Sustain Energy Rev 2018;82:126–55. doi:10.1109/IREC.2016.7478902.

[2] Chauhan A, Saini RP. A review on Integrated Renewable Energy System based power generation for stand-alone applications: Configurations, storage options, sizing methodologies and control. Renew Sustain Energy Rev 2014;38:99–120. doi:10.1016/j.rser.2014.05.079.

[3] Arul PG, Ramachandaramurthy VK, Rajkumar RK. Control strategies for a hybrid renewable energy system: A review. Renew Sustain Energy Rev 2015;42:597–608. doi:10.1016/j.rser.2014.10.062.

[4] Upadhyay S, Sharma MP. A review on configurations, control and sizing methodologies of hybrid energy systems. Renew Sustain Energy Rev 2014;38:47–63. doi:10.1016/j.rser.2014.05.057.

[5] Fathima AH, Palanisamy K. Optimization in microgrids with hybrid energy systems - A review. Renew Sustain Energy Rev 2015;45:431–46. doi:10.1016/j.rser.2015.01.059.

[6] Olatomiwa L, Mekhilef S, Ismail MS, Moghavvemi M. Energy management strategies in hybrid renewable energy systems: A review. Renew Sustain Energy Rev 2016;62:821–35. doi:10.1016/j.rser.2016.05.040.

[7] Torreglosa JP, García P, Fernández LM, Jurado F. Energy dispatching based on predictive controller of an off-grid wind turbine/photovoltaic/hydrogen/battery hybrid system. Renew Energy 2015;74:326–36. doi:10.1016/j.renene.2014.08.010.

[8] Tesfahunegn SG, Ulleberg, Vie PJS, Undeland TM. Optimal shifting of Photovoltaic and load fluctuations from fuel cell and electrolyzer to lead acid battery in a Photovoltaic/hydrogen standalone power system for improved performance and life time. J Power Sources 2011;196:10401–14. doi:10.1016/j.jpowsour.2011.06.037.

[9] Ipsakis D, Voutetakis S, Seferlis P, Stergiopoulos F, Papadopoulou S, Elmasides C. The effect of the hysteresis band on power management strategies in a stand-alone power system. Energy 2008;33:1537–50. doi:10.1016/j.energy.2008.07.012.

[10] Zhang F, Thanapalan K, Procter A, Carr S, Maddy J, Premier G. Power management control for off-grid solar hydrogen production and utilisation system. Int J Hydrogen Energy 2013;38:4334–41. doi:10.1016/j.ijhydene.2013.01.175.

[11] Athari MH, Ardehali MM. Operational performance of energy storage as function of electricity prices for on-grid hybrid renewable energy system by optimized fuzzy logic controller Operational performance of energy storage as function of electricity prices for on-grid hybrid renew. Renew Energy 2016;85:890–902. doi:10.1016/j.renene.2015.07.055.

[12] García P, Torreglosa JP, Fernández LM, Jurado F. Optimal energy management system for stand-alone wind turbine/photovoltaic/ hydrogen/battery hybrid system with supervisory control based on fuzzy logic. Int J Hydrogen Energy 2013;38:14146–58. doi:10.1016/j.ijhydene.2013.08.106.

[13] Bordons C, García-Torres F, Valverde L. Gestión Óptima de la Energía en Microrredes con Generación Renovable. RIAI - Rev Iberoam Autom e Inform Ind 2015;12:117–32. doi:10.1016/j.riai.2015.03.001.

[14] Talebian ME, Plant P, Sobhani S, Borzooi A. New Hybrid System of Fuel Cell Power Plant and Wind Turbine for Household Consumption 2013:2–7.

[15] Wang X, Tong C, Palazoglu A, El-Farra NH. Energy Management for the Chlor-Alkali Process with Hybrid Renewable Energy Generation using Receding Horizon Optimization. Proc 53rd IEEE Conf Decis Control 2014:4838–43.

[16] Velarde P, Maestre JM, Ocampo-Martinez C, Bordons C. Application of robust model predictive control to a renewable hydrogen-based microgrid. 2016 Eur Control Conf ECC 2016 2017:1209–14. doi:10.1109/ECC.2016.7810454.

[17] Valverde L, Bordons C, Rosa F. Power management using model predictive control in a hydrogen-based microgrid. IECON 2012 - 38th Annu Conf IEEE Ind Electron Soc 2012:5669–76. doi:10.1109/IECON.2012.6389059.

[18] Valverde L, Rosa F, Bordons C, Guerra J. Energy Management Strategies in hydrogen Smart-Grids: A laboratory experience. Int J Hydrogen Energy 2016;41:13715–25. doi:10.1016/j.ijhydene.2016.05.279.

[19] Gaouzi K, El Fadil H, Rachid A, Belhaj FZ, Giri F. Constrained model predictive control for DC-DC buck power converters. Proc 2017 Int Conf Electr Inf Technol ICEIT 2017 2018;2018-Janua:1–5. doi:10.1109/EITech.2017.8255245.

[20] Nassourou M, Puig V, Blesa J, Ocampo-Martinez C. Economic model predictive control for energy dispatch of a smart micro-grid system. 2017 4th Int Conf Control Decis Inf Technol

CoDIT 2017 2017;2017-Janua:944–9. doi:10.1109/CoDIT.2017.8102719.
[21] Bruni G, Cordiner S, Mulone V, Rocco V, Spagnolo F. A study on the energy management in domestic micro-grids based on model predictive control strategies q. Energy Convers Manag 2015;102:50–8. doi:10.1016/j.enconman.2015.01.067.
[22] Lautenschlager B, Kruppa K, Lichtenberg G. Convexity Properties of the Model Predictive Control Problem for Subclasses of Multilinear Time-Invariant Systems**This work was partly supported by the project OBSERVE of the Federal Ministry for Economic Affairs and Energy, Germany. IFAC-PapersOnLine 2015;48:148–53. doi:10.1016/j.ifacol.2015.11.275.
[23] Liu L, Ling D, Wu Y, Zheng Y. Process model quality monitoring of model predictive controller. Chinese Control Conf CCC 2017:4391–6. doi:10.23919/ChiCC.2017.8028049.
[24] Benne M, Grondin D, Damour C, Hilairet M, Kbidi F. Energy Management System in Micro-Grid with Storage and Hydrogen Production. IECON 2018 - 44th Annu Conf IEEE Ind Electron Soc 2018. doi:10.1109/iecon.2018.8591204.
[25] Fu C, Lin J, Song Y, Zhou Y, Mu S, Lv KG, et al. Model predictive control of an integrated energy microgrid combining power to heat and hydrogen. IEEE Conf. Energy Internet Energy Syst. Integr., 2017, p. 1–6.
[26] Sevilla FRS, Park C, Knazkins V, Korba P. Model predictive control of energy systems with hybrid storage. IEEE Power Energy Soc Gen Meet 2016;2016-Novem:1–5. doi:10.1109/PESGM.2016.7741339.
[27] Trifkovic M, Sheikhzadeh M, Nigim K, Daoutidis P. Modeling and control of a renewable hybrid energy system with hydrogen storage. IEEE Trans Control Syst Technol 2014;22:169–79. doi:10.1109/TCST.2013.2248156.
[28] Pereira M, Limon D, Alamo T, Valverde L, Bordons C. Economic Model Predictive Control of a smartgrid with hydrogen storage and PEM fuel cell . IECON 2013 - 39th Annu Conf IEEE Ind Electron Soc 2013:7920–5. doi:10.1109/IECON.2013.6700456.
[29] Pereira M, Munoz De La Pena D, Limon D. Robust economic model predictive control of a community micro-grid. 2016 IEEE 55th Conf Decis Control CDC 2016 2016;100:2739–44. doi:10.1109/CDC.2016.7798676.
[30] Acevedo-Arenas CY, Correcher A, Sánchez-Díaz C, Ariza E, Alfonso-Solar D, Vargas-Salgado C, et al. MPC for optimal dispatch of an AC-linked hybrid PV/wind/biomass/H2 system incorporating demand response. Energy Convers Manag 2019;186:241–57. doi:10.1016/J.ENCONMAN.2019.02.044.
[31] Petrollese M, Valverde L, Cocco D, Cau G, Guerra J. Real-time integration of optimal generation scheduling with MPC for the energy management of a renewable hydrogen-based microgrid. Appl Energy 2016;166:96–106. doi:10.1016/j.apenergy.2016.01.014.
[32] Clarke WC, Manzie C, Brear MJ. An economic MPC approach to microgrid control. 2016 Aust Control Conf AuCC 2016 2017:276–81. doi:10.1109/AUCC.2016.7868202.
[33] Parisio A, Rikos E, Glielmo L. Stochastic model predictive control for economic/environmental operation management of microgrids: An experimental case study. J Process Control 2016;43:24–37. doi:10.1016/j.jprocont.2016.04.008.
[34] Zhang Y, Meng F, Wang R, Zhu W, Zeng XJ. A stochastic MPC based approach to integrated energy management in microgrids. Sustain Cities Soc 2018;41:349–62. doi:10.1016/j.scs.2018.05.044.
[35] Parisio A, Rikos E, Tzamalis G, Glielmo L. Use of model predictive control for experimental microgrid optimization. Appl Energy 2014;115:37–46. doi:10.1016/j.apenergy.2013.10.027.
[36] Pereira M, Limon D, De La Pe??a DM, Valverde L, Alamo T. Periodic Economic Control of a Nonisolated Microgrid. IEEE Trans Ind Electron 2015;62:5247–55. doi:10.1109/TIE.2015.2404815.
[37] Garcia F, Bordons C. Regulation service for the short-term management of renewable energy microgrids with hybrid storage using Model Predictive Control. IECON Proc (Industrial Electron Conf 2013:7962–7. doi:10.1109/IECON.2013.6700463.
[38] Garcia-torres F, Bordons C. Optimal Economical Schedule of Hydrogen-Based Microgrids With Hybrid Storage Using Model Predictive Control. IEEE Trans Ind Electron 2015;62:5195–207. doi:10.1109/TIE.2015.2412524.
[39] Pereira M, Limon D, Alamo T, Valverde L. Application of Periodic Economic MPC to a Grid-Connected Micro-Grid. IFAC-PapersOnLine 2015;48:513–8. doi:10.1016/j.ifacol.2015.11.330.
[40] Salazar J, Valverde L, Tadeo F. Predictive Control of a Renewable Energy Microgrid with Operational Cost Optimization. IECON 2013 - 39th Annu Conf IEEE Ind Electron Soc 2013:7950–5. doi:10.1109/IECON.2013.6700461.
[41] Luzi M, Vaccarini M, Lemma M. A tuning methodology of Model Predictive Control design for

energy efficient building thermal control. J Build Eng 2019;21:28–36. doi:10.1016/j.jobe.2018.09.022.

[42] Blet N, Megías D, Serrano J, Prada C de. Nonlinear Mpc Versus Mpc Using on-Line Linearisation — a Comparative Study. IFAC Proc Vol 2002;35:147–52. doi:10.3182/20020721-6-ES-1901.00593.

[43] Wojsznis W, Gudaz J, Blevins T, Mehta A. Practical approach to tuning MPC. ISA Trans 2007;42:149–62. doi:10.1016/s0019-0578(07)60121-9.

[44] Garcia-Torres F, Valverde L, Bordons C. Optimal Load Sharing of Hydrogen-Based Microgrids with Hybrid Storage Using Model-Predictive Control. IEEE Trans Ind Electron 2016;63:4919–28. doi:10.1109/TIE.2016.2547870.

[45] Xing X, Xie L, Meng H. Cooperative energy management optimization based on distributed MPC in grid-connected microgrids community. Int J Electr Power Energy Syst 2019;107:186–99. doi:10.1016/j.ijepes.2018.11.027.

[46] Ilhan ZO, Wehner WP, Schuster E. Model predictive control with integral action for the rotational transform profile tracking in NSTX-U. 2016 IEEE Conf Control Appl CCA 2016 2016:623–8. doi:10.1109/CCA.2016.7587899.

[47] Camacho EF, Bordons C. Model predictive control. Second edition. London: Springer; 2007. doi:10.1007/978-0-85729-398-5.

[48] Rossiter JA, Valencia-Palomo G. Feed forward design in MPC. 2009 Eur Control Conf 2018:737–42. doi:10.23919/ecc.2009.7074491.

[49] Ikonen E. Model Predictive Control and State Estimation 2013.

[50] Garriga JL, Garriga JL, Soroush M. Model Predictive Control Tuning Methods : A Review Model Predictive Control Tuning Methods : A Review. Ind Eng Chem Res 2013;49:3505–15. doi:10.1021/ie900323c.

4.6. Congress 1

Cell Voltage Monitoring All in One. A new low cost solution for degradation analysis on Polymer Electrolyte Fuel Cells

F.J. Vivas, A. De las Heras, F. Segura, J.M. Andújar

Presented in:

Event: European Hydrogen Energy Conference
Organiser: Spanish hydrogen Association
Date: 14/03/2018 – 16/03/2018
Place: Málaga, Spain.

4.7. Congress 2

Optimal energy management strategy of a hybrid renewable energy system with hydrogen generation and storage

F.J. Vivas, A. De las Heras, F. Segura, J.M. Andújar

Presented in:

Event: World Hydrogen Energy Conference
Organiser: Spanish hydrogen Association
Date: 13/06/2016 – 16/06/2016
Place: Zaragoza, Spain.
ISSN: 9781510838352

4.8. Congress 3

A new simulator for hybrid renewable generation systems. A new solution for technological and economic analysis and energy/hydrogen management strategies

F.J. Vivas, A. De las Heras, F. Segura, J.M. Andújar

Presented in:

Event: World Hydrogen Energy Conference
Organiser: Spanish hydrogen Association
Date: 13/06/2016 – 16/06/2016
Place: Zaragoza, Spain.
ISSN: 9781510838352

4.9. Congress 4

Configuration of a fuel cell system. Clues to choose between a modular or single stack-based design

F.J. Vivas, A. De las Heras, F. Segura, J.M. Andújar

Presented in:

Event: 42nd Annual Conference of IEEE Industrial Electronics Society

Organiser: IEEE Power & Energy Society®

Date: 24/10/2016 – 27/10/2016

Place: Florence, Italy.

ISBN: 978-1-5090-3474-1

4.10. Congress 5

A proposal of energy management strategy on hybrid renewable system with hydrogen backup

F.J. Vivas, A. De las Heras, F. Segura, J.M. Andújar

Presented in:

Event: 7th International Renewable Energy Congress

Organiser: IEEE Power & Energy Society®

Date: 22/03/2016 – 24/03/2016

Place: Hammamet, Tunisia.

Chapter 5

General conclusions

Chapter 5. General conclusions

The experimental research comprising this Thesis has allowed obtaining several major highlights and conclusions that are described hereinafter:

Every day it becomes more evident that there is a need to migrate from a centralized electric model to a distributed model. Distribution systems based on fossil fuels require importing resources and producing pollution. Migration models based on renewable energies will allow generation of a low level of emissions and less dependence on oil.

Attending to the concept of Smart Grid, these systems are closely related to the use of renewable generation systems. Despite the benefits of this technology, its dependence on environmental resources makes it impossible to guarantee the energy balance between generation and demand at all times. For this, the hybridization of systems is shown as a technical and viable solution to solve or mitigate the problems associated with this type of technologies. In the hybridization task, the use of different types of energy storage systems like battery and hydrogen-based system is promising solution. Hydrogen-based storage systems usually faces more stable power imbalances and, consequently, acts as a long-term storage system.

The use of this type of hybrid systems poses a complexity in terms of energy management due to the high number of parameters and factors to be taken into account in order to guarantee optimum energy distribution, depending on the application and the energy status of the system.

In this sense, certain aspects associated with the current operation of the systems, such as the system topology, the need for a battery charge voltage controller, the degradation of the equipment, the hydrogen-based system dynamics, the systems losses associated with the working point, or parameters related to the quality of the electricity supply must be considered.

In order to ensure a proper operation mode of hybrid systems based on renewable energy, guaranteeing demand and increasing system performance, it is necessary to use energy management strategies. This leads to the need of a control system to manage the energy supplied by each source, ensuring safe operation and fulfilling the design objectives. This control system must be based on a proper energy management strategy that guarantees the load supply, increases the lifetime of the elements, reduces the operating costs, and therefore maximizes the system performance, providing a technical and economical feasible solution. According to above, the design criteria of these strategies will determine the behaviour of the whole system, so it is very important to define a proper energy management strategy.

There is a large amount of scientific literature in which different solutions are presented regarding energy management algorithms aimed at controlling this type of systems.

Depending on the type of algorithm used, the different solutions can be included in three clearly differentiated groups; methods based on heuristic techniques, where the use of hysteresis-based strategies prevails; methods based on artificial intelligence; and methods based on optimization algorithms and multiobjective problem solving.

Within the last group, and with high growth in the last decade, the use of model-based predictive controllers (MPC) stands out. The advantages over other types of techniques are clear; it allows the use of multivariable control techniques, allowing solving multiobjective constrained optimization problems, as well as implementing a control strategy based on a prediction horizon, which allows the system to adapt the response of the controller based on future events, improving the system response to merely passive control techniques.

For the design and use of predictive control techniques, it is crucial to have an accurate model of the micro grid that allows having enough knowledge about it to design and analysis the controller. In this sense, the particularity and high complexity of the models widely used in the scientific literature, makes the process of designing controllers oriented to the implementation of management strategies a complicated task.

With the aim of simplifying the modelling task and centralizing design efforts exclusively at the level of supervision and management of the system, this Thesis presents a methodological foundation to obtain a generalized model of the whole micro grid. The modelling methodology used is based on the operating philosophy of an EMS, developing a general formulation based on the operating powers of each device, according to the main parameters of the plant, which allows a sufficient level of abstraction for its generalization and use in any other micro grid with a similar configuration, regardless of technology, or working power range of the equipment used.

The proposed discretized state-space model includes all the necessary parameters for the control of a real plant, including the terms associated with the energy status of the system, battery operating voltage, as well as technical and economic parameters, such as degradation, losses or operating cost, in order to define a system cost function that allows its generality for any type of application or design criteria. This general model extended to all the operating range of the micro grid and guarantees a better approximation with respect to those models mostly used in the scientific literature because those one are linearized systems around a single operating point.

The features of the generalized model obtained from the proposed methodology (model based on the entire operating range of each device and inclusion of the technical and economic parameters) help to define multi-objective optimization problems, as well as serving as a knowledge base in the design and implementation of model-based controllers.

The experimental results on each device and on the complete hydrogen-based micro grid allow validating the correct behaviour of the proposed model under long-term simulations.

Despite the large number of works that explore the use of predictive control techniques for applications similar to the one presented, it is important to emphasize that the vast majority is focused on simulation works, which obviates certain important parameters related to real system management, such as the control of battery charging voltage, necessary to guarantee a safe and efficient operation of the batteries. On the contrary, those experimental works make use of simple, linearized models around a single work point, which has a negative impact on the quality of the model, and therefore on the response of the controller.

Although different works can be found in which the theory of predictive control is applied to hydrogen-based micro grids, most present particularized solutions for the topology and application in question, greatly hindering their dissemination and reproduction in other cases. These works present particular solutions, which focus on the short-term operation of the plant, ignoring certain technical-economic criteria, crucial for the optimization and operation of real plants, both short and long term.

In order to respond to the lack of general solutions based on predictive control applied to renewable sources-based micro grid, this Thesis presents a methodological foundation to design a MPC controller that can be applied to renewable sources-based micro grid with hydrogen as backup. The methodology is universal enough that it can be used independently of the micro grid topology.

The resolution of the multi-objective optimization problem has been carried out through the use of a generalized quadratic cost function, whose weighting factors have been calculated taking into account the role of each device in the micro grid, and technical and economic parameters based on the performance of the real devices, including considerations related to battery charging strategy, system performance, operating degradation or system cost in accordance with the selected topology and application both in the short and long-term.

The intrinsic difficulty in optimizing the multi-objective functions as well the high number of parameters to be optimized make the tuning process a highly complex task. Although there is no mathematical method to calculate the weighting factors, because they depends strongly on the micro grid topology and final application, different cause-effect relationships have been explained and guidelines have been given that facilitate the tuning process.

Similarly, in order to consider the short and long term optimization of the system, limited by the concept of the sliding horizon related to predictive control techniques, additional control techniques are used, which act directly on the process tuning of the controller parameters. In this sense, based on the history of the system, the parameters of the controller are recalculated, if necessary, acting directly on the weighting parameters, in such a way that it allows adapting the dynamic response or energy distribution according to the controller design criteria.

The results obtained in the simulation and practical cases show the validity of the model and tuning methodology of the MPC controller offering a powerful tool to other researchers in the tasks of designing, controlling and managing micro grids with renewable generation and hydrogen as an energy vector.

Chapter 6

Other scientific contributions

CHAPTER 6: OTHER SCIENTIFIC CONTRIBUTIONS

Las ponencias a Congresos, relacionadas más abajo, que forman parte del capítulo 6 "Other scientific contributions" han sido retirados de la tesis debido a restricciones relativas a derechos de autor.

- Ríos, J., Enrique, M., Vivas, F.J., Andújar, J.M.: "Comparative analysis of the efficiency of a classic MPPT system with location of sensors at the output of the converter, compared to the traditional approach of measurements at the output of the generator". En: International Congress on Engineering and Sustainability in the XXI century (Faro, Portugal. 2019).

- J.J. Caparrós, J.J., Vivas, F.J., Segura, F., Andújar, J.M.: "Optimized Balance of Plant for a medium-size PEM electrolyzer. Design, Modelling and Control". En: EUROSIM 2019 (Logroño, Spain. 2019).

- López; E., Sáenz; J., Vivas, F.J., Isorna, F., Ridao, M.A., Bordons, C., Hernández, E., Efes, A.: "Evaluation of fuel cell/battery passive hybrid power systems for unmanned vehicles". En: European Hydrogen Energy Conference (Málaga, Spain. 2019).

- Heras, A. de las, Vivas, F.J., Segura, F., Andújar, J.M.: "In the path of H2020 targets. A new proposal and experimental case to reduce the cost of fuel cells. European Hydrogen Energy Conference (Málaga, Spain. 2019).

- Heras, A. de las, Vivas, F.J., Segura, F., Andújar, J.M.: "Keys for the best selection of the Balance of Plant configuration in a fuel cell system based on a PE stack". En: 21st World Hydrogen Energy Conference (WHEC. Zaragoza, Spain. 2016). ISBN 9781510838352

- Heras, A. de las, Vivas, F.J., Segura, F., Andújar, J.M.: "A review of BoP configurations for PEFCs. Experimental study of a suitable topology". En: 7th International Renewable Energy Congress (Hammamet, Tunisia. 2016)

Chapter 6. Other scientific contributions

6.1. Contribution 1

Evaluation of fuel cell/battery passive hybrid power systems for unmanned vehicles

E. López; J. Sáenz; F. José Vivas; F. Isorna; M. A. Ridao; C. Bordons; E. Hernández; A. Efes

Published in:

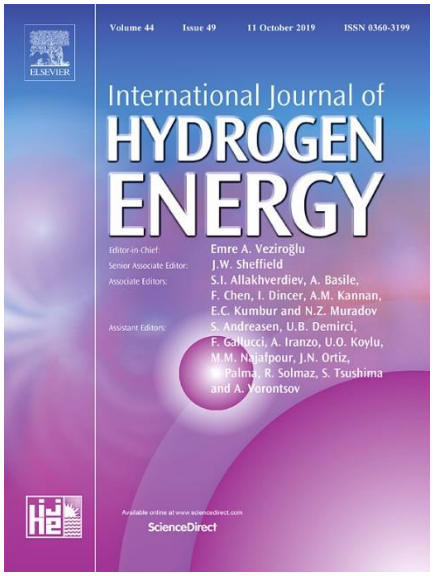

Journal: International Journal of Hydrogen Energy
Editorial: ELSEVIER
Editor-in-Chief: T. Nejat Veziroglu
Reference: Vol. 44, Issue 25, pp. 12772-12782
Year: 2018
ISSN: 0360-3199
DOI 10.1016/j.ijhydene.2018.10.107

Category	Journal Rank / Total journals	Quartile
Energy & Fuels	31 / 103	Q2
Electrochemistry	48 / 148	Q2
Chemistry	8 / 26	Q2
Impact Factor (2018)	4.084	
Citations	3	

INTERNATIONAL JOURNAL OF HYDROGEN ENERGY 44 (2019) 12772–12782

Available online at www.sciencedirect.com

ScienceDirect

journal homepage: www.elsevier.com/locate/he

Experimental evaluation of a passive fuel cell/battery hybrid power system for an unmanned ground vehicle

Eduardo López González [a,*], *Jaime Sáenz Cuesta* [a], *Francisco J. Vivas Fernandez* [a], *Fernando Isorna Llerena* [a], *Miguel A. Ridao Carlini* [b], *Carlos Bordons* [b], *Emili Hernandez* [c], *Alberto Elfes* [c]

[a] *Instituto Nacional de Técnica Aeroespacial (INTA), Ctra. S. Juan-Matalascañas, km. 34, 21130, Mazagón (Huelva), Spain*

[b] *Universidad de Sevilla, Escuela Técnica Superior de Ingeniería, Departamento de Ingeniería de Sistemas y Automática, Camino de los Descubrimientos, s/n, 41092, Sevilla, Spain*

[c] *Commonwealth Scientific and Industrial Research Organization (CSIRO), Data61, Robotics and Autonomous Systems, QCAT, 1 Technology Court, Pullenvale, QLD 4069, Australia*

ARTICLE INFO

Article history:
Received 13 July 2018
Received in revised form
20 September 2018
Accepted 12 October 2018
Available online 22 November 2018

Keywords:
Electrical energy storage
Unmanned vehicles
Fuel cells
Hybrid power systems
Electric propulsion

ABSTRACT

Unmanned vehicles are increasing the performance of monitoring and surveillance in several applications. Endurance is a key issue in these systems, in particular in electric vehicles, powered at present mainly by batteries. Hybrid power systems based on batteries and fuel cells have the potential to achieve high energy density and specific energy, increasing also the life time and safe operating conditions of the power system. The objective of this research is to analyze the performance of a passive hybrid power system, designed and developed to be integrated into an existing Unmanned Ground Vehicle (UGV). The proposed solution is based on six LiPo cells, connected in series, and a 200 W PEM fuel cell stack, directly connected in parallel to the battery without any limitation to its charge. The paper presents the characterization of the system behavior, and shows the main results in terms of performance and energy management.

Introduction to passive hybrid power systems in unmanned vehicles

Unmanned vehicles offer multiple possibilities in industrial, scientific and security applications, due to their ability to provide high quality data in real-time, at a lower cost than other techniques. On-board energy storage is one of the most relevant issues in the design, development and operation of unmanned platforms due to its influence on the performance and capabilities of the vehicle [1,2]. A majority of current unmanned vehicles are powered with internal combustion engines, mainly UAVs and UGVs, but in other applications (e.g. UUVs and microUAVs) electric propulsion is the only available option, which requires suitable energy storage systems to

* *Corresponding author.*
E-mail address: lopezge@inta.es (E. López González).
https://doi.org/10.1016/j.ijhydene.2018.10.107

Nomenclature

BMS	Battery Management System
CSIRO	Commonwealth Scientific and Industrial Research Organization
DC	Direct Current
EMS	Energy Management System
INTA	Spanish National Institute for Aerospace Research
IUFCV	"Improving efficiency and operational range in low-power unmanned vehicles through the use of hybrid fuel-cell power systems" Project
LHV	Lower Heating Value
OCV	Open Circuit Voltage
PEM	Proton Exchange Membrane
SOC	State of Charge
UGV	Unmanned Ground Vehicle
UAV	Unmanned Aerial Vehicle
UUV	Unmanned Underwater Vehicle
USV	Unmanned Surface Vehicle

Abbreviations

E	Energy
I	Current
m	Mass
P	Power
t	Time
V	Voltage

List of indices

batt	Battery
FC	Fuel cell
H_2	Hydrogen
load	Load
diode	Diode

provide high specific energy and power density, to increase life time (number of charging and discharging cycles) and to ensure safe operating conditions, among other requirements. In a similar way to other electric vehicles, most electric unmanned vehicles use lead-acid or Li-ion batteries at present. Despite the rapid progress of these technologies [3] issues remain, and the use of hybrid configurations, combining different energy storage technologies is seen as a promising option to overcome the existing gaps for power systems in electric vehicles [4]. The main advantages of hybrid power systems with respect to battery-based ones are the possibility of achieving higher specific energy while providing redundancy in power supply, which reduces the probability of energy failure, and improves system performance. In the case of power systems based on fuel cells and batteries, several research works have tested and evaluated systems based on both configurations in mobile and stationary applications [5–16].

In general, hybrid power systems are classified in two architectures: active, with control elements (typically using DC/DC converters); and passive, with a direct coupling among the system components. The choice of the most adequate configuration for a given application depends on the vehicles power and energy requirements, weight and volume constraints as well as the characteristics of the fuel cell system and batteries. The active configuration allows a decoupling of sizing and operating conditions on batteries and fuel cell using DC/DC converters, allowing a more precise control of the power system thanks to the control and management of such converters. Their main disadvantages are the more complex system topology, reduced efficiency due to voltage loss, system cost, and higher weight and volume. Passive configurations with direct connections to the DC bus offer the advantages of lower losses, reduced cost and simpler architecture. However, active power control is not possible in this configuration, due to the absence of converters. This could be managed by an external control system, allowing modifications in the operating conditions of the batteries and/or the fuel cell. In consequence, careful design and integration of fuel cells and batteries is required to ensure a similar voltage range operation and proper charging conditions of the batteries from the fuel cell [6,17,18]. Table 1 shows a comparison of active and passive hybrid power systems, with batteries and a fuel cell, summarizing the main advantages and disadvantages for each configuration.

There are also several possible architectures in passive configuration systems, depending on whether the fuel cell is able to charge the batteries without any restriction (Fig. 1a), if there are charging regulation requirements during this process (Fig. 1b), or even if it is not possible to charge the batteries from the fuel cells (Fig. 1c).

Using the configuration depicted in Fig. 1a (direct coupling of fuel cell and batteries) the batteries are the main source to supply power to the load, while the fuel cell supplements the power supplied by the batteries, operating as a "range extender" system. In this operation mode, the fuel cell generates energy when the state of charge (SOC) and the battery voltage reach a predefined minimum value. Once this minimum voltage is reached, the energy generated by the fuel cell is injected into the DC bus that connects the power system to

Table 1 – Comparison between active and passive fuel cell/battery hybrid power system.

	Advantages	Disadvantages
Active configuration	• Decoupling of sizing and operating conditions on batteries and fuel cell • More precise control of the power system	• More complex system topology • Losses in the DC/DC converters • Higher system cost • Higher weight and volume
Passive configuration	• Lower losses • Reduced cost • Simpler architecture, lower risk of failure • Lower weight and volume	• Active power control is not possible. Fuel cell operates at the voltage set by batteries. • Careful design and integration of fuel cell system and batteries to fit the requirements of the load is needed

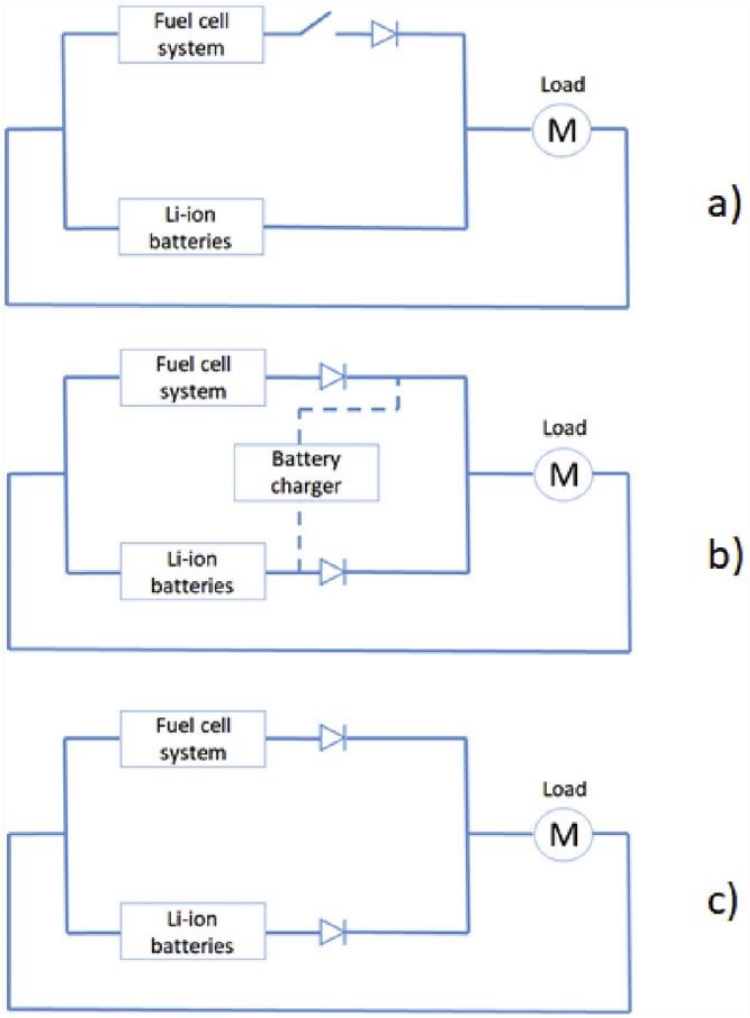

Fig. 1 – Passive hybrid fuel cell/batteries power system configurations.

the electric load. Depending on the energy balance, part of the energy is used to supply the demand while the rest is used to charge the batteries.

In this operation mode, the demanded power load profile largely determines the design of the fuel cell and its nominal power when operating in the battery voltage range. The voltage of the battery sets the fuel cell current, according to its polarization curve. Maximum battery current values, as well as suitable charging/discharging criteria from the safety, performance and durability points of view, have to be taken into account in the design and selection of the right batteries for the system. The passive configuration offers a relatively simple architecture, providing power self-regulation of fuel cells and batteries through appropriate design and selection of both components, at the expense of careful monitoring and supervision of the system in operation.

Taking into account these general characteristics, hybrid power systems based on batteries and fuel cells are considered a suitable option to power unmanned vehicles, mainly to increase the operational range of these platforms. Active and passive hybrid power systems have been already evaluated for unmanned vehicles in several demonstration projects [18–30]. Most of fuel cell/battery power systems demonstrated in small unmanned aerial vehicles correspond to passive configurations, usually according to the scheme depicted in Fig. 1b, with the fuel cell as main power source, and the battery supporting the operation of the fuel cell when the power load is higher than the power supplied by the fuel cell [18,20–24,31–35]. Nevertheless, its application in UGVs has received less attention [36–39].

This paper addresses the use of a passive hybrid power system in a UGV , based on the direct coupling of a fuel cell and Li-ion batteries, without restrictions to the charging of the battery from the fuel cell, with the goal to improve the capabilities and performance of these platforms in real applications. A demonstration of this configuration in an existing

UGV is proposed, and preliminary results, regarding the experimental evaluation of the system on a test bench, are presented and discussed. The main contributions of this research are related to the understanding of the joint performance of fuel cell and batteries in a direct coupling, without charging regulation of the battery, operating under demanding load profiles taken from real data. In this topology, the battery plays a fundamental role as the main power source, acting at the same time as a buffer that minimizes the effect of load variations on the fuel cell, which acts as a "range extender". This configuration and operation mode present an alternative approach to passive hybrid systems for unmanned vehicles, reported in previous experimental works, mainly in small UAVs, where the fuel cell covers the main power demand of the vehicle, being supplemented by batteries at high load [23,24,40].

The first part of the paper offers information about hybrid power systems, introducing the architecture of passive systems based on fuel cells and batteries, and their use in unmanned vehicles. The next section details the development of a passive hybrid fuel cell/battery power system, specifically designed to fulfill the load and endurance requirements of an existing unmanned ground vehicle (UGV), as well as the test and experimental evaluation of the system. The last section exposes the conclusions and future work.

Testing and characterization of passive hybrid systems for unmanned ground vehicles

This research work is developed in the framework of the project "Improving efficiency and operational range in low-power unmanned vehicles through the use of hybrid fuel-cell power systems (IUFCV)" [41,42]. The objective of this project is the increase of the operational range of three existing unmanned vehicles, two UGVs and one UUV, using hybrid power systems based on batteries and fuel cells. These platforms and hybrid power systems will be evaluated in real applications.

Power load profile for the unmanned ground vehicle

The UGVs used in the project are an all-terrain Husky UGV from Clearpath Robotics [43] provided by the Robotics and Autonomous Systems Group at CSIRO, and a Summit XL UGV from Robotnik [44], owned by the Energy Area of INTA. The goal of this project is to increase the endurance on both platforms up to seven hours of continuous usage on field missions, maintaining its core payload, speed capabilities thought the mission execution.

Both platforms will integrate hybrid power systems based on batteries and fuel cell to accomplish these technical targets. The development and testing works presented in the article correspond to the Summit platform. Similar methodology will be applied to the other UGV in the short term. The Summit XL UGV (Fig. 2) is used at INTA for testing multiple power systems configurations and technologies, as well as for integrating sensors and simulate missions defined by different end-users. The main characteristics of this platform, according to the manufacturer, are as follows:

Fig. 2 – Summit XL platform (INTA).

- Weight: 45 kg
- Maximum payload: 20 kg
- Speed: 3 m/s
- Drive system: 4 wheel, 4 brushless motors
- Batteries: 8 × 3.2 V, 15 Ah LiFePO4
- Endurance (nominal/idle): 5/20 hours

Taking into account the limitations of the UGV in terms of available weight and volume, the proposed systems should be as simple as possible in terms of components, trying to achieve the maximum specific energy and energy density with these restrictions, but offering at same time enough warranties to provide the necessary energy and power to fulfill the required missions. Passive hybrid power systems, without DC/DC converters, seem in this case a suitable solution, if designed and sized according to the technical specification of the vehicle. This passive hybrid system is based on open cathode - air cooled Polymer Electrolyte Membrane (PEM) fuel cells, and Li-ion batteries. Compressed hydrogen and metal hydrides will be the hydrogen storage technologies used in the platform. In the first phase, the battery and fuel cell of the hybrid power system designed for the Summit XL UGV were integrated and tested in a test station.

In order to evaluate the performance of the passive hybrid power system under power demand profiles similar to those used by the platforms in real scenarios and missions, the vehicle performed intensive tests under different driving conditions and types of terrain. The power consumption profiles were obtained by measuring the voltage and current in the 8 $LiFePO_4$ batteries connected in series provided by the platform. These driving tests considered the vehicle in: standby mode (idle), smooth driving on flat terrain (with low accelerations and few turns), and more aggressive driving trials on flat terrain with frequent turns and strong accelerations. From the power perspective, the smooth driving is commonly used in autonomous surveillance missions while the aggressive maneuvers are typically required in off-road navigation tasks. The measured load profiles show that the vehicle maximum power peak is around 600 W. Most of the

missions combine different terrain and driving modes. The average power varies from a minimum of around 38 W when the vehicle is in stand-by (idle, with the only consumption of the on-board electronic equipment), to a maximum of 200 W when driving agressively on flat terrain . During these tests in the real conditions required by INTA, combining different driving modes, the real autonomy of the vehicle was around 2 hours, lower than the autonomy specified by the manufacturer in its nominal conditions. Fig. 3 depicts the power curves for smooth and aggressive driving of the vehicle in a flat terrain.

Based on these real profiles, a standard basic mission profile was created, combining the power at stand-by (corresponding to the minimum power consumption of the vehicle), power peaks and several power up and down ramps, representatives of the variations in the vehicle's load profiles analyzed above. This basic profile, covering all these cases and measured variations of the load, has a duration around 300 s. In order to estimate the performance of the system during the targeted operating period (more than 7 hours on the Summit XL), this basic profile was repeated throughout the seven-hours period to create a long-term test profile for the test bench. Fig. 4 illustrates this basic profile.

From this basic load profile, repeated during seven hours, the total energy consumed in this period was calculated, giving a value of around 1 kWh. This is the minimum electrical energy that the power system has to store, in the battery and the hydrogen storage system, and supply to the vehicle.

Development of passive hybrid power system

The passive hybrid power system, designed, developed and evaluated for the Summit XL UGV, integrates an open cathode, metal bipolar plates PEM fuel cell stack, with fan, from the manufacturer BCH, model TH-200. This stack has 30 cells, is air-cooled and able to supply 200 W at 24 V [45] and six 6 KOKAM Ultra High Energy NMC LiPo cells (27 Ah nominal capacity (C), max. charge 27 A (1C), max. discharge 54 A (2C),

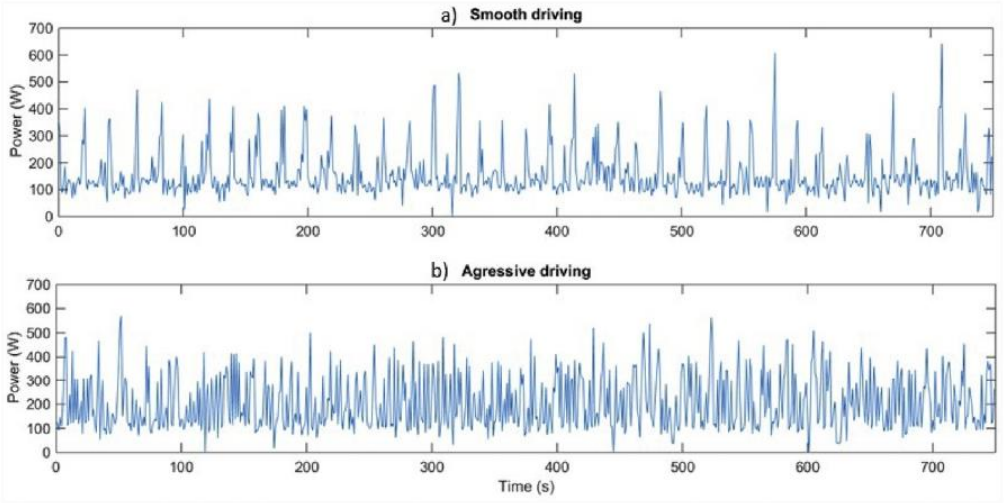

Fig. 3 – Summit XL UGV load profile - Smooth (a) and aggressive driving (b) in flat terrain.

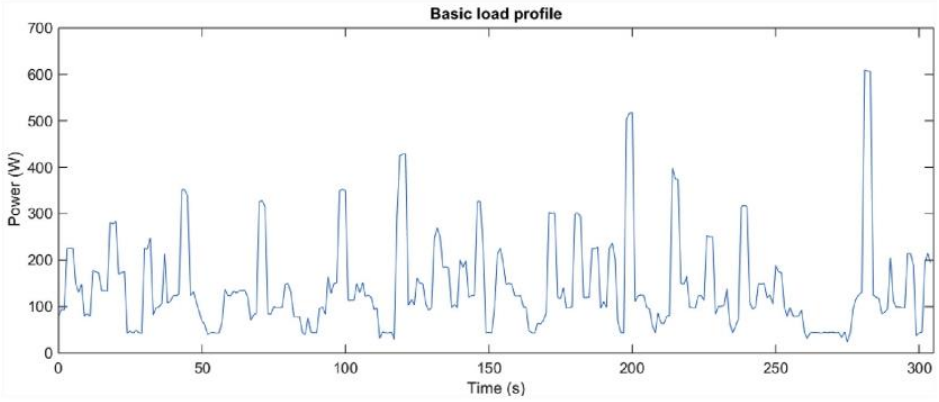

Fig. 4 – Summit XL UGV Basic load profile.

peak discharge 108 A (4C)) connected in series (22.2 V nominal voltage, 25.2 V max. voltage, 16.2 V min. voltage at pack level) [46]. The stack and the batteries, jointly with the hydrogen storage system and a custom developed Energy Management System (EMS), which integrates the functions of a typical Battery Management System (BMS) and the monitoring and control of the fuel cell system, are the main components of the proposed passive power system, which will replace the existing $LiFePO_4$ battery pack in the vehicle. The battery, the fuel cell and the hydrogen storage system were selected and developed to achieve a specific energy higher than 180 Wh/kg and to store at least 1 kWh of electrical energy, equivalent to seven hours of autonomy in the vehicle operating under the basic load profile.

The fuel cell and the batteries were previously tested and characterized in a test bench, in order to obtain the polarization curves (voltage and power vs. current) and the charging-discharging curve respectively (Figs. 5 and 6).

According to Fig. 5, the OCV of the fuel cell is 37.5 V, and the maximum power achieved, at 15.3 A, is 324 W. In these conditions, the fuel cell generates 12.25 A at 24 V, supplying 294 W of power. This value is higher than the nominal values specified by the manufacturer (200 W at 24 V).

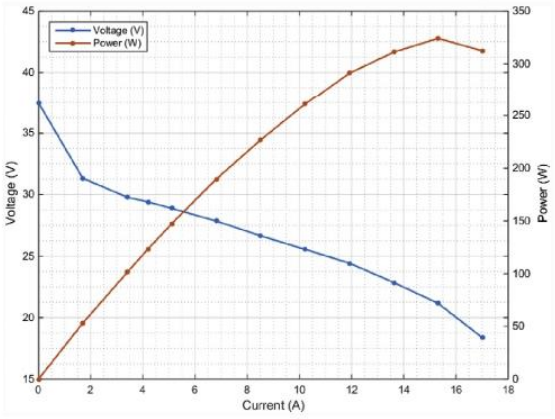

Fig. 5 – Polarization curves of the BCH-T200 fuel cell stack.

Fig. 6 shows the characterization curve of one battery cell, corresponding to a charging step at 5.5 A, up to a maximum voltage of 4.2 V, a discharging step at 2,7 A (0.1 C) until a minimum voltage of 2.7 V, and finally a charging step until the maximum voltage. The measured capacity (C) from this cell and test was 26.91 Ah.

The hybrid system was connected in a direct coupling configuration between the fuel cell stack and the batteries, without limitation to the charge of the batteries from the fuel cell (thanks to the characteristics of the battery in terms of maximum charging/discharging current and capacity) according to the scheme depicted in Fig. 1a. Fig. 7 shows the electric circuit of this passive hybrid power system.

This architecture allows the simplest passive system, avoiding the use of battery charger or similar device. In this configuration, power sharing between battery and fuel cell depends only on the battery voltage (and SOC). The tests were performed in an ARBIN BT-ML 60 V-100 A battery test station [47], programmed to repeat the basic load profile shown in Fig. 4 in a cyclic mode, at least during seven hours. In a first phase, the fuel cell (fan and purges) was managed with a control board supplied by the manufacturer jointly with the stack. Other data from batteries and fuel cell were measured and acquired in a suitable SCADA included in the experimental set-up, as well as in the battery test station, which were also programmed to ensure the operation of the batteries in the voltage range specified by the manufacturer. Fig. 8 depicts this experimental set-up.

Testing of passive hybrid power system for summit XL

Fig. 9 shows voltage and current of the fuel cell/battery power system during the +7 htest.

Fig. 9 illustrates the operation associated to Fig. 1a in section Introduction to passive hybrid power systems in unmanned vehicles. Three clearly-defined steps are observed in the figure:

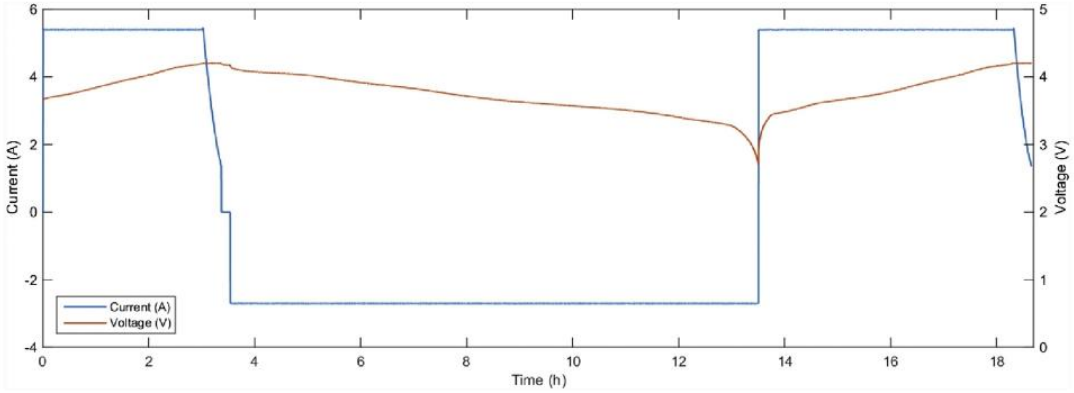

Fig. 6 – Characterization curve of a KOKAM Ultra High Energy NMC cell.

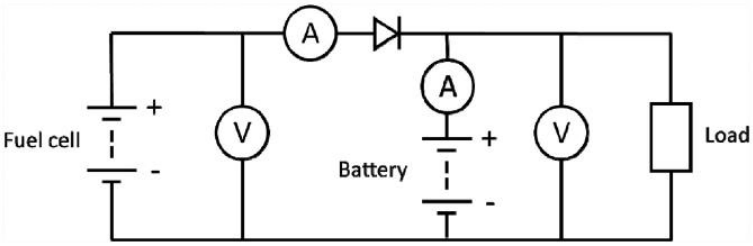

Fig. 7 – Electric circuit of the passive hybrid power system.

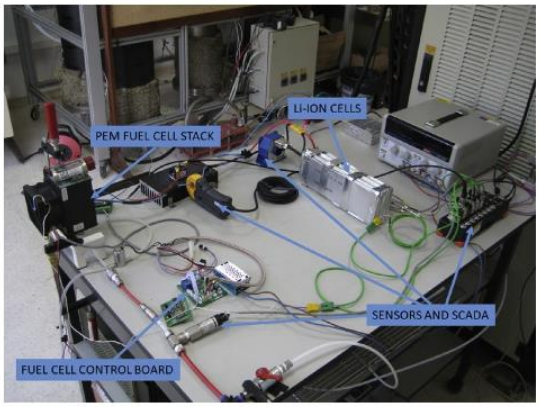

Fig. 8 – Experimental set-up of the passive hybrid fuel cell/battery power system.

a) Step 1

At the beginning of the operation, the load is initially powered only from the battery. In these conditions:

$$\begin{aligned} &V_{load} = V_{batt} \\ &I_{load} = I_{batt} \\ &P_{load} = P_{batt} \\ &E_{batt.1} = \int_{t_o}^{t_1} P_{batt} \cdot dt = E_{load.1} \end{aligned} \quad (1)$$

This step had a duration of 2.45 hours, from t_0 to t_1, and it finished when the battery achieved a predefined minimum voltage of 21.5 V.

b) Step 2

The fuel cell operated jointly with the battery, powering the load and charging the battery. This step started at t_1, when the battery achieved the minimum voltage threshold mentioned above, set to ensure a safe operation of the fuel cell, according to the manufacturer's specifications. In these conditions:

$$V_{load} = V_{batt} = V_{FC} - V_{diode}$$

$$\text{If } P_{load} < P_{FC}, I_{load} = I_{FC} - I_{batt}, P_{load} = P_{FC} - P_{batt} \quad (2)$$

$$\text{If } P_{load} > P_{FC}, I_{load} = I_{FC} + I_{batt}, P_{load} = P_{FC} + P_{batt}$$

$$\text{In general, } E_{FC.2} = E_{load.2} \pm E_{batt.2}$$

where:

$$E_{FC.2} = \int_{t_1}^{t_2} P_{FC} \cdot dt$$

$$E_{batt.2} = \int_{t_1}^{t_2} P_{batt} \cdot dt$$

From t_1, the fuel cell voltage was the sum of the battery voltage plus the diode voltage (approximately a constant value of 0.82 V in this range of operation). The fuel cell operated until the battery voltage achieved a predefined value, 24.5 V in this test, which assured a high SOC of the battery. This voltage

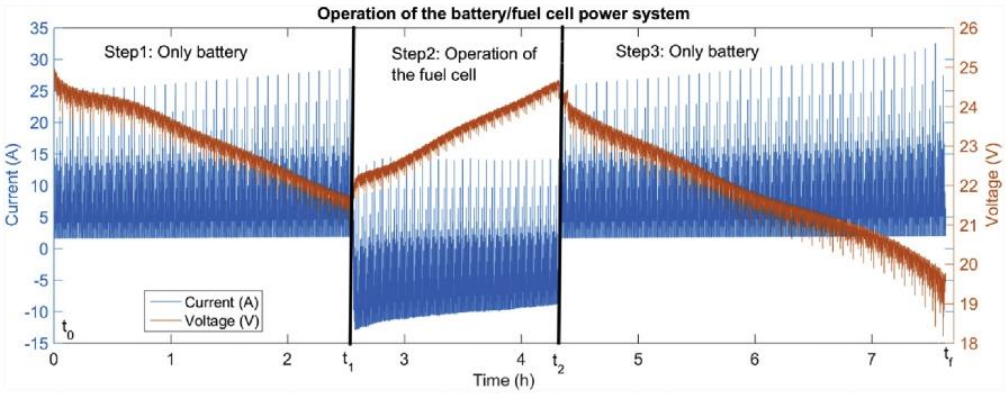

Fig. 9 – Operation of the battery/fuel cell power system for Summit XL UGV.

value was also set considering the hydrogen available in the storage system and the energy provided by the fuel cell, taking into account the minimum energy needed for seven hours of operation of the vehicle under the basic load profile. This step lasted 2.08 hours, from t_1 to t_2.

c) Step 3

Once the battery is recharged to the voltage achieved at t_2 it assumes all the vehicle power load until the voltage drops around 18 V, at t_f. This value was still far from the minimum voltage of the battery pack (16.2 V), but was considered a conservative limit to avoid the total discharge of battery in these first tests, as well as to operate in the voltage range of the on-board DC/DC converters of the Summit platform, used to power its internal electronic systems. As such, not all the available energy in the battery was consumed in the experiment. The operating conditions of the power system are the same as detailed in Eq. (1), with:

$$E_{batt,3} = \int_{t_2}^{t_f} P_{batt} \cdot dt = E_{load,3} \quad (3)$$

The duration of this step, from t_2 to t_f, was 3.1 hours.

The total duration of the test was 7.6 hours, corresponding to 2.08 hours of the joint operation of the fuel cell and the battery, and 5.55 hours to the operation only with the battery. Fig. 10 depicts in detail the evolution of voltages and currents in the operation period of the fuel cell.

Battery and fuel cell voltage curves have a similar shape, being the difference the voltage drop at the diode, with a constant increase as the LiPo cells are recharged and their voltage increases. In this voltage range, the average power of the fuel cell (291.8 W) was greater than the average power load (153.2 W). Consequently, the energy generated in the fuel cell was enough to power the UGV and recharge the battery simultaneously when the fuel cell power was higher than the load. Because of this, the battery current curves show positive values when it is charged and negative when is discharged. The current of the fuel cell remained always positive, while the current from/to the battery changed rapidly, from negative (charging) to positive (discharging) values, depending on the demand profile of the vehicle. The fuel cell current decreased smoothly as the battery voltage increased and the battery was charged. The battery buffered all the demand variations, supplying energy when the requested power exceeded the power generated by the fuel cell, or when being charged because of an energy excess generated by the fuel cell respect to the demanded power. The maximum battery current reached in this charging process was 12.7 A. The charging rate for the 27Ah battery was less than 0.5 C, according to the manufacturer's requirements for safe battery charging. Similarly, the maximum battery discharging current during this period was 14.7 A, which is slightly higher than 0.5 C, and much lower than the maximum discharge current specifications (54 A for continuous discharge and 108 A for peak discharge). The fuel cell current variation was almost linear, from a maximum value of 14.7 A at the beginning of its operation to a minimum value of 10.4 A at its end. The fuel cell voltage values agree with the expected ones, according to the polarization curve (Fig. 5).

In terms of power, Fig. 11 shows the power provided by the battery and the fuel cell, as well as the total power demanded by the vehicle. The total power corresponds to the pattern load profile previously explained. The basic load profile is highlighted in the total power curve, and corresponds to the profile depicted in Fig. 4. Most of the battery power corresponds to the charging process, with a maximum of 282 W. The battery power also presents discharge peaks around 300 W, with a maximum of 341 W. These peaks were generated by the vehicle power demand, and its maximum reaches 610 W. Since the fuel cell power varied almost linearly from 336 W at the beginning of the operation to 264 W at the end, all the additional power, around 50% during these discharge peaks, was supplied by the battery. The contribution of the battery to the total power allowed to the hybrid fuel cell/battery system to provide higher power density than power systems based exclusively on fuel cells [40].

In terms of energy, taking into account the three steps previously defined, the total energy supplied to the system would be:

$$E_{load} = E_{load,1} + E_{load,2} + E_{load,3} \quad (4)$$

Total energy consumption in the 7.6 hours test (E_{load}) was 1065 Wh. During the fuel cell and battery joint operation period, the total energy produced in the fuel cell (E_{FC}) was 608.4 Wh, with a measured hydrogen consumption of 47.1 g. 51% of this energy (308.03 Wh) was used to charge the batteries, and the remaining 49% (300.35 Wh) was used in the energy demand of the vehicle. During this period, the battery

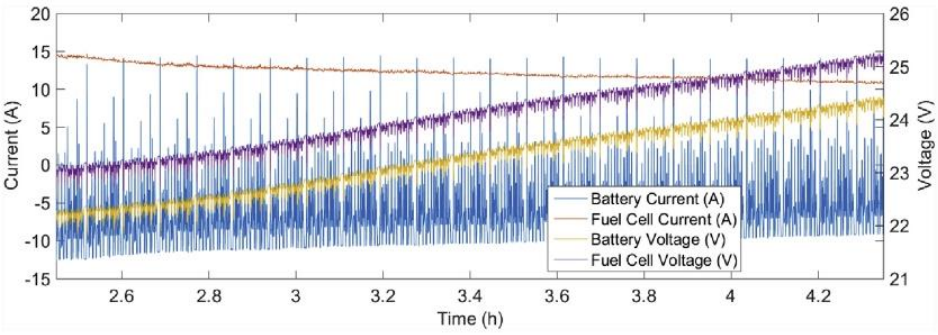

Fig. 10 – Voltage and current evolution.

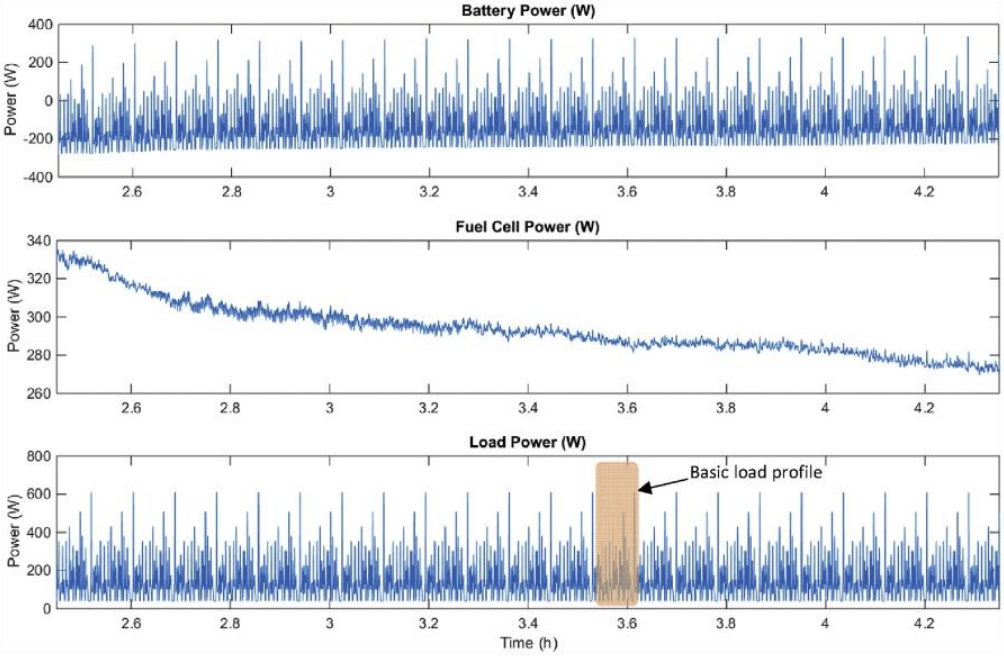

Fig. 11 – Battery, fuel cell and load power.

had an energy output of 18.84 Wh when discharging, mainly due to the peaks in the vehicle load.

The energy supplied by the fuel cell to the battery was in the same order of the energy provided by the battery to the vehicle prior to the operation of the fuel cell (around 327 Wh). Consequently, the battery SOC at the end of fuel cell's operation was almost the same as the SOC at the beginning of the long term test (t_0), when the battery was fully charged. The average fuel cell efficiency over the operating period was calculated as shown in Eq. (5):

$$\eta = \frac{E_{FC}}{E_{H_2}} \tag{5}$$

E_{H2} is the energy content of the hydrogen consumption, and it is calculated as shown in Eq. (6):

$$E_{H_2} = m_{H_2} \cdot LHV_{H_2} \tag{6}$$

E_{FC} was the energy generated by the fuel cell (608.4 Wh), m_{H2} the mass of hydrogen consumed during the test (47.1 g) and LHV_{H2} the lower heating value of hydrogen (120.1 MJ/kg or 33.3 Wh/g). With these values, the average fuel cell efficiency was 39%. A more adequate selection of the operating voltage range in fuel cell and battery could achieve higher efficiency when adjusting the fuel cell voltage range around the maximum efficiency point.

Conclusions and future work

This paper has analyzed the main characteristics of hybrid power systems based on batteries and fuel cells using a passive architecture. After considering different passive configurations, a direct coupling between fuel cell and batteries showed to be most suitable for the considered application because of its simplicity, in terms of components, and flexibility, in terms of operation.

The proposed solution is based on six LiPo cells, connected in series, and a 200 W PEM fuel cell stack, directly connected in parallel to the battery without any limitation to its charge. In a first version, the system was monitored and managed with a control board of the fuel cell stack and a suitable SCADA developed for the tests. A specific Energy Monitoring and management System (EMS) is being developed, and it will be integrated in further versions of the systems. The hybrid power system was tested under a pattern load profile obtained from power consumption data in different real missions of one of these UGVs. The duration of the whole test (7.6 hours) was greater than the minimum period targeted in the project to operate the vehicle (7 hours), and notably greater than the autonomy provided by the original batteries of the vehicle in missions with similar load profile (around 2 hours). The results showed good performance of the fuel cell and the battery during the tests of the hybrid system, which operated the fuel cell when the battery reached a low voltage threshold, around the two hour mark of continuous operation. During the operation, around 49% of the energy produced by the fuel cell was used by the vehicle, and the remaining 51% recharged the battery. The design of the system allowed to the battery to cover the peaks when the required power was higher than that generated in the fuel cell. Battery charging and discharging currents were around 13–14 A (i.e., around 0.5 C), fulfilling the specifications of the manufacturer. In these conditions, the voltage of the fuel cell was set by the voltage at the DC bus; the fuel cell current, voltage and power presented

a smooth variation from the maximum values at the beginning of its operation to the end, which resulted in greater durability of the power system. The average fuel cell efficiency achieved in the tests was 39%.

It is important to highlight that, to guarantee a suitable joint operation of the fuel cell and the battery, careful design, selection and development of both components is required. Based on the experimental data, the next step will be focused on voltage range optimization, which will increase the efficiency and durability of the whole system, as well as minimize fuel cell degradation. Further steps will include integration in the hybrid power system of the hydrogen storage system and the energy management system (EMS). In a first estimation, considering a 3 l compressed hydrogen type III cylinder, operating at 200 bar, as hydrogen storage, the specific energy in the hybrid power system would be around 200 Wh/kg, achieving the technical target of the project (180 Wh/kg). The definitive power systems installed in the UGV will be evaluated in field test under real operating conditions, in order to assess its advantages/disadvantages, in terms of cost, risk of failure, specific energy and energy density, with other possible technical solutions.

Acknowledgments

The authors would like to acknowledge the NATO Science for Peace and Security Program for partially funding this work through the project "Improving efficiency and operational range in low-power unmanned vehicles through the use of hybrid fuel-cell power systems" (IUFCV), Ref. 985079.

REFERENCES

[1] euRobotic aisbl. European Robotics technology platform, strategic research agenda for robotics in Europe 2014-2020. 2014.
[2] U.S. department of defense unmanned systems roadmap 2007–2032. 2007.
[3] Hannan MA, Hoque MM, Mohamed A, Ayob A. Review of energy storage systems for electric vehicle applications: issues and challenges. Renew Sustain Energy Rev 2017;69:771–89.
[4] Keil P, Hofmann M, Horsche MF, Pichlmaier S, Jossen A, Zimmermann T. Review of system topologies for hybrid electrical energy storage systems. J Energy Storage 2016;8:78–90.
[5] Andreasen SJ, Ashworth L, Menjón Remón IN, Kær SK. Directly connected series coupled HTPEM fuel cell stacks to a Li-ion battery DC bus for a fuel cell electrical vehicle. Int J Hydrogen Energy 2008;33:7137–45.
[6] Bernard J, Hofer M, Hannesen U, Toth A, Tsukada A, Büchi FN, et al. Fuel cell/battery passive hybrid power source for electric powertrains. J Power Sources 2011;196:5867–72.
[7] Serincan MF. Validation of hybridization methodologies of fuel cell backup power systems in real-world telecom applications. Int J Hydrogen Energy 2016;42:19129–40.
[8] Zhang X, Liu L, Dai Y, Lu T. Experimental investigation on the online fuzzy energy management of hybrid fuel cell/battery power system for UAVs. Int J Hydrogen Energy 2018;43(21):10094–103.
[9] Fathabadi H. Combining a proton exchange membrane fuel cell (PEMFC) stack with a Li-ion battery to supply the power needs of a hybrid electric vehicle. Renew Energy 2019;130:714–24.
[10] Wang Y-X, Ou K, Kim Y-B. Modeling and experimental validation of hybrid proton exchange membrane fuel cell/battery system for power management control. Int J Hydrogen Energy 2015;40(35):11713–21.
[11] Wang Y-X, Ou K, Kim Y-B. Power source protection method for hybrid polymer electrolyte membrane fuel cell/lithium-ion battery system. Renew Energy 2017;111:381–91.
[12] Roda V, Carroquino J, Valiño L, Lozano A. Remodeling of a commercial plug-in battery electric vehicle to a hybrid configuration with a PEM fuel cell. Int J Hydrogen Energy 2018;43(35):16959–70.
[13] Hwang JJ, Chang WR. Characteristic study on fuel cell/battery hybrid power system on a light electric vehicle. J Power Sources 2012;207:111–9.
[14] Das HS, Tan CW, Yatim AHM. Fuel cell hybrid electric vehicles: a review on power conditioning units and topologies. Renew Sustain Energy Rev 2017;76:268–91.
[15] Belmonte N, Luetto C, Staulo S, Rizzi P, Baricco M. Case studies of energy storage with fuel cells and batteries for stationary and mobile applications. Challenges 2017;8:9. https://doi.org/10.3390/challe8010009.
[16] Chen Y-S, Lin S-M, Hong B-S. Experimental study on a passive fuel cell/battery hybrid power system. Energies 2013;6:6413–22. https://doi.org/10.3390/en6126413.
[17] Samsun RC, Krupp C, Baltzer S, Gnörich B, Peters R, Stolten D. A battery-fuel cell hybrid auxiliary power unit for trucks: analysis of direct and indirect hybrid configurations. Energy Convers Manag 2016;127:312–23.
[18] Nishizawa A, Kallo J, Garrot O, Weiss-Ungethüm J. Fuel cell Li-ion battery and direct hybridization system for aircraft applications. J Power Sources 2013;222:294–300.
[19] Gross T, Poche A, Ennis K. Beyond demonstration: the role of fuel cells in DoD's energy strategy. LMI; 2011.
[20] Dudek M, Raźniak A, Lis B, Kawalec M, Krauz M, Wójcik T. Power sources involving ~ 300W PEMFC fuel cell stacks cooled by different media. Energy Fuels 2016. E3S Web of Conferences 14, 01042 (2017).
[21] Gong A, Palmer JL, Brian G, Harvey JR, Verstraete D. Performance of a hybrid, fuel-cell-based power system during simulated small unmanned aircraft missions. Int J Hydrogen Energy 2016;41:1141–11426.
[22] Renau J, Sanchez F, Lozano A, Barroso J, Barreras F. Analysis of the performance of a passive hybrid powerplant to power a lightweight unmanned aerial vehicle for a high altitude mission. J Power Sources 2017;356:124–32.
[23] Dudek M, Tomczyk P, Wygonik P, Korkosz M, Bogusz P, Lis B. Hybrid fuel cell-battery system as a main power unit for small unmanned aerial vehicles (UAV). Int J Electrochem Sci June 2013;8(6):8442–63.
[24] Verstraete D, Gong A, Lu DD-C, Palmer JL. Experimental investigation of the role of the battery in the AeroStack hybrid, fuel-cell-based propulsion system for small unmanned aircraft systems. Int J Hydrogen Energy 2015;40(3):1598–606.
[25] Mendez A, Leo TJ, Herreros MA. Current state of technology of fuel cell power systems for autonomous underwater vehicles. Energies 2014;7:4676–93.
[26] González-Espasandín O, Leo TJ, Navarro-Arévalo E. Fuel cells: a real option for unmanned aerial vehicles propulsion. Hindawi Publish Corp Sci World J 2014;2014. Article ID 497642.

[27] Sohn S-I, Oh J-H, Lee Y-S, Park D-H, Oh I-K. Design of a fuel-cell-powered catamaran-type unmanned Surface vehicle. IEEE J Ocean Eng APRIL 2015;40(2):388–96.
[28] Savvaris A, Xie Y, Malandrakis K, Lopez M, Tsourdos A. Development of a fuel cell hybrid-powered unmanned aerial vehicle. In: 24th mediterranean conference on control and automation. MED; 2016.
[29] Swider-Lyons KE, Stroman RO, Gould BD, Rodgers JA, MacKrell J, Schuette M, et al. Hydrogen fuel cells for small unmanned air vehicles. ECS Transac 2014;64(3):963–72.
[30] Gong A, Verstraete D. Fuel cell propulsion in small fixed-wing unmanned aerial vehicles: current status and research needs. Int J Hydrogen Energy 2017;42:21311–33.
[31] Lee B, Park P, Kim C, Yang S, Ahn S. Power managements of a hybrid electric propulsion system for UAVs. J Mech Sci Technol 2012;26(8):2291–9.
[32] Donateo T, Ficarella A, Spedicato L. Fuel cell based-on powertrain to hybridize small unmanned aerial vehicles. In: European Fuel Cell Technology & Applications Conference; 2017.
[33] Lapeña-Rey N, Blanco JA, Ferreyra E, Lemus JL, Pereira S, Serrot E. A fuel cell powered unmanned aerial vehicle for low altitude surveillance missions. Int J Hydrogen Energy 2017;42:6926–40.
[34] Verstraete D, Lehmkuehler K, Gong A, Harvey JR, Brian G, Palmer JL. Characterisation of a hybrid, fuel-cell-based propulsion system for small unmanned aircraft. J Power Sources 2014;250:204–11.
[35] Kim T, Kwon S. Design and development of a fuel cell-powered small unmanned aircraft. Int J Hydrogen Energy 2012;37:615–22.
[36] Protonex powers UGV for record mission duration. Fuel Cell Bull June 2009;2009(6):3.
[37] Baldic J, Osenar P, Lauder N, Launie P. Fuel cell systems for long duration electric UAVs and UGVs, Proceedings SPIE Defense, Security, and Sensing. 2010. Orlando, Florida, United States.
[38] Broderick JA, Tilbury DM, Atkins EM. Control of a lead-acid battery/fuel cell hybrid power system for a UGV: experimental report, Automotive Research Center. University of Michigan, Tech. Rep.; 2014.
[39] Bugár M, Ferencey V. Control management system of the hybrid - electric power sources simulation for unmanned ground vehicle, 2016. Levoca: Cybernetics & Informatics (K&I); 2016. p. 1–6. https://doi.org/10.1109/CYBERI.2016.7438631.
[40] Gong A, Verstraete D. Role of battery in a hybrid electrical fuel cell UAV propulsion system. In: 52nd Aerospace Sciences Meeting. AIAA SciTech; 2014.
[41] http://iufcv.com/objectives/. [Accessed in November, 2018].
[42] López E, Isorna F, Ridao MA, Bordons C, Elfes A, Hernández E. Proyecto IUFCV: incremento de la autonomía en vehículos no tripulados mediante el uso de sistemas híbridos de potencia con pila de combustible. Boletín de Observación Tecnológica en Defensa nº 2017;53. 1.er trimestre.
[43] https://www.clearpathrobotics.com/husky-unmanned-ground-vehicle-robot/. [Accessed in November, 2018].
[44] https://www.robotnik.eu/mobile-robots/summit-xl/. [Accessed in November, 2018].
[45] http://www.bchpower.com/en/QingNengDianDui_v109.html#. [Accessed in November, 2018].
[46] http://kokam.com/cell/. [Accessed in November, 2018].
[47] https://www.arbin.com/products/battery-testing/module-testing/. [Accessed in November, 2018].

6.2. Contribution 2

From the cell to the stack. A chronological walk through the techniques to manufacture the PEFCs core

A. De las Heras, F.J. Vivas, F. Segura, J.M. Andújar

Published in:

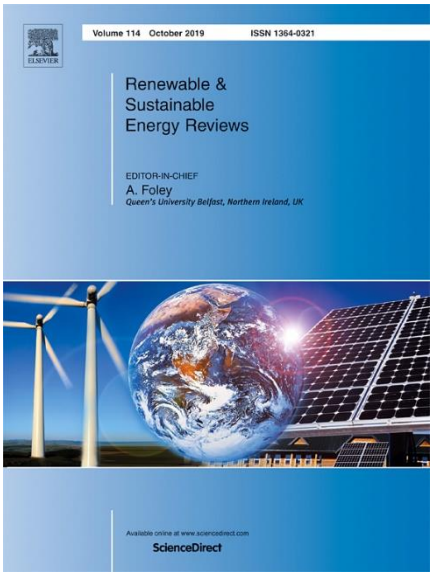

Journal: Renewable and Sustainable Energy Reviews
Editorial: ELSEVIER
Editor-in-Chief: Aoife M. Foley
Reference: Vol. 96, Part 1, pp. 29-45
Year: 2018
ISSN: 1364-0321
DOI 10.1016/j.rser.2018.07.036

Category	Journal Rank / Total journals	Quartile
Energy & Fuels	7 / 103	Q1
Green & sustainability science & technology	1 / 35	Q1
Impact Factor (2018)	10.556	
Citations	3	

Renewable and Sustainable Energy Reviews 96 (2018) 29–45

Contents lists available at ScienceDirect

Renewable and Sustainable Energy Reviews

journal homepage: www.elsevier.com/locate/rser

From the cell to the stack. A chronological walk through the techniques to manufacture the PEFCs core

A. De las Heras*, F.J. Vivas, F. Segura, J.M. Andújar

Grupo de Investigación de Control y Robótica TEP-192, Departamento de Ingeniería Electrónica, de Sistemas Informáticos y Automática, Escuela Técnica Superior de Ingeniería, Universidad de Huelva, Spain

ARTICLE INFO

Keywords:
Polymer electrolyte fuel cell
Catalyst deposition processes
Bipolar plates manufacturing processes
Manufacturing method review

ABSTRACT

In the recent decades, researchers have been focussing more and more on renewable energy because of the known climate crisis that will occur in the near future. One possible solution is the use of fuel cells that generate clean energy. Regarding fuel cell technologies, polymer electrolyte fuel cells (PEFCs) are widely used for portable, stationary or automotive applications as well as backup systems for emergency situations. To build a full PEFC stack, a single cell is used, which is then stacked with more similar cells (the number of cells depends on the electrical power required) and are then integrated into the final product. In a cell, there are two parts that deserve special attention: membrane electrode assembly (MEA) and bipolar plates (BPs). This paper is dedicated to carry out detailed review of processes involved in these two parts, describing the catalyst deposition techniques and BPs manufacturing methods. Finally, a discussion of how to assemble the cells to build a stack of suitable power is included. The review shows the different techniques in chronological order to be able to understand where the fuel cells technology started, and all of the new developments that have been made over time. Each of the techniques has been studied separately in order to provide a comprehensive analysis of the various possible methods found in the scientific literature. After a description and analysis of each technique, a comparative evaluation has been carried out to highlight the most important characteristics of each technique. The review also shows that for fuel cells manufacturing technology to achieve good rates of accuracy, mass production and homogeneity, research should be aimed at achieving less restrictive manufacturing and environmental conditions, and equipment is required with lower costs.

1. Introduction

In the last decade, research is focused on renewable energy, especially owing to the concerns of society about the environmental problems [1]. An attempt is being made to replace conventional energy sources with renewable energy sources (RES) to avoid damaging the environment [2]. Lately, RES (which include biomass, hydropower, geothermal, solar, wind and marine energy) are receiving more attention and currently provide up to 14% of the total world energy demand [3]. The main drawbacks of these energy sources are the energy cost and the low production of energy due to the specific environmental milieus for each geographic location [4] and not all types of RES are available in all locations [5]. Therefore, fuel cells technology might solve some of the drawbacks because their electrical production does not depend on the environmental conditions or location and the only requirement is to have available hydrogen.

Nowadays, with respect to fuel cells, many technologies are being developed for different applications. For example, Alkaline Fuel Cell (AFC) technology is only used for space applications as a result of the electrolyte poisoning with CO_2 [6]. The phosphoric acid fuel cell (PAFC) technology is suitable to the stationary cogeneration market [6,7]. Its disadvantages are the high operating temperature and the need for long warm-up periods [8]. The solid oxide fuel cell (SOFC) and molten carbonate fuel cell (MCFC) technologies [9] are suitable to large-scale MW grid applications in spite of their technical inconveniences such as: the electrolyte control, a limited lifespan of the cell due to corrosion, high sensibility to sulphur, electrolyte losses and high costs [10]. The direct methanol fuel cell (DMFC) technology is being considered for portable power generators [11], although one of the major concern is to improve the catalyst performance [12]. Lastly, the polymer electrolyte fuel cell (PEFC) technology is probably receiving the most attention. This is due to its good properties such as high power density, low operating temperature, zero emissions, easy operation, simplified design and relatively quick start-up and shut-down

* Corresponding author.
E-mail address: ainhoa.delasherasjimenez@gmail.com (A. De las Heras).

https://doi.org/10.1016/j.rser.2018.07.036
Received 21 December 2016; Received in revised form 17 July 2018; Accepted 20 July 2018

Nomenclature

AC-PEFC	air-cooled polymer electrolyte fuel cell
AFC	alkaline fuel fell
BoP	balance of plant
BP	bipolar plate
CCM	catalyst coated membrane
CCS	catalyst coated substrate
CL	catalyst layer
CNC	computer numerical control
DMFC	direct methanol fuel cell
EDM	electrical discharge machining
GDE	gas diffusion electrode
GDL	gas diffusion layer
IBAD	ion beam assisted deposition
MEA	membrane electrode assembly
MCFC	molten carbonate fuel cell
MW	megawatts
PAFC	phosphoric acid fuel cell
PE	polymer electrolyte
PEFC	polymer electrolyte fuel cell
PEM	polymer electrolyte membrane
Pd	palladium
Pt	platinum
PVD	physical vapour deposition
R&D	research and development
RES	renewable energy sources
SOFC	solid oxide fuel cell
TPB	three-phase boundary

functionality [13,14]. PEFCs are suitable to a wide range of applications including portable, stationary and automotive power delivery [15] as well as in backup systems for emergency situations (e.g. earthquakes, terrorist attacks).

A typical cell of a PEFC system is formed by a sandwiched structure that consists of six main parts (Fig. 1), from the outermost to the innermost: (1) end plate (x2) for providing support to the cells assembly; (2) current collector (x2) for current collection and delivery to load [16]; (3) bipolar plate (BP) (x2) for separating the individual cells, delivering the reactant gases, providing an electrical connection, removing the water by-product, dissipating the reaction heat and carrying the clamping force [17,18]; (4) gasket for avoiding leaks of reaction gases; (5) gas diffusion layer (GDL) (x2) for providing a barrier to liquid water, keeping the catalyst layer (CL) partially hydrated and distributing the gases properly [19]; and finally (6) membrane electrode assembly (MEA) for conducting positive hydrogen ions (protons), but no electrons [10,20,21].

From a single cell with similar structure to that shown in Fig. 1, a stack is built by assembling a determined number of BPs and MEAs, depending on the electrical power required. Regarding the manufacturing of the stack, BPs are the responsible for the 40% of the total stack cost [22] and for around the 80% of the stack weight [23–26]. In the same way, in each cell the MEA requires another 40% of the total stack cost, which is divided into two parts: 96% for the material and 4% for the fabrication process [22]. Therefore, in a PEFC system, the stack is undoubtedly the most expensive, heaviest and largest component. Inside the stack, the process used for the MEAs manufacturing and the technique used for the BP implementation determines the stack's weight, volume and cost (Fig. 2).

The aim of this paper is to carry out a detailed chronological review of manufacturing processes involved in above-cited these two key parts (MEA and BP). Current literature hardly includes summaries of the manufacturing techniques related to PEFCs; and there are hardly any papers that do so in chronological order to showcase the path development these systems have undertaken. Likewise, the study presented in [14] analyses the existing PEFCs manufacturing techniques but it only provides a review of alternatives for MEAs and BPs within the scope of vehicle propulsion. This work leaves out manufacturing techniques for other common applications such as micro-power, stationary or back-up power. In contrast, the review carried out in [27] focuses on a variety of strategies to develop advanced GDLs justifying their role in an effective management of water in PEFCs. Nevertheless, according to Fig. 2a and b, regarding cost and weight, GDL is the least significant part in the PEFC structure. However, a key part in a PEFC structure is the BPs as a whole. In this sense, [24] gives a comprehensive overview of the most common designs for the flow fields, but does not include a review on how to manufacture the full BPs.

With the aim of complementing and completing the reviews done in these cited works, this paper describes the catalyst deposition techniques and BPs manufacturing methods; and it analyses the current and future direction of the R&D activities for reducing the weight and volume of the whole stack. The review is based on the order in which the different techniques have appeared. Each of the techniques has been independently studied to provide a more comprehensive analysis of the alternatives found in the literature. After performing a description and analysis of each technique, a comparative evaluation has been developed to highlight the most important features of each one. The review also shows that several features associated with the MEA or BPs such as precision, mass production and homogeneity require a deeper research focused on guaranteeing less restrictive environmental and operating conditions and cheaper equipment. The review of the state of the art shows the advantages and disadvantages of the different methods involved in the manufacturing process, and it also shows how disadvantages of older manufacturing techniques became challenges for new methods resulting in better commercial products for the market.

Contrary to what happens in most of the review papers that can be found in the scientific literature, the aim of this work is not to describe in depth each of the actual methods that can be used for catalyst deposition, BPs manufacturing or stack assembly. The goal of this work is to give an overview about the different techniques classified according to their nature and what the user has at his disposal to design and manufacture a fuel cell right now.

The rest of this paper is written as follows: Section 2 focuses on the different catalyst deposition methods in a MEA. First deposition techniques (manual techniques like Spraying) lead to others based on pattern transfer like Screen Printing or Decal Transfer. Thanks to the

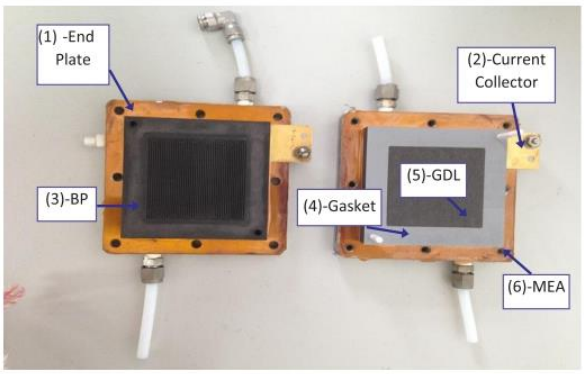

Fig. 1. Single fuel cell with a 50 cm^2 active area from Teledyne™ with three-channel parallel serpentine flow fields (channels of 0.76 mm wide and deep). Graphite bipolar plate's layout is cross-flow with horizontal channels in both anode and cathode.

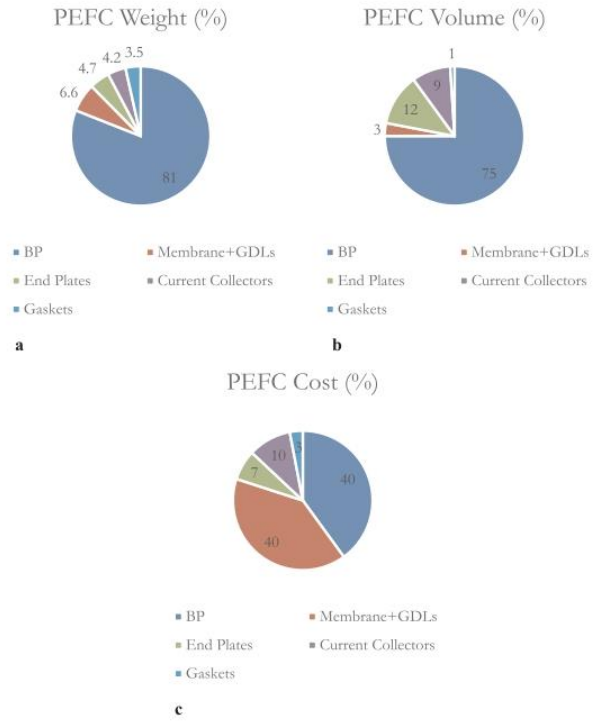

Fig. 2. a. Weight distribution in a PEFC stack. b. Volume distribution in a PEFC stack. c. Cost distribution in a PEFC stack.

technology development, automated process such as doctor blade or electrodeposition allow achieving better cell performance at lower catalyst loadings. Similarly, the most common BPs manufacturing techniques are reviewed in Section 3. As such, the first techniques in which the mould is built under pressure are discussed, followed by techniques based on casting or electro-milling methods. The last step to obtain a fuel cell stack is to assemble a number of single cells built from a (MEA + BPs) structure, as it is shown in Fig. 1. Section 4 reviews the actual assembly techniques showing the main parts of a stack assembly station. Finally, Sections 5 and 6 focus on the discussion of the research work carried out and conclusions, respectively.

2. Catalyst deposition techniques. Old times old techniques, new times new techniques

Regarding other fuel cell technologies described in Section 1, polymer electrolyte (PE) fuel cells have some advantages. They can work at low temperature and they also have other important features such as reduced catalyst loading, bifunctional properties of catalyst based on electrocatalyst alloy, and efficient protons transport using Nafion® membranes. Thanks to these properties, they are going to eclipse other low temperature fuel cell technologies as alkaline and phosphoric fuel cells [28].

In the manufacturing of a PEFC system, the main step is to build the stack that consists of assembling individual cells, one joined to another, convened like slices in a sandwich bread. A scheme of a single PE cell is shown in Fig. 1. The MEA can be considered the core of the cell. This is really important for the whole performance of the PEFC; so many efforts are focused on improving its characteristics and reducing its manufacturing costs (as authors discussed in Section 1, the MEA is one of the most expensive components in the cell and consequently in the stack). A MEA is comprised of GDL, CL and proton exchange membrane (PEM), see Fig. 3. The MEA manufacturing process involves the catalyst deposition supported by platinum (Pt) or Pt alloys [29]. Therefore, the majority of the known techniques for the catalyst deposition seek to reduce the utilisation of Pt to catalyse the oxidation (hydrogen) and reduction (oxygen) reactions, or to substitute the Pt for other less expensive noble metals [30].

According to the scientific literature consulted, a MEA can be manufactured by the following three main methods: (1) catalyst coated membrane (CCM) in which CLs are deposited onto a membrane directly; (2) decal transfer CCM in which coating CL is deposited on a substrate and then transferred onto a membrane; and (3) catalyst coated substrate (CCS) which deposits CL on a GDL. A GDL with CL is called a gas diffusion electrode (GDE). To complete the process, a CCM is sandwiched between two GDEs to obtain the MEA [31]. Regarding these MEA fabrication methods, the most extended methods are CCM and Decal Transfer CCM. Subsequently, this section focuses on reviewing techniques associated to these MEA manufacturing methods [31].

In a MEA, the electrochemical reaction occurs in the CL that needs a three-phase boundary (TPB). In the TPB, the catalyst, the electrolyte and the gas are all in physical contact. The fuel cell performance is affected by the TPB area [32]. In addition, this is mainly dominated by the catalyst deposition method and the properties of the catalyst ink. Therefore, the CL deposition technique and the formula of the catalyst ink are responsible for the fuel cell performance and cost. For mass

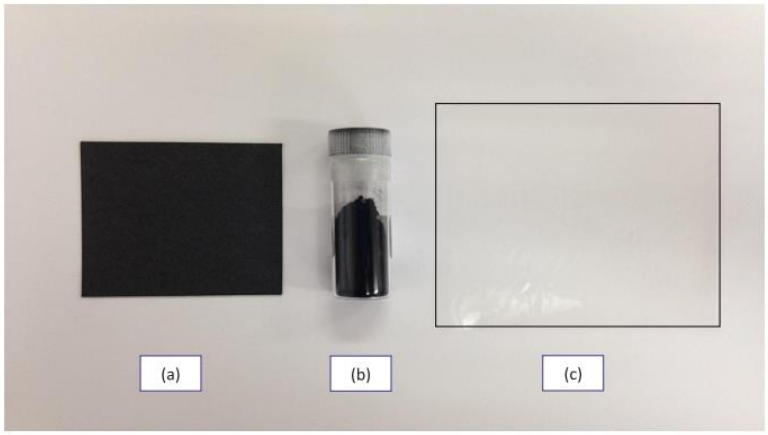

Fig. 3. Images of components needed to manufacture a MEA: (a) GDL, (b) catalyst (Pt) and (c) proton exchange membrane.

production in particular, the catalyst ink costs approximately 34% of the total stack cost [33].

Regardless of the MEA manufacturing method, the first step is to prepare the catalyst ink. It consists of mixing a carbon-supported Pt catalyst, isopropyl alcohol and an ionomer solution in H^+ form [34], and thereafter the catalyst ink is deposited over the CL. One of the objectives is to obtain a MEA with a low Pt content without sacrificing the cell performance. Therefore, it is very important to decrease the Pt catalyst loading to reduce the cost of the anode and cathode electrodes [35].

2.1. The eighties. Hand techniques

Going back to 1950 [36], a material called Teflon (polytetrafluoroethylene or PTFE) became available. It was the first material used in fuel cells with Pt electrodes and acid electrolyte. Along the 1960s and 1970s, high loadings of 4–40 mg cm^{-2} Pt and Pd black catalyst were used to make MEAs [37]. In order to provide ionic transport to the catalyst site, the PTFE-bound CLs are typically impregnated through spraying or brushing. This was a breakthrough in the 1980s, when these deposition techniques were able to reduce the Pt loading of prior PEFCs by a factor of 10: from 4 to 0.4 mg cm^{-2} [38].

When spraying deposition is used in MEA manufacturing (Fig. 4), the prepared ink is deposited on both sides of the membrane (anode and cathode) and then, it is dried at 70 °C prior to be assembled with wet-proofed carbon paper [39]. The required time for the surface drying process depends on the ink, which is sprayed on the membrane, and the temperature depends on the boiling point of the solvent of the solution [40].

Sun et al. [41] use the CCM spraying method to manufacture a MEA. The first step is (1) the membrane treatment that consists of pre-treating the Nafion® (the electrolyte material which replaces the PTFE) with H_2O_2 and H_2SO_4 solutions to eliminate the contaminants (organic and inorganic). The following step is (2) the preparation of the catalyst ink that consists of a solution formed by a commercial Pt/C catalyst powder, isopropyl alcohol and Nafion®. Then, the mixture is sonicated for 1 h. Afterwards, ethylene glycol (EG) is added and the mixture is sonicated for 1 h more. The last step is (3) the preparation of CCMs. The catalyst ink is spread onto one side of the MEA by a spraying gun at 70 °C, over a hot plate, using a set speed and N_2 as the driving gas. After spraying one side of the membrane, it is necessary to dry it at 100 °C for 10 min in air. The other side of the membrane is treated similarly and both sides are dried in a vacuum oven at 100 °C to remove the EG from the membrane.

Otherwise, Kim et al. [34] also use the spraying method to fabricate a MEA without hot pressing and pre-treatments. In this work, the steps proceeded as follows: (1) catalyst inks were prepared by mixing a carbon-supported Pt catalyst, isopropyl alcohol and a Nafion ionomer. Then, (2) the mixture was sonicated for 1 h and, after that, (3) the cover sheet is removed from the membrane. Next, (4) a system is used to spray the catalyst ink onto one side of the membrane while the attached backing film acts as a support. (5) The treated side of the membrane has to be dried for 1 h at 55 °C. Afterwards, (6) the backing film is removed and the other side of the membrane is treated similarly. Finally, (7) the MEA is dried for 8 h under atmospheric conditions without heat treatment. This method is simple and suitable for small-sized MEAs. However, it is unsuitable for ultra-low Pt catalyst loading (< 0.5 mg cm^{-2}) and the deposition uniformity is not easily controlled. [40].

2.2. The nineties. Transfer printing techniques

Alternatively, the CL can be applied using a transfer printing method in which the CL is cast to a PTFE blank. The CL is then decaled onto the membrane. This process is mainly used to manufacture MEAs in an easy way in a research laboratory [42]. In his 1993 patent, Wilson [43] described the thin-film technique for manufacturing CLs in PEFCs with catalyst loadings lower than 0.35 mg cm^{-2}. In this method, the hydrophobic PTFE, traditionally employed to bind the CL, is replaced with hydrophilic perfluorosulfonate ionomer (Nafion).

2.2.1. Screen printing

The screen printing method consists of setting ink across a print matrix to be deposited on the surface [44], see Fig. 5. To sum it up, there are free volumes between the wires in each screen print matrix preparation. The printing ink permeates the free volume and it is fixed at the printing substrate.

Wang et al. [45] suggest a practical application of the method. The first step is to grind the paste with solutions, organic solvents. Next, the paste is put into a small plastic container to be mixed with a high-speed blender; then, the catalyst paste is applied to the membrane with the screen printer. In the scientific literature, most of the works related to the manufacture of MEAs were focused on Solid Oxide Cells [46,47] instead of MEAs for PEFCs.

The screen printing method is simple and effective. The only tool necessary to carry out the technique is a paintbrush, although it presents certain disadvantages. The main one being, it is uneasy to control the uniformity of deposited catalyst ink on the electrode; it depends on the person who uses the materials, while a lot of time is required to complete the process [48].

2.2.2. Decal transfer

The decal transfer method is also called the indirect CCM method that is expected to be suitable to the mass production of MEAs for PEFCs. This method has continuous film processes [49]; CLs are coated on thin-film substrates, transferred to the membrane, and the decal substrates are removed after baking. The problem might be that the heat treatment process can produce structural changes [34].

Decal transfer is effective to fabricate membranes because of its low interfacial resistance. This known method is adequate to scale production and it is based on four main steps: catalyst slurry manufacturing, slurry drying onto a substrate; catalyst layer hot-pressing onto a membrane; and substrate removal. Before the transfer of the catalyst loading, the membrane is treated with a liquid through brushing and the excess of liquid is removed by using a vacuum plate. After this, the following step is to transfer the CL from the substrate to the membrane. The catalyst coated substrate is pressed onto a membrane without liquid treatment at 110 °C and 6 MPa, and the hot-pressing step is at 240 °C, Fig. 6 [50–52].

2.3. Beginnings of the 21st century. Electro-mechanized techniques

Conventional deposition methods, described up to now, have the disadvantage of leaving inactive sites because the catalyst is not distributed uniformly. Remembering that the electrochemical reaction in the fuel cell is limited only by the interface between the PE (e.g., Nafion) and the Pt catalyst exposed to the reactants. For this reason, techniques based on machining and electrodepositions have been suggested by a number of researchers with the main intention of depositing

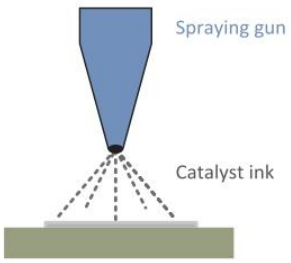

Fig. 4. Schematic diagram of Spraying-applied process.

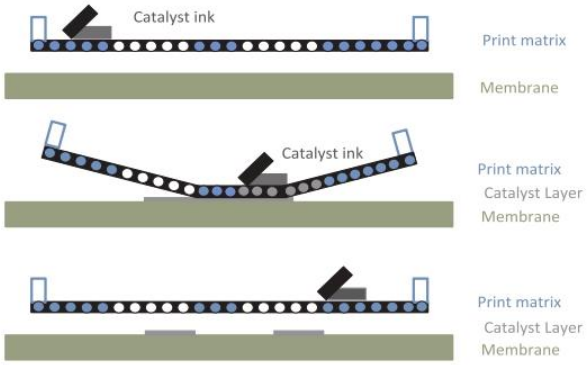

Fig. 5. Schematic diagram of the screen printing process.

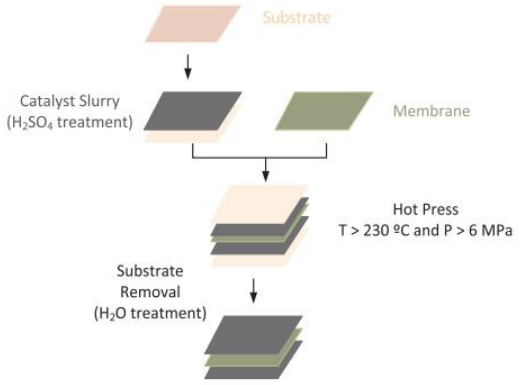

Fig. 6. Schematic diagram of conventional decal transfer method.

small Pt particles at the polymer electrolyte/electrode interface. Pt ions are diffused through the thin Nafion layer and have only electrodeposited at the regions with proper ionic and electronic conductivities.

2.3.1. Sputter deposition

Common vacuum deposition methods include chemical vapour deposition, physical or thermal vapour deposition, and sputtering. Sputtering is commonly employed to form CLs and is known for providing denser layers than the alternative evaporation methods [53].

This technique exhibits a reduction of catalyst loading up to ultra-low levels and a reduction of the cost [54,55]. Alvisi et al. [54] exhibit how Pt films are put on GDE substrates with a commercial RF magnetron sputtering system (SISTEC LS5000). There is a fixed distance between the target and the substrate. The sputtering deposition system is based on a stainless steel in pure Argon.

Natarajan et al. [56] describe the method of sputter deposition to manufacture a PEM in order to improve the performance and catalyst utilisation. In their work, the Pt sputtering target used is a piece of 99.99% Pt foil. The sputtering is carried out under an Argon atmosphere at room temperature with a distance about 55 mm (between the target and electrodes) and a bleeding gas pressure of 0.2 mbar. For a single layer sputtering standard process, the film is deposited for a period of 100 s with a sputter-current of approximately 40 mA. The desired number of layers is reached by repeating the sequence of the process. The catalyst ink consists of a mixture of Pt/C powder and Nafion solution. Then, the following step is to mix and achieve a homogeneous ink that is painted on the GDL to reach the desired Pt loading. Hereafter, the membrane and electrodes require hot pressing to complete the manufacturing. The hot pressing machine requires 130 °C and 1000 psi (Fig. 7).

2.3.2. Doctor blade

In this case, a quantity of the catalyst slurry is deposited on the membrane in front of the blade using a micropipette, and a spreader is used then to spread the catalyst slurry on the membrane. The doctor blade method (Fig. 8) is capable of getting high precision and reproducibility in catalyst loading. This method is more precise and faster than the hand painting processes (screen printing and spraying) and a smooth glass is used to contain the substrate [57]. However, coating the catalysts onto the membrane can be detrimental because the solvents and suspension agents used in the slurry may be absorbed in the membrane. These processing agents may prevent proton transport in the membrane or cause low transport of water through the membrane [58].

2.3.3. Electrospraying deposition

Middelman et al. [59], of Nedstack® fuel cell technology, reported on the development of a CL based on a controlled morphology to enhance performance. Middelman increased the mobility of the CL with high temperatures and chemical additives. Then, an electric field was employed as the driving force to orient the strands.

The electrohydrodynamic atomization of electrospray is a promising method to optimise the Pt loading and it is suitable to electrodes mass production with ultra-low Pt loadings. This technique is based on the atomization of a liquid or suspension subjected to an electric field. It is used to make CLs with high catalyst dispersion. Martin et al. [60] describe the system as follows: the liquid suspension flow rate is controlled inside a capillary tube into the needle by a syringe pump. An electrical potential difference between the needle and the substrate is imposed. The suspension reaches the charged droplets spray, and the electric field helps these charged droplets to get the substrate, while the solvent is evaporated along the flight. During the evaporation, the droplet suffers a Coulomb explosion and breaks up into smaller droplets. Fig. 9 shows a schematic diagram of the process.

Wang et al. [61] show a different process for electrospraying deposition, which comprises a combination of electrospinning and electrospraying process to produce CLs for PEFCs. In this simultaneous process, the Pt/C nanoparticles are deposited by two different needles to get unique nanoparticle/nanofiber electrodes. This combination of processes achieves higher level of control of Pt loading than other electrodes fabrication techniques.

2.3.4. Dual ion-beam assisted deposition (DUAL IBAD)

While the principal aim of all previous alternatives is to improve the charge transfer efficiency at the interface, the dual ion-beam assisted deposition (DUAL IBAD) involves a series of vacuum deposition steps with adequate selection of solvents and carbon blacks.

This technique exhibits some advantages such as good metal efficiency, very low loading of the catalyst based on nanoparticles and low temperature [68].

Dual IBAD consists of the combination between physical vapour deposition (PVD) and ion-beam bombardment. An electron-beam evaporator is used to generate vapour of coating atoms which are deposited on the substrate and ions are accelerated into the growing PVD film at

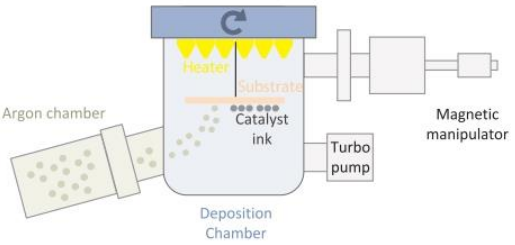

Fig. 7. Schematic diagram of sputter deposition.

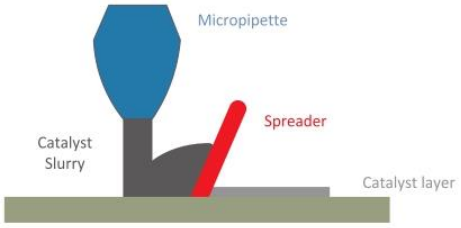

Fig. 8. Schematic diagram of the doctor blade process.

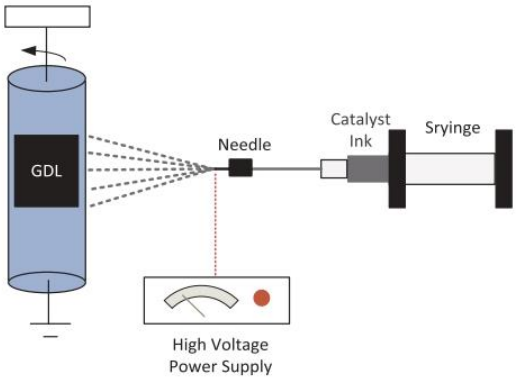

Fig. 9. Schematic diagram of electrospraying deposition.

energies of several hundred to several thousand electron volts (500–2000 eV) [42].

This method requires a relatively lower Pt loading and higher Pt utilisation. Dual IBAD is expected to be an alternative technology to overcome many of the problems of other methods such as electrodeposition and sputter deposition. In this method, the electrode has a significantly different morphology in which low-density Pt deposits are formed by varying depths of penetration into the GDL, exhibiting a gradual change towards increasing crystalline character [69].

2.4. Present. Drop-on-demand technologies

The latest technologies nearly allow deciding the catalyst particle location, with the advantage that these drop-on-demand technologies can deposit the catalyst without contact between the printer head and the substrate. This feature results in high precision values and consequently low Pt loading. Another important attribute of drop-on-demand-based manufacturing is the exceptional reproducibility combined with the unique ability to adapt the manufacturing process to evolving designs or applications. This characteristic may be used to achieve the very low cell failure rates needed to maintain acceptable levels of failure in assembled stacks.

2.4.1. Inkjet printing

Inkjet printers use an electrostatic field to direct the flight of ink droplets [62], and in case of large-scale inkjet printers, they can utilise multiple cartridges capable of holding a variety of solutions (various "colours") for multiple applications or for variations of MEA composition as well as across a specific printed electrode area. The most important parameters are the ink viscosity and surface tension, as well as the particle size. The energy of each printed drop must be sufficient to overcome the viscous flow and surface tension of the ink, yet the viscosity must be low enough to allow the ink reservoir to refill it quickly.

This technique has a good potential to control Pt loading. It is not a conventional process for MEAs manufacturing. Inkjet printing (Fig. 10) is a catalyst application method for PE cells and it has a high precision for controlling the catalyst deposition for ultra-low Pt loadings. Better results are shown in Pt utilisation than the conventional catalyst deposition methods such as screen printing and spray painting [63]. This technique is based on a drop-on-demand printing method. The printed dot is produced from the nozzles of the inkjet printer that ejects ink onto the substrate. Ink ejection speeds are between 5 and 10 m s^{-1} and nozzles are set about 1 mm over the substrate [62]. Towne et al. [62] suggest how to apply this method using a modified printer. In their work, they use the ink cartridges that are cleaned and refilled with the catalyst ink using a syringe. Then, the membrane is put inside a cellulose acetate sheet to be fed through the printer using the paper feed platen. Software is used to control the parameters and less than 1 min is needed to dry the MEA.

2.4.2. Ultrasonic spraying

The main drawbacks of some deposition catalyst methods are: (i) heating, i.e. oxidative treatment is required in order to 'clean' the Pt particles from preparative chemical contamination, (ii) these treatments can greatly affect the surface structure/morphology of the Pt particles, and (iii) the presence of inactive Pt sites for electrochemical reactions at the TPB is often observed [35]. Millington et al. [35] report, for the first time, the use of ultrasonic-spray for the fabrication of PEFC electrodes (GDEs). Five types of GDL were coated with catalyst ink by the ultrasonic-spray method and their performances were compared.

This method has many advantages to fabricate ultra-low Pt loadings MEAs such as precision and controllability. But the main disadvantages are its high cost and that it is unsuitable to high viscosity ink [64]. Su et al. [31] describe the process which consists in putting the catalyst ink in a glass vial and mixes it through an ultrasonic bath. After this, the catalyst ink is ultrasonically sprayed onto the GDL as gas diffusion electrode. With ultrasonic spraying, possible agglomerates in the suspension are broken up resulting in homogenous distribution of the catalyst, resulting in higher efficiency of the fuel cell.

This process consists on mixing the catalyst ink and spraying it onto the GDL ultrasonically using a spray instrument operating at 120 kHz. A sonicated syringe is used (60 kHz) to put inside the catalyst ink previous to atomization in the noodle and sprayed a set flow rate. This step is repeated as many times as necessary to achieve the required Pt catalyst loading. The last step is to dry the fabricated GDEs at 50 °C for 15 min (Fig. 11).

Finally, in order to summarize and order everything analysed thus far, Table 1 shows a chronological classification of catalyst deposition techniques highlighting their main characteristics according to their chronological appearance, noticing some features as well as their

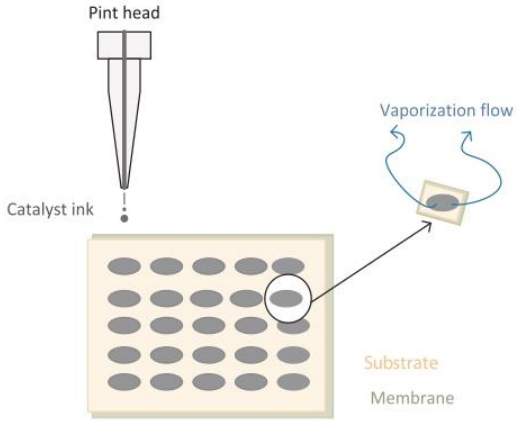

Fig. 10. Schematic diagram of the inkjet printing process.

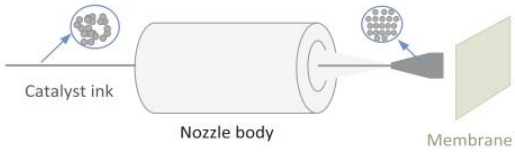

Fig. 11. Schematic diagram of the catalytic-mix formation for ultrasonic spraying deposition.

properties.

3. Bipolar plates manufacturing. Techniques development at the same time that new materials appearance

As we have already commented, MEA and BPs are the basic components of a PEFC [18,71]. Bipolar plates are responsible around 60–80% of the total weight, 30–45% of stack cost [25] and 70–80% of stack volume [26,72] in a typical PEFC stack, Fig. 2.

In spite of recent technical advances, the development and production of PEFC systems are still expensive [73]. The main cost of the fuel cell stack are the electrolyte membrane, the Pt catalyst deposition and the BPP manufacture [25,73,74]. In particular, for BPs depending on the manufacturing technology, their cost is expected to be up to 37%; below 100 €/kW and 15 €/kW for stationary and automotive applications, respectively [73]. The BPs have six basic functions over the fuel cell structure, Fig. 12: (1) separating the individual cells; (2) delivering the reactant gases; (3) providing an electrical connection; (4) removing the water by-product; (5) dissipating the heat of the reaction; and (6) carrying the clamping force [75,76].

For these purposes, BPs should have some characteristics to make them suitable for these functions such as (1) high electrical conductivity ($> 100\,S\,cm^{-1}$), (2) low permeability ($< 2{\cdot}10^{-6}\,cm^3\,(cm^2\,s)^{-1}$), (3) high corrosion resistant ($< 16\,\mu A\,cm^{-2}$), (4) flexural strength (> 59 MPa), (5) tensile strength (> 41 MPa), (6) impact strength ($> 40.5\,J\,m^{-1}$), (7) crush strength (> 4200 kPa), (8) high thermal conductivity ($> 10\,W\,m^{-1}\,K^{-1}$), (9) chemical, electrochemical and thermal stability, (10) low thermal expansion coefficient and (11) inexpensive material and processing costs [17,77,78].

Fig. 12 can identify possible patterns to design the flow channels like straight-parallel (cathode) and multiple serpentine (anode). Other forms include grid-pin or biomimetic designs based on natural flow field like animal lungs or plants xylem [79]. Each design has its own characteristics, for instance: parallel and grid-pin patterns offer many paths from input to output, but the reactant will flow along the path of least resistance. Therefore, in case of channel blockage, such as the formation of water droplets, very common at the cathode side, will worsen the fuel cell performance.

By contrast, designs based on one single flow channel such as serpentine avoid the above commented problem but require high-pressure supply to avoid fluctuations in the current density due to the long flow path. As a solution, designs such as multiple serpentine or biomimetic emerge with the aim of finding a trade-off between advantages and disadvantages.

Additionally, in Fig. 12 making a cross section shape of the BPs, channels can be distinguished with triangular geometry on the cathode side and rectangular geometry on the anode side. This can be justified on the basis of the research work carried out by Akhtar et al. [80], in which they demonstrate that channels with triangular shape accumulate less water and channels with rectangular shape can remove more easily any blockage. This makes triangular and rectangular geometries ideal for the cathode side (electricity and water production) and anode side (the hydrogen must flow from inlet to outlet along the serpentine), respectively.

Apart from the BPs design, the manufacturing process is another issue to take into account. This will depend on the BPs material. Nowadays, BPs can be classified into five categories according to the material used in the manufacturing process: (1) non-porous graphite BPs, (2) coated metallic BPs, (3) polymer-carbon composite BPs [81], (4) carbon-carbon BPs [25] and (5) porous/foam metal BPs [82–84]. Currently, the most extended used are the first three [81]. This is because of the technology to manufacture carbon-carbon BPs is not mature like the few works found in the scientific literature show [85]. In contrast, porous/foam metal BPs are being more investigated recently due to its good properties such as high porosity, controllable permeability, higher specific surface area, capillarity, etc. [86,87].

Non-porous graphite BPs have been traditionally used because of their intrinsic high electrical conductivity, chemical stability [23,71] and thermal stability leading to good corrosion resistance, which is especially important in PEFCs characterised by aggressive operating environment with a pH of 2–3 (remember the anode reaction in the fuel cell: $H_2 \rightarrow H^+ + 2e^-$). This exposure to an acidic environment makes the material properties worse in applications such as stationary, in which more than 40,000 h of reliable operation are required [73]. Moreover, they are brittle, they lack mechanical resistance and need machining in the flow field channels design, which increases the manufacturing costs [23,71].

There are other alternatives to graphite such as coated metallic and polymer-carbon composite BPs. The former incorporates the advantages of metallic materials such as high electric and thermal conductivity, excellent strength and low production cost [23]. However, due to above mentioned corrosive environment in the fuel cell, metallic BPs are protected with coating layers giving rise to their name (coated metallic BPs).

In contrast, the polymer-carbon composite BPs (metal-based and carbon-based) combine porous graphite, polycarbonate plastic and stainless steel for metallic-based, and if carbon-based BPs polycarbonate is replaced by thermoplastic resin. In any case, the polymer-carbon composite BPs try to combine the advantages of the different materials used (graphite, polycarbonate or resin and stainless steel), resulting in an excellent chemical and thermal stability, easy malleability and cost-effective manufacturing process [73,88].

This BPs classification according to the material used in the manufacturing process allows introducing the techniques for the flow field channels design [14]. Then, in non-porous graphite BPs, traditionally the most used material, a conventional technique as compression moulding was initially used. More recently, machined techniques such as CNC milling have made possible the manufacturing of miniature BPs, specifically designed for low and ultra-low power PEFCs applications.

Additionally, when BPs started to be developed using metals (aluminium, stainless steel, titanium or nickel), apart from using conservative techniques such as stamping, other techniques used in metallurgy were incorporated to the BPs manufacturing process (injection moulding, investment casting and UV lithography). In the last years, of course CNC milling has been also used in the design of flow field channels for coated metallic BPs. Apart from the flow field design, the protective coating layer (as above mentioned) is deposited following techniques similar to those used for catalyst deposition that authors have already described in Section 2 (painting, sputtering, vapour deposition, etc.). For porous/foam metal BPs, the methods used are the same that those used for metals BPs such as investment casting, electrodeposition or metal vapour deposition [87]. It is possible to inject gas or gas-releasing blowing agents or to produce super-saturated metal-gas solutions to form pore spaces. A popular method used is to get foam metals from molten metals by making gas bubbles into the liquid to form pore spaces [82].

Bipolar plates, based on polymer-carbon composite, combine with some previous techniques. Stamping is used for the flow field channel design over the stainless steel, while graphite powder and resin (in case of carbon based, and polycarbonate plastic in case of metal-based) are moulded using previously mentioned techniques such as compression or injection. Following, a chronological review about the most common

Table 1
Processes of catalyst deposition ordered chronologically.

Period	Method	Ref.	Pt (mg cm^{-2})	Power (W)	Equipment	Properties
80s	**Spraying** 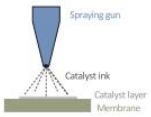	[34,39–41,65]	0.3 mg_{Pt} cm^{-2} (anode) 0.4 mg_{Pt} cm^{-2} (cathode)	430 mW mg_{Pt}^{-1}	Spraying gun	• Unsuitable for ultra-low catalyst loading (< 0.5 mg_{Pt} cm^{-2}) • More ink, longer time to dry • Not easy to control the uniformity • Middle precision • Tolerable for small-sized MEAs • Simple • Effective
90s	**Screen Printing** 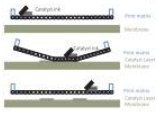	[44–48]	0.4 mg_{Pt} cm^{-2} (cathode) 0.6 mg_{Pt} cm^{-2} (anode)	800 mW mg_{Pt}^{-1}	Paint brush	• Not easy to control the uniformity (depends on the person) • Requires a lot of time • Not suitable for ultra-low catalyst loading (< 0.5 mg_{Pt} cm^{-2}) • Simple • Effective • Tolerable for small-sized MEAs
	Decal Transfer 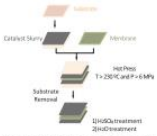	[34,50–52]	0.340–0.420 mg_{Pt} cm^{-2}	1 W mg_{Pt}^{-1}	Decal substrates	• Heat treatment can cause structural changes • Mass production • Low interfacial resistance • Effective
Early 21st century	**Sputter Deposition** 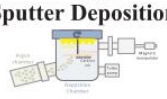	[54–56,66]	0.01–0.16 mg_{Pt} cm^{-2}	85 W mg_{Pt}^{-1}	Magnetron sputtering system	• Strict atmosphere control • Vacuum conditions required • Not easily adaptable to bulk production • Ultra-low catalyst loading • Cost reduction
	Doctor Blade 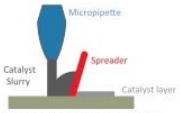	[57,58]	0.125 mg_{Pt} cm^{-2}	5 W mg_{Pt}^{-1}	Micropipette Spreader	• Not for mass production • High precision • Reproducibility • Fast • Efficient • Control of thickness
	Electrospraying deposition 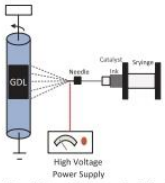	[60,61]	0.052 mg_{Pt} cm^{-2} -0.022 mg_{Pt} cm^{-2}	42 W mg_{Pt}^{-1}	NeedleSyringe pump	• Necessary improve reproducibility and evaluate its capabilities • Ultra-low Pt loading • High catalyst dispersion • Suitable for mass production • No vacuum requirements • Easily scalable to any size • Simple experimental set up
	Dual Ion Beam Assisted Deposition	[67–69]	0.04 – 0.12 mg_{Pt} cm^{-2}	3.862 W mg_{Pt}^{-1}	Electron beam evaporator	• Expensive • Not for mass production • Good efficiency of the metal • Very low loading of the catalyst • Low temperature
Present	**Inkjet Printing** 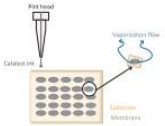	[48,62]	0.020 mg_{Pt} cm^{-2}	16 W mg_{Pt}^{-1}	Inkjet printer	• Expensive • No conventional • High precision • Fast • Mass production
	Ultrasonic Spraying 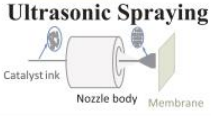	[31,35,64,70]	0.232 mg_{Pt} cm^{-2} (cathode) 0.155 mg_{Pt} cm^{-2} (cathode)	1.69 W mg_{Pt}^{-1} 2.36 W mg_{Pt}^{-1}	Glass vial spray instrument	• High cost • Not suitable for high viscosity ink • Ultra-low Pt loading • Precise • Controllable

techniques used in the BPs manufacturing process is presented. We would like to point that the given date for locating each technique correspond with the date that the technique is formally analysed in the scientific literature in applications related to BPs manufacturing for their further application in PEFCs.

3.1. The seventies. Mould under pressure to obtain the workpiece

As commented in Section 2, fuel cells technology began to be developed along the second half of the twentieth century. In particular, it was driven into the seventies when researchers started to focus their

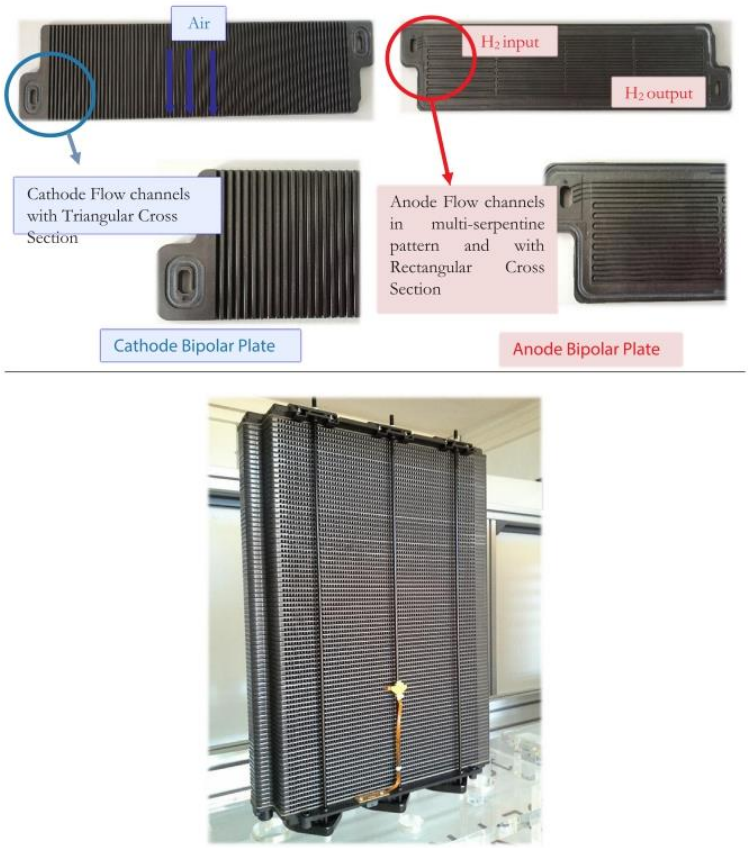

Fig. 12. Cathode bipolar plate (on the left), anode bipolar plate (on the right) and a medium power stack of 3.4 kW from Ballard®.

works on obtaining from the fuel cells their best performance with the lowest catalyst loading over the membrane. At the same time, for the BPs manufacturing processes such as stamping and compression moulding were used.

3.1.1. Stamping moulding

Stamping process is one of the most common production processes to fabricate metallic BPs [89], because of its short processing cycle [90] and inexpensive cost [25]. In this case, two dies (male and female) are needed, which are filled with the chosen material and pressure is applied to the upper die to deform the material plastically in the desired shape [91] (Fig. 13).

Heo et al. [92] show a detailed description of the stamping method that consists of inserting the fabricated preform into a steel mould preheated to 150 °C for 30 s. The stamping process is applied causing the melted phenol resin to infiltrate into the voids of the preform. In this work, the optimal stamping pressure (20 MPa) and the optimal curing time (3 min) are studied. Moreover, this process requires both male and female dies for forming the flow field channels.

3.1.2. Compression moulding

Compression moulding [93] teams with stamping process to be suitable for mass production [94–96]. The difference in this process is that the female die is only needed, which is pressurized with a heated fluid (Fig. 14). Concerning the process conditions, it is important to point out that the micro-channels depth increases with increasing compression pressure. The main advantages of this process for manufacturing BPs are its good surface topology, uniform thickness distribution and tight dimensional tolerance [25].

Jung-Chung et al. [97] present a study in which micro-flow channels with a high aspect ratio are formed by increasing the forming pressure during the process. Nevertheless, this work improves the forming pressure via a novel patented apparatus to enable a two-stage pressure increase in the process; therefore, the working pressure can reach 1000 MPa.

Finally, although these two processes (stamping and compression moulding) are characterised by its simplicity and reduced processing time, they present two main drawbacks in the BPs production: (1) formed defects can appeared such as wrinkle and rupture during the process, and (2) an uniform flow distribution along the channels during PEFC operation is not guaranteed.

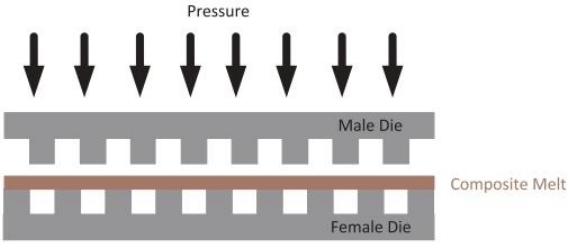

Fig. 13. Stamping scheme for the BPs manufacturing process.

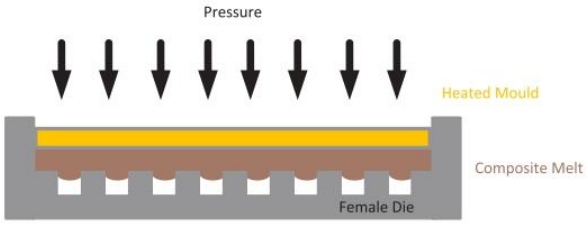

Fig. 14. Compression moulding scheme for BPs manufacturing process.

3.2. The eighties-nineties. Casting methods to fill the mould

When new materials (coated metallic) began to be used for the BPs manufacturing process [98], techniques based on casting were incorporated such as injection moulding and investment casting.

3.2.1. Injection moulding

This process consists in three basic steps (Fig. 15): (1) the molten metal is ladled into the pouring hole of the shoot sleeve; (2) the plunger is moved toward the mould at established speed (v_1) and the vacuum pump starts working, and (3) the plunger is moved slowly ($v_2 < v_1$) to the end of the sleeve ejecting a pressure around 50 MPa. This process is suitable for manufacturing BPs with arbitrarily complicated shapes and mass production is possible because of its short process cycle time (around 30–60 s) and potentially low manufacturing costs [99].

3.2.2. Investment casting

The investment casting process [14] begins with the fabrication of a sacrificial mould, normally ceramic-based with the same basic geometrical shape as the workpiece. Once the mould is finished, it is heated and filled with molten metal, creating the metal casting (Fig. 16). When the casting has cooled sufficiently, the mould shell is chipped away from the solidified workpiece [100,101].

This process is capable of producing pieces with complex shapes [102], but due to the pattern scarify, a new mould is necessary for each BP fabrication cycle. For transforming molten metals into porous/foam metals, a popular method is to make gas bubbles into the liquid to form pore space. An easy way to realise this is to inject gas or to add foaming agents into the melted metals [82,87].

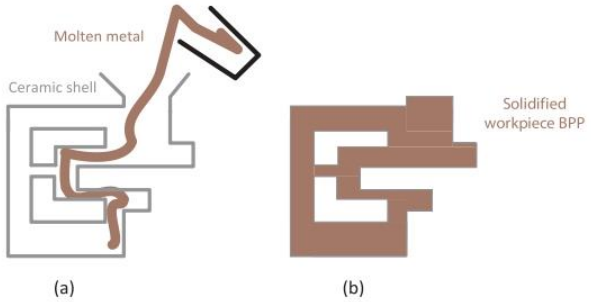

Fig. 16. Investment casting scheme for the BPs manufacturing process: (a) preheated mould and filled with molten metal; and (b) solidified workpiece after chipping away the ceramic shell.

3.3. First steps inward the 21st century. High precission methods for small size plates

It is well known that fuel cells technology is especially suitable for stationary and mobile applications, but for the first half of this century one of the challenges has been to adapt this technology to be used in portable applications as the products of the so-called 3C Industry. For this purpose, it is essential to develop miniature fuel cells that include a stack characterised by its mechanical strength and reduced volume. Then, in basis on their properties, the coated-metallic BPs satisfy these requirements and they may be designed to obtain sheets with 100 μm-thick [72].

3.3.1. Micro-electrical discharge machining (Micro-EDM)

With micro-EDM, the flow field channels are formed by electrical erosion over the conductive material [103]. Applying electrical pulses, electrodes (work and tool piece) take the desired shape and through the supply of a dielectric liquid, both electrodes are insulated and the non-desired material is removed (Fig. 17a). Additionally, due to the tool and workpiece do not contact each other, adverse effects derived from mechanical force and vibrations are minimized.

As it can be deduced, micro-EDM is a point processing technique; thus, among its disadvantages are time consuming and intensive labour. To overcome these drawbacks, we should think in an area-processing technique in which the electrode changes from a rod form to a cuboid (Fig. 17b). This simple innovation receives the name of die-sinking micro-EDM [72] and, in this case, the processing path is a single

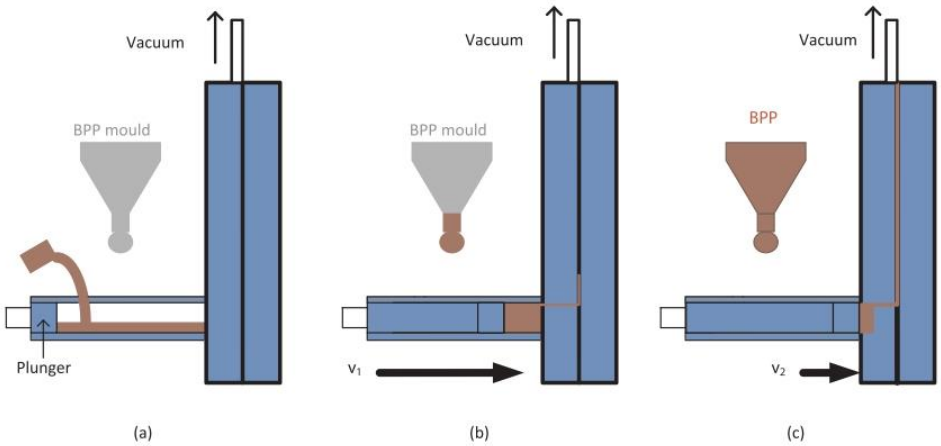

Fig. 15. Injection moulding scheme for the BPs manufacturing process: (a) plunger moving at low speed region; (b) casted material filling the mould; and (c) work piece ready.

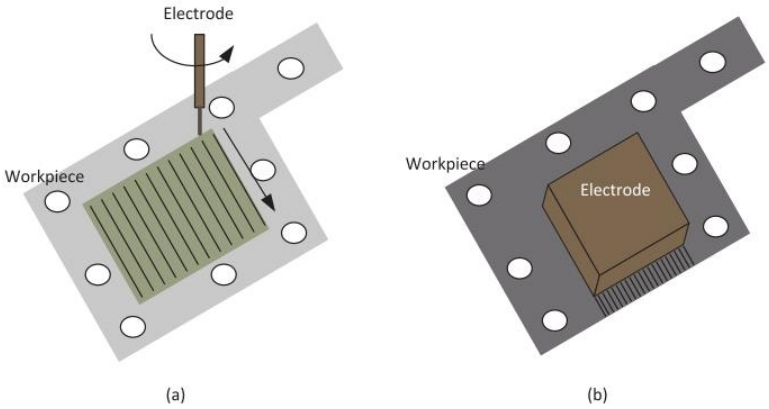

Fig. 17. (a) Micro-EDM scheme and (b) die-sinking micro-EDM.

direction and the flow field channels are formed in one-step, turning the slow micro-EDM technique into a fast process.

3.3.2. UV lithography

Following with the aim of developing miniature fuel cells, another alternative technology is the UV lithography [104]. This technology is suitable to coated-metallic BPs that, because of their strength, the plates coalesce three functions: to distribute the reactant gases as they do the flow field channels; to catch the electrical current as the current collectors do; and to compress the cell assembly as the end plates do. This makes them suitable for designs focused on small fuel cells.

UV lithography is a technology based on a nanoscale metallic deposition process, which can create precise and detailed forms. Over a substrate, normally stainless steel, a photoresist is deposited. The photoresist has been designed with the desired flow field channel shape, and after UV-exposure during 50s, the un-exposed area is etched away leaving photoresist with flow field pattern (Fig. 18).

Finally, as in the previous study of catalyst deposition techniques, Table 2 summarises and sorts chronologically the studied BPs manufacturing techniques, highlighting their main technical characteristics and properties.

4. Stack assembly techniques. The sandwiched structure

Coming back to Fig. 1, at the beginning of the paper, the authors have presented the well-known sandwiched structure of a PE cell made up the MEA and BPs, apart from the other auxiliary elements such as end plates, gaskets and current collectors. Next, a number of cells will be assembled (resulting in the *Stack*) to achieve the voltage and power level required by the final application. In this assembling process, the stack, end plates and the bolts are mounted on a stack assembly station (Fig. 19) to give as result a stack with similar appearance to that shown in Fig. 12.

In this connecting method (tie-rod and bolt), the clamping load plays an important role because the excessive assembly may cause plastic deformation or porosity variation and damage to the GDL. By contrast, poor assembly may result in a high contact electrical resistance at the interface between the GDL and the BP, as well as leakage of water or fuel at the sealed interfaces [110].

Apart from this, even considering a proper clamping load is applied over the whole end plate, some variation in the channels height derived from the BP manufacturing process (Fig. 20) would induce severely uneven contact pressure in different regions of the whole stack. As a result, fuel cell performance is reduced by the dimensional error [111].

Regarding the scientific literature, most of the works focus on studying the effects of various configurations of the bolt and its clamping torque on the PEFC performance on the basis of experiments [20,112,113] and the finite elements theory [114,115]. However, PEFCs assembling methodologies are proposed in very few studies. A sample of them are the following, Lin et al. [110] present a comprehensive methodology to obtain the optimal clamping load for a given PEFC stack. In addition, Qiu et al. [111] propose a feasible and effective methodology for the study of assembly design, calculating the optimal clamping displacement/pressure. In contrast to the variety of catalyst deposition and BPs manufacturing techniques, the stack assembly process can be reduced to that shown in Fig. 19.

5. Discussion

Based on the previously presented data in the process of manufacturing a fuel cell stack, there are two main parts that make up the highest percentage from the point of view of cost, weight and volume. These parts are the MEA because of catalyst deposition and the BPs. This paper presents a review on the most relevant techniques for catalyst deposition in a MEA, and a description of the main methods used in the manufacturing of BPs. This review has been presented in chronological order to aid in the understanding of the solutions that have come forth to face this scientific challenge (Fig. 21).

The catalyst deposition techniques, the most conventional process, which dates back to the 1980s is spraying, characterised by its simplicity and effectiveness. However, it is difficult to control the uniformity of the deposition because it depends on the person performing the deposition, rather than on a machine. Therefore, it is not suitable for ultra-low catalyst loading and it does not allow sufficient precision. Additionally, the more ink amount the membrane has, the longer time it takes for the membrane to dry.

In the following decade, scientists began to use screen printing and

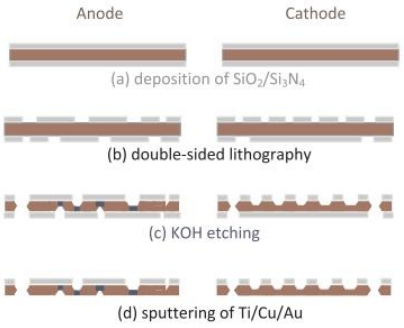

Fig. 18. UV Lithography scheme.

Table 2
Summary of bipolar plates manufacturing processes ordered chronologically.

Period	Process	Refs.	Process Steps	Plate Dimensions	Channel Dimensions	Operation Temperature	Properties
70s	Stamping 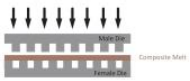	[25,90–92]	Three	70 × 70 mm 100 × 100 mm	1.5 mm (width) 0.5 mm (depth)	150 °C	• Common process • Require both (male and female) die • Complex physical process • Fast • Inexpensive • Mass production • Difficulty precision • Forming defects appear • Optimal stamping pressure: 20 MPa • Optimal curing time 3 min
	Compression Moulding 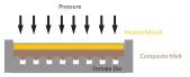	[18,25,94–97]	Two	70 × 70 mm 40 × 40 mm	0.75 mm (width, depth, land area)	80 °C	• Good surface topology • Uniform thickness distributions • Tight dimensional tolerance • Mass production • Working pressure: 55.2 MPa, 82.7 MPa, 843 MPa
80s-90s	Injection Moulding 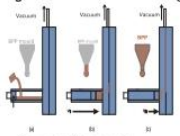	[17,73,92,99]	Three	25 × 25 cm 25 × 25 cm	1.2 mm (width) 1.5 mm (depth)	250 °C	• Low cost bipolar plates • Mass production • Low productivity • Insufficient electrical conductivity • Tensile strength: 15.85 MPa
	Investment Casting 	[82,87,100–102]	Four		1.5 mm (width) 0.75 mm (depth)	250 °C	• BP with complex shapes • Reduced cost • Not suitable for small sizes • Working pressure: 1 atm
Nowadays	Micro EDM 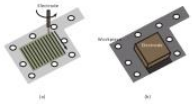	[72,103,105–108]	One	4 × 4 cm 6 mm (thick)	300 μm (width) 300 μm (depth) 200 mm (length)	Room temperature	• Higher aspect ratio • Higher degree of precision • Precision up to sub-micron • Suitable for micro-scaled flow channels • Efficient method • Not useful for mass production • Working pressure: 1 atm
	UV-lithography 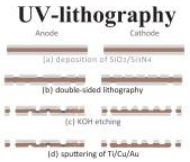	[104,109]	Eight	4 × 4 cm 2.6 mm (thick)	100 μm (width) 200 μm (depth)	120 °C	• Suitable for producing metallic BPs with micro-features • Risk of precision loss due to number of manufacturing steps • Lack of substrate properties due to non-uniform thickness • Working pressure: 1 atm

decal transfer methods. These are simple techniques in which the CL is applied using a transfer printing method. Unfortunately, the uniformity of the CL is not easily controlled and, especially in the decal transfer technique, heat treatment can cause structural changes.

At the turn of the 21st century, processes that are more complex began to appear. These processes are based on more complex deposition techniques such as sputter deposition, the use of a doctor blade, electrospraying deposition and Dual IBAD. These methods require more complex equipment as a magnetron sputtering system or an electron beam evaporator; thus, the process costs increase substantially because of the equipment. Otherwise, these processes present several advantages such as better efficiency, reproducibility and high precision (because the catalyst deposition on the membrane is controlled by the equipment instead of the user). It is important to point out that the same system performance is reached, while keeping the catalyst loading ultra-low.

The most recent techniques are oriented towards drop-on-demand technologies such as inkjet printing and ultrasonic spraying, which are advantageous because of their high precision values and consequently low Pt loading. These techniques allow a customisable GDE, where the only major variable to control is the viscosity of the ink.

Regarding the cost of the catalyst process, spraying techniques are the most inexpensive because the only tool used is a spray gun, which can be used for manufacturing several cells. Screen printing, decal transfer and doctor blade are more expensive because they require the use of a print matrix and a paint brush, thin-film substrates and a micropipette and spreader, respectively. Especially for decal transfer, it is necessary to use a new thin-film substrate every time a cell is manufactured. In the rest of techniques, the cost increases because complex equipment for the manufacturing is needed. The cost of the equipment increases from the inexpensive equipment such as inkjet printing (which uses a printer), electrospraying deposition (which uses an electrospray) to more sophisticated equipment and more expensive as well, sputter (which uses the equipment of the Fig. 7), Dual IBAD (which uses an electron-beam evaporator) and ultrasonic spraying (which uses an ultrasonic bath and an ultrasonic spray). However, the more expensive the equipment is, the less catalyst is used. A summary on the catalyst deposition techniques is shown in Table 3. The most

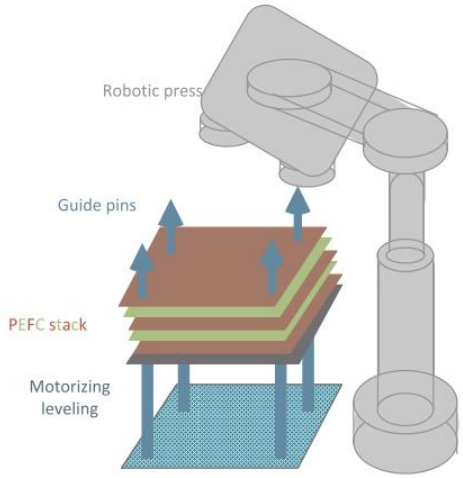

Fig. 19. Conceptual scheme of a stack assembly station.

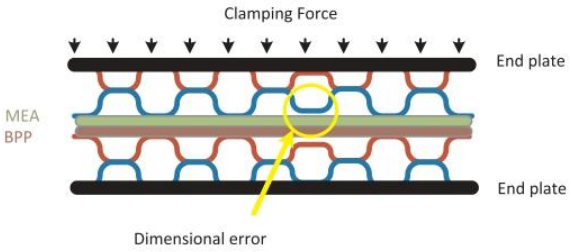

Fig. 20. Schematic diagram of a dimensional error associated to channel height.

important advantages and disadvantages, and the relative cost of each process, are included.

Apart from the catalyst, there are other basic elements that play an important role in a PEFC stack as the BPs. Their roles are very important because they are responsible for separating the individual cells, delivering the reactant gases, maintaining an electrical connection, removing the water by-product, dissipating the heat of the reaction and providing the clamping force.

The handmade deposition catalyst techniques are the prelude of the first BPs manufacturing processes such as the stamping and compression moulding in which the mould is put under pressure to obtain the workpiece. These techniques are simple and suitable for mass production, in spite of the medium-high pressure required for most of them (higher than 15 MPa).

During the eighties and nineties, with the arrival of new materials for BPs like coated-metallic, the high pressure-based methods are replaced by casting methods like injection moulding and investment casting. These techniques facilitate the manufacturing of BPs with arbitrarily complicated shapes. Nevertheless, these techniques require a relatively high working temperature of around 250 °C and they are unsuitable for small BPs sizes.

Nowadays, with the aim of making the fuel cells technology competitive for the 3 C Industry, new BPs manufacturing methods have begun to appear such as micro-EDM and UV lithography. These techniques allow developing miniature BPs with high precision rate in the flow field channels at room temperature and pressure.

In the assembly process, the clamping load plays an important role because both excessive and poor assembly may cause variation in the electro-physical-chemical properties of the MEA+GDLs structure and BP surface, as well as leakage of water or fuel at the sealed interfaces. In this sense, several studies are referenced where a design methodology is proposed to obtain the optimal clamping load for a given PEFC stack.

Regarding the cost of BPs manufacturing, the most simple and inexpensive techniques are stamping (which uses two dies: male and female), compression moulding (which uses a female die and a heated fluid) and investment casting (which uses a ceramic-based with some basic geometrical shape as the final piece). However, new tools are needed for each different BP. Otherwise, injection moulding uses the equipment of Fig. 15, which is more expensive than the tools used in the above-named techniques, but the equipment can be used for manufacturing different BPs. In micro-EDM and UV-lithography, the cost of the equipment increases, because micro-EDM uses electrical erosion equipment and UV-Lithography includes photo-resist and UV equipment. Therefore, it is important to consider what pieces are needed for each method, initial cost must be considered along usage plans and whether or not new pieces must be made for each type of BP in order to optimise cost. The summary of the most important advantages and disadvantages and the cost of the process is included in Table 4.

Finally, Fig. 22 orders the catalyst deposition and BPs manufacturing techniques from the most inexpensive to the most expensive.

6. Conclusions

The process of manufacturing a fuel cell stack starts with the MEA catalyst deposition of each cell. Afterwards, the BPs are manufactured and, finally, each cell is stacked to create the finished product. In a PE cell, the MEA and BPs are responsible for more than 80% of the total weight, volume and cost. Therefore, taking into account the most

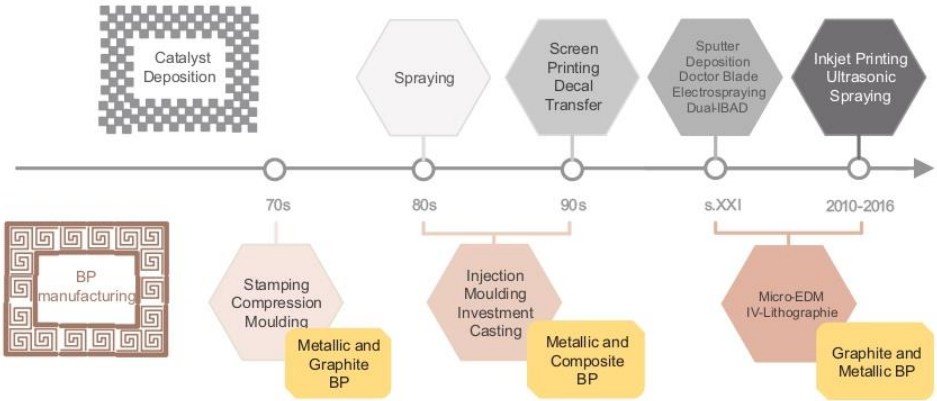

Fig. 21. Timeline classification of catalyst deposition and BPs manufacturing techniques.

Table 3
Catalyst manufacturing processes comparative: advantages, disadvantages and cost.

Catalyst Deposition Method	Advantages	Disadvantages	Cost
Spraying	• Tolerable for small-sized MEAs • Simple • Effective	• Not suitable for ultra-low catalyst loading ($< 0.5\ mg_{Pt}\ cm^{-2}$) • More ink, longer time to dry • Not easy to control the uniformity • Middle precision	• Inexpensive
Screen Printing	• Simple • Effective • Tolerable for small-sized MEAs	• Not easy to control the uniformity (depends on the person) • Require a lot of time • Not suitable for ultra-low catalyst loading ($< 0.5\ mg_{Pt}\ cm^{-2}$)	• Middle price
Decal Transfer	• Mass production • Low interfacial resistance • Effective	• Heat treatment can cause structural changes	• Middle price
Sputter Deposition	• Ultra-low catalyst loading • Cost reduction	• Strict atmosphere control • Vacuum conditions required • Not easily adaptable to bulk production	• Expensive
Doctor Blade	• High precision • Reproducibility • Fast • Efficient • Control of thickness	• Not for mass production	• Expensive
Electrospraying deposition	• Ultra-low Pt loading • High catalyst dispersion • Suitable for mass production • No vacuum requirements • Easily scalable to any size • Simple experimental set up	• Necessary improve reproducibility and evaluate its capabilities	• Expensive
Dual Ion Beam Assisted Deposition	• Good efficiency of the metal • Very low loading of the catalyst • Low temperature	• Not for mass production	• Very expensive
Inkjet Printing	• No conventional • High precision • Fast • Mass production		• Very expensive
Ultrasonic Spraying	• Ultra-low Pt loading • Precise • Controllable	• Not suitable for high viscosity ink	• Very expensive

Table 4
BPs manufacturing processes comparative: advantages, disadvantages and cost.

BP Manufacturing Process	Advantages	Disadvantages	Cost
Stamping	• Common process • Fast • Inexpensive • Mass production	• Three steps • High temperature operation (150 °C) • High pressure operation • Complex physical process • Difficult precision • Forming defects appear	• Inexpensive
Compression Moulding	• Two steps • Good surface topology • Uniform thickness distributions • Mass production	• High pressure operation • Tight dimensional tolerance • High temperature operation (80 °C)	• Inexpensive
Injection Moulding	• Low cost bipolar plates • Mass production	• Three steps • High temperature (250 °C) • High pressure • Low productivity • Insufficient electrical conductivity	• Middle price
Investment Casting	• Atmospheric pressure • BP with complex shapes	• Four steps • High temperature (250 °C) • Not suitable to small sizes • Common process	• Very expensive
Micro EDM	• One step • Room temperature • Atmospheric pressure • Higher aspect ratio • Higher degree of precision • Precision up to sub-micron • Micro-scaled flow channels • Efficient method	• Not for mass production	• Very expensive
UV-lithography	• Atmospheric pressure • Metallic BP with micro-features	• Suitable for producing metallic BP with micro-features • Risk of precision loss because of the steps • Lack of substrate properties	• Very expensive

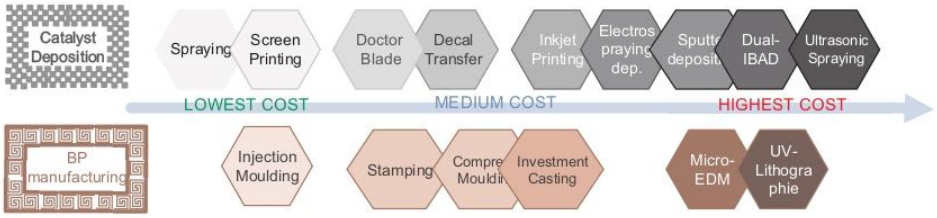

Fig. 22. Cost classification of catalyst deposition and BPs manufacturing techniques.

important matters involved in a PEFC, the presented work has developed a chronological review focusing on reviewing the catalyst deposition processes, BPs manufacturing methods and assembly techniques proposed. The goal of this work is to provide an overview about the different kinds of techniques that are available to design and manufacture a fuel cell and, from it, a whole stack. This review shows how far the fabrication technologies have advanced in the last 50 years – from new materials to improved techniques. However, this does bring higher cost. In order to reduce them, many of the catalyst deposition techniques that have been discussed aim at reducing the amount of catalyst necessary without losing performance to be able to lower cost of manufacturing. Nevertheless, there is often a problem: the reduction of the raw materials increases the cost of the necessary equipment for an effective manufacturing.

As for the bipolar plates, six main types have been brought to mind this review: graphite, polymer-carbon, composite, metallic, carbon-carbon and porous/foam metal bipolar plates. Taking into account the properties required for BPs (high electrical conductivity, high thermal conductivity, good mechanical properties, thermal stability, chemical stability and low cost), the main materials used for the bipolar plates manufacturing are graphite, metal and composite. This review was carried out based on a classification of manufacturing techniques according to their nature, from the oldest and simplest to the most recent and complicated process. Their advantages and disadvantages were studied concerning both materials and manufacturing process to discern which is the most suitable regarding the final application. Additionally, advantages, disadvantages and cost are compared amongst different methods involved in the manufacturing process.

Finally, this review presents a state of the art related to processes involved in the manufacturing and assembly of PEFC stacks. The chronological layout has been prepared to display the advances that have been carried out through history, so that developments can be easily deduced. This paper also shows that it is relatively easy to build a PEFC stack by hand without any of the complicated machinery generally used for its manufacturing.

Acknowledgements

This work is a contribution of the DPI2017–85540-R Project supported by the Spanish Ministry of Economy and Competitiveness and by the European Union Regional Development Fund.

References

[1] de Vries BJM, Van Vuuren DP, Hoogwijk MM. Renewable energy sources: their global potential for the first-half of the 21st century at a global level: an integrated approach. Energy Policy 2007;35:2590–610.
[2] Menanteau P, Finon D, Lamy M. Prices versus quantities: choosing policies for promoting the development of renewable energy," vol. 31, no. 2003, pp. 799–812; 2010.
[3] Panwar NL, Kaushik SC, Kothari S. Role of renewable energy sources in environmental protection: a review. Renew Sustain Energy Rev 2011;15(3):1513–24.
[4] Kleijn R, Van Der Voet E. Resource constraints in a hydrogen economy based on renewable energy sources: an exploration. Renew Sustain Energy Rev 2010;14(9):2784–95.
[5] Carrasco JM, et al. Power-electronic systems for the grid integration of renewable energy sources: a survey. IEEE Trans Ind Electron 2006;53(4):1002–16.
[6] Ralph TR. 'Principles of fuel cells,'. Platin Met Rev 2006;50(2):200–1.
[7] Yang JC, Park YS, Seo SH, Lee HJ, Noh JS. Development of a 50 kW PAFC power generation system. J Power Sources 2002;106:68–75.
[8] Smith JA, Nehrir MH, Gerez V, Shaw SR. A broad look at the workings, types, and applications of fuel cells. IEEE Power Eng Soc Summer Meet 2002;1:70–5.
[9] Tomczyk P. MCFC versus other fuel cells-Characteristics, technologies and prospects. J Power Sources 2006;160:858–62.
[10] Narayanan V, Mahasalkar R, Gadgil P, Gokhale K, Kothwal M, Snehal, Wind Power Generation by Windmill, Two Days Natl. Semin. Altern. Energy Sources, p. 1–164; 2005.
[11] Mollá S, Compañ V. Polymer blends of SPEEK for DMFC application at intermediate temperatures. Int J Hydrog Energy 2014;39:5121–36.
[12] Patel PP, et al. High performance and durable nanostructured TiN supported Pt50–Ru50 anode catalyst for direct methanol fuel cell (DMFC). J Power Sources 2015;293:437–46.
[13] Devrim Y, Devrim H, Eroglu I. Development of 500 W PEM fuel cell stack for portable power generators. Int J Hydrog Energy 2015;40(24):7707–19.
[14] Mehta V, Cooper JS. Review and analysis of PEM fuel cell design and manufacturing. J Power Sources 2003;114:32–53.
[15] Meyer Q, et al. Optimisation of air cooled, open-cathode fuel cells: current of lowest resistance and electro-thermal performance mapping. J Power Sources 2015;291:261–9.
[16] Zhang J, et al. High temperature PEM fuel cells. J Power Sources 2006;160:872–91.
[17] Kuo JK, Chen CK. A novel Nylon-6-S316L fiber compound material for injection molded PEM fuel cell bipolar plates. J Power Sources 2006;162:207–14.
[18] Taherian R. A review of composite and metallic bipolar plates in proton exchange membrane fuel cell: materials, fabrication, and material selection. J Power Sources 2014;265:370–90.
[19] Jordan LR, Shukla AK, Behrsing T, Avery NR, Muddle BC, Forsyth M. Diffusion layer parameters influencing optimal fuel cell performance. J Power Sources 2000;86:250–4.
[20] Lee WK, Ho CH, Van Zee JW, Murthy M. Effects of compression and gas diffusion layers on the performance of a PEM fuel cell. J Power Sources 1999;84:45–51.
[21] Siegel C. Review of computational heat and mass transfer modeling in polymer-electrolyte-membrane (PEM) fuel cells. Energy 2008;33:1331–52.
[22] Carlson EJ, Kopf P, Sinha J, Sriramulu S, Yang Y. Cost analysis of PEM fuel cell systems for transportation. Natl. Renew. Energy Lab.; 2005. [p. NREL/SR-560-39104].
[23] Hermann A, Chaudhuri T, Spagnol P. Bipolar plates for PEM fuel cells: a review. Int J Hydrog Energy 2005;30:1297–302.
[24] Li X, Sabir I. Review of bipolar plates in PEM fuel cells: flow-field designs. Int J Hydrog Energy . 2005;30(4):359–71.
[25] Dundar F, Dur E, Mahabunphachai S, Koç M. Corrosion resistance characteristics of stamped and hydroformed proton exchange membrane fuel cell metallic bipolar plates. J Power Sources 2010;195:3546–52.
[26] Jin CK, Kang CG. Fabrication by vacuum die casting and simulation of aluminum bipolar plates with micro-channels on both sides for proton exchange membrane (PEM) fuel cells. Int J Hydrog Energy 2012;37(2):1661–76.
[27] Park S, Lee JW, Popov BN. A review of gas diffusion layer in PEM fuel cells: materials and designs. Int J Hydrog Energy 2012;37(7):5850–65.
[28] Steele BCH, Heinzel A. Materials for fuel-cell technologies. Nature . 2001;414(6861):345–52.
[29] Gasteiger HA, Kocha SS, Sompalli B, Wagner FT. Activity benchmarks and requirements for Pt, Pt-alloy, and non-Pt oxygen reduction catalysts for PEMFCs. Appl Catal B Environ 2005;56(MARCH 2005):9–35.
[30] Ralph TR, et al. Low cost electrodes for proton exchange membrane fuel cells - Performance in single cells and Ballard stacks. J Electrochem Soc 1997;144(11):3845–57.
[31] Su H, Jao T, Barron O, Pollet BG, Pasupathi S. Low platinum loading for high temperature proton exchange membrane fuel cell developed by ultrasonic spray coating technique. J Power Sources 2014;267:155–9.
[32] Jao TC, Jung GB, Ke ST, Chi PH, Chan SH. Diagnosis of PTFE-Nafion MEA degradation modes by an accelerated degradation technique., 35(14), 1274–1283. Int J Energy Res 2011;35(14):1274–83.
[33] James BD, Huya-Kouadio JM, Houchins C, Cassidy H, DeSantis DA. Mass production cost estimation of direct H2 PEM fuel cell systems for automotive applications: 2011 Update, Strateg. Anal., no. September; 2012.
[34] Kim KH, et al. "The effects of Nafion® ionomer content in PEMFC MEAs prepared by a catalyst-coated membrane (CCM) spraying method. Int J Hydrog Energy 2010;35(5):2119–26.

[35] Millington B, Whipple V, Pollet BG. A novel method for preparing proton exchange membrane fuel cell electrodes by the ultrasonic-spray technique. J Power Sources 2011;196(20):8500–8.
[36] Andújar JM, Segura F. Fuel cells: history and updating. A walk along two centuries. Renew Sustain Energy Rev 2009;13:2309–22.
[37] Penner SS. Assessment of research needs for advanced fuel-cells. Energy 1986;11(1–2):R3–229.
[38] Weber MF, Mamiche-Afara S, Dignam MJ, Pataki L, Venter RD. Sputtered fuel cell electrodes. J Electrochem Soc 1987;134(6):1416–9.
[39] Prasanna M, Cho EA, Lim TH, Oh IH. Effects of MEA fabrication method on durability of polymer electrolyte membrane fuel cells. Electrochim Acta 2008;53:5434–41.
[40] Hsu CH, Wan CC. An innovative process for PEMFC electrodes using the expansion of Nafion film. J Power Sources 2003;115:268–73.
[41] Sun L, Ran R, Wang G, Shao Z. Fabrication and performance test of a catalyst-coated membrane from direct spray deposition. Solid State Ion 2008;179:960–5.
[42] Wilson MS, Valerio JA, Gottesfeld S. Low platinum loading electrodes for polymer electrolyte fuel cells fabricated using thermoplastic ionomers. Electrochim Acta 1995;40(3):355–63.
[43] Wilson MS. Membrane catalyst layer for fuel cells. 5. 1993. p. 777.
[44] Bonifácio RN, Paschoal JOA, Linardi M, Cuenca R. Catalyst layer optimization by surface tension control during ink formulation of membrane electrode assemblies in proton exchange membrane fuel cell. J Power Sources 2011;196:4680–5.
[45] Wang W, Chen S, Li J, Wang W. Fabrication of catalyst coated membrane with screen printing method in a proton exchange membrane fuel cell. Int J Hydrog Energy 2015;40(13):4649–58.
[46] Kluczowski R, Krauz M, Kawalec M, Ouweltjes JP. Near net shape manufacturing of planar anode supported solid oxide fuel cells by using ceramic injection molding and screen printing. J Power Sources . 2014;268:752–7.
[47] Pijolat C. Printed films. Elsevier; 2012.
[48] Taylor AD, Kim EY, Humes VP, Kizuka J, Thompson LT. Inkjet printing of carbon supported platinum 3-D catalyst layers for use in fuel cells. J Power Sources 2007;171:101–6.
[49] Wilson MS, Gottesfeld S. Thin-film catalyst layers for polymer electrolyte fuel cell electrodes. J Appl Electrochem 1992;22(1):1–7.
[50] Jeon S, et al. Effect of ionomer content and relative humidity on polymer electrolyte membrane fuel cell (PEMFC) performance of membrane-electrode assemblies (MEAs) prepared by decal transfer method. Int J Hydrog Energy 2010;35(18):9678–86.
[51] Liang X, Pan G, Xu L, Wang J. A modified decal method for preparing the membrane electrode assembly of proton exchange membrane fuel cells. Fuel 2015;139:393–400.
[52] Yoon YJ, Kim TH, Kim SU, Yu DM, Hong YT. Low temperature decal transfer method for hydrocarbon membrane based membrane electrode assemblies in polymer electrolyte membrane fuel cells. J Power Sources 2011;196(22):9800–9.
[53] Cavalca CA, Arps JH, Murthy M. Fuel cell membrane electrode assemblies with improved power outputs and poison resistance. 6. 2001. p. 000.
[54] Alvisi M, Galtieri G, Giorgi L, Giorgi R, Serra E, Signore MA. Sputter deposition of Pt nanoclusters and thin films on PEM fuel cell electrodes. Surf Coat Technol 2005;200:1325–9.
[55] Cavarroc M, et al. Performance of plasma sputtered fuel cell electrodes with ultra-low Pt loadings. Electrochem Commun 2009;11(4):859–61.
[56] Natarajan SK, Hamelin J. High-performance anode for polymer electrolyte membrane fuel cells by multiple-layer Pt sputter deposition. J Power Sources 2010;195(22):7574–7.
[57] Park IS, Li W, Manthiram A. Fabrication of catalyst-coated membrane-electrode assemblies by doctor blade method and their performance in fuel cells. J Power Sources 2010;195(20):7078–82.
[58] Mench MM. Fuel cell engines. 1st ed John Wiley & Sons, Inc; 2008.
[59] Middelman E. Improved PEM fuel cell electrodes by controlled self-assembly. Fuel Cells Bull . 2002;2002(11):9–12.
[60] Martin S, Garcia-Ybarra PL, Castillo JL. Electrospray deposition of catalyst layers with ultra-low Pt loadings for PEM fuel cells cathodes. J Power Sources 2010;195:2443–9.
[61] Wang X, Richey FW, Wujcik KH, Elabd YA. Ultra-low platinum loadings in polymer electrolyte membrane fuel cell electrodes fabricated via simultaneous electrospinning/electrospraying method. J Power Sources 2014;264:42–8.
[62] Towne S, Viswanathan V, Holbery J, Rieke P. Fabrication of polymer electrolyte membrane fuel cell MEAs utilizing inkjet print technology. J Power Sources 2007;171:575–84.
[63] Wang Z, Nagao Y. Effects of Nafion impregnation using inkjet printing for membrane electrode assemblies in polymer electrolyte membrane fuel cells. Electrochim Acta 2014;129:343–7.
[64] Huang TH, Shen HL, Jao TC, Weng FB, Su A. Ultra-low Pt loading for proton exchange membrane fuel cells by catalyst coating technique with ultrasonic spray coating machine. Int J Hydrog Energy 2012;37:13872–9.
[65] Strong A, Thornberry C, Beattie S, Chen R, Coles SR. Depositing catalyst layers in polymer electrolyte membrane fuel cells: a review. J Fuel Cell Sci Technol 2015;12(6).
[66] Insights into potential substitutes for costly platinum in fuel cell catalysts. [Online]. Available: http://phys.org/news/2015-04-insights-potential-substitutes-costly-platinum.html. [Accessed: 12-Oct-2016]; 2016.
[67] Ramaswamy N, et al. Enhanced activity and interfacial durability study of ultra low Pt based electrocatalysts prepared by ion beam assisted deposition (IBAD) method. Electrochim Acta 2009;54(2009):6756–66.
[68] Saha MS, Gullá AF, Allen RJ, Mukerjee S. High performance polymer electrolyte fuel cells with ultra-low Pt loading electrodes prepared by dual ion-beam assisted deposition. Electrochim Acta 2006;51:4680–92.
[69] Wee JH, Lee KY, Kim SH. Fabrication methods for low-Pt-loading electrocatalysts in proton exchange membrane fuel cell systems. J Power Sources 2007;165:667–77.
[70] Fuel Cell Catalyst Coatings Using Ultrasonic Spray. . [Online]; 2016. Available: ⟨http://www.sono-tek.com/fuel-cell-catalyst-coating-overview/⟩. [Accessed 10 September 2016].
[71] Antunes RA, Oliveira MCL, Ett G, Ett V. Corrosion of metal bipolar plates for PEM fuel cells: a review. Int J Hydrog Energy 2010;35(8):3632–47.
[72] Hung JC, Chang DH, Chuang Y. The fabrication of high-aspect-ratio micro-flow channels on metallic bipolar plates using die-sinking micro-electrical discharge machining. J Power Sources 2012;198:158–63.
[73] Müller A, Kauranen P, Von Ganski A, Hell B. Injection moulding of graphite composite bipolar plates. J Power Sources 2006;154:467–71.
[74] Carlson EJ, Kopf P, Sinha J, Sriramulu S, Yang Y. Cost analyses of fuel cell systems for transportation, Rep. to Dep. Energy, 2001, p. Ref. No. DESC02-98EE50526.
[75] Jiang B, Stübler N, Wu W, Li Q, Ziegmann G, Meiners D. Manufacturing and characterization of bipolar fuel cell plate with textile reinforced polymer composites. Mater Des 2015;65:1011–20.
[76] Koraishy B, Meyers J, Wood K. Manufacturing of membrane electrode assemblies for fuel cells. Res Net 2010:1–13.
[77] Cunningham BD, Baird DG. Development of bipolar plates for fuel cells from graphite filled wet-lay material and a compatible thermoplastic laminate skin layer. J Power Sources 2007;168:418–25.
[78] Cunningham BD, Huang J, Baird DG. Development of bipolar plates for fuel cells from graphite filled wet-lay material and a thermoplastic laminate skin layer. J Power Sources 2006.
[79] Hamilton PJ, Polle BG. Polymer Electrolyte Membrane Fuel Cell (PEMFC) flow field plate: design, materials and characterisation. Fuel Cells 2010;10(4):489–509.
[80] Owejan JP, Trabold TA, Jacobson DL, Arif M, Kandlikar SG. Effects of flow field and diffusion layer properties on water accumulation in a PEM fuel cell. Int J Hydrog Energy 2007;32:4489–502.
[81] Liu Y, Hua L. Fabrication of metallic bipolar plate for proton exchange membrane fuel cells by rubber pad forming. J Power Sources 2010;195(11):3529–35.
[82] Yuan W, Tang Y, Yang X, Wan Z. Porous metal materials for polymer electrolyte membrane fuel cells - A review. Appl Energy 2012;94:309–29.
[83] Kumar A, Reddy RG. Modeling of polymer electrolyte membrane fuel cell with metal foam in the flow-field of the bipolar/end plates. J Power Sources 2003;114(1):54–62.
[84] Kumar A, Reddy RG. Materials and design development for bipolar/end plates in fuel cells. J Power Sources 2004;129(1 SPEC. ISS):62–7.
[85] Koç M, Mahabunphachai S. Feasibility investigations on a novel micro-manufacturing process for fabrication of fuel cell bipolar plates: internal pressure-assisted embossing of micro-channels with in-die mechanical bonding. J Power Sources . 2007;172(2):725–33.
[86] Parvanian AM, Panjepour M. Mechanical behavior improvement of open-pore copper foams synthesized through space holder technique. Mater Des 2013;49:834–41.
[87] Banhart J. Manufacture, characterization and application of cellular metals and metal foams. Prog Mater Sci 2001;46:559–632.
[88] Kim M, Choe J, Lim JW, Lee DG. Manufacturing of the carbon/phenol composite bipolar plates for PEMFC with continuous hot rolling process. Compos Struct 2015;132:1122–8.
[89] Grehier A, Cheron J. Fuel Cells 1977;4(037):023.
[90] Li X, Bassiuny AM. Transient dynamical analysis of strain signals in sheet metal stamping processes. Int J Mach Tools Manuf 2008;48:576–88.
[91] Jin CK, Koo JY, Kang CG. Fabrication of stainless steel bipolar plates for fuel cells using dynamic loads for the stamping process and performance evaluation of a single cell. Int J Hydrog Energy 2014;39(36):21461–9.
[92] Heo SI, Oh KS, Yun JC, Jung SH, Yang YC, Han KS. Development of preform moulding technique using expanded graphite for proton exchange membrane fuel cell bipolar plates. J Power Sources 2007;171:396–403.
[93] Fleming DK, Leitz FB. Bipolar collector plates. 3. 1971. p. 942.
[94] Turan C, Cora ON, Koç M. Effect of manufacturing processes on contact resistance characteristics of metallic bipolar plates in PEM fuel cells. Int J Hydrog Energy 2011;36:12370–80.
[95] Hu Q, Zhang D, Fu H, Huang K. Investigation of stamping process of metallic bipolar plates in PEM fuel cell - Numerical simulation and experiments. Int J Hydrog Energy 2014;39(25):13770–6.
[96] Aginagalde A, Orus A, Esnaola JA, Torca I, Galdos L, García C. Warm hydroforming of lightweight metal sheets, AIP Conf. Proc., vol. 908, no. July 2015, 2007, pp. 1175–1180.
[97] Hung JC, Lin CC. Fabrication of micro-flow channels for metallic bipolar plates by a high-pressure hydroforming apparatus. J Power Sources 2012;206:179–84.
[98] Borup NE, Vanderborgh RL. Design and testing criteria for bipolar plate materials for PEM fuel cell applications. In MRS Proceedings., vol. 393; 1995.
[99] Heinzel A, Mahlendorf F, Niemzig O, Kreuz C. Injection moulded low cost bipolar plates for PEM fuel cells. J Power Sources 2004;131(1–2):35–40.
[100] S. Takahashi, Method of manufacturing carbon fibre-reinforced carbon elongated structural components, 5 112 442; 1992.
[101] Burke JT. Investment casting technique for the formation of metal matrix composite bodies and products produced thereby (30 March 1993) An investment shell, 5 197 528; 1993.
[102] Lim C, Clegg A. "The production and evaluation of metal-matrix composite castings produced by a pressure-assisted investment casting process. J Mater Process

Technol 1997;67(1):13–8.
[103] Hung JC, Yang TC, Li KC. Studies on the fabrication of metallic bipolar plates - Using micro electrical discharge machining milling. J Power Sources 2011;196(4):2070–4.
[104] Lee SJ, Chen YP, Huang CH. Electroforming of metallic bipolar plates with micro-featured flow field. J Power Sources 2005;145(2):369–75.
[105] Lee SJ, Lee CY, Yang KT, Kuan FH, Lai PH. Simulation and fabrication of micro-scaled flow channels for metallic bipolar plates by the electrochemical micro-machining process. J Power Sources 2008;185:1115–21.
[106] Lee YM, Lee SJ, Lee CY, Chang DY. The multiphysics analysis of the metallic bi-polar plate by the electrochemical micro-machining fabrication process. J Power Sources 2009;193:227–32.
[107] Landolt D, Chauvy PF, Zinger O. Electrochemical micromachining, polishing and surface structuring of metals: fundamental aspects and new developments. Electrochim Acta 2003;48:3185–201.
[108] Jin CK, Kang CG. Fabrication process analysis and experimental verification for aluminum bipolar plates in fuel cells by vacuum die-casting. J Power Sources 2011;196(20):8241–9.
[109] Wang X, Zhu Y, Shen C, Zhou Y, Wu X, Liu L. A novel assembly method using multi-layer bonding technique for micro direct methanol fuel cells and their stack. Sens Actuators A Phys 2012;188:246–54.
[110] Lin P, Zhou P, Wu CW. A high efficient assembly technique for large proton exchange membrane fuel cell stacks: part II. Applications. J Power Sources 2010;195:1383–92.
[111] Qiu D, Yi P, Peng L, Lai X. Assembly design of proton exchange membrane fuel cell stack with stamped metallic bipolar plates. Int J Hydrog Energy 2015;40(35):11559–68.
[112] Wang X, Song Y, Zhang B. Experimental study on clamping pressure distribution in PEM fuel cells. J Power Sources 2008;179(1):305–9.
[113] Nitta I. Inhomogeneous compression of PEMFC gas diffusion layers. Helsinki University of Technology Faculty; 2008.
[114] Taymaz I, Benli M. Numerical study of assembly pressure effect on the performance of proton exchange membrane fuel cell. Energy 2010;35(5):2134–40.
[115] Zhang L, Liu Y, Song H, Wang S, Zhou Y, Hu SJ. Estimation of contact resistance in proton exchange membrane fuel cells. J Power Sources 2006;162(2):1165–71.

6.3. Contribution 3

How the BoP configuration affects the performance in an Air-Cooled Polymer Electrolyte Fuel Cell. Keys to design the best configuration

A. De las Heras, F.J. Vivas, F. Segura, J.M. Andújar

Published in:

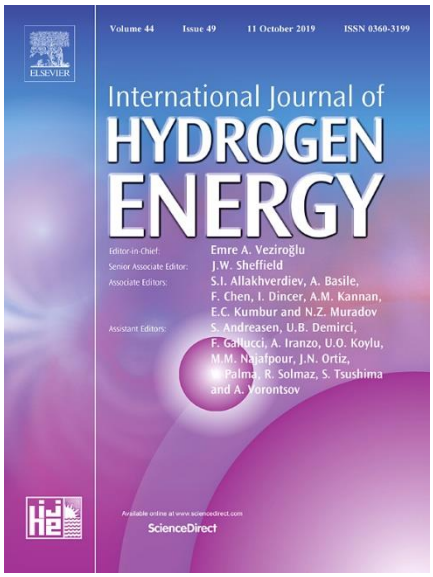

Journal: International Journal of Hydrogen Energy
Editorial: ELSEVIER
Editor-in-Chief: T. Nejat Veziroglu
Reference: Vol. 42, Issue 17, pp. 12841-12855
Year: 2017
ISSN: 0360-3199
DOI 10.1016/j.ijhydene.2016.11.051

Category	Journal Rank / Total journals	Quartile
	24 / 97	Q1
Electrochemistry	42 / 146	Q2
Chemistry	8 / 28	Q2
Impact Factor (2017)	3.581	
Citations	2	

INTERNATIONAL JOURNAL OF HYDROGEN ENERGY 42 (2017) 12841–12855

Available online at www.sciencedirect.com

ScienceDirect

journal homepage: www.elsevier.com/locate/he

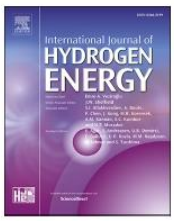

How the BoP configuration affects the performance in an air-cooled polymer electrolyte fuel cell. Keys to design the best configuration

A. de las Heras[*], *F.J. Vivas*, *F. Segura*, *J.M. Andújar*

Grupo de Investigación de Control y Robótica TEP-192, Departamento de Ingeniería Electrónica, de Sistemas Informáticos y Automática, Escuela Técnica Superior de Ingeniería, Universidad de Huelva, Carretera Huelva – Palos de la Frontera, 21819, La Rábida – Palos de la Frontera, Huelva, Spain

ARTICLE INFO

Article history:
Received 19 July 2016
Received in revised form
28 October 2016
Accepted 7 November 2016
Available online 29 November 2016

Keywords:
Air cooled polymer electrolyte fuel cell
BoP configurations
Fuel subsystem design
Experimental study

ABSTRACT

Air Cooled Polymer Electrolyte fuel cells (AC-PEFC) are recently receiving especial attention because they offer the possibility to integrate the oxidant and cooling subsystems in just one. This feature reduces not only the fuel cell weight, volume and cost but also the control complexity. In these fuel cells, the Oxidant/Cooling subsystem along with three others (*Fuel*, *Electrical* and *Control*) make up the Balance of Plant (BoP), which together with the stack comprise the full fuel cell. It is common to find works focused on analysing the influence of the Oxidant/Cooling subsystem on the fuel cell. Nevertheless, studies in which the Fuel subsystem (it is responsible for providing the hydrogen for its reduction–oxidation reaction with oxygen to form water) is investigated are hard to find on the scientific literature. It seems like the Fuel subsystem configuration would not have influence over the whole system performance. Contrary to what one might think, and in basis on experimental results, this paper shows how the fuel cell performance is conditioned by the Fuel subsystem configuration. The aim of this paper is to present a comprehensive experimental study of an AC-PEFC paying particular attention, so unexplored so far, to Fuel subsystem configuration, giving the keys for the most suitable BoP configuration which guarantees the best performance, with the easiest BoP design and the lowest complexity.

Introduction

As it is widely known, Polymer Electrolyte Fuel Cell (PEFC) is a promising technology due to its high power density, low operating temperature, low pollution level, quiet operation, lower corrosion, simplification of stack design and relatively quick start-up and shut-down [1–3]. Although in the past decades there has been a huge progress in the PEFC field, researchers still continue developing their researches in areas related to new cell designs for better performance, cost reduction, or optimized cold-start characteristics [4]. One of the reason of this continuous research works is because PEFCs are suitable for a wide range of applications, including portable, stationary and automotive power delivery [5–10] and they are having more and more importance in backup systems for emergency situations (e.g. earthquakes, terrorist attacks).

* *Corresponding author.*
E-mail address: ainhoa.delasherasjimenez@gmail.com (A. de las Heras).
http://dx.doi.org/10.1016/j.ijhydene.2016.11.051

Nomenclature

AC	Air Cooled
BoP	Balance of Plant
BPP	Bipolar Plates
DEA	Dead-End Anode
DMFC	Direct Methanol Fuel Cell
FC	Fuel Cell
FTA	Flow-Through Anode
GDLs	Gas Diffusion Layers
MEA	Membrane Electrode Assembly
PE	Polymer Electrolyte
PEFC	Polymer Electrolyte Fuel Cell
P_{H2}	Hydrogen Pressure
λ	Stoichiometric rate

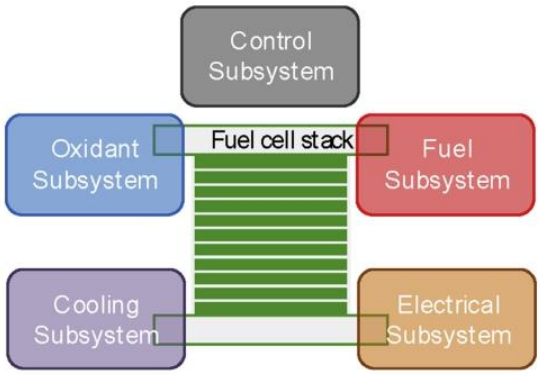

Fig. 2 – Scheme of a PEFC fuel cell integrated by the stack + BoP (Oxidant, Fuel, Cooling, Electrical and Control subsystems).

A typical PEFC is formed by six main parts (Fig. 1) from the outermost to the innermost: End Plates, Current Collectors, Bipolar Plates (BPP), Gaskets, Gas Diffusion Layers (GDLs) and Membrane Electrode Assembly (MEA) [11]. For the design of a PEFC from the stack (built by assembling single cells with similar structure to that shown in Fig. 1), it is necessary to incorporate additional subsystems. Generally these can be classified in five groups: *Oxidant*, *Fuel*, *Cooling*, *Electrical* and *Control*, Fig. 2. All of them make up the Balance of Plant (BoP) and they handle the PEFC works properly [12,13]. The role of these subsystems is to supply reactants (oxygen and hydrogen at the appropriate flow and pressure for electrochemical reaction), remove the heat generated in the stack and maintain it at the temperature recommended by the manufacturer, eliminate the water produced, connect the stack to electric load and process information from sensors to control the actuators [14,15].

Previous efforts for the development of PEFC have demonstrated that a reliable design of the BoP is essential for the fuel cell stack operation as it determines the full fuel cell performance. In the BoP design, it is important to optimize the different subsystems, as well as example an oversized BoP configuration results in an increase in parasitic loss, system volume, weight and noise level [16].

Regarding the scheme of Fig. 2, the authors of this study have used an AC-PEFC stack, which integrate Oxidant and Cooling subsystems into one single. This allows that there are no liquid in the Cooling subsystem, thus facilitating and simplifying the BoP integration because they do not need pipes, valves, pumps and heat exchangers, contributing to reduce weight, volume and cost. Another feature of the stack used in this work is that it does not require high inlet hydrogen pressure; indeed, it can operate at pressures close to ambient. This second feature provides security because it is not necessary to work with high hydrogen supply pressure and less stringent requirements in the hydrogen transfer circuit (connections, pipelines, etc.).

Several authors have developed different BoP configurations [15,17–26], and in all these case authors justify the chosen configuration in basis on the conditions required by their systems.

In this sense, there are not too many works in which different configurations are analysed, discussing their advantages and disadvantages. Then Youngseung Na et al. [27]

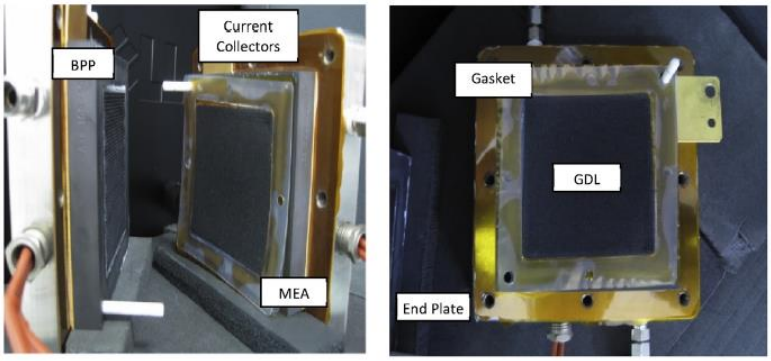

Fig. 1 – Single fuel cell with a 50 cm^2 active area from Teledyne™, with three-channel parallel serpentine flow fields (channels of 0.76 mm wide and deep). Graphite bipolar plate's layout is cross-flow, with horizontal channels in both anode and cathode.

propose a new experimental technique to improve the performance and stability of the DMFC system under air-blowing conditions, and Kim et al. [28] show two types of Oxidant subsystem (a gas recirculation subsystem with and without a recycle blower). On the other hand, Hinaje et al. [29] evidence the behaviour of a fuel cell system as a current source, in which the current is directly controlled by the hydrogen flow rate. Rodatz et al. [30] show an exhaustive evaluation among the five most important types of the fuel subsystems. Going deeper in this way, Chen et al. [31] summarise all these Fuel subsystem configurations in two groups: Dead-End Anode (DEA) and Flow-Through Anode (FTA) operation mode. In any case, independently of the number of groups done all authors agree with the idea that a DEA Fuel subsystem configuration requires fewer auxiliary components compared to traditional FTA, Fig. 3.

The FTA operation with hydrogen flow control depends on a recirculation loop to maintain a high hydrogen utilization and enhanced convective transport. So this configuration requires additional equipment such as an ejector/blower, a water separator/demister and an anode humidifier. These components add weight, volume, and cost to the system.

Regarding DEA operation, it is possible to adjust the hydrogen inlet stoichiometry to one by regulating the inlet pressure (so it would not be needed the hydrogen recirculation) and the anode channel pressure would remain constant. That is, DEA operation depends on upstream pressure regulation instead of the hydrogen mass flow control. Chen et al. [31] try to control the hydrogen inlet pressure by scheduling the purge interval. The final goal of that work was to improve the output power at time that the hydrogen losses are reduced. Simulation results shown the fuel cell efficiency improvement.

Now, giving a further step we proposes six different configurations for the Fuel subsystem in DEA operation. The basic devices which take part in the hydrogen line are a mass flow meter, a pressure sensor and a purge valve. Around these devices, we will put a proportional control valve and experimental results allow us to corroborate some proposals presented previously. Then, we see for example suggestions as the hydrogen mass flow control is not suitable for the DEA operation. Another key point is the way to regulate the hydrogen inlet pressure (and consequently to adjust the hydrogen inlet stoichiometry), which is usually carried out by means the purge interval schedule. However there may be other alternatives (especially when it comes a stack with low inlet pressure). From these we can configure a half-dozen proposals and we can draw some keys to select the most suitable to optimize the AC-PEFC operation.

This paper is organized as follow. AC-PEFC characterization is done in Section II, explaining its main features as well as giving its experimental polarization and power curves. Section III describes the different BoP configurations implemented, showing each diagram and pointing out the particularities of each one. Next, experimental results obtained from each configuration as well as some discussions about

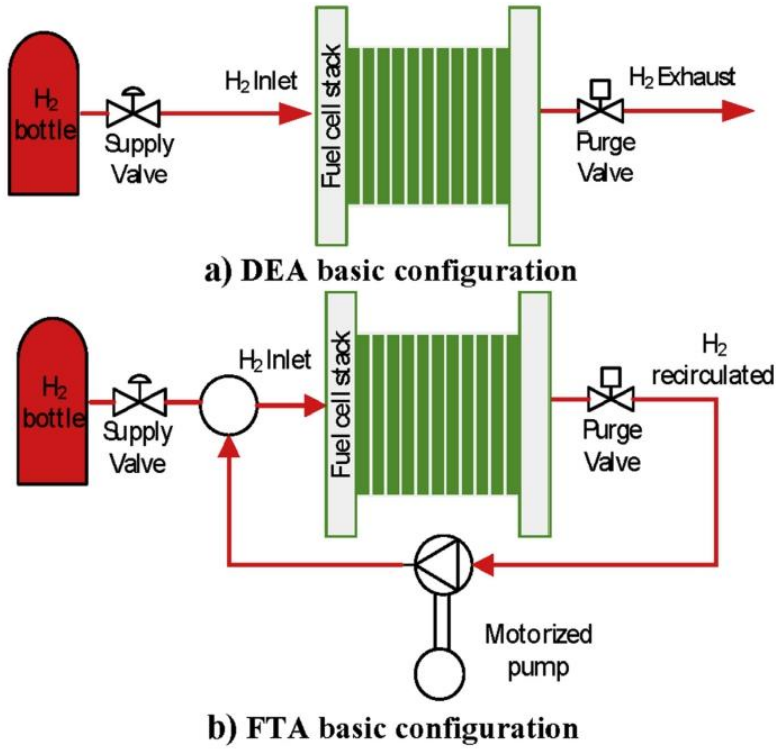

Fig. 3 – Scheme of DEA versus FTA Fuel subsystem configurations.

them are summarised in Section IV and V respectively. Finally, Section VI draws the main conclusions derived from the experimental study.

System characterization

The fuel cell under study is based on the FCgen-1200ACS stack model from Ballard®. This stack is characterised by it is air-cooled and it does not need external air humidification. The operation mode is dead-end using dry hydrogen without humidification. The inlet hydrogen pressure can vary from 1.16 to 1.56 bars. The stack is constituted by 80 cells and, according to manufacturer's data, it can reach up to 3.4 kW [32].

This stack has been used to build a AC-PEFC (Fig. 4) where the (BoP) has been developed according to [17]. The AC-PEFC shown in Fig. 4 has been developed by authors and constitutes an excellent test bench to carry out all kinds of tests on a real system [17].

The configuration of our Oxidant/Cooling subsystem is very simple and effective, consists of an adjustable flow fan (model EbmPapst™ DV6224TDA) and a stack temperature sensor (Ts) included in the own stack (see Fig. 4a and b). Following Fig. 4a, at the fuel input the Fuel subsystem is made up of the hydrogen storage bottle, and a manual pressure regulator to reduce the high pressure from the bottle to pressure range recommended by the stack manufacturer. Additionally, a mass flow meter to measure the hydrogen

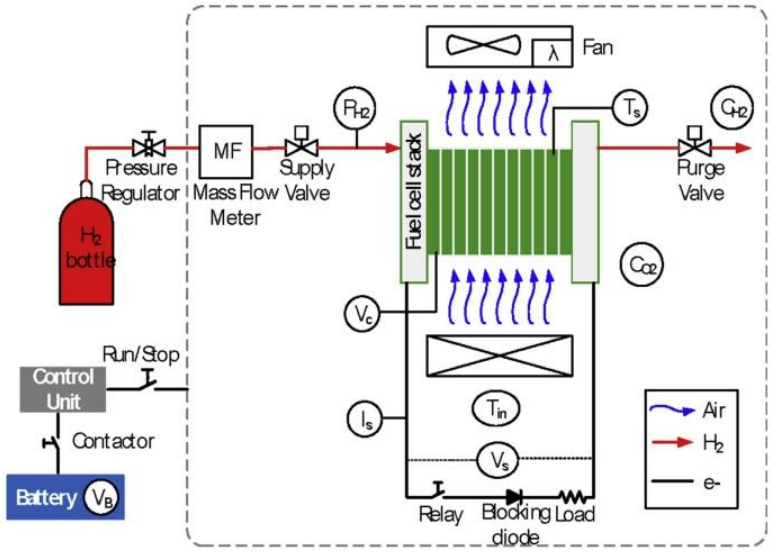

a) AC-PEFC diagram (stack + BoP).

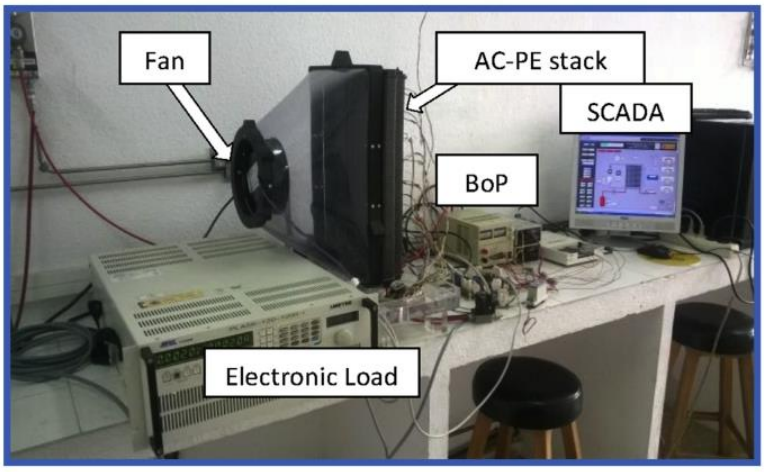

b) AC-PEFC real implementation (stack + BoP).

Fig. 4 – Diagram and real implementation of the AC-PEFC under study.

INTERNATIONAL JOURNAL OF HYDROGEN ENERGY 42 (2017) 12841–12855

consumption, a supply valve to control the hydrogen entry and a hydrogen pressure sensor (P_{H2}) to measure the inlet anode pressure, complete the hydrogen input line. In the hydrogen outlet, a purge valve evacuates inert gases.

Then, once the AC-PEFC (stack + BoP) has been introduced, the first step is to characterize it. For this purpose the FCTESTNET/FCTESQA PEFC power stack performance testing procedure has been followed [33]. We can see (see Fig. 5) that the maximum stack power achieves 3 kW when the load current rises up to 75 A, while the stack voltage drops to 40 V (0.5 V for every cell, total 80, the limit specified by the manufacturer's recommendations). Moreover, the hysteresis phenomenon over the polarization curve (different upward and downward paths) can be easily distinguished [34]. Regarding hydrogen consumption, Fig. 6 compares the real hydrogen flow consumed with the hydrogen flow required for a proper operation according to manufacturer's data. It deserves to point out that in basis on real measures taken with the mass flow meter (see Fig. 4a), the real hydrogen flow rate follows a polynomial curve depending on load current according to (1):

$$Flow_{Hydrogen}(slpm) = 0.645 \cdot I_s - 0.00038 \cdot I_s^2 \quad (1)$$

where I_s is the stack current which coincides with the load current.

BoP configurations study. Proposals for the fuel subsystem

Now, after the AC-PEFC characterization different BoP configurations will be studied and analysed in basis on the AC-PEFC response. This study consists on acting over different devices which integrate the hydrogen line (mass flow meter and hydrogen pressure sensor in the fuel inlet line and purge valve in the fuel outlet line). The way to have influence over the AC-PEFC will be placing a proportional control valve around the above-mentioned devices.

Then, the first two proposals for the BoP configuration are based on locating the proportional control valve downstream and upstream the mass flow meter (Fig. 7). This proportional control valve will allow controlling the hydrogen flow taking into account (1).

The first test will lie in adjusting the proportional control valve according to (2) which it is an empirical equation slightly below respect to real flow rate (1). The goal is to know if an AC-PEFC stack with DEA operation can work when the hydrogen flow input is limited, even if the flow restriction is very small compared to real flow.

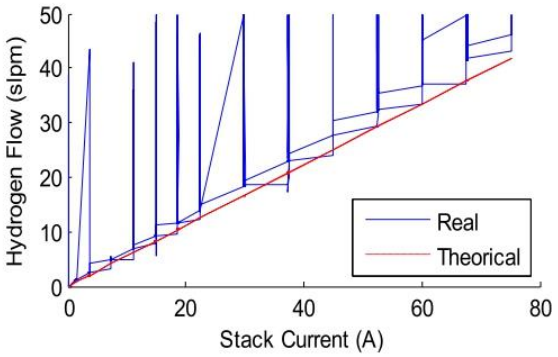

Fig. 6 – Hydrogen flow consumption: measured value versus value provided by manufacturer.

$$Valve_{controlbelow}(slpm) = 0.63 \cdot I_s - 0.00033 \cdot I_s^2 \quad (2)$$

In the same way, the second test consists in adjusting the proportional control valve according to (3), a new empirical equation slightly above respect to real flow rate (1). In this case, we could compare the system performance when there is no restriction in the hydrogen flow input.

$$Valve_{controlabove}(slpm) = 0.65 \cdot I_s - 0.00038 \cdot I_s^2 \quad (3)$$

In the next two configurations, the proportional control valve is located downstream and upstream the hydrogen pressure sensor (P_{H2}) in the fuel inlet line (Fig. 8). In this case, the aim will not be to control the hydrogen flow but the hydrogen pressure. Then, we could draw some conclusions comparing the effects over the AC-PEFC performance when the hydrogen flow is controlled respect to the performance obtained when the control is applied over the hydrogen input.

Finally, the last two configurations consider the proportional control valve located downstream and upstream the hydrogen pressure sensor (P_{H2}), but in this case in the fuel outlet line (Fig. 9).

Then, with the proposed six configurations for the Fuel subsystem in an AC-PEFC, we could know what configuration favours a better system performance and how the control over some variables like hydrogen flow, inlet hydrogen pressure or

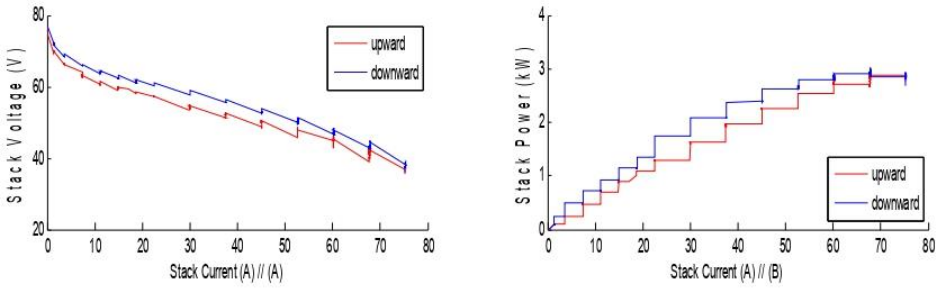

Fig. 5 – Polarization and power curves. A: stack voltage (V) vs stack current (A). B: stack power (kW) vs stack current (A).

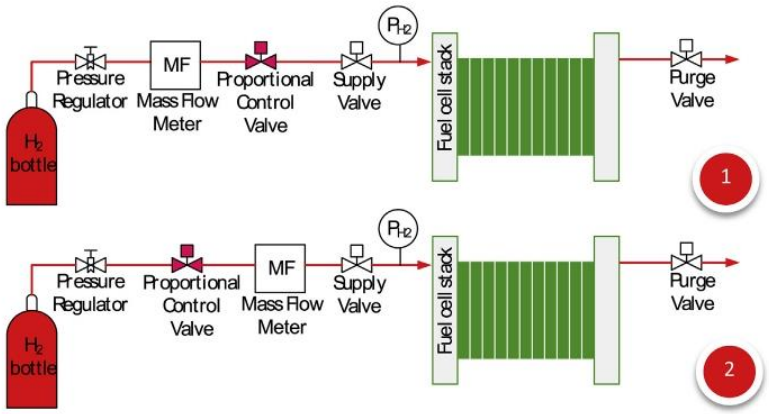

Fig. 7 – Configurations 1 and 2: Proportional control valve downstream and upstream the mass flow meter.

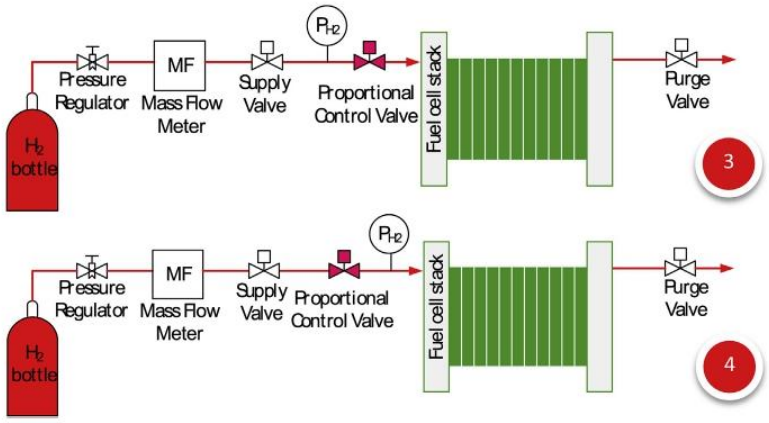

Fig. 8 – Configurations 3 and 4: Proportional control valve downstream and upstream the hydrogen pressure sensor over the fuel inlet line.

outlet hydrogen pressure can affect this performance when it comes to DEA operation.

Experimental results

Once the different configurations have been presented, they have been implemented on the test bench shown in Fig. 4. Next, experimental results obtained from each configuration will be revealed.

Configurations 1 and 2: Proportional control valve downstream and upstream the mass flow meter

In this case, the role of the proportional control valve is to establish the hydrogen input flow rate. As it has been previously commented, firstly the control valve will be placed downstream the mas flow and adjusted in the way that the hydrogen flow rate is slightly below (2) the real hydrogen flow rate (1). In this case, experimental results (Fig. 10) show that the restriction in the hydrogen input flow provokes the stack cannot provide the demanded power dropping it to zero. Notice that this restriction causes hydrogen starvation generating continuous airbags inside the fuel line and consequently leaks of hydrogen pressure. Regarding the cell structure shown in Fig. 1, in both sides of the MEA (anode and cathode), the air acts as reducing and oxidant agent, so no reaction takes place in the cell.

By against, keeping the proportional control valve downstream the mass flow meter but adjusted to allow passing more hydrogen than the real flow rate (3), experimental results (Fig. 11) show that proportional control valve is invisible in this configuration. That is, the hydrogen flow rate follows the load profile; the hydrogen pressure is keeping next to established value. Peaks on hydrogen pressure and flow coincide with hydrogen purges and air is supplied gradually more and more at time that the load current rises. Remember that the air must oxygenates and cools the stack when this is warming due to current increase. Then, we can conclude that in this configuration, proportional control valve can be

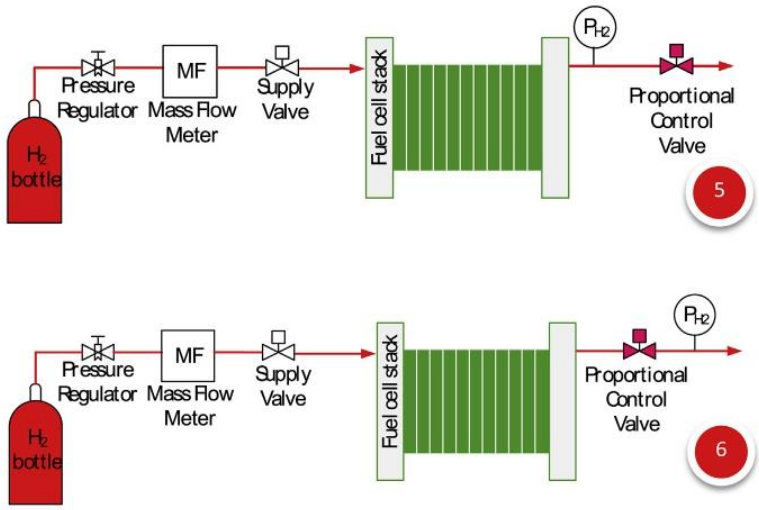

Fig. 9 – Configurations 5 and 6: Proportional control valve downstream and upstream the hydrogen pressure sensor over the fuel outlet line.

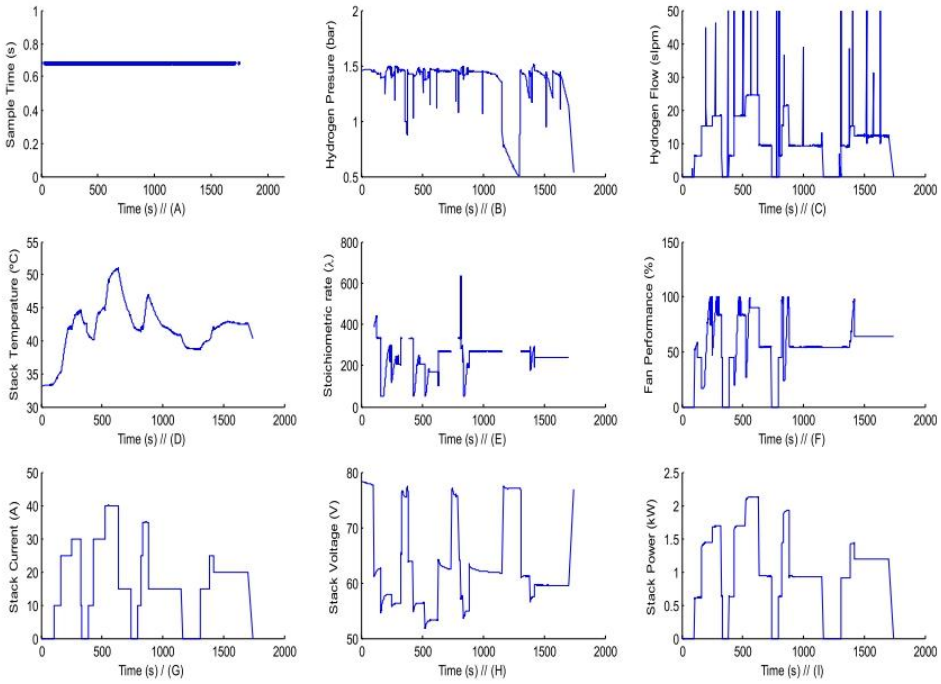

Fig. 10 – AC-PEFC performance when the proportional control valve is placed downstream the mass flow meter and adjusted slightly below. From left to right and from top to bottom: (A)-Sample Time (s), (B)-Hydrogen Pressure (bar), (C)-Hydrogen Flow (slpm), (D)-Stack Temperature (°C), (E)-Air Stoichiometric Rate (λ), (F)-Fan Performance (%), (G)-Stack Current (A), (H)-Stack Voltage (V) and (I)-Stack Power (kW).

removed from de BoP design because does not have any influence respect to system performance obtained from the original configuration shown in Fig. 4a.

Next, the proportional control valve is placed upstream the mass flow meter, and again adjusted slightly below (Fig. 12) and above (Fig. 13) the real hydrogen flow rate. When the proportional control valve is adjusted to control the input hydrogen flow slightly below, again the system stops working because of the hydrogen lack in the inlet line (Fig. 12), the hydrogen flow drops to zero and consequently the hydrogen

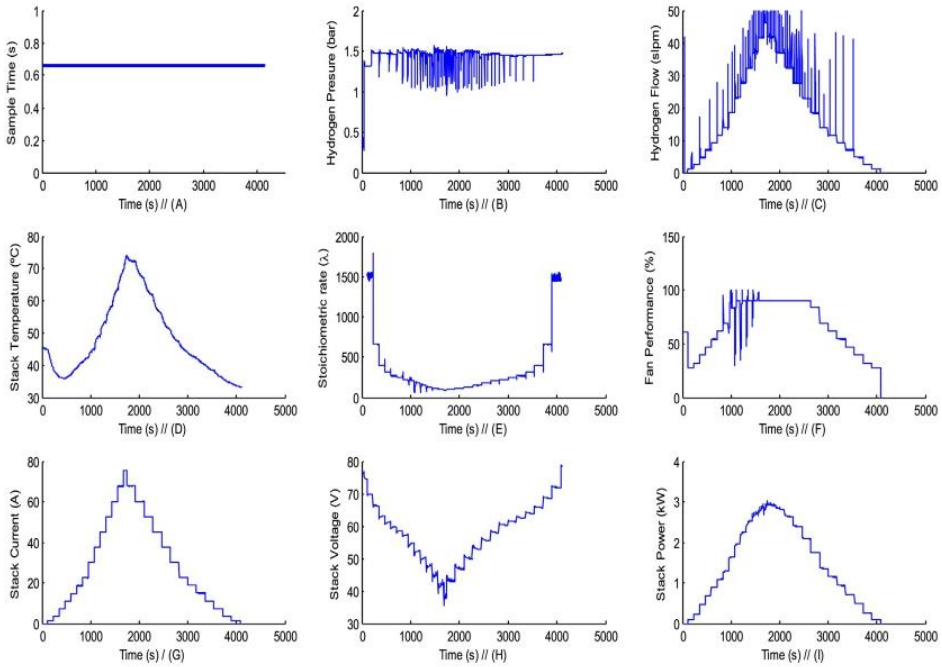

Fig. 11 – AC-PEFC performance when the proportional control valve is placed downstream the mass flow meter and adjusted slightly above. From left to right and from top to bottom: (A)-Sample Time (s), (B)-Hydrogen Pressure (bar), (C)-Hydrogen Flow (slpm), (D)-Stack Temperature (°C), (E)-Air Stoichiometric Rate (λ), (F)-Fan Performance (%), (G)-Stack Current (A), (H)-Stack Voltage (V) and (I)-Stack Power (kW).

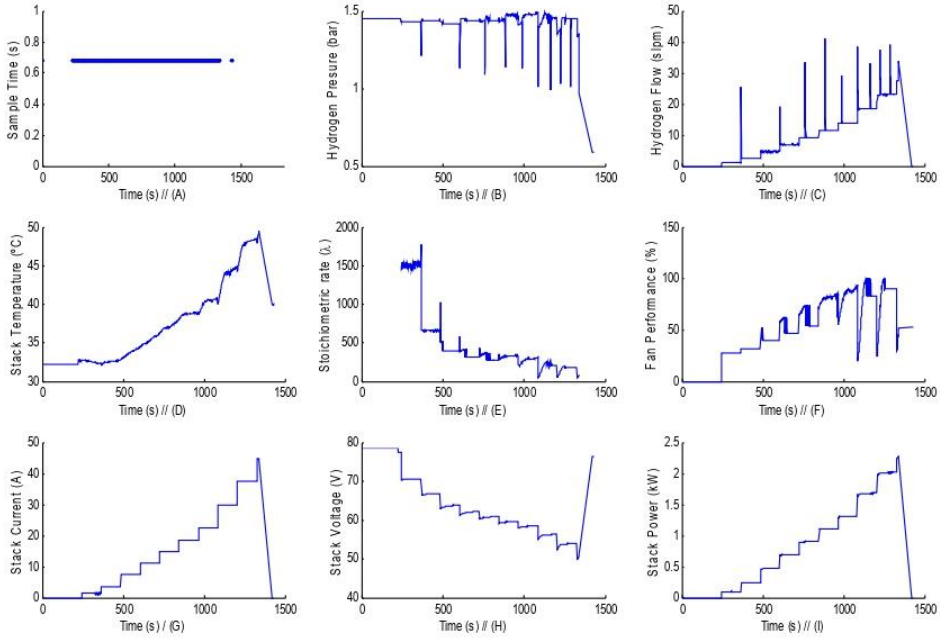

Fig. 12 – AC-PEFC system performance when the proportional control valve is placed upstream the mass flow meter and adjusted slightly below. From left to right and from top to bottom: (A)-Sample Time (s), (B)-Hydrogen Pressure (bar), (C)-Hydrogen Flow (slpm), (D)-Stack Temperature (°C), (E)-Air Stoichiometric Rate (λ), (F)-Fan Performance (%), (G)-Stack Current (A), (H)-Stack Voltage (V) and (I)-Stack Power (kW).

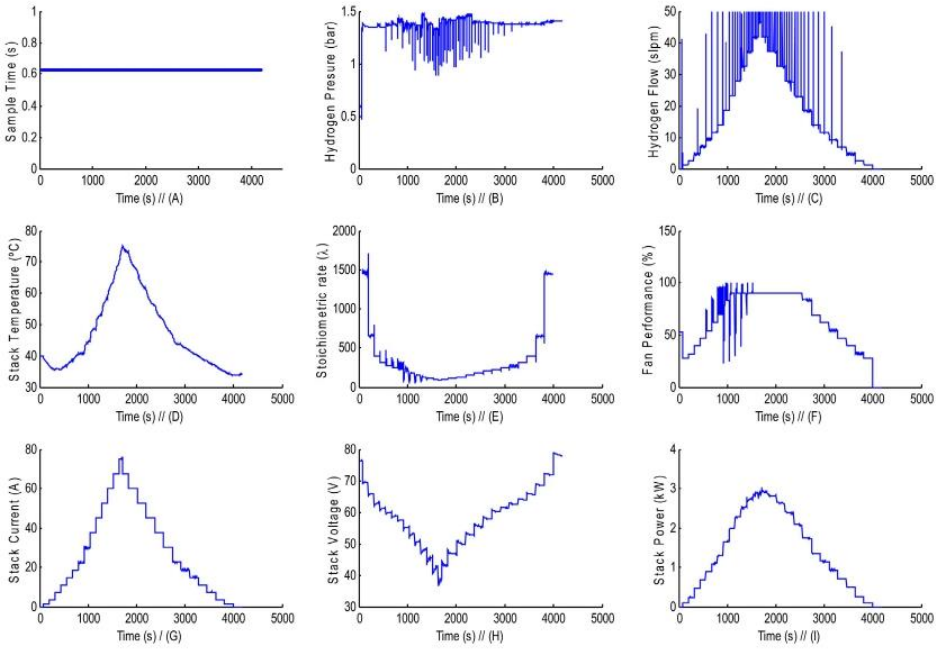

Fig. 13 – AC-PEFC system performance when the proportional control valve is placed upstream the mass flow meter and adjusted slightly above. From left to right and from top to bottom: (A)-Sample Time (s), (B)-Hydrogen Pressure (bar), (C)-Hydrogen Flow (slpm), (D)-Stack Temperature (°C), (E)-Air Stoichiometric Rate (λ), (F)-Fan Performance (%), (G)-Stack Current (A), (H)-Stack Voltage (V) and (I)-Stack Power (kW).

pressure, stack current and power as well. If the control valve is adjusted according to (3), experimental results are similar to that obtained in Fig. 11, when the valve was placed downstream the mass flow meter.

Configurations 3 and 4: Proportional control valve downstream and upstream the pressure sensor in the fuel inlet line

Putting the proportional control valve around the pressure sensor in the fuel inlet line, the goal is to control the hydrogen input pressure. When the control valve is located downstream the pressure sensor, the scheme (Fig. 8-Configuration 3) looks like the feed-forward structure. Then, the control valve tries to anticipate to perturbations in the measure. This is what precisely happens during the first load steps (Fig. 14); along the way up of the load current, as consequence of the first load step, the hydrogen flow must increase. The stack consumes more hydrogen so the hydrogen pressure falls lightly (at $t = 50$ s), and the control valve tends to be completely closed to soften the pressure drop. Then, during the following load step, as current rises again the control valve continues closed in order to accumulate hydrogen in the fuel inlet line and achieve the established pressure value. This situation is responsible for the AC-PEFC shutdown; control valve closed, hydrogen doesn't enter in the anode and no reaction happens in the fuel cell.

In the second case, experimental results show effectively the pressure average value is fixed along the length of the test (Fig. 15). But it can be observed hydrogen pressure path is far to be stable, it presents continuous peaks even more frequent and deeper than in previous configurations. This is due to inter-relation between the hydrogen purge, pressure sensor and control valve. Hydrogen purge rate is fixed at 2300 A s (manufacturer's recommendation), and during the purge the hydrogen escapes freely; so the pressure drops with the purge. Then, the pressure sensor located just above (but in the inlet line) detects the pressure drop and consequently the control valve must act to correct the deviation. The control valve action affects over the hydrogen pressure which responds with an overshoot, and just next, another purge causing another hydrogen drop. These continuous undershoots and overshoots can be observed in Fig. 15B. What is common in those suitable configurations shown up to now (Figs. 11, 13 and 15) is the hydrogen pressure peaks are more frequent in the middle of the test (around $t = 2000$ s). Obviously, according to purge rate, higher current values means purges more frequent.

Configurations 5 and 6: Proportional control valve downstream and upstream the pressure sensor in the fuel outlet line

Putting the proportional control valve around the pressure sensor in the fuel outlet line, the goal is to control the hydrogen pressure along the whole anode (from the input to the output). The first of these configurations locates the proportional control valve downstream the hydrogen pressure sensor in the fuel outlet line. This configuration shows that

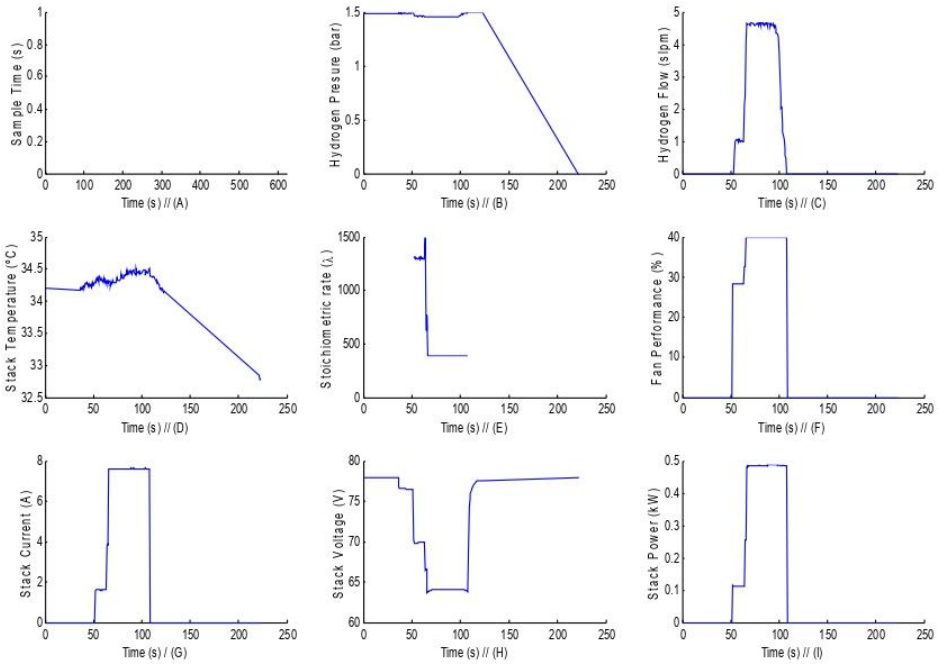

Fig. 14 – AC-PEFC system performance when the proportional control valve is placed downstream the pressure sensor in the fuel inlet line. From left to right and from top to bottom: (A)-Sample Time (s), (B)-Hydrogen Pressure (bar), (C)-Hydrogen Flow (slpm), (D)-Stack Temperature (°C), (E)-Air Stoichiometric Rate (λ), (F)-Fan Performance (%), (G)-Stack Current (A), (H)-Stack Voltage (V) and (I)-Stack Power (kW).

the PEFC system performance (Fig. 16) is similar to that obtained from Configuration 3 (Fig. 12). Again, the control valve tries to anticipate perturbations in the measure. As consequence of the increase in the load demand, the hydrogen flow must increase. The stack consumes more hydrogen, the hydrogen pressure falls and the control valve tends to be completely closed to soften the pressure drop.

However, when the proportional control valve is placed upstream the hydrogen pressure sensor in the fuel outlet line, experimental studies (Fig. 17) show that the goal is achieved: to maintain the hydrogen pressure along the whole fuel line fixed at the established value. Even more, in this case stack doesn't suffer continuous hydrogen pressure undershoots and overshoots as it happened in previous configurations. This is because now control valve acts like purge valve, but it purges hydrogen only when the hydrogen pressure begins to be deviated from the fixed value. That is hydrogen purge rate does not follow manufacturer's recommendations (2300 A s), but it depends on pressure variations. The risk of this apparent "good" configuration is that the purge rate is independent of the relation current–time. This implies inert gases are not removed properly from the anode side, leading in the long term to damage the membrane of the cells which integrate the PE stack.

Another issue which also requires attention is the hydrogen flow. As it can be observed in Fig. 17, in this case, hydrogen flow does not follow the load profile but it directly rises up to almost the maximum flow (40 slpm, see Fig. 6). As it can be observed in Fig. 17, initial pressure value is above the reference (1.48 bar vs 1.36 bar), so the control valve opens up to reduce the real value. This means to waste hydrogen, increasing the inlet flow. After that, hydrogen flow increases a little up to the highest value to allow the stack to supply the nominal power.

Finally, before moving onto the next section we would like to comment some aspects about the Oxidant/Cooling subsystem performance. As it has been commented in Section II, the main device of this subsystem is a speed adjustable fan which is responsible for providing enough air to oxygenate and cool the stack. From experimental results (Figs. 11, 13, 15 and 17), we can observe that in those viable configurations (Configuration 1, 2, 4 and 6) fan performance (speed percentage) raises at time that load current is going up to, in order to provide the air required for the stack reaction and to maintain the increasing stack temperature inside the range recommended by the manufacturer. When the fan performance is close to the maximum and the load current continues raising, the air stoichiometric rate (required air flow/total air flow) remains above the minimum recommended ($\lambda > 20$). Due to high stack temperature achieved at highest current values, the fan performance is kept at maximum even when the load current starts to drop; quick cooling process to maintain the stack temperature inside the recommended range at time that current falls.

When the stack temperature descends enough, it is not necessary to let the fan working at maximum so the fan speed is going to be reduced gradually. In the last configuration (Fig. 17), fan performance shape is slightly different to the rest;

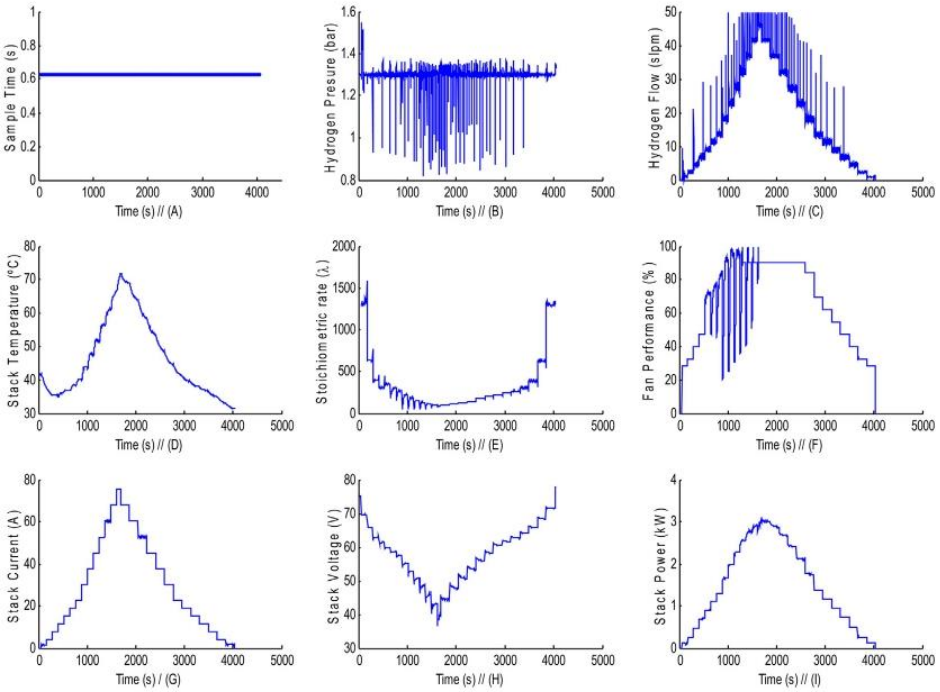

Fig. 15 – AC-PEFC system performance when the proportional control valve is placed upstream the pressure sensor in the fuel inlet line. From left to right and from top to bottom: (A)-Sample Time (s), (B)-Hydrogen Pressure (bar), (C)-Hydrogen Flow (slpm), (D)-Stack Temperature (°C), (E)-Air Stoichiometric Rate (λ), (F)-Fan Performance (%), (G)-Stack Current (A), (H)-Stack Voltage (V) and (I)-Stack Power (kW).

it does not follow the load profile. This is due precisely to load profile; in this last case maximum current value is achieved after t = 200 s, later than in previous tests. Then, before t = 200 s if load current is not too high and stack temperature is inside the range, fan does not need to be accelerate to avoid cells flooding.

Discussion

In this paper, a half-dozen of possible configurations are proposed for the Fuel subsystem in an AC-PEFC. The diagram of the Fuel subsystem includes three basic devices: a mass flow meter, a pressure sensor and a purge valve. The different configurations are obtained adding a proportional control valve locating it downstream and upstream these basic devices. All the possible configurations have been implemented over the test bench shown in Fig. 4. Experimental results show that not all configurations are suitable and not all suitable configurations show identical AC-PEFC performance.

Among configurations no suitable, we can include those where the control valve is located around the mass flow meter and it is adjusted with a mass flow equation slightly below the measured real value, both downstream and upstream (Figs. 10 and 12). This conclusion corroborates one of the hypothesis suggested at the beginning of the paper, in Section I: the hydrogen mass flow control is not suitable for the DEA operation.

Moreover, configurations no suitable are also these where the control valve is placed downstream the hydrogen sensor both in the inlet and outlet fuel line (Configurations 3 and 5). This allow us to elucidate that configurations where the set sensor + actuator keeps the feed-forward structure do not guarantee neither pressure control nor proper stack performance.

By contrast, within the group of suitable configurations we can include all those which do not imply restrictions in the hydrogen mass flow, and all these where the hydrogen pressure is controlled with the set actuator + sensor (similar to a feed-back structure), configurations 1, 2, 4 and 6. Among these last configurations, hydrogen flow differs from one to another. This depends on the way to realise the pressure control and hydrogen purge. When the hydrogen pressure is controlled in the fuel inlet line and the purge rate is adjusted following the manufacturer's recommendations, the hydrogen consumption is optimised and we can observe how the hydrogen flow profile seems the load current profile (Figs. 11, 13 and 15). By contrast, when the hydrogen pressure is controlled in the fuel outlet line and the hydrogen purge depends on the pressure deviations, the hydrogen flow rises (Fig. 17), reducing the AC-PEFC efficiency (considering efficiency as the ratio between the electrical energy provided by the stack and the hydrogen supplied to stack).

Finally, these last configurations also differs in the way the hydrogen pressure responds along the time. In case the hydrogen pressure is controlled in the fuel inlet line, the

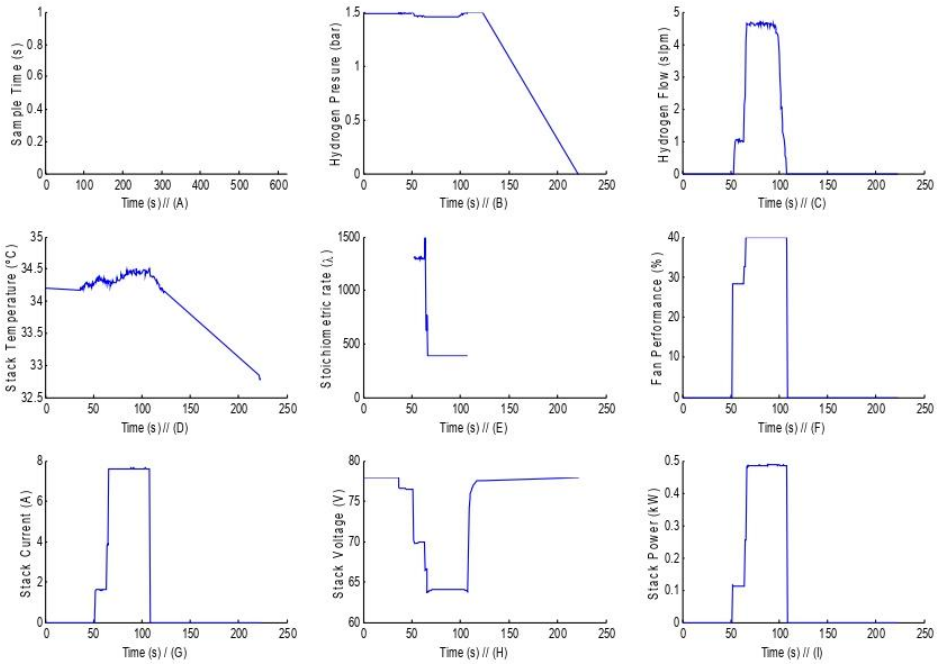

Fig. 16 – AC-PEFC system performance when the proportional control valve is placed downstream the pressure sensor in the fuel outlet line. From left to right and from top to bottom: (A)-Sample Time (s), (B)-Hydrogen Pressure (bar), (C)-Hydrogen Flow (slpm), (D)-Stack Temperature (°C), (E)-Air Stoichiometric Rate (λ), (F)-Fan Performance (%), (G)-Stack Current (A), (H)-Stack Voltage (V) and (I)-Stack Power (kW).

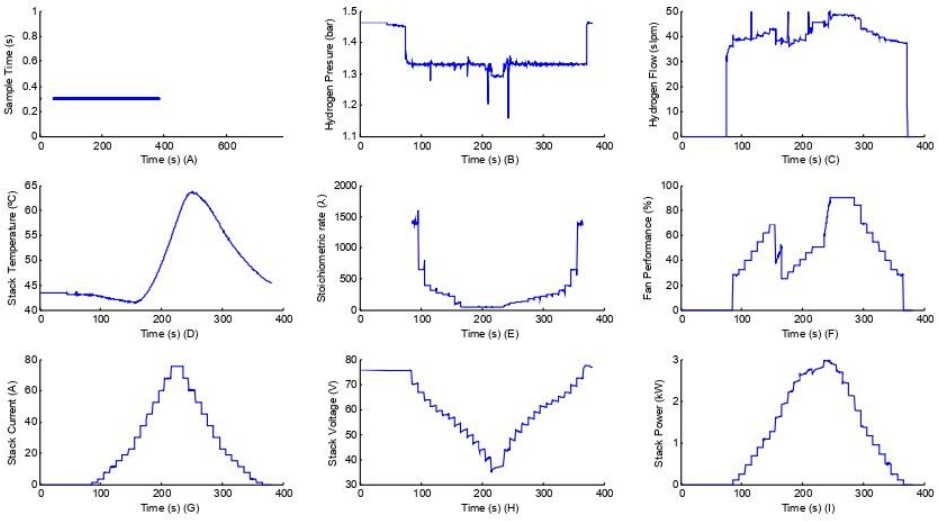

Fig. 17 – AC-PEFC system performance when the proportional control valve is placed upstream the pressure sensor in the fuel outlet line. From left to right and from top to bottom: (A)-Sample Time (s), (B)-Hydrogen Pressure (bar), (C)-Hydrogen Flow (slpm), (D)-Stack Temperature (°C), (E)-Air Stoichiometric Rate (λ), (F)-Fan Performance (%), (G)-Stack Current (A), (H)-Stack Voltage (V) and (I)-Stack Power (kW).

hydrogen purge follows the established rate; the pressure suffers continuous peaks derived from the purge rate and the action of the control valve. But in case the hydrogen pressure is controlled in the fuel outlet line, the hydrogen pressure evolution is a flat line, excepting some peaks derived from the pressure drops due to high power demand.

Table 1 summarises the main characteristics of the configurations analysed in this paper regarding aspects like

INTERNATIONAL JOURNAL OF HYDROGEN ENERGY 42 (2017) 12841–12855

Table 1 – Summary of analysed configurations.

# Configuration	Structure	Variable to control	Suitable	Stable Hydrogen pressure	Reduced Hydrogen consumption	Inert Gases Removed	Efficiency
1a	Control valve downstream the mass flow 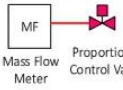	$\dot{M}_{H2}$	✗				
1b	Control valve downstream the mass flow meter, adjusted slightly above 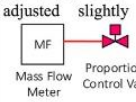	$\dot{M}_{H2}$	✓	✗	✓	✓	✓
2a	Control valve upstream the mass flow meter, adjusted slightly below 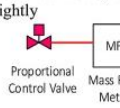	$\dot{M}_{H2}$	✗				
2b	Control valve upstream the mass flow meter, adjusted slightly above 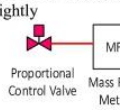	$\dot{M}_{H2}$	✓	✗	✓	✓	✓
3	Control valve downstream the pressure sensor in the fuel inlet line 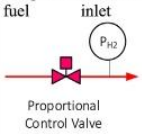	P_{H2}	✗				
4	Control valve upstream the pressure sensor in the fuel inlet line 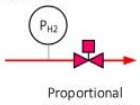	P_{H2}	✓	✗	✓	✓	✓
5	Control valve downstream the pressure sensor in the fuel outlet line 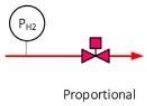	P_{H2}	✗				
6	Control valve upstream the pressure sensor in the fuel outlet line 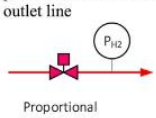	P_{H2}	✓	✓	✗	✗	✗

ability to maintain stable the hydrogen pressure, hydrogen consumption, possibility to remove inert gases as frequent as manufacturer recommends, AC-PEFC efficiency (refereeing provided electrical power respect to hydrogen consumption) and definitely the suitability of the proposed configurations.

Conclusions

This paper presents a comprehensive experimental analysis of six possible configurations of the Fuel subsystem in an AC-PEFC. It has been justified that studies in which the Fuel subsystem is investigated are hard to find on the scientific literature. It seems like the Fuel subsystem configuration would not have influence over the whole system performance. Contrary to what one might think, and in basis on experimental results, this paper has shown how the AC-PEFC performance is conditioned by the Fuel subsystem configuration.

To carry out the study, the AC-PEFC has been previously characterised in a test bench developed by authors.

After that, different Fuel subsystem configurations have been analysed in basis on the AC-PEFC response.

Regarding experimental results, we can assert that Fuel subsystem configurations where the hydrogen mass flow is restricted, even if the mass flow rate is slightly below the real mass flow, are not suitable.

Within the group of suitable configurations are those that do not involve restrictions in the hydrogen mass flow, and all these where the hydrogen pressure is controlled with the set actuator + sensor (feed-back structure).

Moreover, within these last configurations, hydrogen flow response depends on the way to realise the pressure control and hydrogen purge. When the hydrogen pressure is controlled in the fuel inlet line, the purge rate can follows the manufacturer's recommendations and the hydrogen consumption is optimised seeming the load current profile. In case the hydrogen pressure is controlled in the fuel outlet line, the hydrogen purge only happens when there are deviations in the pressure measure. And this causes the hydrogen flow rises.

As conclusion we can say that in an AC-PEFC with DEA operation mode there is not a specific configuration of the Fuel subsystem which could be called the "best configuration". As it has been demonstrated, each configuration has its own advantages. Then for example, if we expect to have a precise control of the pressure in the hydrogen line, the best option is to control the hydrogen pressure in the outlet line and hydrogen will be only purged when pressure measure varies from the reference value. However, if we want to obey manufacturer's recommendations in relation to purge rate (guaranteeing the inert gases removing), and optimise the hydrogen flow consumption, hydrogen pressure will suffer continues peaks derived from the periodic purges.

Finally, main characteristics of analysed configurations have been summarised in Table 1, making easier to compare them for an overview before to implement the BoP of an AC-PEFC.

REFERENCES

[1] Mehta V, Cooper JS. Review and analysis of PEM fuel cell design and manufacturing. J Power Sources 2003;114:32–53.

[2] Sammes N. Fuel cell technology: reaching towards commercialization. Springer Sci Bus Media 2006. ISBN 13: 978-1-85233-974-6.

[3] Faghri BSM. Transport phenomena in fuel cells, vol. 19. WIT Press; 2005.

[4] Siegel C. Review of computational heat and mass transfer modeling in polymer-electrolyte-membrane (PEM) fuel cells. Energy 2008;33:1331–52.

[5] Varigonda S, Kamat M. Control of stationary and transportation fuel cell systems: progress and opportunities. Comput Chem Eng Sep. 2006;30(10–12):1735–48.

[6] Vasallo MJ, Bravo JM, Andújar JM. Optimal sizing for UPS systems based on batteries and/or fuel cell. Appl Energy 2013;105:170–81.

[7] Segura F, Durán E, Andújar JM. Design, building and testing of a stand alone fuel cell hybrid system. J Power Sources 2009;193:276–84.

[8] Özgirgin E, Devrim Y, Albostan A. Modeling and simulation of a hybrid photovoltaic (PV) module-electrolyzer-PEM fuel cell system for micro-cogeneration applications. Int J Hydrogen Energy October 2015;40:15336–42.

[9] Nguyen HQ, Aris AM, Shabani B. PEM fuel cell heat recovery for preheating inlet air in standalone solar-hydrogen systems for telecommunication applications: an exergy analysis. Int J Hydrogen Energy October 2016;41:2987–3003.

[10] Lui JX, Laghrouche S, Ahmed F-S, Wack M. PEM fuel cell air-feed system observer design for automotive applications: an adaptive numerical differentiation approach. Int J Hydrogen Energy 2014;39(30):17210–21.

[11] Zhang J, Xie Z, Zhang J, Tang Y, Song C, Navessin T, et al. High temperature PEM fuel cells. J Power Sources 2006;160:872–91.

[12] Zhang G, Kandlikar SG. A critical review of cooling techniques in proton exchange membrane fuel cell stacks. Int J Hydrogen Energy 2012;37(3):2412–29.

[13] Wang Y-X, Xuan D-J, Kim Y-B. Design and experimental implementation of time delay control for air supply in a polymer electrolyte membrane fuel cell system. Int J Hydrogen Energy Oct. 2013;38(30):13381–92.

[14] Cordner M, Matian M, Offer GJ, Hanten T, Spofforth-Jones E, Tippetts S, et al. Designing, building, testing and racing a low-cost fuel cell range extender for a motorsport application. J Power Sources 2010;195(23):7838–48.

[15] Ahn JW, Choe SY. Coolant controls of a PEM fuel cell system. J Power Sources 2008;179:252–64.

[16] Han HS, Cho C, Kim SY, Hyun JM. Performance evaluation of a polymer electrolyte membrane fuel cell system for powering portable freezer. Appl Energy 2013;105:125–37.

[17] Segura F, Andújar JM. Step by step development of a real fuel cell system. Design, implementation, control and monitoring. Int J Hydrogen Energy 2015;40(15):5496–508.

[18] Philipps F, Simons G, Schiefer K. Dynamic investigation of PEFC stacks in interaction with the air supply system. J Power Sources Mar. 2006;154(2):412–9.

[19] Kim Y-B. Improving dynamic performance of proton-exchange membrane fuel cell system using time delay control. J Power Sources 2010;195(19):6329–41.

[20] Himanen O, Hottinen T, Tuurala S. Operation of a planar free-breathing PEMFC in a dead-end mode. Electrochem Commun 2007;9:891–4.

[21] Eckl R, Zehtner W, Leu C, Wagner U. Experimental analysis of water management in a self-humidifying polymer electrolyte fuel cell stack. J Power Sources 2004;138:137–44.
[22] del Real AJ, Arce A, Bordons C. Development and experimental validation of a PEM fuel cell dynamic model. J Power Sources 2007;173:310–24.
[23] Hwang JJ, Zou ML. Development of a proton exchange membrane fuel cell cogeneration system. J Power Sources 2010;195:2579–85.
[24] Gerbec M, Jovan V, Petrovčič J. Operational and safety analyses of a commercial PEMFC system. Int J Hydrogen Energy 2008;33:4147–60.
[25] Soupremanien U, Le Person S, Favre-Marinet M, Bultel Y. Tools for designing the cooling system of a proton exchange membrane fuel cell. Appl Therm Eng 2012;40:161–73.
[26] Marcinkoski J, James BD, Kalinoski JA, Podolski W, Benjamin T, Kopasz J. Manufacturing process assumptions used in fuel cell system cost analyses. J Power Sources 2011;196(12):5282–92.
[27] Na Y, Suh J, Song I, Choi K-H, Choi H, Kim KB, Park J-Y. Stable operation of air-blowing direct methanol fuel cell stacks through uniform oxidant supply by varying fluid flow fixtures and developing the flow sensor. Int J Hydrogen Energy 2011;36(15):9205–15.
[28] Kim BJ, Kim MS. Studies on the cathode humidification by exhaust gas recirculation for PEM fuel cell. Int J Hydrogen Energy 2012;37(5):4290–9.
[29] Hinaje M, Rael S, Caron JP, Davat B. An innovating application of PEM fuel cell: current source controlled by hydrogen supply. Int J Hydrogen Energy 2012;37(17):12481–8.
[30] Rodatz P, Tsukada A, Mladek M, Guzzella L. Efficiency improvements by pulsed hydrogen supply in PEM fuel cell systems. World Congr 2002;15(1):1509.
[31] Chen J, Siegel JB, Stefanopoulou AG, Waldecker JR. Optimization of purge cycle for dead-ended anode fuel cell operation. Int J Hydrogen Energy Apr. 2013;38(12):5092–105.
[32] Fuel cell stack product manual and integration guide. 2011.
[33] Antoni L. FCTESTNET/FCTESQA PEFC power stack performance testing procedure I. Polarisation curve test method. 2009.
[34] Hou J. A study on polarization hysteresis in PEM fuel cells by galvanostatic step sweep. Int J Hydrogen Energy 2011;36(12):7199–206.

6.4. Contribution 4

Air-cooled fuel cells: Keys to design and build the oxidant/cooling system

A. De las Heras, F.J. Vivas, F. Segura, M.J. Redondo, J.M. Andújar

Published in:

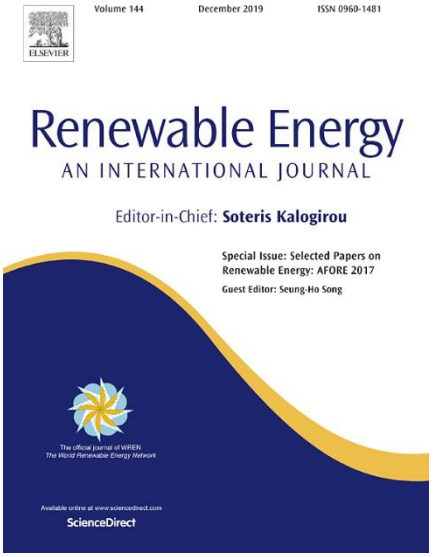

Journal: Renewable Energy
Editorial: ELSEVIER
Editor-in-Chief: Soteris Kalogirou
Reference: Vol. 125, pp. 1-20
Year: 2018
ISSN: 0960-1481
DOI 10.1016/j.renene.2018.02.077

Category	Journal Rank / Total journals	Quartile
Energy & Fuels	17 / 103	Q1
Green & sustainability science & technology	7 / 35	Q1
Impact Factor (2018)	5.439	
Citations	9	

Renewable Energy 125 (2018) 1–20

Contents lists available at ScienceDirect

Renewable Energy

journal homepage: www.elsevier.com/locate/renene

Air-cooled fuel cells: Keys to design and build the oxidant/cooling system

A. De las Heras*, F.J. Vivas, F. Segura, M.J. Redondo, J.M. Andújar

Grupo de Investigación de Control y Robótica TEP-192, Departamento de Ingeniería Electrónica, de Sistemas Informáticos y Automática, Escuela Técnica Superior de Ingeniería, Universidad de Huelva.Carretera Huelva, Palos de la Frontera, 21819, La Rábida, Palos de la Frontera, Huelva, Spain

ARTICLE INFO

Article history:
Available online 19 February 2018

Keywords:
Air cooled polymer electrolyte fuel cell
BoP configurations
Oxidant/cooling subsystem design
Experimental study
Performance improvement

ABSTRACT

In the field of energy, hydrogen as an energetic vector is becoming increasingly important. Specifically, fuel cells powered by hydrogen are becoming an alternative in automotive and other fields because of their ability to produce electricity without any pollution. Therefore, at this time there is a very active research field. A fuel cell can be described as a scale down industrial plant that consists of different subsystems whose purpose is to make the stack works properly. Air Cooled Polymer Electrolyte Fuel Cells (AC-PEFC) are receiving special attention due to their potential to integrate the oxidant and cooling subsystems into one, which in term gives the fuel cells their capability to reduce its weight, volume, cost and control complexity. In these fuel cells, the Oxidant/Cooling subsystem is of crucial importance and along with three others (*Fuel*, *Electrical* and *Control* subsystems) make up the Balance of Plant (BoP), which together with the stack comprise the full fuel cell system. The aim of this paper is to present a comprehensive experimental study of an AC-PEFC paying particular attention to the Oxidant/Cooling subsystem configuration. According to the scientific literature, this subsystem has not received the same attention as other subsystems like the *Fuel* and *Control* subsystems. However, a suitable design and size is critical for the proper functioning of the stack. The analysis carried out in this paper tries to solve some problems that can appear if the design of the Oxidant/Cooling subsystem has not been optimized. These problems are related to important aspects such as the performance and the efficiency of the whole system and temperature distribution over the stack.

1. Introduction

Polymer Electrolyte Fuel Cells (PEFCs) are a promising technology to produce electricity from hydrogen for stationary power generation due to its operational strength such as high power density, low operating temperature, low corrosion, quiet operation, stack design simplification, relatively quick start up and shut down and especially by its zero emission capability [1–4]. In the past decades, there has been a huge progress in the PEFC field but researchers are still focused on new cell designs, cost reduction and performance improvement. PEFC technology is having more and more importance because it is suitable for a wide range of applications, including portable, stationary and automotive power delivery [5–8] and lately it is being more used in backup systems for emergency situations (e.g. earthquakes, terrorist attacks). Configuration or hybridization of generation systems around the PEFC can be miscellaneous [6] [7,9], as well as its control modes [10].

For the configuration of a PEFC system, apart from the stack it is necessary to include additional subsystems for the proper system operation. Generally these systems can be divided into five main groups which form the Balance of Plant (BoP): 1- Oxidant subsystem: it supplies air/oxygen at the appropriate conditions for the oxidant reaction, 2-Fuel subsystem: it supplies hydrogen at the appropriate conditions for the reduction reaction, 3-Cooling subsystem: it removes the heat produced in the stack and keeps it at the temperature recommended by the manufacturer and removes the water produced, 4-Electrical subsystem: it connects the stack to electric load, and 5-Control subsystem: it processes information from sensors so as to control the actuators, Fig. 1 [11–13].

When it comes to develop a PEFC system, researchers conclude that an appropriate design of the BoP is essential to the proper PEFC stack operation and influences on the performance of the whole system. Therefore, according to the BoP design, it is important to

* Corresponding author.
E-mail address: ainhoa.delasherasjimenez@gmail.com (A. De las Heras).

https://doi.org/10.1016/j.renene.2018.02.077
0960-1481/

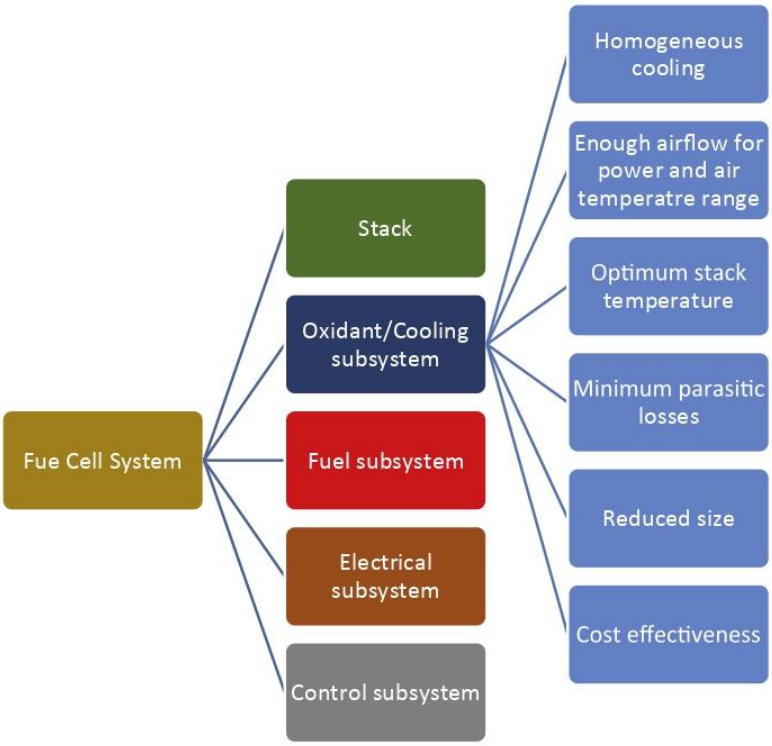

Fig. 1. Conceptual scheme of an AC-PEFC system and challenges in the design and manufacture of the oxidant/cooling subsystem.

optimize the main subsystems avoiding an oversized BoP configuration which usually results in an increase of parasitic losses, system volume, weight and noise level [14].

While the PEFC is operating, the stack temperature changes along the time and with the load demand. The temperature has influence on electrochemical reaction rate and water and reactant transport. Low temperatures might produce membrane flooding and because of that, it might appear operating problems due to membrane resistivity variation. Otherwise, high temperatures might produce membrane thermal stress and cathode catalyst inactivity, resulting in membrane degradation. In basis on this, we can deduce that the Cooling subsystem plays an important role for reliable and efficient stack operation, besides the few papers found in the scientific literature focused in this question [13].

In this work, authors we develop the experimental study using an Air Cooled Polymer Electrolyte (AC-PE) stack. This kind of stacks integrates Oxidant and Cooling subsystems into one single avoiding the liquid parts in the Cooling subsystem. This results in facilitating and simplifying the BoP integration because they do not need pipes, valves, pumps and heat exchangers, contributing to reduce weight, volume and cost. Apart from this, the stack used in this work does not require high inlet hydrogen pressure (it can operate near ambient pressure) and this provides security because it is not necessary to operate with high hydrogen supply pressures and less stringent requirements in the hydrogen transfer circuit (connections, pipelines, etc.).

The implementation of the Oxidant/Cooling subsystem is commonly based on a forced-air convection design with one or several fans. This design requires especial consideration of the stack characteristic curves and the fan/s. Ideally, the operating point intersection between the stack and the fan characteristic curves should be located in the optimal operating region of the fan; and be sufficiently far away from any unstable region [15].

Different BoP configurations have been developed in several works [13,16–25], and the chosen configuration is justified in basis on the required particular conditions by the authors. However, there are not too many works in which different configurations are analysed, discussing their advantages and disadvantages. Thus, Kim et al. [26] show two types of Oxidant/Cooling subsystems (a gas recirculation subsystem with and without a recycle blower). Sasmito et al. [15] present a model in which the results indicate that some factors such as fan power and type, single fan or fans in series, stack length, and separate air-coolant channels have a significant impact on the operating point and the stack performance. Meyer et al. [27] point out that in an cathode AC-PEFC, the air blowers present the largest parasitic load having a direct influence on the stack performance and its temperature.

Based on the bibliography consulted to establish the state of the art of this paper and in our own experience of more than 10 years dealing with PEFCs, we can set six challenges in the design and manufacture of the oxidant/cooling subsystem (Fig. 1): 1) To be able to cool the stack homogeneously, 2) To provide sufficient airflow range to control the PEFC temperature, under a range of power and room/coolant air temperature, 3) To place the stack at optimum temperature, 4) To reduce the auxiliary power consumption, 5) To do all this within a certain sized box, and finally but not least important 6) To do it cost effectively.

In this paper, authors try to expand the current experimental studies published in the scientific literature, and they present a detailed experimental analysis of three different configurations for the Oxidant/Cooling subsystem in an AC-PEFC.

Our study departs from one configuration based on the own

stack's manufacturer proposal. From here, we raise two new configurations to enhance the initial, including different ways of controlling the fan/s contained within the configurations. As it has been reported in previous works [27], the operating performance of this class of PEFCs is conditioned by the coolant air-flow rate, because both the air flow and the room air temperature determine the operating temperature of a given air-cooled fuel cell, at a certain power output. Then the study developed in this paper allow us to analysis what configuration guarantees a better system performance, attending to those six challenges presented in Fig. 1, at time that the stack achieves the highest power working inside its operating temperature range and air stoichiometric rate. Moreover, this experimental study will show us what configuration requires a lowest number of devices or the most complex control system. Additionally, once the best configuration has been identified, it has been checked at different room temperatures to prove it guarantees the oxidant/cooling requirements by the stack.

The structure of the paper is as follow: Section 2 exposes the main features of the test bench developed by authors and used during all the experimental tests. Section 3 presents the proposed Oxidant/Cooling subsystem designs, pointing out the particularities of each one. Next, experimental results obtained from each configuration as well as some discussions about them are summarised in Section IV and V respectively. Finally, Section 6 draws the main conclusions derived from the experimental study.

2. Materials and methods

The test bench for this study (an AC-PEFC system) has been design and built around an air-cooled FCgen-1200ACS stack model from Ballard®, Fig. 2. Additionally, Table 1 summarizes the stack experimental parameters.

The used stack does not need external air humidification and it has a dead-end operation mode; it is used with dry hydrogen without humidification as well. The inlet hydrogen pressure can be varied from 1.16 to 1.56 bars. The stack is made up by 80 cells and it can reach up to 3.4 kW, according to manufacturer's data [28,29]. This stack has been integrated with a BoP configuration developed by authors according to [16]; the instrumentation specifications can be accessed in Table 2. The system shown in Fig. 2 presents a handy test bench to carry out all kinds of tests on a medium power

Table 1
Stack experimental parameters.

Variable	Definition	Range
V_{cell} (V)	Cell Voltage	0.647–1.005
I_S (A)	Stack Current	0–75
T_{opt} (°C)	Optimal Operating Temperature	26.01–65.76
T_S (°C)	Stack Temperature	6–75
T_{in} (°C)	Inlet Air Temperature	10–40
Q_{stack} (slpm)	Stack Required Air flow	0–18656.63
Q_{cell} (slpm)	Cell Required Air Flow	0–237.20
q_{cell} (W)	Heat Produced by Cell	0–45.56
E (V)	Max. Cell Voltage product water vapor	1.2545
λ	Inlet Air Flow/Consumed Air Flow	20–200
C (slpm) slpm/A*cell	Air Cell Consumption	0.0167
n_{cell}	Number of cells	80
RH/%	Relative Humidity	5–100
P_{H2} (kPa)	Inlet Hydrogen Pressure	116–156

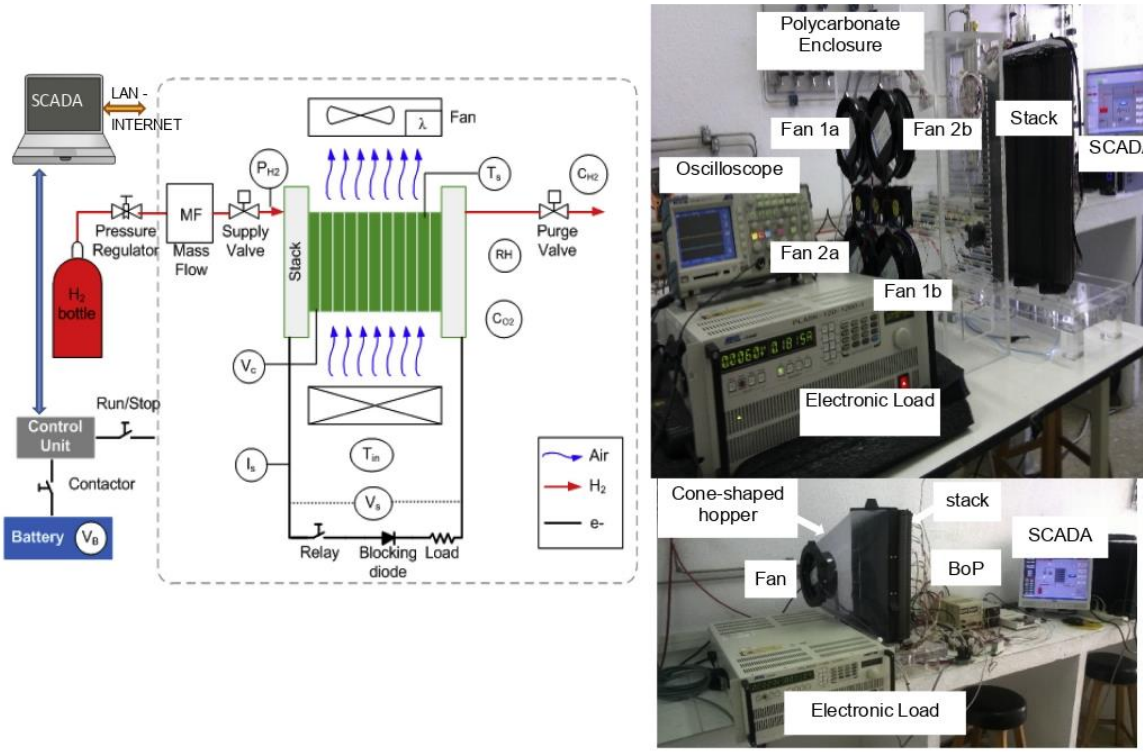

a) Test bench diagram. b) Up and c) Down. Oxidant/Cooling subsystem configurations.

Fig. 2. Diagram and real implementation of the test bench for AC-PEFCs.

Table 2
Instrumentation specifications.

Component	Manufacturer-Model	Quantity
Fuel cell stack	Ballard-FCS1020ACS	1
Oxidant/Cooling Subsystem		
Fan	Embpast-6224TD (Configuration 1 and 2)	4
	Embpast-6224TDA (Configuration 3)	1
Inlet air temperature sensor	Burkert-8400 Accuracy ± 1.5%	1
Fuel cell temperature sensor	Maruta P/N NCP15WF104F03RC Accuracy ± 1%	Included in stack
Oxigen sensor	Figaro-KE50, Accuracy ± 1%	1
Fuel Subsystem		
Valve supply	Burkert-6013	1
Purge valve	Burkert-6606	1
Pressure sensor	Burkert-8314, Accuracy ± 0.3%	1
Hydrogen sensor	Figaro-FCM6812, Accuracy ± 0.2%	1
Electrical Subsystem		
Current sensor	LEM LA 55-P, Accuracy ± 0.9%	1
Stack voltage sensor	LEM-LV 25-P, Accuracy ± 0.8%	
Bloking diode	Vishay-T85HFL	1
Relay	Panasonic-AEV18012	1
Control system		
Microprocessor	Arduino ATMega256	1
Battery	Exide-GF 12 094 Y	1

real AC-PEFCs [16].

Paying special attention to the Oxidant/Cooling subsystem (blue line in Fig. 2a), it includes an adjustable flow fan, an inlet air temperature sensor (T_{in}), and a stack temperature sensor (Ts) built-in the own stack. The manufacturer only includes a stack temperature sensor in the own stack and thermographies of the stack are not facilitated in the manuals. The air stoichiometric coefficient (λ) must be adjusted by the control unit to optimize the system performance. Additionally, a concentration oxygen sensor (C_{O2}) is included to prevent low concentrations of oxygen in the surrounding atmosphere, and a relative humidity sensor (RH) to avoid operating under overly dry room conditions.

Following Fig. 2a, at the fuel input, the Fuel subsystem (red line) is composed by the hydrogen storage bottle, and a manual pressure regulator to reduce the high pressure from the bottle up to the pressure range recommended by the manufacturer's data. In addition it is available a mass flow meter to measure the hydrogen consumption, a supply valve to control the hydrogen entry and a hydrogen pressure sensor (P_{H2}) to measure the inlet anode pressure forming the hydrogen input line. In the hydrogen outlet, although the used stack for tests is designed for dead-ended operation, that is all the fuel enters the anode is used up (fuel stoichiometry: 1), in practice water vapor, nitrogen and other inert gases can be collected in the anode, so this side must be purged periodically. For this reason, a purge valve avoids the accumulation of inert gases for a proper operation of the system and to prevent unsafe room conditions. Finally, a concentration hydrogen sensor (C_{H2}) has been included.

The Electrical subsystem (black line in Fig. 2a) comprises a stack current sensor (Is), stack voltage sensor (Vs) and a cells voltage measurement system (Vc). Additionally, a relay is added to isolate the fuel cell system from the electronic load and a blocking diode to avoid reversal currents.

In addition to the above elements and in order to make all test bench subsystems works properly, with the aim to get the best performance of the stack, a control unit has been developed. It takes care of receiving all the information from sensors and decides what to do every moment: to open the supply valve, to open the purge valve, to run the fan, to connect or disconnect the electrical load, and so on.

On the other hand, it is necessary to note that the system does not produce electricity instantaneously, even more during the start-up the stack can't provide electrical power but the BoP needs to be supply. Therefore, an auxiliary source needed to guarantee the electrical supply to BoP. This is the role of the battery shown in Fig. 2a, where the battery voltage sensor V_B warns of its state.

At this point, it is very important to mention that the management of the test bench requires a complex control system. To this end, a supervisory control and data acquisition (SCADA) has been developed. Its function is to carry out the high-level supervisory management of the test bench. It is hosted in a PC and it is provided with a data network connection for remote management, as well as graphical user interfaces. It can also manage others peripheral devices (PIDs, sensors, actuators and so on) by the control unit (see Fig. 2a). This means that, by the SCADA, we can have absolute control of the test bench as well as process all its information.

Fig. 2b and c represent the real configurations of the test bench where this experimental study will be carried out. These configurations are the result of a design analysis which will be discussed below.

Finally, to conclude this section, we must mention that the thermographies shown in this paper has been made with a TESTO® 875-1i camera, with a matrix of 120 × 160 sensors and a thermal resolution (NETD) < 50 mK. Temperature range: −30 °C to +100 °C.

3. Oxidant/cooling subsystem designs

Now, after the explanation in the previous section of the features of the test bench (AC-PEFC system), different Oxidant/Cooling subsystem architectures will be designed and built. Taking into account the manufacturer's recommendation, uniform flow rate is achieved by using fans to pull air through the stack instead of mounting fans at the air inlet and blowing air through the stack. This allows the negative pressure zone created at the air outlet will act to distribute airflow evenly through the stack, eluding the flooding phenomena [29]. With this way of working of the fans, it is assumed that the phenomenon of flooding will not appear, because the supplied air is sufficient to avoid it. The configuration of each one are the following:

- Configuration 1: Four fans covering the cathode area of the stack working two by two without flow control.
- Configuration 2: Four fans covering the cathode area of the stack working two by two with flow control.
- Configuration 3: One single speed controlled fan.

For configurations 1 and 2, with 4 fans (Fig. 2b), authors have proposed their designs in basis on stack's manufacturer recommendations [28,29]. Manufacturer advices to use one single fan for stack sizes of 45 cells or less (Fig. 3a), and two fans in other case (remember that the stack under study has 80 cells). For stack sizes higher than 45 cells the diagram for the fans stand proposed by manufacturer is shown in Fig. 3b, standard configuration, [29]. Then according to these recommended designs, authors have minimally changed it with the aim to improve the Oxidant/Cooling subsystem that is the stack air-breathing system. Putting four fans instead of two, a higher coverage of the stack cathode is guaranteed so the air can arrive at the cells located both at the top and bottom, and at the ends rightmost and leftmost of each cell. This can be seen in Fig. 2b and it has been built over a polycarbonate rectangular-shaped enclosure. The fans selection has been done in basis on the air stoichiometric requirements of the stack [15,16] and they correspond to fan model EbmPapst® DV6224TD. This enclosure has been used to stand the four fans that integrate the Oxidant/Cooling subsystem.

Regarding configuration 3 with only a fan, the aim of the authors has been to improve the air breathing of the stack and its temperature distribution over the cathode. This third configuration tries to sort out the problem observed in configurations 1 and 2: the air follow preferential paths surrounding the stack instead of crossing it for its cooling.

To carry out the configuration 3, a cone-shaped hopper has been designed and built. This additional tool allows to canalise the air flow in the best homogeneous way as possible (Fig. 2c), forcing the air to blow through the stack instead of surrounding it. Additionally, it has been put properly around the stack without leaving any space between the stack and the hopper avoiding preferential paths of the air flow.

The homogeneous flow is got minimizing the turbulence which will occur in the exit of the flow adapter. To select the high of the hopper (distance between the stack and the fan), authors have compared three possible distances: 20 cm, 25 cm and 30 cm. Experimental results obtained from the three cases are practically the same.

The fan selection has been done in basis on the air stoichiometric requirements of the stack [15,16], and it consists on the adjustable flow fan model EbmPapst® DV6224TDA. The chosen fan is capable of withstanding the maximum pressure drop and supplying the maximum air flow required by system [30].

In summary, regarding to the first two configurations, the third presents two changes to try to enhance the Oxidant/Cooling subsystem. The first change is it uses one single fan instead of four, simplifying the design, minimizing the BoP cost and weight and reducing the auxiliary power consumption and the control complexity. The second change is to use a flow adapter (cone-shaped hopper) instead of a rectangular-shaped enclosure avoiding preferential paths.

Figs. 4–6 represent in schematic form the mode of operation for each of the configurations. In Fig. 4 (configuration 1) the four fans are divided into two groups (GROUP 1-fans in blue line and GROUP 2-fans in orange line). The first group of fans is always working when the fuel cell system is operating and the second group of fans starts to work in case of the stack temperature is higher than the optimal temperature value. The optimal temperature value depends on the operating point in which the stack is operating and according to manufacturer data [28,29].

Fig. 5 represents the second configuration, which is similar to the first one (the actual assembly is again Fig. 2b) but in this case, both groups of fans will be controlled in basis on the difference between the real stack temperature value and the optimal stack temperature value recommended by the manufacturer.

Finally, Fig. 6 represents the last configuration with a flow adapter (cone-shaped hopper) and a speed adjustable fan.

4. Experimental results

The different configurations designed have been implemented on the test bench, as shown in Fig. 2. Once the test bench is set up for each configuration, its SCADA governs, by the control unit, all the Oxidant/Cooling subsystem operation (and in general all the fuel cell subsystems and their operations) in each configuration. From it, you can set setpoints; capture, process and show all data, in different ways and in different formats. In the following, we will discuss the results obtained for each Oxidant/Cooling subsystem configuration.

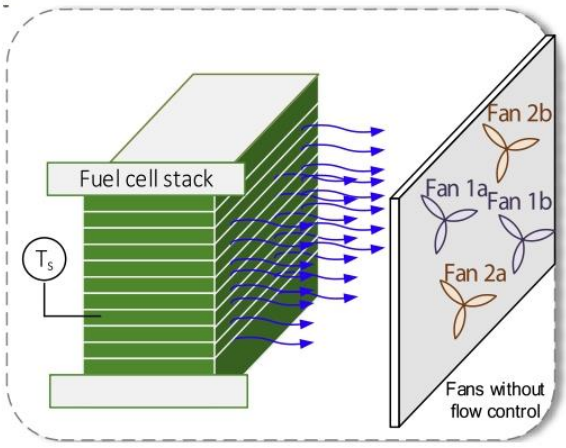

Fig. 4. Configuration 1: Four fans working two by two without flow control.

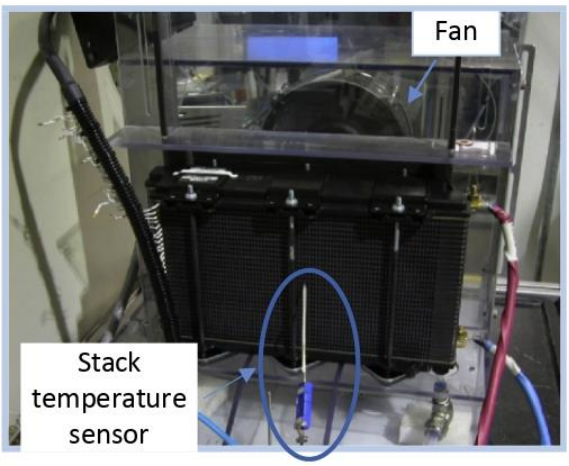

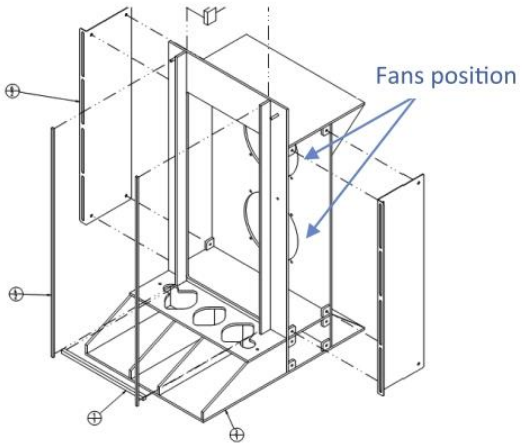

Fig. 3. a. Fan enclosure proposed by manufacturer for stack sizes equal or lower than 45 cells (standard configuration) Fig. 3b. Fan stand design proposed by manufacturer for stack sizes higher than 45 cells (standard configuration).

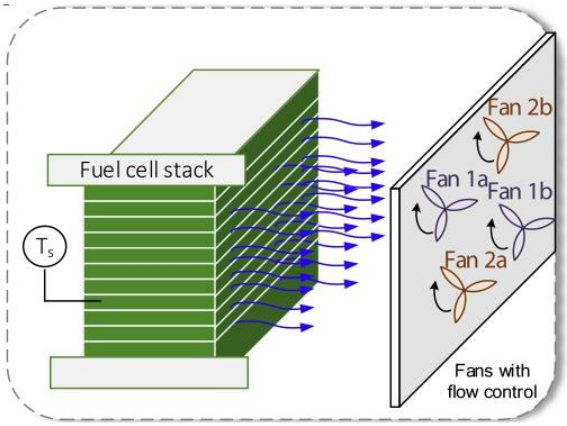

Fig. 5. Configuration 2: Four fans working two by two with flow control.

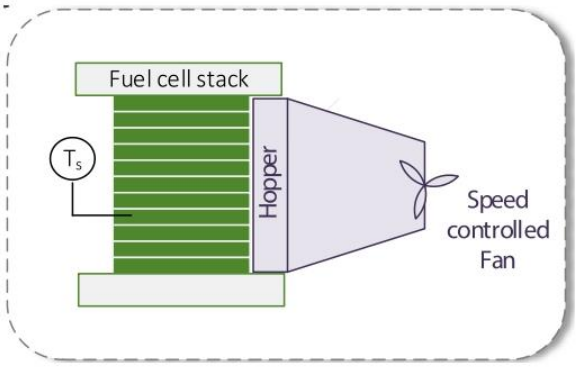

Fig. 6. Configuration 3: One single speed controlled fan inside a cone-shaped hopper.

a) Configuration 1: Four fans covering the cathode area of the stack working two by two without flow control.

For this configuration, the test bench is set up as in Fig. 2b. Fig. 8 shows the flow chart of the operation with this configuration. The experimental analysis starts comparing the real stack temperature with the optimal and robust stack temperature recommended by the manufacturer, expression (1) and (2) respectively, [29].

$$Topt = 0.46\, I_{stack} + 33.63 \quad (1)$$

$$Trob = 0.53\, I_{stack} + 26.01 \quad (2)$$

where,

Topt : Optimal stack temperature (ºC) recommended by manufacturer for legacy operating conditions (air inlet temperature from 10 °C to 40 °C).

Trob: Optimal stack temperature (ºC) recommended by manufacturer for robust operation over wide air inlet temperature range (−20 °C−52 °C). Keeping the stack near this operating temperature, the stack performance and cell stability are achieved.

The aim to compare the real stack temperature with optimal and robust temperature provided by the manufacturer, it is to show that oxidant configurations proposed in this work satisfies $Trob < T_{real} <$

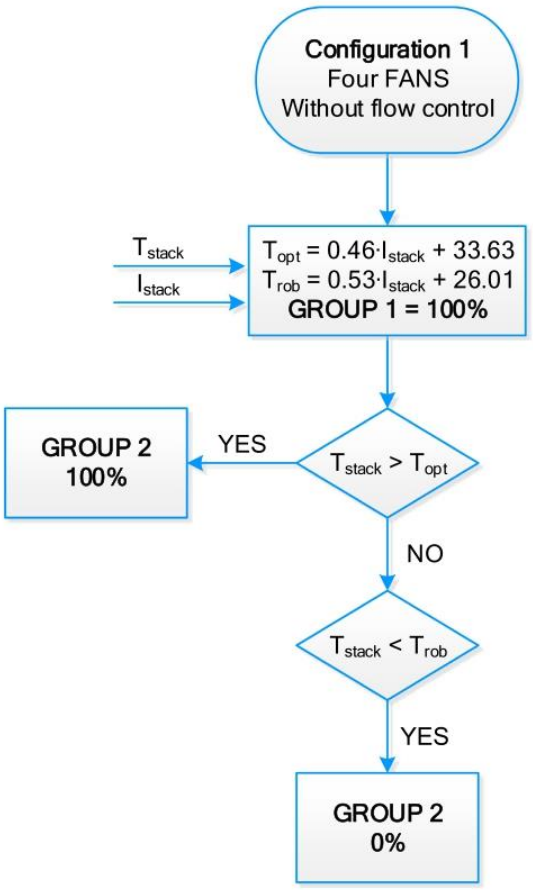

Fig. 7. Flow chart of configuration 1: Four fans working two by two without flow control.

T_{opt} even when initial room temperature is below stack temperature (it is also called *cold start*).

Then, according to the control logic shown in Fig. 7, the first group of fans is always working, and if the stack temperature is higher than the optimal stack temperature at the actual stack current value, the second groups of fans starts to work as well. However if the stack temperature is lower than optimal temperature and also lower than the robust temperature, the control unit does not put in work the second group of fans, keeping in operation only the first one. This situation corresponds with the case where the stack temperature is near the recommended values and the stack operates under acceptable operating conditions. In this case, the first group of fans is kept in operation because they are needed to supply the airflow required by the electrochemical reaction in the stack. In this configurations, fans operating mode is ON/OFF. This means that all the fans will be working at the maximum accepted value, without any control over the fan speed. As an advantage of this configuration, we can highlight its simplicity, but it cannot offer the possibility to adjust the air stoichiometry rate.

Next, we are going to analyse the fuel cell response attending to stack temperature, hydrogen pressure, voltage, current and power supplied by the fuel cell. To do this the AC-PEFC has been subjected to a multi steps load profile (10 A–30 A – 50 A).

Comparing the stack temperature with the optimal and robust

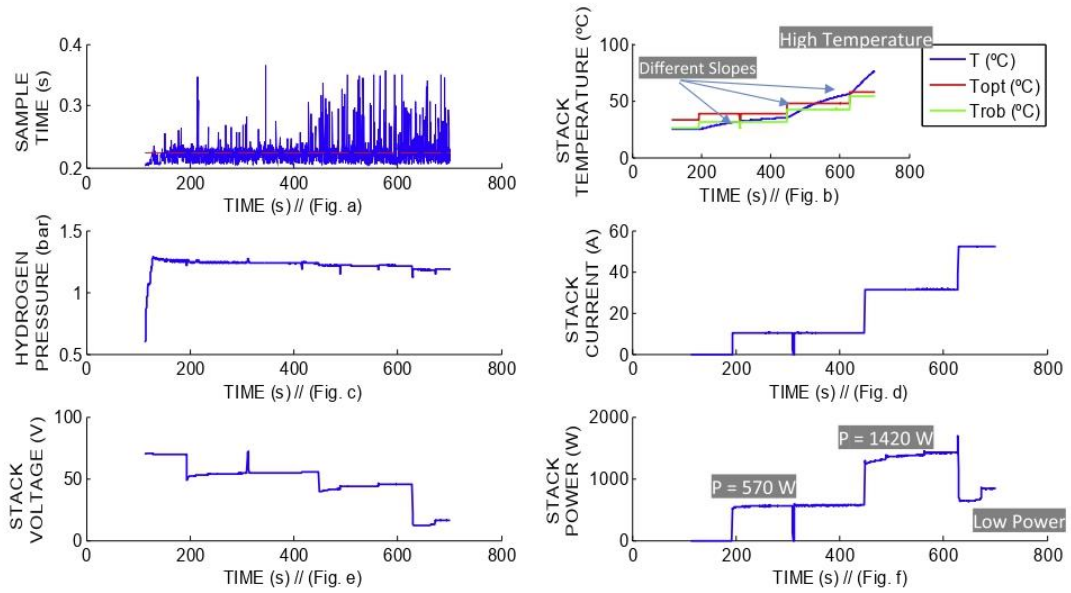

Fig. 8. AC-PEFC response for Configuration 1. From left to right and from top to bottom: (a)-Sample Time (s), (b)-Stack Temperature (°C), (c)-Hydrogen Pressure (bar), (d)-Stack Current (A), (e)-Stack Voltage (V) and (f)-Stack Power (W).

temperature recommended by the manufacturer (Fig. 8b), we can deduce that during the first load steps, the stack temperature keeps between the established margins of robust and optimal temperature, recommended by manufacturer. However, the time interval that the stack temperature is between the robust and optimal temperature is decreasing when the load current is increasing.

Another test done over the developed AC-PEFC with the configuration 1 is a thermography analysis with a thermal imager model Testo 875-1i, with a range of −30 °C to +100 °C and ±2% accuracy). This analysis allows us to evaluate if the configuration under study is suitable or no as optimal Oxidant/Cooling subsystem. For this purpose, a thermography has been taken at the beginning of each load step. Authors have chosen the thermography as an alternative to use multiple thermocouples placed in the cooling channels by simplicity in the temperature diagnosis. In case of an air-cooled fuel cell as this, the cathode is designed with multiple channels for cooling, so this would lead to an extra-wired structure with one thermocouple located in each cooling channel. Additionally, thermocouples need to be in contact with the surface, but this is not easy in an 80-cells stack with 40 cooling channels each cell. Fig. 9a, b and 9c and Tables 3a, b and c show a no uniform temperature distribution.

At the beginning of the operating time interval (Fig. 9a) the stack temperature distribution is considerably no homogenous with a difference of 6.6 °C (Table 3a: M1 regarding M7) between the hottest and the coldest point. However, as the load current increases the difference of temperature between the hottest and the coldest point is more significant achieving at 13.8 °C (Table 3c: M4 regarding M10).

When the load current is 10 A (Table 3a), the higher temperature values can be found, in this order, in M1, M4, M2 and M5. In the case of 30 A (Table 3b), in M4, M5 and M1. Finally, for 50 A, in M4, M5, M1 and M2 (Table 3c). Notice that the hottest spots locations for configuration 1 are always on the upper left corner of the stack.

b)Configuration 2: Four fans covering the cathode area of the stack working two by two with flow control.

This second configuration aims to improve the AC-PEFC performance allowing to control the four fans. This will be done varying the fans speed taking into account the difference between the stack temperature and the optimal and robust temperature recommended by the manufacturer. For this configuration, the test bench is set up as in Fig. 2b.

Fig. 10 shows the flow chart of the operation with configuration 2. This is delimited by three stages. The experimental analysis starts calculating the difference between the stack temperature value and the optimal temperature at the operating point. Additionally, the variable called *LIMIT* presents the maximum value allowed for the difference between the stack temperature and the optimal temperature. In this case authors have established that $LIMIT = 3$. This value corresponds approximately to the difference.

$(Topt - Trob)/2$, when $I_{stack} = 0$. Then, in basis on the comparison between this temperatures difference and the allowable limit, the control system decides to activate one or two groups of fans and the speed they must rotate. The action carried out at each state is described as follow:

- State 0: the stack temperature value is well below the optimal temperature taking into account the established limit. Therefore, in this stage the stack needs to be warmed so fans will be switched off to avoid cooling the stack. The stack takes the air for breathing from the surrounding.
- State 1: the temperatures difference is inside the range of $\pm LIMIT$. This means that the stack temperature is found between the accepted ranges recommended by the manufacturer. Therefore, it is necessary to keep the stack temperature inside this range. Therefore, GROUP 1 is put in working. The fan speed will be adjusted according to the expressions (3) and (4).

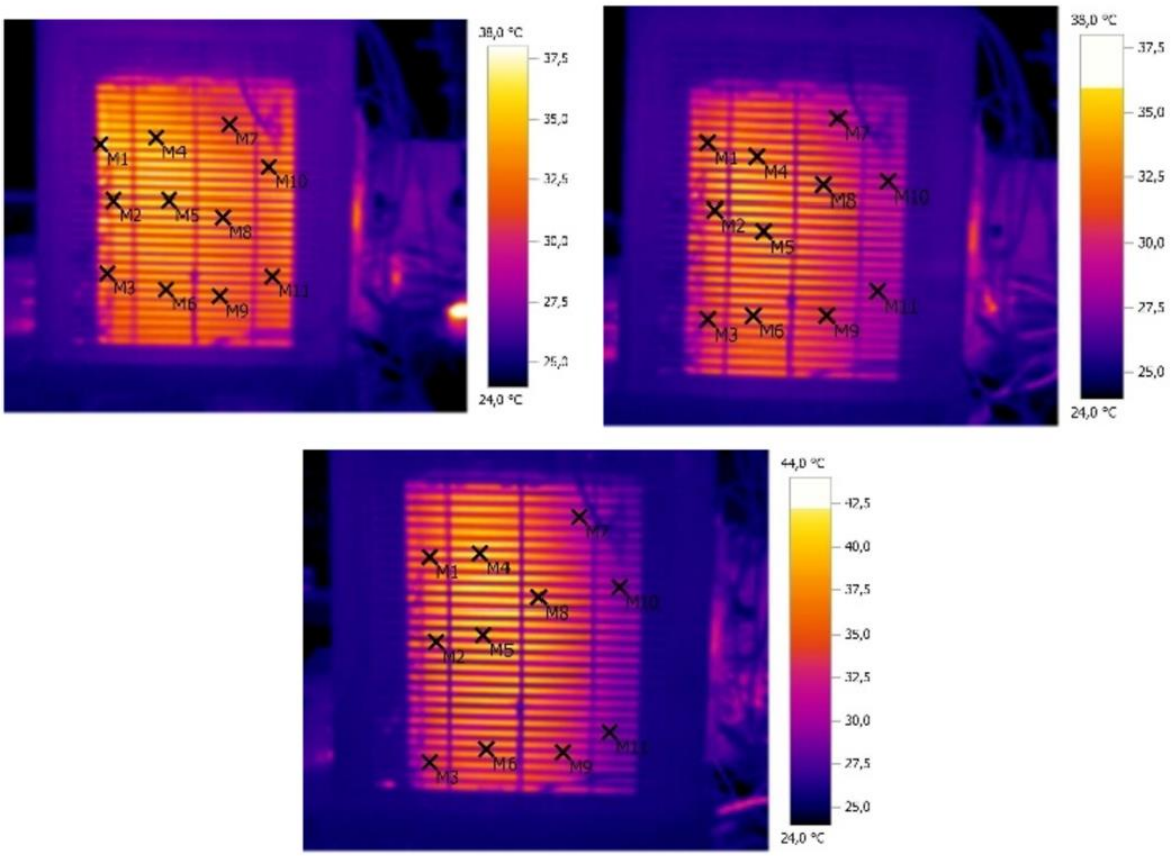

Fig. 9. a. Configuration 1: Thermography at 10 A. Fig. 9b. Configuration 1: Thermography at 30 A. Fig. 9c. Configuration 1: Thermography at 50 A.

Table 3a
Stack temperature points (Config. 1–10 A).

Point	Temp. (°C)	Emis	Ref. Temp. (°C)
M1	36.2 ± 2	0.94	25.0
M2	34.5 ± 2	0.94	25.0
M3	31.8 ± 2	0.94	25.0
M4	35.7 ± 2	0.94	25.0
M5	34.5 ± 2	0.94	25.0
M6	30.9 ± 2	0.94	25.0
M7	29.6 ± 2	0.94	25.0
M8	30.4 ± 2	0.94	25.0
M9	34.0 ± 2	0.94	25.0
M10	33.9 ± 2	0.94	25.0
M11	31.6 ± 2	0.94	25.0

Table 3b
Stack temperature points (Config. 1–30 A).

Point	Temp. (°C)	Emis	Ref. Temp. (°C)
M1	33.0 ± 2	0.94	25.0
M2	31.5 ± 2	0.94	25.0
M3	31.7 ± 2	0.94	25.0
M4	35.2 ± 2	0.94	25.0
M5	34.8 ± 2	0.94	25.0
M6	29.1 ± 2	0.94	25.0
M7	30.3 ± 2	0.94	25.0
M8	27.8 ± 2	0.94	25.0
M9	30.7 ± 2	0.94	25.0
M10	29.6 ± 2	0.94	25.0
M11	27.8 ± 2	0.94	25.0

$$DIF = (DIF - 2\ .LIMIT)K_1 \tag{3}$$

$$Fan_{Speed}(\%) = 100\ \frac{DIF}{2\ .LIMIT} + 50 \tag{4}$$

- State 2: the temperatures difference is far above the defined *LIMIT*. This means than the stack temperature is higher than the optimal temperature taking into account the *LIMIT*. Therefore, both fans groups (GROUP 1 and GROUP 2) must to be activated.

In this state, the fan speed will be adjusted according to the expressions (5) and (6).

$$DIF = DIF\ .\ K_2 \tag{5}$$

$$Fan_{Speed}(\%) = 100\frac{DIF}{2\ .\ LIMIT} + 50 \tag{6}$$

where $K_1 = 1$ and $K_2 = 2$, are variables related to how much the error should be increased and therefore how quickly we expect the control acts. Authors in basis on system response have chosen these constant values.

Table 3c
Stack temperature points (Config. 1–50 A).

Point	Temp. (°C)	Emis	Ref. Temp. (°C)
M1	35.2 ± 2	0.94	25.0
M2	35.0 ± 2	0.94	25.0
M3	34.0 ± 2	0.94	25.0
M4	41.5 ± 2	0.94	25.0
M5	40.9 ± 2	0.94	25.0
M6	29.9 ± 2	0.94	25.0
M7	28.6 ± 2	0.94	25.0
M8	31.6 ± 2	0.94	25.0
M9	30.4 ± 2	0.94	25.0
M10	27.7 ± 2	0.94	25.0
M11	28.1 ± 2	0.94	25.0

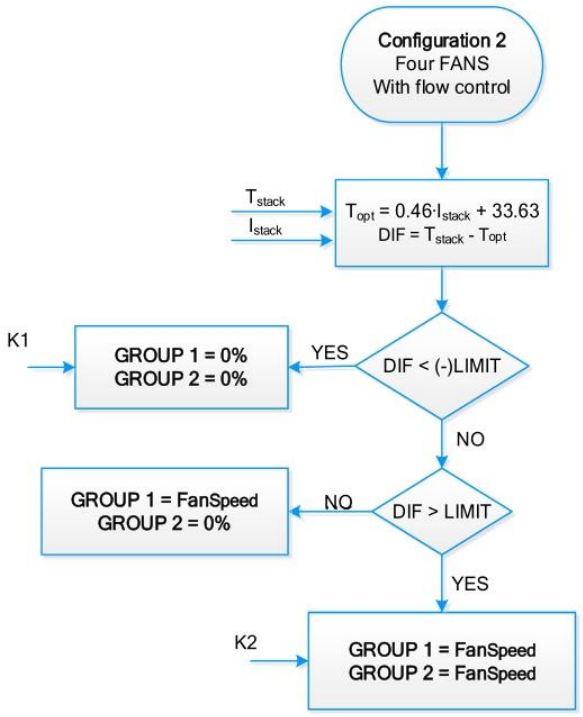

Fig. 10. Flow chart of configuration 2: Four fans working two by two with flow control.

Like in the Configuration 1, the study of the dynamic stack behaviour will be done using a multi steps load profile (10A–30A – 50A).

The fuel cell response is going to be analysed attending to stack temperature, voltage, current, power, hydrogen pressure and a multi steps load profile (10 A–30 A – 50 A) is used. From Fig. 11b, we can see how the stack temperature changes when no current is demanded by the load; this is because the previous study was done before this one, so the stack is still warmed. Therefore, we can appreciate how the configuration is capable of decreasing the stack temperature from 60 °C (due to the previous test) up to 30 °C, which is the optimal temperature for the first load current step. The time when the load changes can be guessed perfectly over the stack temperature response. Moreover, like in the previous configuration, it is noticed that the stack temperature slope does not depend on the step amplitude difference but on the actual current value at this time. That is for the step between 10 A–30A, the amplitude step (20 A) is similar to the step amplitude between 30 A–50 A. However, the temperature slope and curvature are different. The curvature slopes are 0.05 and 0.1 for 30 and 50 A, respectively.

Another observation we can do about Fig. 11 is the stack electrical performance: attending to stack voltage response, when load demand rises up to 50 A, the stack voltage does not drop and the power supplied reaches above 2000 W avoiding air-starvation problem. Therefore, for this configuration it does not seem to be air supply problems.

Additionally, comparing the stack temperature with the optimal and robust temperature recommended by the manufacturer (Fig. 11b), we can deduce that the stack temperature is controlled between the robust and optimal temperature during almost all the load demand. Just in the last load step, the stack temperature is slightly above the range recommended by the manufacturer.

Similarly to configuration 1, now with configuration 2 a thermography analysis has been done as well, in order to evaluate if the configuration under study is suitable or not as optimal Oxidant/Cooling subsystem. For this purpose, a thermography has been taken at the beginning of each load step. Fig. 12a, b and c; and Tables 4a, b and c show a better uniform temperature distribution regarding configuration 1.

In the first operating time interval (Fig. 12a) the stack temperature distribution is significantly no homogenous with a difference of 5.6 °C (Table 4a: M1 regarding M11) between the hottest and the coldest point. However, as the load current increases, the difference of temperature between the hottest and coldest point increases, achieving at 10.3 °C (Table 4b: M4 regarding M10) and 18.1 °C (Table 4c: M4 regarding M9).

When the load current is 10 A (Table 4a), the higher temperature values can be found, in this order, in M1, M5, M2 and M6. In the case of 30 A (Table 4b), in M4, M1, M6 and M2. Finally, for 50 A, in M4, M1 and M5 (Table 4c). Again, note that the hottest spots locations for configuration 2 are always on the left side of the stack.

c) Configuration 3: One single speed controlled fan.

In this case, the control logic results from a combination of the two previous control diagrams. Similarly, it calculates the difference between the stack temperature and the optimal temperature at the operating point and establishes the LIMIT value (in this third case authors have established that LIMIT = 3).

The action carried out at each state is described as follow (Fig. 13):

- State 0: when the difference between the stack temperature and the optimal temperature is lower that (–) LIMIT, the stack far to be cooled it needs to be warmed. An excess of cooling could originate flooding of the membrane, affecting the stack performance. In configuration 2 all the fans were switched off, but in this case the fan is kept at its minimum controllable speed (700 min^{-1}), which is 15% of the minimum speed according to datasheet [31], with the aim to avoid the air starvation problem, supplying the minimum amount of air needed by the stack for breathing.
- State 1: when the temperatures difference is inside the range of ± LIMIT, the stack temperature is found between the accepted ranges. Then, with the aim to keep the stack temperature inside this range, the fan speed is adjusted according to expressions (7).

$$Fan_{Speed}(\%) = 100 \ \frac{DIF}{2 \ . \ LIMIT} + 50 \qquad (7)$$

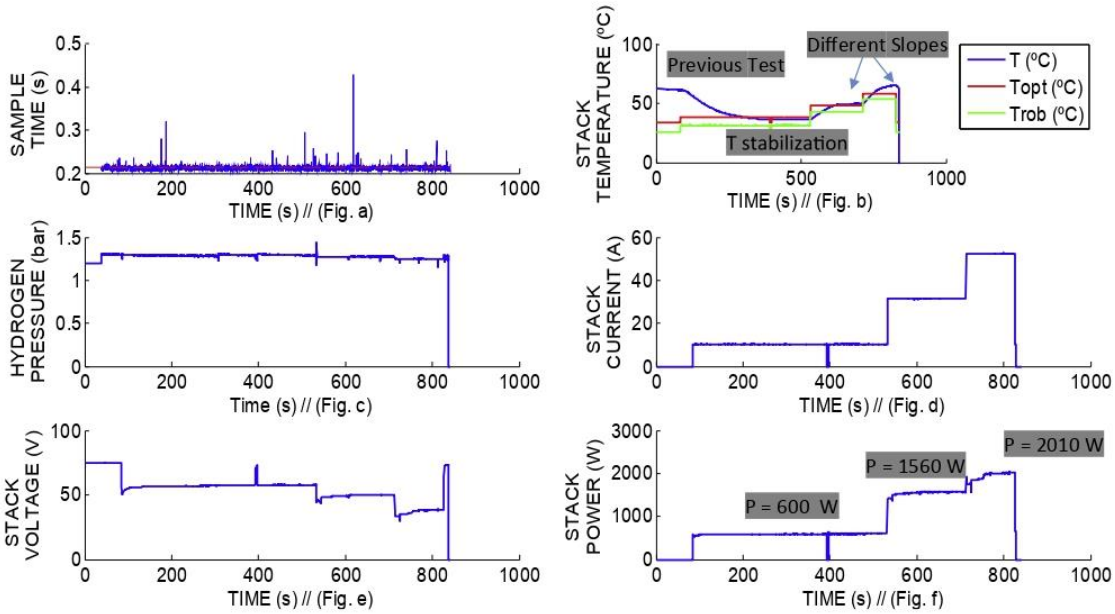

Fig. 11. AC-PEFC for Configuration 2. From left to right and from top to bottom: (a)-Sample Time (s), (a)-Stack Temperature (ºC), (c)-Hydrogen Pressure (bar), (d)-Stack Current (A), (e)-Stack Voltage (V) and (f)-Stack Power (W).

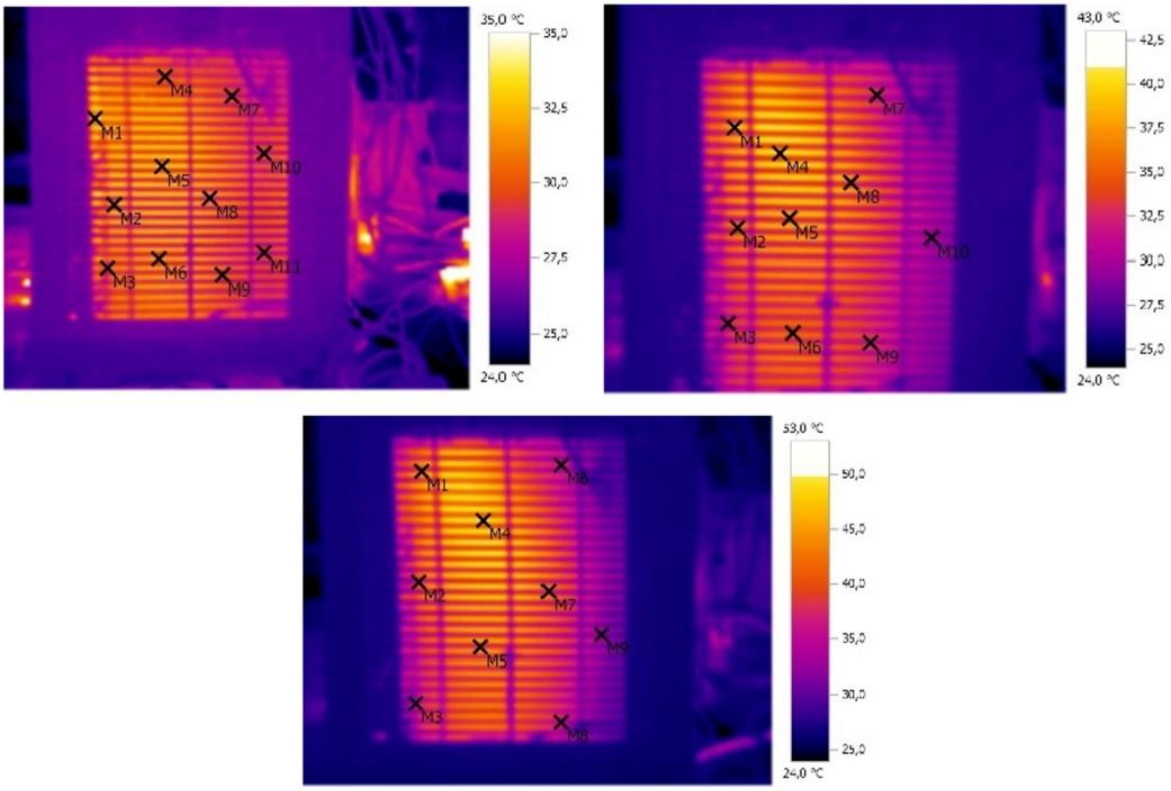

Fig. 12. a. Configuration 2: Thermography at 10 A. Fig. 12b. Configuration 2: Thermography at 30 A. Fig. 12c. Configuration 2: Thermography at 50 A.

Table 4a
Stack temperature points (Config. 2–10 A).

Point	Temp. (°C)	Emis	Ref. Temp. (°C)
M1	33.6 ± 2	0.94	26.5
M2	32.3 ± 2	0.94	26.5
M3	30.3 ± 2	0.94	26.5
M4	29.4 ± 2	0.94	26.5
M5	33.2 ± 2	0.94	26.5
M6	32.3 ± 2	0.94	26.5
M7	28.3 ± 2	0.94	26.5
M8	28.3 ± 2	0.94	26.5
M9	29.7 ± 2	0.94	26.5
M10	28.3 ± 2	0.94	26.5
M11	28.0 ± 2	0.94	26.5

Table 4b
Stack temperature points (Config. 2–30 A).

Point	Temp. (°C)	Emis	Ref. Temp. (°C)
M1	38.3 ± 2	0.94	26.5
M2	34.7 ± 2	0.94	26.5
M3	33.0 ± 2	0.94	26.5
M4	40.2 ± 2	0.94	26.5
M5	33.7 ± 2	0.94	26.5
M6	34.8 ± 2	0.94	26.5
M7	32.0 ± 2	0.94	26.5
M8	33.2 ± 2	0.94	26.5
M9	30.9 ± 2	0.94	26.5
M10	29.9 ± 2	0.94	26.5

Table 4c
Stack temperature points (Config. 2–50 A).

Point	Temp. (°C)	Emis	Ref. Temp. (°C)
M1	39.8 ± 2	0.94	26.5
M2	36.4 ± 2	0.94	26.5
M3	34.1 ± 2	0.94	26.5
M4	49.2 ± 2	0.94	26.5
M5	37.5 ± 2	0.94	26.5
M6	36.6 ± 2	0.94	26.5
M7	36.2 ± 2	0.94	26.5
M8	34.4 ± 2	0.94	26.5
M9	31.1 ± 2	0.94	26.5

- Stage 2: finally, when the temperatures difference is far above the defined LIMIT, the fan must rotate at its maximum speed (5500 min^{-1}) to guarantee both the air breathing of the stack and the temperature control.

Additionally to the previous control stages, it is necessary to point out that the control strategy has to be also based in the following: in case of stack model used in this work, the stoichiometric rate of the stack recommended by manufacturer varies between 50 and 200. Due to this range is excessively wide, it can happen that working inside the stoichiometric range, the stack performance was long from the optimal. Based on this, authors propose the control diagram for configuration 3 with the aim to accomplish with the restrictions related to stoichiometric range at time that it pursues to maintain the stack temperature between the recommended values. This condition of stack temperature is more restrictive than the air stoichiometry criterion. In this case, the difference between the optimal and robust temperature is not higher than 7 °C, so the oxidant/cooling subsystem must be controlled with the aim to guarantee this narrow operating temperature margin.

The experimental results obtained for this configuration are shown in Fig. 14. Like in the previous configurations, the study of

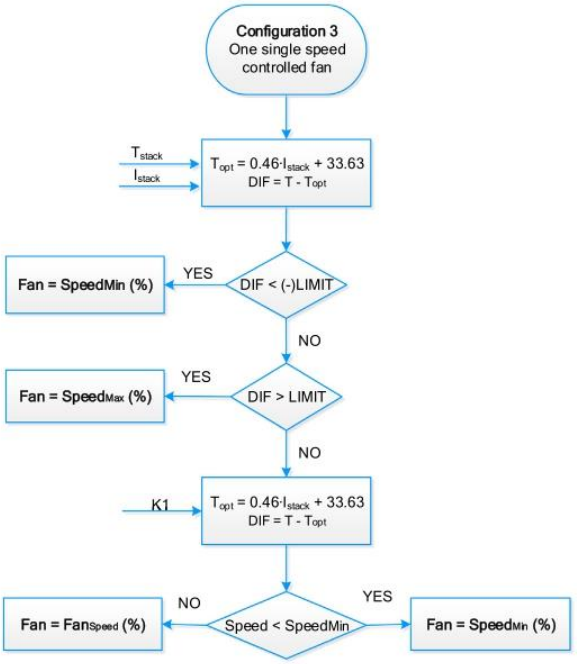

Fig. 13. Flow chart of configuration 3: One single speed controlled fan.

the dynamic stack behaviour will be done using a multi steps load profile (10A–30A– 50A). From Fig. 14, we can point out how the stack temperature remains stabilized when the load demands no current; this is because the stack is cold. The time when the load changes can be guessed perfectly over the stack temperature response. Moreover, for all load currents, it can be pointed out that the stack temperature is between the recommend range (optimal and robust temperature values) and it keeps stabilized in the same way that for 0 A. Unlike to previous configurations, where the stack temperature slope did not depend on the step amplitude difference but on the actual current value, now the temperature slope and curvature are identical at the step between 10 A–30A (amplitude step of 20 A) and at the step between 30 A–50 A.

Another observation we can appreciate over Fig. 14 is the stack electrical performance: attending to stack power response, when load demand rises up to 50 A, the stack power does not drop abruptly like it happened in configuration 1 (remember Fig. 8), but it achieves more than 2500 W.

Regarding the thermography analysis that has been done to evaluate if the configuration under study is suitable or not as optimal Oxidant/Cooling subsystem, in this case like in the previous ones, a thermography has been taken at the beginning of each load step. Fig. 15a, b and c, and Tables 5a, b and c, show uniform temperature distribution. In the first operating time interval (Figure 15a) the stack temperature distribution is practically homogenous with a difference of 0.8 °C (Table 5a: M5 regarding M6) between the hottest and the coldest point. As the load current increases, the difference of temperature between the hottest and the coldest point increases slightly, achieving at 1.1 °C (Table 5b: M5 regarding M3) and 1.4 °C (Table 5c: M5 regarding M3).

Regarding the results obtained up to now, we can have some relevant data to foresee what configuration fulfils the six requirements that the oxidant/cooling system must guarantee. Just as a reminder, they were (Fig. 1): 1) To be able to cool the stack

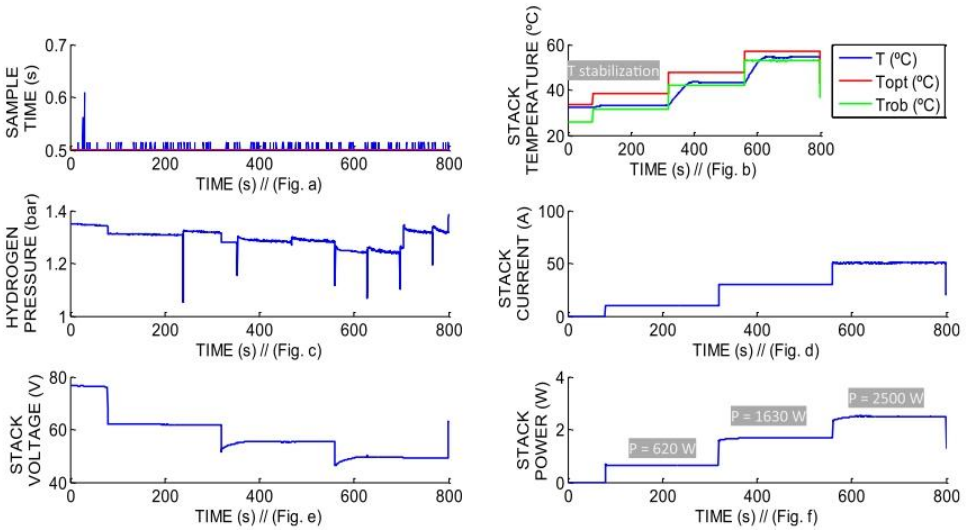

Fig. 14. AC-PEFC for Configuration 3. From left to right and from top to bottom: (a)-Sample Time (s), (b)-Stack Temperature (ºC), (c)-Hydrogen Pressure (bar), (d)-Stack Current (A), (e)-Stack Voltage (V) and (f)-Stack Power (W).

homogeneously, 2) To provide sufficient airflow range to control the PEFC temperature under a range of power and room/coolant air temperature, 3) To place the stack at optimum temperature, 4) To reduce the auxiliary power consumption, 5) To do all this within a certain sized box, and finally but not least 6) To do it cost effectively.

Based on the tests performed, it is clear that the only configuration able to meet the requirements is the configuration 3. However, we still have to prove that it provides sufficient airflow range to control the PEFC temperature, under a range of power and room/coolant air temperature. The previous test has been carried out

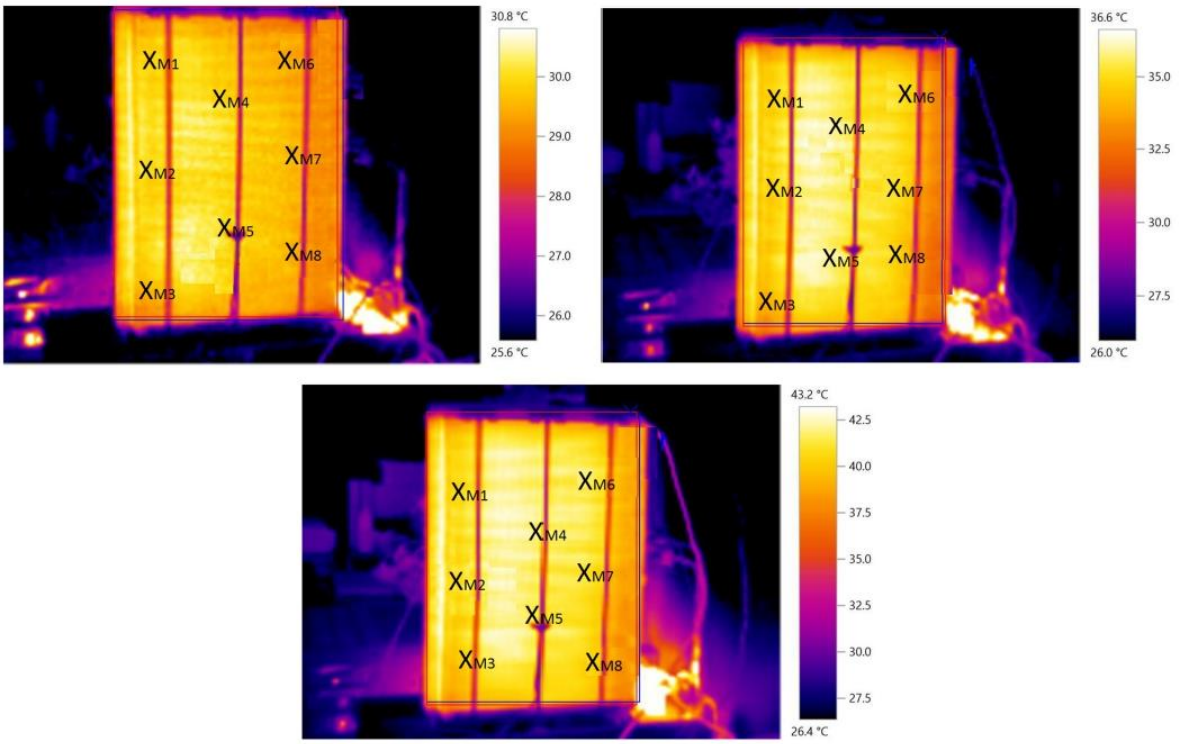

Fig. 15. a. Configuration 3: Thermography at 10 A. Fig. 15b. Configuration 3: Thermography at 30 A. Fig. 15c. Configuration 3: Thermography at 50 A.

Table 5a
Stack temperature points (Config. 3–10 A).

Point	Temp. (ºC)	Emis	Ref. Temp. (ºC)
M1	30.2 ± 2	0.94	23
M2	30.5 ± 2	0.94	23
M3	30.1 ± 2	0.94	23
M4	30.6 ± 2	0.94	23
M5	30.8 ± 2	0.94	23
M6	30.0 ± 2	0.94	23
M7	30.7 ± 2	0.94	23
M8	30.2 ± 2	0.94	23

Table 5b
Stack temperature points (Config. 3–30 A).

Point	Temp. (ºC)	Emis	Ref. Temp. (ºC)
M1	35.9 ± 2	0.94	23
M2	36.5 ± 2	0.94	23
M3	35.7 ± 2	0.94	23
M4	36.6 ± 2	0.94	23
M5	36.8 ± 2	0.94	23
M6	36.0 ± 2	0.94	23
M7	36.7 ± 2	0.94	23
M8	36.3 ± 2	0.94	23

Table 5c
Stack temperature points (Config. 3–50 A).

Point	Temp. (ºC)	Emis	Ref. Temp. (ºC)
M1	42.2 ± 2	0.94	23
M2	43.1 ± 2	0.94	23
M3	42.0 ± 2	0.94	23
M4	43.2 ± 2	0.94	23
M5	43.4 ± 2	0.94	23
M6	42.6 ± 2	0.94	23
M7	43.3 ± 2	0.94	23
M8	42.1 ± 2	0.94	23

with a fix room temperature of 23 °C and an initial stack temperature of 33 °C.

Then, with the aim to probe that the developed oxidant/cooling subsystem provides sufficient air in a room temperature range, a last test will be done over configuration 3. Now the room temperature has been lowered to 13 °C, which logically brings a significant drop in stack temperature. The results of this new test are shown in Fig. 16.

Regarding Fig. 16, we can observe that stack reaches the temperature recommended by the manufacturer at the end of the first step, due to its low starting temperature. In fact, as you can see in Fig. 16b, it takes about 6 min for the temperature to be inside the window (*Top* − *Trob*). From here, the behaviour of the stack temperature is becoming more and more suitable. Nevertheless, in basis on power output, the stack performance is not affected. Then we can advance that the stack can provide the design power even when its starting temperature is below the design temperature.

Regarding the thermographies (Figures 17a, b and c; and Tables 6a, b and c, at the beginning the difference of Tables 5a and 6a, is practically the same as the drop in room temperature. This is, around 10 °C. However, as the stack is working, the gap is coming reduced, and at the end of the test, it is only around 5 °C.

5. Discussion

In the red-ox reaction that takes place in a fuel cell, the hydrogen energy is transformed into electrical power and heat. A stack temperature control non-optimized will lead to a fuel cell where the most of the hydrogen energy is converted into heat, resulting an inefficient system. However, a temperature control in which the aims is not only to adjust the air stoichiometry but to fix the stack temperature between the recommended ranges, provides a better fuel cell efficiency: with the same hydrogen consumption, it supplies higher electrical power.

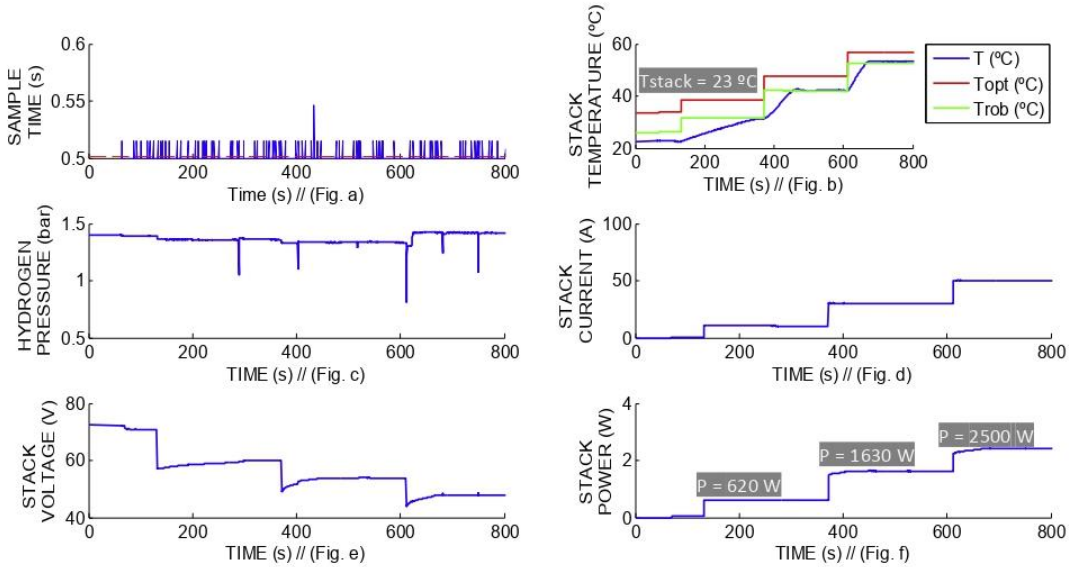

Fig. 16. AC-PEFC for Configuration 3: Test 2. From left to right and from top to bottom: (a)-Sample Time (s), (b)-Stack Temperature (ºC), (c)-Hydrogen Pressure (bar), (d)-Stack Current (A), (e)-Stack Voltage (V) and (f)-Stack Power (W).

Table 6a
Stack temperature points (Config. 3–10 A).

Point	Temp. (°C)	Emis	Ref. Temp. (°C)
M1	20.3 ± 2	0.94	13
M2	20.1 ± 2	0.94	13
M3	20.0 ± 2	0.94	13
M4	19.8 ± 2	0.94	13
M5	20.2 ± 2	0.94	13
M6	19.1 ± 2	0.94	13
M7	19.0 ± 2	0.94	13
M8	20.3 ± 2	0.94	13
M9	19.7 ± 2	0.94	13
M10	19.5 ± 2	0.94	13

Table 6b
Stack temperature points (Config. 3–30 A).

Point	Temp. (°C)	Emis	Ref. Temp. (°C)
M1	30.8 ± 2	0.94	13
M2	31.5 ± 2	0.94	13
M3	30.0 ± 2	0.94	13
M4	30.6 ± 2	0.94	13
M5	32.6 ± 2	0.94	13
M6	31.9 ± 2	0.94	13
M7	30.4 ± 2	0.94	13
M8	32.0 ± 2	0.94	13
M9	30.0 ± 2	0.94	13
M10	23.7 ± 2	0.94	13

Table 6c
Stack temperature points (Config. 3–50 A).

Point	Temp. (°C)	Emis	Ref. Temp. (°C)
M1	36.5 ± 2	0.94	13
M2	37.6 ± 2	0.94	13
M3	36.5 ± 2	0.94	13
M4	36.1 ± 2	0.94	13
M5	38.6 ± 2	0.94	13
M6	37.9 ± 2	0.94	13
M7	35.8 ± 2	0.94	13
M8	37.0 ± 2	0.94	13
M9	36.6 ± 2	0.94	13
M10	29.8 ± 2	0.94	13

In this work, for developed configurations 1 and 2, with 4 fans (Fig. 2b), authors have proposed these designs in basis on stack's manufacturer recommendations based on a polycarbonate enclosure around the stack. This structure serves as stand to support four fans that cover the area of the stack cathode. Regarding configuration 3 with only a fan (Fig. 2c), the design aim of the authors has been to improve the air breathing of the stack and its temperature distribution over the cathode. This third configuration tries to sort out the problem observed in configurations 1 and 2: the air follows preferential paths surrounding the stack instead of crossing it for its cooling. In this sense, authors have proposed a design consisting on a speed controllable fan, which is inserted in a cone-shaped hopper built to facilitate the air blow through the stack and avoiding preferential paths of the airflow.

In configuration 1 the fans operate in ON/OFF mode. In configuration 2, the fans are controlled based on the difference between the stack temperature and the optimal temperature recommended by manufacturer. In configuration 3, the single fan works with variable speed, under a control law whose purpose is to maintain the stack temperature within the window of suitable operating temperatures of the stack. Someone might wonder why the authors have not designed a controller, such as a PID for example that can track the optimum temperature (it would have even been easier than the proposed solution). The answer is that the heating process is not controlled, it depends on the power requested to the stack at any time, and the cooling process, based on ventilation, does not allow to follow a set point exactly; consequently, it is better, more practical and efficient, to work in a window of allowed values.

The three proposed configurations have been tested under the same conditions and load profile. The goal to compare proposed configurations is to verify the fulfilment of the six design challenges proposed at the beginning of the work. These challenges are:

1) To be able to cool the stack homogeneously.
2) To provide sufficient airflow range to control the PEFC temperature, under a range of power and room/coolant air temperature.
3) To place the stack at optimum temperature.
4) To reduce the auxiliary power consumption.
5) To do all this within a certain sized box, and
6) To do it cost effectively.

Analysing the experimental results, we can observe that in configuration 1 (Fig. 8), the stack temperature does not change when no current is demanded by the load. Next, stack temperature starts to increase as load current gets higher. The time when the load changes can be guessed perfectly over the stack temperature response. Moreover, we can notice, the stack temperature slope does not depend on the step amplitude difference but on the actual current value at this time. That is, for the step between 10 A–30 A, the amplitude step (20 A) is similar to the step between 30 A–50 A. However, the temperature slopes and curvatures are different. The curvature slopes are 0.1 °C/A at 10 A, 0.05 °C/A at 30 A and 0.4 for 50 A.

Another observation we can do over Fig. 8 is the electrical performance of the fuel cell. Attending to voltage response, when load demand rises up to 50 A, the stack voltage drops significantly reducing the power supplied by the stack below 1000 W. Attending to the real AC-PEFC implementation and the BoP configuration

Table 7
Analysis of Oxidant/Cooling system parameters.

Configuration		Air required Air_{stack} (m³/h)	Heat Generated Q_{stack_heat} (W)	Air Volume needed for cooling $\dot{V}_s$·(m³/h) [λ[a]]	Total Air Pressure drop ΔP_{total} (Pa)	Fan operating point
# 1	10 A	0.79	470	132.73 [166.59]	44.43	OFF: 0
	30 A	2.39	1560	179.75 [75.19}	52.69	ON: 5500 rpm
	50 A	3.98	4500	270.06 [67.78]	69.43	
# 2	10 A	0.79	450	112.72 [141.41]	41.40	0–5500 rpm
	30 A	2.39	1505.7	177.04 [74.06]	52.22	According to control
	50 A	3.98	2990	215.33 [54.04]	59.58	algorithm (Fig. 10)
# 3	10 A	0.79	380	109.46 [137.38]	40.84	700–5500 rpm
	30 A	2.39	1370	164.44 [68.79]	50.18	According to control
	50 A	3.98	2500	211.81 [53.16]	58.53	algorithm (Fig. 13)

[a] λ is the stoichiometric rate and it is defined as:λ = air flow needed for cooling/air flow required for oxidant reaction.

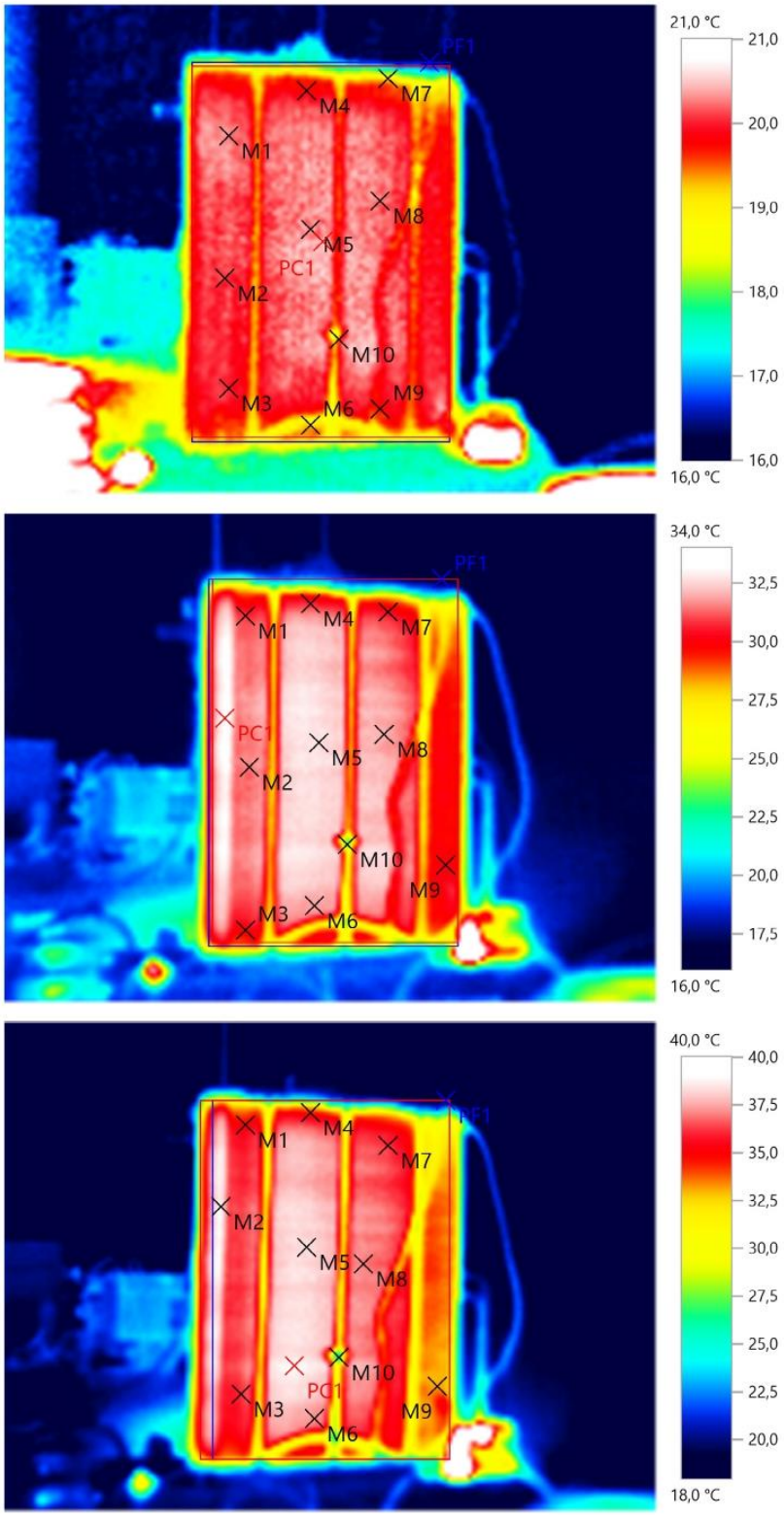

Fig. 17. a. Configuration 3. Test 2: Thermography at 10 A. Fig. 17b. Configuration 3. Test 2: Thermography at 30 A. Fig. 17c. Configuration 3. Test 2: Thermography at 50 A.

(Fig. 2), two reasons could be the origin of this: a wrong hydrogen supply or an inefficient oxidant supply system. They are the only two agents involved in the stack red-ox reaction. Attending to hydrogen pressure response (Fig. 8c), it has been kept fixed along the whole test so this leads us to think the high temperature achieved by the stack (Fig. 8b) is due to an improper air-breathing and the oxidant/cooling system is inefficient. Remember that the air-starvation problem can affect the electrical resistivity of the membrane because the membrane is very dry to allow passing ions across itself.

Based on the above, configuration 1 is an inefficient Oxidant/Cooling subsystem. The stack temperature increases continually (Fig. 8b) because the Oxidant/Cooling subsystem is not capable of maintaining the stack temperature value between the recommended ranges. Therefore, the system requires a better control over the fans to adjust properly the stack temperature as well as to supply the air needed for breathing. Additionally, there is a clear air-starvation problem, reducing considerably the fuel cell efficiency. The thermography images taken along the load profile (Fig. 9a, a and 9c) show clearly how the airflow surrounds the stack following preferential paths because the hottest spots locations are always (regardless of the power demanded) on the upper left corner of the stack (see also values on Tables 3a, b and c). So, a diagonal-shape operating mode for fans activated two by two is not recommended.

Regarding configuration 2, it solves the air-starvation problem presented by configuration 1. Besides, it shows a better stack temperature response (Fig. 11). It increases continually as load current rises and it is closer to the optimal temperature (Fig. 11b) than configuration 1, but most of the time it is still outside. Regarding the fuel cell efficiency, this is better than in previous configuration. However, the stack temperature distribution is still no uniform; note that the hottest spots locations for configuration 2 are always on the left side of the stack (please, see Fig. 12a, b and 12c; and Tables 4a, b and c). In fact, the no-uniformity in the stack temperature is even more noticeable than in configuration 1. This can be appreciated in the thermographies at different load current values. Table 4c shows that there is a difference greater than 18 °C between the hottest and the coldest point at the same time in the same stack.

Finally, the last proposed configuration avoids the preferential paths because the cone-shaped hopper is totally adapted to the stack avoiding the space between the stack and the structure for the air flow. Therefore, the airflow is forced to cross the stack in order to cool it. In this case, experimental results show the stack temperature is fairly well adjusted to optimal temperature, guaranteeing both the stack oxygenation and cooling (please, see Figs. 14 and 15, and Tables 5a, b and C). That is, both air-starvation and no-homogeneous cooling problems from configurations 1 and 2 are solved. As consequence, this design guarantees both the more proper air breathing subsystem for the stack and the best fuel cell efficiency. Additionally, thermography images demonstrate the best temperature distribution is around the stack cathode area.

Up to now, with the tests done over configurations 1, 2 and 3 we can advance what configuration best fulfils the six requirements that the oxidant/cooling system must guarantee (see Fig. 1). The last question that has been addressed in this paper is the oxidant/cooling subsystem capability. As it was introduced, one of the requirements is to provide enough airflow under different power outputs and room temperatures. On the other hand, as it is demonstrated in Ref. [15], the airflow rate needs are higher for stack cooling than for oxygenation. Therefore, if the stack cooling is guaranteed, the stack oxygenation will be too. In this regard, the cooling airflow rate depends on the difference between the stack and air temperature; higher difference, higher airflow needs. Then, the fan selection [15] was done considering the highest temperature the stack could achieve (66 °C at nominal power). Then, the first test applied over configuration 3 confirms the design is suitable for supplying enough airflow to oxygenate and cool the stack at a certain room temperature. The second test completes the first one showing the proper stack oxygenation and cooling for a room temperature range. Regarding this (please see Figs. 16 and 17 and Table 6a, b, c), it is clear that air starvation (deficiency of configuration 1) and high stack temperatures (deficiency of configurations 1 and 2) have more negative effect on the stack performance than a cool starting. In a real application, in case the user desires to start working inside the temperature range, it is advisable to wait a few minutes to warm the stack.

The effects of a proper design of the Oxidant/Cooling subsystem can be observed directly over the stack performance. Then, if the stack is operated at temperatures above optimal one, the membrane will dry out and become more electrically resistive, reducing

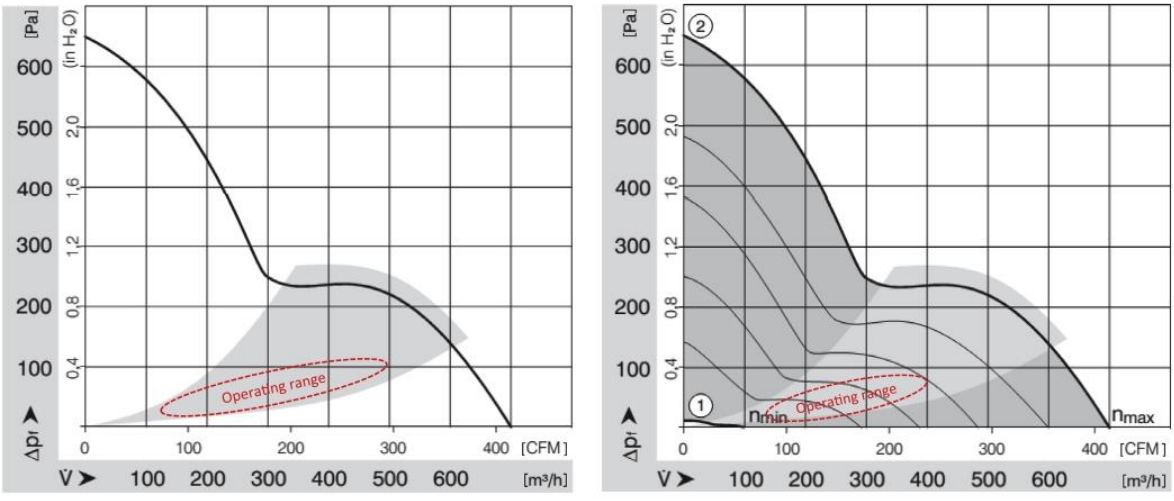

Fig. 18. a. Air chart for fan model Embpast-6224TD (Configuration 1 and 2). Fig. 18bAir chart for fan model Embpast-6224TD (Configuration 3).

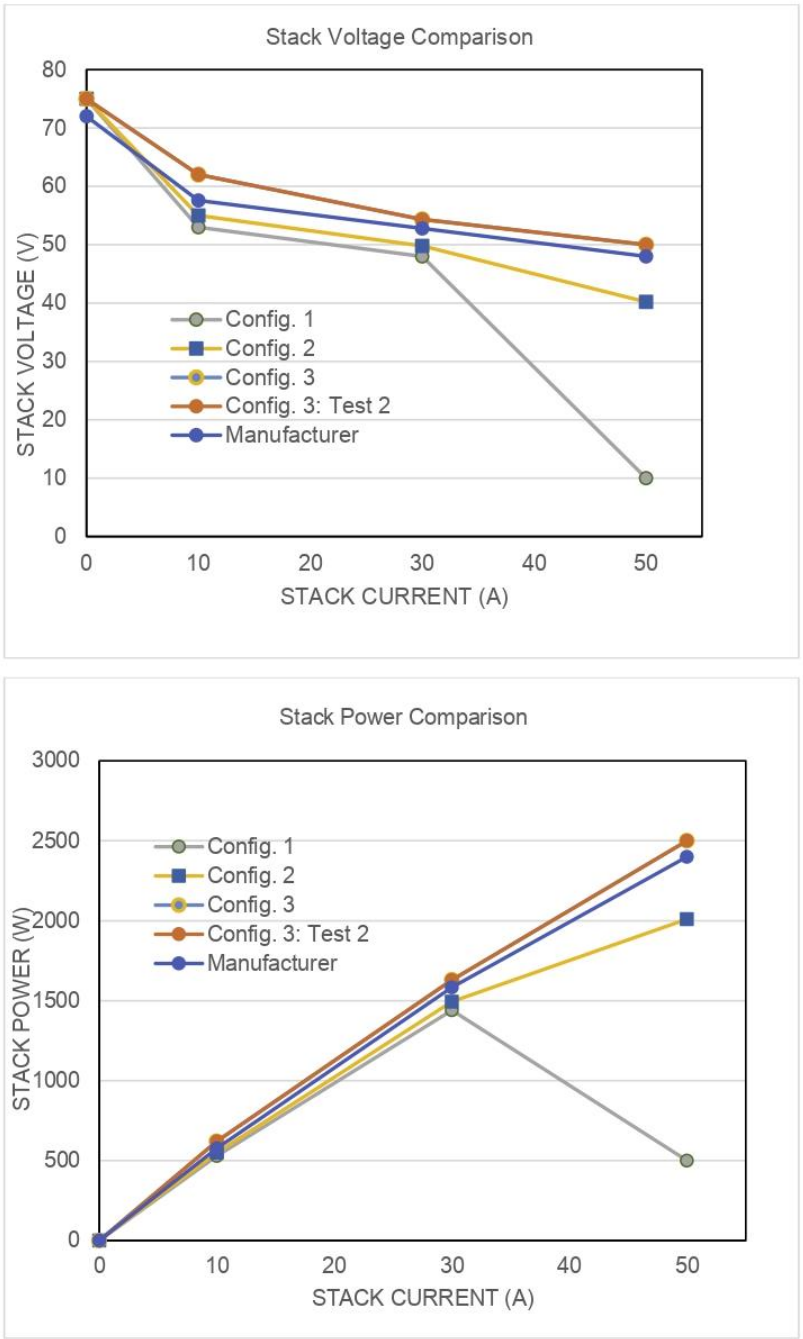

Fig. 19. a. Stack Voltage Comparison. Figure 19b. Stack Power Comparison. Fig. 19c. Stack Temperature Comparison.

the stack performance. This is the case of configurations 1 and 2. Even at extreme temperatures, the membrane can become damaged, resulting in irreversible performance losses. Specifically, in configuration 1 due to an improper air-breathing and inefficient oxidant/cooling system, stack suffers air-starvation problem. This provokes there is no sufficient air for the redox reaction in the membrane (oxygen and hydrogen mix to form electricity and water) and, consequently the voltage will decrease significantly, decreasing too the power provided by the stack.

By contrast, if the stack is operated at temperatures well below optimal value, the membrane will be over-humidified, resulting in the presence of liquid water in the cells. Too much water can cause

anode flooding, where the water blocks reactants from reaching the catalyst layer. This can also cause irreversible performance loss though localized fuel starvation and cell reversals. For this reason, the temperature control system developed in configuration 3 keeps the stack temperature very close to the optimum value. That is, in configuration 3, the one that shows the best stack performance, there are no situations of air-starvation, nor dry or flooded membrane.

Paying attention to thermographies we can observe configuration 1 point out clearly that the airflow surrounds the stack following preferential paths because the hottest spots appear on the upper left corner of the stack. With regard to the difference between the coldest and hottest point at highest current value (50A), it has been justified than it can achieve more than 13 °C, respect to the value 73 °C, given by the temperature sensor provided into the stack by the manufacturer. Therefore, the stack temperature distribution in configuration 1 is no uniform at all.

Regarding thermographies obtained from configuration 2, they show how the stack temperature distribution is still no uniform. In this case, the hottest points also appears on the upper left side of the stack, very similar to configuration 1. Moreover, the difference between the coldest and hottest point at highest current value (50A), is worse than in the first configuration, increasing up to 18 °C taking as reference the value of 65 °C given by the temperature sensor.

In the last configuration, the third, thermography images point out that the best temperature distribution is around the stack cathode area. In this case, temperature distribution is clearly homogeneous in the two cases (configuration 3-Test 1 and configuration 1-Test 2. The difference between the coldest and hottest point is 1.4 °C, while the value offered by the temperature sensor is 65 °C. Then, we can conclude that the best configuration, besides it involves a more complex control into the fan, is configuration 3. It guarantees the best air breathing and cooling into the stack, homogenous temperature distribution and the best stack performance.

Once the three proposed configurations have been discussed separately, now we are going to compare the main factors defined by the oxidant/cooling subsystem design. These factors are the air mass required for oxidant reaction, the heat generated by the stack, the air flow needed for cooling the stack and the fan operating point.

Based on Table 7, we can see that air required by oxidant reaction increases when current rises, and it is much lower than the air flow required for cooling the stack. It is proved that in all the cases, the stoichiometric rate keeps inside the range recommended by the manufacturer (50–200). Additionally, we can observe that the less efficient configuration (#1) is the one that implies highest heat production in the stack. From this, configuration 2 and 3 reduces gradually the heat generation, and therefore the air required for cooling decreases too.

Regarding the fan speed, it is adjusted according to the control algorithm. The fan operating point can be known taking into account the pressure drop that the air flowing through the stack experiences and the air flow needed for cooling. Fig. 18a and b shows the fan/s operating range, in the three cases, is inside of nominal operating area defined by the fan manufacturer.

Where (equations expressed below have been obtained from manufacturer data [29,30],

- $Air_{stack} = 0.000996 \cdot I_s \cdot n_{cell}$ is the air flow required for oxidant reaction (m^3/h).
- $Q_{stack\_heat} = n_{cell} \cdot (1.25\ V - V_{cell}) \cdot I_s$ is the heat generated by the stack (W).
  - o n_{cell} is the number of cells that integrates the stack (80).
  - o $V_{cell} = V_{stack}/n_{cell}$ is the cell voltage (V).
  - o I_s is the number stack current (A).
- $\dot{V}_s = \frac{Q_{stack\_heat}}{(T_s - T_{amb}) \cdot C_p \cdot \rho_{air}}$ is the air volume flow needed for stack cooling (m^3/h).
  - o T_s is the stack temperature (ºC).
  - o T_{amb} is the ambient temperature (23 °C).
  - o C_p is air heat capacity (1012 J/(Kg·K)).
  - o ρ_{air} is the air density (1.29 kg/m^3).
- $\Delta P = \cdot P_s + \cdot P_{ducting}$ is the total pressure drop that the air flowing experiences (Pa).
  - o $P_s = \frac{0.0592 \cdot (T_s+273)^{1.5}}{T_s+393} \cdot \frac{\dot{V}_s}{(n_{cell}+1)}$ is the pressure drop through the stack (Pa), with $\dot{V}_s$ expressed in l/min.
  - o $P_{ducting}$ is the ancillary air pressure drop such as the ducting (no higher than 24 Pa)

Before to conclude, we are going to compare the performances obtained from each configuration with the standard configuration recommended by the manufacturer. Then, Fig. 19a shows the stack voltage obtained in each case, and from it, we can deduce the configuration that allows obtaining the best performance from the stack is the one that guarantees the best breathing/cooling to the stack (configuration 3). Fig. 19b shows that configuration 3 allows extracting from the stack more power than the power offered according to standard configuration proposed by manufacturer.

The last comparison is related to stack temperature. As we can observe from Fig. 19c, those configurations where the stack is properly cooled, the stack temperature is very close to optimal temperature and it matches with configurations that offer higher power rates. As a result, worse temperature control involves worse stack performance.[1]

Finally, Table 8 summarizes the main characteristics of the proposed configurations and the standard configuration proposed by the manufacturer, attending to parameters for accomplishing the challenges posed as goals of the presented work in relation to the oxidant/coolant subsystem. These parameters are:

- Number of fans which integrate the subsystem.
- Size of the enclosure.
- Total weight.
- Cost, calculated as unitary cost * number of units.
- Auxiliary power consumption, calculated as unitary power consumption * number of units.
- Possibility of airflow control.
- Homogenous temperature distribution. Taking into account the stack in made up by 80 cells, the maximum difference between the hottest and coldest point to consider the temperature distribution as uniform is fixed at 2 °C; this corresponds with a rate of 0,025 °C/cell
- And finally, fuel cell system efficiency, calculated as “Output Electrical Power/Hydrogen Consumed)

In basis of them, Table 8 offers a comparative of requirements achieved by each proposal, showing that configuration 3 accomplishes all of them.

[1] Regarding stack temperature response, differences at the beginning of each test are justified because stack has been subjected to different initial conditions.

Table 8
Summary of the performances obtained from the proposed Oxidant/Cooling subsystems and from the manufacturer standard configuration.

Configuration	Structure	Number of fans	Size (W x L x H) (mm)	Weight (gr)	Cost (€)	Auxiliary Power Consumption (W)	Air flow Control	Homogenous Temperature Distribution	AC-PEFC Efficiency (Electrical power/H2 consumption)
1	Four fans without control 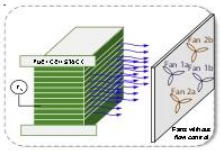	4	400 × 200 × 600	3280	799.36	364.8	No	No	30%
2	meter, adjusted slightly below Four fans with control 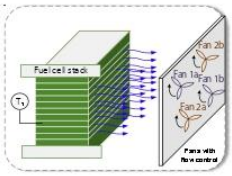	4	400 × 200 × 600	3280	799.36	364.8	Yes	No	42%
3	One single speed controlled fan 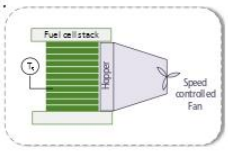	1	350 × 250 × 440	820	199.84	91	Yes	Yes	50%
Manufacturer proposal	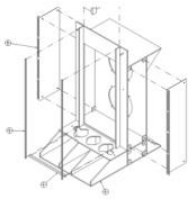	2	400 × 200 × 600	410	399.7	182.4	No	No	45%

6. Conclusion

This paper presents a comprehensive experimental study of three possible configurations of the Oxidant/Cooling subsystem in an AC-PEFC. This presented study justifies that the authors are trying to enhance the Oxidant/Cooling subsystem. Contrary to what one might think, and based on experimental results, this paper has shown how the Oxidant/Cooling subsystem can condition the stack operation. It is really important to control the stoichiometric rate between the values recommended by the manufacturer's data to avoid the stack deterioration.

This work departs from six challenges in the design and manufacture of the oxidant/cooling sub-system in an AC-PEFC: 1) to be able to cool the stack homogeneously, 2) to provide sufficient airflow range to control the PEFC temperature, under a range of power and room/coolant air temperature, 3) to place the stack at optimum temperature, 4) to reduce the auxiliary power consumption, 5) to do all this within a certain sized box, and last but not least 6) to do so cost effectively.

In order to overcome the challenges posed, the presented work departs from a configuration based on manufacturer recommendations and trying to improve the stack temperature control including some changes which could make to enhance the system operation.

To carry out the study, different configurations for the Oxidant/Cooling subsystem have been designed, built and analysed based on the AC-PEFC responses. Proposed configurations are based on influencing on different devices which integrate the Oxidant/Cooling subsystem (fan/s, distance, enclosure design, flow adapter, and so on). Different variables have been analysed from the AC-PEFC system with the different configurations applied to the Oxidant/Cooling subsystem. This has been complemented by introducing different thermography at different stack current values to study the temperature distribution over the stack cathode area.

Three configurations have been carried out: four fans covering the cathode area of the stack working two by two without flow control, four fans covering the cathode area of the stack working two by two with flow control, and one single fan with speed controlled. The first two are housed in a polycarbonate rectangular-shaped enclosure that covers the entire stack. The third has been placed in a cone-shaped hopper also covering the entire stack. This cover is adapted to the stack geometry.

With regard to the experimental results, we can assert that the first two proposals present a diminished airflow distribution because the airflow follows preferential paths due to the space. This space is found between the polycarbonate enclosure and the stack, and the airflow follows these paths instead of crossing the stack and cooling it.

References

[1] F. Barbir, PEM Fuel Cells: Theory and Practice, Elsevier Academic Press, New York, 2012.
[2] U. Kunze, J. Paschos, O. Stimming, Fuel Cell Comparison to Alternate Technologies, in Fuel Cells, Springer, 2013, pp. 77–95.
[3] EG&G Technical Services, Fuel cell handbook, seventh, U.S: Department of Energy, 2004, p. 427.
[4] M. Andersson, S.B. Beale, M. Espinoza, Z. Wu, W. Lehnert, A review of cell-scale multiphase flow modeling, including water management, in polymer electrolyte fuel cells, Appl. Energy 180 (2016) 757–778.
[5] D. Guida, M. Minutillo, Design methodology for a PEM fuel cell power system in a more electrical aircraft, Appl. Energy (Nov. 2016).
[6] M.J. Vasallo, J.M. Bravo, J.M. Andújar, Optimal sizing for UPS systems based on batteries and/or fuel cell, Appl. Energy 105 (2013) 170–181.
[7] F. Segura, E. Durán, J.M. Andújar, Design, building and testing of a stand alone fuel cell hybrid system, J. Power Sources 193 (2009) 276–284.
[8] S. Cordiner, V. Mulone, A. Giordani, M. Savino, G. Tomarchio, T. Malkow, G. Tsotridis, A. Pilenga, M.L. Karlsen, J. Jensen, Fuel cell based Hybrid Renewable Energy Systems for off-grid telecom stations: data analysis from on field demonstration tests, Appl. Energy (2016).
[9] J.J.B.M.J. Vasallo, J.M. Andújar, C. García, A methodology for sizing backup fuel-cell/battery hybrid power systems, Ind. Electron. IEEE Trans. 57 (6) (2010) 1964–1975.
[10] F. Segura, J.M. Andújar, Power management based on sliding control applied to fuel cell systems: a further step towards the hybrid control concept, Appl. Energy 99 (2012) 213–225.
[11] A. Gomez, A. Raj, A.P. Sasmito, T. Shamim, Effect of operating parameters on the transient performance of a polymer electrolyte membrane fuel cell stack with a dead-end anode, Appl. Energy 130 (2014) 692–701.
[12] G. Zhang, S.G. Kandlikar, A critical review of cooling techniques in proton exchange membrane fuel cell stacks, Int. J. Hydrogen Energy 37 (3) (2012) 2412–2429.
[13] J.W. Ahn, S.Y. Choe, Coolant controls of a PEM fuel cell system, J. Power Sources 179 (2008) 252–264.
[14] H.S. Han, C. Cho, S.Y. Kim, J.M. Hyun, Performance evaluation of a polymer electrolyte membrane fuel cell system for powering portable freezer, Appl. Energy 105 (2013) 125–137.
[15] A.P. Sasmito, E. Birgersson, K.W. Lum, A.S. Mujumdar, Fan selection and stack design for open-cathode polymer electrolyte fuel cell stacks, Renew. Energy 37 (1) (2012) 325–332.
[16] F. Segura, J.M. Andújar, Step by step development of a real fuel cell system. Design, implementation, control and monitoring, Int. J. Hydrogen Energy 40 (15) (2015) 5496–5508.
[17] F. Philipps, G. Simons, K. Schiefer, Dynamic investigation of PEFC stacks in interaction with the air supply system, J. Power Sources 154 (2) (Mar. 2006) 412–419.
[18] Y.-B. Kim, Improving dynamic performance of proton-exchange membrane fuel cell system using time delay control, J. Power Sources 195 (19) (2010) 6329–6341.
[19] O. Himanen, T. Hottinen, S. Tuurala, Operation of a planar free-breathing PEMFC in a dead-end mode, Electrochem. Commun. 9 (2007) 891–894.
[20] R. Eckl, W. Zehtner, C. Leu, and U. Wagner, "Experimental analysis of water management in a self-humidifying polymer electrolyte fuel cell stack," J. Power Sources, vol. 138, no. 1–2, pp. 137–144.
[21] H.-W. Wu, A review of recent development: transport and performance modeling of PEM fuel cells, Appl. Energy 165 (2016) 81–106.
[22] R.C. Samsun, J. Pasel, H. Janßen, W. Lehnert, R. Peters, D. Stolten, Design and test of a 5 kWe high-temperature polymer electrolyte fuel cell system operated with diesel and kerosene, Appl. Energy 114 (2014) 238–249.
[23] M. Gerbec, V. Jovan, J. Petrovčič, Operational and safety analyses of a commercial PEMFC system, Int. J. Hydrogen Energy 33 (2008) 4147–4160.
[24] U. Soupremanien, S. Le Person, M. Favre-Marinet, Y. Bultel, Tools for designing the cooling system of a proton exchange membrane fuel cell, Appl. Therm. Eng. 40 (2012) 161–173.
[25] J. Marcinkoski, B.D. James, J. a Kalinoski, W. Podolski, T. Benjamin, J. Kopasz, Manufacturing process assumptions used in fuel cell system cost analyses, J. Power Sources 196 (12) (2011) 5282–5292.
[26] B.J. Kim, M.S. Kim, Studies on the cathode humidification by exhaust gas recirculation for PEM fuel cell, Int. J. Hydrogen Energy 37 (5) (2012) 4290–4299.
[27] Q. Meyer, A. Himeur, S. Ashton, O. Curnick, R. Clague, T. Reisch, P. Adcock, P.R. Shearing, D.J.L. Brett, System-level electro-thermal optimisation of air-cooled open-cathode polymer electrolyte fuel cells: air blower parasitic load and schemes for dynamic operation, Int. J. Hydrogen Energy 40 (no. 46) (2015) 16760–16766.
[28] Q. Wu, H. Li, W. Yuan, Z. Luo, F. Wang, H. Sun, X. Zhao, H. Fu, Performance evaluation of an air-breathing high-temperature proton exchange membrane fuel cell, Appl. Energy 160 (2015) 146–152.
[29] FCgen ® -1020ACS/FCvelocity ® -1020ACS Fuel Cell Stack. Product Manual and Integration Guide, 2010.
[30] Ballard Putting Fuel Cells to Work FCgen ® -1020ACS Fuel Cell Stack FCvelocity ® -1020ACS Fuel Cell Stack Product Manual and Integration Guide, 2014.
[31] Ebmpapst, Product Data Sheet DV6224 TDA, 2012.

6.5. Contribution 5

An Energy Management Strategy and Fuel Cell Configuration Proposal for a Hybrid Renewable System with Hydrogen Backup

F.J. Vivas, A. De las Heras, F. Segura, J.M. Andújar

Published in:

Journal: International Journal of Energy Optimization and Engineering
Editorial: IGI-Global
Editor-in-Chief: Pandian Vasant
Reference: Vol. 6, Issue 1, pp. 1-22
Year: 2017
ISSN: 2160-9500
DOI 10.4018/IJEOE.2017010101
International peer review journal with open access.
Journal indexed in Web Of Science

International Journal of Energy Optimization and Engineering
Volume 6 • Issue 1 • January-March 2017

An Energy Management Strategy and Fuel Cell Configuration Proposal for a Hybrid Renewable System with Hydrogen Backup

Francisco José Vivas Fernández, University of Huelva, Huelva, Spain
Ainhoa de las Heras Jiménez, University of Huelva, Huelva, Spain
Francisca Segura Manzano, University of Huelva, Huelva, Spain
José Manuel Andújar Márquez, University of Huelva, Huelva, Spain

ABSTRACT

This paper presents a new and optimal proposal of energy management strategy for a solar panels/wind turbines/fuel cell/battery/alkaline electrolyzer on grid hybrid power system. These new proposal takes into account technical and economical optimization parameters, improving the system performance, the lifetime of different elements and reducing operation and maintenance cost. The features of the proposed energy management strategy are compared over other strategies found in the scientific literature. Additionally, another key parameter like fuel cell modularity has been considered. That is the effect over the whole system performance of using a single fuel cell with high rate power (P_{FC}) versus a modular configuration built from n stacks with P_{FC}/n rate power each one. Then, joining the new proposed strategy with the optimization parameter regarding the fuel cell modularity, it is possible to get the best solution for this kind of hybrid systems.

KEYWORDS

Energy Management, Fuel Cell Configuration, Hybrid Renewable, Hydrogen Backup, Simulator

1. INTRODUCTION

Nowadays it is an increasingly environmental problem the use of an energy system based on fossil fuels. Despite the efforts of governments and research teams, renewables energies have a number of associated problems such as dependence on environmental conditions, lifetime, high price, etc. In order to reduce these problems, the use of hybrid systems is presented as a technically feasible optimal solution. Recently, the use of hydrogen as an energy vector has been presented as a viable solution to improve the performance of hybrid system (García, Torreglosa, Fernández, & Jurado, 2013).

The proper energy management of hybrid systems requires the design of a control system and energy management strategy. For this reason, different works have been presented in order to make an optimal management, increasing system performance, providing a real alternative to current energy production. Most of these works are based on strategies whose sole propose is to keep the load as long as possible. The main target of these strategies is to ensure the power balance. This parameter is presented therefore as the only decision criteria to operate the system. These strategies base their efforts on maintaining the demand, ignoring technical or economic criteria associated with the proper operation of the equipment and its operating regimes. The use of fuel cell and electrolyzer is determined by the power balance, generating or absorbing energy based on the amount of excess/deficit

DOI: 10.4018/IJEOE.2017010101

International Journal of Energy Optimization and Engineering
Volume 6 • Issue 1 • January-March 2017

energy. Strategies with grid connected configurations, use the grid as an active element of the system increasing security by having a solution in situations of excessive excess or defect energy (Ahmed, 2012), (Alkano, Kuiper, & Scherpen, 2015), (Mohammadi & Nafar, 2013), (Tesfahunegn, Ulleberg, Vie, & Undeland, 2011), (Giannakoudis, Papadopoulos, Seferlis, & Voutetakis, 2010). In isolated topologies, it will depend on the use of short-term energy storage elements. In most applications, batteries or supercapacitors operate in the first instance in situations of excess or defect energy, absorbing or supplying energy respectively. The use of fuel cells and electrolyzers is determined by the maximum or minimum predetermined operating margins for the above equipment (Sun, Lian, Wang, & Li, 2009), (Li, Jiao, & Wang, 2013), (Osman Haruni, Negnevitsky, Haque, & Gargoom, 2013), (Tégani, Aboubou, Ayad, Becherif, & Bahri, 2014), (Feroldi, Degliuomini, & Basualdo, 2013), (Mbarek, Belhadj, Le, & Tunis, 2009), (Bizon, Oproescu, & Raceanu, 2015).

In the same way, there are different works with strategies which objectives include some technical decision factors. The main target of these strategies is to reduce the degradation of the more critical equipment during the system operation. These elements are battery, electrolyzer and fuel cell. The solutions adopted in the literature are diverse and depend on the main goal to study. Strategies which choose to increase battery life, operate it with very low depths of discharge, a fixed load condition or a narrow range of SOC (Alkano et al., 2015), (Sacarisen & Parvereshi, n.d.), (Ipsakis et al., 2008). Other strategies are based on overcurrent control, improving the battery charge process (Kim et al., 2014). Strategies which choose to increase the electrolyzer lifetime are based on operate it with minimal power point. The use of this parameter will increase the performance but with low purity of products (Alkano et al., 2015), (Dash & Bajpai, 2015), (Uzunoglu, Onar, & Alam, 2009).

In order to reduce the degradation of the fuel cell versus dynamic conditions, it will operate in stable power (Brka, Kothapalli, & Al-Abdeli, 2015), (Dursun & Kilic, 2012).

On the other hand, to reduce the negative effect of starts-stops cycles of electrolyzer and fuel cell, two different solutions are adopted in the literature. The first one determines the start-stop points of the equipment according to the hysteresis of the SOC (Karami, Moubayed, & Outbib, 2014)], (Dash & Bajpai, 2015), (Sacarisen & Parvereshi, n.d.). The second one uses generation and demand forecast to determine, based on the current system status, what element will be necessary in the next work cycle and its power reference (F. Segura, Durán, & Andújar, 2009), (Hussain, Member, Bingham, & Stone, n.d.). Such strategies have the disadvantage of relying of the precision of the forecast. Finally, (Behzadi & Niasati, 2015) presents a strategy which priority is based on the accumulated degradation for each element. The element with lower degradation will absorb or supply energy when it is necessary.

Other strategies have only economic goals, ignoring some real problems associated with the equipment degradation. The solutions adopted in the literature (Bordons, García-Torres, & Valverde, 2015), (Heymann & Bessa, 2015), (Zhou, 2008), (García, Torreglosa, Fernández, & Jurado, 2014), (Zhang et al., 2013), (Patsios, Antonakopoulos, Chaniotis, & Kladas, 2010), (Trifkovic, Marvin, Sheikhzadeh, & Daoutidis, 2013) are based on the use of different cost functions associated with the charge or discharge of the elements, which determine an optimization problem. The use of different algorithms will be used to calculate the solution of optimization problem.

Finally, this kind of strategy seeks to increase system performance, based on the proper supply to demand. Technical and economic criteria are taken into account to increase equipment life and reduce maintenance costs. This strategy has an optimal solution for a technical and economic point of view, compared to traditional generation alternative systems. The solutions adopted in the literature (Castañeda, Cano, Jurado, Sánchez, & Fernández, 2013), (Wang, Tong, Palazoglu, & El-farra, 2014) are based on nonlinear optimization problems, using cost and equipment depreciation and useful life functions.

On the other hand, most of studied hybrid systems (Ahmed, 2012; Das, Esmaili, Xu, & Nichols, 2005; Eid, 2014) consider a fuel cell as energy backup element to ensure the load demand and system stability as secondary long-time backup. In all these cases the fuel cell system is built from a single stack, and hardly we can find works, (El-Shatter, Eskander, & El-Hagry, 2006), which mention the

International Journal of Energy Optimization and Engineering
Volume 6 • Issue 1 • January-March 2017

possibility of including a modular fuel cell instead of a single fuel cell for a better adaptation to supply the required energy.

Regarding the fuel cell operation, stacks can be deteriorating in start-up/stop cycles, load changes and run-time operation.

In order to take into account all the technical and economic requirements necessary for guaranteeing an optimal system response, authors propose a strategy based on battery (BAT), SOC hysteresis and optimum operating points of electrolyzer (ELEC) and optimal configuration of fuel cells (FC). Additionally, a hydrogen management strategy is supplied, in order to obtain the maximum performance in the generation, storage and consumption subsystems.

Finally, a sensitivity analysis will be performed in order to compare the results obtained from the proposed strategy with regard to other solutions adopted in technical literature.

In the next section, the proposed hybrid system is studied. In Section 3, the energy management strategy is presented. The designed simulator and the models used for each subsystem are discussed in Section 4. The results and discussions are presented in Sections 5 and 6 respectively. Finally, conclusions are presented in Section 7.

2. PROPOSED HYBRID POWER SYSTEM

The hybrid system presented in this work consists mainly of two different sources of renewable energy, solar panels (PV) and wind turbines (WT) as primary and secondary energy sources. As a last resort, the injection of the grid can be used in case of energy deficit in the system.

Similarly, it has a number of loads which must be guaranteed at all times. The primary load is modelled as a DC variable load, which represents any possible profile in any application. There is a secondary load whose function is to ensure the energy balance in situations of excess production. This load is represented by an electrolyzer, which can convert the electrical energy into chemical energy with the use of hydrogen like energy vector. In extreme cases, the grid can be considered like another load, in case of over production.

Additionally, there are needed energy backup elements to ensure the load demand and system stability in situations of energy deficit. In this case, a batteries bank (BAT) is used as primary short/medium-time backup energy, and a fuel cell system (FC) as secondary long-time backup energy.

In the same way, is necessary the use of hydrogen backup technologies. For this target, the use of metal hydrides tanks and high pressure tanks are used in this topology.

Finally, all the elements of the system are connected to an internal DC bus. In order to assure an optimal connection, DC/DC converters are used to keep sources at his optimal operation point, and to assure the nominal output voltage to the correct DC bus connection.

The architecture of the proposed hybrid renewable system installed at the University of Huelva is shown in Fig. 1.

3. ENERGY MANAGEMENT STRATEGY

To operate, integrate and interconnect all the elements of the presented distributed generation system, ensuring safe operating regime and fulfilling the objectives, it is necessary a control system to manage the energy inside. Proper energy management strategy, enable us to supply the demand, increase the lifetime of the elements, reduce operating costs, and therefore, maximize system performance, providing a viable technical and economical solution.

The main targets of the proposed energy management strategy are guarantee the demand at all time, operate the system in order to increase the lifetime of different elements and reduce the operation and maintenance costs, and finally the optimal hydrogen management in its three different phases: production, storage and consumption. For this reason, is necessary the development of two different strategies, the first one a power management strategy, and the second one a hydrogen management strategy.

International Journal of Energy Optimization and Engineering
Volume 6 • Issue 1 • January-March 2017

Figure 1. Architecture of proposed hybrid power system

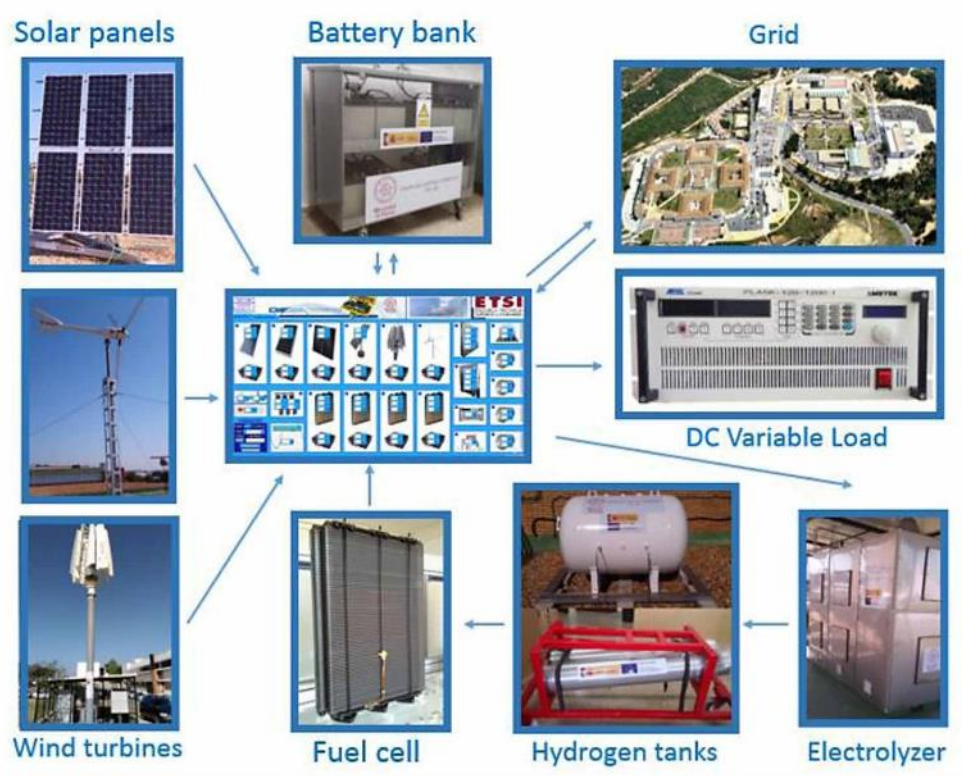

3.1. Power Management Strategy

The power management strategy has the target of operate the system in an optimal operation point, fulfilling the objectives presented previously. In order to get it, the power balance at all the time must to assure the demand. Then the power balance equation can thus be written as (1):

$$P_{net} = P_{PV} + P_{WT} - P_{load} - P_{losses,} \quad (1)$$

where P_{net} is the net power, P_{PV}, P_{WT}, is the power generated by solar panels and wind turbines; and P_{load}, P_{losses}, are the demand and electrical loses inside the system respectively.

Additionally, in order to operate the system in an optimal operation point, taking into account the lifetime of the elements, is necessary to know the disadvantages of each component.

The use of fuel cells in dynamic start/stop cycling and variable loads conditions, increase the degradation of active area in electrodes, with a fast oxidation and dissolution of platinum layer, resulting in mass transport losses and therefore, resulting in voltage losses (Bae et al., 2012; Borup, Davey, Garzon, Wood, & Inbody, 2006; Janssen, Sitters, & Pfrang, 2009; Kannan, Kabza, & Scholta, 2015; Lin et al., 2015; Mohammed Jourdan, Mounir, & Marjani, 2014; Oyarce et al., 2014; Uno & Tanaka, 2011; Yu et al., 2012). These losses affect the stack performance.

On the other hand, the batteries lifetime depends on the depth of discharge (DOD) and operation conditions, so it is necessary to guarantee the use of them under security margins (Sacarisen & Parvereshi, n.d.),(Ng, Moo, Lin, & Hsieh, 2008). Finally, the use of an electrolyzer under very low power operation points or dynamic start/stop conditions, can suffer extra deterioration in electrolyte, and also operate in very low efficiency operation point (Ziogou et al., 2013; Miland & Ulleberg, 2012).

International Journal of Energy Optimization and Engineering
Volume 6 • Issue 1 • January-March 2017

In order to solve the majority of the above problems, different operation conditions are presented:

1. Hysteresis band for battery state of charge (SOC) for the start/stop conditions of fuel cells (blue) and electrolyzer (red), in order to reduce the cycling of these elements (Ulleberg, 2004). To develop this strategy, is necessary to define different SOC operation points:
   - **SOCmax:** Maximum charge status must be guaranteed to work safely. This value matches the battery SOC at which the electrolyzer should start, because the state of charge is the maximum allowed.
   - **SOCmin:** Minimum state of charge must be guaranteed throughout the lifetime of the battery. This value coincides with the start conditions of fuel cells.
   - **SOCelemin, SOCfcmax:** SOC value which indicates the stop condition of electrolyzer and fuel cells respectively.
   - **SOCH2:** Minimum SOC value which indicates the stop condition for the hydrogen recharge from high pressure tanks to metal hydrides tanks. This value is necessary because the load process absorbs energy, so will affect to the remaining energy of the system in situations of low SOC value.
   - **SOClow:** Minimum battery state of charge. The grid will supply demand and the fuel cell will be disconnected in order to save energy from battery.

   A scheme of the proposed SOC hysteresis band strategy is shown in Fig. 2.
2. Fixed power operation point for fuel cell depending on the hydrogen stock. This condition will improve the lifetime of fuel cell (Janssen et al., 2009; Mohammed Jourdan et al., 2014), despite increasing the hydrogen consumption and the battery operation time.
3. All hydrogen produced depends on the overall performance of generation, given by the product of the performance of the primary generators (solar and wind), and the electrolyzer. Solar performance is very low, so it is necessary to work with the best electrolyzer performance as possible. In order to get this target, minimum power point for electrolyzer is necessary, in order to guarantee the highest performance operation conditions. To assure it, in case the excess of energy is not enough to reach the minimum power to start the electrolyzer, batteries will supply the necessary energy to reach it.
4. Use of batteries bank as main element of the hybrid system because of its capacity for rapid response to transients. This condition will improve the use of batteries respect the rest of elements, which are more expensive and more vulnerable to transients.
5. DOD of batteries bank must to guarantee an optimal technical and economical solution, providing the best configuration taking into account the operation and maintenance costs of the different elements, and the influence that DOD has in its operation conditions.

3.2. Hydrogen Management Strategy

Fuel cells require around 14 slpm of hydrogen/kW, and this required flow must be provided by hydrogen tanks to hold the fuel cell operating point. Then, the discharge flow of metal hydrides tanks will determine the maximum possible power supplied by the FC. The purpose of the hydrogen management strategy is to determine the priority of charge/discharge of metal hydrides tanks, in order to give the best solution.

The charge of metal hydrides tanks will be make through a high pressure tank, whose function is create a reserve of hydrogen between electrolyzer and metal hydrides tanks, in order to guarantee a constant hydrogen input flow towards the fuel cell system. This process needs extra energy, so it will happen only under $SOC>SOC_{H2}$ condition. On the other hand, the discharge of metal hydrides tanks also needs energy, so it is necessary to take into account that this process will occur in deficit energy situations, aggravating the consumption problem.

International Journal of Energy Optimization and Engineering
Volume 6 • Issue 1 • January-March 2017

Figure 2. SOC operation conditions

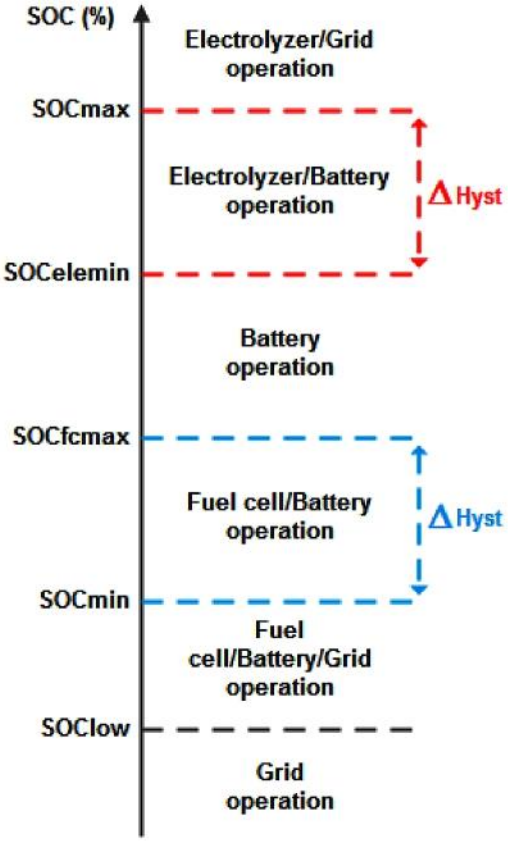

The optimal solution is one that prioritizes the use of equipment with greater capacity of charge/discharge. The use of this type of solution ensures bigger stock and consequently higher hydrogen output flow, and therefore greater response of fuel cell power generation. The extra energy consumption during metal hydride tanks charging will not be a problem, because this situation only happens in case of energy excess. In the same way, the extra energy consumption in discharging situations should be provided with the extra power that the fuel cells have to produce.

3.3. Proposed Energy Management Strategy

The system operation can be formulated as follows: PV and WT will supply the load as much as possible. In energy deficit conditions, batteries and subsequently fuel cell, will supply the necessary energy, according to hysteresis operation mode and hydrogen stock. The grid will act when not all the resources of the system are enough to guarantee the demand, keeping the battery SOC over the lower established limit.

On the other hand, in energy excess conditions, batteries and subsequently electrolyzer will absorb the excess of energy, based on hysteresis operation mode and hydrogen stock. The grid could be considered as extraordinary load when the excess of energy is higher than the system capability to absorb energy. The flowcharts, which represent the described strategy for discharge and charge operation modes are presented in Figures 3 and 4 respectively.

International Journal of Energy Optimization and Engineering
Volume 6 • Issue 1 • January-March 2017

Figure 3. Flux diagram for discharge operation mode

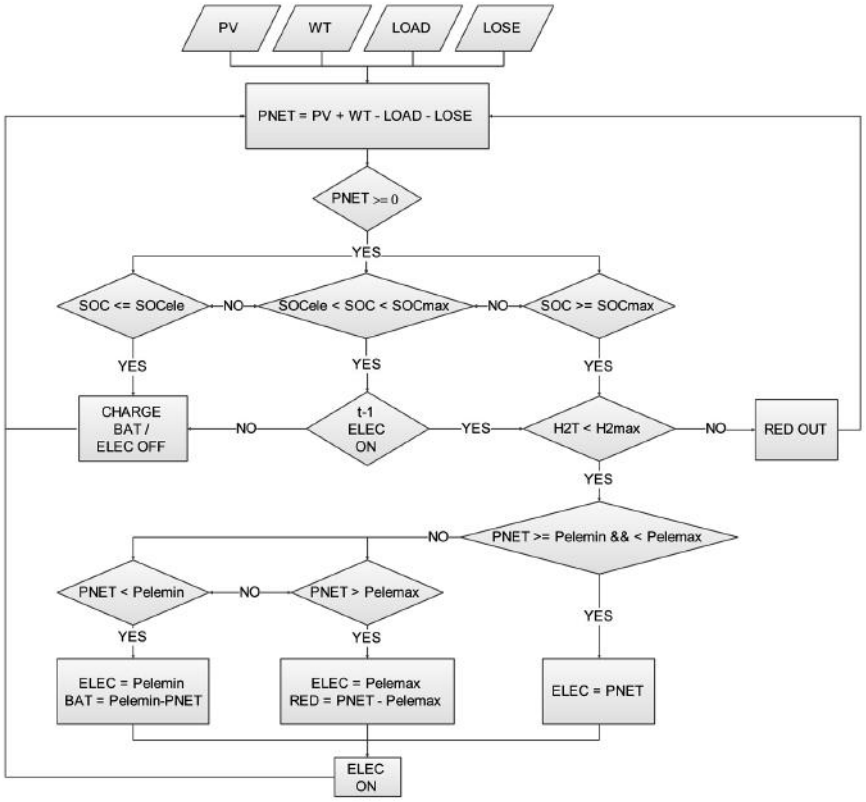

Figure 4. Flux diagram for charge operation mode

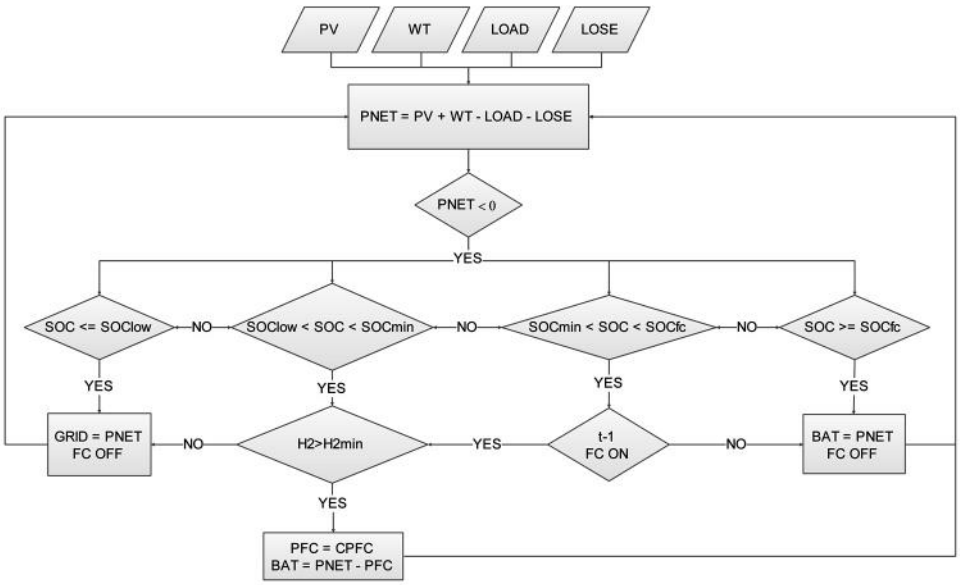

International Journal of Energy Optimization and Engineering
Volume 6 • Issue 1 • January-March 2017

The hydrogen load-download process will occur under electrolyzer and fuel cell operation respectively. The hydrogen will be extracted from metal hydride tanks until they reach their minimum value.

The number of hydrogen tanks downloading in parallel will depend on fuel cell requirements.

On the other hand, the metal hydride tanks will absorb hydrogen while they do not reach their maximum value, and the battery SOC is over the $SOCH_2$ limit previously established.

The priority to load and download the different hydrogen tanks was presented previously. The flowcharts which represent the described hydrogen download-load operations are presented in Figure 5.

The proposed energy management strategy has been developed and tested in Matlab/Simulink environment simulator. This simulator is described in the next section.

4. SIMULATOR

The developed simulator described in this section tries to solve the integration of all components of the proposal hybrid system, as well as the implementation management strategies. A general view of the simulator is shown in Fig 6.

Figure 5. Flowcharts for hydrogen download-load operation

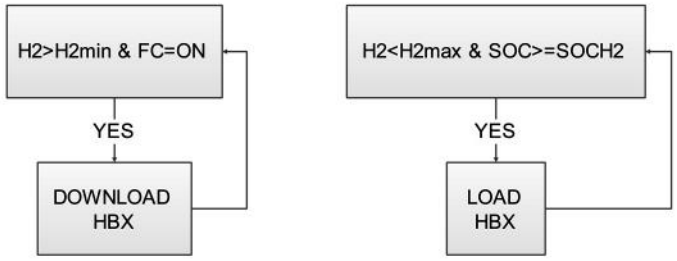

Figure 6. Simulator general view

International Journal of Energy Optimization and Engineering
Volume 6 • Issue 1 • January-March 2017

The target of this simulator is to test the system in order to get the pros and cons of the different management strategies and fuel cell configurations, in order to get the optimal solution. To do this, the simulator calculates lifetime and power points of each element, and finally, develops different energy management strategies based on power balance, SOC and hydrogen stock.

The simulator is based on power parameters of each element, and uses empirical weather conditions (solar radiation and wind speed), measured by sensors used by TEP-92 researcher group. In the same way, the time step used is less than one second, in order to test the dynamic response of different elements.

Next, models used by the simulator to represent each element are described below.

4.1. Solar Panels

A photovoltaic panel is composed of the union in series and parallel photovoltaic cells. The model used for solar panels is based on linear approximation between solar radiation energy and the maximum power production (3), taken into account MPPT control laws and the effect of temperature in solar production (2).

$$P_{PV}(G,T) = P_{PVmax}(G/G_{nom}) \quad (2)$$

$$P_{PVmax}(T) = (G*\eta_{PV})*(1+ K_{TP}(T_c - 25\ ºC)) \quad (3)$$

where:

G: Solar radiation (W/m^2)
G_{nom}: Solar radiation in STC conditions (W/m^2)
P_{PVmax}, P_{PV}: Maximum / instant power (W)
η_{PV}: Module efficiency (%)
K_{TP}: Power temperature coefficient (%/K)
T_c: Solar Cell temperature (ºC)

4.2. Wind Turbines

A wind turbine is an aerodynamic machine which converts the kinetic energy from the air, to electrical energy, throw aerodynamic load and an electrical generator. The model used in this case is based in power curve of wind turbines, presented below:

$$0;\ v \le v_a, \quad (4)$$

$$C_p(1/2)\rho A v^3;\ v_a < v < v_n, \quad (5)$$

$$P_N;\ v_n \le v \le v_p, \quad (6)$$

$$0;\ v_p < v, \quad (7)$$

where:

v: Wind speed (m/s)
v_a: Start speed (m/s)
v_n: nominal design speed (m/s)
v_p: Stop speed (m/s)
P_N: Rated power of the wind turbine (W)

International Journal of Energy Optimization and Engineering
Volume 6 • Issue 1 • January-March 2017

A: rotor area (m^2)
C_p: Belt coefficient
ρ: Air density (kg / m^3)

4.3. Fuel Cells

A fuel cell is an electrochemical device in which electrical energy is produced through oxidation and reduction of hydrogen and oxygen in the anode and cathode respectively, according to the following reactions:

$$\text{Anode: } 2H_2 \rightarrow 4H^+ + 4e^- \quad (8)$$

$$\text{Cathode: } O_2 + 4e^- + 4H^+ \rightarrow 2H_2O \quad (9)$$

In this case, the model is based in a transfer function of first order, trying to model the fuel cell in ohmic operation region, and neglecting any transient effect. This can be a good approximation, because the fuel cell will operate always in fix power point inside this region (Osman Haruni et al., 2013), presenting a linear relationship between current and power.

In the same way, hydrogen consumption will obey a linear dependence with current, following Faraday's Law.

$$m_{H2} = (I \cdot t)/(zF) \quad (10)$$

where:

m_{H2}: Hydrogen consumption (mol/s)
I: Current (A)
t: Time (s)
z: Nº electrons in the reaction
F: Faraday constant (96485 C/mol)

Finally, the effects of cycling and operation time losses have been taken account to calculate the output power along lifetime. These parameters have been taken from technical datasheet.

4.4. Electrolyzer

An alkaline electrolyzer is a device capable of splitting water into hydrogen and oxygen through the passage of a DC electric current between two separate electrodes. The reactions occurring at the anode and cathode are presented below:

$$\text{Anode: } 2OH\ aq \rightarrow 1/O_2\ g + H_2O + 2e \quad (11)$$

$$\text{Cathode: } H_2O + 2e^- \rightarrow 1/2H_2 + 2\ OH\ aq \quad (12)$$

The model used to determine the hydrogen production, is based in Faraday's Law (10); different auxiliary loads have been taken into account in order to reduce the electrolysis power.

4.5. Batteries

A lead-acid battery is an electrochemical device, with the ability to transform electrical energy into chemical energy during charging process, and vice versa, during the discharching process.

International Journal of Energy Optimization and Engineering
Volume 6 • Issue 1 • January-March 2017

In the case of lead-acid battery, the reactions taking place inside are:

$$An: Pb + SO_4^{-2} \leftrightarrow PbSO_4 + 2e \quad (13)$$

$$Ca: PbO_2 + SO_4^{-2} + 4H^+ + 2e^- \leftrightarrow PbSO_4 + 2H_2O \quad (14)$$

The model of the battery is represented by the equation which allow calculate the SOC. To get it, it has been assumed that the battery voltage is constant, so the current can be calculated like the relationship between the battery power and its nominal voltage. This can be a good approximation in case battery operates in nominal area, where voltage is fix respect to the current.

$$SOC(t) = SOC(t\text{-}1) \pm (i(t)\Delta t / Q_{nom}(t)) \quad (15)$$

4.6. Hydrogen Tanks

The hydrogen storage units through metal hydride base their operation on reversible covalent bonds between the metal (M) and hydrogen (H_2), over pressure and temperature conditions.

Charge/discharge reactions in metal hydrides are defined below:

$$Load: M + nH_2 \rightarrow MH_{2n} + heat \quad (16)$$

$$Unload: MH_{2n} + heat \rightarrow M + nH_2 \quad (17)$$

The model of hydrogen tanks is represented by a variable load, which models the thermal energy needed to produce the reactions.

4.7. Economic Analysis

The economic analysis is based on operation and maintenance costs (CO&M) associated with fuel cell, electrolyzer and battery operation. In order to calculate the total CO&M, it has been assumed different operation and maintenance costs per hour for fuel cell and electrolyzer.

In the same way, the remaining life of battery and fuel cell has been calculated, in order to attribute a partial cost of the current use of these elements. To do this, a model presented in (Layadi, Champenois, Mostefai, & Abbes, 2015) has been used to determine the remaining life of the battery depending of DOD operation conditions. The remaining life of fuel cell has been calculated depending of current degradation and the maximum degradation recommended in technical datasheet.

The results of the economic analysis allow us to compare different energy management strategies, and also different operation parameters.

5. SIMULATION RESULTS

In this section two different simulations are presented in order to study the effect of different energy management strategies and fuel cell configurations on the overall system performance. The simulations will be made with different hybrid system parameters. The first simulation made with higher values of generation and demand in order to demonstrate clearly the influence of the energy management strategies over the system response. In basis on the optimal energy management strategy obtained, the second simulation is going to demonstrate the best fuel cell configuration (modular o single stack) to obtain the highest system performance.

International Journal of Energy Optimization and Engineering
Volume 6 • Issue 1 • January-March 2017

5.1. Energy Management Strategy

In this section, results from different simulations of different energy management strategies on the proposal system are presented.

Simulations have been realized under the same weather and load conditions during one year, keeping the hybrid system topology. In this case, it will be used a modular fuel cell topology. The hybrid system parameters used in all simulations are shown in Table 1.

The energy management strategy described in Section 3 (A) has been tested with the developed simulator. In order to guarantee the benefits, it have been simulated three other energy management strategies which have been selected from the scientific literature, which represent strategies which don't take into account the criteria of minimum power to the electrolyzer (B) (Karami et al., 2014),(Dash & Bajpai, 2015); hysteresis band in the battery management (C) (Changrong & Jih-Sheng, 2007), (Dursun & Kilic, 2012); and finally, a strategy which only take into account the power balance (D) (Ahmed, 2012),(Sun et al., 2009). Additionally, these strategies (A, B, C, and D) have been simulated for different SOC cases (I and II) in order to realize a sensitive analysis with all the parameters. A brief of strategies specifications is shown in Table 2.

In order to compare the benefits of the different strategies, there have been analysed the operating parameters of the principal vulnerable elements: fuel cell and electrolyzer start/stop cycles, operation time, and also battery cycles. In addition, an energy analysis has been also made in order to explain the relationship between life-energy parameters, and strategies used at each simulation.

Finally, a sensitive analysis has been development based on the hysteresis bandwidth. This study pretends to demonstrate the effect of different SOC cases over the system response. The simulation results are presented in Figures 6-7 and Table 3.

Table 1. Hybrid system parameters

Element	Parameters	Weather conditions
PV	16.2 kW	G_{max}=750 W/m^2
WT	6.8 kW	Wind Speed mean=3.75 m/s
FC	9.2 Kw / Loss 0.1 V	Localization parameters
BAT	400 V, 100 Ah, SOC_{H2} = 85%	Latitude=37º
ELEC 1	11 kW	Installation param.
ELEC 2	5 kW	Mounting solar angle 35º
LOAD	1.5 kW	Simulation time
HM & HPT	13 Nm^3 2.5/1.5 Nm^3/h 1 Nm^3	365 days
Element	**Cost Parameters**	
BAT	C0=7650 €	
FC	C0=8000 €; CO&M=0.6 €/h	
ELEC	C0=75000 €; CO&M=0.1 €/h	
GRID	CIN=0.136 €/kWh – COUT=-0.0274 €/kWh	

International Journal of Energy Optimization and Engineering
Volume 6 • Issue 1 • January-March 2017

Table 2. Brief of strategies specifications

Case	SOC_{max}	SOC_{elemin}	SOC_{fcmax}	SOC_{min}
I	95	90	80	75
II	95	90	70	65
Strategy	**Param.**			
A	Hyst and Pmin	C	Pmin	
B	Hyst	D	None	

5.2. Fuel Cell Configuration

In this section, results from different simulations for different fuel cell configurations on the proposal system are presented. For this simulations it has been used the strategy A and medium hysteresis values (Table 4), which represent the optimal energy management strategy respect the other strategies studied (please, see Table 3 and Discussion section).

The experimental study carried out is based on a FC system built around the air-cooled 80-cells PE stack model FCgen-1200ACS from Ballard whose system is developed in (Francisca Segura & Andújar, 2015). As it has been demonstrated in (Francisca Segura & Andújar, 2015) even when a stack is new, that is, without having been used, it is very common that its performance does not meet the expected theoretical behaviour. Then the power curve used for simulation is based on experimental data obtained from laboratory (Fig. 7).

Figure 7. Fuel cell power curve for 3.4 kW (experimental) and 6.8 kW (estimated) stack

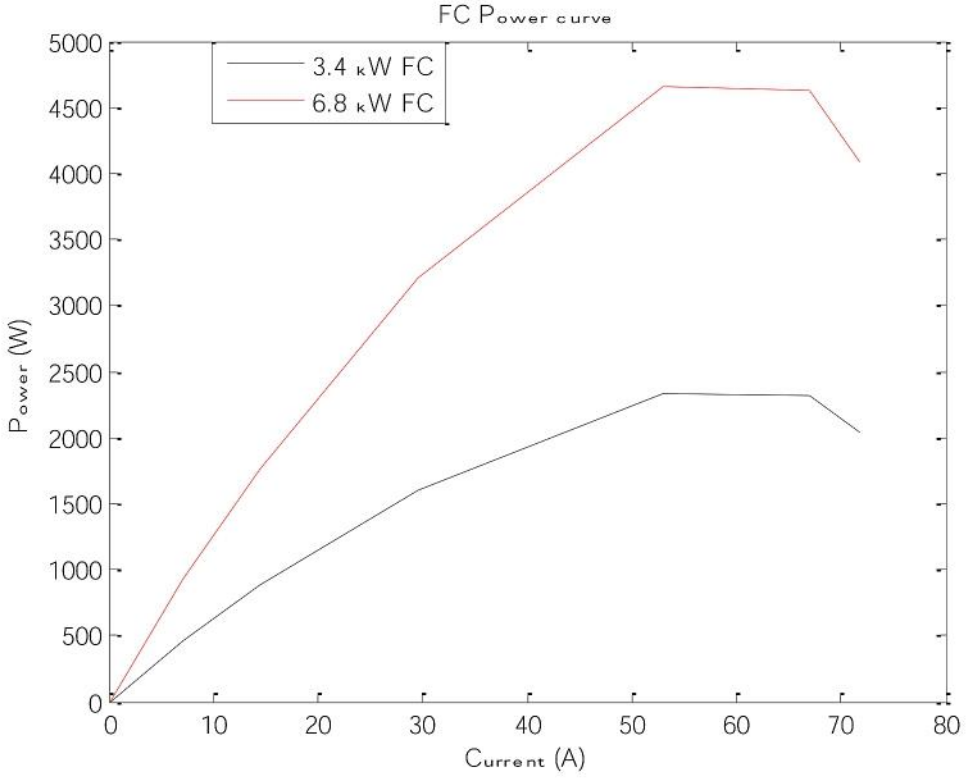

International Journal of Energy Optimization and Engineering
Volume 6 • Issue 1 • January-March 2017

Table 3. Energy/life parameters results

Case		Eout (kW/h)	Ein (kW/h)	Ebat (kW/h)	Efc/Loss (kW/h)	Eelec (kW/h)	CYC/Tfc (h)	CYC/Telec (h)	CYC bat	CO&M (€)	H2 (Nm^3)
I	A	11870.60	436.38	1117.33	443.29/0.58	2277.70	180/193.39	128/682.94	142	1788.20	284.32
	B	11884.35	223.24	884.99	450.38/0.44	1409.08	192/197.08	110/619.08	113	1136.84	177.76
	C	11680.91	416.00	1079.04	436.24/10.16	2104.36	3208/195.01	1818/680.34	92	23230.2	265.478
	D	11687.36	412.63	1048.86	435.51/10.21	2094.57	3225/194.72	228/800.33	92	4167.89	264.24
II	A	12238.27	295.51	1261.08	370.44/0.45	1479.54	154/162.26	104/493.43	114	1525.02	186.66
	B	12234.07	243.07	1213.79	370.85/0.43	1435.07	159/162.19	99/651.11	113	1471.37	181.05
	C	12128.06	275.66	1211.89	368.15/6.89	1515.28	2511/163.25	1244/468.13	71	15969.67	193.18
	D	12132.15	272.81	1193.62	365.88/6.79	1508.71	2475/163.03	175/565.26	71	3141.25	190.34

Table 4. Hybrid system parameters

Simulation time: 1 year			
Element	**Resource**	**BAT SOC**	**(%)**
PV	5 kW	SOCmax	95
WT	2 kW	SOCelemin	90
Metal Hydride	13 Nm^3	SOCfcmax	75
ELEC	5 kW, 1 Nm^3	SOCmin	70
BAT	400 V, 100 Ah	SOCH2	85
Equipment cost	**Units**		
FC O&M cost	0.6 €/h		
ELEC O&M cost	0.1 €/h		
Input energy Cost	0.136 €/kWh		
Output energy Cost	-0.0274 €/kWh		
FC Cost	8000 € (3.4 kW) 16000 € (6.8 kW)		
ELEC Cost	75000 €		
BAT Cost	7650 €		
Equipment degradation	**Units**		
Runtime FC losses	12 µV/cell/h		
Start/stop FC losses	30 µV/cell/cyc		
Estimated FC lifetime (max degradation)	100 mV/cell		
Estimated ELEC lifetime	5000 cycles		

Moreover, an estimated power curve will be developed for a 6.8 kW stack from the previous power curve (Fig. 4). In order to calculate it, a lineal relation between the number of cells and the power supply is assumed. This consideration can be accepted because the same type of cells is used.

Additionally, an estimated curve of the stack efficiency is presented (Fig. 8). The curve is obtained in basis on the chemical energy contained in hydrogen consumed.

International Journal of Energy Optimization and Engineering
Volume 6 • Issue 1 • January-March 2017

Figure 8. Fuel cell efficiency

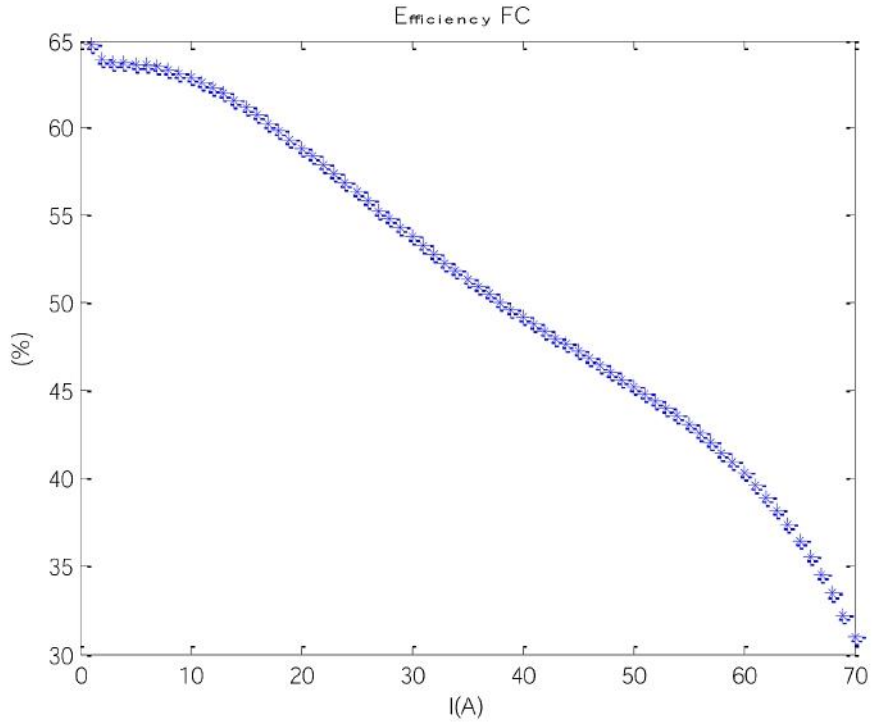

The stack efficiency calculated from the ratio between the input power and the power available at the output of the stack. The input power corresponds with the hydrogen heating power, which is the product among the hydrogen consumption (kg), the Lower Heating Value (LHV) which is 120 MJ/kg, the current (I) and the number of cells (*n*).

Otherwise, the available output power is the product among voltage (*V*), current (*I*) and number of cells (*n*), (Eq. 18).

$$Effic = P_{H2}/P_{out} = (H_{2cons} * \text{LHV} * I * n)/(V * I * n) \quad (18)$$

It is worth noting from Fig. 5 that higher fuel cell efficiency is achieved at low currents (around 65%) and it decreases when current increases to half (30%).

The hybrid system parameters used in these simulations are based on the proposed energy management strategy. For this simulation, different costs and degradation parameters have been obtained from commercial datasheets. These parameters are shown in the Table 4.

To study the system cost and lifetime, two possible fuel cell configurations are going to be analysed:

Configuration Modular: a modular fuel cell system with 6.8 kW rate power made up by two 3.4 kW stacks working at 2 kW every stack.

Configuration Single: a fuel cell system made up by a single 6.8 kW stack working at 4 kW.

The purpose of the analysed configurations is to compare the use of a modular fuel cell system with respect a fuel cell built from a high power single stack regarding different operating situations.

The optimal configuration will show the best results attending to technical and economic criteria. The results obtained from simulation are shown in Table 5.

International Journal of Energy Optimization and Engineering
Volume 6 • Issue 1 • January-March 2017

Table 5. Energy/life parameters results

Fuel Cell Configuration	Ein (kW/h)	Eout (kW/h)	Ebat (kW/h)	Efc (kW/h) --- Loss (mW/h/cell)	Eelec (kW/h)	CYC/Tfc (h)	CYC/Telec (h)	CYC bat	CO&M (€)	H2 (Nm^3)
Modular	960.04	2547.64	2600.72	187.42 --- 586.89 (FC1) 308.11 (FC2)	1282.13	54/72.36 35/21.36	136/843.24	130	3092.80	158.96
Single	959.22	2602.21	2615.8	188.09 --- 460	1286.99	56/47.02	137/846.15	137	3256.98	159.56

6. DISCUSSION

6.1. Energy Management Strategy

According to results shown in Table 3, the use of hysteresis strategy will help to reduce the number of start/stop cycles of fuel cell and electrolyzer, reducing degradation and power losses, resulting in cost reduction.

A minimum power operation point for electrolyzer will result in getting higher hydrogen production in less operation time. This condition also produces a higher use of backup energy, reducing the energy stock, so this results in a mayor energy deficit. The energy input from grid will be higher in these conditions.

In the same way, the energy output to grid decreases, because it is used more energy for electrolysis production. All parameters are shown in Table 3 cases A-B and C-D.

Strategies which use higher DOD for batteries bank operation conditions, will produce a mayor use of it. These strategies can reduce the number of start/stop cycles of fuel cell, reducing hydrogen consumption. This situation also results in more excess of energy, because the required energy for electrolysis decreases in the same way that the hydrogen stock increases. The cost will be reduced, because the fuel cell and electrolyzer lifetime will be increased.

On the other hand, the use of lower DOD, will produce a minor use of the batteries bank. These strategies will increase the use of fuel cell, and the use of electrolyzers, in order to generate enough hydrogen. In the same way, the energy deficit will increase, and it is necessary introduce more energy from the grid. The cost of this strategy will increase because of CO&M for fuel cell and electrolyzer. The battery life is higher than the last configuration.

Because all previously explained, medium DOD strategies will improve the system, and also reduce the overall cost. This DOD also coincides with recommended operation values for lead-acid batteries.

A sensitive analysis based on hysteresis bandwidth is presented in Figures 9-10.

The effect of increase or reduce the hysteresis bandwidth evidences some effects on energy and cost parameters.

Regarding Fig. 9, the use of higher SOCelemin will determine a higher backup energy in batteries because the electrolyzer operation will finish earlier than other configurations, so the grid input energy will be reduced and the energy excess will be increased. In the same way, the use of electrolyzer will be decreased, provoking a minor hydrogen stock. On the other hand, the start/stop cycles will be increased, so it will produce extra deterioration and higher operation and maintenance cost for the electrolyzer.

Finally, the effects over fuel cell will be determined because of the reduction of hydrogen stock. The fuel cell will suffer a little underproduction.

The use of lower SOCelemin will provoke higher use of batteries and electrolyzer because the operation time is longer than other configurations. The hydrogen stock will be increased, so the

International Journal of Energy Optimization and Engineering
Volume 6 • Issue 1 • January-March 2017

fuel cell can operate more time. In the same way, and the output energy decreases due to the extra utilization of electrolyzer. On the other hand, according to Fig. 10 the use of higher SOCfcmax, will determine a higher use of the fuel cell and associated extra deterioration due to run time.

Increasing the SOCfcmax, also produces a higher backup energy in batteries, because the fuel cell will turn off after than other SOC values, charging them. This effect results in a higher capacity to produce hydrogen by electrolysis. The use of electrolyzer will be increased, and also the hydrogen production. The extra energy will decrease, because it is necessary to generate more hydrogen to assure the higher use of fuel cells.

Low values of SOCfcmax will increase the number of start/stop cycles, so it also will increase the fuel cell degradation and overall cost.

The use of medium SOCfcmax will reduce the overall cost because of the reduction of extra deterioration and operation and maintenance cost of the fuel cell. This justifies the medium SOC values chosen during simulations for fuel cell configuration (Table 4).

In basis on these results, authors can conclude that the optimal SOC selection has influence over technical and economic aspects like operation time, lifetime, number of start/stop cycles and cost.

6.2. Fuel Cell Configuration

According to results shown Table 5, in both configurations the fuel cell operates at similar power levels so the fuel cell achieves similar efficiency values is similar (please see Fig. 7 and 8).

In Configuration Single, the limit of hysteresis is reached quickly by high power operation, so there is an increase of the number battery cycles (5%), therefore, the deterioration is increased.

From Configuration Modular, the use of a modular fuel cell system built from two stacks produces a more adapted response than the Configuration Single, so it allows using the hydrogen resource property, and increasing the fuel cell operation time, increasing also runtime degradation respect the second case.

Despite the higher utilization and degradation showing in Configuration Modular, the relationship between degradation vs fuel cell cost is still lower than in Configuration Single (3082.80 € vs 3256.98 €). Thanks to this, the Configuration Modular shows a better economical response with the same overall system performance, presenting an annual cost reduction of 5% respect to Configuration Single.

Moreover, this use of a modular fuel cell system built from two stacks, is a more suitable configuration because in case of failure of a stack, there is available another one (in this case where there are used two stacks), in case of having a problem such as an excessive deterioration of breakable of any of the cells which form the stack.

The utilization of modular fuel cell system join to an energy strategy based on battery hysteresis band and minimum power operation point condition for electrolyzer presents the most viable solution from technical and economical point of view.

7. CONCLUSION

Energy management strategies are necessary to operate a hybrid system based on renewable energy sources fulfilling all the technical and economic targets. In order to improve the performance of the hybrid system, a new energy management strategy has been described and tested with a developed simulator presented in this paper.

According to results, the strategy based on battery hysteresis band will improve the lifetime of the fuel cell and electrolyzer, reducing their operation and maintenance costs. The study of different hysteresis bandwidths reveals the importance of this parameter, in order to improve the system response. In the same way, the use of minimum power operation point condition for electrolyzer will increase the hydrogen stock, but it also will increase the energy deficit inside the system.

International Journal of Energy Optimization and Engineering
Volume 6 • Issue 1 • January-March 2017

Figure 9. SOCelemin analysis for first load profile

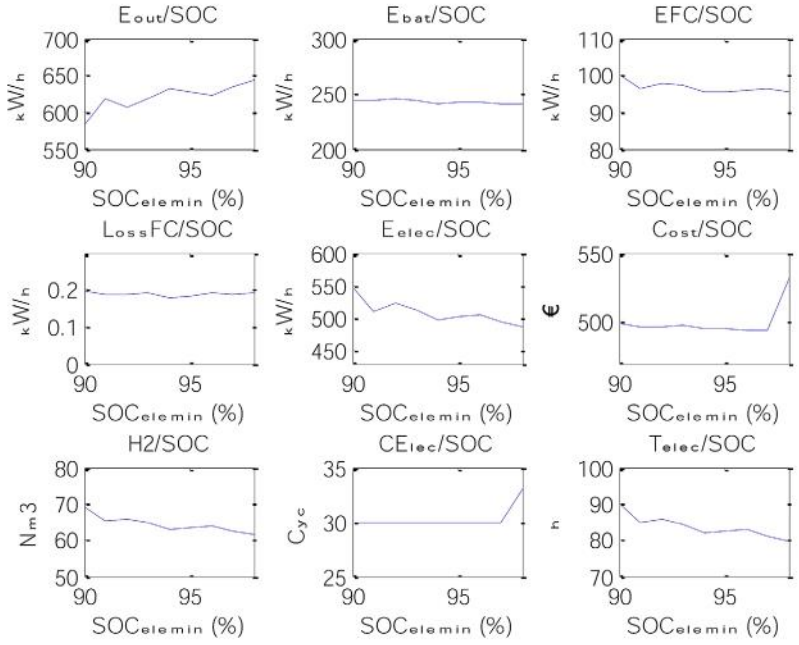

Figure 10. SOCfcmax analysis for first load profile

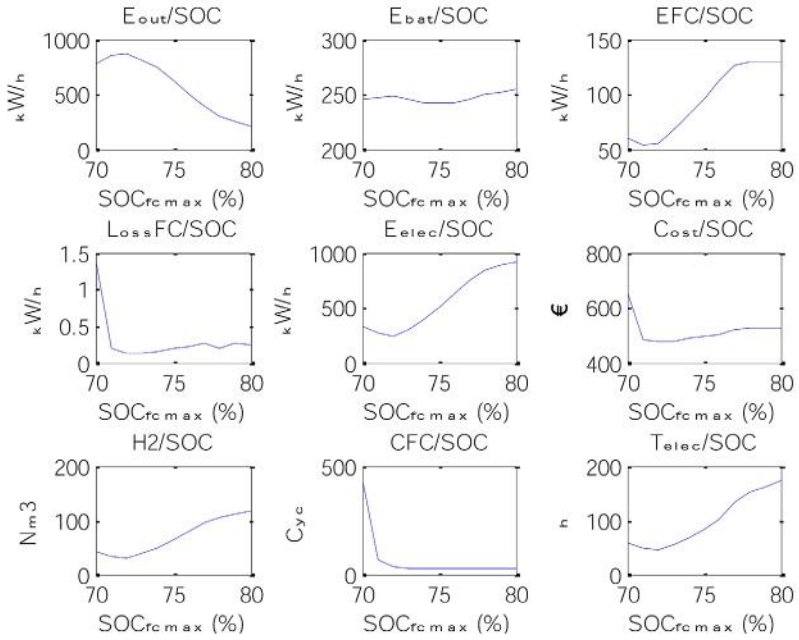

International Journal of Energy Optimization and Engineering
Volume 6 • Issue 1 • January-March 2017

The use of strategies based on medium DOD will reduce the utilization of fuel cell, so it will avoid an extra degradation of it. In the same way, it will improve the battery lifetime respect other strategies. The overall cost will be reduced by the optimal use of it.

The features of the proposed energy management strategy have been compared with other strategies and authors notice the need to include extra analysis to get the optimal SOC values for operation based on hysteresis bandwidth. The use of medium values for hysteresis bandwidth demonstrates an optimal configuration from a technical and economic point of view.

Finally, the use of a modular fuel cell system built from several stacks demonstrates to be the best option from a technical and economic point of view. This configuration allows safer operation mode and assumable operation deterioration, reducing the system operation cost.

To conclude, the importance of choosing an optimal energy management strategy as well as the fuel cell configuration have influence over critical technical and economic aspects like operation time, lifetime, number of start/stop cycles and cost.

International Journal of Energy Optimization and Engineering
Volume 6 • Issue 1 • January-March 2017

REFERENCES

Ahmed, N. A. (2012). On-Grid Hybrid Wind / Photovoltaic / Fuel Cell Energy System.

Alkano, D., Kuiper, I., & Scherpen, J. M. a. (2015). Distributed MPC for Power-to-Gas facilities embedded in the energy grids.

Bae, S. J., Kim, S.-J., Park, J. I., Park, C. W., Lee, J.-H., Song, I., & Park, J.-Y. et al. (2012). Lifetime prediction of a polymer electrolyte membrane fuel cell via an accelerated startup–shutdown cycle test. *International Journal of Hydrogen Energy*, *37*(12), 9775–9781. doi:10.1016/j.ijhydene.2012.03.104

Behzadi, M. S., & Niasati, M. (2015). Comparative performance analysis of a hybrid PV/FC/battery stand-alone system using different power management strategies and sizing approaches. *International Journal of Hydrogen Energy*, *40*(1), 538–548. doi:10.1016/j.ijhydene.2014.10.097

Bizon, N., Oproescu, M., & Raceanu, M. (2015). Efficient energy control strategies for a Standalone Renewable/Fuel Cell Hybrid Power Source. *Energy Conversion and Management*, *90*, 93–110. doi:10.1016/j.enconman.2014.11.002

Bordons, C., García-Torres, F., & Valverde, L. (2015). Gestión Óptima de la Energía en Microrredes con Generación Renovable. *Revista Iberoamericana de Automática E Informática Industrial RIAI, 12*(2), 117–132. http://doi.org/<ALIGNMENT.qj></ALIGNMENT>10.1016/j.riai.2015.03.001

Borup, R. L., Davey, J. R., Garzon, F. H., Wood, D. L., & Inbody, M. a. (2006). PEM fuel cell electrocatalyst durability measurements. *Journal of Power Sources, 163*(1), 76–81. Doi:10.1016/j.jpowsour.2006.03.009

Brka, A., Kothapalli, G., & Al-Abdeli, Y. M. (2015). Predictive power management strategies for stand-alone hydrogen systems: Lab-scale validation. *International Journal of Hydrogen Energy*, *40*(32), 9907–9916. doi:10.1016/j.ijhydene.2015.06.081

Castañeda, M., Cano, A., Jurado, F., Sánchez, H., & Fernández, L. M. (2013). Sizing optimization, dynamic modeling and energy management strategies of a stand-alone PV/hydrogen/battery-based hybrid system. *International Journal of Hydrogen Energy*, *38*(10), 3830–3845. doi:10.1016/j.ijhydene.2013.01.080

Changrong, L., & Jih-Sheng, L. (2007). Low frequency current ripple reduction technique with active control in a fuel cell power system with inverter load. *IEEE Transactions on* Power Electronics, *22*(4), 1429–1436. doi:10.1109/TPEL.2007.900594

Das, D., Esmaili, R., Xu, L., & Nichols, D. (2005). An Optimal Design of a Grid Connected Hybrid Wind / Photovoltaic / Fuel Cell System for Distributed Energy Production. *Proceedings of the 31st annual conference of the IEEE industrial electronics society '05*. Doi:10.1109/IECON.2005.1569298

Dash, V., & Bajpai, P. (2015). Power management control strategy for a stand-alone solar photovoltaic-fuel cell–battery hybrid system. *Sustainable Energy Technologies and Assessments*, *9*, 68–80. doi:10.1016/j.seta.2014.10.001

Dursun, E., & Kilic, O. (2012). Comparative evaluation of different power management strategies of a stand-alone PV/Wind/PEMFC hybrid power system. *International Journal of Electrical Power & Energy Systems*, *34*(1), 81–89. doi:10.1016/j.ijepes.2011.08.025

Eid, A. (2014). Utility integration of PV-wind-fuel cell hybrid distributed generation systems under variable load demands. *International Journal of Electrical Power & Energy Systems*, *62*, 689–699. doi:10.1016/j.ijepes.2014.05.020

El-Shatter, T. F., Eskander, M. N., & El-Hagry, M. T. (2006). Energy flow and management of a hybrid wind/PV/fuel cell generation system. *Energy Conversion and Management*, *47*(9-10), 1264–1280. doi:10.1016/j.enconman.2005.06.022

Feroldi, D., Degliuomini, L. N., & Basualdo, M. (2013). Energy management of a hybrid system based on wind–solar power sources and bioethanol. *Chemical Engineering Research & Design*, *91*(8), 1440–1455. doi:10.1016/j.cherd.2013.03.007

International Journal of Energy Optimization and Engineering
Volume 6 • Issue 1 • January-March 2017

García, P., Torreglosa, J. P., Fernández, L. M., & Jurado, F. (2013). Optimal energy management system for stand-alone wind turbine/photovoltaic/hydrogen/battery hybrid system with supervisory control based on fuzzy logic. *International Journal of Hydrogen Energy*, *38*(33), 14146–14158. doi:10.1016/j.ijhydene.2013.08.106

García, P., Torreglosa, J. P., Fernández, L. M., & Jurado, F. (2014). Improving long-term operation of power sources in off-grid hybrid systems based on renewable energy, hydrogen and battery. *Journal of Power Sources*, *265*, 149–159. doi:10.1016/j.jpowsour.2014.04.118

Giannakoudis, G., Papadopoulos, A. I., Seferlis, P., & Voutetakis, S. (2010). Optimum design and operation under uncertainty of power systems using renewable energy sources and hydrogen storage. *International Journal of Hydrogen Energy*, *35*(3), 872–891. doi:10.1016/j.ijhydene.2009.11.044

Osman Haruni, a., Negnevitsky, M., Haque, M. E., & Gargoom, A. (2013). A novel operation and control strategy for a standalone hybrid renewable power system. *IEEE Transactions on Sustainable Energy, 4*(2), 402–413. Doi:10.1109/TSTE.2012.2225455

Heymann, F., & Bessa, R. (2015). Power-to-Gas potential assessment of Portugal under special consideration of LCOE. *2015 IEEE Eindhoven PowerTech. PowerTech*, *2015*. doi:10.1109/PTC.2015.7232586

Hussain, E. K., Member, S., Bingham, C. M., & Stone, D. (n. d.). Hybrid Stand-Alone Renewable Energy System with High Fuel-cell Efficiency and Unity Power Factor.

Ipsakis, D., Voutetakis, S., Seferlis, P., Stergiopoulos, F., Papadopoulou, S., & Elmasides, C. (2008). The effect of the hysteresis band on power management strategies in a stand-alone power system. *Energy*, *33*(10), 1537–1550. doi:10.1016/j.energy.2008.07.012

Janssen, G. J. M., Sitters, E. F., & Pfrang, A. (2009). Proton-exchange-membrane fuel cells durability evaluated by load-on/off cycling. *Journal of Power Sources*, *191*(2), 501–509. doi:10.1016/j.jpowsour.2009.02.027

Jourdan, M., Mounir, H., & Marjani, A. El. (2014). Compilation of Factors Affecting Durability of Proton Exchange Membrane Fuel Cell (PEMFC). *Proceedings of theInternational Renewable and Sustainable Energy Conference (IRSEC)* (pp. 542–547). http://doi.org/ doi:10.1109/IRSEC.2014.7059906

Kannan, A., Kabza, A., & Scholta, J. (2015). Long term testing of start–stop cycles on high temperature PEM fuel cell stack. *Journal of Power Sources*, *277*, 312–316. doi:10.1016/j.jpowsour.2014.11.115

Karami, N., Moubayed, N., & Outbib, R. (2014). Energy management for a PEMFC-PV hybrid system. *Energy Conversion and Management*, *82*, 154–168. doi:10.1016/j.enconman.2014.02.070

Kim, J., Kim, M., Kang, T., Sohn, Y. J., Song, T., & Choi, K. H. (2014). Degradation modeling and operational optimization for improving thelifetime of high-temperature PEM (proton exchange membrane) fuel cells. *Energy*, *66*, 41–49. doi:10.1016/j.energy.2013.08.053

Layadi, T. M., Champenois, G., Mostefai, M., & Abbes, D. (2015). Lifetime estimation tool of lead–acid batteries for hybrid power sources design. *Simulation Modelling Practice and Theory*, *54*, 36–48. doi:10.1016/j.simpat.2015.03.001

Li, X., Jiao, X., & Wang, L. (2013). Coordinated power control of wind-{PV}-fuel cell for hybrid distributed generation systems. *Proceedings of theSICE Annual Conference (SICE '13)* (pp. 150–155).

Lin, R., Cui, X., Shan, J., Técher, L., Xiong, F., & Zhang, Q. (2015). Investigating the effect of start-up and shut-down cycles on the performance of the proton exchange membrane fuel cell by segmented cell technology. *International Journal of Hydrogen Energy*, *40*(43), 14952–14962. doi:10.1016/j.ijhydene.2015.09.042

Mbarek, E., Belhadj, J., Le, B. P., & Tunis, B. (2009). Photovoltaic Wind hybrid system integrating a Permanent Exchange Membrane Fuel Cell (PEMFC). *International Multi-Conference on Systems, Signals and Devices 2009*, (1), 1–6. http://doi.org/<ALIGNMENT.qj></ALIGNMENT>10.1109/SSD.2009.4956782

Miland, H., & Ulleberg, Ø. (2012). Testing of a small-scale stand-alone power system based on solar energy and hydrogen. *Solar Energy*, *86*(1), 666–680. doi:10.1016/j.solener.2008.04.013

Mohammadi, M., & Nafar, M. (2013). Fuzzy sliding-mode based control (FSMC) approach of hybrid micro-grid in power distribution systems. *International Journal of Electrical Power & Energy Systems*, *51*, 232–242. doi:10.1016/j.ijepes.2013.03.009

Ng, K. S., Moo, C. S., Lin, Y. C., & Hsieh, Y. C. (2008). Investigation on intermittent discharging for lead-acid batteries. *Proceedings of the2008 IEEE Power Electronics Specialists Conference* (pp. 4683–4688). http://doi.org/ doi:10.1109/PESC.2008.4592707

Oyarce, A., Zakrisson, E., Ivity, M., Lagergren, C., Ofstad, A. B., Bodén, A., & Lindbergh, G. (2014). Comparing shut-down strategies for proton exchange membrane fuel cells. *Journal of Power Sources*, *254*, 232–240. doi:10.1016/j.jpowsour.2013.12.058

Patsios, C., & Antonakopoulos, M., Chaniotis, a., & Kladas, a. (2010). Control and analysis of a hybrid renewable energy-based power system. *Proceedings of the XIX International Conference on Electrical Machines - ICEM 2010*, 1–6. http://doi.org/ doi:10.1109/ICELMACH.2010.5608086

Sacarisen, S. P., & Parvereshi, J. J. P. (n. d.). *Improved Lead-Acid Battery Management Techniques.*

Segura, F., & Andújar, J. (2015). Modular PEM Fuel Cell SCADA & Simulator System. *Resources*, *4*(3), 692–712. doi:10.3390/resources4030692

Segura, F., Durán, E., & Andújar, J. M. (2009). Design, building and testing of a stand alone fuel cell hybrid system. *Journal of Power Sources*, *193*(1), 276–284. doi:10.1016/j.jpowsour.2008.12.111

Sun, X. S. X., Lian, Z. L. Z., Wang, B. W. B., & Li, X. L. X. (2009). A Hybrid renewable DC microgrid voltage control. *2009 IEEE 6th International Power Electronics and Motion Control Conference, 3*, 725–729. http://doi.org/ doi:<ALIGNMENT.qj></ALIGNMENT>10.1109/IPEMC.2009.5157480

Tégani, I., Aboubou, A., Ayad, M. Y., Becherif, M., & Bahri, M. (2014). Power flow management in WT/FC/SC hybrid system using flatness based control. *Proceedings of the3rd International Symposium on Environment Friendly Energies and Applications EFEA '14*. http://doi.org/ doi:10.1109/EFEA.2014.7059962

Tesfahunegn, S. G., Ulleberg, Ø., Vie, P. J. S., & Undeland, T. M. (2011). Optimal shifting of Photovoltaic and load fluctuations from fuel cell and electrolyzer to lead acid battery in a Photovoltaic/hydrogen standalone power system for improved performance and life time. *Journal of Power Sources*, *196*(23), 10401–10414. doi:10.1016/j.jpowsour.2011.06.037

Trifkovic, M., Marvin, W., Sheikhzadeh, M., & Daoutidis, P. (2013). Dynamic Real-Time Optimization and Control of a Hybrid Energy System.

Ulleberg, Ø. (2004). The importance of control strategies in PV–hydrogen systems. *Solar Energy*, *76*(1-3), 323–329. doi:10.1016/j.solener.2003.09.013

Uno, M., & Tanaka, K. (2011). Pt/C catalyst degradation in proton exchange membrane fuel cells due to high-frequency potential cycling induced by switching power converters. *Journal of Power Sources*, *196*(23), 9884–9889. doi:10.1016/j.jpowsour.2011.08.030

Uzunoglu, M., Onar, O. C., & Alam, M. S. (2009). Modeling, control and simulation of a PV/FC/UC based hybrid power generation system for stand-alone applications. *Renewable Energy*, *34*(3), 509–520. doi:10.1016/j.renene.2008.06.009

Wang, X., Tong, C., Palazoglu, A., & El-farra, N. H. (2014). Energy Management for the Chlor-Alkali Process with Hybrid Renewable Energy Generation using Receding Horizon Optimization.*Proceedings of the 53rd IEEE Conference on Decision and Control* (pp. 4838–4843). doi:10.1109/CDC.2014.7040144

Yu, Y., Li, H., Wang, H., Yuan, X.-Z., Wang, G., & Pan, M. (2012). A review on performance degradation of proton exchange membrane fuel cells during startup and shutdown processes: Causes, consequences, and mitigation strategies. *Journal of Power Sources*, *205*, 10–23. doi:10.1016/j.jpowsour.2012.01.059

Zhang, F., Thanapalan, K., Procter, A., Carr, S., Maddy, J., & Premier, G. (2013). Power management control for off-grid solar hydrogen production and utilisation system. *International Journal of Hydrogen Energy*, *38*(11), 4334–4341. doi:10.1016/j.ijhydene.2013.01.175

Zhou, K. (2008). Optimal energy management strategy and system sizing method for stand-alone photovoltaic-hydrogen systems. *International Journal of Hydrogen Energy*, *33*(2), 477–489. doi:10.1016/j.ijhydene.2007.09.027

Ziogou, C., Ipsakis, D., Seferlis, P., Bezergianni, S., Papadopoulou, S., & Voutetakis, S. (2013). Optimal production of renewable hydrogen based on an efficient energy management strategy. *Energy*, *55*, 58–67. doi:10.1016/j.energy.2013.03.017

6.6. Contribution 6

Comparative analysis of the efficiency of a classic MPPT system with location of sensors at the output of the converter, compared to the traditional approach of measurements at the output of the generator

J. Ríos, J.M. Enrique, F.J. Vivas, J.M. Andújar

Presented in:

Event: International Congress on Engineering and Sustainability in the XXI century

Organiser: Universidade do Algarve

Date: 09/10/2019 – 11/09/2019

Place: Faro, Portugal.

6.7. Contribution 7

Optimized Balance of Plant for a medium-size PEM electrolyzer. Design, Modelling and Control

J.J. Caparrós, F.J. Vivas, F. Segura, J.M. Andújar

Presented in:

Event: EUROSIM 2019

Organiser: University of La Rioja, EUROSIM Federation of European Simulation Societies, Comité Español de Automática

Date: 01/07/2019 – 05/07/2019

Place: Logroño, Spain.

6.8. Contribution 8

Evaluation of fuel cell/battery passive hybrid power systems for unmanned vehicles

E. López; J. Sáenz; F. José Vivas; F. Isorna; M. A. Ridao; C. Bordons; E. Hernández; A. Efes

Presented in:

Event: European Hydrogen Energy Conference
Organiser: Spanish hydrogen Association
Date: 14/03/2018 – 16/03/2018
Place: Málaga, Spain.

6.9. Contribution 9

In the path of H2020 targets. A new proposal and experimental case to reduce the cost of fuel cells

A. De las Heras, F.J. Vivas, F. Segura, J.M. Andújar

Presented in:

Event: European Hydrogen Energy Conference
Organiser: Spanish hydrogen Association
Date: 14/03/2018 – 16/03/2018
Place: Málaga, Spain.

6.10. Contribution 10

Keys for the best selection of the Balance of Plant configuration in a fuel cell system based on a PE stack

A. De las Heras, F.J. Vivas, F. Segura, J.M. Andújar

Presented in:

Event: World Hydrogen Energy Conference
Organiser: Spanish hydrogen Association
Date: 13/06/2016 – 16/06/2016
Place: Zaragoza, Spain.
ISSN: 9781510838352

6.11. Contribution 11

A review of BoP configurations for PEFCs. Experimental study of a suitable topology

A. De las Heras, F.J. Vivas, F. Segura, J.M. Andújar

Presented in:

Event: 7th International Renewable Energy Congress

Organiser: IEEE Power & Energy Society®

Date: 22/03/2016 – 24/03/2016

Place: Hammamet, Tunisia.

List of Tables

List of Tables

List of Figures

List of Figures

Chapter 4. Results & Methods